August 2004 Volume 207 • Number 1

THE BIOLOGICAL BULLETIN

Published by the Marine Biological Laboratory

Woods Hole, Massachusetts


WHEN IT COMES TO INPUT/OUTPUT FLEXIBILITY, NOTHING WILL GET YOU TO AN IMAGE FASTER.
SCIENCE
UTILITY
VEHICLE.
IX81
MOTORIZED
INVERTED
MICROSCOPE.
OLYMPUS
ROCKET SCIENCE™.
olympusamerica.com/microscopes 800-455-8236
OLYMPUS
Your Vision, Our Future
the Olympus BioScapes Digital Imaging Competition
Deadline September 7, 2004
Visit www.olympusbioscapes.com

Cover

Many benthic marine invertebrates produce planktonic larvae that are dispersed by tides and currents. Even if, by chance, these larvae arrive timely at a location close to an appropriate substratum, specific behavioral responses must be evoked that will lead them to settle and to complete their metamorphosis to the adult form. These critical larval behaviors, and thus successful recruitment, are now known to be induced by chemical cues—some adsorbed to surfaces, others soluble—generated in the environment.

The illustration on the cover shows a pair of nudibranchs (*Phestilla sibogae*) crawling and eating on their characteristic habitat—and prey—*Porites compressa*, an abundant coral in Hawaiian reefs. *Phestilla* has been a superior model for studying larval responses to chemical cues that lead to successful settlement. This small nudibranch (<3 cm) can be conveniently, rapidly, and repeatedly reared in the laboratory throughout the year, and its metamorphosis is well understood. More important, its larvae are induced to settle by a small polar molecule released by *Porites*, its coral substrate and source of food. Furthermore, details of the signal-transduction pathway, including the location of the receptor that induces metamorphosis, are also known.

In nature, however, the interaction between larva and cue occurs in a real environment, and the reef—comprising coral and other types of attached plant and animal species—is a very complex physical habitat indeed. The wave-driven, turbulent flow of seawater over and through the reef disperses the chemical cue released from the coral in extremely fine filaments that swirl in essentially clean water. The *Phestilla* larvae, mixed with cue by the turbulence, enter and leave filaments at high frequency, so each encounter with the cue is very brief. In this issue of *The Biological Bulletin* (p. 28), M. G. Hadfield and M. A. R. Koehl consider for the first time, and in detail, these instantaneous responses of *Phestilla* larvae to encounters with a soluble settlement cue.

As shown in the inset on the cover, individual larvae (shell length, 210 μm) were stuck to the tip of a fine insect pin and inserted into a mini-flume; the flow rate toward the larva was adjusted to equal that of a larva freely swimming in still water. Filaments of fluorescein-tagged seawater (green area in both panels), with or without cue, were produced and could be moved over and past a larva, simulating its passage into and out of a natural filament. In clean water (left panel), the larva quickly extends its foot and velum (the larval swimming organ) from the shell, beats its cilia, and "swims." In a filament containing seawater with settlement cue (right panel), it partially retracts into its shell and would sink if it weren't tethered. These rapid responses to a dissolved settlement cue can enhance the rapid transport of microscopic larvae to the substratum, even in the wave-driven, turbulent flow across a coral reef.

The image of *Phestilla sibogae* (with egg masses) on coral was taken by Robin B. Kinnel; the two images of a tethered larva in the mini-flume are from Figure 2 (p. 32) in the paper by Hadfield and Koehl and were taken by the authors. The cover design was drafted by M. Lynn Milstead (The Whitney Laboratory, University of Florida) and completed by Beth Liles (Marine Biological Laboratory).

THE
BIOLOGICAL BULLETIN
AUGUST 2004

Published by
Marine Biological Laboratory
Woods Hole, Massachusetts

http://www.biolbull.org

Editor's Note

Availability of MBL Annual Report

The Annual Report of the Marine Biological Laboratory, which in the past has been published in the August issue of the journal, is now available on the MBL website. It can also be obtained from the MBL Communications Office or through the MBL WHOI Library. Contact information is given below.

Marine Biological Laboratory
7 MBL Street
Woods Hole, MA 02543-1015

MBL website
http://www.mbl.edu

MBL Communications Office
telephone: 508-289-7423
e-mail: comm@mbl.edu

MBL WHOI Library
telephone: 508-289-7002
e-mail: library@mbl.edu

CONTENTS

VOLUME 207, NO. 1: AUGUST 2004

PHYSIOLOGY AND BIOMECHANICS

DEVELOPMENT AND REPRODUCTION

NEUROBIOLOGY AND BEHAVIOR

CELL BIOLOGY

RESEARCH NOTE

THE BIOLOGICAL BULLETIN

THE BIOLOGICAL BULLETIN is published six times a year by the Marine Biological Laboratory, 7 MBL Street, Woods Hole, Massachusetts 02543.

Subscriptions and similar matter should be addressed to Subscription Administrator, THE BIOLOGICAL BULLETIN, Marine Biological Laboratory, 7 MBL Street, Woods Hole, Massachusetts 02543. Subscription includes both print and online journals. Subscription per year (six issues, two volumes): $325 for libraries; $120 for individuals. Subscription per volume (three issues): $165 for libraries; $70 for individuals. Back and single issues (subject to availability): $75 for libraries; $25 for individuals.

Communications relative to manuscripts should be sent to Michael J. Greenberg, Editor-in-Chief, or Pamela Clapp Hinkle, Managing Editor, at the Marine Biological Laboratory, 7 MBL Street, Woods Hole, Massachusetts 02543. Telephone: (508) 289-7149. FAX: 508-289-7922. E-mail: pclapp@mbl.edu.

http://www.biolbull.org

THE BIOLOGICAL BULLETIN is indexed in bibliographic services including *Index Medicus* and MEDLINE, *Chemical Abstracts, Current Contents, Elsevier BIOBASE/Current Awareness in Biological Sciences*, and *Geo Abstracts*.

Printed on acid free paper,
effective with Volume 180, Issue 1, 1991.

POSTMASTER: Send address changes to THE BIOLOGICAL BULLETIN, Marine Biological Laboratory, 7 MBL Street, Woods Hole, MA 02543.

Periodicals postage paid at Woods Hole, MA, and additional mailing offices.
ISSN 0006-3185

INSTRUCTIONS TO AUTHORS

The Biological Bulletin accepts outstanding original research reports of general interest to biologists throughout the world. Papers are usually of intermediate length (10–40 manuscript pages). A limited number of solicited review papers may be accepted after formal review. A paper will usually appear within four months after its acceptance.

Very short, especially topical papers (less than 9 manuscript pages including tables, figures, and bibliography) will be published in a separate section entitled "Research Notes." A Research Note in *The Biological Bulletin* follows the format of similar notes in *Nature*. It should open with a summary paragraph of 150 to 200 words comprising the introduction and the conclusions. The rest of the text should continue on without subheadings, and there should be no more than 30 references. References should be referred to in the text by number, and listed in the Literature Cited section in the order that they appear in the text. Unlike references in *Nature*, references in the Research Notes section should conform in punctuation and arrangement to the style of recent issues of *The Biological Bulletin*. Materials and Methods should be incorporated into appropriate figure legends. See the article by Lee (October 2003, Vol. **205:** 99–101) for sample style. A Research Note will usually appear within two months after its acceptance.

The Editorial Board requests that regular manuscripts conform to the requirements set below; those manuscripts that do not conform will be returned to authors for correction before review.

1. ***Manuscripts.*** Manuscripts, including figures, should be submitted in quadruplicate, with the originals clearly marked. (Xerox copies of photographs are not acceptable for review purposes.) Please include an electronic copy of the text of the manuscript. Label the disk with the name of the first author and the name and version of the wordprocessing software used to create the file. If the file was not created in some version of Microsoft Word, save the text in rich text format (rtf). The submission letter accompanying the manuscript should include a telephone number, a FAX number, and (if possible) an E-mail address for the corresponding author. The original manuscript must be typed in no smaller than 12 pitch or 10 point, using double spacing (*including* figure legends, footnotes, bibliography, etc.) on one side of 16- or 20-lb. bond paper, 8 by 11 inches. Please, no right justification. Manuscripts should be proofread carefully and errors corrected legibly in black ink. Pages should be numbered consecutively. Margins on all sides should be at least 1 inch (2.5 cm). Manuscripts should conform to the *Council of Biology Editors Style Manual*, 5th Edition (Council of Biology Editors, 1983) and to American spelling. Unusual abbreviations should be kept to a minimum and should be spelled out on first reference as well as defined in a footnote on the title page. Manuscripts should be divided into the following components: Title page, Abstract (of no more than 200 words), Introduction, Materials and Methods, Results, Discussion, Acknowledgments, Literature Cited, Tables, and Figure Legends. In addition, authors should supply a list of words and phrases under which the article should be indexed.

2. ***Title page.*** The title page consists of a condensed title or running head of no more than 35 letters and spaces, the manuscript title, authors' names and appropriate addresses, and footnotes listing present addresses, acknowledgments or contribution numbers, and explanation of unusual abbreviations.

3. ***Figures.*** The dimensions of the printed page, 7 by 9 inches, should be kept in mind in preparing figures for publication. We recommend that figures be about 1 times the linear dimensions of the final printing desired, and that the ratio of the largest to the smallest letter or number and of the thickest to the thinnest line not exceed 1:1.5. Explanatory matter generally should be included in legends, although axes should always be identified on the illustration itself. Figures should be prepared for reproduction as either line cuts or halftones. Figures to be reproduced as line cuts should be unmounted glossy photographic reproductions or drawn in black ink on white paper, good-quality tracing cloth or plastic, or blue-lined coordinate paper. Those to be reproduced as halftones should be mounted on board, with both designating numbers or letters and scale bars affixed directly to the figures. All figures should be numbered in consecutive order, with no distinction between text and plate figures and cited, in order, in the text. The author's name and an arrow indicating orientation should appear on the reverse side of all figures.

Digital art: The Biological Bulletin will accept figures submitted in electronic form; however, digital art must conform to the following guidelines. Authors who create digital images are wholly responsible for the quality of their material, including color and halftone accuracy.

Format. Acceptable graphic formats are TIFF and EPS. Color submissions must be in EPS format, saved in CMKY mode.

Software. Preferred software is Adobe Illustrator or Adobe Photoshop for the Mac and Adobe Photoshop for Windows. Specific instructions for artwork created with various software programs are available on the Web at the Digital Art Information Site maintained by Cadmus Professional Communications at http://cpc.cadmus.com/da/

Resolution. The minimum requirements for resolution are 1200 DPI for line art and 300 for halftones.

Size. All digital artwork must be submitted at its actual printed size so that no scaling is necessary.

Multipanel figures. Figures consisting of individual parts (*e.g.,* panels A, B, C) must be assembled into final format and submitted as one file.

Hard copy. Files must be accompanied by hard copy for use in case the electronic version is unusable.

Disk identification. Disks must be clearly labeled with the following information: author name and manuscript number; format (PC or Macintosh); name and version of software used.

Color: The Biological Bulletin will publish color figures and plates, but must bill authors for the actual additional cost of printing in color. The process is expensive, so authors with more than one color image should—consistent with editorial concerns, especially citation of figures in order—combine them into a single plate to reduce the expense. On request, when supplied with a copy of a color illustration, the editorial staff will provide a pre-publication estimate of the printing cost.

4. ***Tables, footnotes, figure legends, etc.*** Authors should follow the style in a recent issue of *The Biological Bulletin* in preparing table headings, figure legends, and the like. Because of the high cost of setting tabular material in type, authors are asked to limit such material as much as possible. Tables, with their headings and footnotes, should be typed on separate sheets, numbered with consecutive Arabic numerals, and placed after the Literature Cited. Figure legends should contain enough information to make the figure intelligible separate from the text. Legends should be typed double spaced, with consecutive Arabic numbers, on a separate sheet at the end of the paper. Footnotes should be limited to authors' current addresses, acknowledgments or contribution numbers, and explanation of unusual abbreviations. All such footnotes should appear on the title page. Footnotes are not normally permitted in the body of the text.

5. ***Literature cited.*** In the text, literature should be cited by the Harvard system, with papers by more than two authors cited as Jones *et al.*, 1980. Personal communications and material in preparation or in press should be cited in the text only, with author's initials and institutions, unless the material has been formally accepted and a volume number can be supplied. The list of references following the text should be headed Literature Cited, and must be typed double spaced on separate pages, conforming in punctuation and arrangement to the style of recent issues of *The Biological Bulletin*. Citations should include complete titles and inclusive pagination. Journal abbreviations should normally follow those of the U. S. A. Standards Institute (USASI), as adopted by BIOLOGICAL ABSTRACTS and CHEMICAL ABSTRACTS, with the minor differences set out below. The most generally useful list of biological journal titles is that published each year by BIOLOGICAL ABSTRACTS (BIOSIS List of Serials; the most recent issue). Foreign authors, and others who are accustomed to using THE WORLD LIST OF SCIENTIFIC PERIODICALS, may find a booklet published by the Biological Council of the U.K. (obtainable from the Institute of Biology, 41 Queen's Gate, London, S.W.7, England, U.K.) useful, since it sets out the WORLD LIST abbreviations for most biological journals with notes of the USASI abbreviations where these differ. CHEMICAL ABSTRACTS publishes quarterly supplements of additional abbreviations. The following points of reference style for THE BIOLOGICAL BULLETIN differ from USASI (or modified WORLD LIST) usage:

A. Journal abbreviations, and book titles, all underlined (for *italics*)

B. All components of abbreviations with initial capitals (not as European usage in WORLD LIST *e.g., J. Cell. Comp. Physiol.* NOT *J. cell. comp. Physiol.*)

C. *All* abbreviated components must be followed by a period, whole word components *must not* (*i.e., J. Cancer Res.*)

D. Space between all components (*e.g., J. Cell. Comp. Physiol.*, not *J.Cell.Comp.Physiol.*)

E. Unusual words in journal titles should be spelled out in full, rather than employing new abbreviations invented by the author. For example, use *Rit Vísindafjélags Íslendinga* without abbreviation.

F. All single word journal titles in full (*e.g., Veliger, Ecology, Brain*).

G. The order of abbreviated components should be the same as the word order of the complete title (*i.e.*, *Proc.* and *Trans.* placed where they appear, not transposed as in some BIOLOGICAL ABSTRACTS listings).

H. A few well-known international journals in their preferred forms rather than WORLD LIST or USASI usage (*e.g.*, *Nature, Science, Evolution* NOT *Nature, Lond., Science, N.Y.; Evolution, Lancaster, Pa.*)

6. ***Sequences.*** By the time a paper is sent to the press, all nucleotide or amino acid sequences and associated alignments should have been deposited in a generally accessible database (*e.g.*, GenBank, EMBL, SwissProt), and the sequence accession number should be provided.

7. ***Reprints, page proofs, and charges.*** Authors may purchase reprints in lots of 100. Forms for placing reprint orders are sent with page proofs. Reprints normally will be delivered about 2 to 3 months after the issue date. Authors will receive page proofs of articles shortly before publication. They will be charged the current cost of printers' time for corrections to these (other than corrections of printers' or editors' errors). Other than these charges for authors' alterations, *The Biological Bulletin* does not have page charges.

Reference: *Biol. Bull.* **207:** 1–16. (August 2004)

Propagation and Perception of Bioluminescence: Factors Affecting Counterillumination as a Cryptic Strategy

SÖNKE JOHNSEN[1,*], EDITH A. WIDDER[2], AND CURTIS D. MOBLEY[3]

[1]*Biology Department, Duke University, Durham, North Carolina 27708;*
[2]*Marine Science Division, Harbor Branch Oceanographic Institution, Ft. Pierce, Florida 34946;*
and [3]*Sequoia Scientific Inc., Bellevue, Washington 98005*

Abstract. Many deep-sea species, particularly crustaceans, cephalopods, and fish, use photophores to illuminate their ventral surfaces and thus disguise their silhouettes from predators viewing them from below. This strategy has several potential limitations, two of which are examined here. First, a predator with acute vision may be able to detect the individual photophores on the ventral surface. Second, a predator may be able to detect any mismatch between the spectrum of the bioluminescence and that of the background light. The first limitation was examined by modeling the perceived images of the counterillumination of the squid *Abralia veranyi* and the myctophid fish *Ceratoscopelus maderensis* as a function of the distance and visual acuity of the viewer. The second limitation was addressed by measuring downwelling irradiance under moonlight and starlight and then modeling underwater spectra. Four water types were examined: coastal water at a depth of 5 m and oceanic water at 5, 210, and 800 m. The appearance of the counterillumination was more affected by the visual acuity of the viewer than by the clarity of the water, even at relatively large distances. Species with high visual acuity (0.11° resolution) were able to distinguish the individual photophores of some counterilluminating signals at distances of several meters, thus breaking the camouflage. Depth and the presence or absence of moonlight strongly affected the spectrum of the background light, particularly near the surface. The increased variability near the surface was partially offset by the higher contrast attenuation at shallow depths, which reduced the sighting distance of mismatches. This research has implications for the study of spatial resolution, contrast sensitivity, and color discrimination in deep-sea visual systems.

Received 15 December 2003; accepted 17 April 2004.

* To whom correspondence should be addressed. E-mail: sjohnsen@duke.edu

Abbreviations: MTF, modulation transfer function; OTF, optical transfer function; PSF, point spread function.

Introduction

Counterillumination is a common form of crypsis in the open ocean (Latz, 1995; Harper and Case, 1999; Widder, 1999). Its prevalence is due to the fact that, because the downwelling light is orders of magnitude brighter than the upwelling light, even an animal with white ventral coloration appears as a black silhouette when viewed from below (Johnsen, 2002). This is particularly disadvantageous because an object is detectable at a far greater distance when viewed from below than when viewed from any other angle (Mertens, 1970; Johnsen, 2002). Aside from extremely transparent tissue, which is not easy to achieve in larger species with complex tissues, the way to overcome this disadvantage is for the ventral surface to emit light that matches the downwelling light in intensity, spectrum, and angular distribution. Indeed, this solution is nearly ubiquitous in nontransparent mesopelagic species, particularly in crustaceans, fish, and squid (Young and Roper, 1976; Herring, 1977, 1985; Widder, 1999).

Counterilluminating species have evolved complex strategies to match the intensity, spectrum, and angular distribution of the downwelling light (Denton *et al.*, 1972; Young and Mencher, 1980; Herring, 1983; Widder, 1999). One aspect that is poorly understood, however, is the spatial distribution of the photophores (Young and Roper, 1976). While some species (*e.g.*, the cookie cutter shark *Isistius*

brasiliensis) have many small photophores that evenly illuminate the ventral surface, most have a smaller number of isolated photophores that produce uneven illumination (*e.g.*, Fig. 2d). Thus, even if the photophores match the spectrum and intensity of the downwelling light perfectly, the counterilluminator will be visible when viewed at a distance that allows these individual sources to be discerned. To investigate this problem, the effects of the intervening water and the viewer's visual acuity on the perceived image of the counterillumination must be understood.

This study examines the effects of underwater light scattering and visual acuity on the perceived images of counterillumination signals. The effects are modeled with Monte Carlo methods and image transfer theory, using data collected from water types ranging from shallow coastal water to the deep mesopelagic zone (800 m). Three visual systems, with high, medium, and low acuity, are also examined. The goal is to determine under which conditions counterilluminators are still visible and what implications this has for both camouflage and visual detection under low-light conditions.

Materials and Methods

General principles of image transfer

The perceived image of a counterilluminating animal viewed from a distance is affected by three factors: absorption and scattering by the water and the acuity of the viewer's eye. The water and associated particulates potentially dim and blur the image, and the acuity of the eye determines the resolution of the perceived image.

The effect of the first factor is generally modeled in the following way. First, the optical effects of the water on the image of a point source are calculated. The image of a point source is known as the point spread function (PSF) (Mertens and Replogle, 1977). The point source is then convolved with a given image to determine the appearance of the image after it passes through the water. In a convolution, each point in the image is replaced by its product with the point spread function (Fig. 1). Fortunately, this computationally expensive procedure can be streamlined using the convolution theorem, which states that for any two images I_1 and I_2, the convolution of I_1 with I_2 is equal to the inverse Fourier transform of the product of the Fourier transforms of the two images: that is,

$$I_1 * I_2 = \mathcal{F}^{-1}[\mathcal{F}(I_1) \cdot \mathcal{F}(I_2)], \quad \text{(Fig. 1)} \quad \text{(Equation 1)}$$

where * denotes convolution, and $\mathcal{F}(I)$ and $\mathcal{F}^{-1}(I)$ are the Fourier and inverse Fourier transforms of an image I (Goodman, 1996). Let I_1 be the image of the counterillumination, and I_2 be the point spread function. Substituting into equation (1) gives

$$\text{image} * \text{PSF} = \mathcal{F}^{-1}[\mathcal{F}(\text{image}) \cdot \mathcal{F}(\text{PSF})]. \quad \text{(Equation 2)}$$

The Fourier transform of the point spread function is gen-

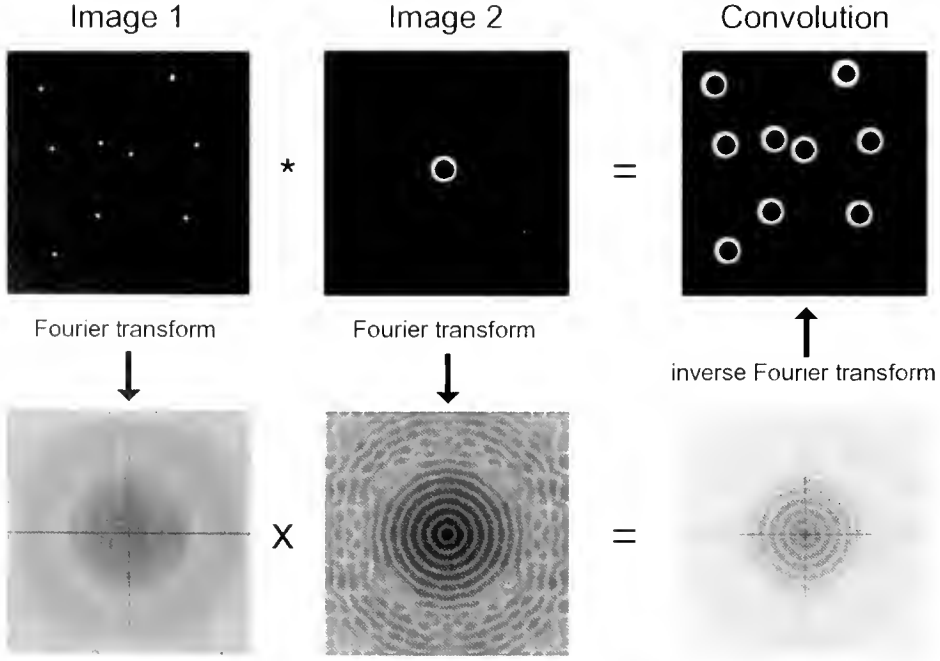

Figure 1. The convolution of image 1 and image 2 (denoted by the "*" operator) can be calculated by multiplying the Fourier transforms of the two images and then calculating the inverse Fourier transform of the product.

erally referred to as the optical transfer function (OTF). Due to the convolution theorem, the OTF of a whole system is simply the product of the OTFs of the various components in the system (Goodman, 1996). Thus, for this study

$$\text{image}_{\text{final}} = \mathcal{F}^{-1}[\mathcal{F}(\text{image}_{\text{initial}}) \cdot \text{OTF}_{\text{water}} \cdot \text{OTF}_{\text{eye}}], \quad \text{(Equation 3)}$$

where $\text{image}_{\text{final}}$ is the perceived image and $\text{OTF}_{\text{water}}$ and OTF_{eye} are the optical transfer functions of the water and eye respectively. A final, convenient implication of the convolution theorem is that the OTF of x meters of optically homogeneous water is equal to the OTF of 1 meter of water to the x^{th} power. Thus, one need only calculate the PSF for one distance. This property, known as the linearity assumption, does not hold in extreme cases (*e.g.*, very large x), but is appropriate for the situations examined in this study (Jaffe, 1992). The equation for underwater image transfer is then

$$\text{image}_{\text{final}}(x) = \mathcal{F}^{-1}[\mathcal{F}(\text{image}_{\text{initial}}) \cdot (\text{OTF}_1)^x \cdot \text{OTF}_{\text{eye}}], \quad \text{(Equation 4)}$$

where $\text{image}_{\text{final}}(x)$ is the perceived image viewed from a distance of x meters, and OTF_1 is the optical transfer function of the water over a distance of 1 meter.

Although Eq. (4) correctly describes the propagation of a two-dimensional image, it requires modification when used in the context of counterillumination, because the background radiance is affected by the entire three-dimensional light field and changes as the viewer moves down and away from its target. From Mertens (1970), the degradation of contrast of a large image underwater (*i.e.*, the OTF at zero spatial frequency) is

$$\text{OTF}(0) = \frac{C_x}{C_0} = e^{-(c - K_L)x}, \quad \text{(Equation 5)}$$

where C_x and C_0 are contrast at x and 0 meters viewing distance, c is the beam attenuation coefficient, and K_L is the attenuation coefficient of the background radiance. In the case of upward viewing, K_L equals K_{Ld}, the attenuation coefficient of direct downward radiance (Johnsen, 2002).

The correct OTF for objects being viewed from below is obtained by normalizing the original OTF so that OTF(0) equals $e^{-(c - K_{Ld})x}$ (Mertens, 1970). Thus the final equation for the propagation of images viewed from below is

$$\text{image}_{\text{final}}(x) = \mathcal{F}^{-1}\left[\mathcal{F}(\text{image}_{\text{initial}}) \cdot \left(e^{-(c - K_{Ld})} \cdot \frac{\text{OTF}_1}{\text{OTF}_1(0)}\right)^x \cdot \text{OTF}_{\text{eye}}\right]. \quad \text{(Equation 6)}$$

The OTF is a complex-valued function and difficult to interpret. Therefore, its magnitude, known as the modulation transfer function (MTF), is often also calculated. The MTF is quite useful because it gives the fraction of remaining image contrast as a function of spatial frequency. For example, MTF(4) = 0.5 implies that 50% of the original image contrast remains for detail that has a spatial frequency of 4 cycles per degree.

Images examined

Images of the ventral bioluminescence of two counterilluminating species were used: (1) the enoploteuthid squid *Abralia veranyi* (Rüppell, 1844) (eye-flash squid), and (2) the myctophid fish *Ceratoscopelus maderensis* (Gunther, 1864) (horned lanternfish) (Fig. 2A, B). The two were chosen to provide a range of photophore spacing. Counterillumination in *A. veranyi* is finely detailed; that of *C. maderensis* is relatively coarse (Fig. 2C, D). *A. veranyi* was collected at depth, using the *Johnson-Sea-Link* research submersible fitted with 11-liter acrylic plastic cylinders with hydraulically activated, sliding lids. *C. maderensis* was collected at night, using an opening/closing Tucker trawl (4.3-m^2 opening, ¼ inch knotless nylon mesh) fitted with a thermally insulated collecting container. Specimens were manually stimulated to bioluminesce, and then were recorded with a Dage ISIT image-intensified video camera (*A. veranyi*) or Intevac GenIISys image intensifier system and CCD video camera (*C. maderensis*). Images that show how the counterilluminating animals appear from below (Fig. 2E, F) were created by combining the bioluminescence images with silhouettes of the animals obtained from normal illumination photographs (taken immediately after the intensified images). Non-illuminating portions of the animals are shown as black because this is how they appear against the downwelling light (Johnsen, 2002). The natural posture of *A. veranyi* is unknown. Although observers in submersibles generally find mesopelagic squid with their fins folded and their arms and tentacles placed over their heads (Vecchione and Roper, 1991; Fig. 2A), this is may be a response to the perceived threat from the submersible. In the silhouette chosen, the fins and appendages were extended to examine their effect on visibility.

The backgrounds were set to a brightness equal to the average brightness of the counterilluminating animal (minus the fins, arms, and tentacles in the case of the squid). Because these relative values allow the animal to blend with the background most easily, it is assumed that they approximately match what would be observed in the field. The backgrounds for the *C. maderensis* images are darker because the average brightness of the animal is darker (due to the wider spacing of the photophores). Note that these figures show *relative* brightnesses, chosen to maximize visibility on the printed page. The *absolute* brightnesses are of

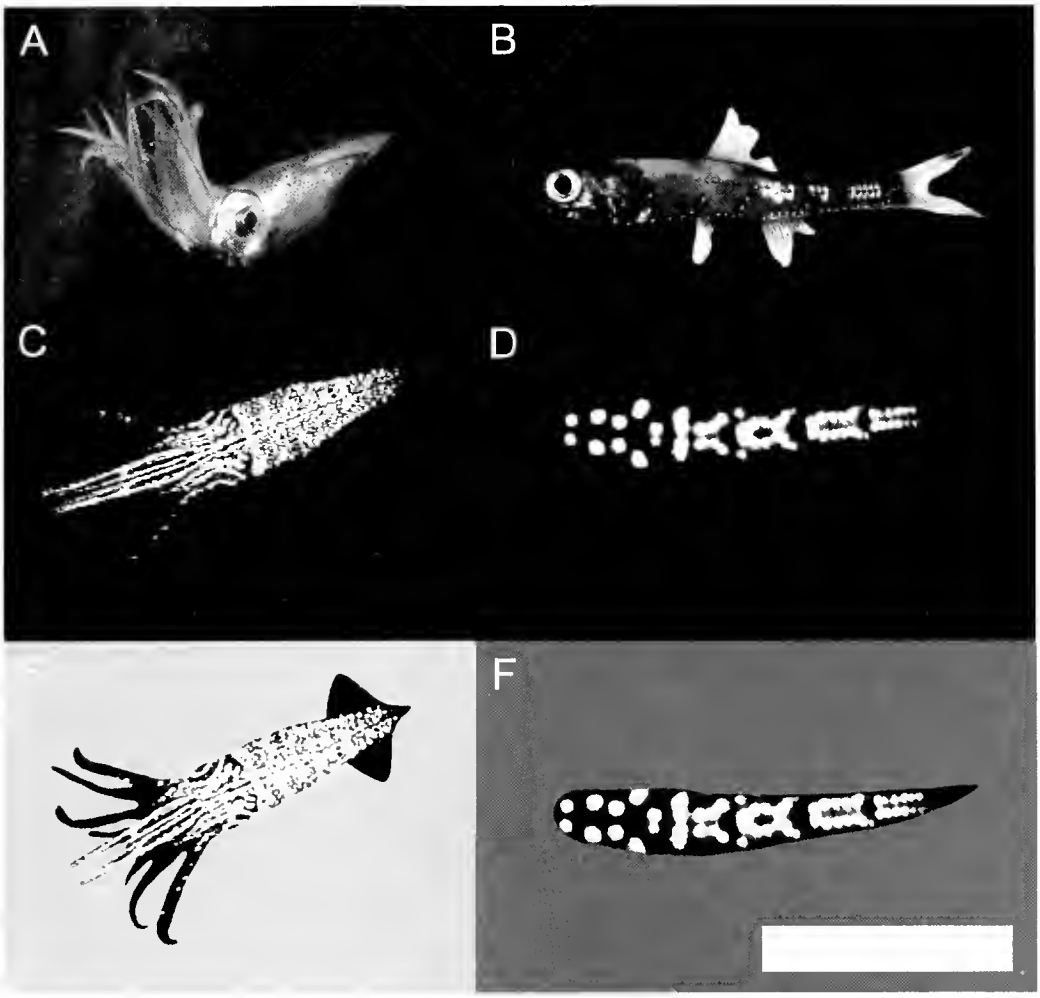

Figure 2. (A) The eye-flash squid *Abralia veranyi*. (B) The horned lanternfish *Ceratoscopelus maderensis*. (C) Counterillumination of *A. veranyi*. (D) Counterillumination of *C. maderensis*. (E) Counterillumination of *A. veranyi* as viewed from below against the downwelling light. (F) Counterillumination of *C. maderensis* as viewed from below against the downwelling light. Scale bar is 5 cm. Background in (E) and (F) is set to the average brightness of the counterilluminating animal. Panel B courtesy of Marine Biological Laboratory Digital Archive, Flescher Fish Collection.

course much dimmer (far beyond the reach of printed paper) and can only be seen by the dark-adapted eye.

The intensified images are not perfect representations of the actual counterillumination. The resolution of the images is low, and the photophore signals are slightly expanded due to "blooming" of the image at the detector array. In addition, although counterillumination is more stable than other bioluminescent signals, the images are static representations of potentially variable light emission. Indeed, a subset of the ventral photophores in *A. veranyi* was not lit in the studied image (Herring *et al.*, 1992). This relatively low number of small photophores most likely would not change a spatial distribution that is already quite uniform. However, they may play a role in spectral changes. In *C. maderensis*, all the ventral photophores were emitting during the image exposure.

Calculation of point spread functions and attenuation coefficients

The PSFs in this study were determined using Monte Carlo software (BSFPSF ver. 1.1., developed by CDM). Five million simulated photons were tracked from an isotropic point source (of unit power) to their point of intersection with a sphere of radius 1 m. Although a PSF is defined as the image of a cosine point source, the use of an isotropic point source achieves the same result because scattering in natural waters is primarily in a forward direction (Mertens and Replogle, 1977; confirmed by preliminary calculations). Due to the symmetry of an isotropic point source, calculations could be completed in far less time than if a cosine point source were used.

The radiance distribution of the simulated photons at the

intersection with the 1-m sphere is the PSF. The three factors (besides distance) affecting the PSF are (1) the absorption coefficient a, (2) the scattering coefficient b, and (3) the phase function γ. The first and second factors specify how often a photon is absorbed or scattered by the water and associated particulates. The third factor specifies the angular distribution of the scattered light. Absorption and attenuation coefficients were obtained for four water types: (1) coastal water at 5-m depth, (2) oceanic water at 5-m depth, (3) oceanic water at 210-m depth, and (4) oceanic water at 800-m depth (Table I). Absorption and scattering coefficients for coastal water were obtained by Dr. Heidi Sosik (Woods Hole Oceanographic Institution, Woods Hole, MA) using a dual-path, multiband absorption/attenuation meter (ac-9, WETLabs Inc.) at a site 80 km from the coast of Portsmouth, New Hampshire (42°47′N 70°05′W, 1106 local time, 30 June 2000) (see Johnsen and Sosik, 2003, for details). Optical coefficients in oceanic water (Jerlov type 1) at 5 m and 210 m were obtained by Drs. Andrew Barnard, Scott Pegau, and Ronald Zaneveld (College of Oceanic and Atmospheric Sciences, Oregon State University, Corvallis, Oregon) using the same equipment in the equatorial Pacific (1005 local time, 30 April 1996; 0°0′N 177°21′W). Optical coefficients in oceanic water at 800-m depth were obtained from Capone *et al.* (2002). In all cases, absorption and beam attenuation coefficients were measured at 412, 440, 488, 510, 532, 555, 650, and 676 nm. Although point spread functions were calculated for all eight wavelengths, for clarity only those at 412, 488, 555, and 650 nm are analyzed and discussed in this study. While the 5-m coastal measurement is somewhat specific to measurement site, the three oceanic measurements are typical of most oceanic waters, particular those at 210 and 800 m.

Because the ac-9 absorption-attenuation meter has detectors of finite size, light scattered over small angles was collected by the detector and incorrectly interpreted as unscattered. Thus, scattering was underestimated by a small amount. If one assumes that the scattering matches Petzold's phase function, then the scattering coefficient is underestimated by approximately 20%. Again, preliminary results showed that this had negligible effect on the blurring of the image, though it would have resulted in slightly greater attenuation of the contrast of the whole image. The ac-9 meter also does not measure certain factors that may influence image propagation, such as marine snow and refractive index inhomogeneities. The large particles of marine snow will limit the long-range visibility of small objects by direct occlusion, and refractive index inhomogeneities may slightly increase scattering at very small angles (below the resolution limit of the visual systems examined) (Bogucki *et al.*, 1998).

The phase function γ was chosen to be the commonly used "average particle" function (Mobley *et al.*, 1993) based on measurements by Petzold (1977). In productive coastal waters, most of the light is scattered by living phytoplankton, which have a backscatter fraction of 0.01 or less (*e.g.*, Ulloa *et al.*, 1994). However, in clear oceanic water, isotropic scattering by the water itself is a significant fraction of the total scattering, and the total backscatter fraction can be as large as 0.04 (Mobley, 1994). We chose Petzold's average particle phase function (Mobley *et al.*, 1993), which has a backscatter fraction of 0.018, about midway between the two extremes. Preliminary results showed that, because scattered light was extremely dim compared to the unscattered direct beam, the choice of phase function made no notable difference.

PSF values were calculated up to 10°, at 0.05° intervals. Although the PSF from 0 to 1° was calculated using Monte Carlo methods, computational limits (due to the small size of the angular bins receiving scattered photons) prevented accurate calculations at substantially higher angles for the given number of initial photons. Therefore, the PSF from 1° to 10° was estimated by fitting the PSF from 0.45° to 1° to a power function and then extrapolating by 0.05° increments up to an angle of 10° (see Voss, 1991, for justification).

The optical transfer functions of the eyes were modeled as the Gaussian curve:

$$\mathrm{OTF}(\nu) = e^{-3.56\cdot(R\nu)^2} \qquad \text{(Equation 7)}$$

where ν is the spatial frequency (in cycles/degree) and R is the spatial resolution (Warrant, 1999). This function, often used to model the OTF of visual systems, results in a barely

Table I

Absorption and scattering coefficients (a and b respectively) used in the Monte Carlo calculation of point spread functions

Wavelength (nm)	Coastal water at 5-m depth		Oceanic water at 5-m depth		Oceanic water at 210-m depth		Oceanic water at 800-m depth	
	a	*b*	*a*	*b*	*a*	*b*	*a*	*b*
412	0.29	0.26	0.035	0.11	0.060	0.018	0.027	0.020
488	0.15	0.21	0.038	0.098	0.035	0.013	0.027	0.014
555	0.11	0.19	0.073	0.091	0.077	0.0094	0.072	0.0060
650	0.37	0.15	0.36	0.085	0.36	0.014	0.36	0.014

detectable contrast of 2.8% ($= e^{-3.56}$) at the spatial resolution of the eye. The spatial resolutions of three mesopelagic fish were chosen to span a wide range of visual acuity: (1) $R = 0.11°$ (the "lovely hatchetfish" *Argyropelecus aculeatus*), (2) $R = 0.23°$ (the spookfish *Opisthoproctus soleatus*), and (3) $R = 0.50°$ (the myctophid fish *Lampanyctus festivus*) (Collin *et al.*, 1997; Wagner *et al.*, 1998). *A. aculeatus* and *O. soleatus* both have upward-viewing tubular eyes; *L. festivus* has lateral-viewing eyes and so probably does not search for overhead, counterilluminating prey.

The acuity of these species was measured from the density of their retinal ganglion cells (which accounts for spatial summation). Because these counts also include displaced ganglion cells, they may slightly overestimate acuity. The predicted acuity also assumes a well-focused image, but this is generally the case for the foveal regions of deep-sea eyes (Warrant and Locket, 2004). Increasing spatial summation will also lower the acuity. Finally, it is important to note that these spatial resolutions do not include potential blurring of a moving image due to large temporal summation. Since long temporal summation times are common at depth (Frank, 1999) and animals do drift relative to one another in the water, the actual spatial resolution in certain situations may be less than that predicted by retinal morphology.

The minimum contrast threshold is the smallest percentage variation in radiance that can be detected. This value for fish is approximately 1%–2% in bright light, but it rises as depth increases (Douglas and Hawryshyn, 1990). Though few direct measurements have been made, the threshold at mesopelagic light levels appears to range from about 25% to 50% (*e.g.*, threshold for the Atlantic cod *Gadus morhua* at 650-m depth is approximately 50% (Anthony, 1981)). We therefore set the minimum contrast threshold at 33%, while accepting that depth, water clarity, and special visual adaptations make the actual threshold highly variable.

The attenuation coefficients of direct downward radiance K_{Ld} were calculated by modeling the underwater radiance distribution using radiative transfer software (Hydrolight 4.2, Sequoia Scientific Inc., Bellevue, WA, www.hydrolight.info). The inherent optical properties required by the software were obtained from measured vertical profiles of chlorophyll concentration and absorption and scattering coefficients from the four water types examined (see Johnsen, 2002; and Johnsen and Sosik, 2003, for details). The sun was assumed to be at the zenith on a clear day with no wind.

Measurement of moonlight and starlight spectra

Nocturnal spectra under moonlight and starlight were measured using a spectrometer with a highly sensitive photomultiplier detector (OL-754-PMT, Optronics Laboratories Inc., Orlando, FL). Moonlight spectra were measured in air on a barrier island in Florida during full moon (moon was at its peak elevation). An integrating sphere was used to collect light from all regions of the sky. Starlight spectra were measured on a moonless night on a completely darkened ship in the center of the Gulf Stream (latitude ~27°N) to ensure a complete absence of light pollution. To minimize light loss, the integrating sphere was removed and the entrance slit of the spectrometer (~30° angular field) was aimed at the zenith. The downwelling irradiance at 5-m depth under moonlight and starlight was calculated using the above-described radiative transfer software, with the correct skylight spectrum as an input.

Results

Point spread and optical transfer functions of the water types and visual resolutions

The point spread functions in all four water types were extremely narrow, with the radiance at zero degrees 2–3 orders of magnitude larger than the radiance at higher angles (at a distance of 5 m) (Fig. 3). With increasing water clarity and depth, this effect became more pronounced. The wavelength dependence of the PSF was complex, depending on the relative numbers of scattering and absorption events.

In all four water types, the modulation transfer function was primarily affected by the visual resolution of the viewer's eye (Fig. 4). However, the MTFs in near-surface waters decreased at higher spatial frequencies (independently of the decrease due to visual acuity limitations), indicating some blurring by the water (Fig. 4A, B). The MTFs within a given water type had similar shapes and differed primarily in magnitude (set by $\mathrm{MTF}(0) = e^{-5(c - K_{Ld})}$). This magnitude had a complicated wavelength dependence, being proportional to wavelength in near-surface waters and inversely proportional to wavelength in deep waters.

Perceived images

The perceived images were dramatically affected by the visual resolution of the viewer and, to a lesser extent, by scattering and absorption by the water (Figs. 5, 6). When viewed at 0.11° resolution, *Ceratoscopelus maderensis* and *Abralia veranyi* had a contrast greater than 33% at distances up to 4 to 8 m (though the visibility of the latter was primarily due to the unlit fins and appendages). However, when viewed at 0.5° resolution, the contrast of the counterillumination was greater than 33% only up to a distance of 1 to 2 m. The individual photophores of *C. maderensis* were distinguishable up to 2 m at 0.11° resolution, and the general pattern of photophores was distinguishable up to 2 m at lower resolutions. The general pattern of the photophores of

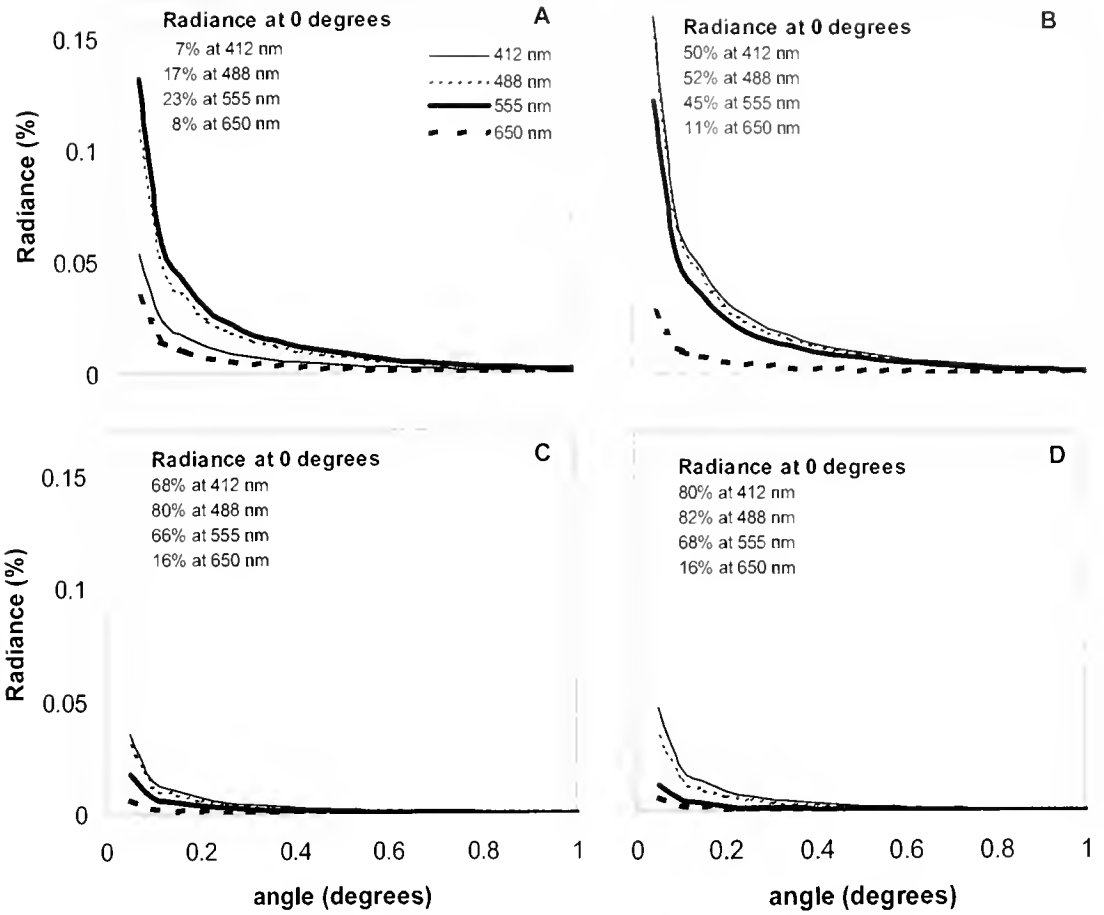

Figure 3. Radiance *vs.* angle for a point source viewed from a distance of 5 m (point spread function). The radiance is normalized by the radiance of a point source viewed at 5 m in a medium that does not scatter or absorb light. (A) Coastal water at 5-m depth. (B) Oceanic water at 5-m depth. (C) Oceanic water at 210-m depth. (D) Oceanic water at 800-m depth. The normalized radiances at zero degrees are given numerically rather than graphically because they are far higher than the other values.

A. veranyi was evident at 1 m at 0.11° resolution, but not at lower resolutions.

The counterillumination of both species is visible at roughly twice the distance in the clearest conditions studied (at 488 nm in oceanic water at 800-m depth) as it is in the most turbid conditions (at 412 nm in coastal water at 5-m depth) (Fig. 5A *vs.* 5B, Fig. 6A *vs.* 6B). The difference was entirely due to the difference in MTF(0) between the two water types (95% *vs.* 37% at a distance of 5 m) and not to significantly increased blurring of fine detail.

Variation of background spectra and wavelength dependence of contrast attenuation

The background spectra at shallow depths under moonlight and starlight differed substantially in both coastal and oceanic waters, particularly at shorter wavelengths (Fig. 7A, B). Under starlight, the spectrum narrowed and the peak wavelength was long-shifted (by 40 to 80 nm depending on the water type and what is considered the true peak). The background spectra were also affected substantially by depth, even at mesopelagic depths. As the depth increased from 200 to 800 m, the spectra of the downwelling irradiance narrowed slightly and the peak wavelength shifted from 490 nm to 480 nm (Fig. 7C).

General contrast attenuation was relatively rapid and wavelength-independent at 5-m depth in both coastal and oceanic waters, with sighting distances (proportional to $1/c - K_{Ld}$) only 5%–20% of those in deeper waters (Fig. 7D). At greater depths, sighting distance was highly dependent on wavelength. At these depths, sighting distance increased with wavelength, until it reached a peak at a wavelength about 30 nm longer than that of the peak wavelength of downwelling irradiance. After this peak, the sighting distance decreased rapidly with wavelength. For wavelengths greater than 600 nm, the sighting distances at depth were less than those near the surface.

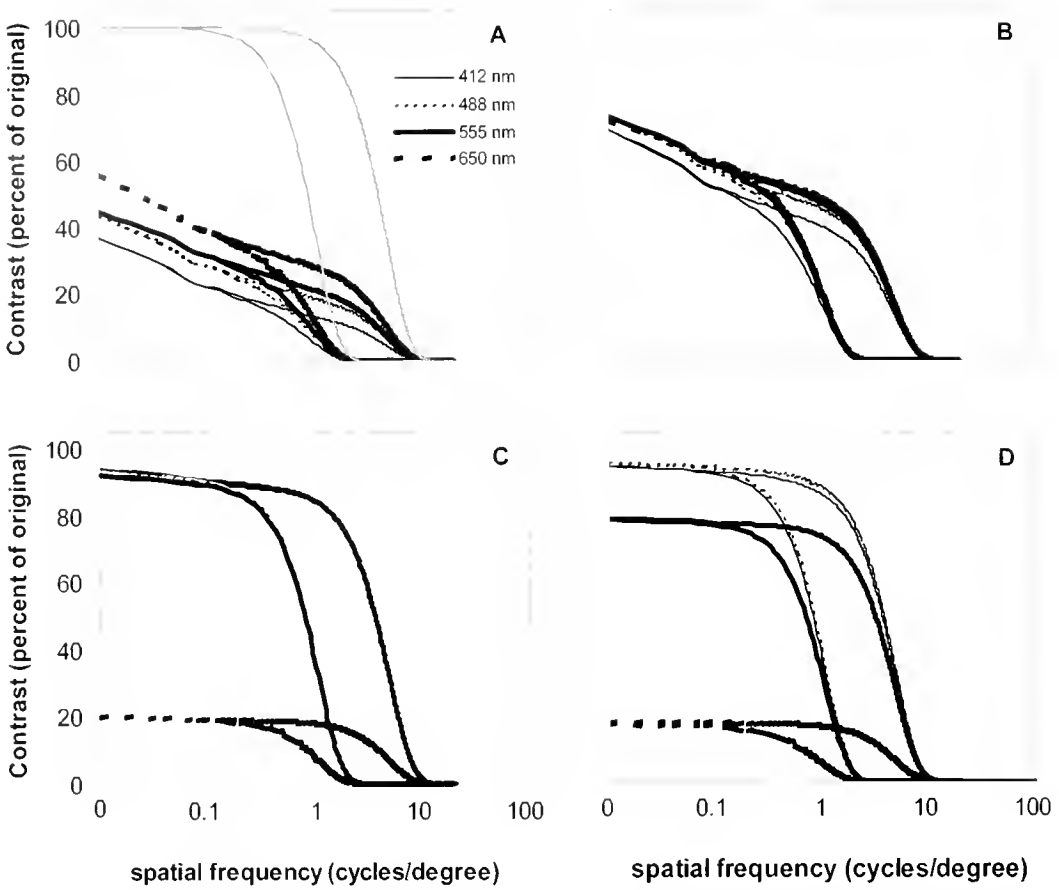

Figure 4. Contrast as a function of spatial frequency for an object viewed from a distance of 5 m (modulation transfer function, MTF). The contrast is normalized by the contrast at a distance of 0 m. (A) Coastal water at 5-m depth. (B) Oceanic water at 5-m depth. (C) Oceanic water at 210-m depth. (D) Oceanic water at 800-m depth. The MTF is shown for two visual systems, one with 0.11° resolution and one with 0.5° resolution. At a spatial frequency of approximately 0.4 cycles/deg, the data split, with the lower trace denoting 0.5° resolution. The two gray lines in (A) denote the MTF for the eyes alone. Because the MTF at 0 cycles/deg is important, the graphs include this point despite being logarithmic.

Discussion

This study shows that a counterilluminating individual faces a number of difficulties. First, an acute eye (0.11° resolution) with moderate contrast sensitivity (33%) can detect the photophore patterns of both *Abralia veranyi* and *Ceratoscopelus maderensis* at distances greater than 1 m. Second, even the water at the relatively turbid shallow coastal site blurred the counterillumination signals very little. Although all four water types did lower the overall contrast of the counterilluminator, the attenuation rate was quite low, particularly at mesopelagic (>200 m) depths. Finally, the spectrum of downwelling background light varied considerably with depth in the mesopelagic zone and was strongly affected by the source of nocturnal illumination at the shallow depths. This suggests that counterilluminating photophores must be spaced closely together when viewed by visually acute species, and that matching the background spectrum may be more difficult than previously considered. From the predator's point of view, this study suggests that high spatial resolution and color discrimination in the blue-green portion of the spectrum are highly advantageous for detecting counterilluminating prey. However, since both of these characteristics reduce sensitivity, they also have a cost that must be balanced.

The remainder of the paper explores these limitations in detail. It is important to note that, despite these limitations, counterillumination dramatically decreases the visibility of the individual. The visibility of *A. veranyi* at distances greater than 1 m is entirely due to the unlit fins, tentacles, and arms (Fig. 5), which may be held above and against the body to minimize their silhouette (Fig. 2A). The visibility of these unlit regions at distances of at least 8 m highlights the impressive crypsis afforded by counterillumination. In addition, in certain cases the goal may not be complete cryp-

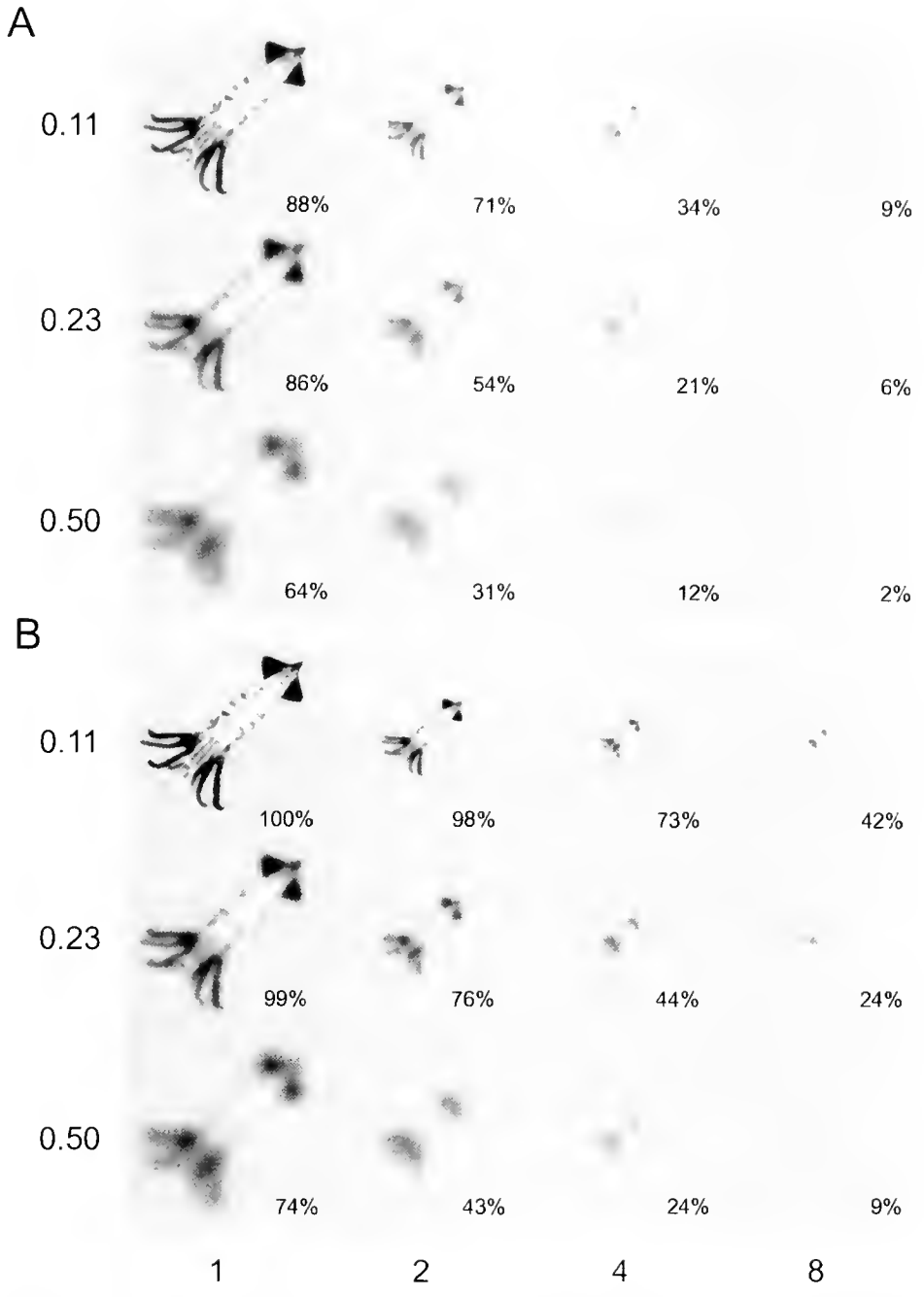

Figure 5. Counterillumination of *Abralia veranyi* viewed from distances of 1, 2, 4, and 8 m by animals with eyes of 0.11°, 0.23°, and 0.5° resolution. (A) Counterillumination is viewed at a wavelength of 412 nm in coastal water at 5-m depth (the optical conditions that had the greatest effect on image propagation). (B) Counterillumination is viewed at a wavelength of 488 nm in oceanic water at 800-m depth (the optical conditions that had the least effect on image propagation). The percentages indicate the maximum contrast in each image. All images are scaled in size for viewing distance, and the backgrounds are all set equal. To see the absolute brightness values in the image, view the figure under dim illumination so that the printed background matches the brightness at the relevant depth. For example, to see what the counterillumination looks like at depths of 200, 300, and 400 m, view the figure under civil twilight, full moonlight, and half-moonlight respectively.

sis, but a bioluminescent analog of disruptive coloration. The individual photophores may break up the silhouette so that it appears as a number of small objects rather than as one large, recognizable outline. This tactic is common and highly successful in benthic and terrestrial habitats where the background is complex (Lythgoe, 1979). Its effective-

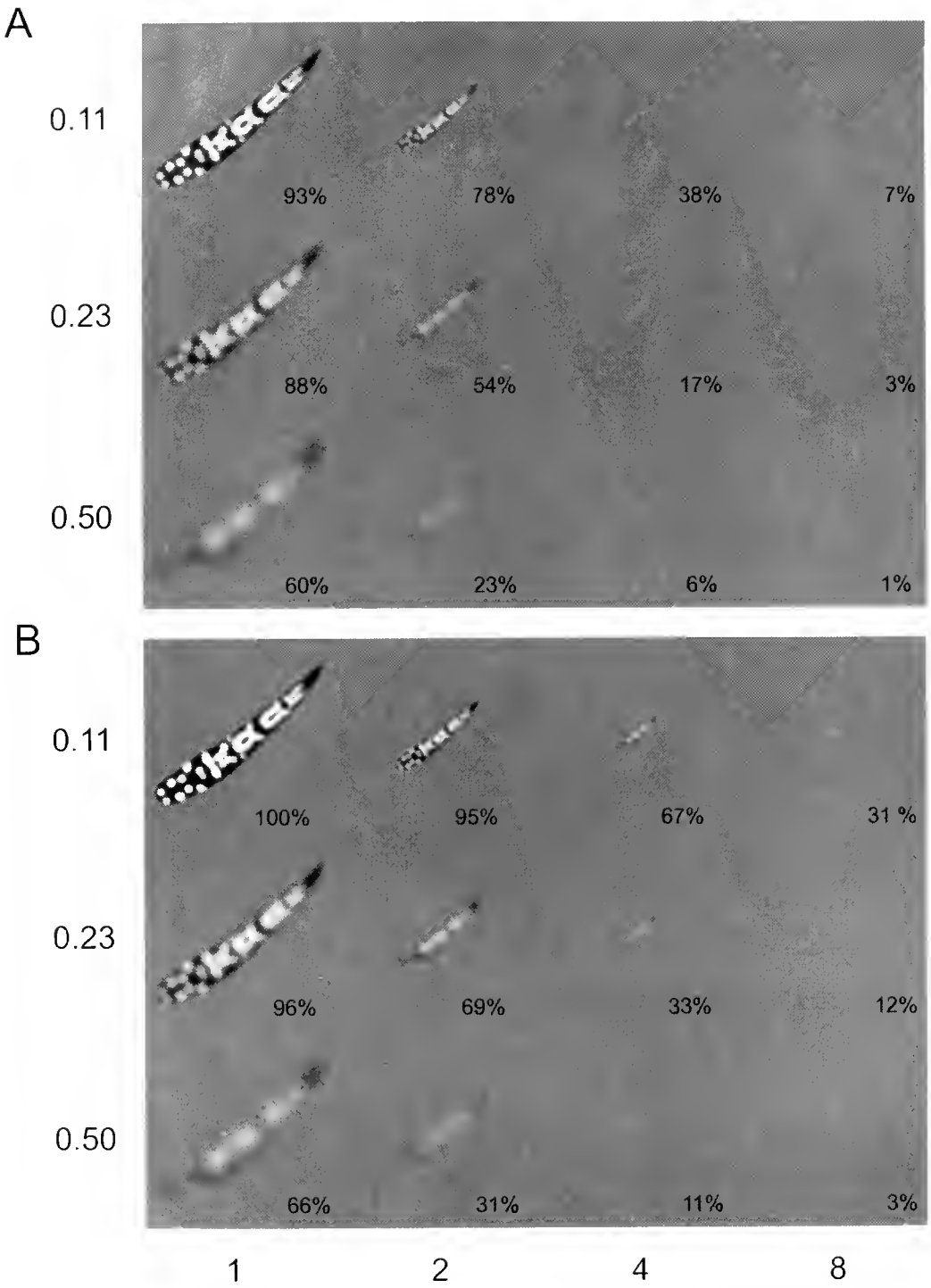

Figure 6. Identical to Figure 5, except that the counterillumination signal is generated by *Ceratoscopelus maderensis*.

ness in pelagic environments, where the background is very uniform, is uncertain. Finally, the ability of the predator to recognize the perceived image as potential prey depends on pattern recognition, a higher level of visual processing that is poorly understood in oceanic species.

Effects of intervening water on counterillumination

Despite the authors' initial expectations, the water had little effect on the appearance of the counterillumination. This was due to several factors. First, even in the worst case

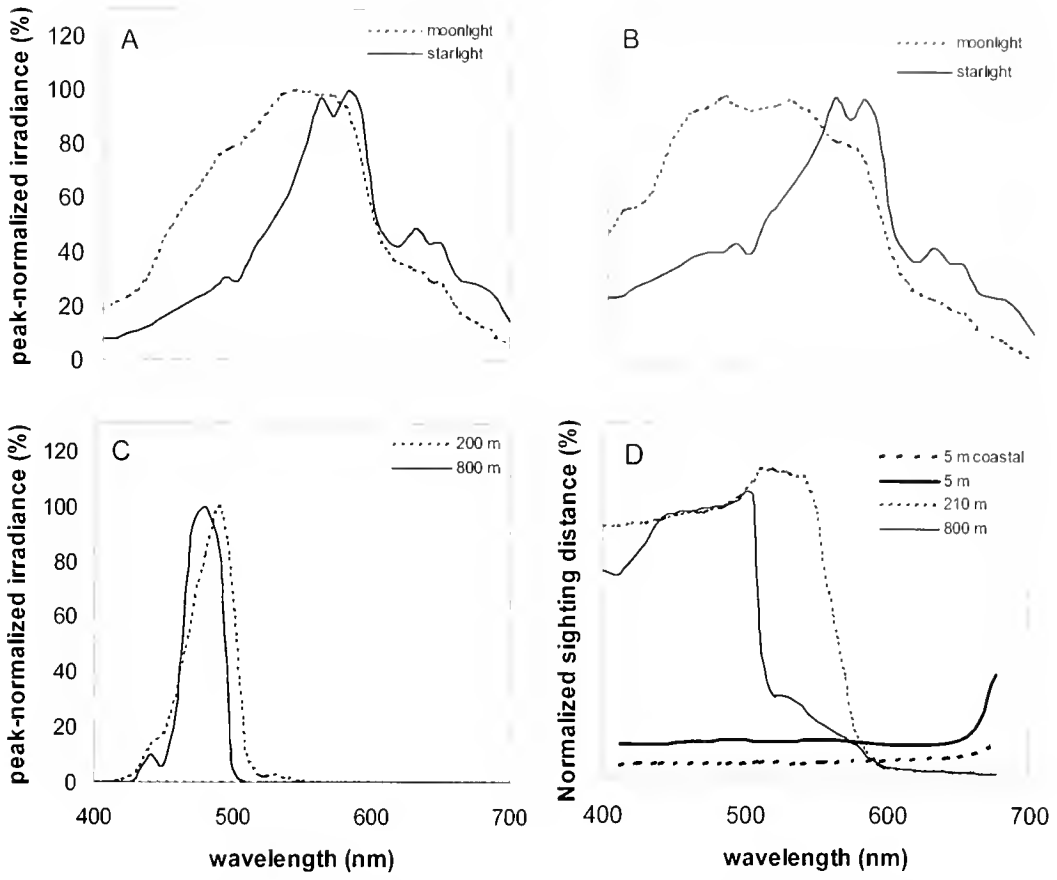

Figure 7. (A) Downwelling irradiance (normalized by peak) at 5-m depth in coastal water under moonlight and starlight. (B) Same as (A), but in oceanic water. (C) Downwelling daytime irradiance at depths of 200 and 800 m. (D) Sighting distance of a counterilluminator, normalized by sighting distance in mesopelagic waters at 480 nm. Because all published bioluminescence spectra are calibrated in energy units (instead of quanta), (A), (B) and (C) are calibrated in relative energy units.

(412-nm light in coastal water at 5-m depth), 8% of the photons were neither scattered nor absorbed after traveling 5 m ($=e^{-5(a\,+\,b)} = e^{-5(0.29\,+\,0.26)}$). The viewer perceives these uncollided photons as all arriving from one point (which has a radius determined by the spatial resolution of the eye), so the perceived radiance of this unscattered light is quite high. In contrast, the scattered photons, although more numerous (92% in this case), are scattered over a larger angular area and so have a lower radiance. Second, for a photon to contribute to image blurring, it must be scattered but not absorbed by the water. Because highly scattering waters also tend to be highly absorbing (see Table 1), many scattered photons are absorbed before they can reach the eye and thus cannot contribute to image blurring. This is in sharp contrast to atmospheric scattering (*e.g.*, due to haze or fog), which can be high while absorption is negligible (Bohren and Huffman, 1998). Finally, light scattering in water is strongly biased in the forward direction. In the phase function used in this study, more than 50% of the scattered photons are deflected less than 5° (Petzold, 1977). Thus, the halo of scattered light surrounding the image of a point source is quite narrow. This also differs from the atmospheric case, where light is often scattered over relatively large angles (Bohren and Huffman, 1998). For all the above reasons, the images in all the water types examined did not lose a substantial amount of fine detail. There are, of course, considerably more turbid marine waters (very close to shore or to river plumes, coccolithophore blooms, *etc.*). Counterilluminators, however, are seldom found in these locations.

A parameter that was greatly affected by the water was the attenuation of the contrast of the entire scene (*e.g.*, MTF(0)). The attenuation coefficient depends on the viewing angle of the predator and for upward viewing is $c - K_{Ld}$ (see Eq. 5). This coefficient is far smaller than the attenuation coefficients for viewing an object horizontally or from above (c, and $c + K_{Ld}$ respectively), so objects viewed from below are visible at much longer distances (Johnsen, 2002). This result derives from the fact that, as a viewer moves down and away from a counterilluminator, the background

dims almost as quickly as the signal does, thus maintaining the contrast. The unusual wavelength dependence of the attenuation of counterillumination occurs because c and K_{Ld} vary somewhat independently. At shorter wavelengths, $c - K_{Ld}$ increases slightly with wavelength; at longer wavelengths at depth, c increases rapidly with wavelength, while K_{Ld} remains more or less constant. This is because almost all long-wavelength light at depth is due to Raman scattering, in which a small portion of the blue-green light is converted into longer wavelength light (Marshall and Smith, 1990; Johnsen, 2002). Because this Raman-scattered light is produced *de novo* from shorter wavelength light, it has roughly the same attenuation coefficient as that light, and so the difference between c and K_{Ld} can grow quite large. But because the long wavelength light is extremely dim, it may not be of visual significance, particularly at mesopelagic depths.

A curious feature of this wavelength dependence is that the wavelength of least contrast attenuation is about 30 nm longer than the peak wavelength of the downwelling light. The lower contrast attenuation at these wavelengths allows for a slightly longer sighting distance (proportional to $1/c - K_{Ld}$: 12.5% longer at 210 m; 5.5% longer at 800 m) than at the peak wavelength. Because the spectral responses of most deep-sea visual systems are relatively flat (Douglas *et al.*, 1998), this shift may be inconsequential.

Effect of variation in background illumination

The fact that the spectrum of the background changes with depth has been examined before (*e.g.*, Young and Mencher, 1980). This study confirms that, even at mesopelagic depths, the spectrum changes substantially with depth. While a 10-nm shift in the peak wavelength appears minor, it causes large shifts in the intensity of the off-peak light because the wavelength distributions are quite narrow. For example, if the peak intensities are set equal at 100% (as in Fig. 7C), the difference between the downwelling irradiance at depths of 200 and 800 m is 62% at 500 nm and 32% at 470 nm.

A previously unconsidered issue is the effect of the nocturnal illumination source. Many counterilluminators are vertical migrators and can be found near the surface at night (the downwelling irradiance at 5-m depth under moonlight and starlight equals that found during the middle of the day at 300 and 500 m respectively). The background illumination then depends on whether the moon is present. Over a complete lunar cycle, the moon is above the horizon for about half of the nocturnal hours. Because the moon reflects all wavelengths more or less equally (Munz and McFarland, 1977), the spectrum of the night sky with the moon present is similar to the spectrum of daylight (though dimmer by about 6 orders of magnitude, and slightly red-shifted due to background starlight). When the moon is not present, the illumination has three primary components: (1) starlight, mostly due to dim red stars invisible to the naked eye, (2) scattering of sunlight by dust in the plane of the solar system, and (3) emission spectra from gases in the upper atmosphere (*e.g.*, airglow) (Munz and McFarland, 1977). The final irradiance spectrum is strongly red-shifted. Whereas the spectral shift from moonlight to starlight is minor at mesopelagic depths, it is quite obvious in near-surface waters (Fig. 7A, B), particularly in blue, oceanic waters. Since very few marine species are known to have long-wavelength sensitivity at scotopic light levels, the implications of the spectral shifts at these wavelengths are unknown. However, the shifts at blue-green wavelengths (450–500 nm) are also substantial, and can be detected by nearly all deep-sea visual systems. Although certain counterilluminating species alter the spectra of their emitted light with ambient temperature or depth (Young and Mencher, 1980; Young and Arnold, 1982; Herring *et al.*, 1992), adaptations to the spectral shift caused by the presence or absence of the moon are unknown.

Implications for counterillumination

The clarity of the water and the spectral variation due to depth and the presence or absence of the moon have several important implications for counterilluminators. First, since it is unlikely that light scattering by the water will combine the light from the individual photophores into an even light field, an animal with few, widely spaced light organs is at a disadvantage, particularly when the background light levels are relatively high. Furthermore, the fewer the photophores, the brighter they must be to balance out the unlit regions of the ventral surface. In this study, the photophores of *C. maderensis* had to be 175% brighter than the background radiance, whereas the more finely distributed photophores of *A. veranyi* had to be only 34% brighter. For this reason, a counterilluminator viewed by a high-resolution eye will appear as a signal both brighter and darker than the background (*i.e.*, bright photophores on a silhouetted body). This may explain why shallower species generally have more finely spaced photophores, since acute vision is only possible at higher levels of illumination (Widder, 1999; Warrant and Locket, 2004).

A second important implication of this study is that counterillumination is potentially more successful at shallower depths. Due to the greater contrast attenuation at shallow depths, any mismatch with the background is detectable at only 5%–20% of the distance at which the same mismatch would be detectable in deeper waters. This increase in contrast attenuation may offset the disadvantage due to the variable spectra and angular distribution found near the surface.

Finally, because contrast attenuation is relatively constant over a wide range of wavelengths (Fig. 7D), and because

contrast sensitivity decreases rather slowly with decreasing illumination (Warrant, 1999), a counterilluminator ideally must match the downwelling spectrum from about 450 to 520 nm at depth and over a somewhat greater wavelength range near the surface. However, a survey of published photophore spectra shows that this is not the case (Fig. 8). Photophores involved in counterillumination do have spectral characteristics different from those used for other purposes, but the pattern is far from intuitive. In fish, counterilluminating photophores produce light with roughly the same peak wavelength (but with a narrower spectrum) as those of non-counterilluminating photophores. In decapods, the peak is red-shifted and the spectrum narrower in counterilluminating *versus* non-counterilluminating photophores. In squid and a few fish, counterilluminating photophores emit light at a longer (and occasionally shorter) wavelength than the non-counterilluminating photophores. Interestingly, the spectra of the counterilluminators, despite being quite clustered (suggesting natural selection), seldom match the downwelling spectrum. Some are 10–20 nm too blue, and others are 10–30 nm too red. This suggests that they may be visible to predators whose color discrimination

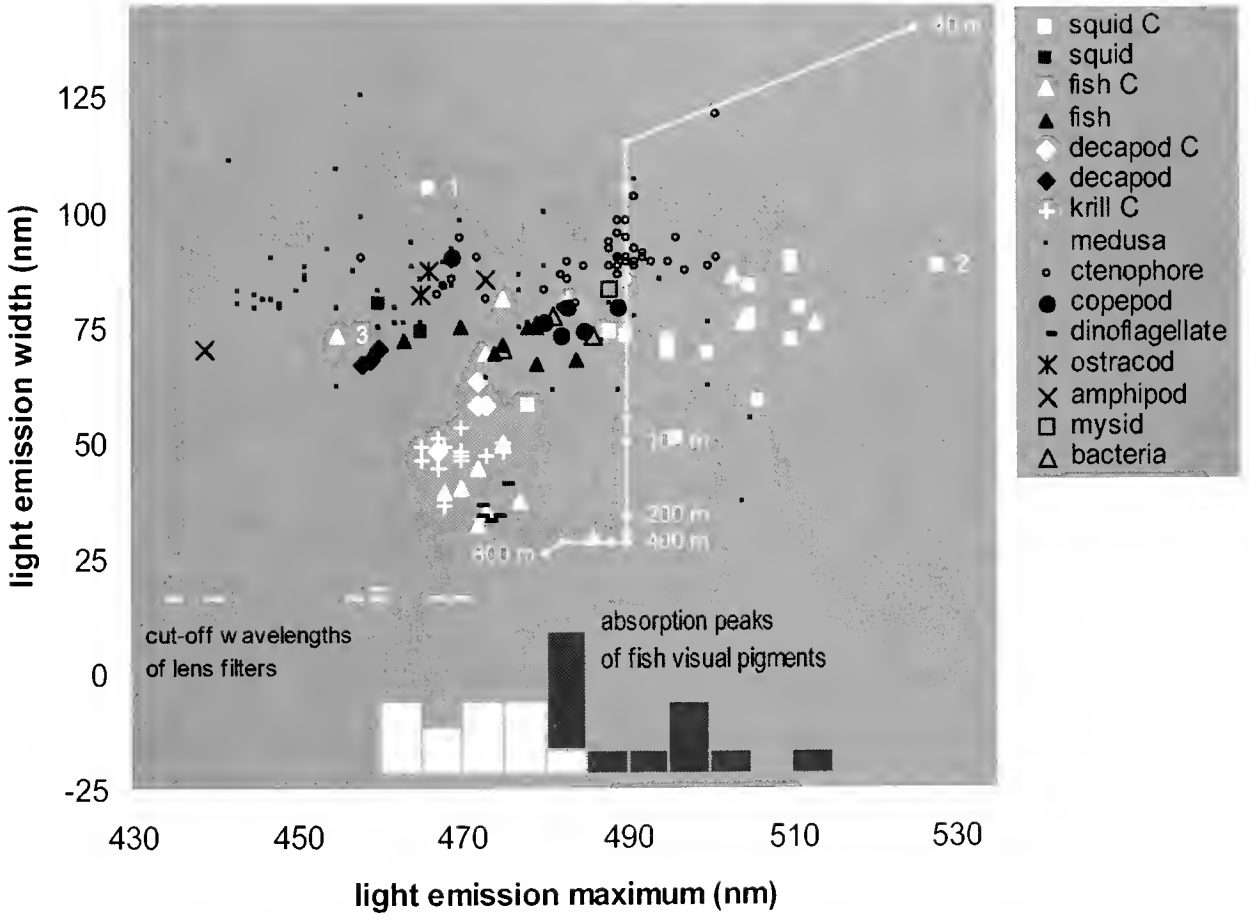

Figure 8. Peak wavelength *vs.* emission width (full-width half-max, FWHM) for the light emissions from various species. White symbols denote photophores involved in counterillumination. Black symbols denote photophores and other luminous sources used for other tasks (warning, luring, etc.). The outliers among the counterilluminators are [1]*Abraliopsis falco* (enoploteuthid squid), [2]*Teuthowenia megalops* (cranchiid squid), [3]*Isistius brasiliensis* (cookie-cutter shark). White line shows peak wavelength and FWHM for downwelling light as a function of depth (depth intervals are 10 m down to 100 m, and then 100 m for depths down to 800 m). Bar chart is a histogram of visual pigment absorption peaks for deep-sea fish eyes known to have multiple pigments in the blue-green portion of the spectrum (data from Douglas *et al.*, 1998). The white bars are the short-wavelength pigments; the black bars are the long-wavelength pigments. The gray symbols show the cut-off wavelengths for the filters in the lenses of seven species of deep-sea fish (data from Douglas and Thorpe, 1992). Photophore spectral data taken from Nicol (1960), Swift *et al.* (1973, 1977), Biggley *et al.* (1981), Herring (1983), Denton *et al.* (1985), Widder *et al.* (1983), Herring *et al.* (1992, 1993), and Haddock and Case (1999). Because the published bioluminescence spectra are calibrated in energy units (instead of quanta), the downwelling light curve is calibrated in relative energy units.

at blue and green wavelengths is good owing to multiple visual pigments or ocular filters.

Although about 15 deep-sea species (including fish, alciopid polychaetes, oplophorid shrimp, and the squid genus *Watasenia*) are known to have multiple visual pigments, most deep-sea species apparently are monochromatic, with a relatively flat spectral response near the maximum wavelength (due to the extreme thickness of their photoreceptors) (Douglas *et al.*, 1998). Therefore the spectral mismatches seen in Figure 8 may not be detectable as a color shift by many predators (excepting those possessing color filters). For a counterilluminator facing a color-blind predator, the relevant issue is that the light emitted from the photophores is attenuated more quickly than the downwelling light, due to higher absorption at non-peak wavelengths. Therefore, even if the emitted light perfectly matches the background intensity at one distance, the counterillumination will become darker than the background at a greater distance. The difference between the attenuation coefficients at 470 nm and 480 nm is small. Therefore, this issue is likely to be insignificant for the krill, fish, and decapods whose photophores emit at 470 nm. The close clustering of the spectra of these species remains puzzling, but may be an evolutionary strategy to prevent predators from developing a species-specific search image. This is analogous to the "selfish herd" effect, in which identical individuals in large aggregations reduce their chance of predation (Hamilton, 1971; Bond and Al Kamil, 2002).

The light emitted by squid photophores that peaks at 510 nm will be attenuated significantly more quickly than the downwelling light, potentially leading to the detection of the squid, but these measured spectra may not be representative of the natural spectra. As mentioned above, certain squid can change the spectrum of their counterillumination depending on temperature. Since the spectral measurements were not done *in situ* and often required a fair bit of manipulation, the squid may have been at a higher temperature and thus produced light to match shallower and therefore greener water. In fact, the published spectra of all counterilluminators must be treated with some caution because very few of the animals were measured while they were passively counterilluminating, but instead were being manually stimulated to emit light. Because manual stimulation tends to turn on all available photophores in an attention-getting signal that is assumed to act as a "burglar alarm" (Widder, 1999), the measured spectrum may include light from photophores that are not active during counterillumination, altering the spectrum.

Effects of visual resolution and color discrimination on perceived image

Although the range of water types commonly inhabited by counterilluminators had little effect on their visibility, the range of visual acuities of potential predators had a dramatic effect. Because light scattering by the water had little effect on the appearance of the counterillumination signal, acute vision can detect the individual photophores and is therefore highly advantageous. Indeed, many deep-sea species are known to have far greater resolution ($\sim 10\times$) in the dorsal viewing region than in other directions (Collin *et al.*, 1997; Wagner *et al.*, 1998; Land, 1999; Warrant and Locket, 2004). For example, although the spatial resolution for upward viewing in the hatchet fish *Argyropelecus aculeatus* is 0.11° (see Materials and Methods), the spatial resolution over the rest of visual field is 0.7°–1.7° (Collin *et al.*, 1997). In contrast, the myctophid *Lampanyctus festivus*, which has lateral-viewing eyes, has a relatively constant and low visual acuity (0.5°) over the entire visual field (Wagner *et al.*, 1998). Because this increased spatial resolution decreases sensitivity (and hence ability to detect contrast), it has an associated cost. Warrant and Locket (2004) analyzed the benefits and costs of high spatial resolution as a function of what is being viewed; they determined that high spatial resolution should be selected for in eyes that search overhead for small, silhouetted objects. While they do not explicitly consider the spatial pattern of counterillumination, the same principles apply.

The high spectral variation of the background light and the spectral mismatches seen in Figure 8 suggest that good color discrimination in the blue-green would be extremely advantageous. As mentioned above, certain deep-sea species probably have good color discrimination at blue and green wavelengths. Indeed, the peaks of these pigments seem to support the hypothesis of Douglas *et al.* (1998) that one pigment matches the counterilluminator's spectrum and one matches the downwelling light (Fig. 8). In addition, certain species with only one visual pigment have multibanked retinas. The filtering of the light by the vitread banks alters the spectrum of the light reaching the sclerad banks, changing their sensitivity and theoretically allowing for color discrimination (Denton and Locket, 1989). Finally, the lenses of certain deep-sea species have yellow filters that can also increase the contrast of a counterilluminator against the background (Munz, 1976; Douglas and Thorpe, 1992).

Conclusions

Although counterillumination is a ubiquitous and successful cryptic strategy, the clarity of the water implies that the camouflage can be broken by species with acute vision at longer distances than anticipated. In addition, the background to be matched depends not only on depth, but also on the source of nocturnal illumination. While spectral variation is greatest near the surface, contrast attenuation is also greatest. These results suggest several fruitful avenues for future research, including further analysis of the conflicting constraints of visual sensitivity and spatial resolu-

tion, a determination of how counterilluminators that can change spectral emissions choose the correct spectrum (despite being color-blind), and investigation of a possible relationship between the resolution of ventral photophore patterns and the acuity of potential predators.

Acknowledgments

The authors thank Drs. Eric Warrant, Tamara Frank, Steven Haddock, Richard Young, Roger Hanlon, and Peter Herring for a critical reading of earlier versions of the manuscript, and Drs. Craig Bohren, Jules Jaffe, Robert Maffione, Ken Voss, and Ron Zaneveld for helpful discussions. This work was funded in part by grants from the Office of Naval Research to EAW and SJ (N00014-02-1-0949) and to CDM. This is contribution number 1557 of the Harbor Branch Oceanographic Institution.

Literature Cited

Anthony, P. D. 1981. Visual contrast thresholds in the cod *Gadus morhua*. *J. Fish Biol.* **19:** 87–103.

Biggley, W. H., T. Napora, and E. Swift. 1981. The color of bioluminescent secretions from decapod prawns in the genera *Oplophorus* and *Systellaspis* (Caridea). Pp. 66–71 in *Bioluminescence: Current Perspectives*, K. H. Nealson, ed. Burgess Publishing, Minneapolis, MN.

Bogucki, D. J., J. A. Domaradzki, D. Stramski, and J. R. Zaneveld. 1998. Comparison of near-forward scattering on oceanic turbulence and particles. *Appl. Optics* **37:** 4669–4671.

Bohren, C. F., and D. R. Huffman. 1998. *Absorption and Scattering by Small Particles*. John Wiley & Sons, New York.

Bond, A. B., and A. C. Kamil 2002. Visual predators select for crypticity and polymorphism in virtual prey. *Nature* **415:** 609–613.

Capone, A., T. Digaetano, A. Grimaldi, R. Habel, D. Lo Presti, E. Migneco, R. Masullo, F. Moro, M. Petruccetti, C. Petta, P. Piatelli, N. Randazzo, G. Riccobene, E. Salusti, P. Sapienza, M. Sedita, L. Trasatti, and L. Ursella. 2002. Measurements of light transmission in deep sea with the AC9 transmissometer. *Nucl. Instr. Meth. Phys. Res.* **487:** 423–434.

Collin, S. P., R. V. Hoskins, and J. C. Partridge. 1997. Tubular eyes of deep-sea fishes: a comparative study of retinal topography. *Brain Behav. Evol.* **50:** 335–357.

Denton, E. J., and N. A. Locket. 1989. Possible wavelength discrimination by multibank retinae in deep-sea fishes. *J. Mar. Biol. Assoc. UK* **69:** 409–435.

Denton, E. J., J. B. Gilpin-Brown, and P. G. Wright. 1972. The angular distribution of the light produced by some mesopelagic fish in relation to their camouflage. *Proc. R. Soc. Lond. B* **182:** 145–158.

Denton, E. J., P. J. Herring, E. A. Widder, M. F. Latz, and J. F. Case. 1985. The roles of filters in the photophores of oceanic animals and their relation to vision in the oceanic environment. *Proc. R. Soc. Lond. B* **225:** 63–97.

Douglas, R. H., and C. W. Hawryshyn. 1990. Behavioral studies of fish vision: an analysis of visual capabilities. Pp. 373–418 in *The Visual System of Fish*, R. H. Douglas and M. B. A. Djamgoz, eds. Chapman and Hall, New York.

Douglas, R. H., and A. Thorpe. 1992. Short-wave absorbing pigments in the ocular lenses of deep-sea teleosts. *J. Mar. Biol. Assoc. UK* **72:** 93–112.

Douglas, R. H., J. C. Partridge, and N. J. Marshall. 1998. The eyes of deep-sea fish. I. Lens pigmentation, tapeta and visual pigments. *Prog. Retin. Eye Res.* **17:** 597–636.

Frank, T. M. 1999. Comparative study of temporal resolution in the visual systems of mesopelagic crustaceans. *Biol. Bull.* **196:** 137–144.

Goodman, J. W. 1996. *Introduction to Fourier Optics*. McGraw Hill, New York.

Haddock, S. H. D., and J. F. Case. 1999. Bioluminescence spectra of shallow and deep-sea gelatinous zooplankton: ctenophores, medusae, and siphonophores. *Mar. Biol.* **133:** 571–582.

Hamilton, W. D. 1971. Geometry for the selfish herd. *J. Theor. Biol.* **31:** 295–311.

Harper, R. D., and J. F. Case. 1999. Disruptive counterillumination and its anti-predatory value in the plainfish midshipman *Porichthys notatus*. *Mar. Biol.* **134:** 529–540.

Herring, P. J. 1977. Luminescence in cephalopods and fish. *Symp. Zool. Soc. Lond.* **38:** 127–159.

Herring, P. J. 1983. The spectral characteristics of luminous marine organisms. *Proc. R. Soc. Lond. B* **220:** 183–217.

Herring, P. J. 1985. Bioluminescence in the crustacea. *J. Crustac. Biol.* **5(4):** 557–573.

Herring, P. J., E. A. Widder, and S. H. D. Haddock. 1992. Correlation of bioluminescence emissions with ventral photophores in the mesopelagic squid *Abralia veranyi* (Cephalopoda: Enoploteuthidae). *Mar. Biol.* **112:** 293–298.

Herring, P. J., M. I. Latz, N. J. Bannister, and E. A. Widder. 1993. Bioluminescence of the poecilostomatoid copepod *Oncaea conifera*. *Mar. Ecol. Prog. Ser.* **94:** 297–309.

Jaffe, J. S. 1992. Validity and range of linear approximations in underwater imaging. Pp. 388–396 in *Ocean Optics XII*, G. D. Gilbert, ed. The International Society of Optical Engineering, Bellingham, WA.

Johnsen, S. 2002. Cryptic and conspicuous coloration in the pelagic environment. *Proc. R. Soc. Lond. B* **269:** 243–256.

Johnsen, S., and H. M. Sosik. 2003. Cryptic coloration and mirrored sides as camouflage strategies in near-surface pelagic habitats: implications for foraging and predator avoidance. *Limnol. Oceanogr.* **48:** 1277–1288.

Land, M. F. 1999. Compound eye structure: matching eye to environment. Pp. 51–71 in *Adaptive Mechanisms in the Ecology of Vision*, S. N. Archer, M. B. A. Djamgoz, E. R. Loew, J. C. Partridge, and S. Vallerga, eds. Kluwer Academic, Boston.

Latz, M. I. 1995. Physiological mechanisms in the control of bioluminescent countershading in a midwater shrimp. *Mar. Freshw. Behav. Physiol.* **26:** 207–218.

Lythgoe, J. N. 1979. *The Ecology of Vision*. Clarendon Press, Oxford.

Marshall, B. R., and R. C. Smith. 1990. Raman scattering and in-water optical properties. *Appl. Optics* **29:** 71–84.

Mertens, L. E. 1970. *In-Water Photography: Theory and Practice*. John Wiley, New York.

Mertens, L. E., and R. S. Replogle. 1977. Use of point spread and beam spread functions for analysis of imaging systems in water. *J. Opt. Soc. Am.* **67:** 1105–1117.

Mobley, C. D. 1994. *Light and Water: Radiative Transfer in Natural Waters*. Academic Press, New York.

Mobley, C. D., B. Gentili, H. R. Gordon, Z. Jin, G. W. Kattawar, A. Morel, P. Reinersman, K. Stamnes, and R. H. Stavn. 1993. Comparison of numerical models for computing underwater light fields. *Appl. Optics* **32:** 7484–7504.

Munz, W. R. A. 1976. On yellow lenses in mesopelagic animals. *J. Mar. Biol. Assoc. UK* **56:** 963–976.

Munz, F. W., and W. N. McFarland. 1977. Evolutionary adaptations of fishes to the photic environment. Pp. 194–274 in *The Visual System of Vertebrates*, F. Crescitelli, ed. Springer-Verlag, New York.

Nicol, J. A. C. 1960. Spectral composition of the light of the lantern-fish, *Myctophum punctatum*. *J. Mar. Biol. Assoc. UK* **39:** 27–32.

Petzold T. J. 1977. Volume scattering functions for selected ocean waters. Pp. 150–174 in *Light in the Sea*, J. E. Tyler, ed. Dowden, Hutchinson, and Ross, Stroudsberg, PA

Swift, E., W. H. Biggley, and H. H. Seliger. 1973. Species of oceanic dinoflagellates in the genera *Dissodinium* and *Pyrocystis*: interclonal and interspecific comparisons of the color and photon yield of bioluminescence. *J. Phycol.* **9:** 420–426.

Swift, E., W. H. Biggley, and T. Napora. 1977. The bioluminescence emission spectra of *Pyrosoma atlanticum*, *P. spinosum* (Tunicata), *Euphausia tenera* (Crustacea) and *Gonostoma sp.* (Pisces). *J. Mar. Biol. Assoc. UK* **57:** 817–823.

Ulloa, O., S. Sathyendranath, and T. Platt. 1994. Effect of the particle-size distribution on the backscattering ratio in seawater. *Appl. Optics* **33:** 7070–7077.

Vecchione, M., and C. F. E. Roper. 1991. Cephalopods observed from submersibles in the western north Atlantic. *Bull. Mar. Sci.* **49:** 433–445.

Voss, K. J. 1991. Simple empirical model of the oceanic point spread function. *Appl. Optics* **30:** 2647–2651.

Wagner, H. J., E. Frochlich, K. Negishi, and S. P. Collin. 1998. The eyes of deep-sea fish II. Functional morphology of the retina. *Prog. Retin. Eye Res.* **17:** 637–685.

Warrant, E. J. 1999. Seeing better at night: life style, eye design, and the optimum strategy of spatial and temporal summation. *Vision Res.* **39:** 1611–1630.

Warrant, E. J., and N. A. Locket. 2004. Vision in the deep sea. *Biol. Rev. Camb. Philos. Soc.* (In press).

Widder, E. A. 1999. Bioluminescence. Pp. 555–581 in *Adaptive Mechanisms in the Ecology of Vision*, S. N. Archer, M. B. A. Djamgoz, E. R. Loew, J. C. Partridge, and S. Vallerga, eds. Kluwer Academic, Boston.

Widder, E. A., M. I. Latz, and J. F. Case. 1983. Marine bioluminescence spectra measured with an optical multichannel detection system. *Biol. Bull.* **165:** 791–810.

Young, R. E., and J. M. Arnold. 1982. The functional morphology of a ventral photophore from the mesopelagic squid, *Abralia trigonura*. *Malacologia* **23:** 135–163.

Young, R. E., and F. M. Mencher. 1980. Bioluminescence in mesopelagic squid: diel color change during counterillumination. *Science* **208:** 1286–1288.

Young, R. E., and C. F. E. Roper. 1976. Bioluminescent countershading in midwater animals: evidence from living squid. *Science* **191:** 1046–1048.

Reference: *Biol. Bull.* **207:** 17–27. (August 2004)

Effect of Zooid Spacing on Bryozoan Feeding Success: Is Competition or Facilitation More Important?

MARNEY C. PRATT*

Department of Biology, Duke University, Durham, North Carolina 27708-0338

Abstract. Most Recent bryozoan species are encrusting sheets, and many of these colonies have densely packed feeding zooids. In this study, I tested whether tight packing of feeding zooids affects food capture. Colonies of a bryozoan with an encrusting sheet form (*Membranipora membranacea*) were dissected to produce individuals whose feeding zooids were (1) closely packed, (2) more widely spaced, or (3) isolated. For each type, rates of particle ingestion were measured in still water and in a freestream velocity of 2.7 cm s^{-1}. Ingestion rate increased when zooids were closest together, probably because of reduced refiltration and increased feeding current strength farther from the lophophores. The mean incurrent velocity within 0.02 cm above the center of the lophophore was 0.28 cm s^{-1} regardless of zooid spacing; however, when the incurrent velocity was measured more than 0.1 cm from the lophophores, zooids that were close together or spaced one zooid's width apart had significantly faster incurrent velocities than single zooids. Flow visualization suggests that isolated zooids and those spaced far apart refilter more water than zooids that are close together. These results along with the observed trend of increased zooid integration over evolutionary time suggest that the benefits of increasing coordination outweigh the consequences of intrazooid competition.

Introduction

Bryozoan colonies can take many forms, but most Recent species are encrusting sheets (McKinney and Jackson, 1991). Whether the encrusting sheet has come to be the dominant bryozoan colony form because it is advantageous is unclear. Although the phylogeny of bryozoans is far from resolved, the encrusting sheet form is found across the higher levels of the taxon, which suggests that convergence is likely. The growth pattern of an encrusting sheet is relatively simple and may also be relatively simple to evolve from multiple origins. While encrusting sheets are generally thought of as superior spatial competitors to runners (Buss, 1979b; Jackson, 1979; Bishop, 1989), the functional advantage of the encrusting sheet form has rarely been demonstrated experimentally.

The zooids in encrusting sheets are generally densely packed in a two-dimensional layer, and all of them stay in contact with the substratum (Fig. 1). This configuration has some potential benefits as well as costs. Since the zooids are on the substratum and do not project far from it, they experience the slower water velocities associated with the velocity gradient that exists close to the substratum. Therefore, the zooids are protected from the higher forces of fast flow, and they need little structural support. However, they can also experience a higher rate of sedimentation as well as a lower flux of food particles that result in a lower rate of food capture. The growth of encrusting sheets can theoretically be infinite, and in practice growth is generally limited only by the availability of substratum or food. For example, most encrusting colonies continue to grow as long as space and food are available, but some encrusting colonies, often called spots, show determinate growth and become reproductive at a very small size in habitats where space or food is limiting (Bishop, 1989; Okamura *et al.*, 2001). On the one hand, since the entire area of an encrusting colony is in contact with the substratum, the colony can take up a large amount of the available space and may be able to exclude competitors. On the other hand, encrusting sheets can be susceptible to overgrowth by some competitors. An advantage of having the feeding zooids close together in a sheet is the opportunity for coordinated feeding currents, but disadvantages of this configuration are the potential for more competition or for interference among the feeding currents of closely neighboring zooids. While any or all of these

Received 4 December 2003; accepted 12 May 2004.

* Present Address: Coastal Studies Center and Department of Biology, Bowdoin College, 6775 College Station, Brunswick, ME 04011. E-mail: mpratt@bowdoin.edu

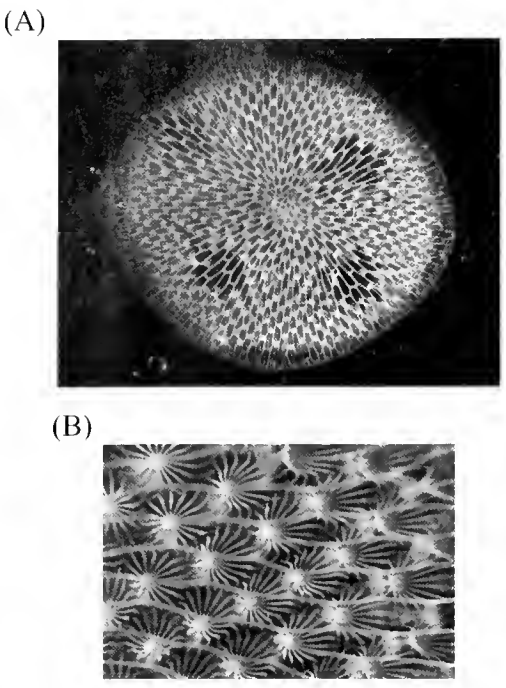

Figure 1. (A) Top view of a *Membranipora membranacea* colony. Note the darker spaces in the interior of the colony; these are the areas of excurrent flow called excurrent chimneys. (B) A closer top view of a group of feeding zooids with lophophores extended. Note that the lophophores are packed very tightly.

trade-offs could be important, the focus of this study is on the effect of zooid spacing on food acquisition.

Bryozoans use a ciliated crown of tentacles called a lophophore to create a feeding current that brings water laden with food down through the center of the crown toward the mouth and out through the base (Fig. 2). Food particles, which are generally phytoplankton, are transported to the mouth by a combination of mechanisms, including beat reversals of lateral cilia (Strathmann, 1973, 1982), tentacle flicks (Borg, 1926; Bullivant, 1968a; Strathmann, 1973; Larsen and Riisgård, 2002), other behaviors involving the tentacles (Winston, 1978), and bulk flow (Bullivant, 1968a; Best and Thorpe, 1983; McKinney *et al.*, 1986). Particle capture can be influenced by many factors such as temperature (Riisgård and Manríquez, 1997), particle concentration (Best and Thorpe, 1983, 1986b; Riisgård and Manríquez, 1997), presence of neighboring colonies (Okamura, 1984, 1985, 1988; Best and Thorpe, 1986a, b), particle size (Okamura, 1987, 1990), and colony size (Okamura, 1984, 1985).

Feeding zooids can show a wide variety of behaviors at the level of the individual (Winston, 1978, 1979; Shunatova and Ostrovsky, 2001) and the colony (Winston, 1978, 1979; Shunatova and Ostrovsky, 2002). At both levels, volumetric incurrent flow must equal volumetric excurrent flow according to the principle of continuity, where volumetric flow is equal to the velocity multiplied by the cross-sectional area (Dick, 1987). Individual zooids, or those spaced very widely apart, do not experience interference in their incurrent or excurrent flows. In colonies where zooids are closer together, there may be substantial interference among the incurrent or excurrent flows. In encrusting sheets where zooids are packed tightly together, a canopy of lophophores creates a large incurrent space. The excurrent space is below the lophophore canopy, and water that enters this space will escape the colony at the periphery. As an encrusting sheet colony increases in size, the perimeter of the colony does not increase as fast as the total area, so the total cross-sectional area of the excurrent space decreases relative to the incurrent space. Having less excurrent area increases pressure in the interior of the colony, which could result in slower incurrent velocities and thus a decreased feeding rate. Some colonies stay small enough to have sufficient excurrent area on the perimeter relative to incurrent area; others create local excurrent spaces, called excurrent chimneys, in the interior of the colony (Fig. 1). The importance of having sufficient excurrent space in a colony is generally agreed upon, but how much is enough is not known, and whether there is substantial interference among feeding currents in the interior of a colony regardless of the amount of excurrent space remains unclear.

Mathematical models have been developed to determine whether or not neighboring feeding zooids interfere with or enhance each other's feeding currents. These two models complement each other in that one (Grünbaum, 1995) concentrates more on what happens to the flow below the lophophore canopy, while the other (Eckman and Okamura, 1998) focuses more on the flow above the colony. However, the conclusions the authors draw from their models differ. Grünbaum's (1995) model suggests that a large negative interaction in the excurrent flows in the area beneath the lophophore canopy increases the relative pressure in the

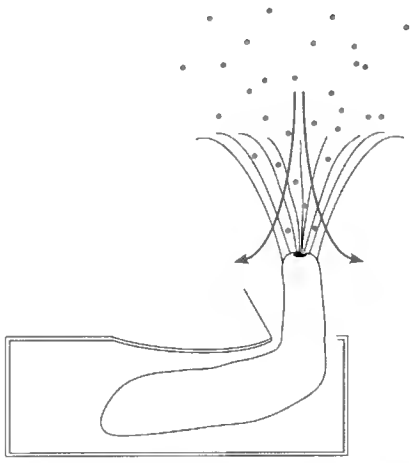

Figure 2. A schematic drawing of a single bryozoan zooid in side view. The small circles represent food particles (phytoplankton cells) that are being drawn down through the lophophore toward the mouth, which is at the base of the lophophore. Arrows indicate the direction of water flow.

interior of the colony. He concludes that this pressure below the lophophores should increase resistance to water flow and greatly reduce feeding currents. Thus, for this growth form to persist, other factors must make this colony form advantageous. In contrast, the model proposed by Eckman and Okamura (1998) suggests that as long as there is sufficient excurrent space, the combined ciliary currents produced by densely packed feeding zooids increase feeding rate. While both models agree that excurrent space is needed in the interior of a colony as it grows, controversy remains over the existence of interference or augmentation of feeding currents among zooids in encrusting sheets in nature. The purpose of this study was to test experimentally whether zooid spacing affects feeding rate. Since encrusting sheets are the dominant colony form and feeding success is crucial to acquiring the necessary energy for all other life processes, I hypothesize that closely packed zooids have greater feeding success than zooids that are spaced farther apart.

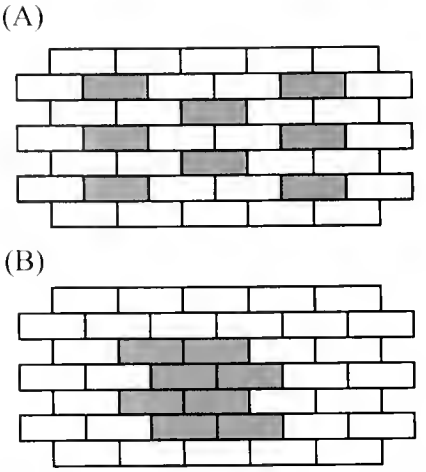

Figure 3. Schematic drawings of how dissections were performed to create the spaced (A) and close (B) zooid treatments (top view). The white boxes indicate where zooids were removed; the gray boxes indicate the live feeding zooids that were left untouched.

Materials and Methods

Bryozoan collection and maintenance

Membranipora membranacea (Linnaeus, 1767) usually grows as an encrusting sheet and is most often found on large macroalgae such as kelps. *Membranipora* was chosen for this study because it is tolerant of manipulations and its feeding zooids are densely packed (Fig. 1). Previous work indicates that *Membranipora* tends to have a higher ingestion rate than many other bryozoan species (Pratt, 2003), possibly due to the feeding advantage of its densely packed feeding zooids.

Colonies of *Membranipora* growing on the red alga *Mazzealla splendens* were collected from the floating docks at the Friday Harbor Laboratories in Friday Harbor, Washington. Large colonies were peeled off the algae, cut into pieces, and placed on glass slides (1 cm × 3 cm) in dishes of seawater. The colony pieces were allowed to grow onto the slides until they were firmly attached (usually 1–2 days). The slides were then placed in slide racks and hung off the floating docks so the bryozoans could feed in their natural habitat until needed for experiments. Colony pieces from the same original individual colony were recorded as being from the same clone and were later randomly assigned to different treatments.

Manipulations of zooid spacing

To create colonies with different spacing but the same total number of zooids, larger colony pieces were dissected down to eight zooids that were either spaced more widely ("spaced" treatment) or at their normal spacing ("close" treatment) (Fig. 3). To create the spaced treatment, all the surrounding zooids were dissected away (removing both the polypides and zooid walls with fine forceps) so that the remaining eight zooids were each isolated and surrounded by a zooid's width of space on all sides. In addition to the spaced treatment with eight zooids in each treatment, I dissected some colonies down to a single zooid to represent a treatment in which there was no interference from neighboring zooids. Portions of colonies with zooids of a similar size were chosen for these dissections to eliminate potential effects of zooid size. To survive, bryozoan colonies must be able to tolerate damage from predators or abrasion. After neighboring zooids have been removed, the remaining zooids can bud and replace the removed zooids. Therefore, I have assumed that the dissections did not adversely affect the feeding ability of the remaining zooids once they were given a few days to recover from the dissections.

Feeding experiments

All feeding experiments were conducted in a recirculating flow tank (working section 70 cm × 10.2 cm × 18 cm, after Vogel and LaBarbera [1978]) filled to a depth of 13 cm with 0.45-μm filtered seawater. Experiments were run at one of two freestream velocities, 0 and 2.7 cm s^{-1}, and the tank was kept in a cold room at 12 °C to maintain a constant water temperature similar to *Membranipora*'s natural habitat. Although some water motion usually remained in the tank, the ambient velocity was assumed to be near stagnant (0 cm s^{-1}) when the flow tank was turned off and allowed to settle for at least 10 min. The freestream velocity of 2.7 cm s^{-1} (± 0.06 cm s^{-1} SD) was estimated by taking the mean of velocities between 2.5 and 4.5 cm above the bottom. At the freestream velocity of 2.7 cm s^{-1}, there was a linear relationship between velocity (U, cm s^{-1}) and height above the bottom (z, cm) when $z < 1$ cm such that $U = (2.7)\,z$ ($R^2 = 0.95$) and shear velocity (U^*, where $U^* = (\nu\, dU/dz)^{1/2}$ (Vogel, 1994)) was 0.18 cm s^{-1}. Thus, the

ambient velocity in the horizontal direction at the top of an average lophophore (~0.11 cm) was 0.30 cm s^{-1}. Encrusting bryozoans such as *Membranipora* that live on large macroalgae most likely feed in the linear velocity gradient (or viscous sublayer) that exists close to the substratum (Lidgard, 1981; Grünbaum, 1995; Larsen *et al.*, 1998). Thus, the flow conditions used here are likely to be similar to what *Membranipora* colonies experience naturally.

The size and concentration of particles were chosen to be close to those quantified in the field and used in other studies (Bullivant, 1968b; Winston, 1979; Okamura, 1984, 1985; Pratt, 2003). The food particles used were blue-dyed polystyrene beads (mean diameter = 10.3 μm, SD = 0.94 μm, density = 1050 kg m^{-3}) at a concentration of 1000 beads ml^{-1}. Bryozoans have been shown to ingest large quantities of beads (Okamura, 1984, 1985), and observations of *Membranipora* zooids feeding on beads show that they do not reject the beads (pers. obs.). Concentrations were measured using a nanoplankton counting meter.

The glass slides were positioned flush with the bottom of the flow tank so only the bryozoans protruded into the flow. After feeding for 10 min, colonies were removed, fixed in formalin, rinsed in 70% EtOH, and cleared in 50% glycerol. The number of beads ingested by each zooid in the colony was counted using a compound microscope at 100×.

Flow visualization

Flow visualization was used to compare the incurrent velocities of the close, spaced, and single-zooid treatments when there was no ambient velocity. The water in the tank was seeded with particles that were about 20 μm in diameter and nearly neutral in buoyancy (cornstarch particles). To approximate a two-dimensional view, the flow field was illuminated with a 1-mm-thick laser light sheet (Lasiris SNF laser, 100 mW, 670 nm, focusable single line with 20° fan angle). Videos were recorded using a digital video camera (Sony DCR TRV900 with two +4 diopter close-up filters) with the optical axis perpendicular to the light sheet. The flow was analyzed by manually tracking particles from one video frame to the next. Only particles that entered the center of a lophophore were tracked. Once a particle was chosen, it was tracked from as far away from the lophophores as it was visible until it entered the lophophore. For the close and spaced treatments, particles were tracked for lophophores in the center of the colony.

Data analysis

Feeding rate with two spacing treatments and clone as a random factor. The first analysis of variance (ANOVA) tested the effect of zooid spacing and velocity on zooid ingestion rate for only the two treatments with eight zooids. There were not enough single zooids of the same clones as the close and spaced treatments to include the single treatment in the analysis and still test the effect of clone, so the single treatment was excluded from this analysis. The dependent variable used in the ANOVA model was zooid ingestion rate, which is the number of beads ingested by a zooid divided by the length of the experiment (10 min). Since the dependent variable was measured on the zooid level, colony was used as a random blocking factor. I also used three different genetic individuals that were split into the different treatments, so clone was also included as a random blocking factor in the model. The data were analyzed with a mixed ANOVA model (SAS 8.02, PROC MIXED) where spacing (close and spaced) and velocity (0 and 2.7 cm s^{-1}) were classified as fixed effects, and clone and colony were classified as random effects.

Feeding rate with all three spacing treatments. The second ANOVA was similar to the first except that clone was excluded as a random factor and the single zooid treatment was added as a level in the fixed spacing factor. *A priori* and *a posteriori* tests were also included in the analysis. Orthogonal polynomial tests can be used to run what is essentially a regression on treatment means to test for trends in the dependent variable as a function of the treatment effects (Quinn and Keough, 2002). *A priori* orthogonal polynomial tests were performed to assess whether zooid ingestion changed as a linear or quadratic function of zooid spacing. *A posteriori* pairwise comparisons were performed using the Tukey-Kramer adjustment.

Flow visualization. Incurrent velocity as a function of distance from the lophophores was measured for four particles for each of two colonies for each spacing treatment at 0 cm s^{-1}. Mixed-model analysis of covariance (ANCOVA) tests (SAS 8.02, PROC MIXED) were used to compare how the different spacing treatments (close, spaced, and single) affected the incurrent velocity with distance from the lophophore as the covariate. First, the slopes were compared using the following model:

$$Y_{ijkm} = \mu + \alpha_i + \beta_i X_{ijkm} + c_{j(i)} + d_{k(j(i))} + \varepsilon_{ijkm}, \quad \text{(Equation 1)}$$

where Y_{ijkm} = the value of the response variable (incurrent velocity in cm s^{-1}), μ = the overall mean incurrent water velocity, i = the levels of the spacing factor (1 = close, 2 = single, 3 = spaced), j = the number of colonies (two colonies per spacing treatment), k = the number of particles tracked (four particles per colony per spacing treatment), m = the observations of particle velocity at a particular distance from the lophophores, α_i = the intercept (fixed effect) of the i^{th} spacing treatment, β_i = the slope for the i^{th} spacing treatment, X_{ijkm} = the distance from the lophophore (cm) of the m^{th} observation of the k^{th} particle in the j^{th} colony of the i^{th} spacing treatment, $c_{j(i)}$ = the random effect of the j^{th} colony in the i^{th} spacing treatment, $d_{k(j(i))}$ = the

random effect of the k^{th} particle of the j^{th} colony in the i^{th} spacing treatment, and ε_{ijkm} = the unexplained random error. If the slopes had not been found to be significantly different (*i.e.*, if $P > 0.05$), then the slopes among spacing treatments would have been set as equal to each other, and the intercepts would have been compared using the following:

$$Y_{ijkm} = \mu + \alpha_i + \beta X_{ijkm} + c_{j(i)} + d_{k(j(i))} + \varepsilon_{ijkm}, \quad \text{(Equation 2)}$$

where β is the common slope for all levels of the spacing factor. However, since the slopes differed, the data were split into three subset ranges of the covariate: (1) $0 < D \leq 0.05$, (2) $0.05 < D \leq 0.1$, and (3) $0.1 < D \leq 0.15$ where D is the distance (in cm) from the lophophore. ANCOVA tests using Equation 2 were done separately on each of the three subset ranges, and the Tukey-Kramer adjustment was used for *a posteriori* pairwise contrasts. Incurrent velocities were log-transformed in all analyses.

Results

Feeding experiments

Feeding rate with two spacing treatments and clone as a random factor. The zooids in the close treatment had significantly higher mean zooid ingestion rates than the zooids in the spaced treatment, but velocity and the interaction between velocity and zooid spacing did not have a significant effect on ingestion rate (Fig. 4). A significant amount of variation in zooid ingestion rate was contributed by the colony and clone random factors ($P < 0.0001$).

Feeding rate with all three spacing treatments. Spacing and velocity had significant effects on zooid ingestion rate, but the interaction between spacing and velocity did not (Fig. 5). As in the above analysis, the random colony factor significantly increased the variation in ingestion rate ($P < 0.0001$). Mean zooid ingestion rate was significantly higher at 2.7 cm s^{-1} than at 0 cm s^{-1} when spacing treatments were pooled, but ingestion rate was not significantly different between velocities within any of the spacing treatments (Table 1). There was a significant linear trend in spacing: zooid ingestion rate increased as zooids were spaced closer together (Fig. 5). Both the close and spaced treatments had significantly greater mean zooid ingestion rates than single zooids when velocity treatments were pooled (Table 1). However, when the data were analyzed for each velocity separately, the differences among spacing treatments were not quite as strong as when velocity treatments were pooled (Table 1). Both the single and spaced zooids had all the zooids surrounding them removed, yet the spaced zooids had significantly higher mean ingestion rate than the single zooids, which suggests that the dissection process itself did not adversely affect feeding performance.

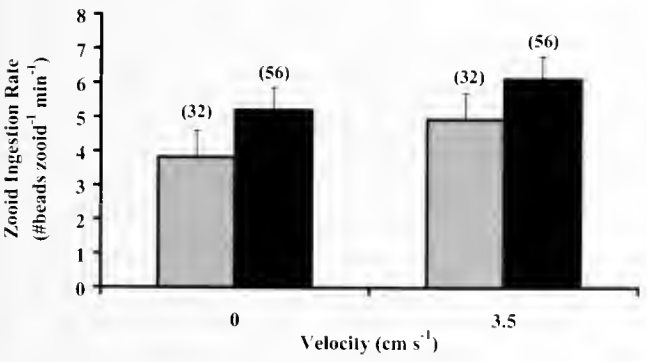

Figure 4. Zooid ingestion rate in two free-stream velocities for two zooid spacing treatments. Spaced zooids: gray bars; close zooids: black bars. Ingestion rate was greatest for closely spaced zooids ($P = 0.0361$). Velocity ($P = 0.1157$) and the interaction between velocity and spacing ($P = 0.8697$) did not significantly affect ingestion rate. Bars represent the least squares means ± one standard error of the least squares mean, and the number of zooids in each treatment is shown in parentheses.

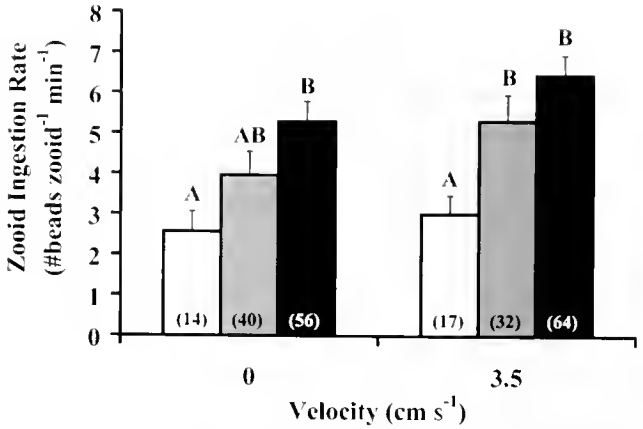

Figure 5. Zooid ingestion rate in two free-stream velocities for three zooid spacing treatments. Single zooids: open bars; spaced zooids: gray bars; close zooids: black bars. Overall, spacing ($P < 0.0001$) and velocity ($P = 0.0293$) significantly affected ingestion rate, whereas the interaction between spacing and velocity did not have a significant effect ($P = 0.6562$). Ingestion rate increased linearly ($P < 0.0001$) but not quadratically ($P = 0.5405$) as zooids were spaced closer together. Bars with the same letter were not significantly different from each other in pairwise comparisons (see Table 1 for statistics). Bars represent the least squares means ± one standard error of the least squares mean, and the number of zooids in each treatment is shown in parentheses.

Flow visualization

ANCOVA tests revealed that the two random factors, colony and particle, each significantly increased the variation in incurrent velocity ($P < 0.0001$). Incurrent velocity scaled significantly differently with distance from the lophophores among treatments (Fig. 6), so the data were divided into three subset ranges of distance from the lophophores: (1) 0–0.05 cm, (2) 0.05–0.10 cm, and (3) 0.10–

Table 1

A posteriori pairwise comparisons testing the effects of zooid spacing and water velocity on zooid ingestion rate

	Spacing pooled	Within-spacing treatments		
		Close	Spaced	Single
0 *vs.* 2.7 cm s^{-1}	0.0293	0.5579	0.6340	0.9863
	Velocity pooled	Within-velocity treatments		
		0 cm s^{-1}	2.7 cm s^{-1}	
Close *vs.* Spaced	0.0782	0.5008	0.7234	
Close *vs.* Single	< 0.0001	0.0045	< 0.0001	
Spaced *vs.* Single	0.0048	0.4614	0.0510	

Three zooid spacing treatments (close, spaced, single) and two velocities (0, 2.7 cm s^{-1}) were used in this analysis. Zooid ingestion rate is the number of beads eaten per zooid per minute. All values in the table represent the *P* value for the given pairwise comparison.

0.15 cm. Separate ANCOVA tests on each subset revealed that spacing had an increasingly significant effect on incurrent velocity when the particles were further away from the lophophores (Table 2). Pairwise *a posteriori* tests revealed that the close and spaced treatments had significantly faster incurrent velocities than the single zooid treatment when the particles were greater than 0.1 cm from the lophophores, but this difference disappeared as the particles got closer to the lophophores (Table 2). Conversely, the incurrent velocities of the close and spaced treatments never differed significantly (Table 2). Since the incurrents very close to the lophophores (within 0.05 cm) were never significantly different among any of the spacing treatments (Table 2), the assumption that the dissections did not affect zooid feeding is supported. The mean incurrent velocity within 0.02 cm of the lophophore for all three treatments was 0.28 cm s^{-1} (± 0.08 cm s^{-1} SD).

Discussion

Tightly spaced zooids have a feeding advantage

The results of this study demonstrate that ingestion rate increases when zooids are closer together. This difference was especially strong when the ingestion rates of isolated zooids were compared with the ingestion rates of the closely spaced zooids in natural *Membranipora membranacea* colonies. Thus, these results support the conclusions of Eckman and Okamura (1998) rather than those of Grünbaum (1995).

At least in small colonies, what happens above the colony (refiltration and the incurrent velocity far from the lophophores) may thus be more important than what happens

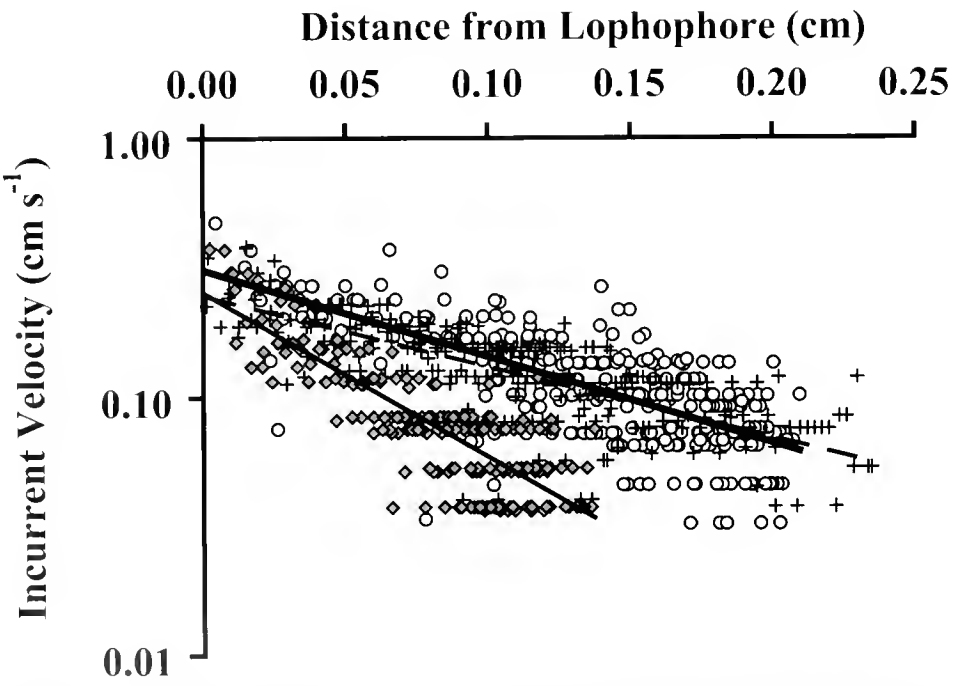

Figure 6. Velocity of particles traveling in the incurrent flow of bryozoan zooids, measured as a function of distance from the lophophores for three zooid spacing treatments. Close zooids: plus signs, thick dashed line; spaced zooids: open circles, thick solid line; and single zooids: gray diamonds, thin solid line. Lines represent standard least squares regressions for each treatment (close: $\ln y = -6.33x - 1.40$; spaced: $\ln y = -7.72x - 1.17$; single: $\ln y = -14.63x - 1.37$). Analysis of covariance revealed significant differences among the slopes of these lines ($P < 0.0001$).

Table 2

A posteriori *analysis of covariance comparing the effects of zooid spacing on log-transformed incurrent velocity as a function of distance from the lophophore*

		$0 < D \leq 0.05$	$0.05 < D \leq 0.1$	$0.1 < D \leq 0.15$
Type 3 Tests of Fixed Effects	Spacing	0.5427	0.0516	0.0252
	Distance	< 0.0001	< 0.0001	< 0.0001
Pairwise Contrasts	Close *vs.* Spaced	0.8340	0.7200	0.6484
	Close *vs.* Single	0.6790	0.0646	0.0435
	Spaced *vs.* Single	0.5429	0.0673	0.0254

Three zooid spacing treatments (close, spaced, single) were used in this analysis. All values represent *P* values. *D*, distance from the lophophore (cm).

below the lophophore canopy within the colony. This is not to say that the pressure that can build up under the lophophore canopy is not important; indeed, both mathematical models agree that, as a colony grows, excurrent chimneys are needed to keep some balance between incurrent and excurrent flow. However, as long as there is enough excurrent space to relieve the pressure built up under the lophophore canopy as the colony grows, then external conditions and refiltration seem to be more important.

Consequently, the feeding advantage of tightly packed zooids most likely results from a reduction in refiltration and an increase in the strength of the feeding current farther from the lophophores (Eckman and Okamura, 1998). If excurrent water is reintroduced above the lophophore and mixes with the incurrent water, the concentration of particles in the incurrent water will be reduced. Avoiding refiltration of excurrent water should increase the particle flux through the lophophores and increase the particle ingestion rate. In addition, increased incurrent velocity farther from the lophophores should result in increased particle capture because the feeding current reaches farther into the water column to regions of higher particle flux due to faster ambient water velocities and increased turbulent mixing.

This study provides evidence of both reduced refiltration and increased feeding current strength farther from the lophophores. Because incurrent velocities were never significantly different with height between the close and spaced zooids, the most likely explanation for the greater ingestion rate measured in the close zooids is that less refiltration occurs when zooids are closer together. Overall, zooids spaced farther apart may be "leakier," so that more particles escape between them. Flow visualization revealed that particles approaching the outer edges of the lophophore often escaped between or just above the tips of the tentacles, but when zooids were close together, neighboring zooids often caught the escaping particle. When zooids were farther apart, many particles were observed to slip between zooids uncaught (Fig 7). Both the spaced and close zooids had significantly higher zooid ingestion rates than the single zooids; and while this may be partly a result of greater refiltration by isolated zooids, it is also likely to be due to slower incurrent velocities for the single-zooid treatment when a particle was more than 0.1 cm from the lophophores (Figs. 6, 7). Flow visualization revealed that at the freestream flow of 2.7 cm s^{-1}, the spaced and close treatments both could capture particles up to 0.07 cm above the lophophores (traveling downstream at ~ 0.49 cm s^{-1}), while the isolated zooids could only capture particles up to 0.04 cm above them (traveling downstream at ~ 0.41 cm s^{-1}) (Fig. 7). Thus, isolated zooids have effectively weaker incurrents than those of the zooids in the spaced and close treatments.

These results support the assumption that closely spaced zooids create faster, more vertically directed feeding currents (Figs. 6, 7). Models of bryozoan feeding currents have assumed that the shape of the incurrent water flow over an isolated zooid is an inverted cone, whereas the shape over zooids that are tightly packed is cylindrical (Grünbaum, 1995; Eckman and Okamura, 1998). To conform with the principle of continuity (Vogel, 1994), the velocity at a given distance from the lophophore should be lower in a conical incurrent than in a cylindrical one. Similarly, measurements of the feeding current velocities in *Electra pilosa* suggest that the combined feeding currents of two lophophores are faster and more vertically directed than the currents of an isolated lophophore (Larsen and Riisgård, 2002).

My data on incurrent velocities agree well with other published measurements of *Membranipora* colonies. The average incurrent velocity less than 0.02 cm from the lophophore for all treatments in this study was 0.28 cm s^{-1}. Values of incurrent velocities cited in the literature for *Membranipora* include a mean of 0.25 cm s^{-1} (Lidgard, 1981) and a maximum of 0.24 cm s^{-1} (Larsen and Riisgård, 2001) for zooids in a colony, as well as a mean and standard deviation of 0.258 ± 0.08 cm s^{-1} for isolated zooids (Riisgård and Goldson, 1997).

Importance of spacing and flow velocities to suspension feeders

Although this is the first time that the effect of zooid spacing on feeding success has been tested in bryozoans,

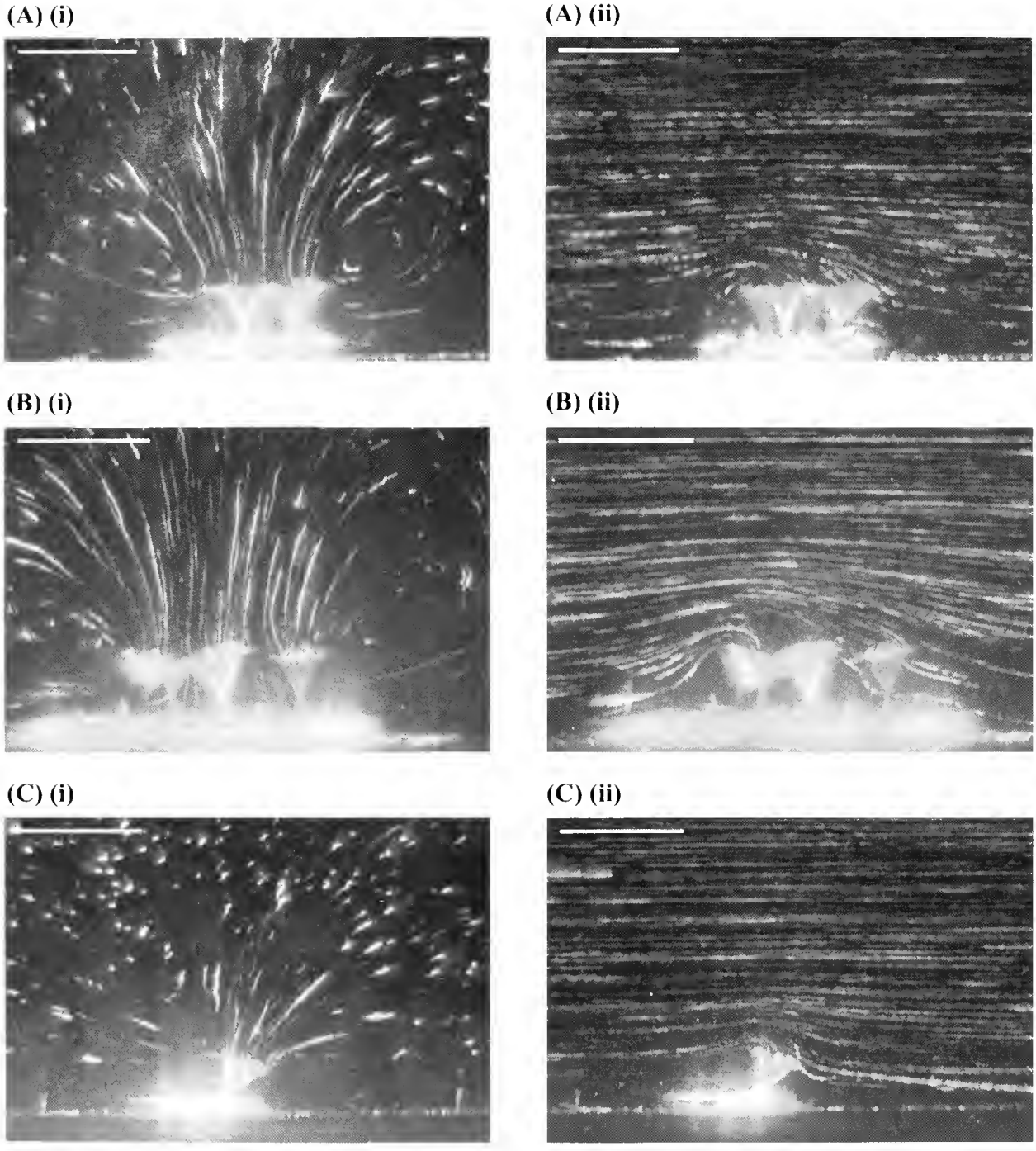

Figure 7. Example of flow around colonies at (i) 0 cm s^{-1} and (ii) 2.7 cm s^{-1} free-stream velocity. Colonies were dissected to create three treatments: (A) 8 zooids close together, (B) 8 zooids further apart, and (C) isolated zooids. These pictures were created by overlapping 180 frames of video (~6 s) using a macro in Scion Image ver. 3b (macro developed by M. von Dassow, University of California Berkeley). Images are taken from the side with freestream flow (when 2.7 cm s^{-1}) coming from the left to right. Scale bars are 0.2 cm.

studies on other suspension feeders have investigated the effects of individual or zooid or polyp spacing on feeding success. For example, phoronids are not colonial, but these lophophorate suspension feeders can live in very dense aggregations (up to 20,000 m^{-2}) (Johnson, 1997). On the basis of studies of growth and of flow around neighboring phoronids, Johnson (1990, 1997) predicted increased feeding success when there is an upstream neighbor; however, this advantage disappeared when the upstream neighbor was within one lophophore's diameter (~1 cm).

The presence of neighbors is also important for nonciliary suspension feeders. For example, upstream neighbors were found to decrease prey capture in the sea anemone *Metridium senile* (Anthony, 1997). One species of acorn barnacle, *Semibalanus balanoides*, had higher particle capture rates in the middle of a dense aggregation than in solitary individuals or those on the edge of a dense aggregation (Bertness *et al.*, 1998); another acorn barnacle, *Balanus amphitrite*, had higher particle capture rate upstream and at the peak of hill-shaped clusters than did barnacles located downstream (Pullen and Labarbera, 1991). Having different species as neighbors also may influence feeding success. Feeding performance was higher in mixed assemblages of three species of hydropsychid caddisfly larvae than in species monocultures (Cardinale *et al.*, 2002).

The spacing of neighbors or polyps can have different effects depending on the ambient flow velocity. The influence of neighbor colonies on feeding rate has been investigated in both arborescent and encrusting colonies of bryozoans in different flow velocities. The presence of a large upstream neighbor decreased the feeding rate of small conspecific colonies of an arborescent bryozoan (*Bugula stolonifera*) in both a relatively slow (1–2 cm s^{-1}) and a fast (10–12 cm s^{-1}) ambient velocity (Okamura, 1984). Conversely, the presence of a neighbor colony 1–5 mm upstream increased the feeding rate of conspecific colonies of an encrusting bryozoan (*Conopeum reticulum*) in a relatively slow velocity (1–2 cm s^{-1}) (Okamura, 1985). Encrusting colonies of *Electra pilosa* have reduced feeding rates when surrounded by *Alcyonidium hirsutum* colonies at a relatively slow flow (1–2 cm s^{-1}), but they have increased rates when surrounded by *A. hirsutum* or *Flustrellidra hispida* colonies at a relatively fast flow (10–12 cm s^{-1}) (Okamura, 1988). Similarly, dense aggregations of branches of the scleractinian coral *Madracis mirabilis* have high food capture at higher flow rates, but more spaced aggregations of branches have their highest food capture rate at intermediate flow velocities (Sebens *et al.*, 1997).

Previous experiments on medium-sized (0.51 ± 0.19 cm^2) *Membranipora membranacea* colonies suggest that the zooid ingestion rate increases until the average free-stream velocity reaches about 2.7 cm s^{-1}, and then decreases (Pratt, 2003). The results of this study also suggest that the ingestion rate increases when velocity increases from 0 to 2.7 cm s^{-1}. If additional velocities between 0 and 2.7 cm s^{-1} were tested, I would expect a significant linear trend in zooid ingestion rate as a function of velocity. Although ambient velocity did not alter the significance of spacing to relative ingestion rate in this study, it may be that differences would occur at a wider range of flow. Alternatively, colonies can respond to flow with phenotypic plasticity, in which zooids become smaller in faster flow (Okamura and Partridge, 1999); however, the colony must be exposed to that velocity for a long time.

Implications and significance of zooid spacing

Although the results of this study suggest that ingestion rate increases with decreased distance between zooids, the relevance of this phenomenon to the fitness of bryozoan colonies remains to be demonstrated. There is some evidence that *Membranipora* has a higher feeding rate and thus a higher growth rate than other native species in the Pacific Northwest (Pratt, 2003). This relatively high feeding rate may be a consequence of the efficient colonywide filter created by closely packed zooids. Perhaps the high feeding rate and growth rate of this species have contributed to its fast and effective invasion of the Gulf of Maine (Berman *et al.*, 1992; Lambert *et al.*,1992; Scheibling *et al.*, 1999).

While the results of this study show that having zooids close together can enhance feeding performance in very small colonies, whether or not this advantage is important in larger colonies is not known. Larger colonies may have higher fitness since fecundity (Hayward, 1973; Hayward and Ryland, 1975; Winston and Jackson, 1984; Jackson and Wertheimer, 1985), growth rate (Lutaud, 1983; Winston and Jackson, 1984; Hughes and Hughes, 1986), and survivorship (Sutherland and Karlson, 1977; Buss, 1981; Russ, 1982; Winston and Jackson, 1984) increase with colony size. Still, increasing colony size must cost something, and some colonies show an upper size limit (spots: Bishop [1989]; Okamura *et al.*, [2001]; plates: Nielsen [1981]; erect branching colonies: Cheetham and Hayek [1983]; Cheetham [1986]). As an encrusting sheet colony grows past a certain size, internal excurrent space is necessary to balance the incurrent and excurrent flows. In fact, chimneys may form in the internal areas of the colony where the per-zooid feeding rate is lowered as a result of the building backpressure under the lophophore canopy as the colony grows (Larsen and Riisgård, 2001). The consequences of these excurrent spaces for feeding performance are not clear. Refiltration of water can decrease particle flux and lower particle capture rates in bryozoans (Grünbaum, 1995; Eckman and Okamura, 1998; Larsen *et al.*, 1998; Larsen and Riisgård, 2002; this study). Concentrating the excurrent flow into a fast jet of water may help prevent refiltration (Lidgard, 1981; M. Pratt, unpubl. data); however, as ambient flow increases, excurrent jets from chimneys may be directed back toward the colony surface and no longer prevent refiltration (M. Pratt, unpubl. data). Ambient flow conditions and how the feeding currents interact with the ambient flow are clearly important in determining bryozoan feeding performance (Lidgard, 1981; Eckman and Okamura, 1998; Larsen *et al.*, 1998; Okamura *et al.*, 2001; Larsen and Riisgård, 2002).

Once a sessile animal such as a bryozoan settles, it cannot relocate to a new habitat if conditions become suboptimal. However, a colony may adapt its shape or size to optimize conditions for feeding. Okamura and Partridge's (1999) study revealed not only that colonies can have smaller

zooids in faster flows to maintain a favorable velocity at the level of the colony, but that these colonies have the same growth rate as colonies with larger zooids in slower flows. Further research exploring the effects of factors such as colony shape and size as well as a wider range of flow conditions on feeding would enhance our understanding of the relationship between feeding performance and surrounding flow conditions.

The fossil record of bryozoans shows an increase in zooid integration over evolutionary time (McKinney and Jackson, 1991), and this study provides evidence for one functional explanation for selection in favor of integrated feeding currents. Traditionally, spatial limitation (Buss, 1979a; Jackson, 1979), dislodgement risk (Cheetham and Thomsen, 1981; Cheetham, 1986), and predation (McKinney and Jackson, 1991) have been identified as major selective factors driving the evolution of colony form in bryozoans. It is becoming increasingly clear that food acquisition also has played a significant role in the evolution of colony form (Eckman and Okamura, 1998; Okamura *et al.*, 2001; this study).

Acknowledgments

I am grateful for comments made by S. Vogel, D. McShea, C. W. Cunningham, W. H. Kier, and E. Shaughnessy on early drafts of this manuscript. Comments from A. S. Johnson, O. Ellers, and two anonymous reviewers were invaluable on later drafts. I would like to thank A. O. D. Willows and staff for providing facilities and support at the Friday Harbor Laboratories. I was supported by an American Dissertation Fellowship from the American Association of University Women, a Wainwright Fellowship from the Friday Harbor Laboratories, and a Doctoral Dissertation Improvement Grant (IBN-0206457) from the National Science Foundation during the course of this research. During manuscript preparation I was supported as the Scholar-in-Residence at Bowdoin College's Coastal Studies Center.

Literature Cited

Anthony, K. R. N. 1997. Prey capture by the sea anemone *Metridium senile* (L): effects of body size, flow regime, and upstream neighbors. *Biol. Bull.* **192:** 73–86.

Berman, J., L. Harris, W. Lambert, M. Buttrick, and M. Dufresne. 1992. Recent invasions of the Gulf of Maine: three contrasting ecological histories. *Conserv. Biol.* **6:** 435–441.

Bertness, M. D., S. D. Gaines, and S. M. Yeh. 1998. Making mountains out of barnacles: the dynamics of acorn barnacle hummocking. *Ecology* **79:** 1382–1394.

Best, M. A., and J. P. Thorpe. 1983. Effects of particle concentration on clearance rate and feeding current velocity in the marine bryozoan *Flustrellidra hispida*. *Mar. Biol.* **77:** 85–92.

Best, M. A., and J. P. Thorpe. 1986a. Effects of food particle concentration of feeding current velocity in six species of marine Bryozoa. *Mar. Biol.* **93:** 255–262.

Best, M. A., and J. P. Thorpe. 1986b. Feeding-current interactions and competition for food among the bryozoan epiphytes of *Fucus serratus*. *Mar. Biol.* **93:** 371–376.

Bishop, J. D. D. 1989. Colony form and the exploration of spatial refuges by encrusting Bryozoa. *Biol. Rev.* **64:** 197–218.

Borg, F. 1926. Studies on recent cyclostomatous Bryozoa. *Zool. Bidr. Upps.* **10:** 181–507.

Bullivant, J. S. 1968a. The method of feeding of lophophorates (Bryozoa, Phoronida, Brachiopoda). *N. Z. J. Mar. Freshw. Res.* **2:** 135–146.

Bullivant, J. S. 1968b. The rate of feeding of the bryozoan, *Zoobotryon verticillatum*. *N. Z. J. Mar. Freshw. Res.* **2:** 111–134.

Buss, L. W. 1979a. Bryozoan overgrowth interactions—the interdependence of competition for space and food. *Nature* **281:** 475–477.

Buss, L. W. 1979b. Habitat selection, directional growth and spatial refuges: why colonial animals have more hiding places. Pp. 459–497 in *Biology and Systematics of Colonial Organisms*, G. Larwood and B. R. Rosen, eds. Academic Press, New York.

Buss, L. W. 1981. Mechanisms of competition between *Onychocella alula* (Hastings) and *Antropora tincta* (Hastings) on an Eastern Pacific rocky shoreline. Pp. 39–49 in *Recent and Fossil Bryozoa*, G. P. Larwood and C. Nielsen, eds. Olsen and Olsen, Fredensborg, Denmark.

Cardinale, B. J., M. A. Palmer, and S. L. Collins. 2002. Species diversity enhances ecosystem functioning through interspecific facilitation. *Nature* **415:** 426–429.

Cheetham, A. H. 1986. Branching, biomechanics and bryozoan evolution. *Proc. R. Soc. Lond. B Biol. Sci.* **228:** 151–172.

Cheetham, A. H., and L. A. C. Hayek. 1983. Geometric consequences of branching growth in adeoniform Bryozoa. *Paleobiology* **9:** 240–260.

Cheetham, A. H., and E. Thomsen. 1981. Functional morphology of arborescent animals: strength and design of cheilostome bryozoan skeletons. *Paleobiology* **7:** 355–383.

Dick, M. H. 1987. A proposed mechanism for chimney formation in encrusting bryozoan colonies. Pp. 73–80 in *Bryozoans: Present and Past*, J. R. P. Ross, ed. Western Washington University Press, Bellingham.

Eckman, J. E., and B. Okamura. 1998. A model of particle capture by bryozoans in turbulent flow: significance of colony form. *Am. Nat.* **152:** 861–880.

Grünbaum, D. 1995. A model of feeding currents in encrusting bryozoans shows interference between zooids within a colony. *J. Theor. Biol.* **174:** 409–425.

Hayward, P. J. 1973. Preliminary observations on settlements and growth in populations of *Alcyonidium hirsutum* (Fleming). Pp. 107–113 in *Living and Fossil Bryozoa*, G. P. Larwood, ed. Academic Press, London.

Hayward, P. J., and J. S. Ryland. 1975. Growth, reproduction, and larval dispersal in *Alcyonidium hirsutum* (Fleming) and some other Bryozoa. *Pubbl. Stn. Zool. Napoli* **39:** 226–241.

Hughes, D. J., and R. N. Hughes. 1986. Metabolic implications of modularity: studies on the respiration and growth of *Electra pilosa*. *Philos. Trans. R. Soc. Lond. B* **313:** 23–29.

Jackson, J. B. C. 1979. Morphological strategies of sessile animals. Pp. 499–555 in *Biology and Systematics of Colonial Organisms*, G. Larwood and B. R. Rosen, eds. Academic Press, New York.

Jackson, J. B. C., and S. Wertheimer. 1985. Patterns of reproduction in five common species of Jamaican reef-associated bryozoans. Pp. 161–168 in *Bryozoa: Ordovician to Recent*, C. Nielsen and G. P. Larwood, eds. Olsen and Olsen, Fredensborg, Denmark.

Johnson, A. S. 1990. Flow around phoronids: consequences of a neighbor to suspension feeders. *Limnol. Oceanogr.* **35:** 1395–1401.

Johnson, A. S. 1997. Flow is genet and ramet blind: consequences of individual, group, and colony morphology on filter feeding and flow. Pp. 1093–1096 in Vol. 2, *Proceedings of the Eighth International Coral Reef Symposium*, Panama, June 24–29, 1996, H. A. Lessios and I. G. Macintyre, eds. Smithsonian Tropical Research Institute, Balboa, Panama.

Lambert, W. J., P. S. Levin, and J. Berman. 1992. Changes in the

structure of a New England (USA) kelp bed: the effects of an introduced species? *Mar. Ecol. Prog. Ser.* **88:** 303–307.

Larsen, P. S., and H. U. Riisgård. 2001. Chimney spacing in encrusting bryozoan colonies (*Membranipora membranacea*): video observations and hydrodynamic modeling. *Ophelia* **54:** 167–176.

Larsen, P. S., and H. U. Riisgård. 2002. On ciliary sieving and pumping in bryozoans. *J. Sea Res.* **48:** 181–195.

Larsen, P. S., S. S. Matlok, and H. U. Riisgård. 1998. Bryozoan filter feeding in laminar wall layers: flume experiments and computer simulation. *Vie Milieu* **48:** 309–319.

Lidgard, S. 1981. Water flow, feeding, and colony form in an encrusting cheilostome. Pp. 135–143 in *Recent and Fossil Bryozoa*, G. P. Larwood and C. Nielsen, eds. Olsen and Olsen, Fredensborg, Denmark.

Lutaud, G. 1983. Autozooid morphogenesis in anascan cheilostomes. Pp. 208–237 in *Treatise on Invertebrate Paleontology, Part G, Bryozoa Revised*, R. A. Robison, ed. University of Kansas and Geological Society of America, Lawrence, KS and Boulder, CO.

McKinney, F. K., and J. B. C. Jackson. 1991. *Bryozoan Evolution.* University of Chicago Press, Chicago.

McKinney, F. K., M. R. A. Listokin, and C. D. Phifer. 1986. Flow and polypide distribution in the cheilostome bryozoan *Bugula* and their inference in *Archimedes*. *Lethaia* **19:** 81–93.

Nielsen, C. 1981. Morphology and reproduction of *Hippodiplosia insculpta* and *Fenestrulina malusii* (Bryozoa, Cheilostomata). *Ophelia* **20:** 91–126.

Okamura, B. 1984. The effects of ambient flow velocity, colony size and upstream colonies on the feeding success of Bryozoa: 1. *Bugula stolonifera*, an arborescent species. *J. Exp. Mar. Biol. Ecol.* **83:** 179–194.

Okamura, B. 1985. The effects of ambient flow velocity, colony size and upstream colonies on the feeding success of Bryozoa: 2. *Conopeum reticulum*, an encrusting species. *J. Exp. Mar. Biol. Ecol.* **89:** 69–80.

Okamura, B. 1987. Particle size and flow velocity induce an inferred switch in bryozoan suspension-feeding behavior. *Biol. Bull.* **173:** 222–229.

Okamura, B. 1988. The influence of neighbors on the feeding of an epifaunal bryozoan. *J. Exp. Mar. Biol. Ecol.* **120:** 105–124.

Okamura, B. 1990. Particle size, flow velocity, and suspension-feeding by the erect bryozoans *Bugula neritina* and *Bugula stolonifera*. *Mar. Biol.* **105:** 33–38.

Okamura, B., and J. C. Partridge. 1999. Suspension feeding adaptations to extreme flow environments in a marine bryozoan. *Biol. Bull.* **196:** 205–215.

Okamura, B., J.-G. Harmelin, and J. B. C. Jackson. 2001. Refuges revisited: enemies *versus* flow and feeding as determinants of sessile animal distribution and form. Pp. 61–93 in *Evolutionary Patterns: Growth, Form, and Tempo in the Fossil Record*, J. B. C. Jackson, S. Lidgard and F. K. McKinney, eds. University of Chicago Press, Chicago.

Pratt, M. C. 2003. Flow, feeding and form: consequences of coloniality in bryozoans. Ph.D. dissertation, Duke University, Durham, NC. 179 pp.

Pullen, J., and M. LaBarbera. 1991. Modes of feeding in aggregations of barnacles and the shape of aggregations. *Biol. Bull.* **181:** 442–452.

Quinn, G. P., and M. J. Keough. 2002. *Experimental Design and Data Analysis for Biologists.* Cambridge University Press, New York.

Riisgård, H. U., and A. Goldson. 1997. Minimal scaling of the lophophore filter-pump in ectoprocts (Bryozoa) excludes physiological regulation of filtration rate to nutritional needs. Test of hypothesis. *Mar. Ecol. Prog. Ser.* **156:** 109–120.

Riisgård, H. U., and P. Manríquez. 1997. Filter-feeding in fifteen marine ectoprocts (Bryozoa): particle capture and water pumping. *Mar. Ecol. Prog. Ser.* **154:** 223–239.

Russ, G. R. 1982. Overgrowth in a marine epifaunal community: competitive hierarchies and competitive networks. *Oecologia* **53:** 12–19.

Scheibling, R. E., A. W. Hennigar, and T. Balch. 1999. Destructive grazing, epiphytism, and disease: the dynamics of sea urchin-kelp interactions in Nova Scotia. *Can. J. Fish. Aquat. Sci.* **56:** 2300–2314.

Sebens, K. P., J. Witting, and B. Helmuth. 1997. Effects of water flow and branch spacing on particle capture by the reef coral *Madracis mirabilis* (Duchassaing and Michelotti). *J. Exp. Mar. Biol. Ecol.* **211:** 1–28.

Shunatova, N. N., and A. N. Ostrovsky. 2001. Individual autozooidal behaviour and feeding in marine bryozoans. *Sarsia* **86:** 112–142.

Shunatova, N. N., and A. N. Ostrovsky. 2002. Group autozooidal behaviour and chimneys in marine bryozoans. *Mar. Biol.* **140:** 503–518.

Strathmann, R. R. 1973. Function of lateral cilia in suspension feeding of lophophorates (Brachiopoda, Phoronida, Ectoprocta). *Mar. Biol.* **23:** 129–136.

Strathmann, R. R. 1982. Cinefilms of particle capture by an induced local change of beat of lateral cilia of a bryozoan. *J. Exp. Mar. Biol. Ecol.* **62:** 225–236.

Sutherland, J. P., and R. H. Karlson. 1977. Development and stability of the fouling community at Beaufort, North Carolina. *Ecol. Monogr.* **47:** 425–446.

Vogel, S. 1994. *Life in Moving Fluids: The Physical Biology of Flow.* Princeton University Press, Princeton, NJ.

Vogel, S., and M. LaBarbera. 1978. Simple flow tanks for research and teaching. *BioScience* **28:** 638–643.

Winston, J. E. 1978. Polypide morphology and feeding behavior in marine ectoprocts. *Bull. Mar. Sci.* **28:** 1–31.

Winston, J. E. 1979. Current-related morphology and behaviour in some Pacific coast bryozoans. Pp. 247–268 in *Advances in Bryozoology*, G. P. Larwood and M. B. Abbott, eds. Academic Press, New York.

Winston, J. E., and J. B. C. Jackson. 1984. Ecology of cryptic coral reef communities: 4. Community development and life histories of encrusting cheilostome bryozoa. *J. Exp. Mar. Biol. Ecol.* **76:** 1–22.

Reference: *Biol. Bull.* **207:** 28–43. (August 2004)

Rapid Behavioral Responses of an Invertebrate Larva to Dissolved Settlement Cue

MICHAEL G. HADFIELD[1,*] AND M. A. R. KOEHL[2]

[1]*Kewalo Marine Laboratory, University of Hawaii, 41 Ahui St., Honolulu, Hawaii 96813; and*
[2]*Department of Integrative Biology, University of California, Berkeley, California 94720-3140*

Abstract. Larvae of the nudibranch *Phestilla sibogae* were used to study whether a natural dissolved settlement cue (from their prey, *Porites compressa*, an abundant coral on Hawaiian reefs) induces behavioral responses that can affect larval transport to suitable settlement sites. As cue and larvae are mixed in the turbulent flow over a reef, cue is distributed in fine-scale filaments that the larva experiences as rapid (seconds) on/off encounters. To examine larval responses in this setting, individual larvae were tethered in a small flume with flow simulating water velocity relative to a freely swimming larva, and their responses to realistic temporal patterns of cue encounter were videotaped. Competent larvae quickly ceased swimming in cue filaments and resumed swimming after exiting filaments. The threshold cue concentration eliciting a response was 3%–17% of concentrations within heads of *P. compressa* in nature. When moving freely in filtered seawater, competent larvae swam along straight paths in all directions at ~0.2 cm s^{-1}, whereas in water conditioned by *P. compressa*, most ceased swimming and sank at ~0.1 cm s^{-1}. The ability of larvae to rapidly respond (by sinking) to brief encounters with dissolved settlement cues can enhance their rapid transport to the substratum, even in wave-driven turbulent flow.

Introduction

Successful larval settlement is critical to the long-term stability of benthic populations and communities. Planktonic larvae of benthic marine invertebrates are dispersed from their birth sites and depend on the vicissitudes of tides and currents to deliver them to suitable locations for recruitment. Once in or near such sites, successful settlement requires appropriate behavioral responses by larvae to reach or get very near the substratum and remain there long enough to complete metamorphosis. More than a half century of laboratory research has amply demonstrated that larvae from many different invertebrate phyla respond to chemical cues generated in the environment by settling in sites that are appropriate for successful metamorphosis, growth, and reproduction (reviewed by Hadfield, 1998; Hadfield and Paul, 2001).

Induction of settlement and metamorphosis by natural external chemical cues has been demonstrated for species as diverse as cnidarians (*e.g.*, Müller, 1973; Hofmann and Brand, 1987; Morse *et al.*, 1988; Morse and Morse, 1991; Leitz *et al.*, 1994; Fleck and Hofmann, 1995), polychaetes (Wilson, 1952; Jensen and Morse, 1990; Pawlik *et al.*, 1991; Hadfield *et al.*, 1994), sipunculans (Rice, 1988), bivalves (Grassle *et al.*, 1992), gastropods (Scheltema, 1961; Morse and Morse, 1984; Hadfield, 1984), barnacles (*e.g.*, Crisp and Meadows, 1962), crabs (Jensen, 1989; Brumbaugh and McConaugha, 1995), echinoids (Pearce and Scheibling, 1990a, 1991), phoronids (Herrmann, 1995), and ascidians (Young and Braithwaite, 1980). The search to understand the chemical nature of these cues has been a major component of research on invertebrate larval settlement (Hadfield and Paul, 2001), although much recent emphasis has been on signal-transduction mechanisms in the larvae (*e.g.*, papers in Clare and Jones, 1998).

Many earlier studies on invertebrate settlement focused on adsorbed, or surface-bound, cues. Crisp, a leader in such studies for more than 35 years, believed that larvae were too small to use dissolved cues to locate appropriate settlement sites (Crisp, 1974). However, studies on sea slugs (Hadfield and Scheuer, 1985; Hadfield and Pennington, 1990; Krug and Manzi, 1999), barnacles (Rittschof, 1985), blue crabs

Received 21 July 2003; accepted 17 May 2004
* To whom correspondence should be addressed. E-mail: hadfield@hawaii.edu

(Welch *et al.*, 1997), oysters (Zimmer-Faust and Tamburri, 1994), ascidians (Young, 1978), echinoids (Burke, 1984; Williamson *et al.*, 2000), and other taxa (reviewed in Hadfield and Paul, 2001) have demonstrated quite clearly that many larvae respond to dissolved chemical cues with decisive settlement from the water column, attachment to the substratum, and metamorphosis. Although less extensive, experimental evidence has also been presented to show that larvae of other opisthobranchs (Bahamondes-Rojas and Dherbonez, 1990; Lambert and Todd, 1994; Lambert *et al.*, 1997), prosobranchs (McGee and Targett, 1989; Boettcher and Targett, 1998), sipunculans (Rice, 1986), and other echinoids (Pearce and Scheibling, 1990b) are induced to settle and metamorphose by dissolved compounds arising from appropriate substrata, prey species, or conspecific individuals. With the exception of efforts by Turner *et al.* (1994), Tamburri *et al.* (1996), and Finelli and Wethey (2003), who studied responses of oyster larvae in unidirectional water flow in flumes, investigations of larval responses to dissolved inducers have been restricted to observations of the frequency of metamorphosis in stationary water.

Dispersion of dissolved settlement cues in marine habitats

A detailed understanding of the dispersion of dissolved substances from the substratum in ambient water flow is needed to determine how dissolved chemical cues affect larval settlement in nature. Many shallow coastal habitats are subjected to wave action, which renders water motion along the substratum oscillatory with high instantaneous velocities and accelerations (*e.g.*, Koehl, 1977; Denny, 1988). Even though instantaneous velocities are high, net advection of dissolved substances in back-and-forth, wave-dominated flow is slow, while turbulent mixing and shear dispersion can be high (Koehl and Powell, 1994). Canopies of attached organisms (*e.g.*, coral, kelp, sea grass) that provide a complex three-dimensional habitat in which many other species live, affect ambient flow and the dispersal of dissolved materials. For example, ambient water movement is retarded by coral reefs (*e.g.*, Black *et al.*, 1990), turbulent mixing in the water right above a reef is increased by the rough surfaces that coral and reef algae present to the flow (*e.g.*, Koehl *et al.*, 1997; Koehl and Dobbins, 1998), and some of the water hitting a reef flows through the porous reef framework rather than over the top of the reef (*e.g.*,Oberdorfer and Buddemeier, 1986; Parnell, 1986; Koehl and Hadfield, 2004). Chemical cues for larval settlement can be retained in water within reef canopies, as demonstrated by Hadfield and Scheuer (1985).

Advection-diffusion models are often used to describe the spatial patterns—on scales of centimeters to kilometers—of the concentration of dissolved substances released from the substratum and dispersed in coastal sites by currents, waves, and turbulent mixing (*e.g.*, Koehl and Powell, 1994; Okubo and Levin, 2001). However, instantaneous (~0.02 s), fine-scale (~200 μm) concentration measurements are required to understand the patterns of cue concentration encountered by larvae a few hundred micrometers in length swimming at a few millimeters per second in the water flowing above a cue-releasing substratum. Such fine-scale patterns of chemical dispersion can be measured by planar laser-induced fluorescence (PLIF) in a laboratory flume (*e.g.*, described by Crimaldi and Koseff, 2001). With this approach, a thin (~1-mm-thick) slice of the flow field is illuminated with a sheet of laser light, and video records are made of the brightness of fluorescent dye released from a substratum into the turbulent flow in the flume. PLIF studies have shown that chemical plumes near substrata in currents and waves are made up of fine filaments of high concentration swirling in clean water (*e.g.*, Crimaldi and Koseff, 2001; Koehl *et al.*, 2001; Mead *et al.*, 2003). The spatial distribution of such fine filaments above a coral reef has been revealed by PLIF measurements of fluorescent dye leaching from the surface of a reef composed of cleaned skeletons of *Porites compressa* in a flume in wave-driven flow (Reidenbach, 2004). Flow in the flume was designed to mimic field measurements of water movement and turbulence over reefs of *P. compressa* in Kaneohe Bay, Hawaii (Koehl and Hadfield, 2004). The resulting PLIF images revealed that microscopic larvae transported in the water above a cue-releasing substratum such as a coral reef may encounter fine filaments (hundreds of micrometers to millimeters in width) of high cue concentration interspersed in cue-less water (Fig. 1), rather than the diffuse gradient of cue concentration (scale of centimeters to meters) assumed in the past (*e.g.*, Crisp, 1974; Eckman *et al.*, 1994).

Research system

To better understand how larvae respond to dissolved settlement cues in habitats characterized by wave-driven, turbulent flow, where chemical cues arising from the substratum are rapidly and unevenly dispersed and diluted, we are investigating the settlement biology of a coral-eating nudibranch, *Phestilla sibogae* Bergh, 1905. This species serves as an excellent model organism for such research because its larvae are specifically induced to settle by a small, polar metabolite from its prey coral *Porites compressa* Dana, 1846 (Hadfield and Pennington, 1990), and because it can be rapidly and repeatedly reared in the laboratory throughout the year. Metamorphosis in the species is well understood at both light- and electron-microscopical levels (Bonar and Hadfield, 1974). The signal-transduction pathway has been extensively studied, including the identification of the site of the metamorphic inducer receptors on the larvae (Hadfield *et al.*, 2000).

The larvae of *P. sibogae* provide a model for larval

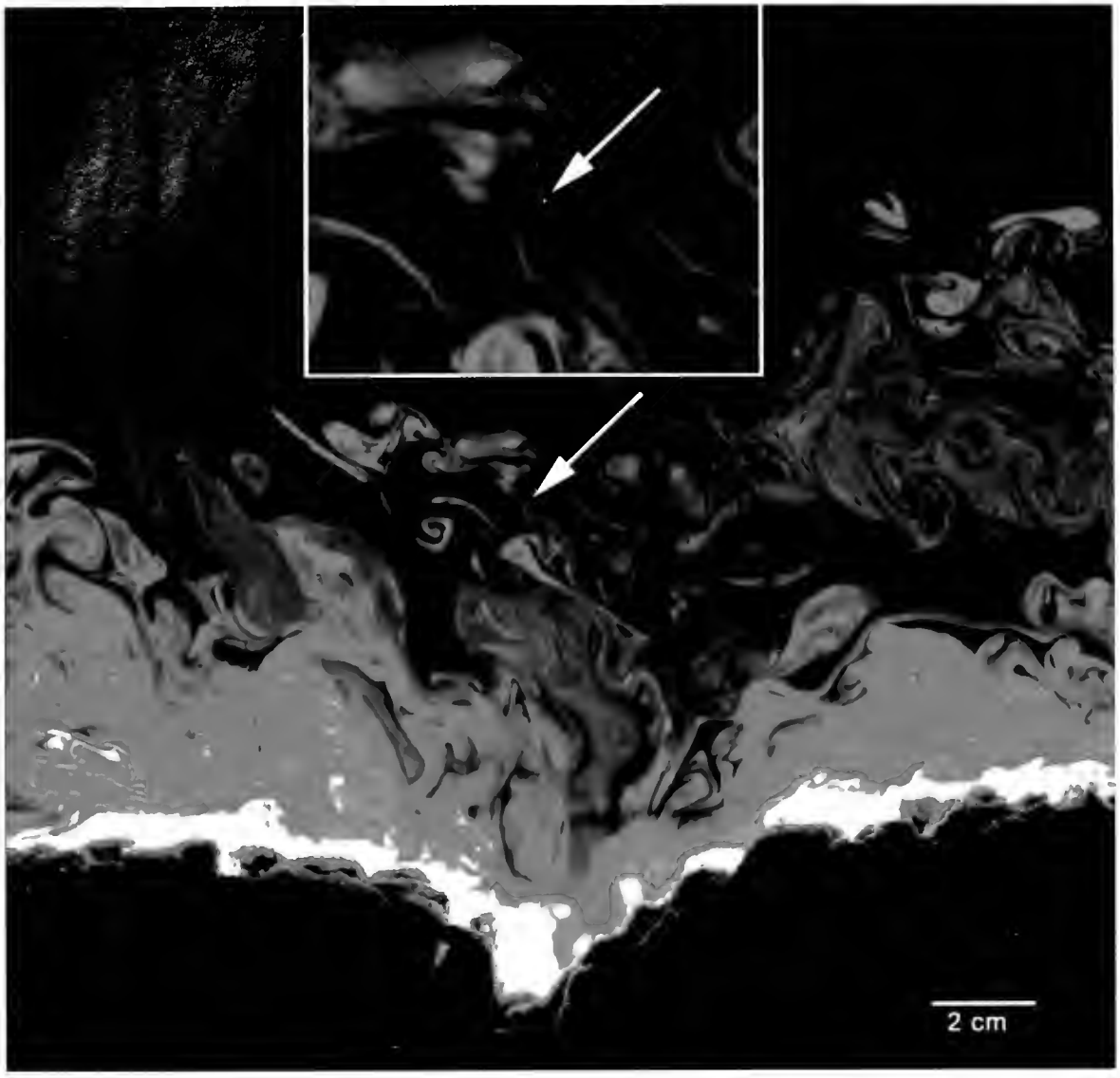

Figure 1. Planar laser-induced fluorescence (PLIF) image of rhodamine dye leaching from the surface of a reef of cleaned skeletons of *Porites compressa* exposed to waves in a flume (single frame of a video made by M. A. Reidenbach and J. R. Koseff, Environmental Fluid Mechanics Laboratory, Dept. of Civil Engineering, Stanford University). The brightness of the dye in the water is proportional to concentration (Crimaldi and Koseff, 2001). The arrow indicates the position of the modeled larva shown on the inset. Inset, segment of the PLIF image magnified 2.85× with a dot representing the size of a larva among the filaments of dye.

settlement into the complex three-dimensional communities of coral reefs. Coral-reef communities include not only the corals themselves, but also many algal species, reef fishes, and a host of invertebrates from many phyla living on and among the corals (Paulay, 1997). Most of the invertebrates in these communities have complex life cycles that include free-living larval stages. For many of the latter, successful recruitment depends on factors similar to those that confront larvae of *P. sibogae*. On Hawaiian reefs, these include the corals (Richmond, 1997), parasitic helminthes whose metacercariae encyst in the coral *Porites compressa* (Aeby, 1998), crustaceans that live on or within specific corals, coralliophilid snails that are obligate symbionts of corals (Kay, 1979), sessile vermetid gastropods (Hadfield *et al.*, 1972), sponges that live among or within the skeletons of the corals (Glynn, 1997), serpulid polychaetes whose tubes become embedded in living coral colonies, polychaetes and asteroids that feed on corals, sipunculans that burrow into coral skeletons, and many others (Paulay, 1997). Gaining information on larval transport into the complex interstices of coral reefs and their retention there will enhance understanding of metapopulation dynamics in all of these forms.

This first step in determining whether larvae of *P. sibogae* can utilize dissolved settlement cues in the turbulent, wave-

driven flow that characterizes coral reefs and many other coastal habitats focuses on the short-term behavioral responses of the larvae to dissolved cues from corals. Specifically, how rapidly do larvae respond behaviorally when they encounter the settlement cue? Larvae of *P. sibogae* require an exposure to cue of 1.5–2.0 h to develop a strong adhesion to a substratum (Koehl and Hadfield, 2004) and of nearly 6 h for metamorphosis to follow (Hadfield, 1977). Since larvae swimming or drifting above a coral reef are never likely to be in concentrations of coral cue long enough for morphogenetic induction to occur, we wanted to learn whether behavioral changes that bring about settlement from the water column occur more rapidly. If sinking or downward swimming behavior occurs rapidly and enhances transport of larvae into a reef, then larvae could remain in the cue-laden water within coral heads sufficiently long for metamorphic induction to occur (Hadfield and Scheuer, 1985).

Objectives of this study

The purpose of this study was to characterize the rapid behavioral responses of competent and precompetent larvae of *Phestilla sibogae* to brief encounters with dissolved chemical cues from *Porites compressa*. By videotaping swimming larvae through a microscope, we were able to monitor the behavior of the cilia, velar lobes, and foot of an individual larva as it entered and exited water containing different concentrations of cue from *P. compressa*. High-magnification video recordings of swimming larvae were made possible by tethering larvae in the field of view of a microscope while exposing them to the same rate of water movement relative to their bodies that they would experience when swimming freely. To translate cue-induced changes in the behavior of a tethered larva into differences in the velocities of untethered larvae, we also made and analyzed video recordings of larvae moving freely in aquaria filled with filtered seawater or seawater containing dissolved cue from *P. compressa*.

Materials and Methods

Culture of larvae for assays of behavior and metamorphosis

Phestilla sibogae is continuously maintained in Hadfield's laboratory at the University of Hawaii's Kewalo Marine Laboratory. Juvenile and adult animals are kept in shallow water tables supplied with flowing seawater, where they are provided with their living prey, *Porites compressa*, collected from the field 1–2 times per month. For this research, egg masses laid on the coral by adult *P. sibogae* were collected on the day they were deposited and maintained in bubbled beakers of filtered seawater in a 25 °C incubator until they hatched 6–7 days after deposition. Larvae were maintained at 25 °C as described in detail by Miller and Hadfield (1986). Competent larvae were typically used for studies on metamorphic induction when they were between 10 and 14 d post-fertilization (3–7 d post-hatching). In the experiments described below, precompetent larvae were tested on the day that they hatched from the egg mass. Each cohort of larvae used was a mixture of larvae from 5–10 different egg masses.

Test solutions

In the experiments on behavior and metamorphosis described below, the following solutions were tested: (i) seawater from the laboratory's continuously flowing system passed through a 0.45-μm Millipore filter (FSW); (ii) standardized strong cue from *P. compressa* ("*Porites* water" [100% PW]), produced by placing healthy branches of *P. compressa* densely in beakers of filtered seawater, aerating them overnight at room temperature (23–25 °C), removing the coral, and decanting the water through a Whatman #50 paper filter (details given in Hadfield and Scheuer, 1985; Hadfield and Pennington, 1990); and (iii) solutions of PW diluted with FSW (30% PW, 10% PW, 5% PW, and 1% PW). The metamorphosis assays described below were conducted in these solutions as well as in "reef water" collected within heads of living *P. compressa* on reefs in Kaneohe Bay, Hawaii, using procedures described in Hadfield and Scheuer (1985).

Tests of induction of metamorphosis

Assays to determine the biological activity of all batches of the solutions listed above were carried out in 30-well microtiter plates, with larvae placed approximately 20 per 2 ml of test solution in a well (Pennington and Hadfield, 1989). The percentage of larvae that metamorphosed after 24 h was tallied for each well and used as a measure of the relative inductive strength of the solution being tested (typically, 90%–100% of larvae metamorphose when exposed for 24 h to 100% PW [Hadfield and Scheuer, 1985; Hadfield and Pennington, 1990]). These tests, which were conducted on the days that behavioral experiments were done, also assessed the metamorphic responsiveness of each cohort of larvae used in the behavioral experiments.

Rapid behavioral responses of tethered larvae to brief encounters with cue filaments

Individual larvae of *Phestilla sibogae* were tethered in a small flume ("mini-flume"), and the water-flow velocity past the animal was adjusted to be about the same as the water velocity relative to an untethered swimming larva (0.2 cm s^{-1}). The acrylic plastic mini-flume had a working section (3 cm wide × 3 cm deep × 14.5 cm long) small enough to permit the larva to be viewed laterally through a

microscope. A steady flow rate of FSW through the flume was maintained by a constant-head tank; velocity was adjusted by raising or lowering the constant-head tank with a lab jack. The mini-flume was a flow-through system; because water was not recirculated through the test section, background levels of test solutions did not build up over the course of an experiment. Velocity past a larva in the mini-flume was measured by videotaping (60 frames s^{-1}) the movement of small, neutrally buoyant particles carried in the moving water. The microscope was focused on the midline of the flume (where the larva was positioned), and, to avoid errors due to parallax, only particles in sharp focus were digitized. Such particle movements in the focal plane of the tethered larva were videotaped using an SPI Minicam mounted on a 20× ocular on a Wild dissecting microscope positioned to give a lateral view of the larva at an objective magnification of 6×. These videos were analyzed using SCION Image software, ver. 1.62, and instantaneous velocities of the particles were calculated (as described below for velocity measurements of freely swimming larvae).

Individual larvae were tethered to the tip of a fine (0.24-mm diameter) stainless steel insect pin so that they could be held in a fixed position in the mini-flume in the field of view of the microscope. The tip of a pin, coated with a thin layer of petroleum jelly, was gently pushed against the dorsal surface of the shell of a submerged larva so that the hydrophobic shell stuck to the pin. The pin and larva were gently lifted from the larval culture dish and positioned with a micromanipulator in the mini-flume so that the larva could "swim" into the flow (*i.e.*, the water flow relative to the tethered larva was the same as the water flow relative to a freely swimming larva) (Fig. 2A). If the larva was positioned on the pin so that it did not contact the pin or the petroleum jelly when it extended its foot and velum from the shell, it quickly expanded its velar lobes and beat its velar cilia in the manner of a freely swimming larva. Only properly tethered larvae showing this "swimming" behavior in clean FSW in the mini-flume were used in our experiments.

Tethered larvae were exposed to filaments of test solutions (FSW, 100% PW, 30% PW, 10% PW, 5% PW, or 1% PW) labeled with 0.05% or 0.1% fluorescein that were carried past them in the flowing water (Fig. 2B, C). These filament encounters were designed to mimic the exposure to filaments of cue that a freely swimming larva would encounter in the turbulent flow above a coral reef (Fig. 1) (Koehl *et al.*, 2000). A computer simulation of larval motions (due to swimming, ambient waves, and turbulence) through the changing concentration fields recorded in PLIF videos (Reidenbach, 2004) was used to calculate the cue concentrations encountered by larvae as a function of time (Strother *et al.*, 2001). As a larva moves through the water, it passes into and out of cue filaments, and thus experiences an on-off temporal pattern of encounters with cue. Larvae close to the reef encounter filaments more often than do those higher above the reef (see Fig. 1). In the experiments reported here, a repeatable pattern of alternating exposure to test solution for 3–5 s (to simulate moving through a filament) and to clean FSW for 4–6 s was used so that larval responses to different test solutions could be compared

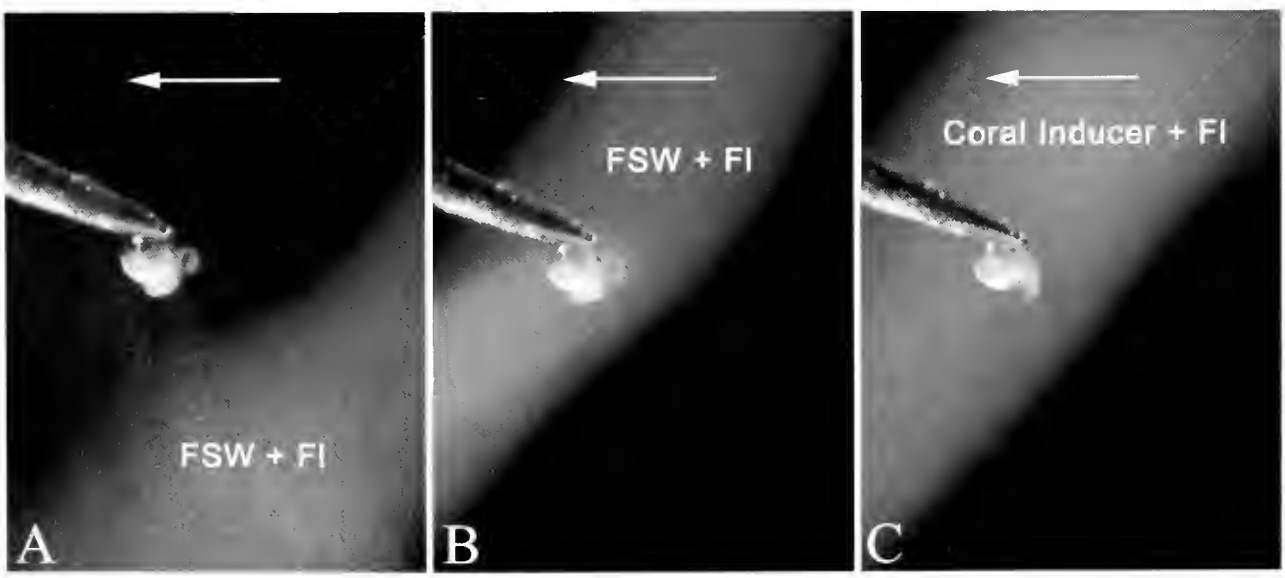

Figure 2. Photomicrographs of tethered larvae in the mini-flume. (A) Larva swimming in flowing seawater, with a filament of filtered seawater with fluorescein below larva. (B) Larva swimming in control filament (fluorescein in FSW). (C) Larva retracted in response to filament of seawater saturated with coral metabolites. FSW, filtered seawater; Fl, fluorescein. Arrow shows direction of seawater flow. The larval shell is about 210 μm long.

under standardized conditions. Filament exposures of such durations are typical at heights of about 5–8 cm above a reef dominated by *Porites compressa* (Koehl *et al.*, 2000; Strother *et al.*, 2001). A narrow stream, or filament, of test solution was gently released into the water through a syringe needle (bore diameter of 0.5 mm) positioned perpendicular to the flow upstream from the larva by a micromanipulator. The filament of test solution was carried downstream toward the larva by the flowing water in the mini-flume (*i.e.*, not by injection pressure), as though the larva were swimming toward the filament. An infusion pump (syringe pump model No. 351, Sage Instruments, Inc., Cambridge, MA) was used to produce a slow, steady rate of solution injection. By moving the syringe needle up and down slightly with the micromanipulator, the filament could be directed onto the larva (to simulate passage into a cue filament; Fig. 2C) or below the larva (to simulate passage out of a filament and into a band of clean water; Fig. 2A). Each larva was exposed to 18–21 filaments of a given test solution.

Both competent and precompetent tethered larvae were tested for responses to fluorescein-labeled FSW and PW. The behavior of the tethered larvae was recorded at 60 frames s^{-1} by the videocamera mounted on the ocular of the dissecting microscope positioned to observe the larvae in lateral view at 100×. Instantaneous responses could be observed, including cessation and resumption of beating of velar cilia, and partial or complete retraction or re-extension of the velum or foot. Frame-by-frame analyses of these video records permitted us to measure (to the nearest 0.017 s) the time when the edge of a filament encountered or left the chemoreceptive organ of a larva (Hadfield *et al.*, 2000) and the onset or cessation of any of these larval behaviors. These measurements were used (1) to calculate the lag time for larval responses to entering or leaving a cue filament and (2) to determine the percentage of filaments of test solution that caused a larva to react.

Effects of settlement cue (PW) on behavior of freely swimming larvae

The behavior of freely swimming larvae of *P. sibogae* was observed in acrylic plastic aquaria, 17.6 cm tall, 14 cm wide, and 4.5 cm thick, filled with either 100% PW or FSW at ~24 °C. An aquarium was set up in a darkroom, and a vertical plane midway between the front and back walls of the aquarium was illuminated by fluorescent lights shining through a 1-mm-wide slit on each side of the aquarium. The spectral range of the light in the water, determined with an LI-1800 underwater spectroradiometer (LI-COR, Inc., Lincoln, Nebraska), had peaks of irradiance at wavelengths of 400–725 nm, with the highest values at 550–650 nm. Similar measurements in shallow water in Kaneohe Bay, Hawaii (site of our field studies for this project), yielded high spectral irradiance at 325–700 nm, with greatest values at 350–600 nm (Gulko and Jokiel, 1995). Although these overlapping spectra are not identical, preliminary tests with newly hatched larvae of *P. sibogae* revealed that they swam toward the fluorescent lights in our aquaria, just as they do toward natural light (Miller and Hadfield, 1986). Miller and Hadfield (1986) determined that precompetent larvae of *P. sibogae* are attracted to light over a wide range of intensities (47–890 $\mu E\ m^{-2}\ s^{-1}$) in both the vertical and horizontal planes. As larvae of *P. sibogae* become metamorphically competent, their positive phototaxis weakens, until they become indifferent to light over the same range of intensities (Miller and Hadfield, 1986); trial tests with competent larvae in filtered seawater in the aquaria revealed the same response trend to the fluorescent lights.

For each "run," one of the test solutions was poured into an aquarium and allowed to come to rest, then larvae that had been in FSW were added to the aquarium, and the trajectories of larvae in the solution were videotaped at 60 frames s^{-1}. A Sony Hi8 Handycam TR101 video camera was mounted on a tripod and positioned sufficiently close to the aquarium that the field of view was an area 8.5 cm wide and 6.5 cm high in the lower half of the aquarium. The area filmed was equidistant from the side walls and the floor of the aquarium so that behavioral reactions to surfaces were not included in our analysis. The larvae in the vertical plane of illuminated water were clearly visible as bright spots in a dark field. For each run, about 300 larvae in 25 ml of water were gently poured into the aquarium. Videotaping began when larvae were introduced into the test water in the aquarium, but we waited 1 min before digitizing larval paths from the tapes. This provided the larvae with 1 min of exposure to the chemical cues, and allowed time for convection caused by adding the larvae to be sufficiently damped that larval swimming and sinking velocities were faster than convective velocities. Trajectories of all larvae that moved through the field of view during the subsequent 2 min were digitized using SCION Image software (sampling frequency 0.2 s) (Fig. 3). Because the movement of only those larvae in the illuminated plane in the aquarium could be digitized, errors due to parallax and to underestimation of velocity by digitizing larvae swimming toward or away from the camera were minimized.

Larval motion was quantified by analysis of trajectories such as those illustrated in Figure 3. "Instantaneous speed" was calculated by dividing the distance that a larva traveled between video frames by the time interval between those frames. The mean instantaneous speed for each larva was calculated using all of the instantaneous velocities measured for the trajectory of that larva. The length of the path followed by the larva was calculated as the sum of all the instantaneous speeds divided by the total duration of that individual's trajectory in the illuminated field of view. A vector was drawn between the first and last positions of a

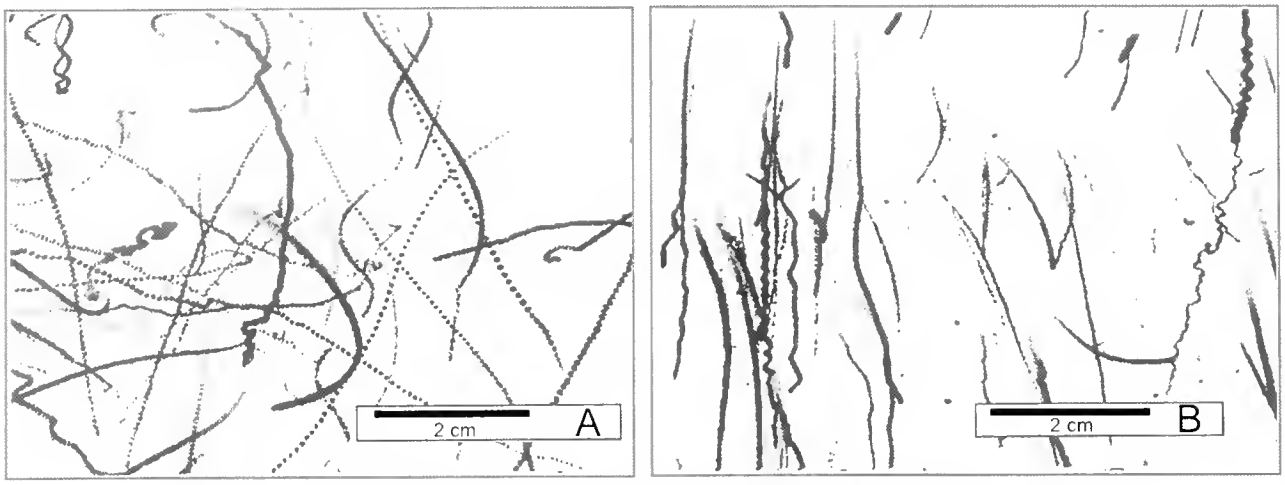

Figure 3. Trajectories of swimming or sinking larvae digitized from videotapes (duration = 50 s, sampled every 0.2 s). (A) Larvae moving in filtered seawater. (B) Larvae moving in settlement cue (seawater saturated with metabolites from the coral *Porites compressa*).

larva along its trajectory. The angle of the vector (where 0° was up, 90° was lateral to the left or right, and 180° was down) represented the net direction of movement by that larva. The length of the vector was the net displacement by the larva. We calculated "straightness index," a measure of straightness of the path followed by a larva, by dividing the net displacement of the larva by the length of the path followed by that individual. The "resultant speed" of the larva was calculated by dividing the net displacement of the larva by the duration of that individual's trajectory. As illustrated by the intersecting trajectories of the larvae in Figure 3A, the paths of individual larvae were not altered by the motions of the other larvae in the aquarium.

Sinking rate of dead larvae

The gravitational fall velocities of dead larvae of *P. sibogae* were measured to compare the passive sinking speeds of larvae with the velocities of larvae that moved downward in the experiments described above. Individually, actively swimming competent (11-day-old) larvae were gently captured from a culture beaker with a Pasteur pipette and transferred to a dilute solution of formalin (10 drops of 10% formalin solution in 35 ml of filtered seawater) to kill them. Prior to testing, each larva was inspected under a dissecting microscope to determine that it was entire and that its ciliary locomotion had ceased. These observations also revealed that every larva tested had retracted completely into its shell. Gravitational fall velocities of individual larvae that had reached terminal velocity while sinking through filtered seawater at 27 °C were measured using the technique described by Butman *et al.* (1988a).

Statistical analyses

ANOVA and Bonferroni/Dunn tests were conducted using Statview 5.0 statistical software, and means and standard deviations were calculated using Microsoft Excel 98 software.

Results

Metamorphosis in various concentrations of cue from Porites compressa

The biological activity of the *P. compressa* water (PW) used in our experiments was determined by metamorphosis assays using competent larvae of *Phestilla sibogae*. The results of these assays for 100% PW, 30% PW, and filtered seawater (FSW) are shown in Figure 4, where they are compared with results of metamorphosis assays for water collected within heads of *P. compressa* in Kaneohe Bay ("reef water"). No larvae underwent metamorphosis in FSW. Rates of metamorphosis in reef water were not significantly different from those we measured in 30% PW and were in the same range as those reported for reef water by Hadfield and Scheuer (1985), whereas metamorphosis rates in 100% PW were significantly higher, and those in FSW were significantly lower (ANOVA, Bonferroni/Dunn, significance level 5%). Therefore, 30% PW provides a reasonable laboratory mimic of the biological activity of inducer in water in reefs in the field.

Rapid behavioral responses of larvae to brief encounters with cue from Porites compressa

Tethered larvae "swimming" in the mini-flume (in which they were exposed to the same water motion relative to their

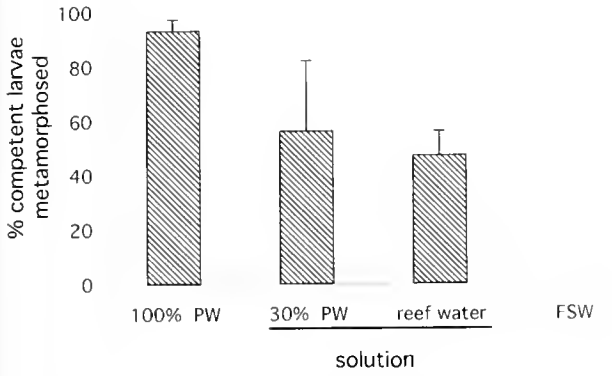

Figure 4. Percent of competent larvae of *Phestilla sibogae* that underwent metamorphosis in various solutions. Four replicate assays were conducted for each sample of a solution, and the mean was calculated for that sample. The mean of those sample means for each type of solution is plotted in this graph; error bars represent one standard deviation. For laboratory-prepared *Porites compressa* water (PW) and filtered seawater (FSW), a sample was taken on each day that experiments were conducted using tethered larvae. "Reef water" samples were collected within heads of *P. compressa* in Kaneohe Bay (n = 4 reefs). The bar below the horizontal axis indicates samples that were not significantly different from each other (ANOVA, Bonferroni/Dunn, significance level 5%).

bodies as they would have experienced if swimming freely through the water) extended their feet and velar lobes and beat their cilia for many hours in FSW (Fig. 2A). Frame-by-frame analysis of videotapes made through a microscope revealed the responses of such larvae "swimming through" filaments of fluorescein-labeled FSW or PW of various concentrations. The larvae continued to "swim" normally through control filaments of fluorescein-labeled FSW (Fig. 2B). In contrast, they often stopped beating their velar cilia and partially retracted their velar lobes upon entering a filament of PW (Fig. 2C). Typically, the larval foot remained at least partially extended, a posture important for immediate attachment when a settling larva encounters a surface.

The responsiveness of competent and precompetent larvae to encounters with filaments of different concentrations of PW is shown in Figure 5A. Typically, larvae did not retract when exposed to filaments of FSW or 1% PW. In contrast, larvae retracted their velar lobes in response to a high percentage of the filaments they encountered if the PW concentration in the filaments was 100% PW or 30% PW (30% is the concentration wherein metamorphosis-inducing activity is similar to that of water collected from within heads of *P. compressa* in the field). There was no significant difference between the percentage of filaments causing larval retraction in 100% PW and in 30% PW for both competent and precompetent larvae. A significantly lower percentage of filaments of 10% and 5% PW stimulated larvae to retract. There was no significant difference between the responsiveness of competent and precompetent larvae at any of the concentrations of PW.

Although both competent and precompetent larvae stopped "swimming" when they first entered a filament of cue from *P. compressa*, their behavior after that initial contact differed. Whereas competent larvae typically remained retracted while in a filament of PW, precompetent larvae more often re-expanded their velar lobes and re-

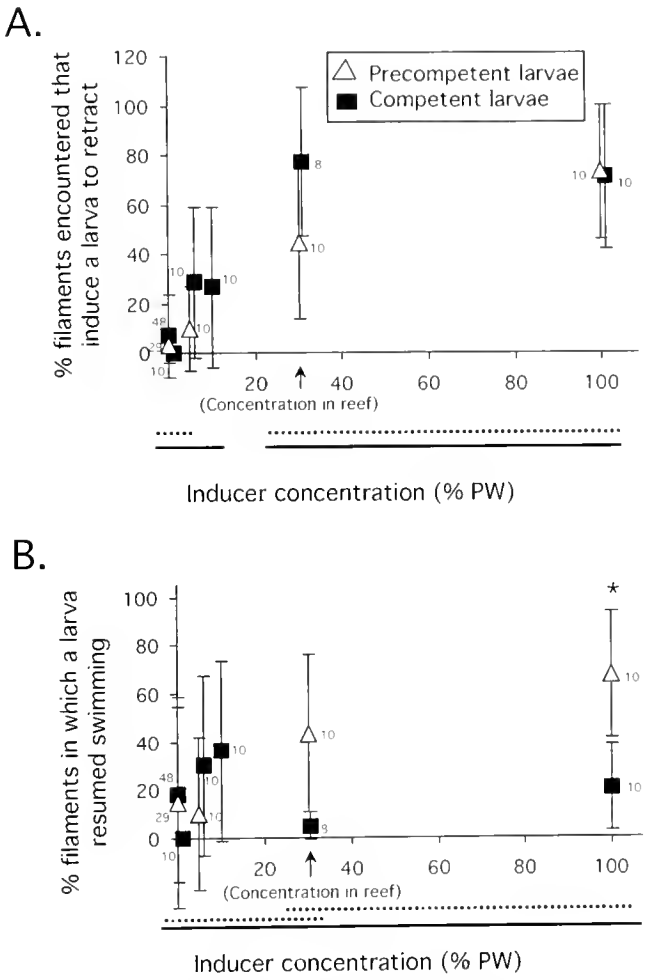

Figure 5. Responses of competent (black squares) and precompetent (open triangles) tethered larvae "swimming" through filaments of fluorescein-labeled filtered seawater or *Porites compressa* water (PW) in a small flume simulating untethered swimming. The small numbers next to each symbol represent the number of larvae in that treatment; error bars indicate one standard deviation. All of the data were compared using an ANOVA followed by Bonferroni/Dunn tests with a significance level of 5%. Solid lines below the horizontal axis indicate concentrations that were not significantly different for the competent larvae, and dotted lines indicate concentrations that were not significantly different for the precompetent larvae. An asterisk above the symbols for a particular concentration indicates that the competent and precompetent larvae were significantly different at that concentration. (A) "Responsiveness" of larvae to brief encounters with PW, measured as the percent of the filaments encountered that cause larvae to retract their velar lobes. (B) Percent of the filaments that stimulated retraction in which larvae re-expanded their velar lobes and resumed ciliary "swimming" while still in the filament.

sumed ciliary "swimming" while still in a PW filament (Fig. 5B).

There were lag times between when larvae first encountered or exited cue filaments and when their behavioral responses occurred. The lag time between the video frame when a filament of PW or FSW first reached a larva's apical sensory organ and the video frame when the cilia stopped beating and the velum started to retract is plotted in Figure 6A for larvae exposed to a range of concentrations of PW. There was no significant difference in this lag time to retraction between competent and precompetent larvae, nor were there any significant differences between the various concentrations of PW tested for competent and for precompetent larvae. Since so few precompetent larvae remained retracted in cue filaments, we were able to statistically analyze the lag times to resume swimming after exiting a filament only for competent larvae (Fig. 6B). We defined the lag time to resume swimming after exiting a filament as the time between the video frame in which a cue filament first moved beyond the upstream lip of the larval shell and the frame in which the cilia resumed beating on a fully re-expanded velum. There was no significant difference between the lag time to resume swimming for competent larvae exposed to filaments of 5%, 10%, 30%, and 100% solutions of PW. Competent larvae sometimes resumed swimming while still in filaments of 1% PW; hence the mean lag time to resume swimming in this weak cue was negative (*i.e.*, they resumed swimming on average about 1 s before exiting a filament).

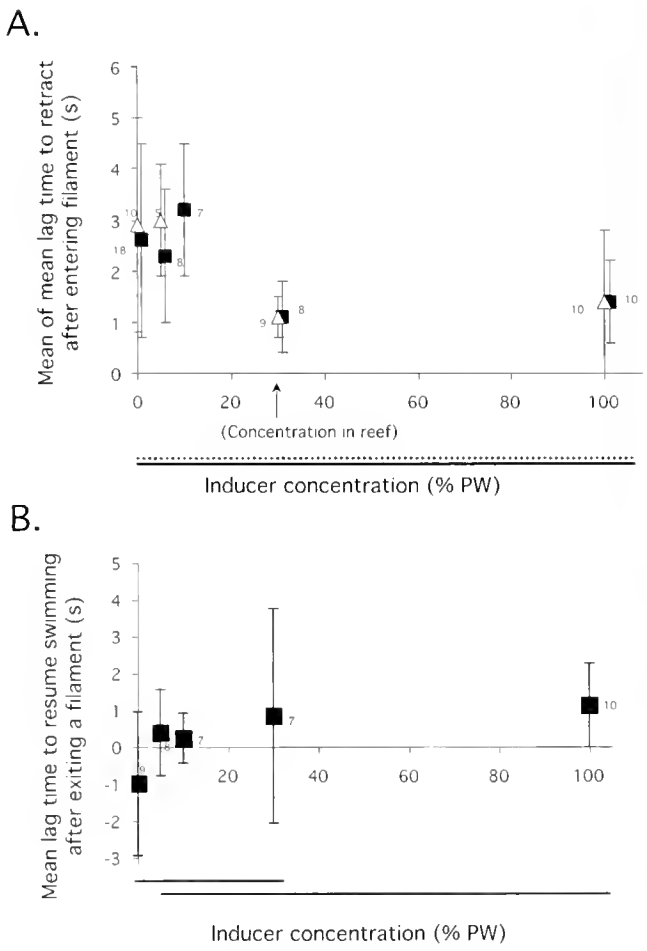

Figure 6. Mean lag times for larvae to respond to entering (A) or exiting (B) a filament, plotted as a function of *Porites compressa* water (PW) concentration for competent (black squares) and precompetent (open triangles) larvae. The small numbers next to each symbol indicate the number of larvae; error bars indicate one standard deviation. For precompetent larvae and competent larvae at PW concentrations of 10% PW, the n values are smaller than in Fig. 5 because not all of the larvae tested retracted when they encountered filaments. For each larva that retracted in each treatment, the mean lag time for all of its retractions was calculated, and the mean lag time for all its resumptions of "swimming" was calculated. The values plotted here are the means of those individual mean lag times. Statistical analyses (ANOVA, Bonferroni/Dunn, significance level 5%) were done as described in Fig. 5. Lines below different concentrations indicate that there was no significant difference between those concentrations for competent larvae (solid lines) and precompetent larvae (dotted lines). (A) Mean lag time to stop swimming. There were no significant differences between precompetent and competent larvae at any of the concentrations tested. (B) Mean lag time of competent larvae to resume swimming. Negative values indicate that larvae resumed swimming before exiting the filaments.

Speeds and trajectories of freely moving larvae in FSW and PW

If larvae were not tethered, those with beating velar cilia swam through the water, while those with retracted velar lobes sank. The data for swimming or sinking speeds and path straightness of competent larvae are plotted in Figure 7 and summarized in Table 1, where the statistical analyses are described. Significantly more larvae moved downward in PW than in FSW, as illustrated in Figure 3 and documented in Table 1. Our data underestimate the proportion of larvae moving downward, because many of the sinking larvae had already reached the bottom of the aquarium when the digitized section of each video began. Not only were the instantaneous speeds (Fig. 7A) of larvae in PW significantly slower than those of larvae in FSW, but so were the net speeds (Fig. 7B), since there was no significant difference between the straightness of the paths along which larvae in PW or FSW moved (Fig. 7C; Table 1).

Precompetent larvae swam faster and were less likely to move downward than competent larvae. Measurements of the motions of freely swimming precompetent larvae in aquaria containing FSW or 100% PW are plotted in Figure 8. We observed that precompetent larvae swam toward the light slits at the sides of our aquaria; hence only a small percentage of them moved downward in FSW (mean = 2%, SD = 1, n = 2 runs, number of larvae per run: 152 and 97). In contrast, competent larvae swam in many different directions in FSW in our aquaria, as illustrated in Figure 3a,

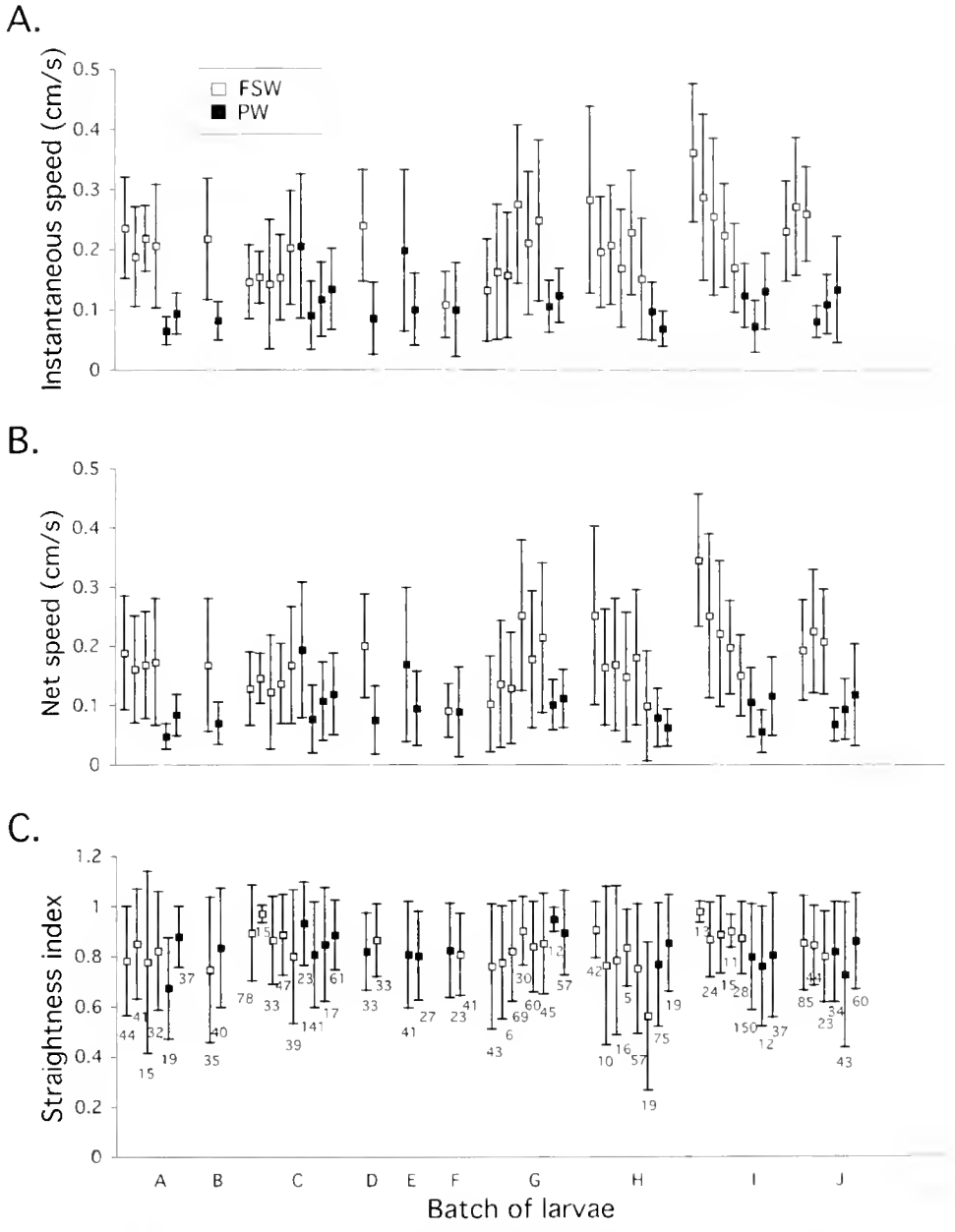

Figure 7. Measurements of competent larvae moving freely in aquaria containing filtered seawater (FSW; open squares) or 100% *Porites compressa* water (PW; black squares). Each symbol represents the mean value calculated for all of the larvae digitized in a run; error bars indicate one standard deviation. The small numbers below each symbol in Fig. 7C indicate the number of larvae digitized in that run in Figs. 7 A, B, and C. The letters along the horizontal axis indicate the cohorts of larvae used for the various runs. Statistical comparisons of these data are reported in Table 1. Since there were no significant differences between the cohorts of larvae (ANOVA, Bonferroni/Dunn, significance 5%), all of the runs were pooled for the analyses reported in Table 1. (A) The mean instantaneous speed for a run plotted here is the mean of the mean instantaneous speeds of all the larvae digitized in that run. (B) Mean net speed for all the larvae in each run. (C) Mean straightness index for all the larvae in each run. A straightness index of 1.0 represents a perfectly straight trajectory, whereas a lower straightness index indicates that a larva changed directions as it moved through the water, traveling along a curved or circuitous trajectory.

and thus significantly more competent larvae moved downward in FSW than did precompetent larvae (ANOVA, df = 32 where each sample was a run, $P < 0.05$). In the run we conducted with precompetent larvae in PW, 8% of the larvae moved downward ($n = 165$ larvae). The instantaneous speeds (mean = 0.32 cm s^{-1}, SD = 0.01, $n = 2$ runs)

Table 1

Movements of freely swimming competent larvae

Treatment	Instantaneous speed (cm s^{-1}) Mean[1] ± SD	Net speed (cm s^{-1}) Mean[1] ± SD	Straightness index Mean[1] ± SD	% larvae going down[2] Mean[1] ± SD	Number of runs[1]
FSW	0.21 ± 0.06	0.18 ± 0.05	0.83 ± 0.08	14 ± 9	32
PW	0.11 ± 0.04	0.10 ± 0.04	0.82 ± 0.07	20[3] ± 10	20
Significantly different?[4]	yes	yes	no	yes	

[1] For each run, a fresh solution was placed in an aquarium, new larvae were added, and all larvae in the field of view of the video were digitized (the numbers of larvae per run are shown in Fig. 7C). The mean values for instantaneous speed, net speed, and straightness index for the larvae in each run were calculated (means and SD values for each run shown in Fig. 7). The means of those run means are shown in this table.

[2] The angle between the net trajectory of a larva (see Methods) and vertical described the direction the larva was moving, where 0° was up, 90° was horizontal to the right or left, and 180° was down. We counted a larva as going down if its direction was 170° to 180°.

[3] These data underestimate the proportion of larvae moving downward, because many of the sinking larvae had already reached the bottom of the aquarium when the digitized section of each video began.

[4] ANOVA, Bonferroni/Dunn, significance level 5%.

and net speeds (0.27 cm s^{-1}, SD = 0.02, n = 2 runs) of precompetent larvae in FSW were significantly faster than those of competent larvae (Table 1) in FSW (ANOVA, df = 32, $P < 0.05$), whereas their speeds in PW were similar (Figs. 7A, B; 8A, B). The straightness indices of the trajectories of precompetent (Fig. 8C) and competent (Fig. 7C) larvae in both FSW and PW were also similar.

Sinking rates of dead larvae vs. *living larvae responding to PW*

The mean instantaneous sinking rate of living competent larvae moving freely in aquaria of PW was 0.12 cm s^{-1} (SD = 0.03, n = 21 runs). For each run, only larvae whose net direction of movement was 170°–180° (where 90° was lateral right and left, and 180° was down) were counted as sinking, and the mean of their instantaneous velocities was calculated for that run. The mean of those means for 21 runs is the value reported above (total number of sinking larvae measured in all the runs = 660). Sinking rates of living precompetent larvae in an aquarium of PW were measured in one run when 13 of 185 larvae were moving at angles of 170°–180°. The mean instantaneous sinking rate of these precompetent larvae, 0.12 cm s^{-1} (SD = 0.05, n = 13 larvae) was the same as that of the competent larvae in PW.

The mean gravitational fall velocity of dead larvae was 0.33 cm s^{-1} (SD = 0.04, n = 27). It is noteworthy that the passive sinking rate of fully retracted dead larvae of *P. sibogae* was almost three times faster than the speed of living larvae that sank in response to PW with their feet protruding from their shells.

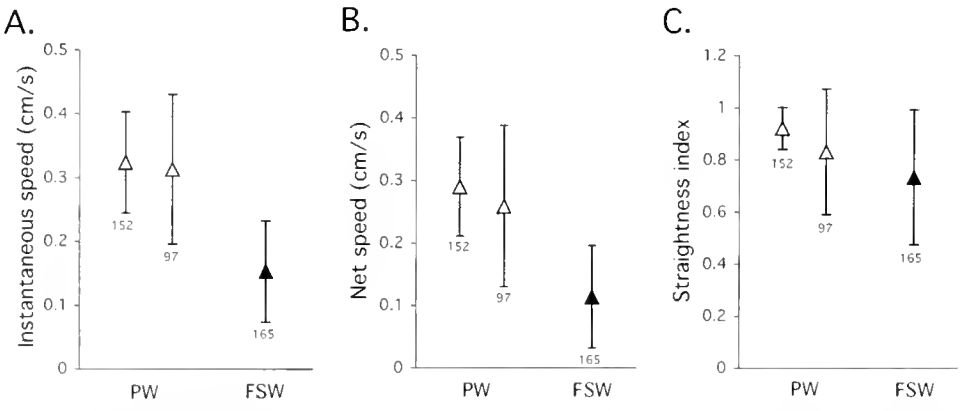

Figure 8. Measurements of precompetent larvae freely moving in aquaria containing filtered seawater (FSW; open triangles) or 100% *Porites compressa* water (PW; black triangles). All larvae were taken from the same cohort. Each symbol represents the mean value calculated for all of the larvae digitized in a run; the small numbers below each symbol indicate the number of larvae digitized in that run; and the error bars represent one standard deviation. (A) Mean instantaneous speeds, (B) net speeds, and (C) straightness indices for each run were calculated as described in Fig. 7; statistical analyses are reported in the text.

Discussion

Although many laboratory studies had revealed that competent larvae of *Phestilla sibogae* metamorphose in response to a dissolved substance from *Porites compressa* (*e.g.*, Hadfield and Pennington, 1990), a process that takes longer than 12 h, the dynamic behavioral responses of larvae of *P. sibogae* to encounters with coral cue had not previously been examined. Clearly, for coral cue to affect larval transport from the water column to the substratum in the turbulent flow across coral reefs, the larval behavioral responses to cue must be more rapid than the processes of metamorphosis. Thus, the present study assessed the behavioral responses of swimming larvae to encounters with water containing coral-produced settlement cue.

Rapid responses of larvae to settlement cue

This study focused on larval behavior over the time scale of tens of milliseconds to minutes. If chemicals are released from a surface in turbulent flowing water or air, fine filaments of fluid containing the chemical are formed in the high shear along the surface and are stirred into the surrounding water or air by swirling eddies (*e.g.*, Crimaldi and Koseff, 2001). Therefore, the distribution of concentrations of the released chemical in the turbulent, flowing fluid is very patchy. The intermittent nature of encounters with odors by insects flying in turbulent air flow has long been recognized (*e.g.*, Murlis, 1986; Murlis *et al.*, 1992; Vickers and Baker, 1992; Mafra-Neto and Cardé, 1994, 1998). Some studies of large benthic crustaceans tracking odor plumes have also documented the fluctuating, intermittent nature of chemical signals transported from a source by turbulent flowing water (reviewed in Weissburg, 2000), and recent PLIF studies have shown the fine-scale filamentous distribution of odors sampled by the olfactory antennules of these animals (Koehl *et al.*, 2000; Mead *et al.*, 2003). As microscopic larvae swim and are carried in the turbulent water flow above benthic habitats, they encounter dissolved substances released from the substratum (*e.g.*, Fig. 1) as a series of on-off pulses on a temporal scale of seconds (Strother *et al.*, 2001, unpubl. data). For this reason, we examined the rapid behavioral responses of swimming larvae exposed to a series of brief encounters, lasting a few seconds each, with filaments of settlement cue. We found that competent larvae of *P. sibogae* rapidly respond by sinking when they encounter a filament of dissolved cue from *Porites compressa*, but resume swimming when they exit the cue filament.

Settlement cue produced in the laboratory

Many studies of metamorphosis in *P. sibogae* have used a standardized "*Porites* water" (100% PW) produced in the laboratory (*e.g.*, Pennington and Hadfield, 1989). While this approach is suitable for studying the process of metamorphosis or isolating the inductive molecules in a chemical signal, investigations of behavioral responses should—if their results are to be useful in future analyses of larval transport and settlement—present larvae with a range of cue concentrations approximating those likely to be experienced in nature. The importance of using ecologically relevant concentrations of odors in studies of chemically mediated behavior is reviewed by Weissburg (2000).

The inductive chemicals in *Porites*-conditioned water (PW) are being isolated and characterized (V. Paul and Hadfield, unpubl.), but there is no chemical assay currently available to measure the molarity of inductive molecules in water samples. We have therefore used a bioassay—induction of metamorphosis—to measure the "strength" of inducer in our water samples. This bioassay has the advantage over a simple concentration measurement of incorporating any enhancement or reduction of cue activity by other substances that may in be in a water sample.

We found that water collected from coral heads in the field had metamorphosis-inducing strength similar to 30% solutions of laboratory-prepared PW. However, we found no significant differences between the instantaneous behavioral responses of larvae exposed to filaments of 100% PW or 30% PW. Furthermore, we found no difference between the adhesive strength of larvae induced to stick to surfaces by exposure to 30% PW or to 100% PW (Koehl and Hadfield, 2004). Thus, although we recommend that studies of larval behavioral responses to settlement cue be conducted at cue strengths comparable to those in nature, in the case of *P. sibogae* we found no difference between the behaviors of larvae in reef concentrations or in higher laboratory concentrations of cue from *P. compressa*.

Since the postures of larvae of *P. sibogae* induced to sink (velum retracted and foot expanded) by 100% PW were the same as those of larvae induced to sink in lower concentrations (5% PW–30% PW), our measurements of the fall velocities of larvae induced to sink in aquaria of 100% PW should be applicable to field conditions (fall velocity depends on the drag slowing the descent of a body, and drag depends on the size and shape of the body; *e.g.*, Vogel, 1994). Similarly, since the swimming velocities of larvae of *P. sibogae* in filtered laboratory seawater were the same as those of larvae in unfiltered water collected in the field upstream of coral reefs (Koehl and Hadfield, unpubl. data), our measurements of larval swimming velocities in filtered seawater should also be comparable to those of larvae in nature.

Downward velocities should be measured using unanesthetized living larvae

The downward velocities of living larvae responding to settlement cue are not necessarily the same as sinking

velocities measured for killed or anesthetized larvae. For example, when a larva of *P. sibogae* responds to coral cue by retracting its velum and sinking, its foot remains extended from the shell. The drag on the protruding foot slows the descent of the living larva relative to that of a fully retracted larva. Conversely, when near the substratum, oyster larvae may actively swim downward at speeds much greater than the sinking velocities of dead larvae (Finelli and Wethey, 2003). Therefore, measuring the sinking rates of anesthetized or dead larvae to determine the downward velocities of living larvae, as has often been done in the past (*e.g.*, Butman *et al.*, 1988a), may produce erroneous conclusions for some species.

Effects of larval behavior on their transport to and retention within a coral reef

On the scale of a larva, dissolved settlement cue released from a coral reef is very patchily distributed, but the frequency, thickness, and concentration of cue filaments are greater near the reef surface than higher above it (Fig. 1) (Reidenbach, 2004). A competent larva of *P. sibogae* responds within 1–2 s on most encounters with filaments of dissolved coral cue above threshold concentration by arresting the beat of its velar cilia, retracting its velum, and sinking. While microscopic larvae swim and sink through the water, the water in which they are moving is also transported toward and away from the reef surface due to the vertical orbital motion of water in waves and to swirling turbulent eddies (Koehl and Hadfield, 2004; Reidenbach, 2004). If the larva sinks, swims, or is transported closer to the reef, its encounters with cue filaments above threshold concentration increase in frequency and duration from one encounter every 10–20 s at a height of 12 cm above the reef to almost continuous exposure 1 cm above the corals (Strother *et al.*, 2001; Strother *et al.*, unpubl. data).

To examine whether the simple behavioral algorithm (sink in cue and swim in cue-free water) used by competent larvae of *P. sibogae* could enhance their settlement rates onto coral reefs exposed to turbulent, wave-driven flow, we employed a computer simulation (Strother *et al.*, 2001; Strother *et al.*, unpubl. data). In this individual-based model, we used measured values of the mean lag times, swimming and sinking velocities, and responsiveness to cue filaments of different concentrations. "Larvae" using this algorithm were randomly placed in the water column in PLIF videos (*e.g.*, Fig. 1) of changing concentrations of dye (an analog for cue) above a reef of *P. compressa* in a flume (Reidenbach, 2004) in wavy, turbulent flow like that measured over *P. compressa* reefs in the field (Koehl and Hadfield, 2004). Each "larva" swam in a particular direction randomly assigned at the beginning of the simulation. At each time step (*i.e.*, video frame), each "larva" swam or sank, depending on the cue concentration of the pixel in which it was located and on the history of cue exposure it had just experienced. The instantaneous net velocity of the "larva" was the vector sum of (i) its sinking or swimming velocity, (ii) the instantaneous velocity of the water at that height above the reef and phase of the wave cycle, and (iii) the random velocity fluctuation due to turbulence at that height and phase (values for ii and iii were measured in the flume; Reidenbach, 2004). The instantaneous net velocity of the "larva" determined its position in the next frame of the video, and so on. These calculations, done for thousands of "larvae," revealed that the simple behavioral algorithm used by the larvae of *P. sibogae* can enhance the rate of larval transport to the reef surface in turbulent, wavy flow by about 30% over that of larvae that do not alter their behavior in response to cue (Koehl *et al.*, 2000; Strother *et al.*, 2001; Strother *et al.*, unpubl. data).

The behavioral responses of competent larvae of *P. sibogae* to cue from *P. compressa* not only improve their transport down to the reef, but also enhance their chances of retention in a suitable habitat. Because larvae sink in cue concentrations like those found in the water between coral branches in *P. compressa* reefs, larvae that have been transported into a reef are likely to remain there, continuing to sink through the slowly moving (Koehl and Hadfield, 2004), cue-laden water within the reef. Furthermore, a larva that sinks in response to cue does so with its foot extended from the shell and thus is able to attach quickly on contact with a surface. Over the course of about 2 h of exposure to cue concentrations like those in coral heads in the field, larvae develop stronger adhesion both to living *P. compressa* tissue and to non-*Porites* surfaces (*e.g.*, coralline algae, glass) (Koehl and Hadfield, 2004), thereby further improving their chances of remaining in a suitable habitat bathed in inducer long enough for metamorphosis to occur.

The observation that precompetent larvae, not yet capable of undergoing metamorphosis, respond with about the same frequency as competent larvae to encounters with filaments of coral cue indicates that the chemosensitivity to the cue arises early in larval development. However, as indicated by the high percentage of times precompetent larvae re-extended their velar lobes and resumed swimming while within a cue filament, the sensitivity to coral cue is probably not sufficiently great to result in settlement and attachment. Furthermore, during daylight hours, the strongly photopositive precompetent larvae swim upward (Miller and Hadfield, 1986). Computer simulation of precompetent larvae in turbulent wave-driven flow above a reef of *Porites compressa* shows that such upward swimming when not responding to cue decreases larval encounters with cue filaments and enhances larval transport off the reef (Strother *et al.*, unpubl. data). By contrast, competent larvae are indifferent to light (Miller and Hadfield, 1986) and remain partially contracted in most of the cue filaments that cause them to stop swimming. Thus, in nature, competent larvae should

sink rapidly toward the coral reef, while precompetent larvae should be carried away.

Comparison of our results with those of other studies of effects of chemical cues on larval settlement in flowing water

Although many shallow coastal habitats are subjected to the oscillatory flow associated with waves, until now studies of the effects of chemical cues on larval transport to or settlement on the substratum have been done in unidirectional flow. The studies have typically determined the settlement positions of larvae onto different types of substrata after transport across the substrata in unidirectional laminar flow (*e.g.*, Butman *et al.*, 1988b; Pawlik *et al.*, 1991; Pawlik and Butman, 1993; Turner *et al.*, 1994). These studies provided solid evidence that larvae can discriminate among available substrata while being transported across them in flowing seawater. Additionally, Tamburri *et al.* (1996) videotaped paths of oyster pediveligers transported in a flume containing seawater only or seawater plus settlement-inducing substances, and reported downward movement of the larvae when the inducers were present. Our study contrasts with these earlier ones by focusing on wave-driven flow, by considering how dissolved cues are distributed on the spatial scale of microscopic larvae, and by examining the rapid behavioral responses of individual larvae to intermittent, brief encounters with cue. We found that larval responses are sufficiently rapid that repeated short encounters with cue filaments in turbulent, wave-driven flow can enhance larval transport into a suitable cue-releasing habitat. The behavior of larvae in cue can also enhance their retention in a flow-slowing, cue-releasing canopy such as a coral reef. Thus, this research on rapid behavioral responses of larvae in wave-driven flow is consistent with earlier studies of larvae in unidirectional flow in suggesting that larvae in flowing water can use chemical cues to enhance their settlement into appropriate habitats.

As in our computer simulations, another model of larval transport to the substratum also predicted enhanced settlement by larvae responding to chemical cues. Eckman *et al.* (1994) developed a one-dimensional model of the flux of larvae settling through a turbulent boundary layer when the vertical speed of the larvae is a function of their depth in the water column. In cases where steep gradients in the downward velocity of larvae occur near the substratum, which Eckman *et al.* (1994) suggested might be produced by larval responses to chemical cues associated with the bottom, settlement rate is enhanced.

Finally, the new data presented here demonstrate that a dissolved chemical cue from the prey coral *P. compressa* causes not only morphological metamorphosis in larvae of *P. sibogae*, a process requiring many hours of exposure (Hadfield, 1977), but also rapid behavioral responses that enhance chances of transport to and retention in a suitable habitat. Hence, settlement is not simply a result of the onset of metamorphosis, but rather is a behavioral phenomenon that results in placement of larvae within coral heads where dissolved cue is strong and consistent enough to induce adhesion to the substratum and metamorphosis (Koehl and Hadfield, 2004).

Acknowledgments

The authors gratefully acknowledge important assistance by students, postdoctoral fellows, research assistants, and visitors in their labs: at Kewalo Marine Laboratory—K. del Carmen, R. Chock, A. Faucci, K. Demain, W. Kelly, B. Nedved, V. Paul, and C. Unabia; at the University of California, Berkeley—B. Acosta, T. Cooper, J. Fong, M. Pong, J. Strother, and G. Wang. We thank M. A. Reidenbach and J. R. Koseff, Environmental Fluid Mechanics Laboratory, Dept. of Civil Engineering, Stanford University, for allowing us to use their PLIF data and the image for Figure 1. The recommendations of three anonymous reviewers led to increased clarity of this paper. This research was supported by National Science Foundation grants OCE-9907545 to MGH and OCE-9907120 to MARK.

Literature Cited

Aeby, G. S. 1998. Behavioral and ecological relationships of a parasite and its host within a coral reef system. *Pacific Sci.* **45:** 263–269.

Bahamondes-Rojas, I., and M. Dherbonez. 1990. Purification partielle de substances glycoconjuguées capables d'induire la metamorphose des larves competentes d'*Eubranchus doriae* (Trinchese, 1879), mollusque nudibranche. *J. Exp. Mar. Biol. Ecol.* **144:** 17–27.

Black, K. P., S. L. Gay, and J. C. Andrews. 1990. Residence times of neutrally buoyant matter such as larvae, sewage or nutrient on coral reefs. *Coral Reefs* **9:** 105–114.

Boettcher, A. A., and N. M. Targett. 1998. Role of chemical inducers in larval metamorphosis of queen conch, *Strombus gigas* Linnaeus: relationship to other marine invertebrate systems. *Biol. Bull.* **194:** 132–142.

Bonar, D. B., and M. G. Hadfield. 1974. Metamorphosis of the marine gastropod *Phestilla sibogae*. I. Light and electron microscopic analysis of larval and metamorphic stages. *J. Exp. Mar. Biol. Ecol.* **16:** 1–29.

Brumbaugh, R. D., and J. R. McConaugha. 1995. Time to metamorphosis of blue crab *Callinectes sapidus* megalopae: effects of benthic macroalgae. *Mar. Ecol. Prog. Ser.* **129:** 113–118.

Burke, R. D. 1984. Pheromonal control of metamorphosis in the Pacific sand dollar, *Dendraster excentricus*. *Science* **225:** 442–443.

Butman, C. A., J. P. Grassle, and E. J. Busky. 1988a. Horizontal swimming and gravitational sinking of *Capitella* sp. 1 (Annelida: Polychaeta) larvae: implications for settlement. *Ophelia* **29:** 43–58.

Butman, C. A., J. P. Grassle, and C. M. Webb. 1988b. Substrate choices made by marine larvae settling in still water and in a flume flow. *Nature* **333:** 771–773.

Clare, A. S., and M. B. Jones, guest editors. 1998. Special issue: Papers from the International Symposium on Settlement and Metamorphosis of Marine Invertebrate Larvae, University of Plymouth, July 1996. *Biofouling* **12(1–3):** 1–269.

Crimaldi, J. P., and J. R. Koseff. 2001. High-resolution measurements

of the spatial and temporal scalar structure of a turbulent plume. *Exp. Fluids* **31:** 90–102.

Crisp, D. J. 1974. Factors influencing the settlement of marine invertebrate larvae. Pp. 177–265 in *Chemoreception in Marine Organisms*, P. T. Grant and A. M. Mackie, eds. Academic Press, London.

Crisp, D. J., and P. S. Meadows. 1962. The chemical basis of gregariousness in cirripedes. *Proc. R. Soc. Lond. B* **156:** 500–520.

Denny, M. W. 1988. *Biology and the Mechanics of the Wave-swept Environment.* Princeton University Press, Princeton, NJ.

Eckman, J. E., F. E. Werner, and T. F. Gross. 1994. Modeling some effects of behavior on larval settlement in a turbulent boundary layer. *Deep-Sea Res.* **41:** 185–208.

Finelli, C. M. and D. S. Wethey. 2003. Behavior of oyster larvae (*Crassostrea virginica*) larvae in flume boundary layer flows. *Mar. Biol.* **143:** 703–711.

Fleck, J., and D. K. Hofmann. 1995. *In vivo* binding of a biologically active oligopeptide in vegetative buds of the scyphozoan *Cassiopea andromeda:* demonstration of receptor-mediated induction of metamorphosis. *Mar. Biol.* **122:** 447–451.

Glynn, P. W. 1997. Bioerosion and coral-reef growth: a dynamic balance. Pp. 68–95 in *Life and Death on Coral Reefs*, C. Birkeland, ed. Chapman and Hall, New York.

Grassle, J. P., P. V. R. Snelgrove, and C. A. Butman. 1992. Larval habitat choice in still water and flume flows by the opportunistic bivalve *Mulinia lateralis*. *Neth. J. Sea Res.* **30:** 33–44.

Gulko, D., and P. L. Jokiel. 1995. Ultraviolet radiation and coral reefs. Hawaii Institute of Marine Biology, Report no. 41. Univ. of Hawaii, Honolulu, HI.

Hadfield, M. G. 1977. Chemical interactions in larval settling of a marine gastropod. Pp. 403–413 in *Marine Natural Products Chemistry*, D. J. Faulkner and W. H. Fenical, eds. Plenum, New York.

Hadfield, M. G. 1984. Settlement requirements of molluscan larvae: new data on chemical and genetic roles. *Aquaculture* **39:** 283–298.

Hadfield, M. G. 1998. The D. P. Wilson lecture, research on settlement and metamorphosis of marine invertebrate larvae: past, present and future. *Biofouling* **12:** 9–29.

Hadfield, M. G., and V. J. Paul. 2001. Natural chemical cues for settlement and metamorphosis of marine invertebrate larvae. Pp. 431–461 in *Marine Chemical Ecology*, J. B. McClintock and W. Baker, eds. CRC Press, Boca Raton, FL.

Hadfield, M. G., and J. T. Pennington. 1990. The nature of the metamorphic signal and its internal transduction in larvae of the nudibranch *Phestilla sibogae*. *Bull. Mar. Sci.* **46:** 455–464.

Hadfield, M. G., and D. Scheuer. 1985. Evidence for a soluble metamorphic inducer in *Phestilla sibogae:* ecological, chemical and biological data. *Bull. Mar. Sci.* **37:** 556–566.

Hadfield, M. G., E. A. Kay, M. U. Gillette, and M. G. Lloyd. 1972. The Vermetidae (Mollusca: Gastropoda) of the Hawaiian Islands. *Mar. Biol.* **12:** 81–98.

Hadfield, M. G., C. Unabia, C. M. Smith, and T. M. Michael. 1994. Settlement preferences of the ubiquitous fouler *Hydroides elegans*. Pp. 65–74 in *Recent Developments in Biofouling Control*, M. Fingerman, R. Nagabhushanam, and R. Sarojini, eds. Oxford and IBH, New Delhi.

Hadfield, M. G., E. A. Meleshkevitch, and D. Y. Boudko. 2000. The apical sensory organ of a gastropod veliger is a receptor for settlement cues. *Biol. Bull.* **198:** 67–76.

Hermann, K. 1995. Induction and regulation of metamorphosis in planktonic larvae: *Phoronis müllerí* (Tentaculata) as archetype. *Helgol. Wiss. Meeresunters.* **49:** 255–281.

Hofmann, D. K., and U. Brand. 1987. Induction of metamorphosis in the symbiotic scyphozoan *Cassiopea andromeda:* role of marine bacteria and of biochemicals. *Symbiosis* **4:** 99–116.

Jensen, G. C. 1989. Gregarious settlement of megalopae of the porcelain crab *Petrolisthes cinctipes* (Randall) and *P. eriomerus* Stimpson. *J. Exp. Mar. Biol. Ecol.* **131:** 223–231.

Jensen, R. A., and D. E. Morse. 1990. Chemically induced metamorphosis of polychaete larvae in both the laboratory and ocean environment. *J. Chem. Ecol.* **16:** 911–930.

Kay, A. E. 1979. *Hawaiian Marine Shells.* Sec. 4, Reef and Shore Fauna of Hawaii, Bishop Museum Press, Honolulu, HI.

Koehl, M. A. R. 1977. Effects of sea anemones on the flow forces they encounter. *J. Exp. Biol.* **69:** 87–105.

Koehl, M. A. R., and E. Dobbins. 1998. Small-scale mixing and transport in and above a coral reef during mass spawning. *EOS Trans. Am. Geophys. Union.* **78:** OS59.

Koehl, M. A. R., and M. G. Hadfield. 2004. Soluble settlement cue in slowly moving water within coral reefs induces larval adhesion to surfaces. *J. Mar. Sys.* (In press: doi:10.1016/j.jmarsys.2003.06.003).

Koehl, M. A. R., and T. M. Powell. 1994. Turbulent transport of larvae near wave-swept rocky shores: does water motion overwhelm larval sinking? Pp. 261–274 in *Reproduction and Development of Marine Invertebrates*, G. S. H. Wilson and S. Stricker, eds. Johns Hopkins Univ. Press, Baltimore, MD.

Koehl, M. A. R., T. M. Powell, and E. L. Dobbins. 1997. Effects of algal turf on mass transport and flow microhabitat of ascidians in a coral reef lagoon. *Proc. 8th Int. Coral Reef Symp.* **2:** 1087–1092.

Koehl, M. A. R., M. G. Hadfield, T. Cooper, M. A. Reidenbach, and J. R. Koseff. 2000. Can larvae of benthic animals use dissolved chemical cues in wave-driven flow? *Am. Zool.* **40(6):** 1089.

Koehl, M. A. R., J. R. Koseff, J. P. Crimaldi, M. G. McCay, T. Cooper, M. G. Wiley, and P. A. Moore. 2001. Lobster sniffing: antennule design and hydrodynamic filtering of information in an odor plume. *Science* **294:** 1948–1952.

Krug, P. J., and A. E. Manzi. 1999. Waterborne and surface-associated carbohydrates as settlement cues for larvae of the specialist marine herbivore *Alderia modesta*. *Biol. Bull.* **197:** 94–103.

Lambert, W. J., and C. D. Todd. 1994. Evidence for a water-borne cue inducing metamorphosis in the dorid nudibranch mollusc *Adalaria proxima* (Gastropoda: Nudibranchia). *Mar. Biol.* **120:** 265–271.

Lambert, W. J., C. D. Todd, and J. D. Hardege. 1997. Partial characterization and biological activity of a metamorphic inducer of the dorid nudibranch *Adalaria proxima* (Gastropoda: Nudibranchia). *Invertebr. Biol.* **116:** 71–81.

Leitz, T., K. Morand, and M. Mann. 1994. Metamorphosin A: a novel peptide controlling development of the lower metazoan *Hydractinia echinata* (Coelenterata, Hydrozoa). *Dev. Biol.* **163:** 440–446.

Mafra-Neto, A., and R. T. Cardé. 1994. Fine-scale structure of pheromone plumes modulates upwind orientation of flying moths. *Nature* **369:** 142–144.

Mafra-Neto, A., and R. T. Cardé. 1998. Rate of realized interception of pheromone pulses in different wind speeds modulates almond moth orientation. *J. Comp. Physiol A* **182:** 563–572.

McGee, B. L., and N. M. Targett. 1989. Larval habitat selection in *Crepidula* (L.) and its effect on adult distribution patterns. *J. Exp. Mar. Biol. Ecol.* **131:** 195–214.

Mead, K. S., M. B. Wiley, M. A. R. Koehl, and J. R. Koseff. 2003. Fine-scale patterns of odor encounter by the antennules of mantis shrimp tracking turbulent plumes in wave-affected and unidirectional flow. *J. Exp. Biol.* **206:** 181–193.

Miller, S. E., and M. G. Hadfield. 1986. Ontogeny of phototaxis and metamorphic competence in larvae of the nudibranch *Phestilla sibogae* Bergh (Gastropoda: Opisthobranchia). *J. Exp. Mar. Biol. Ecol.* **97:** 95–112.

Morse, A. N. C., and D. E. Morse. 1984. Recruitment and metamorphosis of *Haliotis* larvae induced by molecules uniquely available at the surfaces of crustose red algae. *J. Exp. Mar. Biol. Ecol.* **75:** 191–215.

Morse, D. E., and A. N. C. Morse. 1991. Enzymatic characterization of

the morphogen recognized by *Agaricia humilis* (Scleractinian coral) larvae. *Biol. Bull.* **181:** 104–122.

Morse, D. E., N. Hooker, A. N. C. Morse, and R. A. Jensen. 1988. Control of larval metamorphosis and recruitment in sympatric agariciid corals. *J. Exp. Mar. Biol. Ecol.* **116:** 193–217.

Müller, W. A. 1973. Metamorphose-Induktion bei Planulalarven. *Wilhelm Roux's Arch. Dev. Biol.* **173:** 107–121.

Murlis, J. 1986. The structure of odour plumes. Pp. 27–38 in *Mechanisms in Insect Olfaction*, T. L. Payne, M. C. Birch, and C. E. J Kennedy, eds. Clarendon Press, Oxford, United Kingdom.

Murlis, J., J. S. Elkinton, and R. T. Cardé. 1992. Odor plumes and how insects use them. *Annu. Rev. Entomol.* **37:**505–532.

Oberdorfer, J. A., and R. W. Buddemeier. 1986. Coral reef hydrology: field studies of water movement within a barrier reef. *Coral Reefs* **5:** 7–12.

Okubo, A., and S. A. Levin 2001. *Diffusion and Ecological Problems: Modern Perspectives*, 2nd ed. Springer-Verlag, New York.

Parnell, K. E. 1986. Water movement within a fringing reef flat, Orpheus Island, North Queensland, Australia. *Coral Reefs* **5:** 1–6.

Paulay, G. 1997. Diversity and distribution of reef organisms. Pp. 298–353 in *Life and Death of Coral Reefs*, C. Birkeland, ed. Chapman and Hall, New York.

Pawlik, J. R., and C. A. Butman. 1993. Settlement of a marine tube worm as a function of current velocity: interacting effects of hydrodynamics and behavior. *Limnol. Oceanogr.* **38:** 1730–1740.

Pawlik, J. R., C. A. Butman, and V. R. Starczak. 1991. Hydrodynamic facilitation of gregarious settlement of a reef-building tube worm. *Science* **251:** 421–424.

Pearce, C. M., and R. E. Scheibling. 1990a. Induction of metamorphosis of larvae of the green sea urchin, *Strongylocentrotus droebachiensis*, by coralline red algae. *Biol. Bull.* **179:** 304–311.

Pearce, C. M., and R. E. Scheibling. 1990b. Induction of settlement and metamorphosis in the sand dollar *Echinarachnius parma*: evidence for an adult-associated factor. *Mar. Biol.* **107:** 363–369.

Pearce, C. M., and R. E. Scheibling. 1991. Effect of macroalgae, microbial films, and conspecifics on the induction of metamorphosis of the green sea urchin *Strongylocentrotus droebachiensis* (Müller). *J. Exp. Mar. Biol. Ecol.* **147:** 147–162.

Pennington, J. T., and M. G. Hadfield. 1989. Larvae of a nudibranch mollusc (*Phestilla sibogae*) metamorphose when exposed to common organic solvents. *Biol. Bull.* **177:** 350–355.

Reidenbach, M. A. 2004. Boundary layer dynamics in coral reef systems. Ph.D. dissertation. Stanford University, Stanford, CA. 263 pp.

Rice, M. E. 1986. Factors influencing larval metamorphosis in *Golfingia misakiana* (Sipuncula). *Bull. Mar. Sci.* **39:** 362–375.

Rice, M. E. 1988. Observations on development and metamorphosis of *Siphonosoma cumanense* with comparative remarks on *Sipunculus nudus* (Sipuncula, Sipunculidae). *Bull. Mar. Sci.* **42:** 1–15.

Richmond, R. H. 1997. Reproduction and recruitment in corals: critical links in the persistence of reefs. Pp. 175–197 in *Life and Death on Coral Reefs*, C. Birkeland, ed. Chapman and Hall, New York.

Rittschof, D. 1985. Oyster drills and the frontiers of chemical ecology: unsettling ideas. *Am. Malacol. Bull.* **(Special Ed) 1:** 111–116.

Scheltema, R. S. 1961. Metamorphosis of the veliger larvae of *Nassarius obsoletus* (Gastropoda) in response to bottom sediment. *Biol. Bull.* **120:** 92–109.

Strother, J., M. A. R. Koehl, M. Reidenbach, and M. G. Hadfield. 2001. Computer simulations of larval behavior in wave-driven flow predict settling success in response to soluble cues. *Am. Zool.* **41(6):**1598.

Tamburri, M. N., C. M. Finelli, D. S. Wethey, and R. K. Zimmer-Faust. 1996. Chemical induction of larval settlement behavior in flow. *Biol. Bull.* **191:** 367–373.

Turner, E. J., R. K. Zimmer-Faust, M. A. Palmer, M. Luckenbach, and N. D. Pentcheff. 1994. Settlement of oyster (*Crassostrea virginica*) larvae: effects of water flow and a water-soluble cue. *Limnol. Oceanogr.* **39:** 1579–1593.

Vickers, N. J., and T. C. Baker. 1992. Male *Heliothis-virescens* maintain upwind flight in response to experimentally pulsed filaments of their sex pheromone (Lepidoptera, Noctuidae). *J. Insect Behav.* **5:** 669–687.

Vogel, S. 1994. *Life in Moving Fluids*, 2nd Ed. Princeton University Press, Princeton, NJ.

Weissburg, M. J. 2000. The fluid dynamical context of chemosensory behavior. *Biol. Bull.* **198:** 188–202.

Welch, J. M., D. Rittschof, T. M. Bullock, and R. B. Forward, Jr. 1997. Effects of chemical cues on settlement behavior of blue crab *Callinectes sapidus* postlarvae. *Mar. Ecol. Prog. Ser.* **154:** 143–153.

Williamson, J. E., R. De Nys, N. Kumar, D. G. Carson, and P. D. Steinberg. 2000. Induction of metamorphosis in the sea urchin *Holopneustes purpurascens* by a metabolite complex from the algal host *Delisea pulchra*. *Biol. Bull.* **198:** 332–345.

Wilson, D. P. 1952. The influence of the nature of the substratum on the metamorphosis of the larvae of marine animals especially the larvae of *Ophelia bicornis* Savigny. *Ann. Inst. Oceanogr. Monaco* **27:** 49–156.

Young, C. M. 1978. Studies on solitary ascidian larval ecology and functional morphology. M.S. thesis, Brigham Young University, Salt Lake City, UT.

Young, C. M., and L. F. Braithwaite. 1980. Larval behavior and post-settling morphology in the ascidian, *Chelyosoma productum* Stimpson. *J. Exp. Mar. Biol. Ecol.* **42:** 157–169.

Zimmer-Faust, R. K., and M. N. Tamburri. 1994. Chemical identity and ecological implications of a waterborne, larval settlement cue. *Limnol. Oceanogr.* **39:** 1075–1087.

Reference: *Biol. Bull.* **207:** 44–55. (August 2004)

Effects of Odor Flux and Pulse Rate on Chemosensory Tracking in Turbulent Odor Plumes by the Blue Crab, *Callinectes sapidus*

TROY A. KELLER[1] AND MARC J. WEISSBURG[2]

School of Biology, Georgia Institute of Technology, 310 Ferst Dr., Atlanta, Georgia 30332-0230

Abstract. The ability of animals to track through chemical plumes is often related to properties of evanescent odor bursts and to small-scale mixing process that determine burst properties. However, odor plumes contain variation over a range of scales, and little is known about how variation in the properties of the odor signal on the scale of one to several seconds affects foraging performance. We examined how flux and pulse rate interact to modulate the search behavior of blue crabs, *Callinectes sapidus*, locating odor sources in controlled flume flows. Experimental treatments consisted of continuous plumes and plumes with discrete odor pulses at intervals of 2.5 s and 4 s at two fluxes. Crabs experienced diminished search success and reduced search efficiency as flux decreased and the inter-pulse interval lengthened. There often were significant interactions between flux and pulse length, and neither property completely determined search behavior. Thus, over the time span of several seconds, the blue crab chemosensory system is not a simple flux detector. The sensitivity of blue crabs to inter-pulse intervals in the range of several seconds indicates that larger-scale mixing processes, which create odor variation on comparable scales, may exert a significant impact on foraging success in nature.

Introduction

Many aquatic and terrestrial animals orient to fluid-borne chemical plumes to locate predators, prey, mates, or dwelling sites. A common sensory strategy of animals in these environments is to use fine-scale features of odor plumes to extract information on distance and direction (Moore and Atema, 1991; Mafra-Neto and Cardé, 1994; Vickers and Baker, 1994). These plume features, variously termed odor filaments, pulses, or bursts, are the result of turbulent mixing processes that distribute chemicals within the plume. Accordingly, odor stimulation in plumes is evanescent: although turbulent mixing may result in temporal variation in stimulus intensity over a variety of scales, odor filaments typically last less than 1 s and commonly may be less than 200–500 ms (Murlis *et al.*, 1992; Moore *et al.*, 1994; Crimaldi and Koseff, 2001; Webster and Weissburg, 2001).

The time scale of odor fluctuations may not be the same time scale that characterizes either the neural coding of chemical signals or the behavioral response, for several reasons. The physical and molecular events underlying the transduction process set limits on neuronal response times. For example, sensory neurons in crustaceans and insects cannot respond distinctly to odor pulses presented at frequencies exceeding 4 and 10 Hz, respectively (Kaissling *et al.*, 1987; Gomez *et al.*, 1994). Even when sensory systems may be able to encode information rapidly, averaging or integrating over longer periods may increase the signal-to-noise ratio and result in more accurate depiction of stimulus properties. Indeed, temporal averaging is necessary for navigational strategies that rely on mean properties of odor plumes, since stochastic variation in signal intensity in turbulent plumes reduces the accuracy of rapid assessments of local mean concentration (Webster and Weissburg, 2001).

Crustaceans such as crabs and lobsters clearly rely, at least in part, on brief odor pulses as they navigate through turbulent plumes (Moore and Atema, 1991; Weissburg and Zimmer-Faust, 1994; Mead, 2002). However, animals may alter behavior in response to larger-scale flow structures if they integrate information over time scales (*i.e.*, seconds)

Received 15 January 2004; accepted 17 May 2004

[1] Current address: Department of Water Resources, St. Johns River Water Management District, P.O. Box 1429, Palatka, FL 32178.

[2] To whom correspondence should be addressed. E-mail: marc.weissburg@biology.gatech.edu

corresponding to the period over which these structures cause signal variation. Unfortunately, there is little information on how blue crabs or other crustaceans respond to odor signal variation over time scales of one to several seconds. Such information is essential for a meaningful analysis of plume tracking in nature, where large-scale flow structures (*i.e.,* eddies) may interact with small-scale turbulence to produce odor fluctuations on time scales ranging from milliseconds to minutes (Atema, 1995; Weissburg, 2000; Webster and Weissburg, 2001). Thus, this study examined the navigation of blue crabs (*Callinectes sapidus*) in turbulent flow in response to artificially pulsed odor plumes. Pulse rate and flux were varied independently to examine whether crab responses to pulsed plumes varied with the general level of stimulus intensity. The results indicate that flux and pulse rate interact to determine crab foraging behavior, suggesting that small-scale turbulent features are not the only determinants of olfactory-mediated foraging ability.

Methods

Animals

Male and female blue crabs (*Callinectes sapidus* Rathbun, 1896) were collected, using baited traps (Gulf Specimen Supplies), from habitats adjacent to Dickson Bay in Panacea, Florida (30°00′ N, 84°22′ W). Crabs were shipped to Atlanta, Georgia, kept in communal tanks filled with artificial seawater (ASW; Instant Ocean, 33 ppt, 20 °C), and tested within 20 d of collection. Animals were maintained on a cycle of 12 h light and 12 h dark, and fed freshly thawed shrimp *ad libitum* every other day. We withheld food from the crabs about 12 h before testing to ensure that they were not satiated and to standardize the time of last access to food.

The flow and stimulus environment

We characterized blue crab search behavior and hydrodynamics in an indoor, recirculating flume (12.5-m long × 0.75-m wide; total capacity about 3200 gal, or roughly 12,113 l) lined with sand to provide a natural substrate. The working section where foraging trials took place begins about 10 m downstream of the flume entrance. This facility has been described previously, and results in reproducible, realistic, and well-defined flow environments (Keller *et al.,* 2003). Average flow velocity was maintained at 4.9 cm s^{-1} ± 0.08 (mean ± SD) with a water depth of 23.0 cm ± 0.348 (mean ± SD). The vertical velocity profile of our flows showed a good fit to the Law-of-the-Wall equation (Keller *et al.,* 2003), which specifies the expected relationship between flow velocity and height above the substrate in an equilibrium boundary layer (Weissburg, 2000). At this flow speed, the boundary layer shear velocity, u^*, a measure of stress due to turbulent velocity fluctuations (Denny, 1988), was 3.1 mm s^{-1}, calculated using the Law-of-the-Wall (Weissburg and Zimmer-Faust, 1993; Keller *et al.,* 2003). This value conforms well to expectations for turbulence in open channel flows. The Roughness Reynolds number (Re^*), which measures the penetration of turbulent eddies into the boundary layer, was 2.65, which suggests smooth flow (Denny, 1988). These hydrodynamic conditions during behavior trials are well within the range reported for blue crab habitats in the field (*e.g.,* Zimmer-Faust *et al.,* 1995). Trials took place between about 1400 and 1700. Light levels were lowered during trials to minimize visual cues during navigation and to reproduce the low light levels corresponding to early morning and evening periods when foraging activity peaks in the field (Clarke *et al.,* 1999).

Chemical stimuli consisted of a solution prepared by soaking whole, intact (previously frozen) shrimp in ASW drawn from the flume. Shrimp were soaked in ASW for 1 h at a concentration of either 3.5 or 7.0 gm · l^{-1}, and the solutions were prepared immediately before behavioral trials. This odorant solution was released parallel to the flow 2.5 cm above the bed from a 4.7-mm-diameter brass nozzle with a fairing to minimize the flow perturbation.

Dual inputs into the nozzle accommodated an odorless ASW source and the odorant solution. The use of two separate flows allowed us to alternate between odorless and odor-containing solutions to introduce odor pulses into the flume channel. The two flow streams converged at the horizontal arm of the L-shaped nozzle (about 2 in. long), and each was equipped with an in-line flowmeter so that the velocities could be independently controlled. Each flow stream passed through a three-way solenoid valve, and both valves were controlled by a valve driver such that one valve was on (*i.e.,* diverting the flow into the nozzle) when the other was off (diverting the flow into a waste reservoir). A pulse generator (AM Systems) provided the timing signal to the valve driver to control the on-and-off times. Air pressure imparted the necessary force to drive the fluid through the system.

Experiments were run using three patterns of stimulus release for each of the two odorant concentrations. In addition to a continuous odor plume, we also generated pulsed plumes of two types. In the first condition, 2.5 s of odorant release alternated with 2.5 s of odorless ASW. The second condition consisted of alternating 1-s odor pulses and 4-s intervals of odorless ASW. Initial flow visualization experiments suggested that it was difficult to produce coherent pulses using on-or-off times of less than 1 s. The flow rate for the odorless ASW was set to 60 ml min^{-1} to ensure cleanly separated odor pulses. The flow rate for the odorant solution was systematically adjusted to equalize the volume of odorant solution released in each of the three plume types. Release rate for the continuous case was 6 ml · min^{-1}, which corresponded to isokinetic release, as flow

velocity 2.5 cm above the bed is approximately 0.5 cm s^{-1} (Keller *et al.*, 2003). The 2.5-s and 1-s odor pulses were released at rates of 12 and 30 ml min^{-1}, respectively. Since experiments took place in the same water flow speed, a sensor of constant area would experience the same number of stimulus molecules delivered to its surface over the 5-s cycle length for plumes created with solutions of a given odorant concentration. Our manipulations using different pulse lengths and stimulus concentrations therefore decouple the temporal pattern of stimulation from rate of odorant delivery (flux) to crab chemosensors.

Flow visualization

We performed a series of qualitative flow visualizations to roughly characterize the plume conditions. Our methods were designed only to ascertain that pulsing the source results in discrete odor signals that propagate downstream, and are similar to qualitative methods employed in other studies (*e.g.*, Belanger and Willis, 1996); a full analysis of pulse properties requires methods, such as planar laser-induced fluorescence (Webster and Weissburg, 2001), that go well beyond that needed here. Initial visualizations suggested that coherent pulses generated at the nozzle orifice were disrupted as they moved downstream but maintained cohesion for at least 100 cm, setting an approximate (and probably conservative) boundary for pulse coherence. Thus, we photographed the plume as it evolved for roughly 15 cm beginning at a distance of about 85 cm downstream of the nozzle. Pictures of the plume as viewed from above were taken with a digital camera mounted 0.5 m above the middle of the working section, yielding a visualized area of approximately 15 × 10 cm (l × w). A 0.1% fluorescein solution prepared in flume water was illuminated with a 2-cm-thick horizontal light sheet produced by a slide projector and focused on the plume, and photographed against a black sand background. The three release conditions (continuous, 2.5-s pulse, and 1-s pulse) were replicated using the same delivery and flow parameters as in the behavioral trials.

The digital images were converted to high-resolution (1000 × 1500 pixel) jpeg files, then converted to grayscale and inverted using Adobe Photoshop. We selected a random subsection away from the plume (free of visible odor filaments) in each image and used this to determine the background pixel intensity, which then was subtracted from each image. Images were analyzed using the public domain NIH Image program (ver. 4.02; available at http://rsb.info.nih.gov/nih-image/) to produce a frequency histogram of pixel intensity values for each image. An average histogram for each plume condition was constructed from five images, each taken from a separate visualization.

Behavioral experiments

The ability of blue crabs to locate the odor source by navigating through the chemical plumes was tested in the flume, using methods similar to those previously described (Keller *et al.*, 2003). Briefly, blue crabs were carefully moved to the flume and placed in a flow-through acrylic plastic box (27.2-cm long, 19.5-cm wide, 16.5-cm high). Animals were acclimated in the box for 13 min prior to the release of odorant solution from a source located 1.5 m directly upstream of the center of the acrylic box. The front door was raised 2 min later. Trials lasted for a maximum of 15 min and were terminated if the animal successfully found the source and attempted to grab it, or moved either upstream of the source or downstream of the acrylic box. Trials were also terminated if the animal failed to leave the box within 5 min. Release rate and stimulus concentration were varied daily, with three or four trials on any given day. Consequently, no more than 1 l of the stimulus solution was released into the flume, which minimized accumulation of shrimp metabolites. Flume water was filtered through 5-μm particulate filters, activated carbon, nitrate- and phosphate-absorbing media, and UV sterilizers two or three times per week for a period of 12–18 h.

Crab behavior was recorded on videotape using a low-light-sensitive CCD camera mounted about 2 m above the working section of the flume. A watertight backpack containing two red-light-emitting diodes powered by a watch battery was attached to the carapace of each blue crab before behavioral experiments. We assayed the motivational state of animals that failed to find the source by placing them in a small tank (28 cm dia. containing 5 l of flume water) and offering them a single shrimp. Blue crabs that failed to respond to this food within 5 min were designated as unresponsive and were omitted from subsequent analysis. Similar to observations by Weissburg and Zimmer-Faust (1993), the percentage of unresponsive crabs ranged from about 11% to 19%, with no systematic variation across treatments. Each crab was tested only once, for a total of over 150 trials (Table 1) used for behavioral and kinematic analysis.

Table 1

Number of successful and unsuccessful searches as a function of pulse length and source concentration

		Pulse length (seconds)		
Flux*	Search outcome	1	2.5	Continuous
High	Successful	9	11	12
	Unsuccessful	8	10	6
Low	Successful	11	10	10
	Unsuccessful	26	26	13

* High and low flux rates correspond to plumes produced with odorant solutions of 7 and 3.5 g shrimp · l^{-1}, respectively.

The x,y coordinates of the centroid of each light-emitting diode were determined using Motion Analysis software (30 Hz; ver. 3.1; Motion Analysis Corp., Santa Rasa, CA), smoothed using a moving average algorithm (window size = 3 frames), and extracted to produce a 5-Hz time series. The tracks of successful and unsuccessful searches were used to calculate a variety of kinematic parameters of foraging crabs, including walking speed, turning angle, and net-to-gross displacement ratio (NGDR, a measure of path tortuosity; Weissburg and Zimmer-Faust, 1993).

Statistical analysis

Data on crab foraging success in various plume conditions were analyzed using log-likelihood methods for frequency analysis (Sokal and Rohlf, 1981). These methods use maximum likelihood techniques to establish the significance of treatment variables (and their interactions) for determining the frequency of observations in each table cell by attempting to express the logarithm of expected cell frequencies as a linear function of experimental parameters. To examine the influence of pulse length, flux, and their interaction on foraging success, we used LOGLIN, a log-linear analysis procedure for multiway frequency tables that is available in the SYSTAT software package, ver. 10.2 (SYSTAT Software Inc., Richmond, CA).

Analysis of variance (ANOVA) was used to examine the influence of pulse length, flux, and their interaction in determining kinematic parameters for animals that were clearly engaged in olfactory navigation (*i.e.*, successful searchers). Calculation of kinematic variables (speed, NGDR, turning angle, and time spent motionless) was based on the entire path of a given successful or unsuccessful forager. The Bonferroni method was used to establish significance values for multiple *post hoc* tests (Sokal and Rohlf, 1981) to permit comparisons across the three pulse treatments at each flux rate. We performed a similar analysis on unsuccessful searchers, but the ANOVA suggested that plume properties had no impact on behavior (see Results). Finally, we used multiple analysis of variance (MANOVA) to compare overall kinematic behavior of unsuccessful and successful foragers. In this analysis, data were pooled across pulse and flux conditions for each state of search success (see Results).

Results

Flow visualization

Qualitative flow visualization revealed that our system generated pulsed plumes that differed substantially from the continuous case, and documented small differences in spatial variability between plumes generated with 1-s *versus* 2.5-s pulses (Figs. 1, 2). Plumes created with both pulse times were composed of highly intermittent odor bursts interspersed with clean water. The continuous plume was more homogeneous than either of the two pulsed cases, although it still exhibited considerable fine-scale structure that is a general hallmark of plumes created by sources with slow release rates relative to the ambient flow (Webster and Weissburg, 2001). The concentration records along the plume centerline reinforce the perceptions gained from examining the images. The continuous plume showed some variation but had relatively long stretches with moderate dye concentration. In contrast, dye concentration in the pulsed plumes was either extremely high or undetectable. Peak-to-peak distances along the plume centerline ranged between 8 and 15 cm in pulsed plumes, which at a relative flow velocity of 5 cm s^{-1}, produced peak-to-peak intervals of approximately 1.6–3 s. The intermittency factor, defined as the total proportion of the field of view above the detection limit (*i.e.*, with a pixel intensity greater than 0; Chatwin and Sullivan, 1989), was 0.557 ± 0.23, 0.391 ± 0.19, and 0.139 ± 0.24 (mean ± std err), for continuous, 2.5-s, and 1-s pulses, respectively, indicating more signal variability in pulsed plumes as a result of highly coherent dye patches. However, pulsed plumes were more variable even when the effects of signal absence (no detectable dye) were removed. Frequency histograms of dye intensity that include only non-zero pixel values (Fig. 2) indicated that low dye concentrations occurred often in pulsed plumes. In contrast, continuous plumes had a more even distribution of intensity values, a lower frequency of dilute dye, and more frequent cases of intermediate concentration. Thus, continuous cases represented fairly constant stimulation, whereas pulsed plumes represented odor environments in which odor stimulation was highly intermittent, on the scale of one to several seconds. Plumes with the shortest pulses were the most intermittent in space, and therefore would be expected to show the greatest temporal variability as the plume is advected downstream.

Behavior

Success rate. Flux and release properties affected the ability of foraging crabs to navigate through the plume to the source (Table 1). Groups of crabs challenged with various plume types located the source at rates from 67% to 28% depending on the combination of pulse length and flux. In general, a larger flux rate (*i.e.*, plumes produced with the more concentrated stimulus solution) significantly increased the success rate (log-likelihood $\chi^2 = 21.35$, $P < 0.01$, df = 6) relative to the lower flux plumes. Pulsed plumes were less easily tracked by foraging crabs at both high and low fluxes; however, the effect of pulse on success rates was marginally insignificant (log-likelihood $\chi^2 = 13.87$, $P = 0.054$, df = 7). The decrement in foraging success when navigating through pulsed plumes was greater at the higher flux, but the interaction between pulse properties and flux was not

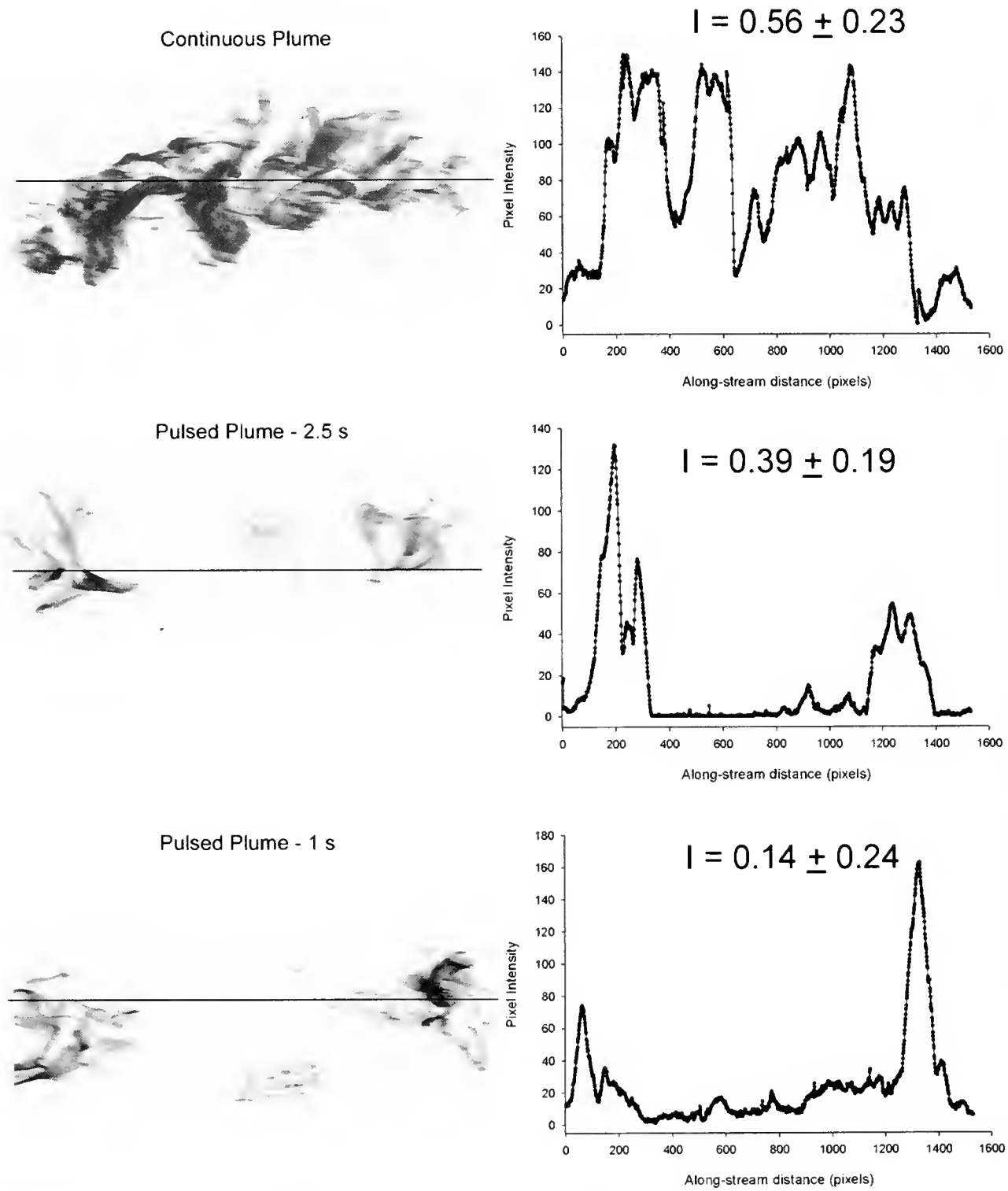

Figure 1. Characteristics for continuous and pulsed odor plumes: a side-by-side comparison of a representative plume image (left panel) and the distribution of pixel intensity values (right panel) along the plume centerline (solid line), for each of the three plume conditions. Pixel intensity values are derived from the digitally processed images, in which higher values indicate greater dye concentration. The intermittence, *I*, defined as the proportion of pixels in the image above the detection threshold (*i.e.*, with a pixel intensity greater than 0; Chatwin and Sullivan, 1989), is given above each graph of pixel intensity. The figure gives the mean *I* (± SEM) based on five images, for each plume type.

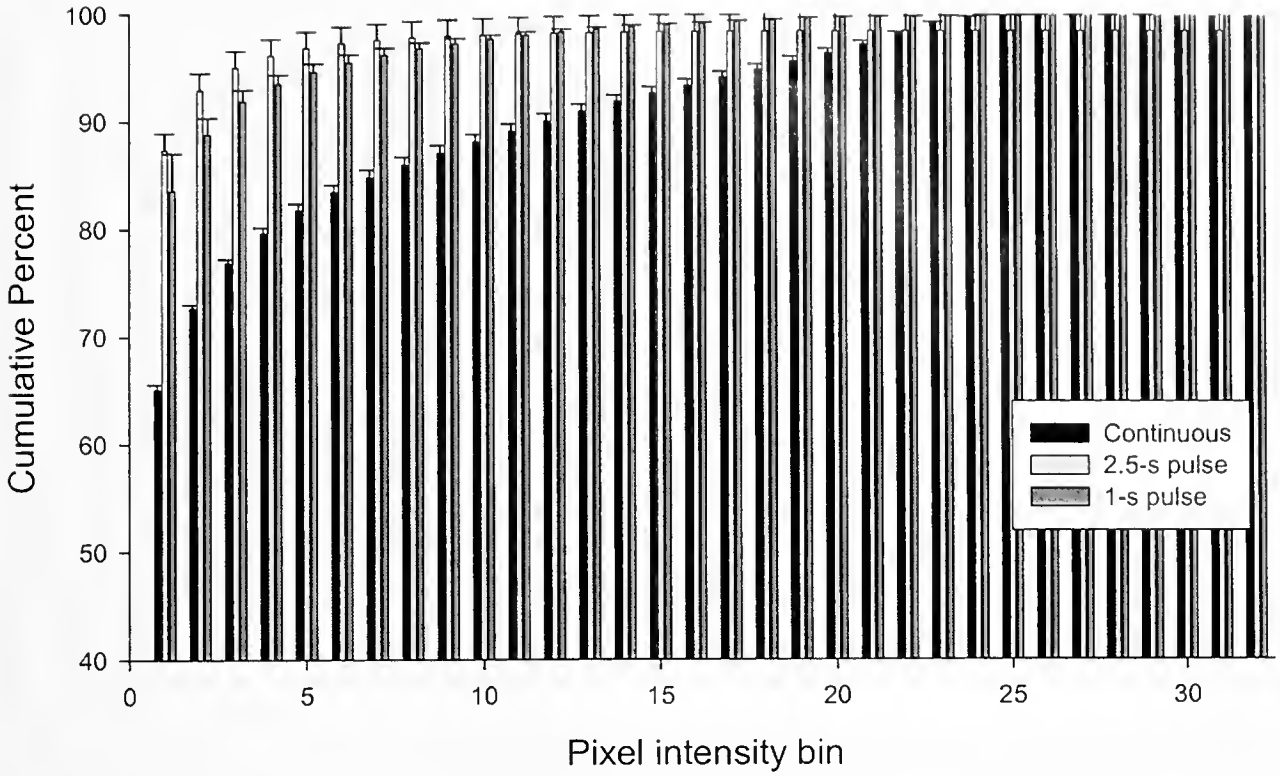

Figure 2. Distribution of pixel intensity values in continuous and pulsed plumes: the average cumulative frequency distribution (± 1 std err) as a function of pixel intensity bin for each plume type. Each bin corresponds to eight pixel intensity values, except for the first bin where the 0 pixel value (no detectable dye) has been omitted. The average frequencies are based on a sample size of five images for each plume type.

significant (pulse *concentration interaction $\chi^2 = 13.25$, $P = 0.066$, df = 7).

Search kinematics. Tracking behavior of crabs was qualitatively similar to that described in a variety of other studies on chemosensory navigation in aquatic crustaceans (Moore *et al.*, 1991; Weissburg and Zimmer-Faust, 1994; Mead, 2002). Animals moved toward the source, sometimes directly, but at other times using circuitous routes involving cross-stream tacks or meanders. Animals occasionally stopped for one to several seconds enroute to the source, but long periods of motionlessness were rare; crabs generally moved consistently upstream until they reached the nozzle and grabbed it with their chelae. Release conditions significantly affected crab foraging behavior (see below). In contrast, the behavior of unsuccessful foragers was remarkably constant and lacked detectable differences in any kinematic parameter (speed, NGDR, stop time, body angle) as a function of pulse length or flux. In fact, the majority of P values for these tests were greater than 0.5, and only one was less than 0.2. Thus, we combined the paths of all unsuccessful foragers for presentation and analysis.

Behavior of successful searchers. ANOVA revealed that flux, pulse length, and their interaction all significantly affected tracking speed for successful searchers ($F_{1,53} = 26.77$, $F_{2,53} = 17.00$, $F_{2,53} = 21.66$, respectively; $P < 0.001$ for all cases). Crabs locomoted extremely quickly under maximally stimulatory conditions (continuous plumes at high fluxes), displaying mean movement rates of approximately 10 cm s^{-1}, which exceeds the mean speed of unsuccessful foragers (Fig. 3). Crabs tracking plumes in most other conditions moved at rates of 4–6 cm s^{-1}, somewhat less than those of unsuccessful foragers. More consistent odor stimulation produced higher mean speeds only at high fluxes, whereas mean speed was similar in pulsed *versus* continuous plumes at low fluxes.

Low rates of movement in particular stimulus-release conditions were associated with increases in motionless periods (Fig. 4). Animals in high-flux plumes rarely paused during odor tracking and even at the shortest pulse length stopped for total periods of less than 5 s. Motionless periods exceeded 5 s in all low-flux plumes, and crabs remained stationary for over 20 s in plumes with short pulse lengths (long inter-pulse intervals). Flux, pulse length, and their interaction all had significant effects on the duration of motionless periods ($F_{1,53} = 12.86$, $P < 0.001$; $F_{2,53} = 23.12$, $P < 0.001$; $F_{2,53} = 4.76$, $P < 0.05$, respectively). The trend for increased motionlessness with decreasing pulse length was nonsignificant at high flux rates, although

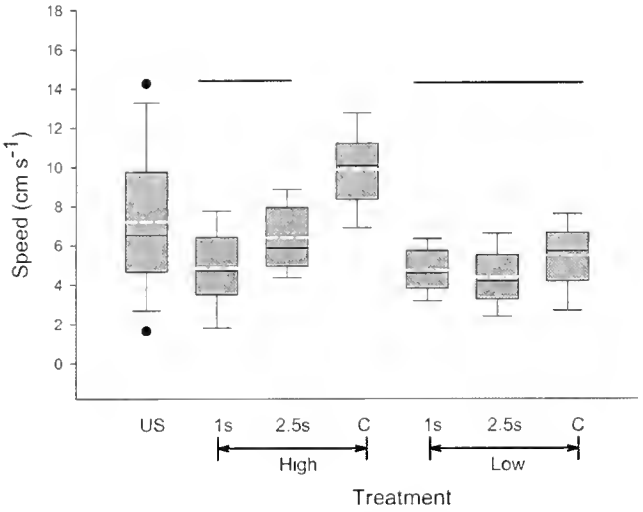

Figure 3. Walking speed statistics for all unsuccessful foragers (US) and for successful foragers in plumes with 1-s and 2.5-s pulses, and continuous plumes, for high-flux and low-flux treatments (*i.e.*, plumes created with odorant solutions of 7 and 3.5 g shrimp · l^{-1}, respectively). The gray box encloses the 25th and 75th percentiles, error bars above and below the box enclose the 90th and 10th percentiles, circles represent points outside of the 90th and 10th percentiles, the black solid line within the box is the median, and the white dashed line is the mean. Lines above the box plots join pulse treatments not significantly different from each other at $P < 0.05$ using Bonferroni adjusted *post hoc* tests. Sample sizes (numbers of paths) for these groups are given in Table 1.

post hoc tests detected significant differences among some treatment groups. The 1-s pulse length induced significantly greater motionlessness in low-flux plumes relative to the other two pulse treatments.

Path linearity varied significantly as a function of pulse length ($F_{2,53} = 5.97$, $P < 0.01$) and the flux rate–pulse length interaction ($F_{2,53} = 3.57$, $P < 0.05$), although there was no significant effect of flux itself ($F_{2,53} = 5.97$, $P < 0.01$). The overall effect of these factors was uniformly moderate path linearity at low fluxes, and moderate to high path linearity in high fluxes, with paths displaying significantly more meander at the shortest pulse length (Fig. 5).

Behavior of successful versus *unsuccessful searchers.* The behavior of unsuccessful searchers occasionally resembled that of successful crab foragers when individual kinematic parameters were examined. For instance, mean speed or stop times for unsuccessful searchers are in the middle of the range displayed by successful searchers. However, it is intriguing to note that even when mean values are similar between these groups, crabs failing to locate the source displayed more uniform behavior. For most kinematic parameters, both the median and the range (expressed as quartiles or percentage limits) indicate that crabs failing to locate the source moved more uniformly than did successful searchers. This is typified by data for path linearity and body angle (Figs. 5, 6), and to a lesser extent by mean stop time (Fig. 4). Median values for both NGDR and body angle are higher than for any other group. The upper and lower quartiles and 10th to 90th percentage limits span a smaller range than in successful searchers operating in any single plume type, and are much smaller than the variation encompassed by successful searchers across the range of different plume types. Mean and median stop times for unsuccessful foragers are lower than for successful foragers in nearly all plume types, and display a very low range as well. These patterns are somewhat surprising if the behavior of unsuccessful animals reflects a failed search attempt. The significant behavioral responses to plume conditions in successful foragers argue for similar behavioral differences among unsuccessful foragers if they are attempting, albeit poorly, to locate the source. Thus, one might reasonably expect a greater degree of variation among the pooled group of unsuccessful searchers compared to that of successful foragers in any given condition.

The MANOVA examining the difference in kinematics between all successful and unsuccessful searchers was highly significant ($F_{3,111} = 1340.97$, $P < 0.001$), indicating that movements differed according to whether animals found the source. Testing the pooled successful forager treatment against unsuccessful foragers is a conservative test for overall differences between animals that locate, or fail to locate, the source. In general, pooling across treatments that display significant differences (*i.e.*, successful foragers) is ill-advised since it compounds error variance

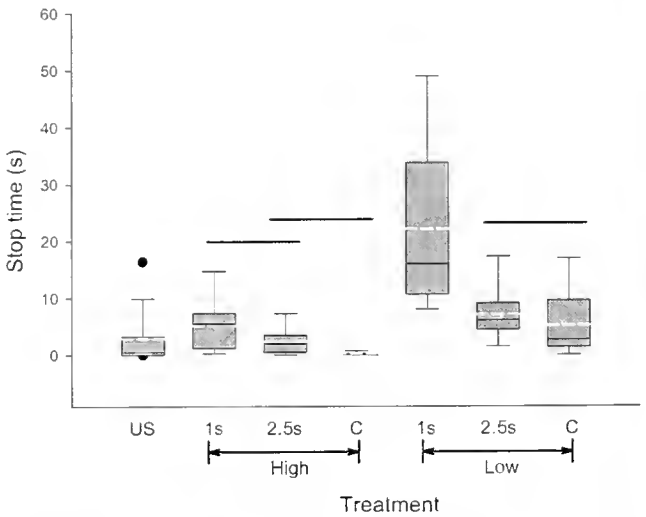

Figure 4. Stop time statistics for all unsuccessful foragers (US) and for successful foragers in plumes with 1-s and 2.5-s pulses, and continuous plumes, for high-flux and low-flux treatments (*i.e.*, plumes created with odorant solutions of 7 and 3.5 g shrimp l^{-1}, respectively). The gray box encloses the 25th and 75th percentiles, error bars above and below the box enclose the 90th and 10th percentiles, circles represent points outside of the 90th and 10th percentiles, the black solid line within the box is the median, and the white dashed line is the mean. Lines above the box plots join pulse treatments not significantly different from each other at $P < 0.05$ using Bonferroni adjusted *post hoc* tests. Sample sizes (numbers of paths) for these groups are given in Table 1.

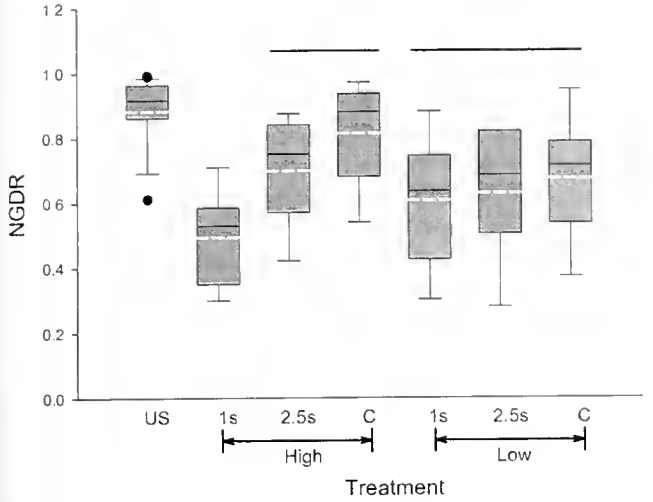

Figure 5. Net-to-gross displacement ratio (NGDR) statistics for all unsuccessful foragers (US) and for successful foragers in plumes with 1-s and 2.5-s pulses, for high-flux and low-flux treatments (*i.e.*, plumes created with odorant solutions of 7 and 3.5 g shrimp l^{-1}, respectively). The gray box encloses the 25th and 75th percentiles, error bars above and below the box enclose the 90th and 10th percentiles, circles represent points outside of the 90th and 10th percentiles, the black solid line within the box is the median, and the white dashed line is the mean. Lines above the box plots join pulse treatments not significantly different from each other at $P < 0.05$ using Bonferroni adjusted *post hoc* tests, with NGDR arcsin-transformed prior to analysis. Sample sizes (numbers of paths) for these groups are given in Table 1.

with variance due to treatment effects, and reduces the power of a test to detect a difference. Angular data require special test methods and could not be included in the MANOVA analysis. However, a Raleigh test (specific for angular data) reveals that successful foragers displayed significantly lower average body angles than crabs failing to find the source ($F_{1,113} = 13.09$, $P < 0.001$), further emphasizing the differences between the behavior of unsuccessful and successful searchers.

Discussion

Turbulent fluid motion has been shown to have a dramatic effect on the behavior of aquatic and terrestrial chemosensory foragers (Weissburg and Zimmer-Faust, 1993; Mafra-Neto and Cardé, 1994; Vickers and Baker, 1994; Moore and Grills, 1999). Investigators have focused on fine-scale mixing processes that produce variation in odor-filament structure as a key feature mediating olfactory-based navigation. The peak odor intensity of filaments and filament duration, rise time (slope), and frequency have been suggested to modulate the ability to track an odor plume to its source in a variety of creatures (Moore and Atema, 1991; Weissburg and Zimmer-Faust, 1994; Atema, 1996). The importance of small-scale mixing in modulating tracking performance is quite clear, even if the importance of particular filament features is still being debated (*e.g.*, Webster *et al.*, 2001; Webster and Weissburg, 2001).

The results presented here indicate that larger-scale odor fluctuations of one to several seconds alter the behavior of animals tracking chemical cues. Animals in plumes with short pulses (long inter-pulse intervals) showed degraded tracking performance. Similarly, field and laboratory studies of pheromone tracking in insects have indicated that larger-scale variation in plume features decreases the initiation and efficiency of search behavior (David *et al.*, 1983; Baker and Haynes, 1987; Zanen *et al.*, 1994). In aquatic creatures as well as in insects, it appears that understanding olfactory-mediated navigation will require us to investigate physical processes that create long-term fluctuations in odor concentration, in addition to examining fine-scale mixing.

Behaviorally relevant signal properties of pulsed plumes. Foraging crabs in pulsed plumes found the source less frequently, reduced their walking speed, spent less time walking, and tacked across-stream more extensively than did animals in continuously released plumes. Interestingly, decreased search success was not simply an extension of inefficient search. Unsuccessful searchers acted in a rather uniform manner as a group, showing behaviors (very straight paths, high body angles) characteristic of animals in the absence of stimulus sources (Weissburg and Zimmer-Faust, 1993, 1994; Weissburg *et al.*, 2003). This suggests that the apparent decrease in search success in pulsed con-

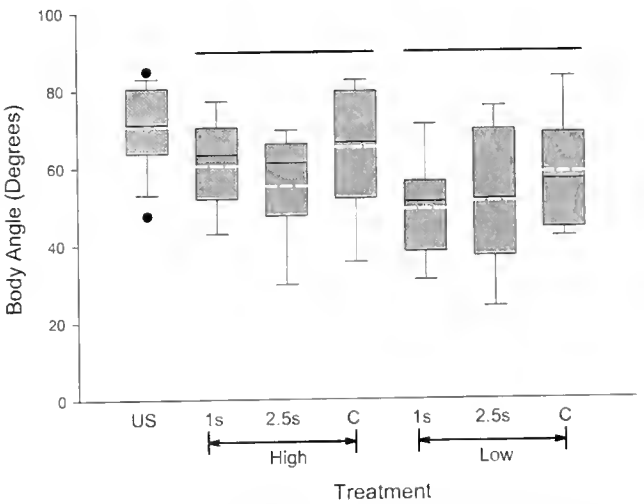

Figure 6. Body angle statistics for all unsuccessful foragers (US) and for successful foragers in plumes with 1-s and 2.5-s pulses, for high-flux and low-flux treatments (*i.e.*, plumes created with odorant solutions of 7 and 3.5 g shrimp l^{-1}, respectively). The gray box encloses the 25th and 75th percentiles, error bars above and below the box enclose the 90th and 10th percentiles, circles represent points outside of the 90th and 10th percentiles, the black solid line within the box is the median, and the white dashed line is the mean. Lines above the box plots join pulse treatments not significantly different from each other by a Raleigh test at $P < 0.05$ using a Bonferroni adjustment. Sample sizes (numbers of paths) for these groups are given in Table 1.

ditions reflects a failure to initiate search, as opposed to an inability to locate the source once search has begun. Thus, blue crabs in pulsed plumes often elect not to search, and they probably experience reduced search success when they do attempt to track to the source.

Our results suggest that the chemosensory system in blue crabs is not a simple flux detector, at least over the time scale of several seconds that is an important level of temporal variation in naturally occurring odor plumes (*e.g.*, Murlis, 1986; Finelli *et al.*, 1999). The performance of blue crabs in different release conditions ought to be similar if flux was the sole determinant of behavior, since plumes created with the same stimulus concentration had equal flux rates over the 5-s cycle length. The deleterious effects of short pulses suggest that the integration of incoming chemical signal strength requires periods substantially longer than the integration time of chemosensory neurons, which in lobsters can code stimulus intensity within several hundred milliseconds (Gomez and Atema, 1996). Integration may act to smooth out random fluctuations in signal intensity, particularly when physiological response times are shorter than the relevant scale of variation of the incoming stimulus. Indeed, it has been suggested that a major advantage of olfactory transduction is that biochemical events at the cellular level act as an integrator so that rapid binding and unbinding of stimulus molecules at the receptor does not result in spurious fluctuations in neuronal output (*i.e.*, action potentials) (Zufall *et al.*, 1994).

Flux was not completely irrelevant to the tracking performance of the crabs, however. Lower flux did indeed produce effects similar to those of plume pulsing; animals in the low-flux (low-concentration) plume walk more slowly, stop more, and find the source less often than crabs in the higher flux plume. Thus, flux can have a significant impact on chemosensory search when superimposed on changes in the longer-term pattern of temporal variation in signal intensity. Unfortunately, few experiments have decoupled flux from pulse rate or inter-pulse interval, so it is currently unclear whether olfactory systems in other animals display similar properties.

Moths, another group of well-studied animals that employ chemosensory tracking, respond to pulsed plumes similarly to blue crabs. Increasing the interval between successive odor pulses decreases the initiation of search flight, decreases flight speed, and increases the extent of cross-wind movement (*i.e.*, cross-wind casting; Vickers and Baker, 1992; Mafra-Neto and Cardé, 1995). Decreased speed and increased casting may enhance the probability that a moth will reacquire the plume if it temporarily loses the signal (Mafra-Neto and Cardé, 1995). Flying arthropods must keep moving to stay aloft, which necessitates cross-wind flight to regain the plume signal. For an animal walking on the sea floor, remaining in the same spot is analogous to casting; a motionless animal has a chance to re-contact the plume, suggesting that increased stopping behavior in pulsed plumes may improve the foraging success of benthic arthropods in intermittent-stimulus environments. At present, we lack the data necessary to clarify the role of stopping *versus* casting in other walking arthropods. Some walking insects increase the extent of cross-stream meanders as plumes become more intermittent (Kanzaki *et al.*, 1992). Such a casting strategy is based on an internally generated counter-turning scheme similar to the one that produces casting of insects when they are aloft (Tobin, 1981; Kanzaki *et al.*, 1992). Other walking insects (Willis and Baker, 1987), as well as benthic crustaceans (Weissburg, 2000), do not use a counter-turn generator, but their response to loss of an odor signal has not been examined. Thus, the extent to which search strategies are molded by evolutionary constraints rather than by a common stimulus environment remains unknown.

One difference in the responses of aquatic and terrestrial arthropods is the maximum interval between odor pulses that still allows the animal to maintain smooth and rapid upstream progress toward the source. Blue crabs responded negatively to inter-pulse intervals that exceed 2.5 s. In contrast, inter-pulse intervals in the range of 0.25 s to 1 s are sufficient to disrupt orientation in moths flying through pheromone plumes (Vickers and Baker, 1992; Mafra-Neto and Cardé, 1995, 1998). Although the difficulty of creating cleanly separated pulses at higher frequencies prevents examination of shorter inter-pulse intervals, it is unlikely that blue crabs respond significantly more quickly to signal offset than current observations suggest, given the relatively slow rate at which primary chemosensory afferents in crustaceans operate. The responses of insect olfactory receptor neurons to brief pulses remain distinct at frequencies of up to at least 10 Hz (Rumbo and Kaissling, 1989; Vickers and Baker, 1992). In contrast, lobster chemosensory neurons fuse signals when the frequencies exceed 4–6 Hz (Gomez *et al.*, 1994). The generally smaller turbulence intensity in aquatic *versus* terrestrial environments (Murlis, 1986; Weissburg, 2000) results in larger mixing lengths. In turn, this larger mixing scale (and more moderate flow speeds) translates into slower variation of odor signals in waterborne plumes, possibly resulting in longer processing times in aquatic animals than in terrestrial ones. Interestingly, the inter-pulse intervals required to disrupt plume-following in the oriental silk moth (*Bombyx mori*) are about 2–3 s (Kanzaki *et al.*, 1992). Silkmoths walk to pheromone sources and are within the low-velocity region of a boundary layer where odor signals are less disrupted by turbulent fluid motion. Thus, odor signals may be more coherent to a walking insect than to its flying brethren, resulting in a reduced sensitivity to short periods of odor absence.

The importance of longer-term signal variation. Investigators have focused on variation in the fine-scale structure of odor filaments as a key feature mediating olfactory-based

navigation. The results presented here indicate that signal variation on the order of one to several seconds also affects both the success rate and the kinematics of animals tracking chemical cues. Thus, understanding olfactory-mediated navigation will require us to investigate physical processes that create long-term fluctuations in odor concentration, in addition to examining fine-scale mixing. Unfortunately, controlled studies on the effects of such longer-term signal variation are rare compared to investigations on filament-scale variation, particularly in aquatic habitats. A few laboratory and field studies (in addition to the study reported here) suggest that odor fluctuations over one to many seconds significantly affect foraging success and behavior (Lapointe and Sainte-Marie, 1992; Keller *et al.*, 2001). Whelks, for instance, are less likely to be caught in baited traps when they are confronted with dramatic changes in current direction (Lapointe and Sainte-Marie, 1992) that likely cause long-term gaps in the odor signal or changes in its intensity.

Turbulence that generates second-scale odor fluctuations is common and may be created by a variety of mechanisms that produce eddies of an intermediate size (*e.g.*, 10–1000 cm), which are generally smaller than the largest scales and greater than the microscale flow structures (1–10 mm) that are primarily responsible for the properties of individual odor filaments. Eddies in this intermediate size range may either cause the entire plume to oscillate cross-stream or else repackage the odor into larger-scale structures, both of which will induce longer-term odor variation. The largest turbulence scales are restricted by the largest flow dimension—for instance, the water depth or channel width (Roberts, 1990). Because energy present in the largest flow features is transferred to successively smaller scales (the Kolmogorov cascade), large turbulent eddies present in open estuaries, embayments, *etc.*, will invariably create eddies of a size sufficient to induce odor variation on the scale of one to several seconds. Alternately, shallow or narrow tidal channels may initially generate eddies in the correct size range. Finally, objects in flow shed vortices at a predictable frequency. The frequency, f, produced by a circular cylinder of diameter d in a flow of velocity U is given by the Strouhal number, St, which is 0.2 over a large range of Reynolds numbers (White, 1991). Thus, $0.2 = fD/U$, so a 10-cm-diameter object will shed vortices at a frequency of 1 Hz in a flow of 50 cm s^{-1}. Given typical flow velocities in tidally dominated systems (*ca.* 1–100 cm $\cdot$ s^{-1}), biological or nonbiological objects (worm tubes, protruding shells, *etc.*) may create turbulence at scales required to disrupt olfactory foraging, at least in blue crabs.

Time-series measurements of odor plumes show fluctuations on a variety of scales that reflect the processes described above. Low-frequency fluctuations (*e.g.*, less than 1 Hz) are often a dominant component of frequency spectra for odor fluctuations in both aquatic and terrestrial environments (Hanna and Insley, 1989; Finelli *et al.*, 1999, 2000; Keller *et al.*, 2001). For instance, the slowest frequency for odor fluctuations in an estuarine tidal channel is about 0.8 Hz, which probably reflects plume cross-stream meander created by the largest eddies in the flow (Finelli *et al.*, 1999).

Many aquatic crustaceans forage most effectively in spatially and temporally coherent plumes (Weissburg, 2000; but see Keller *et al.*, 2001), which may reflect strategies that maximize the speed of navigation at the cost of decreased ability to operate in more complex stimulus environments (Weissburg *et al.*, 2002). Although turbulence may be the primary mechanism producing longer-term odor fluctuations detrimental to olfactory foraging, potential prey may exploit these signal characteristics to mask themselves from their predators. This raises the possibility that predators and prey coupled to one another *via* waterborne signals may be engaged in an arms race similar to that evolved in other systems (Vermeij, 1987); prey rendered apparent to their consumers *via* transmission of fluid-borne chemicals may modulate the release of these signals to evade predation.

Bivalves, which are commonly consumed by crabs and other olfactory predators, mimic quite well the general properties of the signal source used here. Bivalves discharge attractive metabolites from a siphon, and in principle, can modulate the flow to release odor pulses over time scales that degrade the tracking ability of their predators. In fact, any animal capable of actively controlling the release of chemical cues might profit from creating pulsed plumes rather than continuous ones. Prey species, including bivalves, use a variety of mechanisms to detect predators; once a predator is detected, the prey use a suite of strategies to decrease their apparency and vulnerability to their consumers (Cote and Jelnikar, 1999; Leonard *et al.*, 1999; Nakaoka, 2000). It is not known whether anti-predation strategies include the modification of plume signal properties, though bivalve prey exposed to predators often cease pumping entirely (Irlandi and Peterson, 1991; Nakaoka, 2000). Clearly, additional field and laboratory experiments on both predators and potential prey are required to evaluate the significance of longer-term variations in odor signals.

Acknowledgments

The authors thank Elizabeth Wood, Dan Sickbert, Chen Chen, and Jacqueline Stewart for help on the behavioral trials. This work was partially supported by grants from DARPA/ONR (contract #N0014-03-1-0366) and the National Science Foundation (NSF-IBN #0321444) to MJW. Two anonymous reviewers provided comments that increased the clarity and breadth of this work.

Literature Cited

Atema, J. 1995. Chemical signals in the marine environment—dispersal, detection, and temporal signal analysis. *Proc. Natl. Acad. Sci. USA* **92:** 62–66.

Atema, J. 1996. Eddy chemotaxis and odor landscapes: exploration of nature with animal sensors. *Biol. Bull.* **191:** 129–138.

Baker, T. C., and K. F. Haynes. 1987. Manoeuvres used by flying male oriental fruit moths to relocate a sex pheromone plume in an experimentally shifted wind-field. *Physiol. Entomol.* **12:** 263–279.

Belanger, J. H., and M. A. Willis. 1996. Adaptive control of odor-guided locomotion: behavioral flexibility as an antidote to environmental unpredictability. *Adapt. Behav.* **4:** 217–253.

Chatwin, P. C., and P. J. Sullivan. 1989. The intermittency factor of scalars in turbulence. *Phys. Fluids A* **1:** 761–763.

Clarke, M. E., T. G. Wolcott, D. L. Wolcott, and A. H. Hines. 1999. Foraging and agonistic activity co-occur in free-ranging blue crabs (*Callinectes sapidus*): observation of free-ranging animals by ultrasonic telemetry. *J. Exp. Mar. Biol. Ecol.* **193:** 317–327.

Cote, I. M., and E. Jelnikar. 1999. Predator-induced clumping behavior in mussels (*Mytilus edulis* Linnaeus). *J. Exp. Mar. Biol. Ecol.* **235:** 201–211.

Crimaldi, J. P., and J. R. Koseff. 2001. High-resolution measurements of the spatial and temporal scalar structure of a turbulent plume. *Exp. Fluids* **31:** 90–102.

David, C. T., J. S. Kennedy, and A. R. Ludlow. 1983. Finding of a sex pheromone source by gypsy moths released in the field. *Nature* **303:** 804–806.

Denny, M. W. 1988. *Biology and Mechanics of the Wave-swept Environment.* Princeton University Press, Princeton, NJ

Finelli, C. M., N. D. Pentcheff, R. K. Zimmer, and D. S. Wethey. 1999. Odor transport in turbulent flows: constraints on animal navigation. *Limnol. Oceanogr.* **44:** 1056–1071.

Finelli, C. M., N. D. Pentcheff, R. K. Zimmer, and D. S. Wethey. 2000. Physical constraints on ecological processes: a field test of odor-mediated foraging. *Ecology* **81:** 784–797.

Gomez, G., and J. Atema. 1996. Temporal resolution in olfaction: stimulus integration time of lobster chemoreceptor cells. *J. Exp. Biol.* **199:** 1771–1779.

Gomez, G., R. Voigt, and J. Atema. 1994. Frequency filter properties of lobster chemoreceptor cells determined with high-resolution stimulus measurement. *J. Comp. Physiol. A* **174:** 803–811.

Hanna, S. R., and E. M. Insley. 1989. Time series analysis of concentration and wind fluctuations. *Boundary-Layer Meteorol.* **47:** 131–147.

Irlandi, E. A., and C. H. Peterson. 1991. Modification of animal habitat by large plants: mechanisms by which seagrasses influence clam growth. *Oecologia* **87:** 307–318.

Kaissling, K. E., Z. Strausfeld, and E. Rumbo. 1987. Adaptation processes in insect olfactory receptors: mechanisms and behavioral significance. *Annals NY Acad. Sci.* **510:** 104–112.

Kanzaki, R., N. Sugi, and T. Shibuya. 1992. Self-generated zigzag turning of *Bombyx mori* males during pheromone mediated upwind walking. *Zool. Sci.* **9:** 515–527.

Keller, T. A., A. M. Tomba, and P. A. Moore. 2001. Orientation in complex chemical landscapes: Spatial arrangement of odor sources influences crayfish food-finding efficiency in artificial streams. *Limnol. Oceanogr.* **46:** 238–247.

Keller, T. A., I. Powell, and M. J. Weissburg. 2003. Role of appendages in chemically mediated orientation of blue crabs. *Mar. Ecol. Prog. Ser.* **261:** 217–231.

Lapointe, V., and B. Sainte-Marie. 1992. Currents, predators, and the aggregation of the gastropod *Buccinum undatum* around bait. *Mar. Ecol. Prog. Ser.* **85:** 245–257.

Leonard, G. H., M. D. Bertness, and P. J. Yund. 1999. Crab predation, waterborne cues, and inducible defenses in the blue mussel, *Mytilus edulis*. *Ecology* **80:** 1–14.

Mafra-Neto, A., and R. T. Cardé. 1994. Fine-scale structure of pheromone plumes modulates upwind orientation of flying moths. *Nature* **369:** 142–144.

Mafra-Neto, A., and R. T. Cardé. 1995. Effect of the fine-scale structure of pheromone plumes: pulse frequency modulates activation and upwind flight of almond moth males. *Physiol. Entomol.* **20:** 229–242.

Mafra-Neto, A., and R. T. Cardé. 1998. Rate of realized interception of pheromone pulses in different wind speeds modulates almond moth orientation. *J. Comp. Physiol. A* **182:** 563–572.

Mead, K. S. 2002. From odor molecules to plume tracking: an interdisciplinary, multilevel approach to olfaction in stomatopods. *Integr. Comp. Biol.* **42:** 258–264.

Moore, P. A., and J. Atema. 1991. Spatial information in the three-dimensional fine structure of an aquatic odor plume. *Biol. Bull.* **181:** 408–418.

Moore, P. A., and J. L. Grills. 1999. Chemical orientation to food by the crayfish, *Orconectes rusticus*, influence of hydrodynamics. *Anim. Behav.* **58:** 953–963.

Moore, P. A., N. Scholz, and J. Atema. 1991. Chemical orientation of lobsters, *Homarus americanus*, in turbulent odor plumes. *J. Chem. Ecol.* **17:** 1293–1308.

Moore, P. A., M. J. Weissburg, J. M. Parrish, R. K. Zimmer-Faust, and G. A. Gerhardt. 1994. Spatial distribution of odors in simulated benthic boundary layer flows. *J. Chem. Ecol.* **20:** 255–279.

Murlis, J. 1986. The structure of odour plumes. Pp. 27–38 in *Mechanisms in Insect Olfaction*, T. L. Payne, M. C. Birch, and C. E. J. Kennedy, eds. Clarendon Press, Oxford.

Murlis, J., J. S. Elkinton, and R. T. Cardé. 1992. Odor plumes and how insects use them. *Annu. Rev. Entomol.* **37:** 505–532.

Nakaoka, M. 2000. Nonlethal effects of predators on prey populations: predator-mediated change in bivalve growth. *Ecology* **81:** 1031–1045.

Roberts, P. J. W. 1990. Mixing and transport in natural streams. Pp. 99–117 in *Encyclopedia of Fluid Mechanics*, N.P. Cheremisinoff, ed. Gulf Publishing, Boca Raton, FL.

Rumbo, E. R., and K. E. Kaissling. 1989. Temporal resolution of odor pulses by three types of pheromone receptors in *Antheraea polyphemus*. *J. Comp. Physiol. A* **165:** 281–291.

Sokal, R. R., and F. J. Rohlf. 1995. *Biometry.* 3rd ed. W.H. Freeman, New York.

Tobin, T. R. 1981. Pheromone orientation: the role of internal control mechanisms. *Science* **214:** 1147–1149.

Vermeij, G. J. 1987. *Evolution and Escalation: An Ecological History of Life.* Princeton University Press, Princeton, NJ.

Vickers, N. J., and T. C. Baker. 1992. Male *Heliothis virescens* maintain upwind flight in response to experimentally pulsed filaments of their sex pheromone (Lepidoptera, Noctuidae). *J. Insect Behav.* **5:** 669–687.

Vickers, N. J., and T. C. Baker. 1994. Reiterative responses to single strands of odor promote sustained upwind flight and odor source location by moths. *Proc. Natl. Acad. Sci. USA* **91:** 5756–5760.

Webster, D. R., and M. J. Weissburg. 2001. Chemosensory guidance cues in a turbulent odor plume. *Limnol. Oceanogr.* **46:** 1048–1053.

Webster, D. R., S. Rahman, and L. P. Dasi. 2001. On the usefulness of bilateral comparison to tracking turbulent chemical odor plumes. *Limnol Oceanogr.* **46:** 1048–1053.

Weissburg, M. J. 2000. The fluid dynamical context of chemosensory behavior. *Biol. Bull.* **198:** 188–202.

Weissburg, M. J., and R. K. Zimmer-Faust. 1993. Life and death in moving fluids: hydrodynamic effects on chemosensory-mediated predation. *Ecology* **74:** 1428–1443.

Weissburg, M. J., and R. K. Zimmer-Faust. 1994. Odor plumes and how blue crabs use them to find prey. *J. Exp. Biol.* **197:** 349–375.

Weissburg M. J., M. C. Ferner, D. P. Pisut, and D. L. Smee. 2002. Ecological consequences of chemically mediated prey perception. *J. Chem. Ecol.* **28:** 1953–1970.

Weissburg, M. J., C. P. James, D. L. Smee, and D. R. Webster. 2003. Fluid mechanics produces conflicting constraints during olfactory navigation of blue crabs, *Callinectes sapidus*. *J. Exp. Biol.* **206:** 171–180.

White, F. M. 1991. *Viscous Fluid Flow*. McGraw-Hill, New York.

Willis, M. A., and T. C. Baker. 1987. Comparison of maneuvers used by walking versus flying *Grapholita molesta* males during pheromone-mediated upwind movement. *J. Insect Physiol.* **33:** 875–883.

Zanen, P. O., M. W. Sabelis, J. P. Buonaccorsi, and R. T. Cardé. 1994. Search strategies of fruit flies in steady and shifting winds in the absence of food odours. *Physiol. Entomol.* **19:** 335–341.

Zimmer-Faust, R. K., C. M. Finelli, N. D. Pentcheff, and D. S. Wethey. 1995. Odor plumes and animal navigation in turbulent water flow: a field study. *Biol. Bull.* **188:** 111–116.

Zufall, F., S. Firestein, and G. M. Sheperd. 1994. Cyclic nucleotide-gated ion channels and sensory transduction in olfactory receptor neurons. *Annu. Rev. Biophys. Biomol. Struct.* **23:** 577–607.

Reference: *Biol. Bull.* **207:** 56–66. (August 2004)

Cytoskeletal Organization of *Limulus* Amebocytes Pre- and Post-Activation: Comparative Aspects

MARA CONRAD, JOANNA DENOBILE, IRINA CHAIKHOUTDINOV, DOUGLAS ESCRIBANO, KYENG-GEA LEE, AND WILLIAM D. COHEN*

Department of Biological Sciences, Hunter College, New York, NY, and the Marine Biological Laboratory, Woods Hole, Massachusetts

Abstract. One of the major functions of circulating *Limulus* amebocytes is to effect blood coagulation upon receipt of appropriate signals. However, the hypothesis that *Limulus* amebocytes are fundamentally similar to vertebrate thrombocytes and platelets has not been tested sufficiently in previous studies of their cytoskeletal organization. Whereas the earlier data were derived from transmission electron microscopy (TEM) of thin sections of a limited number of cells, improved fluorescence labeling methods that retain cell morphology have now enabled us to survey F-actin and microtubule organization in intact individual amebocytes and in large amebocyte populations pre- and post-activation. Anti-tubulin immunofluorescence showed the marginal band (MB) of microtubules to be ellipsoidal in most unactivated cells, with essentially no other microtubules present. However, minor subpopulations of cells with discoidal or pointed shape, containing corresponding arrangements of microtubules suggestive of morphogenetic intermediates, were also observed. Texas-red phalloidin labeled an F-actin-rich cortex in unactivated amebocytes, accounting for MB and granule separation from the plasma membrane as visualized in TEM thin sections, and supporting earlier models for MB maintenance of flattened amebocyte morphology by pressure against a cortical layer. Shape transformation after activation by bacterial lipopolysaccharide was attributable principally to spiky and spreading F-actin in outer cell regions, with the MB changing to twisted, nuclei-associated forms and eventually becoming unrecognizable. These major pre- and post-activation cytoskeletal features resemble those of platelets and non-mammalian vertebrate thrombocytes, supporting recognition of the *Limulus* amebocyte as a representative evolutionary precursor of more specialized clotting cell types.

Received 30 September 2003; accepted 15 June 2004

* To whom correspondence should be addressed at Department of Biological Sciences, Hunter College, 695 Park Avenue, New York, NY 10021. E-mail: cohen@genectr.hunter.cuny.edu

Abbreviations: DIC, differential interference contrast; LPS, lipopolysaccharide; MB, marginal band; PBS, phosphate-buffered saline; TEM, transmission electron microscopy.

Introduction

Only a single cell type—the granular amebocyte—is believed to circulate in the hemolymph (blood) of *Limulus polyphemus*, the American horseshoe crab. However, the amebocyte is multifunctional with respect to innate immune mechanisms, playing a role in phagocytosis, wound healing, and clotting (Armstrong, 1985a). In its native, or unactivated, state in the circulation, the amebocyte is a flattened ellipsoid, a characteristic shape maintained by a specialized organization of cytoskeletal elements. When amebocytes are suitably activated, exocytosis occurs, and molecular components released from the intracellular granules cause the hemolymph to clot rapidly (Levin and Bang, 1968; Armstrong and Rickles, 1982). *Limulus* amebocytes are exquisitely sensitive to activation by bacterial lipopolysaccharide (LPS; Armstrong, 1980; Ornberg and Reese, 1981), and algal LPS is also effective (Conrad *et al.*, 2001). Such activation is accompanied by marked changes in cell shape, a feature shared by specialized non-mammalian vertebrate clotting cells (nucleated thrombocytes) and by mammalian platelets (Allen *et al.*, 1979; Debus *et al.*, 1981; Lee *et al.*, 2004). This study was aimed at gauging the extent to which the cytoskeletal characteristics of *Limulus* amebocytes, both pre- and post-activation, are shared by vertebrate thrombocytes and platelets.

The existing relevant data about *Limulus* amebocytes

have been obtained principally by transmission electron microscopy (TEM) of thin sections. Copeland and Levin (1985) described the general fine structure of the native circulating amebocyte, including the nucleus, mitochondria, Golgi apparatus, endoplasmic reticulum, and ribosomes. They also reported that granules of two size classes were present, with "large" ones predominant, and that immature forms of the large granules were Golgi-associated and had distinctive matrix patterns not visible in mature granules. Similar TEM observations were made of the organelles and granules in amebocytes of the Asian horseshoe crab *Tachypleus* (Toh *et al.*, 1991).

Cytoskeletal organization within the *Limulus* amebocyte was also observed in thin sections. Marginal bands (MBs) of microtubules were found in the plane of flattening of unactivated cells by Nemhauser *et al.* (1980), similar to the MBs that are characteristic of nearly all vertebrate nucleated erythrocytes and clotting cells (Fawcett and Witebsky, 1964; Shepro *et al.*, 1966; Behnke, 1970; Jagadeeswaran *et al.*, 1999). Subsequently, Cohen and Nemhauser (1985) suggested that these MBs functioned to maintain the flattened ellipsoidal shape of unactivated cells by interaction with a cortical cytoskeletal network, as in mammalian platelets (Debus *et al.*, 1981). Tablin and Levin (1988)—using a TEM fixation method originally devised to reveal F-actin in platelets (Boyles *et al.*, 1985)—observed thin filament arrays in the cortex of unactivated amebocytes. They suggested that MB interaction with the cortical array might constitute a shape-maintaining cytoskeletal tension system in unactivated cells, similar to that proposed earlier for nucleated erythrocytes by Joseph-Silverstein and Cohen (1984, 1985). They also reported that MBs of activated cells relocated to the cell interior together with cortical filament arrays, and that the MBs never completely disassembled.

The present study had two principal objectives: first, to evaluate earlier proposals that the interaction between the MB and cortical thin filament arrays is responsible for maintaining the shape of unactivated amebocytes; and second, to determine whether post-activation cytoskeletal events in *Limulus* amebocytes parallel those of the more specialized clotting cells of vertebrates. Because the TEM methodology used previously limits depth of field and number of cells that can be observed, we turned to fluorescence labeling. This provides the best assessment of cytoskeletal organization in whole single cells and in large cell populations, and it has been applied successfully to mammalian platelets (Debus *et al.*, 1981). Moreover, impetus for the work came from two recent developments: methods for rapid localization of cytoskeletal proteins with improved retention of native cell shape became available (Lee *et al.*, 2002), and the post-activation cytoskeletal sequence for non-mammalian vertebrate thrombocytes was reported for the first time through use of such methods (Lee *et al.*, 2004).

Employing fluorescence localization, we first examined the features of unactivated *Limulus* amebocytes, focusing on the organization of major cytoskeletal elements: F-actin in the cell cortex, and microtubules in the MBs. Then, after LPS-induced activation, the changes undergone by *Limulus* amebocytes were studied in carefully timed post-activation samples. TEM thin sections of both unactivated and activated amebocytes yielded ancillary details. The results provide a more complete picture of the cellular organization and activities of amebocytes than had been obtained previously, revealing basic structural and functional similarities between these ancient, multifunctional chelicerate blood cells and specialized vertebrate clotting cell types.

Materials and Methods

Living material

Specimens of *Limulus polyphemus* provided by the Marine Resources Center of the Marine Biological Laboratory, Woods Hole, Massachusetts were maintained in the Laboratory's running seawater system at ~16 °C or in closed circulating artificial seawater tanks at ~12 °C, and fed clams or mussels periodically. Individual animals were identified by tape labels or rubber bands attached to the tail.

Preparation of cells for subsequent fluorescence labeling

Unactivated cells. Unactivated cells for population surveys were pre-fixed in suspension by dripping ~0.5 ml of blood directly into 0.5 ml of 2% formaldehyde in 3% NaCl (room temperature, ~23 °C). Subsequent steps were performed by gentle centrifugation of the fixed cells in 2-ml siliconized microcentrifuge tubes. After 5 min of pre-fixation, cells were washed in 3% NaCl; extracted and further fixed for 30 min in 0.6% Brij-58, 2% formaldehyde in 3% NaCl; then washed in PBS and blocked for 1 h in 1% BSA in PBS prior to fluorescence labeling.

Activated cells. Activated cells were prepared by exposure to bacterial LPS as follows. Sterile, virgin, 35-mm plastic petri dishes were prepared for production of successive post-activation time samples. Each dish contained 5 ml of 3% sterile, endotoxin-free NaCl and a sterile LPS-free coverslip (pre-baked >4 h, 200 °C; Armstrong, 1985b). The dishes were pre-chilled for 20 min at ~9 °C to inhibit cell activation. An animal was chilled for 2 h at 4 °C and then dried; after its cephalothorax-opisthosome joint was cleaned with 70% ethanol, it was bled by cardiac puncture with a 20- or 21-gauge needle. With the dishes now placed at room temperature (~23 °C), 1 drop of blood (hemolymph) was added to each dish; the large volume ratio of saline to blood diluted hemolymph components that might otherwise activate the cells. To avoid possible distortion of cell shape, the blood was dripped directly from the open end of a syringe needle into the medium, rather than first drawing blood into

a syringe. The dishes were lightly swirled to disperse the cells, which were then allowed to settle for about 3 min and adhere to coverslips. During this process the cells remained unactivated. To activate the cells and induce exocytosis, 3 ml of supernate were removed *via* LPS-free pipette, and 2 ml of 2× concentrated activating medium (20 m*M* $CaCl_2$, 20 μg/ml LPS in 3% NaCl) was added to each dish, to make final concentrations of 10 m*M* $CaCl_2$ and 10 μg/ml LPS in 3% NaCl. The dishes were incubated at room temperature (~23 °C) and, at particular time points (ranging from 30 s to 10 min), coverslips with adhering amebocytes plus any clot-related material were further processed. Following a wash in 3% NaCl, the material was pre-fixed 5 min in 1% formaldehyde in 3% NaCl, extracted and fixed for 30 min in 3% NaCl containing 0.6% Brij-58 and 2% formaldehyde, washed in PBS, and blocked 1 h in 1% BSA in PBS prior to fluorescence labeling.

Fluorescence labeling and observation of cytoskeletal proteins

To label microtubules, samples were incubated in PBS containing a 50:50 mix of mouse monoclonal anti α- and β-tubulins (Sigma T-9026 and T-4046) that had been pre-bound with Zenon Alexa Fluor 488 F_{ab} (Z-25002, 1:1 by mass; Molecular Probes). For F-actin, samples were incubated in 260 n*M* of Texas-red phalloidin, for a minimum of 10 min, followed by a wash in PBS. Nuclei were labeled with 3 μ*M* DAPI (Sigma D-9542). Labeled samples were examined routinely using a Zeiss phase contrast/epi-fluorescence microscope equipped with a Nikon 950 digital camera; some observations were made using DIC optics.

Preparations for transmission electron microscopy

Sample tubes, each containing 2 ml of 10 μg/ml bacterial lipopolysaccharide (LPS; Sigma) in 3% sterile NaCl, were prepared for various periods: 0 (pre-activation), 30 s, 1 min, 2 min, 5 min, and 10 min. Two drops of blood were added to each tube *via* cardiac puncture, as described above. At each time point, 2 ml of 5% glutaraldehyde in 10 m*M* HEPES (pH 6.8) was added, except for the 0-time tube, to which it was pre-added so that the final glutaraldehyde concentration was ~2.5%. Preparations were fixed for 1 h at room temperature (~23 °C), washed three times in Sorensen's phosphate buffer (0.1 *M*, pH 6.8), and post-fixed in 1% osmium tetroxide in the same phosphate buffer for 1 h. Following three washes in phosphate buffer, the material was dehydrated with ethanol, infiltrated using propylene oxide, and embedded in Epon. Thin sections were cut with a diamond knife, stained with aqueous uranyl acetate and Reynold's lead citrate, and examined in a Hitachi H-600 transmission electron microscope.

Results

Cytoskeletal organization in unactivated cells: fluorescence observations

All of the cells observed in both fresh and fixed blood samples from many animals appeared to be granular amebocytes. As seen by DIC or phase contrast microscopy, the cells were typically flattened, nucleated ovoids, 15–20 μm in length, with 1–2-μm oval, refractile granules packing their cytoplasm (Fig. 1). Anti-tubulin immunofluorescence revealed the MB of unactivated cells as one major circumferential microtubule bundle that conformed to the ellipsoidal cell shape (Fig. 2a, b). The MB was restricted to the plane of flattening (Fig. 2d, e), with few other microtubules visible in the cells (Fig. 2f).

Not all of the cells exhibited this typical ovoid amebocyte morphology, however. A few were circular in profile, and contained a circular MB (Fig. 3a, a′). In addition, in samples from every animal examined, a significant percentage of cells tapered to a point at one or both ends (Fig. 3b–d), and the microtubules in these cells were not organized into typical continuous circumferential MBs but rather extended into the pointed ends (Fig. 3b–3d′). The percentage of pointed amebocytes, as determined by counts of more than 1000 cells in 10 animals, ranged from 1.3% to 8.3% (Table 1). In all cases the predominant variant was singly-pointed; doubly-pointed cells were observed in small numbers and in only five of the animals (Table 1), and cells with circular profile were also observed sporadically.

The distribution of F-actin was determined by Texas-red phalloidin binding (Fig. 4). F-actin appeared in some interior regions of unactivated cells, usually in the vicinity of the nucleus. F-actin was also evident in a thickened cortical layer in edge view throughout the cell periphery (Fig. 4b,

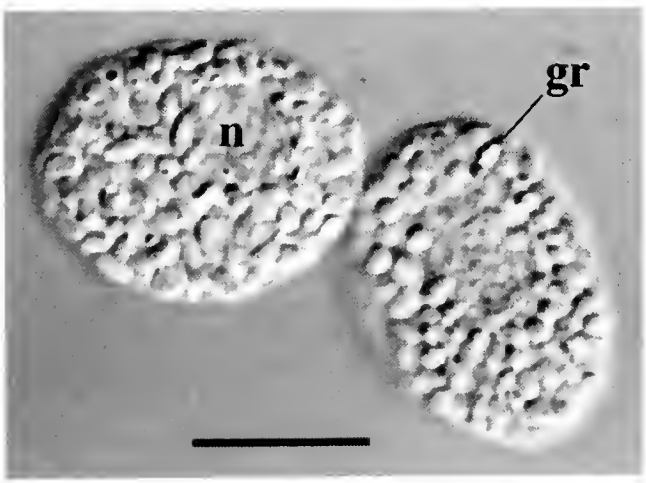

Figure 1. Intact unactivated amebocytes. The cells are flattened ovoids, packed with secretory granules (gr) except in the region occupied by the nucleus (n). DIC image; bar = 10 μm.

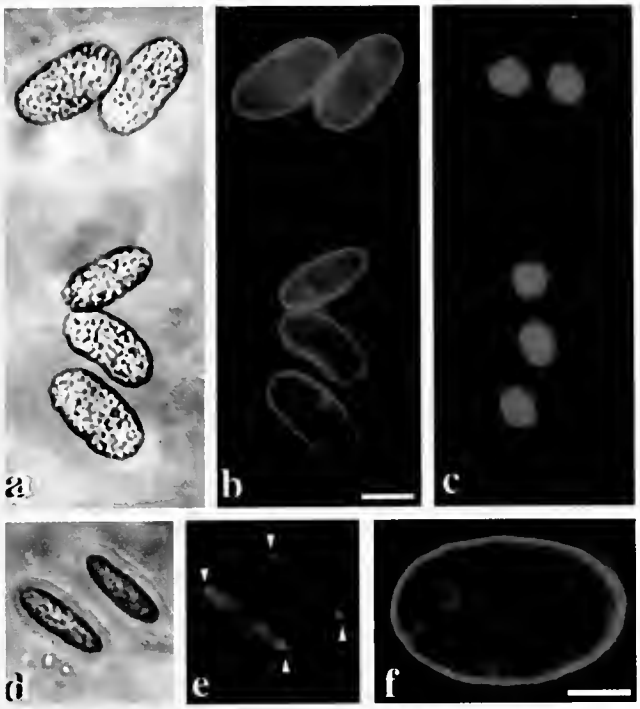

Figure 2. Microtubule distribution in unactivated cells; phase contrast and fluorescence microscopy. (a–c) A field of suspension-labeled cells, observed with phase contrast, anti-tubulin, and DAPI labeling, respectively. The marginal band (MB) in all cells follows ellipsoidal cell contour (a *vs.* b), with nuclei in the interior (c). (d, e) Two cells viewed on edge; phase contrast and anti-tubulin labeling, respectively. Flattened morphology is evident, with MB at the planar extremities (e; arrowheads). (f) Higher magnification view of MB microtubules in another cell. The MB consists of one major circumferential microtubule bundle, with few microtubules evident elsewhere.

arrows), with adjacent hazily labeled areas that are attributable to cortical F-actin being observed in face view.

Additional structural features of unactivated cells: TEM observations

To visualize cytoskeletal elements and cellular organelles in greater detail, fixed, unactivated cells were examined in TEM thin sections (Fig. 5). In addition to the electron-dense granules found throughout the cell, major components visible in survey views included nucleus, mitochondria, and Golgi apparatus; there was no surface-associated canalicular membrane system such as is found in non-mammalian vertebrate thrombocytes and mammalian platelets (Fig. 5a). Examination of numerous mature granules in TEM thin sections showed that those closest to the cell surface were always separated from the plasma membrane by a cytoplasmic gap ~50 nm thick (Fig. 5b, c). At higher magnifications, MB microtubules and centrioles (Fig. 5d–g) were visible, with the MB routinely observed at the cell periphery in various sectional views (*e.g.*, Fig. 5d *vs.* e). In cross

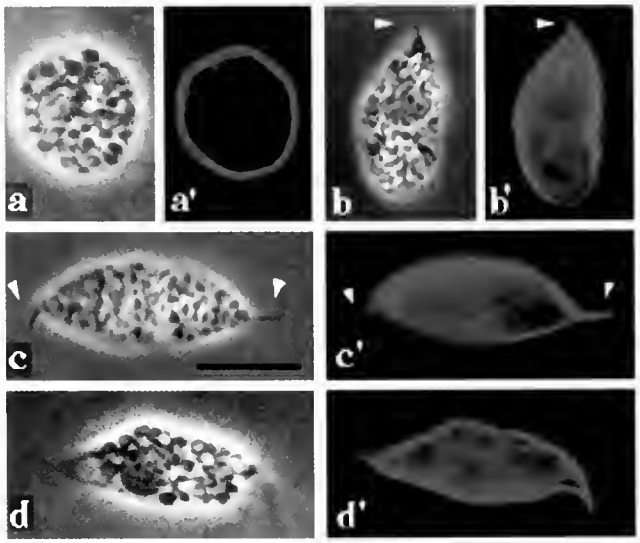

Figure 3. Cytoskeletal variants in the normal unactivated amebocyte population; paired images; phase contrast and fluorescence. (a, a′) Amebocyte, with a circular rather than elliptical profile, and with a circular MB. (b, b′) Singly-pointed amebocyte, with microtubule bundles following the entire cell contour including the pointed tip (arrowheads). This variant type was found in every animal examined (see also Table 1). (c, c′; d, d′) Examples of doubly-pointed cells, with microtubule bundles forming incomplete, doubly-pointed MBs (arrowheads). This variant was found only in some animals. Bar = 10 μm.

sections, the closest approach of MB component microtubules to the plasma membrane was ~50 nm, as in the case of granules (Fig. 5d; arrowheads and white bars).

Centrioles were found regularly, often with both members of a pair in a given section, usually located between the nucleus and Golgi apparatus. Centrioles had classic cylindrical structure, ~0.2 × 0.3 μm, with one closed end (Fig. 5f, arrow) and typical 9 + 0 triplet cross section (Fig. 5g). Centriole pairs were present in both parallel and perpendicular orientation, and when both members of a pair were

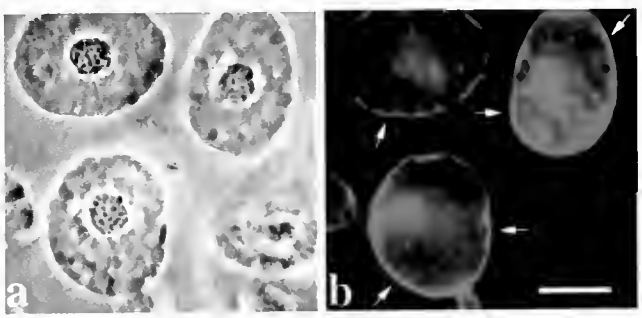

Figure 4. F-actin distribution in unactivated cells; phase contrast and fluorescence microscopy. (a) Phase contrast, several cells with nuclei visible. (b) Same cells as in (a), rhodamine-phalloidin binding by F-actin filaments. F-actin was concentrated principally in regions near the nucleus, and in a cortical layer visible in edge view at the cell periphery (b, arrows). Bar = 10 μm.

Table 1

Percentage of pointed granular amebocytes in hemolymph of 10 animals

Animal no.	No. cells counted	% SP	% DP	Total % pointed
1	1005	3.9	0	3.9
2	1101	6.0	0.6	6.6
3	1348	2.9	0.3	3.2
4	1002	1.3	0	1.3
5	1183	4.5	0.6	5.1
6	1003	8.3	0	8.3
7	1221	4.1	0.2	4.3
8	1037	2.6	0	2.6
9	1137	5.7	1.0	6.7
10	1276	1.8	0	1.8

Key: SP = singly-pointed; DP = doubly-pointed.

Note: Each count was made on more than 1000 cells per animal. Animals were of different sizes and sexes. Cell morphology was preserved by free flow of hemolymph directly into fixative, thus avoiding pipette-induced shearing or contact with slides or coverslips prior to fixation.

present in cross section, their triplets had the same "pinwheel" polarity (Fig. 5g, arrows). Few microtubules were present in the vicinity of the centrioles, which appeared to have no physical connection with the MB.

Cytoskeletal features in LPS-activated cells: fluorescence observations

Anti-tubulin immunofluorescence was used to follow the fate of marginal band microtubules after activation (Fig. 6). At $t = 30$ s the MB was visible at the periphery, but appeared buckled and otherwise distorted in shape (Fig. 6a, a′). At 3 min it was still recognizable, but now highly twisted and physically associated with the nucleus (Fig. 6b). At 7 min the MB was still nucleus-associated but nearly unrecognizable (Fig. 6c, c′), and ultimately it disappeared as such, though some tubulin-containing areas were visible (Fig. 6d, d′).

F-actin was redistributed in a dramatic way following activation (Fig. 7). Shortly after activation, cytoplasmic F-actin content increased in the cell population ($t = 1$ min; Fig. 7a″), while MB microtubules were still visible in distinct but twisted bundles (Fig. 7a′, arrow). At ~5 min, with MBs less distinct, many cells had spiky F-actin-rich protrusions several micrometers in length (Fig. 7b″). At 7 min, the spiky exterior of cells in some regions of the clot was less pronounced, and the F-actin had spread into more circular patterns (Fig. 7c″). However, not all cells responded in this way; at $t = 10$ min, with distinct microtubule bundles no longer present, cells in other clot regions still had numerous long F-actin-containing filopodia that appeared to cross and perhaps touch those of adjacent cells (Fig. 7d″).

Additional structural features of LPS-activated cells: TEM observations

Extensive nuclear deformation and reshaping was evident in thin sections of many cells in clots several minutes after activation (Fig. 8a). Microtubule bundles were no longer seen at the cell periphery, as they were in unactivated amebocytes, but bundles of microtubules were consistently found adjacent to the deformed nuclei (Fig. 8b, arrows). In no instance was a complete internalized MB observed, however. Centrioles remained intact, even in fully exocytosed cells (Fig. 8c), but there was no evidence of centrosomal microtubule organization in their vicinity.

Discussion

Our observations of unactivated amebocyte structure—as revealed by fluorescence localization of microtubules and F-actin—support earlier proposals that a cortical F-actin layer and the marginal band (MB) function together to maintain the shape of these cells. In addition, the cytoskeletal variants that we detected for the first time in the native cell population suggest that biogenesis of *Limulus* amebocytes involves microtubule-based mechanisms similar to those in other MB-containing blood cell types, such as the nucleated erythrocytes of non-mammalian vertebrates. Moreover, although *Limulus* amebocytes are multifunctional, activation by bacterial LPS produces major changes in their cytoskeletal organization that are closely similar to those occurring in vertebrate thrombocytes and mammalian platelets. Each of these points is further discussed below.

The cytoskeleton of unactivated cells

As observed previously by TEM (Nemhauser *et al.*, 1980), unactivated amebocytes have a MB of microtubules in their plane of flattening. In the present work, the MB was readily visualized by combining brief pre-fixation, detergent extraction, and immunofluorescence with Zenon-prelabeled anti-tubulin (Lee *et al.*, 2002). The MB matched the contour of each cell in the plane of flattening (*e.g.*, Fig. 2a–e), and essentially no microtubules were observed elsewhere in the unactivated cell (Fig. 2f).

TEM thin sections revealed a space ~50 nm wide separating both MB and granules from the plasma membrane bilayer (Fig. 5b, c, d). A comparable gap occurs between MB and plasma membrane in granular lobster hemocytes (Cohen *et al.*, 1983), and between the dense granules and plasma membrane of unactivated ("resting") platelets, which fuse only after activation (Morgenstern, 1995). This is evidence of a cortical layer throughout the entire unactivated cell, as illustrated diagrammatically in Figure 9, corresponding to a filamentous layer underlying the plasma membrane, as observed previously in thin sections of ame-

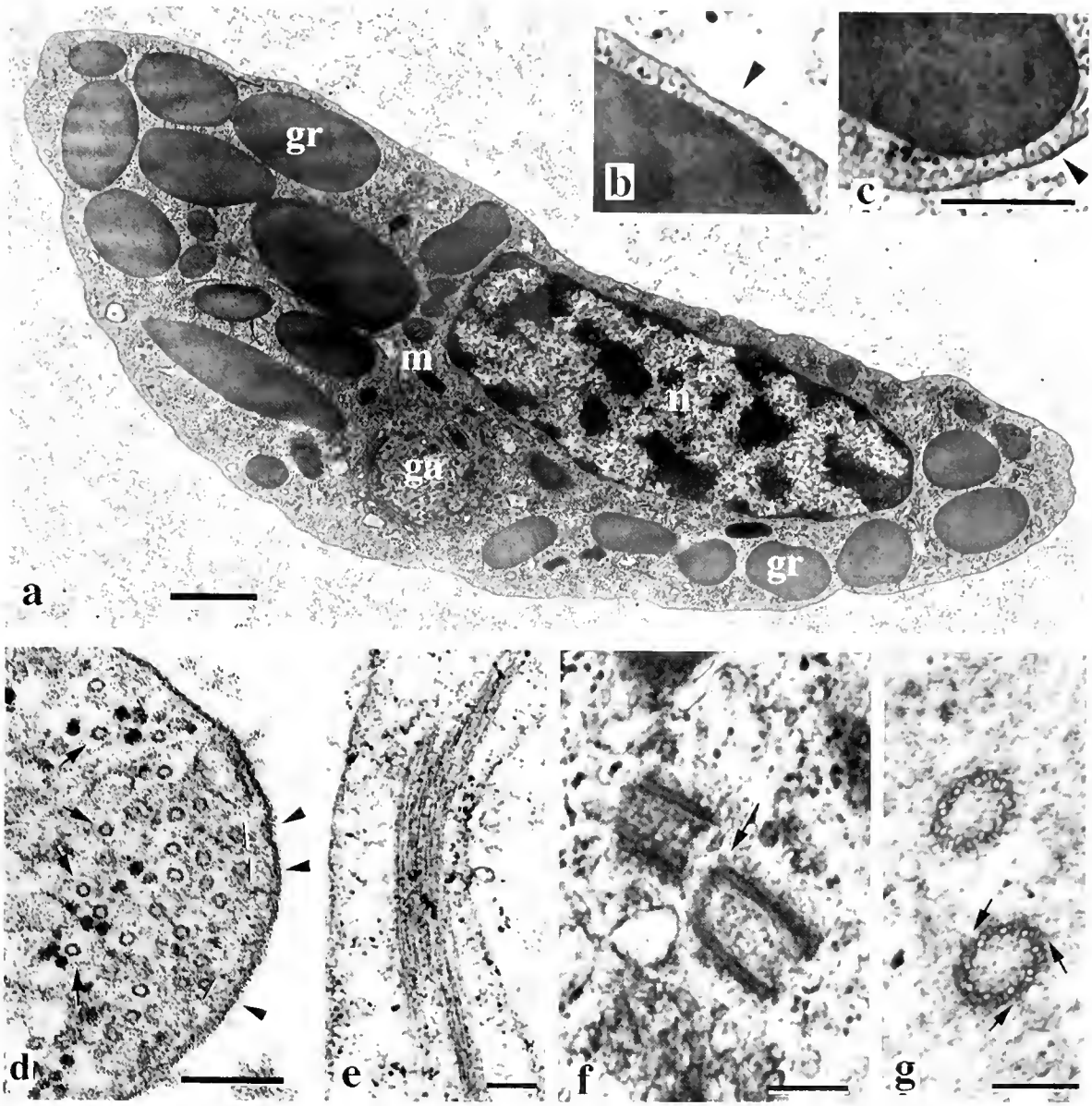

Figure 5. Structure of unactivated cells, TEM thin sections. (a) Longitudinal section overview, showing granules (gr), Golgi apparatus (ga), nucleus (n), mitochondria (m). Note: background material external to cell = fixed hemocyanin. (b, c) Enlarged views of gr-labeled granules in the same cell, showing the granules separated from the plasma membrane by a gap of ~50 nm (arrowheads). (d) Marginal band (MB) of microtubules in cross section, with some of the interior microtubules indicated by arrows; like granules, the outermost MB microtubules of unactivated cells are separated from the plasma membrane by a gap of ~50 nm, as indicated by the white lines (opposite arrowheads). (e) MB microtubules in longitudinal section. (f, g) Centriole pairs, shown in longitudinal and cross section, respectively, are a common feature. Longitudinal view shows typical closure at one end (f, arrow), and the triplet "pinwheel" directionality of pairs is evident in cross-sectional view (g, arrows). Bars: (a) = 1 μm; (b, as in c) = 0.5 μm; (d–g) = 0.2 μm.

bocytes prepared by freeze-substitution (Ornberg, 1985), or by a fixation method that preserves cortical F-actin in platelets (Boyles *et al.*, 1985; Tablin and Levin, 1988).

Because of its binding specificity, phalloidin labeling verifies that an F-actin-rich cortical layer is present in the *Limulus* amebocyte (Fig. 4), as shown previously for F-actin in unactivated platelets and vertebrate thrombocytes (Debus *et al.*, 1981; Lee *et al.*, 2004). Thus, in the *Limulus* amebocyte, the MB appears to act as a flexible frame that maintains unactivated cell shape by pressing from within against an actin-rich, filamentous cortical network (Fig. 9), in agreement with earlier proposals based on thin sections

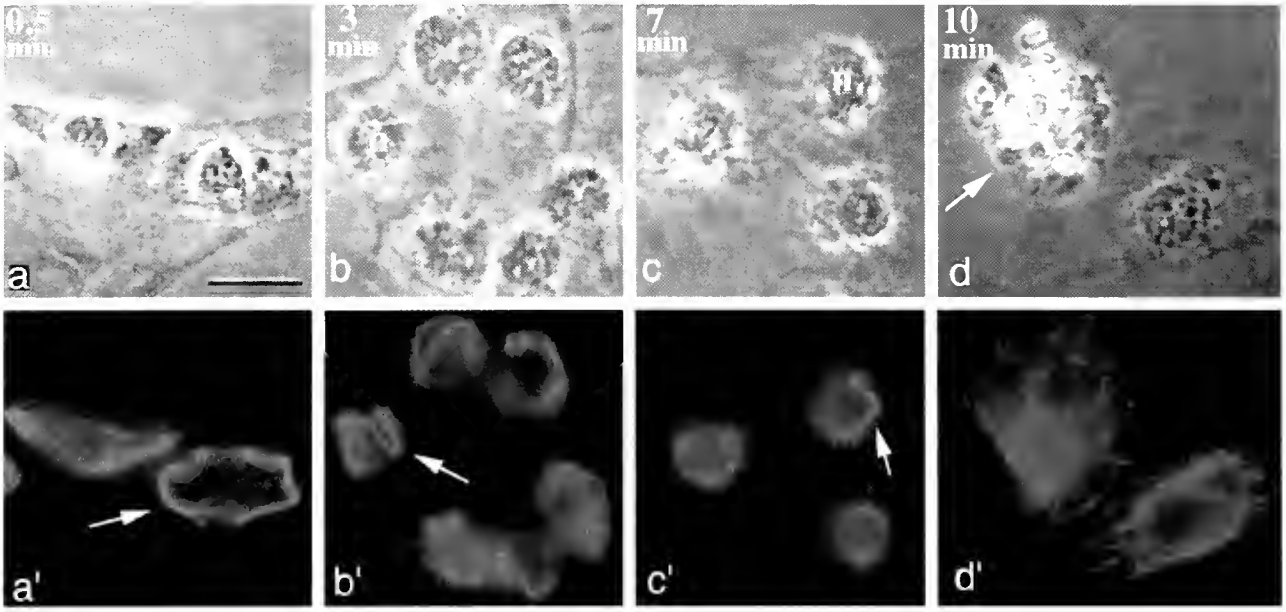

Figure 6. Time-course of microtubule redistribution during clot formation by lipopolysaccharide-activated amebocytes, observed by anti-tubulin immunofluorescence (phase contrast-fluorescence pairs; time of fixation is in upper left corner of phase images a–d). (a, a′) Cells 30-s post-activation; MBs are still at the periphery, somewhat folded and buckled, but still recognizable (e.g., a′, arrow), most granules have already exocytosed, and boundaries of individual cells are beginning to be obscured by the clot as viewed in phase contrast (a). (b, b′) 3 min after activation; microtubules have moved into the interior and are associated with nuclei, many MBs are still recognizable as highly twisted forms (e.g., arrow). (c, c′) 7 min post-activation; MBs are essentially unrecognizable as such, but microtubule bundles are still localized at nuclear surfaces (n; arrow in c′). (d, d′) 10 min post-activation; microtubules have a much more diffuse distribution, even in the few remaining cells in which exocytosis is incomplete (d, arrow). Bar = 10 μm.

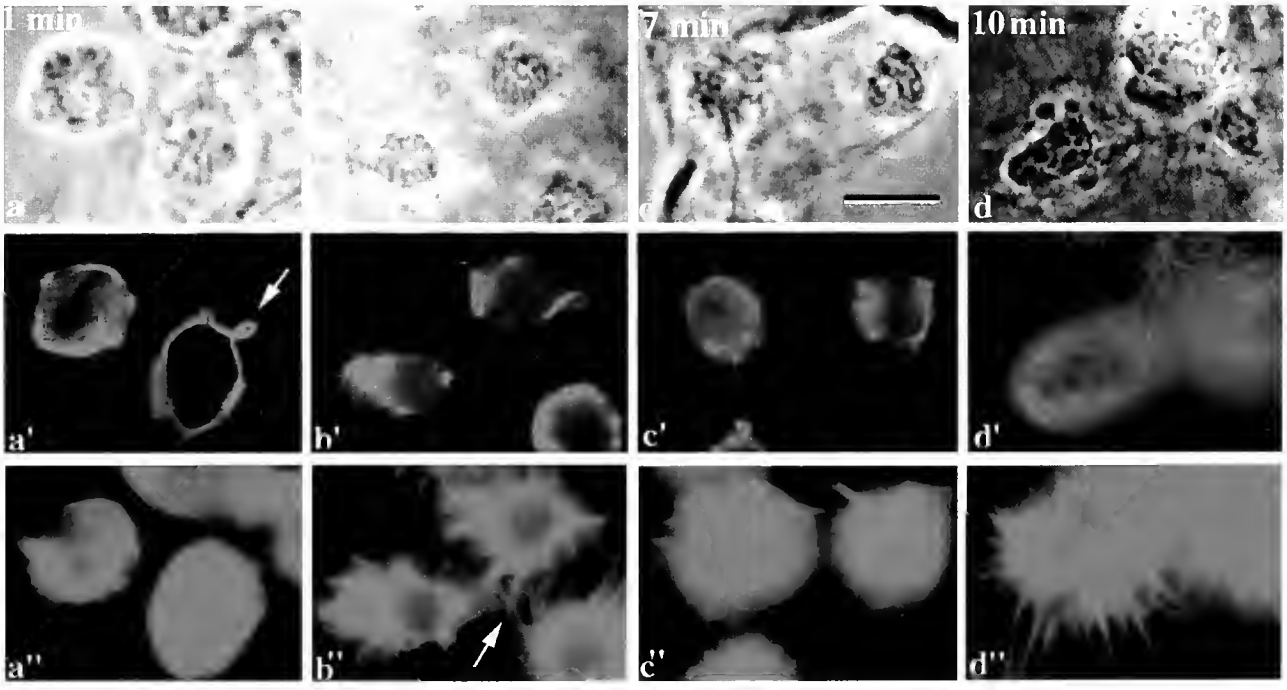

Figure 7. Activation time-course for F-actin redistribution relative to microtubules during clot formation, observed by anti-tubulin and rhodamine-phalloidin fluorescence (phase contrast-fluorescence triplets); time of fixation is in upper left corner of phase micrographs (a–d). Individual cells are not discernible in phase contrast post-activation, with the image mottled by the surrounding clot. (a–a″) $t = 1$ min; exocytotic cells within the clot have become more compact, with marginal bands (MBs) beginning to deform and twist (a′, arrow) and cytoplasmic F-actin distribution in a variable phase (a″). (b–b″) $t = 5$ min; MBs are twisted and located in the interior, closer to nuclei (b′); spiky F-actin-rich protrusions appear on most cells (b″, arrow). (c–c″) $t = 7$ min; MBs have lost recognizability, and microtubule bundles remain in the interior close to nuclei (c′); F-actin has redistributed in a spreading cell pattern, with a few peripheral F-actin-rich protrusions remaining (c″). (d–d″) $t = 10$ min; some variation was noted in different regions of the clot, with this region still containing cells that had long F-actin-rich filopodia. Bar = 10 μm.

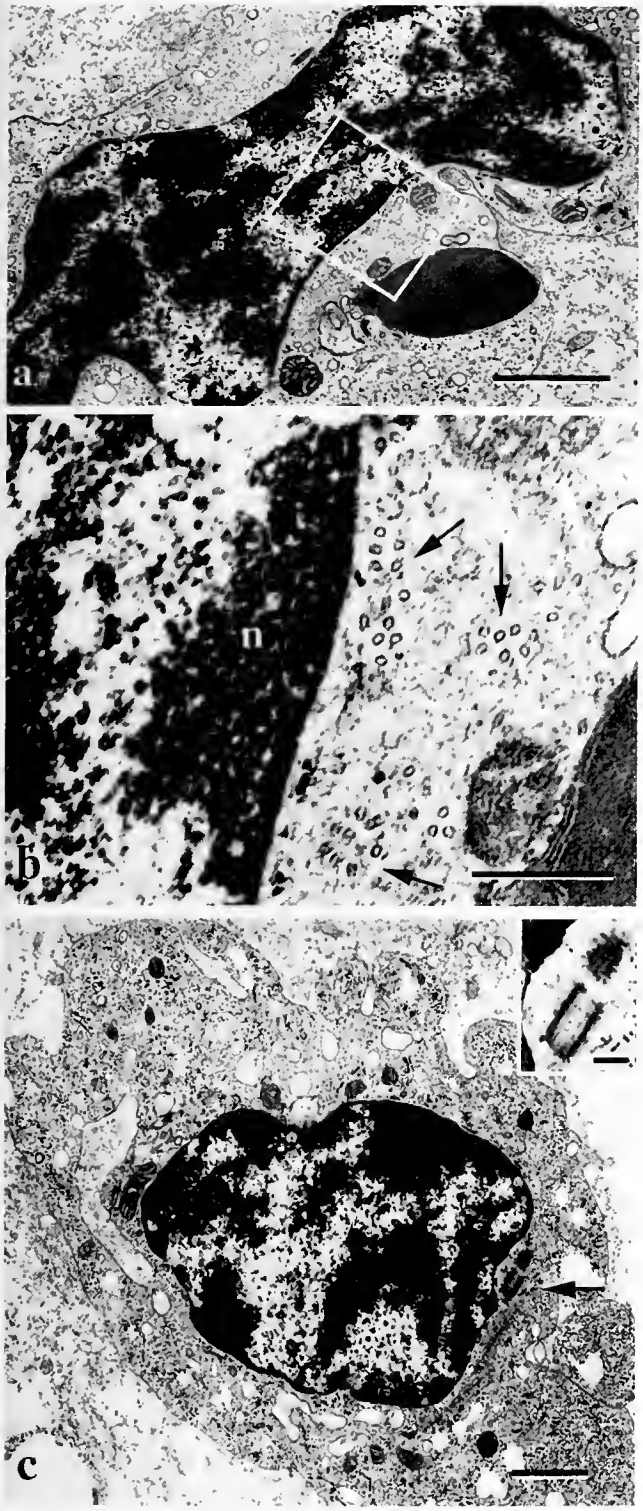

Figure 8. Cytoskeletal and nuclear structure in lipopolysaccharide-activated cells (TEM). (a) ~5 min post-activation; low-magnification view of deformed nucleus. (b) Higher magnification view of area delimited in (a), showing bundles of microtubules adjacent to nucleus (arrows). (c) ~10 min post-activation; exocytosis is complete, with no intact granules remaining. Centrioles (arrow, and inset) remain intact. Bars: (a, c) = 1 μm; (b) = 0.25 μm; (c inset) = 0.2 μm.

(Nemhauser *et al.*, 1980; Cohen and Nemhauser, 1985; Tablin and Levin, 1988). The same mechanism applies to platelets and to non-mammalian thrombocytes (Lee *et al.*, 2004), and it is similar to that proposed previously for the MB-containing nucleated erythrocytes of all non-mammalian vertebrates (Joseph-Silverstein and Cohen, 1984, 1985).

There is, however, one fundamental difference between the MB-containing cytoskeleton of unactivated nucleated erythrocytes and that of invertebrate or vertebrate clotting cells. The erythrocyte system is designed for long-term maintenance of circulating cell shape, with the MB interacting with a filamentous network—the actin-spectrin membrane skeleton—that is highly specialized for stability. In contrast, the cortical layer of the clotting cell—through interaction with the MB—must maintain the unactivated circulating shape for long periods, while remaining at all times responsive to the signals that induce the rapid shape transformations associated with clotting. As shown in the current work with *Limulus* amebocytes, as well as in previous work on platelets and non-mammalian vertebrate thrombocytes, the ultimate effector targeted by such signaling appears to be F-actin.

Unactivated cytoskeletal variants

The presence of minor numbers of discoidal cells containing discoid MBs and pointed cells containing a pointed microtubular cytoskeleton (Fig. 3) raises the possibility that there is more than one blood cell type in *Limulus*. While such amebocytes have not been reported previously, two hemocyte types—granular and nongranular—have been de-

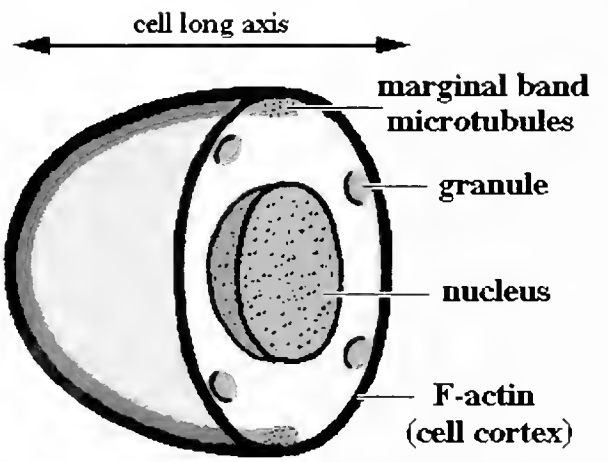

Figure 9. Diagrammatic summary of cytoskeletal features of the unactivated *Limulus* amebocyte; cutaway view with cell thickness exaggerated). The marginal band (MB), enclosed within the F-actin-rich cortical layer in the plane of flattening, is presumed to act as a flexible frame imposing pressure against the cortex to maintain the flattened ellipsoidal shape of unactivated cells. Both the MB and the most peripheral mature granules abut the cortical layer, as illustrated in the cross-sectional view.

scribed for the Asian horseshoe crab *Tachypleus* (Toh *et al.*, 1991). Nongranular hemocytes have not been observed in *Limulus*, but the singly-pointed granular cells constituted ~1%–8% of the population in 10 animals examined, with a few doubly-pointed ones in some (Table 1). Their number and constancy in samples prepared by free flow of blood directly into fixative preclude simple dismissal as a surface-contact or pipetting artifact, but it is highly unlikely that they represent a different cell type. Both singly-pointed and doubly-pointed morphologies (Fig. 3) are reminiscent of forms found previously during MB biogenesis in developing amphibian erythroblasts *in vivo* and *in vitro* (Ginsburg *et al.*, 1989; Twersky *et al.*, 1995; Huang *et al.*, 2001). In addition, discoidal amphibian erythrocytes containing discoidal MBs are reported to precede the generation of ellipsoids (Dorn and Broyles, 1982). Thus the observed variant amebocyte types may be biogenetic intermediates in the formation of ovoid *Limulus* amebocytes. Alternatively, pointed morphology could be produced by mechanically deteriorating cytoskeletons in older cells destined for retirement, and both possibilities remain to be tested. Unfortunately, this problem is made difficult because the sites of amebocyte production and recycling in the adult animal are still unknown.

Post-activation events

Shortly after activation, the MB remained associated with the cell periphery, still with few microtubules evident elsewhere (Fig. 6a, a′). Within a few minutes, however, the MB rapidly lost this association, as twisted microtubule bundles moved to the interior, adjacent to cell nuclei (Fig. 6b, b′, c, c′). In TEM thin sections, these interior bundles of microtubules were consistently found near the nuclear indentations of activated cells (Fig. 8a, b), suggesting that they may be responsible for altering nuclear shape. Though not commonly observed in other systems, microtubule association with nuclear constrictions occurs both in activated non-mammalian thrombocytes (Lee *et al.*, 2004) and in cultured leukemic cells undergoing apoptosis (Pittman *et al.*, 1997). Microtubule function in nuclear remodeling is perhaps best documented for the spermatid manchette in a mechanism involving dynein and kinesin motor proteins (McIntosh and Porter, 1967; Hall *et al.*, 1992), but in the other cases the effector mechanism is unknown. In the activated *Limulus* amebocytes, all recognizable MB microtubules disappeared eventually (Fig. 6d′; Fig. 7d′), in this respect resembling lobster hemocytes spreading on a substrate (Cohen *et al.*, 1983).

Following activation induced by lipopolysaccharide (LPS), the F-actin reorganized and spread outward, producing long, spiky, F-actin-rich filopodia as a major feature (Fig. 7a″ *vs.* 7b″, d″). Though not previously shown to contain F-actin, such spiky filopodia have also been observed in individual LPS-activated spheroidal amebocytes separated on a substratum—that is, not in a clot (Armstrong, 1985a). Thus, formation of such spiky filopodia does not require cell-cell contact. The F-actin in cells in some regions of our clots transformed into flattened discoidal patterns similar to individual surface-spreading non-mammalian vertebrate thrombocytes (Lee *et al.*, 2004) and mammalian blood platelets (Allen *et al.*, 1979). However, in other regions the cells retained spiky F-actin filopodia for longer periods, possibly contributing to the integrity and mechanical properties of the clot, as proposed for platelets (Cohen, 1979). Lack of synchrony or identity in the response of cells throughout the clot is not surprising, since the clots formed *in vitro* had local variations in thickness, cell density, and cell proximity to the clot surface and the surrounding medium.

In contrast to the outward-moving F-actin, the microtubules relocated into the interior and became associated with nuclei (Figs. 6b′, 7b′), in agreement with TEM observations of Tablin and Levin (1988), and in marked similarity to fluorescently localized F-actin and microtubules in activated non-mammalian thrombocytes and in platelets (Debus *et al.*, 1981; Lee *et al.*, 2004). These results support the hypothesis that the microtubules function primarily in the biogenesis and maintenance of unactivated amebocyte morphology, whereas F-actin is involved primarily in motile and morphogenetic functions associated with post-activation shape transformation. Thus, in most respects, the function of major cytoskeletal elements before and after activation of *Limulus* amebocytes closely resembles that of both mammalian blood platelets and non-mammalian nucleated thrombocytes (Allen *et al.*, 1979; Debus *et al.*, 1981; Lee *et al.*, 2004).

With respect to signaling pathways involved in *Limulus* amebocyte exocytotic and cytoskeleton-based activity, some cells that had undergone complete exocytosis were found to contain twisted but nearly intact MBs (*e.g.*, Figs. 6a,′ 7a′). This indicates that MB disorganization *per se* is not a prerequisite for exocytosis. Conversely, complete exocytosis is not a prerequisite for complete MB disorganization (*e.g.*, Fig. 6d, arrow). Thus, bacterial LPS probably triggers several sequences of events that proceed in parallel, but are relatively independent of each other.

Amebocyte multifunctionality

Centrioles were observed in thin sections of unactivated cells with such frequency that we assume a centriole pair to be present in every cell. What might their function be in mature amebocytes? They are not involved in cell division, as mitosis has been observed only in immature amebocyte precursors in early *Limulus* embryos (Coursey *et al.*, 2003), and never in amebocytes of adult animals (*e.g.*, Copeland and Levin, 1985). They are not associated with MB micro-

tubules as in molluscan erythrocytes, in which centrioles function in MB reassembly (Nemhauser *et al.*, 1983), and there are few other cytoplasmic microtubules present. Moreover, the centrioles remain adjacent to the nucleus in cells in which exocytosis is complete (Fig. 8c), with no evidence of centrosomal microtubule nucleation during that process. Are they just "leftovers" from poles of the last mitotic spindle preceding their biogenesis? Not necessarily. As their name suggests, *Limulus* amebocytes are multifunctional cells that can move about the tissues of the animal with pseudopodia, in addition to being carried by the circulation; and they can also engage in limited phagocytosis independent of exocytosis and clotting (Armstrong, 1985a). Centriole-containing centrosomes may well be involved in these activities, as in similar crawling movements of mammalian polymorphonuclear leukocytes and T-cells (Zigmond, 1978; Pryzwansky *et al.*, 1983; Volkov *et al.*, 1998; Abal *et al.*, 2002).

Our TEM thin section observations (Fig. 5) confirmed the general organelle and granule content observed in earlier studies (Copeland and Levin, 1985), as well as the absence of a subsurface membranous canalicular system such as is characteristic of both non-mammalian vertebrate thrombocytes and platelets (*e.g.*, White and Clawson, 1980; Daimon and Uchida, 1985). Why are canaliculi not present in the *Limulus* amebocyte? The canalicular system is a specialized compartment that responds to clotting activation signals by rapid reorganization, and we suggest that the canaliculi of clotting cells represent a degree of differentiation incompatible with the multifunctionality of *Limulus* amebocytes. This raises an important issue with respect to mechanisms of innate immunity and comparative hematology. There appear to be two evolutionary strategies at work: (a) several functions can be encompassed within a single cell type, in which case the cell must be sensitive to a variety of signals and respond to them in various specialized ways *via* separate paths; or (b) functions can be distributed among more specialized cell types, with correspondingly specialized signal receptor systems and fewer intracellular pathways. The *Limulus* amebocyte exemplifies the former, whereas the presence of canaliculi in vertebrate thrombocytes and platelets is symptomatic of the latter.

Acknowledgments

This work was supported by grants from the City University of New York (PSC-CUNY 63215), the Howard Hughes Medical Institute (HHMI) Undergraduate Science Education Program 71100-534602), and the National Science Foundation (NSF 9808368). Special thanks go to Dr. Peter Armstrong, to the reviewers, and to Editor-in-Chief Michael J. Greenberg for substantial scientific and editorial input. This work is a contribution from the Comparative Hematology and Innate Immunity Cluster (CHIIC) of the MBL's Whitman Center.

Literature Cited

Abal, M., M. Piel, V. Bouckson-Castaing, M. Mogensen, J. B. Sibarita, and M. Bornens. 2002. Microtubule release from the centrosome in migrating cells. *J. Cell Biol.* **159:** 731–737.

Allen, R. D., L. R. Zacharski, S. T. Widirstky, R. Rosenstein, L. M. Zaitlin, and D. R. Burgess. 1979. Transformation and motility of human platelets: details of the shape change and release reaction observed by optical and electron microscopy. *J. Cell Biol.* **83:** 126–142.

Armstrong, P. B. 1980. Adhesion and spreading of *Limulus* blood cells on artificial surfaces. *J. Cell Sci.* **44:** 243–262.

Armstrong, P. B. 1985a. Adhesion and motility of the blood cells of *Limulus*. Pp. 77–124 in *Blood Cells of Marine Invertebrates*, W. D. Cohen, ed. Alan R. Liss, New York.

Armstrong, P. B. 1985b. Amebocytes of the American "horseshoe crab," *Limulus polyphemus*: a practical guide. Pp. 253–258 in *Blood Cells of Marine Invertebrates*, W. D. Cohen, ed. Alan R. Liss, New York.

Armstrong, P. B., and F. R. Rickles. 1982. Endotoxin-induced degranulation of the *Limulus* amebocyte. *Exp. Cell Res.* **140:** 15–24.

Behnke, O. 1970. A comparative study of microtubules of disk-shaped blood cells. *J. Ultrastruct. Res.* **31:** 61–75.

Boyles, J., J. E. Fox, D. R. Phillips, and P. E. Stenberg. 1985. Organization of the cytoskeleton in resting, discoid platelets: preservation of actin filaments by a modified fixation that prevents osmium damage. *J. Cell Biol.* **101:** 1463–1472.

Cohen, I. 1979. The contractile system of blood platelets and its function. *Methods Achiev. Exp. Pathol.* **9:** 40–86.

Cohen, W. D., and I. Nemhauser. 1985. Marginal bands and the cytoskeleton in blood cells of invertebrates. Pp. 3–49 in *Blood Cells of Marine Invertebrates*, W. D. Cohen, ed. Alan R. Liss, New York.

Cohen, W. D., I. Nemhauser, and M. F. Cohen. 1983. Marginal bands of lobster blood cells: disappearance associated with changes in cell morphology. *Biol. Bull.* **164:** 50–61.

Copeland, D. E., and J. Levin. 1985. The fine structure of the amebocyte in the blood of *Limulus polyphemus*. I. Morphology of the normal cell. *Biol. Bull.* **169:** 449–457.

Conrad, M. L., R. L. Pardy, and P. B. Armstrong. 2001. Response of the blood cell of the American horseshoe crab, *Limulus polyphemus*, to a lipopolysaccharide-like molecule from the green alga *Chlorella*. *Biol. Bull.* **201:** 246–247.

Coursey, Y., N. Ahmad, B. M. McGee, N. Steimel, and M. Kimble. 2003. Amebocyte production begins at stage 18 during embryogenesis in *Limulus polyphemus*, the American horseshoe crab. *Biol. Bull.* **204:** 21–27.

Daimon, T., and K. Uchida. 1985. Ultrastructural evidence of the existence of the surface connected canalicular system in the thrombocyte of the shark (*Triakis scyllia*). *J. Anat.* **141:** 193–200.

Dehus, E., K. Weber, and M. Osborn. 1981. The cytoskeleton of blood platelets viewed by immunofluorescence microscopy. *Eur. J. Cell Biol.* **24:** 45–52.

Dorn, A. R., and R. H. Broyles. 1982. Erythrocyte differentiation during the metamorphic hemoglobin switch of *Rana catesbeiana*. *Proc. Natl. Acad. Sci. USA* **79:** 5592–5596.

Fawcett, D. W., and F. Witebsky. 1964. Observations on the ultrastructure of nucleated erythrocytes and thrombocytes with particular reference to the structural basis of their discoidal shape. *Z. Zellsforsch. Mirosk. Anat.* **62:** 785–806.

Ginsburg, M. F., L. H. Twersky, and W. D. Cohen. 1989. Cellular

morphogenesis and the formation of marginal bands in amphibian splenic erythroblasts. *Cell Motil. Cytoskel.* **12:** 157–168.

Hall, E. S., J. Eveleth, C. Jiang, D. M. Redenbach, and K. Boekelheide. 1992. Distribution of the microtubule-dependent motors cytoplasmic dynein and kinesin in rat testis. *Biol. Reprod.* **46:** 817–828.

Huang, L-F., L. Levinhar, K-G. Lee, M. Ginsburg, and W. D. Cohen. 2001. *In vitro* morphogenesis of amphibian erythroblasts. *Cell Biol. Internat.* **25:** 1229–1236.

Jagadeeswaran, P., J. P. Sheehan, F. E. Craig, and D. Troyer. 1999. Identification and characterization of zebrafish thrombocytes. *Br. J. Haematol.* **107:** 731–738.

Joseph-Silverstein, J., and W. D. Cohen. 1984. The cytoskeletal system of nucleated erythrocytes. III. Marginal band function in mature cells. *J. Cell Biol.* **98:** 2118–2125.

Joseph-Silverstein, J., and W. D. Cohen. 1985. Role of the marginal band in an invertebrate erythrocyte: evidence for a universal mechanical function. *Can. J. Biochem. Cell Biol.* **63:** 621–630.

Lee, K-G., A. Braun, I. Chaikhoutdinov, J. DeNobile, M. Conrad, and W. D. Cohen. 2002. Rapid visualization of microtubules in blood cells and other cell types in marine model organisms. *Biol. Bull.* **203:** 204–206.

Lee, K-G, T. Miller, I. Anastassov, and W. D. Cohen. 2004. Shape transformation and cytoskeletal reorganization in activated non-mammalian thrombocytes. *Cell Biol. Internat.* **28:** 299–310.

Levin, J., and F. B. Bang. 1968. Clottable protein in *Limulus*; its localization and kinetics of its coagulation by endotoxin. *Thromb. Diath. Haemorrh.* **19:** 186–197.

McIntosh, J. R., and K. R. Porter. 1967. Microtubules in the spermatids of the domestic fowl. *J. Cell Biol.* **35:** 153–173.

Morgenstern, E. 1995. The formation of compound granules from different types of secretory organelles in human platelets (dense granules and alpha-granules). A cryofixation/-substitution study using serial sections. *Eur. J. Cell Biol.* **68:** 183–190.

Nemhauser, I., R. Ornberg, and W. D. Cohen. 1980. Marginal bands in blood cells of invertebrates. *J. Ultrastruct. Res.* **70:** 308–317.

Nemhauser, I., J. Joseph-Silverstein, and W. D. Cohen. 1983. Centrioles as microtubule organizing centers for the marginal band of a molluscan erythrocyte. *J. Cell Biol.* **86:** 286–291.

Ornberg, R. L. 1985. Exocytosis in *Limulus* amebocytes. Pp. 127–142 in *Blood Cells of Marine Invertebrates,* W. D. Cohen, ed. Alan R. Liss, New York.

Ornberg, R. L., and T. S. Reese. 1981. Beginning of exocytosis captured by rapid-freezing of *Limulus* amebocytes. *J. Cell Biol.* **90:** 40–54.

Pittman, S., M. Geyp, M. Fraser, K. Ellem, A. Peaston, and C. Ireland. 1997. Multiple centrosomal microtubule organising centres and increased microtubule stability are early features of VP-16-induced apoptosis in CCRF-CEM cells. *Leuk. Res.* **21:** 491–499.

Pryzwansky, K. B., M. Schliwa, and K. R. Porter. 1983. Comparison of the three-dimensional organization of unextracted and Triton-extracted human neutrophilic polymorphonuclear leukocytes. *Eur. J. Cell Biol.* **30:** 112–125.

Shepro, D., F. A. Belamarich, and R. Branson. 1966. The fine structure of the thrombocyte in the dogfish (*Mustelus canis*) with special reference to microtubule orientation. *Anat. Rec.* **156:** 203–214.

Tahlin, F., and J. Levin. 1988. The fine structure of the amebocyte in the blood of *Limulus polyphemus.* II. The amebocyte cytoskeleton: a morphological analysis of native, activated, and endotoxin-stimulated amebocytes. *Biol. Bull.* **175:** 417–429.

Toh, Y., A. Mizutani, F. Tokunaga, T. Muta, and S. Iwanaga. 1991. Morphology of the granular hemocytes of the Japanese horseshoe crab *Tachypleus tridentatus* and immunocytochemical localization of clotting factors and antimicrobial substances. *Cell Tiss. Res.* **266:** 137–147.

Twersky, L. H., A. Bartley, N. Rayos, and W. D. Cohen. 1995. Immature erythroid cells with novel morphology and cytoskeletal structure in adult *Xenopus. Protoplasma* **185:** 37–49.

Volkov, Y., A. Long, and D. J. Kelleher. 1998. Inside the crawling T cell: leukocyte function-associated antigen-1 cross-linking is associated with microtubule-directed translocation of protein kinase C isoenzymes beta(I) and delta. *J. Immunol.* **161:** 6487–6495.

White, J. G., and C. C. Clawson. 1980. The surface-connected canalicular system of blood platelets—a fenestrated membrane system. *Am. J. Pathol.* **101:** 353–364.

Zigmond, S. H. 1978. Chemotaxis by polymorphonuclear leukocytes. *J. Cell Biol.* **77:** 269–287.

Reference: *Biol. Bull.* **207:** 67–71. (August 2004)

Size and Organic Content of Eggs of Marine Annelids, and the Underestimation of Egg Energy Content by Dichromate Oxidation

BRUNO PERNET[1,*] AND WILLIAM B. JAECKLE[2]

[1]*Friday Harbor Laboratories, 620 University Road, Friday Harbor, Washington 98250; and*
[2]*Illinois Wesleyan University, PO Box 2900, Bloomington, Illinois 61702-2900*

Dichromate oxidation is a simple technique that is often used to estimate the energy content of eggs in studies of marine invertebrate life histories (1). We used this method to measure the energy contents of the eggs of 12 species of marine annelids. In combination with measures of egg ash-free dry weight (AFDW), these data yielded estimates of AFDW-specific energy density that were mostly lower than the average weight-specific energy density of carbohydrates. This seemed unlikely to be correct, as invertebrate eggs typically contain little carbohydrate and instead are composed primarily of energy-dense protein and lipid (1, 2). After validating our methods (by using them to estimate energy content and AFDW of the eggs of a previously studied echinoderm) and reexamining published data on the energy contents of echinoderm eggs, we conclude that dichromate oxidation often underestimates the energy contents of small eggs of marine invertebrates. This systematic error, which is likely related to the tendency of the assay to incompletely oxidize proteins, can only be corrected with substantial independent data on egg biochemical composition. We thus suggest that dichromate oxidation should not be used for routine measurement of the total energy content of marine invertebrate eggs.

Maternal investment of energy per offspring is a variable of fundamental importance in models of the evolution of life histories (3, 4). It is relatively easy to quantify in free-spawning marine invertebrates, where maternal investment is primarily limited to the organic material provided in the egg. Among echinoderms, egg energy and organic content (as AFDW) are both positively correlated with egg volume in interspecific comparisons (1, 5). Few data on relationships between egg size and organic or energy content are available for members of other phyla of invertebrates (1, 6, 7). We measured these variables in 12 species of marine annelids, with the aim of testing hypotheses on differences between annelids and echinoderms in relationships between maternal investment and larval nutritional mode. We used the technique of dichromate oxidation to estimate egg energy content (8, 9). Though it is prone to several problems (10, 11, 12), previous analyses have suggested that dichromate oxidation estimates agree well with those made by other techniques (1, 13), and it is frequently used to measure egg energy content (reviewed in ref. 1). Studied annelid eggs ranged in diameter from 44 to 352 μm (Table 1), and in egg volume from 4×10^{-5} to 2×10^{-2} μl, a range of 2.7 orders of magnitude (calculated as in 14). Both AFDW and energy content were positively correlated with egg volume in interspecific comparisons (by ordinary least squares [OLS] regression: ln[AFDW] on ln[volume], $r^2 = 0.99$; ln[energy] on ln[volume], $r^2 = 0.99$).

However, calculation of AFDW-specific energy densities (Table 1) revealed surprisingly low values: the mean AFDW-specific energy density for eggs of the 12 species was 15.2 mJ/μg (range 10.3–22.5), lower than the average weight-specific energy density of carbohydrates (17.5 mJ/μg [15]). This result might be correct if annelid eggs were composed primarily of carbohydrates. However, all invertebrate eggs whose composition has been studied (primarily those of echinoderms and crustacean arthropods) contain little carbohydrate (less than 5% by weight: 1, 2, 6) and a great deal of relatively energy-dense protein and lipid. Thus, we focused on two other possible explanations for our low estimates of AFDW-specific energy density in annelid

Received 30 April 2004; accepted 23 June 2004.

* To whom correspondence should be addressed, at Department of Biological Sciences, California State University, Long Beach, 1250 Bellflower Blvd, Long Beach, CA 90840-3702. E-mail: bpernet@csulb.edu

Table 1

Egg size, ash-free dry weight (AFDW), energy content, and weight-specific energy density for 12 species of marine annelids

Note that we believe our reported energy contents (and energy densities) are significant underestimates of true values; see text for discussion

Taxon	*n*	Diameter (μm)	Volume (μl)	AFDW (μg)	Energy (mJ)	Energy density (mJ/μg)
Chaetopteridae						
Chaetopterus sp. (FL, plk)	3	94.7 (0.7)	0.00045	0.152 (0.017)	2.19 (0.28)	14.4
Hesionidae						
Ophiodromus pugettensis (WA, plk)	3	85.1 (3.1)	0.00032	0.096 (0.015)	1.01 (0.22)	10.5
Maldanidae						
Axiothella mucosa (FL, lec)	4	212.4 (3.2)	0.005	1.670 (0.275)	33.95 (6.02)	20.3
Nereididae						
Platynereis bicanaliculata (WA, lec)	1	149.0	0.002	0.652	9.5	14.6
Onuphidae						
Kinbergonuphis simoni (FL, lec)	3	351.9 (7.5)	0.023	10.306 (0.738)	231.60 (20.23)	22.5
Pectinariidae						
Pectinaria gouldi (FL, plk)	2	43.7 (1.1)	0.00004	—	0.16 (0.00)	—
Sabellariidae						
Phragmatopoma lapidosa (FL, plk)	4	84.6 (2.9)	0.00032	0.120 (0.033)	1.90 (0.31)	15.8
Sabellaria cementarium (WA, plk)	3	68.8 (3.4)	0.00017	0.067 (0.010)	0.74 (0.03)	11.0
Sabellidae						
Schizobranchia insignis (WA, lec)	3	155.5 (2.7)	0.002	0.895 (0.025)	15.64 (1.78)	17.5
Serpulidae						
Hydroides sanctaecrucis (FL, plk)	3	52.2 (0.5)	0.00007	0.027 (0.003)	0.40 (0.04)	14.8
Protula sp. (FL, lec)	2	86.3 (1.1)	0.00034	0.138 (0.004)	2.07 (0.14)	15.0
Serpula columbiana (WA, plk)	4	69.1 (3.6)	0.00017	0.063 (0.009)	0.65 (0.03)	10.3

Values are means (one standard deviation) of measurements from each of *n* females. "FL" and "WA" refer to the collection location (Florida or Washington); "plk" and "lec" refer to larval nutritional mode (planktotrophic or lecithotrophic).

Collection of adults and eggs. Adults were obtained from around the Smithsonian Marine Station, Fort Pierce, Florida, and the Friday Harbor Marine Laboratories, Friday Harbor, Washington. Details of collection sites are available from the first author. Eggs were obtained from pectinariids, sabellariids, and serpulids by removing them from their tubes, after which they spawned. Nereidids and hesionids were captured as epitokes which spawned in the laboratory after capture. Sabellids spawned after warming of the seawater to room temperature. Maldanids deposited embryos in gelatinous masses attached to parental tubes; recently deposited masses (<12 h old) were obtained by frequent visitation to a marked patch of adults in the field, and embryos were removed from masses by dissection. The onuphids were intratubular brooders, and embryos were obtained by searching through parental tubes. Recently fertilized, single-celled zygotes were used for measurements in all cases except the maldanids and onuphids, where early cleavage stage embryos were used. For simplicity, we hereafter call all these stages "eggs." Eggs were cleaned by passing them through a Nitex sieve with a mesh size slightly larger than the egg diameter to remove any large debris, and collecting them on a sieve with a mesh size smaller than the egg diameter to remove smaller debris. They were rinsed twice and resuspended in filtered seawater (0.45-μm mesh size, FSW). Concentrations of eggs in the final suspension were estimated by counts of eggs or embryos in replicated (4–6×) subsamples of known volumes taken with calibrated micropipettors. The large eggs of maldanids and onuphids were counted directly using a dissecting microscope.

Egg volume. Linear dimensions were estimated by measuring eggs with a compound microscope and ocular micrometer (final magnification usually 400×). In many cases, unfertilized eggs were not spherical at spawning, but became spherical soon after fertilization. A single axis (diameter) was measured for spherical eggs. Eggs of the maldanid were prolate spheroids (oblong-shaped), and two axes were measured. For each female, means of the linear dimensions of 20 eggs were calculated; reported diameters are among-female means of these values for spherical eggs, or the diameters of spheres of equivalent volumes for the maldanid.

Ash-free dry weight. Known numbers of eggs were transferred to 1.5-ml microfuge tubes, with three replicate tubes for each female. Tubes were centrifuged briefly and the supernatant FSW removed. To remove residual seawater, eggs were resuspended in milli-Q filtered H_2O (mqH_2O), immediately centrifuged again, and the supernatant decanted. This rinsing process was repeated once more. Samples were stored at −80 °C for up to a month before further processing. Samples were eventually transferred to pre-ashed foil pans and dried to constant weight at 65–75 °C (6–14 days). Dried samples were weighed with a Cahn electrobalance, then ashed for 5 h at 500 °C. Ashed samples were weighed and AFDW was estimated by subtraction. Per-egg AFDW was obtained by division. Egg AFDW for each female was taken as the mean of three separate measurements; reported values are among-female means. For *Axiothella* and *Phragmatopoma*, AFDW measurements were made on eggs from only three females. Insufficient tissue was available to measure AFDW of eggs of *Pectinaria*.

Energy content. Known numbers of eggs were transferred to 1.5-ml microfuge tubes, with three replicate tubes for each female, and rinsed in mqH2O as described above. Rinsed eggs were transferred to pre-ashed glass test tubes, where they were stored at −80 °C for up to a month before energy assays were conducted. Energy assays were carried out by dichromate oxidation following McEdward and Coulter (9), except that samples and standards were lyophilized prior to assays (preliminary experiments showed that lyophilization had no effect on energy content). For each sample, organic matter was estimated against glucose standards (0–857 μg) as the weight of glucose (μg) yielding equivalent reduction in dichromate. Division of this value by 2.5 gave sample content in equivalents of organic carbon (μg) in glucose, and this was converted to energy content using the relationship 1 μg C = 39 mJ. Per-egg energy content was obtained by division. Egg energy for each female was taken as the mean of three measurements; reported values are among-female means.

Note that eggs for AFDW and energy content measurements for each female were drawn from the same container of eggs of known concentration, and eggs destined for both assays were rinsed in mqH_2O using the same methods. Errors associated with estimating egg concentration or with rinsing eggs should thus be of the same magnitude and direction for both assays for each female, and should cancel in estimates of energy density.

eggs—that we had systematically underestimated egg energy content or overestimated egg AFDW. To distinguish between these possibilities, we estimated the energy content and AFDW of eggs of the sea urchin *Strongylocentrotus droebachiensis* from San Juan Island, Washington, using the same techniques we had used for annelid eggs. Eggs of *S. droebachiensis* had previously been studied by other investigators using several different methods (16, 17, 18), and their data provided a useful check on our methods. The eggs we obtained were 152.25 μm in mean diameter (SD = 1.77, n = 4 females), slightly smaller than those studied by these other workers (157, 156, and 157 μm in refs. 16–18, respectively). Our estimate of egg energy content in *S. droebachiensis* (mean = 8.16 mJ, SD = 0.66, n = 4 females) was similar to the published value obtained by dichromate oxidation (7.02 mJ, calculated from data in 16), and our estimate of egg AFDW (mean = 0.494 μg, SD = 0.074, n = 4 females) was similar to the sole published value (0.531 μg, calculated from data in 17). Again, however, our data yielded a very low AFDW-specific energy density, 16.5 mJ/μg. Our estimate of the energy content of eggs of *S. droebachiensis* is undoubtedly incorrect, as eggs of this species contain substantial protein and lipid but little carbohydrate (17, 19). Indeed, an energy content estimate for eggs of *S. droebachiensis* made by summing the energetic values of measured biochemical components and the remainder fraction was 12.18 mJ, 1.5 times greater than the estimate yielded by dichromate oxidation (17). This higher estimate of energy content yielded a more realistic AFDW-specific energy density of about 23 mJ/μg, which is very similar to the weight-specific energy density of eggs of *S. droebachiensis* measured by another technique, direct calorimetry (22.5 mJ/μg dry weight [18]; note that these authors report *dry weight*-specific energy density, which we expect to be a slight underestimate of *AFDW*-specific energy density). The striking difference in energy content and density estimates made by dichromate oxidation, on the one hand, and biochemical component analyses and direct calorimetry, on the other, led us to suspect that we had consistently underestimated energy contents of our samples due to an error associated with the dichromate oxidation technique itself.

It is also possible that we (and other workers: 17, 18) had consistently overestimated egg AFDW, perhaps because water associated with intracellular salts was not removed by drying at 65–75 °C, but was removed when samples were ashed at 500 °C (20). However, eggs of marine invertebrates contain only small amounts of salts (2, 21), and even if all of these are hydrated, this potential error cannot account for the large underestimates of AFDW-specific energy density we observed (Table 1). Further, our AFDW measurements yield realistic estimates of AFDW-specific energy density when combined with energy content estimates made by biochemical component analysis (17), and these are consistent with those made by direct calorimetry (18), suggesting that we did not seriously overestimate egg AFDW.

We hypothesized that this possible systematic underestimation of energy content by dichromate oxidation might be apparent in published data on egg size and energy content in echinoderms, a phylum in which both dichromate oxidation and biochemical component analyses have been used to estimate egg energy contents. To test this hypothesis, we examined data compiled by McEdward and Morgan (5) on the energy contents of eggs of 47 echinoderm species. Because AFDW is rarely measured in dichromate oxidation studies of egg energy content, we were unable to compare relationships between energy content and AFDW for the two methods; instead, we used egg volume as a measure of egg size. Eggs in this sample fall into two groups: 24 species with planktotrophic larval development and relatively small eggs (75–274 μm diameter), and 23 species with lecithotrophic development and large eggs (496–2799 μm diameter). Inspection of these data (Fig. 1) suggests that for the small eggs of planktotrophic species, energy content estimates made by dichromate oxidation are often lower than those made by biochemical component analysis. For the larger eggs of lecithotrophs, the two methods yield similar estimates. Comparisons of egg volume-specific energy densities support these impressions. Within the planktotrophs, mean volume-specific energy density was significantly lower in species whose egg energy contents were estimated by dichromate oxidation (mean = 4566.1 mJ/μl, SD

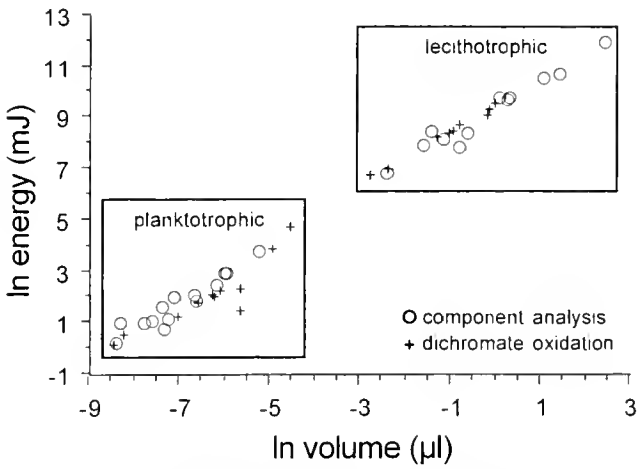

Figure 1. Relationships of egg energy content (estimated by dichromate oxidation [+] or biochemical component analysis [o]) to egg volume in 47 species of echinoderms. Data were taken from McEdward and Morgan (5), with three changes: we replaced their value for the energy content of eggs of *Clypeaster rosaceus* with the higher value recently reported by Miner *et al.* (25); we excluded *Notasterias armata* from our analysis, as McEdward and Morgan (5) concluded that it was an extreme outlier in their dataset; and we excluded *Perknaster fuscus* from our analysis, since published estimates of egg energy content for this species vary considerably (26, 27). None of these modifications significantly affect our conclusions.

=2348.5, $n = 11$) than in those whose egg energy contents were estimated by biochemical component analysis (mean = 7100.5 mJ/μl, SD = 2214.9, $n = 14$; Student's t test, $P = 0.011$). This difference was not evident in the lecithotrophs, where mean volume-specific energy density was similar in both groups (dichromate oxidation mean = 11655.2 mJ/μl, SD = 1303.2, $n = 9$; biochemical component mean = 12893.5 mJ/μl, SD = 3434.8, $n = 13$; t test, $P = 0.318$).

We can think of two explanations for this result. First, many of the data on energy contents of small eggs of echinoderms are derived from studies by only two groups of investigators: Strathmann and Vedder (16), who used dichromate oxidation, and Turner and Lawrence (17), who used biochemical component analysis. It is possible that errors associated with either group, not with the techniques used, produced the apparent differences in egg energy content. However, Strathmann and Vedder's (16) results agree well with ours for eggs of a sea urchin and two annelids (*Sabellaria cementarium* and *Serpula columbiana* [as *S. vermicularis*]); this consistency suggests that the dichromate oxidation results are correct, at least within the limits of the method. And because Turner and Lawrence's (17) data yield realistic estimates of AFDW-specific energy density that are consistent with results from direct calorimetry (18), we do not doubt that they are accurate. Instead, we suggest that dichromate oxidation systematically underestimates the energy content of small eggs. Our reasoning is as follows. Though dichromate oxidation performs well in oxidizing carbohydrates and lipids, it is known to incompletely oxidize proteins, and thus to underestimate energy contributed by proteins (10, 11, 12). In echinoderms, at least, protein concentration varies with egg size, with the smaller eggs of planktotrophs containing proportionally more protein than the larger eggs of lecithotrophs (1). Underestimates of energy content attributed to incomplete oxidation of protein by dichromate oxidation should thus be more severe for smaller eggs, consistent with the pattern that we have observed in previously published data for echinoderms (Fig. 1) and in our data on annelids (Table 1). Note that eggs of 11 of the 12 species of annelids we studied fall in the range of sizes of planktotrophic echinoderm eggs shown in Figure 1. Further, even in the limited size range of annelid eggs we studied, there is a significant positive relationship between AFDW-specific energy density and egg size (by OLS regression, ln[AFDW-specific energy density] on ln[volume], $r^2 = 0.60$), consistent with the hypothesis that underestimates of energy content associated with the technique of dichromate oxidation are more severe for smaller eggs. We believe that the data that we have reported here on egg volume and AFDW in annelids (Table 1) are accurate, but we have no confidence in the accuracy of our energy content or energy density estimates and report them only to illustrate this systematic problem with dichromate oxidation.

These results lead us to suggest that dichromate oxidation should not be used to estimate total egg energy content in marine invertebrates. One problem, illustrated for echinoderms in Figure 1, is that the magnitude of the error associated with incomplete oxidation of protein may vary with egg size. One can try to correct this potential error by independently measuring egg protein content and then applying a correction factor to account for incomplete oxidation of that material, as suggested by several authors (11, 12). However, a second problem may complicate this correction—that is, different proteins appear to be incompletely oxidized to different degrees by dichromate oxidation (12). Thus there is potential error associated not only with variation in protein concentration in eggs, but also with variation in the types of proteins present. Eggs of different species may vary in both types and quantity of protein present (22, 23). These issues, as well as others such as the sensitivity of dichromate oxidation to residual chloride in samples (12), suggest that when estimates of the energy contents of eggs or other protein-rich tissues are desired, other techniques will generally be preferable to dichromate oxidation. If only relative estimates of egg energy content are required for a particular study (*e.g.*, do eggs of species A contain more or less energy than those of species B?), then, because energy content generally appears to be correlated with egg size (1, 6, 7), simple estimates of egg volume may well be sufficient. If absolute measures are required (*e.g.*, for studies of the scaling of energy content with egg size), one can use direct calorimetry (10) or elemental analysis (24), or one can independently measure carbohydrate, protein, and lipid fractions and sum their energetic contributions. The latter technique, in particular, is suitable for analyzing the relatively small amounts of tissue often available in studies of marine invertebrate eggs. Further, though it is more laborious than dichromate oxidation and is subject to its own potential problems (in particular, how to deal with the "remainder" fraction of egg AFDW that is often unaccounted for by the separate component assays: 1, 9), biochemical component analysis has the pleasing property of yielding plausible data on energy content for eggs of all sizes.

Acknowledgments

We thank D. Duggins, K. Fauchald, K. Hayes, W. Lee, S. Reed, H. Reichardt, J. Simon, and C. Staude for help collecting annelids. H. ten Hove kindly identified *Hydroides sanctaecrucis*. Discussions with M. Jacobs, B. Miner, R. Strathmann, and K. Zigler helped to clarify our argument and writing, as did the comments of two reviewers. We thank the Smithsonian Marine Station at Fort Pierce and the Friday Harbor Laboratories for laboratory space and sup-

port. Smithsonian Marine Station at Fort Pierce Contribution #591.

Literature Cited

1. **Jaeckle, W. B. 1995.** Variation in the size, energy content and biochemical composition of invertebrate eggs: correlates to the mode of larval development. Pp. 49–77 in *Ecology of Marine Invertebrate Larvae*, L. McEdward, ed. CRC Press, Boca Raton, FL.
2. **Needham, J. 1963.** *Chemical Embryology*, Vol. 1. Hafner Publishing, London.
3. **Roff, D. A. 1992.** *The Evolution of Life Histories*. Chapman and Hall, New York.
4. **Vance, R. 1973.** On reproductive strategies in marine benthic invertebrates. *Am. Nat.* **107:** 339–352.
5. **McEdward, L. R., and K. H. Morgan. 2001.** Interspecific relationships between egg size and the level of parental investment per offspring in echinoderms. *Biol. Bull.* **200:** 33–50.
6. **Clark, A. 1993.** Egg size and egg composition in polar shrimps (Caridea: Decapoda). *J. Exp. Mar. Biol. Ecol.* **168:** 189–203.
7. **Anger, K., G. S. Moreira, and D. Ismael. 2002.** Comparative size, biomass, elemental composition (C, N, H) and energy concentration of caridean shrimp eggs. *Invertebr. Reprod. Dev.* **42:** 83–93.
8. **Strickland, J. D. H., and T. R. Parsons. 1968.** A practical handbook of seawater analysis. *Bull. Fish. Res. Board Can.* **167:** 1–311.
9. **McEdward, L. R., and L. K. Coulter. 1987.** Egg volume and energetic content are not correlated among sibling offspring of starfish: implications for life-history theory. *Evolution* **41:** 914–917.
10. **Paine, R. T. 1971.** The measurement and application of the calorie to ecological problems. *Annu. Rev. Ecol. Syst.* **2:** 145–164.
11. **Crisp, D. J. 1984.** Energy flow measurements. Pp. 284–372 in *Methods for the Study of Marine Benthos*, N.A. Holme and A.D. McIntyre, eds. Blackwell, London.
12. **Gosselin, L. A., and P. Y. Qian. 1999.** Analysing energy content: a new micro-assay and an assessment of the applicability of acid dichromate assays. *Hydrobiologia* **390:** 141–151.
13. **Strathmann, R. R. 1967.** Estimating the organic carbon content of phytoplankton from cell volume or plasma volume. *Limnol. Oceanogr.* **12:** 411–418.
14. **Prothero, J. 1986.** Methodological aspects of scaling in biology. *J. Theor. Biol.* **118:** 259–286.
15. **Gnaiger, E. 1983.** Calculation of energetic and biochemical equivalents of respiratory oxygen consumption. Pp. 337–345 in *Polarographic Oxygen Sensors*, E. Gnaiger and H. Forstner, eds. Springer-Verlag, New York.
16. **Strathmann, R. R., and K. Vedder. 1977.** Size and organic content of eggs of echinoderms and other invertebrates as related to developmental strategies and egg eating. *Mar. Biol.* **39:** 305–309.
17. **Turner, R. L., and J. M. Lawrence. 1979.** Volume and composition of echinoderm eggs: implications for the use of egg size in life-history models. Pp. 25–40 in *Reproductive Ecology of Marine Invertebrates*, S.E. Stancyck, ed. University of South Carolina Press, Columbia.
18. **Thompson, R. J. 1982.** The relationship between food ration and reproductive effort in the green sea urchin *Strongylocentrotus droebachiensis*. *Oecologia* **56:** 50–57.
19. **McEdward, L. R. 1986.** Comparative morphometrics of echinoderm larvae. I. Some relationships between egg size and initial larval form in echinoids. *J. Exp. Mar. Biol. Ecol.* **96:** 251–265.
20. **Moreno, G., P. Selvakumaraswamy, M. Byrne, and O. Hoegh-Guldberg. 2001.** A test of the ash-free dry weight technique on the developmental stages of *Patiriella* spp. *Limnol. Oceanogr.* **46:** 1214–1220.
21. **Rothschild, L., and H. Barnes. 1953.** The inorganic constituents of the sea-urchin egg. *J. Exp. Biol.* **30:** 534–544.
22. **Byrne, M., A. Cerra, and J. T. Villinski. 1999.** Oogenic strategies in the evolution of development in *Patiriella*. *Invertebr. Reprod. Dev.* **36:** 195–202.
23. **Scott, L. B., W. J. Lennarz, R. A. Raff, and G. A. Wray. 1990.** The "lecithotrophic" sea urchin *Heliocidaris erythrogramma* lacks typical yolk platelets and yolk glycoproteins. *Dev. Biol.* **138:** 188–193.
24. **Gnaiger, E., and G. Bitterlich. 1984.** Proximate biochemical composition and caloric content calculated from elemental CHN analysis: a stoichiometric concept. *Oecologia* **62:** 289–298.
25. **Miner, B. G., J. D. Cowart, and L. R. McEdward. 2002.** Egg energetics for the facultative planktotroph *Clypeaster rosaceus* (Echinodermata: Echinoidea), revisited. *Biol. Bull.* **202:** 97–99.
26. **McClintock, J. B., and J. S. Pearse. 1986.** Organic and energetic content of eggs and juveniles of Antarctic echinoids and asteroids with lecithotrophic development. *Comp. Biochem. Physiol.* **85A:** 341–345.
27. **Shilling, F. M., and D. T. Manahan. 1994.** Energy metabolism and amino acid transport during early development of Antarctic and temperate echinoderms. *Biol. Bull.* **187:** 398–407.

Reference: *Biol. Bull.* **207:** 72–75. (August 2004)

Circatidal and Circadian Rhythms of Locomotion in *Limulus polyphemus*

CHRISTOPHER C. CHABOT[1,*], JEFFREY KENT[1], AND WINSOR H. WATSON III[2]

[1]*Department of Biological Sciences, Plymouth State University, Plymouth, New Hampshire 03264; and*
[2]*Department of Zoology, University of New Hampshire, Durham, New Hampshire 03824*

The nocturnal increases in the sensitivity of the lateral eye of Limulus polyphemus, *the species of horseshoe crab found along the Atlantic coast, have been firmly established as being controlled by an endogenous circadian clock (1, 2, 3) located in the brain (4). Virtually nothing is known, however, about the control of the animal's behavioral rhythms of mating and spawning that are observed in the intertidal zone during high tides in late spring (5, 6, 7). Many other marine species, especially intertidal crabs, exhibit similar rhythmic behaviors that have been demonstrated to be under the control of endogenous clocks that are circatidal (8, 9, 10, 11, 12), circadian (10, 12), or both. While there is some evidence that the activity of juvenile horseshoe crabs is primarily nocturnal (13, 14), and possibly controlled by a circadian clock (14), we know of no published work showing that locomotor activity in the adult is endogenously controlled on either a 12.4-h (circatidal) or 24-h (circadian) basis. We report here that locomotor activity in adult individuals of* L. polyphemus *is endogenously modulated on both a circatidal and a circadian basis and that when the animals are subjected to a light-dark (LD) cycle, most activity occurs at night.*

The locomotor activity of individual adult horseshoe crabs was recorded using activity chambers located in recirculating aquaria. Animals were exposed to three conditions: a 12:12 LD cycle, at 11–14 °C ("fall" conditions, LD_1), a 14:12 LD cycle, at 17–21 °C ("summer" conditions, LD_2), and constant darkness (DD). Typical records of the locomotor activity of three horseshoe crabs exposed to these three different photoperiods are presented in Figure 1. Circatidal rhythms were observed in all animals. While significant activity rhythms (15) in the tidal range (12.4 h) were found in only 3 of 6 animals (*tau* = 12.83 ± 0.78 h [mean ± SEM]) during LD_1, in LD_2, significant tidal rhythms (12.2 ± 0.1 h) were observed in all animals. In some cases in LD_2 (4 of 6 animals), clear free-running rhythms were sometimes apparent, (Fig. 1; middle, bottom panels), while in other cases the activity appeared to synchronize to the LD cycles (Fig. 1: top). In DD, circatidal rhythms (12.6 ± 0.2 h) were found in 5 of 6 animals (Fig. 1; all panels).

Most animals (5 of 6 in LD_1; 6 of 6 in LD_2) exhibited significant rhythms in the circadian range (*tau* = 24.29 ± 0.14 h). Periodogram analyses (15) and visual inspection indicated that 5 of the 6 animals tested synchronized their activity to the initial 12:12 LD cycle (LD_1). The single animal that did not thus synchronize had a very low level of activity. Significantly more activity occurred during the dark phase than the light phase in 4 of 6 animals (Fig. 1; top and bottom [but not middle] panels). The average period (*tau*) for these animals in the daily (24-h) range in LD_1 was 24.12 ± 0.09 h. Upon subsequent exposure to "summer" conditions (LD_2), 3 (of 6) animals remained synchronized to the LD cycle (Fig. 1; top panel). In others (2 of 6), this apparent synchronization was not stable (Fig. 1; middle, days 10–18 and days 29–42) and, in still another animal, the synchronization, if any, was unclear (Fig. 1: bottom). Animals that both synchronized *and* showed a clear onset of activity initiated their activity a significant amount of time (1.7 ± 0.1 h; $P < 0.005$) before the lights went out during LD_2 but not LD_1 (1.1 ± 0.5 h; $P > 0.15$). Significantly more activity occurred during D *versus* L periods in 3 of 6 animals (Fig. 1: top panel only). In constant darkness (DD), all animals also expressed significant circadian rhythms (25.27 ± 0.69 h; Fig. 1, all panels). In addition, the activity patterns of 3 of 6 animals in DD exhibited evidence of entrainment based on the similarity of phasing with the previous LD cycle (Fig. 1; top, middle). *L. polyphemus* was significantly more active overall during LD_2 than during LD_1 and DD ($P < 0.03$). Neither circatidal ($P > 0.78$) nor

Received 12 February 2004; accepted 7 June 2004.

* To whom all correspondence should be addressed. E-mail: chrisc@mail.plymouth.edu

circadian ($P > 0.51$) *tau* values were significantly affected by photoperiod.

Our results provide the first evidence for an endogenous circatidal rhythm in *L. polyphemus*. While field studies (5, 6, 16, 17, 18) and a wealth of anecdotal observations in popular literature have cited the propensity of horseshoe crabs to mate during high tides, this is the first study to demonstrate that an endogenous clock may set the timing for this behavior. Other marine invertebrates, including fiddler crabs and green crabs, have also been shown to possess endogenous circatidal locomotor rhythms that can be entrained by tidally related stimuli (19) such as inundation (20), salinity changes (21), and temperature changes (20). The cues that horseshoe crabs use in their natural habitat to synchronize their mating activities to the natural tidal cycle are currently unknown.

We also provide evidence that the locomotor activity of adult individuals of *L. polyphemus* can be synchronized to an LD cycle, and that these rhythms will persist in constant conditions. This finding is consistent with a previous report showing that juveniles (14) of *L. polyphemus* exhibit circadian rhythms of locomotion. Interestingly, however, whereas 100% of the adult animals in the current study (6 of 6) exhibited significant circadian rhythms in DD, only 40% (2 of 5) of the juvenile animals did (in DD; 14). It is not surprising that *L. polyphemus* exhibits circadian rhythms of locomotion, because circadian modulation of lateral eye visual sensitivity—especially the electroretinogram (ERG)—has been very well documented, and it is clear that horseshoe crabs possess one or more circadian clocks (22, 23, 24, 4, 25, 26, 1, 3). However, we have two reasons to suspect that the timing mechanism that mediates this rhythm of visual sensitivity may be different than the mechanism that controls the timing of locomotion. First, in none of the papers cited above that document circadian control of visual sensitivity is there any mention or indication of a tidal rhythm. Second, although there was clear evidence of rhythmic activity in most of the animals exposed to LD, in several (Fig. 1; middle, bottom panels) the activity was coordinated with the LD cycle only for short periods of time—that is, there was not consistent synchronization or entrainment. This type of modulation of ERG activity also has not been reported in the literature on electroretinograms in *L. polyphemus*.

Our results also indicate that under the laboratory conditions to which our animals were exposed, horseshoe crabs are primarily nocturnally active. Of the animals that appeared stably synchronized to the LD cycle (3 of 6), all were significantly more active during the night than during the day. These findings are consistent with previous studies of locomotor activity in larvae (27) and juveniles (13, 14) as well as with the large body of literature demonstrating greatly increased visual sensitivity at night (3) One field report on a Florida population of *L. polyphemus* also indicates a preference for mating at night (6), but interestingly, other studies in Florida report a preference for diurnal patterns of mating (17). Furthermore, juveniles of *L. polyphemus* in Florida also show a similar preference for diurnal activity in the intertidal zone (5, 16). The issue is further complicated by a study of *L. polyphemus* in Cape Cod, Massaehusetts, in which animals were found mating both during the day and at night (7), which is also the pattern in New Hampshire (Watson, unpubl. obs.) where our animals were caught, and in Maine (S. Schaller, pers. comm., Bar Mills Ecological). While the factors associated with the differences in behavior observed between the studies remain to be determined, it is clear from our study that LD cycles do affect both circadian and circatidal rhythms in the laboratory. Several of our animals did not remain completely entrained when exposed to LD (Fig. 1; middle, bottom panels), suggesting that the LD cycle may be a less important stimulus in the temporal organization of locomotor activity than it is for the physiological rhythm of visual sensitivity. While our results do not directly show that the circatidal activity rhythms observed in *L. polyphemus* actually entrain to LD cycles, the expression of the timing of these rhythms appears to at least be modulated by the LD cycle. Similar modulating effects of LD on circatidal locomotor rhythms have been observed in some species of crabs (19) but not in others (28).

Our results also show that *L. polyphemus* can exhibit clear circatidal rhythms in locomotion in the laboratory, even during nonbreeding times of years (November–February). In the field, the appearance of millions of horseshoe crabs along the eastern seaboard, primarily during April through July, clearly indicates a strong seasonal preference for mating. *L. polyphemus* has been reported to be much less active at other times of the year (18) and, in winter, either to burrow in the mud in or around estuaries or to move to the open ocean where it has been found far out on the continental shelf (29). While annual changes in the timing of behavior (that are often strongly influenced by photoperiod) have been well documented in a wide variety of species (30), we are surprised that circatidal rhythms were expressed during this time of year. Whether horseshoe crabs normally express tidal rhythms throughout the year, but these are not observed, or whether the rhythms we observed were initiated by the longer photoperiod or the increased temperature, remains to be elucidated.

Acknowledgments

We thank Brandy Adams, Jason Lotterhand, Jordan Murphy, and Michael Zegarelli for help in conducting the experiments.

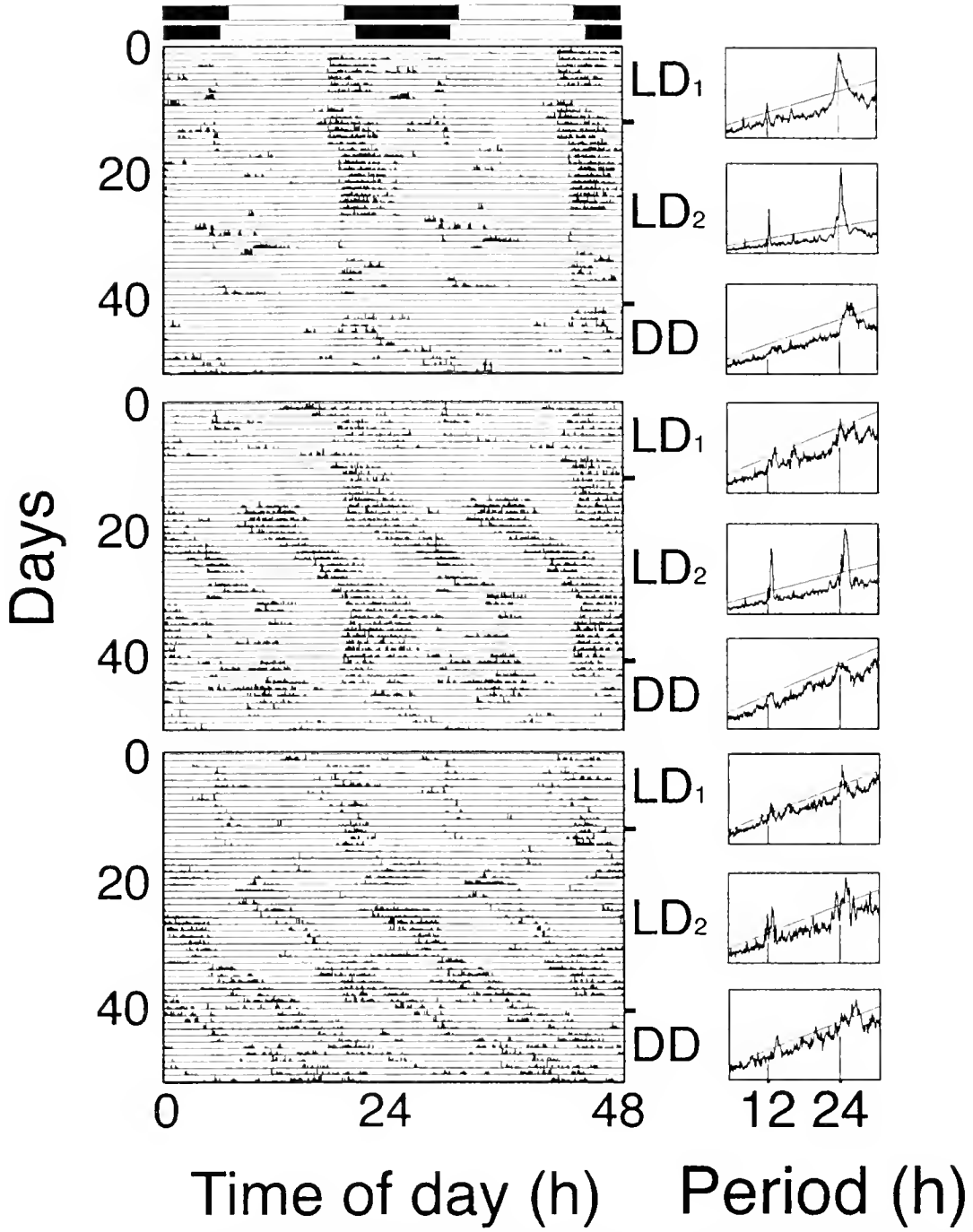

Figure 1. Locomotor activity of 3 (of the 6 tested) individuals of *Limulus polyphemus* housed in activity chambers (39 cm wide × 32 cm long × 9-cm deep) in recirculating aquaria (left panels). Data are double-plotted to facilitate visual inspection. Periodograms corresponding to the respective photoperiods and animals are presented in the right panels. Animals were exposed to three consecutive photoperiods. (1) LD_1 = 12:12 (light source: 20-W broad-spectrum fluorescent bulbs, Simkar Corp., Pittsburgh, PA; light intensity during L = 150 lux/2.8 μmol and during D = 0 lux/0 μmol), with water temperature = 11–14 °C. These conditions simulated fall temperature and photoperiod, during which *L. polyphemus* may be expected not to exhibit tidal rhythms); (2) LD_2 = 14:10; temperature = 17–21 °C. These conditions simulated summer conditions during which *L. polyphemus* would be expected to exhibit tidal rhythms. (3) DD = constant darkness; temperature = 17–21 °C. These conditions were employed to determine whether the rhythms observed in LD would persist in DD. Water was collected at the Jackson Estuarine Laboratory (Durham, NH), and the salinity was kept between 25‰ and 27‰. Although temperature varied either between 17 and 21 °C or 11 and 14 °C, neither temperature nor salinity cycled with periods near 12 or 24 h (HOBO data loggers, Onset, Pocasset, MA). In October 2002, horseshoe crabs (2 females, weighing 519 g and 676 g; 4 males, weighing 197–310 g) were caught in lobster traps in Great Bay, New Hampshire, an area that experiences semidiurnal tides. Immediately after the crabs were brought to the laboratory in Plymouth, New Hampshire, magnets were affixed to their dorsal carapace, between the lateral eyes, using cyanoacrylate glue and duct tape. Magnetic reed

Literature Cited

1. **Powers, M. K., and R. B. Barlow, Jr. 1985.** Behavioral correlates of circadian rhythms in the *Limulus* visual system. *Biol. Bull.* **169:** 578–591.
2. **Herzog, E. H., M. K. Powers, and R. B. Barlow. 1996.** *Limulus* vision in the ocean day and night: effects of image size and contrast. *Vis. Neurosci.* **13:** 31–41.
3. **Barlow, R. B., J. M. Hitt, and F. A. Dodge. 2001.** *Limulus* vision in the marine environment. *Biol. Bull.* **200:** 169–176.
4. **Barlow, R. B., Jr. 1983.** Circadian rhythms in the *Limulus* visual system. *J. Neurosci.* **3:** 856–870.
5. **Rudloe, A. 1979.** *Limulus polyphemus:* a review of the ecologically significant literature. Pp. 27–35 in *Biomedical Applications of the Horseshoe Crab (Limulidae).* E. Cohen, ed. Alan Liss, New York.
6. **Rudloe, A. 1980.** The breeding behavior and patterns of movement of horseshoe crabs, *Limulus polyphemus,* in the vicinity of breeding beaches in Apalachee Bay, FL. *Estuaries* **3:** 177–183.
7. **Barlow, R. B., Jr., M. K. Powers, H. Howard, and L. Kass. 1986.** Migration of *Limulus* for mating: relation to lunar phase, tide height, and sunlight. *Biol. Bull.* **171:** 310–329.
8. **Bennet, M. F., J. Shriner, and R. A. Brown. 1957.** Persistent tidal cycles of spontaneous motor activity in the fiddler crab, *Uca pugnax. Biol. Bull.* **112:** 267–275.
9. **Naylor, E. 1958.** Tidal and diurnal rhythms of locomotor activity in *Carcinus maenas. J. Exp. Biol.* **35:** 602–610.
10. **Palmer, J. D. 1973.** Tidal rhythms: the clock control of the rhythmic physiology of marine organisms. *Biol. Rev.* **48:** 377–418.
11. **Lehmann, U. 1975.** Interpretation of entrained and free-running locomotor activity patterns of *Uca.* Pp. 77–92 in *Biological Rhythms in the Marine Environment,* P. J. DeCoursey, ed. University of South Carolina Press, Columbia, SC.
12. **De Coursey, P. J. 2003.** The behavioral ecology and evolution of biological timing systems. Pp. 67–106 in *Chronobiology: Biological Timekeeping,* J. C. Dunlap, J. J. Loros, and P. J. DeCoursey, eds. Sinauer Associates, Sunderland, MA.
13. **Casterlin, M., and W. Reynolds. 1979.** Diel locomotor activity pattern of juvenile *Limulus polyphemus* Linnaeus. *Rev. Can. Biol.* **38:** 43–44.
14. **Borst, D., and R. B. Barlow. 2002.** Circadian rhythms in locomotor activity of juvenile horseshoe crabs. *Biol. Bull.* **203:** 227–228.
15. **Sokolove, P. G., and W. N. Bushell. 1978.** The chi-square periodogram: its utility for analysis of circadian rhythms. *J. Theor. Biol.* **74:** 131–160.
16. **Rudloe, A. 1978.** Some ecologically significant aspects of the behavior of the horseshoe crab, *Limulus polyphemus.* Ph.D. thesis, The Florida State University, Tallahassee, FL.
17. **Cohen, J. A., and H. J. Brockman. 1983.** Breeding activity and mate selection in the horseshoe crab, *Limulus polyphemus. Bull. Mar. Sci.* **33:** 274–281.
18. **Shuster, C. N., Jr. 2001.** Two perspectives: horseshoe crabs during 420 million years worldwide, and the past 150 years in Delaware Bay. Pp. 17–40 in *Limulus in the Limelight,* J. T. Tanacredi, ed. Kluwer Academic/Plenum Publishers, New York.
19. **Honegger, H. W. 1973.** Rhythmic motor activity responses of the California fiddler crab, *Uca crenulata* to artificial light conditions. *Mar. Biol.* **18:** 19–31.
20. **Williams, B. G., and E. Naylor. 1969.** Synchronization of the locomotor tidal rhythm of *Carcinus. J. Exp. Biol.* **51:** 715–725.
21. **Forward, R. B., J. K. Douglass, and B. E. Kenney. 1986.** Entrainment of the larval release rhythm of the crab *Rhithropanopeus harrissii* by cycles of salinity change. *Mar. Biol.* **90:** 537–544.
22. **Barlow, R. B., Jr., S. J. Bobarski, Jr., and M. L. Brachman. 1977.** Efferent optic nerve fibers mediate circadian rhythms in the *Limulus* eye. *Science* **197:** 86–89.
23. **Chamberlain, S. C., and R. B. Barlow, Jr. 1979.** Light and efferent activity control rhabdom turnover in *Limulus* photoreceptors. *Science* **206:** 361–363.
24. **Barlow, R. B., Jr., S. C. Chamberlain, and J. Z. Levinson. 1980.** *Limulus* brain modulates the structure and function of the lateral eyes. *Science* **210:** 1037–1039.
25. **Kaplan E., and R. B. Barlow, Jr. 1980.** Circadian clock in *Limulus* brain increases and decreases noise of retinal photoreceptors. *Nature* **286:** 393–395.
26. **Chamberlain, S. C., and R. B. Barlow, Jr. 1984.** Transient membrane shedding in *Limulus* photoreceptors: control mechanisms under natural lighting. *J. Neurosci.* **4:** 2792–2810.
27. **Rudloe, A. 1979.** Locomotor and light responses of larvae of the horseshoe crab, *Limulus polyphemus. Biol. Bull.* **157:** 494–505.
28. **Lehmann, U. 1976.** Interpretation of entrained and free-running locomotor activity patterns of *Uca.* Pp. 77–92 in *Biological Rhythms in the Marine Environment,* P. J. DeCoursey, ed. Univ. of South Carolina Press, Columbia, SC.
29. **Shuster, C. N., Jr. 2001.** Tracks and trails. Pp. 17–40 in *Limulus in the Limelight,* J. T. Tanacredi, ed. Kluwer Academic/Plenum Publishers, New York.
30. **Goldman, B., E. Gwinner, F. J. Karsch, D. Saunders, I. Zucker, and G. F. Ball. 2004.** Circannual rhythms and photoperiodism. Pp. 107–144 in *Chronobiology: Biological Timekeeping,* J. C. Dunlap, J. J. Loros, and P. J. DeCoursey, eds. Sinauer Associates, Sunderland, MA.

switches (one per activity chamber) that produced a voltage change whenever a crab passed under one were used to monitor activity. The animals were not fed after being caught and were always individually housed in activity chambers. A "ceiling" (9-cm high) was used to prevent the animals from flipping over and becoming immobilized. In addition, three bricks were placed on the ceiling to weigh it down and to create a shielded, darker area over about half of each activity chamber to provide a shelter. Activity was recorded on a CPU-based data collection system and analyzed using the ClockLab suite of programs for analysis of time-series data (Actimetrics, Evanston, IL). Significance of rhythmicity was determined both visually and by chi-square periodogram analysis ($P < 0.01$; 15). The period (*tau*) in the circadian range for each individual during each experiment was determined by recording the highest significant peak on the periodogram between 22 and 26 h or for circatidal rhythms, between 10 and 14 h. Entrainment to LD cycles was ascertained by visually comparing the onsets of activity during the last several days in LD_2 to the onsets during the first several days in DD. Phase angles were determined by comparing the difference between the onset of the LD cycles and the onset of activity for each animal (as determined by best-drawn eye-fit lines). To determine a preference for activity during L (diurnality) or D (nocturnality), the amount of activity during L and D for each day for each animal was summed. Paired Student's *t*-test or repeated measures ANOVA ($P < 0.05$; Statview, ver. 4.51, Abacus Concepts, Berkeley, CA) was used to determine statistical significance between means.

THE BIOLOGICAL BULLETIN
(www.biolbull.org)
2004 SUBSCRIPTION FORM
(VOLUMES 206-207, 6 ISSUES)

(please print)
NAME: _____
INSTITUTION: _____
ADDRESS: _____
CITY: _____ **STATE:** _____
POSTAL CODE: _____ **COUNTRY:** _____
TELEPHONE: _____ **FAX:** _____
E-MAIL ADDRESS _____

All subscriptions run on the calendar year; price includes both print and online journals

❒ Please send me a 2004 subscription to *The Biological Bulletin* at the rate indicated below:

❒ Individual: $120.00 (6 ISSUES) ❒ Institutional : $325.00 (6 ISSUES)
❒ Individual: $70.00 (3 ISSUES) ❒ Institutional : $165.00 (3 ISSUES)

Check one: ❒ February April June or ❒ August October December

❒ Please send me the following back issue(s): _____

❒ Individual: at $25.00 (PER ISSUE) ❒ Institutional : at $75.00 (PER ISSUE)

Delivery Options

_____ Surface Delivery (Surface delivery is included in the subscription price.)
_____ Air delivery (Please add the correct amount to your payment.)

❒ U.S. and Canada: $46.00 ❒ Mexico: $60.00 ❒ All other locations: $100.00

Payment Options

_____ Enclosed is my check or U.S. money order for $ _____payable to The Marine Biological Laboratory

_____ Please charge my ❒ VISA, ❒ MasterCard ❒ Discover Card $_____

_____ Please send me an invoice. (Note: Payment must be received before subscription commences.)

Account No.: _____ **Exp. Date:** _____

Signature: _____ **Date:** _____

Return this form with your check or credit information to:
Marine Biological Laboratory
Subscription Office ◆ The Biological Bulletin ◆7 MBL Street ◆ Woods Hole, MA 02543-1015

Director/Chief Executive Officer
Marine Biological Laboratory

The Marine Biological Laboratory (MBL), an international research and educational institution founded in 1888 and located in Woods Hole, Massachusetts, invites applications and nominations for the position of Director, who will serve as the institution's Chief Executive Officer.

The MBL is an international resource that provides a stimulating and productive research base for scientists in the areas of basic biology, biomedicine and environmental science. For more than a century, the Laboratory has prepared young biologists for leadership positions in research and teaching through its internationally recognized education programs. The MBL recently completed a visionary strategic plan that stresses interdisciplinary research and innovations in science education, the details of which are available at <http://www.mbl.edu/inside/what/planning/index.html>.

The Laboratory hosts a year-round staff of more than 290 scientists and support personnel, including 69 Ph.D.-level investigators working in more than 30 laboratories and research centers. During the summer months, an additional 1400 scientists and students from 300 institutions worldwide come to the MBL to conduct research and to train in modern techniques through intensive laboratory-based courses.

The Director reports to the Board of Trustees and oversees the scientific direction of the Laboratory, develops fundraising priorities, provides general supervision of the Laboratory, and controls the business of the Corporation. Candidates should have a strong record of scientific leadership, fundraising capability, and a demonstrated ability to form consensus among individuals with different perspectives and to lead them in achieving policy objectives.

It is anticipated that the appointment will commence July 1, 2006. The Marine Biological Laboratory is located in Woods Hole, MA, a village rich with scientific inquiry and discovery as well as one of the most beautiful locations on Cape Cod. Additional information about the MBL is available at <www.mbl.edu>.

Please send nominations or your letter of interest and resumé to:

MBL Director/CEO Search Committee
c/o Human Resources
Marine Biological Laboratory
7 MBL Street
Woods Hole, MA 02543

Review of applications will begin September 1, 2004, and continue until a successful applicant is identified.

The Marine Biological Laboratory is an Affirmative Action/Equal Employment Opportunity Employer

Confused

Convinced.

R&D 100 Winner

Axiovert 200

ApoTome.
The revolution in fluorescence microscopy.

Developed to provide distinct optical sections, ApoTome offers crucial advantages in fluorescence microscopy of thick specimens – enhanced image quality, greater sharpness, more contrast and optical resolution in the axial direction. Impressive benefits rounded off by higher performance and free choice of dyes. Advance the performance level of your digital imaging system to new heights – with revolutionary ease, speed and cost-effectiveness.

Carl Zeiss MicroImaging, Inc. Thornwood, NY. 800-233-2343, www.zeiss.com/apotome.

ZEISS

We make it visible.

October 2004 Volume 207 • Number 2

THE BIOLOGICAL BULLETIN

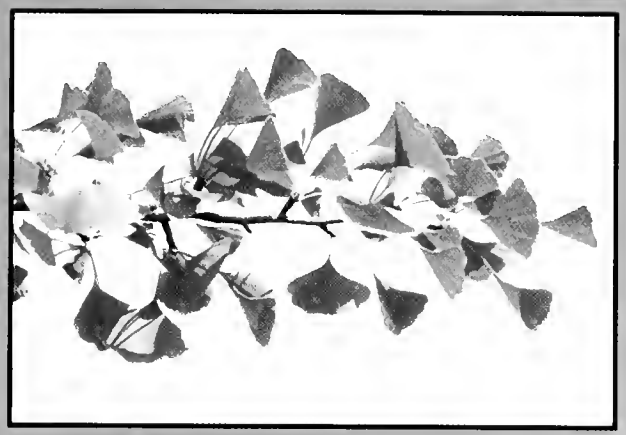

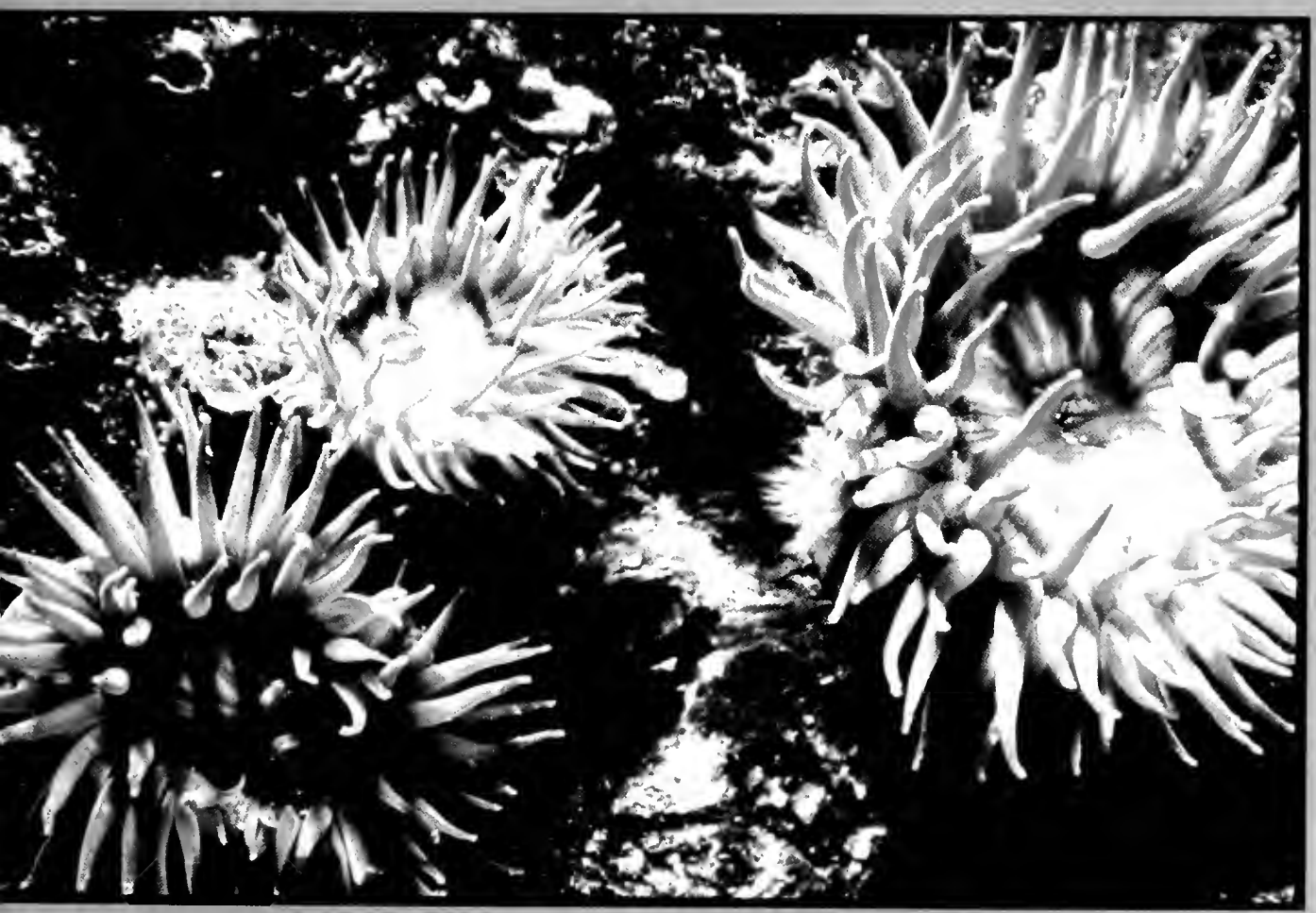

Published by the Marine Biological Laboratory

Woods Hole, Massachusetts

WHEN IT COMES TO LIVE CELL MICROSCOPY,

FOR EVERY ACTION REACTION THERE'S A SIMULTANEOUS ACTION REACTION.

CONFOCAL LASER SCANNING MICROSCOPE.

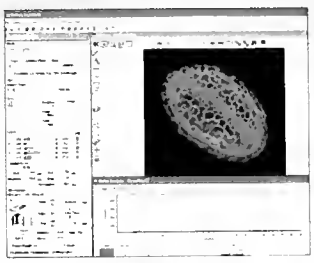

REAL-TIME OBSERVATION

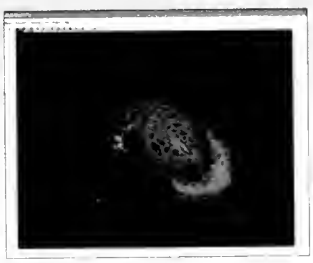

ADVANCED ANALYSIS

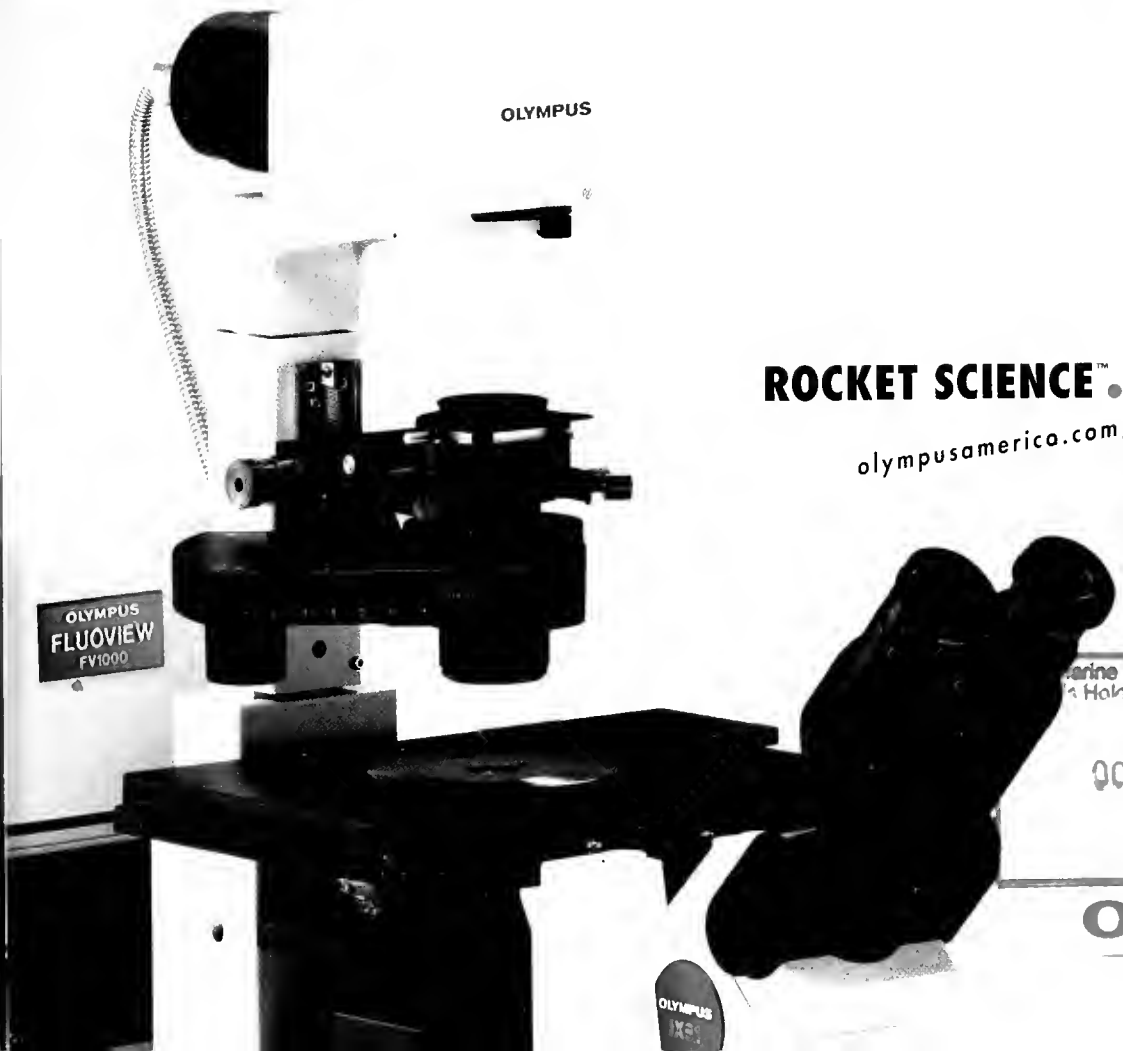

ROCKET SCIENCE™.

olympusamerica.com/microscopes 800-455-8236

OLYMPUS

Your Vision, Our Future

Cover

The larger image on the cover of this issue shows three specimens of *Anthopleura elegantissima*, a sea anemone (disk diameter ~2 cm); the animals were photographed on the rocky shore of San Juan Island, off the coast of Washington. The different colors of the anemones are due to their algal symbionts: the single brown anemone primarily contains the familiar dinoflagellate symbionts from the genus *Symbiodinium* (commonly called "zooxanthellae"), whereas the two green anemones contain algae from the phylum Chlorophyta. The proportion of algal partners in each host is influenced by light and temperature; in particular, the number of anemones hosting chlorophytes increases in the shade and at higher latitudes. But the anemones on the cover are obviously living together and, indeed, could be clone mates; so the basis for the distribution of symbiont types is still uncertain.

Also obscure is the taxonomy of the green algal symbionts in *Anthopleura* species. Previous investigations of these symbionts led to the presumption that they are marine species of the genus *Chlorella*, and that they are therefore related to similar algae associated with freshwater animals such as hydras and sponges, whence the designation "zoochlorellae." But *Chorella* is a paraphyletic taxon; *i.e.*, the species within it do not have a common origin. Thus, the identity of the green symbionts within *Anthopleura* and their relationship with freshwater algae are in question.

In this issue of *The Biological Bulletin* (p. 87), Louise A. Lewis and Gisèle Muller-Parker report on a phylogenetic analysis of 18S rDNA and the *rbcL* gene, which are encoded, respectively, by the nucleus and plastid of green symbionts isolated from *Anthopleura elegantissima*. The results suggest that these symbionts are members of a well-supported but highly divergent clade comprising species of small, spherical green algae—both symbiotic and free-living—which are distinct from species of *Chorella* in freshwater. The clade includes a lichen symbiont (*Coccomyxa glaronensis*), a free-living alga (*Paradoxia*), and the small green endophytes in the gametophytic tissues of *Ginkgo biloba*, a gymnosperm "living fossil." (Ginkgo leaves yellowing against a fall sky appear on the cover.)

Because this newly identified clade of green algae participates in a very wide range of symbiotic interactions, Lewis and Muller-Parker propose that members of the lineage share a genetic predisposition to form symbiotic relationships and are, therefore, potential models for investigating how such associations are established and maintained. Studies of the growth rates, nutrition, and physiological requirements of these algae, both in the host and in culture, should provide insight into the features that promote their symbioses.

The photograph of *Anthopleura elegantissima* was taken in the field by Christopher Wojcik, and the image of the ginkgo leaves was provided by Louise A. Lewis (University of Connecticut). Beth Liles (Marine Biological Laboratory) designed the cover.

THE
BIOLOGICAL BULLETIN
OCTOBER 2004

Published by
MARINE BIOLOGICAL LABORATORY
WOODS HOLE, MASSACHUSETTS

http://www.biolbull.org

CONTENTS

VOLUME 207, NO. 2: OCTOBER 2004

RESEARCH NOTES

SYMBIOSIS AND PARASITOLOGY

DEVELOPMENT AND REPRODUCTION

ECOLOGY AND EVOLUTION

NEUROBIOLOGY AND BEHAVIOR

* * *

THE BIOLOGICAL BULLETIN

THE BIOLOGICAL BULLETIN is published six times a year by the Marine Biological Laboratory, 7 MBL Street, Woods Hole, Massachusetts 02543.

Subscriptions and similar matter should be addressed to Subscription Administrator, THE BIOLOGICAL BULLETIN, Marine Biological Laboratory, 7 MBL Street, Woods Hole, Massachusetts 02543. Subscription includes both print and online journals. Subscription per year (six issues, two volumes): $325 for libraries; $120 for individuals. Subscription per volume (three issues): $165 for libraries; $70 for individuals. Back and single issues (subject to availability): $75 for libraries; $25 for individuals.

Communications relative to manuscripts should be sent to Michael J. Greenberg, Editor-in-Chief, or Pamela Clapp Hinkle, Managing Editor, at the Marine Biological Laboratory, 7 MBL Street, Woods Hole, Massachusetts 02543. Telephone: (508) 289-7149. FAX: 508-289-7922. E-mail: pclapp@mbl.edu.

http://www.biolbull.org

THE BIOLOGICAL BULLETIN is indexed in bibliographic services including *Index Medicus* and MEDLINE, *Chemical Abstracts, Current Contents, Elsevier BIOBASE/Current Awareness in Biological Sciences,* and *Geo Abstracts.*

Printed on acid free paper,
effective with Volume 180, Issue 1, 1991.

POSTMASTER: Send address changes to THE BIOLOGICAL BULLETIN, Marine Biological Laboratory, 7 MBL Street, Woods Hole, MA 02543.

Periodicals postage paid at Woods Hole, MA, and additional mailing offices.
ISSN 0006-3185

INSTRUCTIONS TO AUTHORS

The Biological Bulletin accepts outstanding original research reports of general interest to biologists throughout the world. Papers are usually of intermediate length (10–40 manuscript pages). A limited number of solicited review papers may be accepted after formal review. A paper will usually appear within four months after its acceptance.

Very short, especially topical papers (less than 9 manuscript pages including tables, figures, and bibliography) will be published in a separate section entitled "Research Notes." A Research Note in *The Biological Bulletin* follows the format of similar notes in *Nature.* It should open with a summary paragraph of 150 to 200 words comprising the introduction and the conclusions. The rest of the text should continue on without subheadings, and there should be no more than 30 references. References should be referred to in the text by number, and listed in the Literature Cited section in the order that they appear in the text. Unlike references in *Nature,* references in the Research Notes section should conform in punctuation and arrangement to the style of recent issues of *The Biological Bulletin.* Materials and Methods should be incorporated into appropriate figure legends. See the article by Lee (October 2003, Vol. **205:** 99–101) for sample style. A Research Note will usually appear within two months after its acceptance.

The Editorial Board requests that regular manuscripts conform to the requirements set below; those manuscripts that do not conform will be returned to authors for correction before review.

1. ***Manuscripts.*** Manuscripts, including figures, should be submitted in quadruplicate, with the originals clearly marked. (Xerox copies of photographs are not acceptable for review purposes.) Please include an electronic copy of the text of the manuscript. Label the disk with the name of the first author and the name and version of the wordprocessing software used to create the file. If the file was not created in some version of Microsoft Word, save the text in rich text format (rtf). The submission letter accompanying the manuscript should include a telephone number, a FAX number, and (if possible) an E-mail address for the corresponding author. The original manuscript must be typed in no smaller than 12 pitch or 10 point, using double spacing (*including* figure legends, footnotes, bibliography, etc.) on one side of 16- or 20-lb. bond paper, 8 by 11 inches. Please, no right justification. Manuscripts should be proofread carefully and errors corrected legibly in black ink. Pages should be numbered consecutively. Margins on all sides should be at least 1 inch (2.5 cm). Manuscripts should conform to the *Council of Biology Editors Style Manual,* 5th Edition (Council of Biology Editors, 1983) and to American spelling. Unusual abbreviations should be kept to a minimum and should be spelled out on first reference as well as defined in a footnote on the title page. Manuscripts should be divided into the following components: Title page, Abstract (of no more than 200 words), Introduction, Materials and Methods, Results, Discussion, Acknowledgments, Literature Cited, Tables, and Figure Legends. In addition, authors should supply a list of words and phrases under which the article should be indexed.

2. ***Title page.*** The title page consists of a condensed title or running head of no more than 35 letters and spaces, the manuscript title, authors' names and appropriate addresses, and footnotes listing present addresses, acknowledgments or contribution numbers, and explanation of unusual abbreviations.

3. ***Figures.*** The dimensions of the printed page, 7 by 9 inches, should be kept in mind in preparing figures for publication. We recommend that figures be about 1 times the linear dimensions of the final printing desired, and that the ratio of the largest to the smallest letter or number and of the thickest to the thinnest line not exceed 1:1.5. Explanatory matter generally should be included in legends, although axes should always be identified on the illustration itself. Figures should be prepared for reproduction as either line cuts or halftones. Figures to be reproduced as line cuts should be unmounted glossy photographic reproductions or drawn in black ink on white paper, good-quality tracing cloth or plastic, or blue-lined coordinate paper. Those to be reproduced as halftones should be mounted on board, with both designating numbers or letters and scale bars affixed directly to the figures. All figures should be numbered in consecutive order, with no distinction between text and plate figures and cited, in order, in the text. The author's name and an arrow indicating orientation should appear on the reverse side of all figures.

Digital art: The Biological Bulletin will accept figures submitted in electronic form; however, digital art must conform to the following guidelines. Authors who create digital images are wholly responsible for the quality of their material, including color and halftone accuracy.

Format. Acceptable graphic formats are TIFF and EPS. Color submissions must be in EPS format, saved in CMKY mode.

Software. Preferred software is Adobe Illustrator or Adobe Photoshop for the Mac and Adobe Photoshop for Windows. Specific instructions for artwork created with various software programs are available on the Web at the Digital Art Information Site maintained by Cadmus Professional Communications at http://cpc.cadmus.com/da/

Resolution. The minimum requirements for resolution are 1200 DPI for line art and 300 for halftones.

Size. All digital artwork must be submitted at its actual printed size so that no scaling is necessary.

Multipanel figures. Figures consisting of individual parts (*e.g.*, panels A, B, C) must be assembled into final format and submitted as one file.

Hard copy. Files must be accompanied by hard copy for use in case the electronic version is unusable.

Disk identification. Disks must be clearly labeled with the following information: author name and manuscript number; format (PC or Macintosh); name and version of software used.

Color: The Biological Bulletin will publish color figures and plates, but must bill authors for the actual additional cost of printing in color. The process is expensive, so authors with more than one color image should—consistent with editorial concerns, especially citation of figures in order—combine them into a single plate to reduce the expense. On request, when supplied with a copy of a color illustration, the editorial staff will provide a pre-publication estimate of the printing cost.

4. ***Tables, footnotes, figure legends, etc.*** Authors should follow the style in a recent issue of *The Biological Bulletin* in preparing table headings, figure legends, and the like. Because of the high cost of setting tabular material in type, authors are asked to limit such material as much as possible. Tables, with their headings and footnotes, should be typed on separate sheets, numbered with consecutive Arabic numerals, and placed after the Literature Cited. Figure legends should contain enough information to make the figure intelligible separate from the text. Legends should be typed double spaced, with consecutive Arabic numbers, on a separate sheet at the end of the paper. Footnotes should be limited to authors' current addresses, acknowledgments or contribution numbers, and explanation of unusual abbreviations. All such footnotes should appear on the title page. Footnotes are not normally permitted in the body of the text.

5. ***Literature cited.*** In the text, literature should be cited by the Harvard system, with papers by more than two authors cited as Jones *et al.*, 1980. Personal communications and material in preparation or in press should be cited in the text only, with author's initials and institutions, unless the material has been formally accepted and a volume number can be supplied. The list of references following the text should be headed Literature Cited, and must be typed double spaced on separate pages, conforming in punctuation and arrangement to the style of recent issues of *The Biological Bulletin*. Citations should include complete titles and inclusive pagination. Journal abbreviations should normally follow those of the U. S. A. Standards Institute (USASI), as adopted by BIOLOGICAL ABSTRACTS and CHEMICAL ABSTRACTS, with the minor differences set out below. The most generally useful list of biological journal titles is that published each year by BIOLOGICAL ABSTRACTS (BIOSIS List of Serials; the most recent issue). Foreign authors, and others who are accustomed to using THE WORLD LIST OF SCIENTIFIC PERIODICALS, may find a booklet published by the Biological Council of the U.K. (obtainable from the Institute of Biology, 41 Queen's Gate, London, S.W.7, England, U.K.) useful, since it sets out the WORLD LIST abbreviations for most biological journals with notes of the USASI abbreviations where these differ. CHEMICAL ABSTRACTS publishes quarterly supplements of additional abbreviations. The following points of reference style for THE BIOLOGICAL BULLETIN differ from USASI (or modified WORLD LIST) usage:

A. Journal abbreviations, and book titles, all underlined (for *italics*)

B. All components of abbreviations with initial capitals (not as European usage in WORLD LIST *e.g., J. Cell. Comp. Physiol.* NOT *J. cell. comp. Physiol.*)

C. *All* abbreviated components must be followed by a period, whole word components *must not* (*i.e., J. Cancer Res.*)

D. Space between all components (*e.g., J. Cell. Comp. Physiol.*, not *J.Cell.Comp.Physiol.*)

E. Unusual words in journal titles should be spelled out in full, rather than employing new abbreviations invented by the author. For example, use *Rit Vísindafjélags Islendinga* without abbreviation.

F. All single word journal titles in full (*e.g., Veliger, Ecology, Brain*).

G. The order of abbreviated components should be the same as the word order of the complete title (*i.e., Proc.* and *Trans.* placed where they appear, not transposed as in some BIOLOGICAL ABSTRACTS listings).

H. A few well-known international journals in their preferred forms rather than WORLD LIST or USASI usage (*e.g., Nature, Science, Evolution* NOT *Nature, Lond., Science, N.Y.; Evolution, Lancaster, Pa.*)

6. ***Sequences.*** By the time a paper is sent to the press, all nucleotide or amino acid sequences and associated alignments should have been deposited in a generally accessible database (*e.g.*, GenBank, EMBL, SwissProt), and the sequence accession number should be provided.

7. ***Reprints, page proofs, and charges.*** Authors may purchase reprints in lots of 100. Forms for placing reprint orders are sent with page proofs. Reprints normally will be delivered about 2 to 3 months after the issue date. Authors will receive page proofs of articles shortly before publication. They will be charged the current cost of printers' time for corrections to these (other than corrections of printers' or editors' errors). Other than these charges for authors' alterations, *The Biological Bulletin* does not have page charges.

Reference: *Biol. Bull.* **207:** 77–79. (October 2004)

The Projectile Tooth of a Fish-Hunting Cone Snail: *Conus catus* Injects Venom Into Fish Prey Using a High-Speed Ballistic Mechanism

JOSEPH R. SCHULZ*, ALEX G. NORTON, AND WILLIAM F. GILLY

Hopkins Marine Station, Department of Biological Sciences, Stanford University, 120 Ocean View Blvd., Pacific Grove, California 93950

Conus catus, a fish-hunting cone snail (Fig. 1A), delivers venom into its prey by means of a single-use radular tooth (Fig. 1B). The venom is composed of a potent mix of bioactive peptides that, when injected into a fish through the hollow harpoon-shaped tooth, causes tetanus of the body musculature, resulting in a rigid paralysis (1). Although peptide toxins in the venom have been extensively studied (2), the biomechanical mechanisms of tooth insertion and venom ejection have not been determined. Anatomical observations have led to the suggestion that the radular tooth is pushed into prey by muscles surrounding the proboscis lumen (3). In this paper we show that the radular tooth is not pushed directly by the muscles of the proboscis but rather is propelled by a high-speed ballistic mechanism.

Small specimens of *Conus catus* (Hwass, 1792; <3 cm shell length) have a translucent proboscis allowing radular tooth movements to be visualized *in situ* by using a combination of transmitted-light microscopy with water-immersion optics and high-speed video. Figure 1A illustrates the experimental arrangement. A fish was positioned at the end of a trough where video observations were made. The snail sought the prey by extending its proboscis down a narrow trough in a recording chamber. As the proboscis approaches the fish, hairlike sensory papillae are visible at its tip (Fig. 1C, SP in top panels). Prior to stinging prey, the radular tooth is not held at the end of the proboscis but is positioned with its point 730 μms (about half the length of the tooth) from the end of the proboscis. The tip of the proboscis then contacts the fish, sensing potential prey (Fig. 1C, second panel). The delay between the proboscis first touching the fish and tooth ejection ranged from 240 to 295 ms.

With the proboscis held stationary against the fish, the radular tooth is propelled against a constriction of the proboscis lumen (Fig. 1C, arrowheads in the third panels), presumably by pressurization of the fluid space behind the tooth. The slight movements of the radular tooth against the constriction during this "priming" step peak during the 4–5 ms prior to release of the tooth into the fish (Fig. 2). Priming was a consistent feature with a similar time course in 10 feeding sequences captured by high-speed video.

During the final millisecond, the radular tooth is explosively propelled into the fish (Fig. 1C, fourth panels). This release step propels the base of the tooth (Fig. 1B, asterisk) to the tip of the proboscis, where it is tightly held by a ring of muscles. The minimum velocity of the tooth during release is approximately 3 ms^{-1}, but the actual time course of tooth movement is clearly faster than the maximum recording rate employed (1000 frames per second, shutter speed 1/2000). This extremely rapid event exceeds the maximum velocity (2 ms^{-1}) for discharge of the cnidarian nematocyst (4). Radular tooth release is one of the fastest known prey capture events and has a time course similar to that of the trap jaw response (0.33 to 1 ms) of the ant *Odontomachus* (5).

Immediately following impalement, the end of the proboscis loses its taper and swells with fluid, especially near the tip where a noticeable bulge appears (Fig. 1C, fourth panels). This fluid, which contains the venom peptides, enters an opening at the base of the tooth and is ejected from both the tip of the tooth and the beginning of the largest radular barb (data not shown and ref. 6, 7). Onset of tetanus in the fish prey is seen within 50 ms of impalement.

By gripping the base of the radular tooth, the proboscis is

Received 28 April 2004; accepted 19 July 2004.

* To whom correspondence should be addressed at Department of Biology M-3, Occidental College, Los Angeles, CA 90041-3314. E-mail: jschulz@oxy.edu

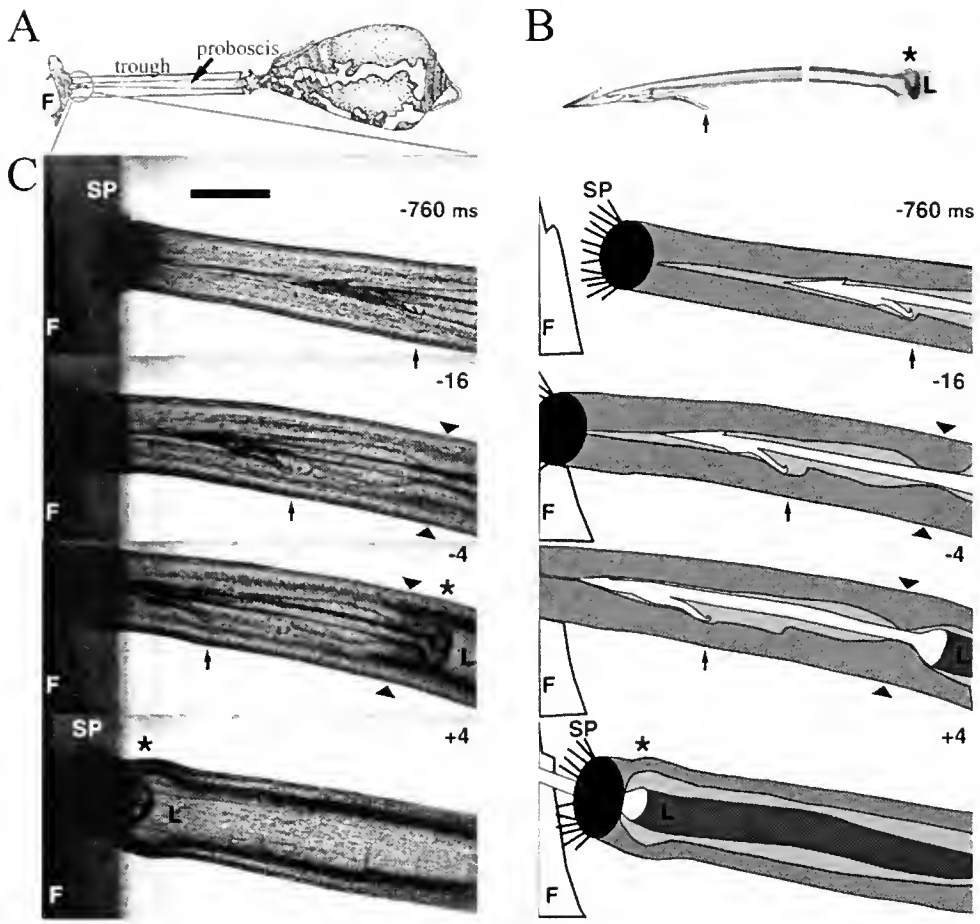

Figure 1. Mechanism of prey capture by *Conus catus*. (A) Left panel: The experimental arrangement for observing prey capture by *C. catus* (1.8 cm shell length, specimens collected on Kauai island, Hawaii). The proboscis extends down a trough in the recording chamber to sting the fish (F). (B) Right panel: Composite photomicrograph of the anterior and posterior sections of an isolated radular tooth. Most of the ligament (L) trailing from the base of the tooth has been omitted. (C) Left panels: Frames from a high-speed video clip of the feeding sequence (times in milliseconds before and after release of the tooth are indicated in the upper right of each panel). Scale bar, 350 μm. Microscopy employed transmitted light and water-immersion optics. Video was sampled at 1000 frames/s (Redlake Imaging, courtesy of Mark Denny, Stanford University). (C) Right panels: Sketches indicating the position of the radular tooth (white) in the proboscis (medium grey) occupying most of the proboscis lumen (light grey). **F** in all panels indicates the location of the fish at the end of the trough. An asterisk above the proboscis indicates the location of the radular tooth base. **SP** indicates the sensory papillae at the tip of the proboscis. Arrowheads indicate the location of the constriction inside the proboscis lumen. Arrows below the proboscis indicate the location of the largest of three barbs on the tooth. **L** indicates the ligament (dark grey, right panels). A collection of stills from a high-speed video (1000 fps) illustrating radular tooth ejection by *Conus catus* can be viewed as a video sequence at <www.mbl.edu/BiologicalBulletin/VIDEO/BB.video.html>. The radular tooth ligament flutters inside the proboscis after tooth ejection.

able to retain control of the stung fish prey while retracting. The paralyzed fish is then engulfed whole, thus completing the feeding sequence. The ligament attached to the base of the radular tooth (Fig. 1C, L fourth panels) moves freely in the proboscis lumen following impalement and therefore apparently does not participate in grasping of the impaled tooth by the proboscis (see supplemental material described in the legend to Fig. 1).

The proboscis acts as a hydrostatic skeleton that allows for coordinated movements in the absence of skeletal structures (3). It is unclear how the proboscis generates the pressure necessary to propel the tooth into prey. One possibility is that the muscles of the proboscis contract the fluid-filled lumen to generate pressure. To explore this possibility, the dimensions of extended proboscises (length 9 to 13 mm) were used to estimate the pressure necessary to accelerate the radular tooth by contraction of the proboscis muscles [minimum acceleration (3000 ms^{-2}) $\times$ proboscis fluid mass $\div$ tooth base surface area = pressure (Pa)]. The minimum pressure necessary was estimated to be 28.2 kPa

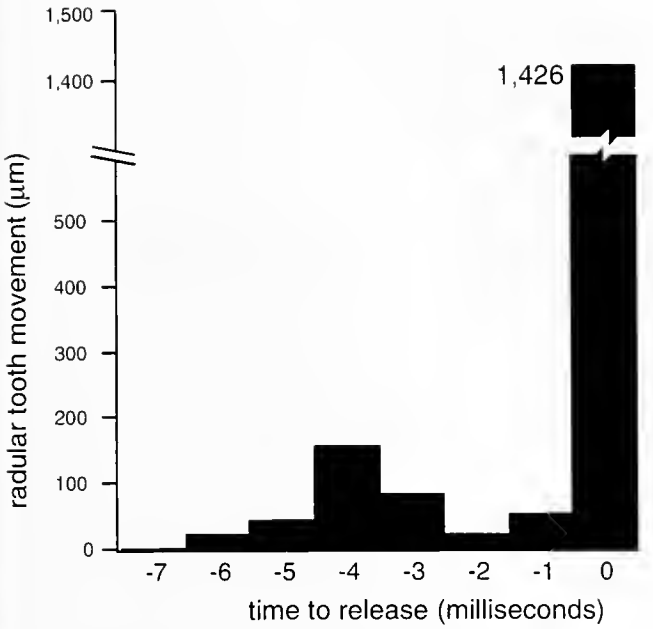

Figure 2. Linear incremental movement (parallel to the chamber trough) of the radular tooth between the times indicated and the previous frame (1000 frames per second). 0 indicates the first frame after release of the radular tooth into the fish.

(0.278 atm). This value falls within the range of the ~10 to 40 kPa recorded as the intra-mantle pressure during escape jetting in the squid *Loligo opalecsens* (8, 9, 10), suggesting that it would be feasible for the proboscis muscles of *Conus catus* to generate the necessary pressure. Although coordinated contraction of the proboscis muscles was not noted during any of the recorded feeding sequences, the radular tooth moves only 1.4 mm during the final millisecond (Fig. 2), so these contractions may be slight. This differs considerably from escape jetting in squid in which mantle contractions are obvious because water mass within the mantle is lost as thrust. Generation of the necessary pressure within the snail's proboscis may also involve contraction of the longitudinal muscles of the proboscis, and these would be more difficult to visualize.

In addition to retaining the radular tooth prior to the release step, the constriction of the proboscis lumen may also aid in the acceleration of the tooth by releasing elastic energy as the base of the tooth passes the stretched constriction. Further analysis of the tissues in this region of the proboscis will be required to determine whether this mechanism is possible.

Conus catus has evolved an effective biomechanical means of tooth ejection based on a ballistic prime-and-release mechanism. This mechanism probably involves contraction of the proboscis muscles to propel the radular tooth into unsuspecting prey and, in combination with a potent mix of venom peptides, makes this cone snail a highly effective predator of fast-moving prey.

Acknowledgments

We thank M. Denny, W.M. Kier, and an anonymous reviewer for valuable advice, M. O'Donnell for assistance with high-speed video; and A. J. Kohn for critical reading of an earlier version of this manuscript. This work was supported by a Kirschstein NIH postdoctoral fellow 5F32NS43938 (J.R.S.) and NSF grant IBN-0131788 (W.F.G.).

Literature Cited

1. **Kohn, A. J. 1956.** Piscivorous gastropods of the genus *Conus*. *Proc. Natl. Acad. Sci. USA* **42:** 168.
2. **Olivera, B. M. 1997.** *Conus* venom peptides, receptor and ion channel targets, and drug design: 50 million years of neuropharmacology. *Mol. Biol. Cell* **8:** 2101.
3. **Greene, J. L., and A. J. Kohn. 1989.** Functional morphology of the *Conus* proboscis (Mollusca: Gastropoda). *J. Zool. Lond.* **219:** 487.
4. **Holstein, T., and P. Tardent. 1984.** An ultrahigh-speed analysis of exocytosis: nematocyst discharge. *Science* **223:** 830.
5. **Gronenberg, W., J. Tautz, and B. Hölldobler. 1993.** Fast trap jaws and giant neurons in the ant *Odontomachus*. *Science* **262:** 561.
6. **James, M. J. 1980.** Comparative morphology of radular teeth in *Conus:* observations with scanning electron microscopy. *J. Molluscan Stud.* **46:** 116.
7. **Kohn, A. J., M. Nishi, and B. Pernet. 1999.** Snail spears and scimitars: a character analysis of *Conus* radular teeth. *J. Molluscan Stud.* **65:** 461.
8. **Gosline, J. M., and R. E. Shadwick. 1982.** The role of elastic energy storage mechanisms in swimming: an analysis of mantle elasticity in escape jetting in the squid, *Loligo opalescens*. *Can. J. Zool.* **61:** 1421.
9. **O'Dor, R. K. 1988.** The forces acting on swimming squid. *J. Exp. Biol.* **137:** 421.
10. **Neumeister, H., B. Ripley, T. Preuss, and W. F. Gilly. 2000.** Effects of temperature on escape jetting in the squid *Loligo opalescens*. *J. Exp. Biol.* **203:** 547.

Reference: *Biol. Bull.* **207:** 80–86. (October 2004)

Octocoral Chemical Signaling Selects and Controls Dinoflagellate Symbionts

KAZUHIKO KOIKE[1], MITSURU JIMBO[1], RYUICHI SAKAI[1], MASAMI KAERIYAMA[1], KOJI MURAMOTO[2], TAKEHIKO OGATA[1], TADASHI MARUYAMA[3,‡], AND HISAO KAMIYA[1,*]

[1] *School of Fisheries Sciences, Kitasato University, Sanriku, Ofunato, Iwate, 022-0101, Japan;*
[2] *Graduate School of Life Science, Tohoku University, Sendai, Miyagi, 981-8555, Japan; and*
[3] *Marine Biotechnology Institute, Heita, Kamaishi, Iwate, 026-0001, Japan*

*Symbioses between zooxanthellae (*Symbiodinium *spp.) and marine invertebrates, including corals, are common in shallow marine environments. The zooxanthellae contribute to host nutrition by translocating photosynthetic products and enabling them to effloresce in oligotrophic conditions. Coral mainly acquire* Symbiodinium *spp. by capturing free-swimming cells from the environment (1). Cultured* Symbiodinium *cells show a diel growth cycle with alternation between motile and non-motile cell stages once a day (2, 3), and the cell divides only during the latter stage (2). When associated with a host, however, cells are arrested in a non-motile stage while healthy cell division is maintained (4). We deduced that host-directed and chemical-based mechanisms are responsible for this phenomenon since SLL-2, a lectin that binds to carbohydrate chains with a* D*-galactosyl moiety, produced by the octocoral* Sinularia lochmodes, *is localized on the cell surface of the* Symbiodinium *harbored in the host (5). Here we describe SLL-2 as the key chemical factor for arresting* Symbiodinium *in the cell-dividing, non-motile stage, while some nonsymbiotic microalgae were even destroyed by SLL-2.*

Symbiotic associations between photosynthetic dinoflagellates (*Symbiodinium* spp.) and invertebrate hosts such as corals are crucial for the survival of the host animals since *Symbiodinium* supplies organic compounds to them and enables them to prosper in the oligotrophic environment that is especially common in tropical and subtropical regions. As in a case of "coral bleaching," however, evacuation of the symbiotic algae leads to the death of the hosts. Thus the host animals must acquire and properly maintain the algae for their survival.

The sexual progeny of host animals can acquire *Symbiodinium* in two ways: vertical transmission (acquisition by maternal inheritance) and horizontal transmission (acquisition from the environment by either larval or adult stages) (1). The latter mode, which dominates (~85%) in cnidarians (6), may allow the animals to acquire *Symbiodinium* cells suited to the environment where they have settled, but how these animals select and acquire *Symbiodinium* is not clear. For the initial infection of *Symbiodinium*, the two main mechanisms that have been suggested are (a) chemotactic attraction of motile *Symbiodinium* to the host's mouth and gastric cavity, then subsequent transmission to the gastrodermal cells (7, 8) and (b) acquisition of *Symbiodinium* cells that have been ingested by the hosts while feeding (8, 9). Regardless of the mechanisms, *Symbiodinium* must at some point be selected, from other nonsymbiotic microalgae or other materials that corals have ingested, by host-directed mechanisms. In the case of *Cassiopeia xamachana*, *Symbiodinium* was phagocytosed by the endodermal cells, and only the cells capturing live *Symbiodinium* were able to escape digestion by avoiding lysosomal fusion (10). Moreover, some "host factors" such as a cell adhesion protein (sym32) (11, 12) or the macerated tissue (6) of a sea anemone (*Anthopleura elegantissima*) were suspected to be involved in symbiotic events. The physiological actions of these host factors on the algae were not understood, however.

Received 28 January 2004; accepted 20 July 2004.

* To whom correspondence should be addressed. E-mail: h.kamiya@kitasato-u.ac.jp

‡ Current address: Marine Biology and Ecology Research Program, Japan Agency for Marine-Earth Science and Technology (JAMSTEC), Natsushima, Yokosuka, Kanagawa, 237-0061, Japan.

We previously found that lectin (SLL-2) isolated from the octocoral *Sinularia lochmodes* was localized densely on the surface of the *Symbiodinium* cells released from the host coral (5). Lectins can recognize specific carbohydrate structures of glycoproteins on the cell surface, and some of them are proposed to mediate interactions between hosts and symbionts. For instance, in the case of rhizobia-legume symbiosis, a number of results support the hypothesis that lectins mediate development of a symbiotic relationship between the bacteria and the plant (13). There are some examples of putative interactions between invertebrate hosts and symbiotic bacteria or algae mediated by lectin from the invertebrate (14, 15). We therefore hypothesize that SLL-2 also plays a role in selecting *Symbiodinium* and possibly in stabilizing the symbiotic relationship. This hypothesis was tested herein by assessing the effect of purified SLL-2 on the diel cycle or cell morphology and cell division of symbiotic and nonsymbiotic microalgal cultures.

For symbiotic microalgae models, the *Symbiodinium* strains P083-2, JCUCS-1, and CS-156 were used. They were all in well-synchronized regular diel alternation between motile and non-motile (coccoid) forms, and more than 70% of the cells were in the motile form during the observation period (9–10 AM). The additions of 10 or 100 μg ml^{-1} of SLL-2 to the cultures of actively swimming *Symbiodinium* affected both the motility and the growth of the algae. Within 1 h after the addition of the lectin (100 μg ml^{-1}), the cells aggregated and formed clumps. For all strains, the number of motile cells dramatically decreased at day 1 (24 h after the addition; Fig. 1a, b, c), and they had begun to transform into stationary coccoid forms (Fig. 2b). Typically, in the presence of 100 μg ml^{-1} protein, nearly 100% of CS-156 and P083-2 cells and 80% to 90% of JCUCS-1 cells were arrested at the coccoid form after day 3; this form persisted throughout the experimental period (one week; Fig. 1a, b, c), and dividing cells were frequently observed (arrows in Fig. 2b). The effect of SLL-2 on cell motility seemed to be concentration-dependent, as the lower concentration (10 μg ml^{-1}) did not affect the motility of JCUCS-1 (Fig. 1b). Following the addition of 10 μg ml^{-1} of SLL-2 to CS-156, 65% of the cells were transformed to the coccoid form at day 1, but the effect was reversible since 50%–70% of the cells were in the motile form on day 2 and thereafter (Fig. 1a). Strain P083-2 was the most sensitive of the *Symbiodinium* strains tested; nearly 100% of the cells were transformed to the stationary coccoid form within 1 day after the treatment, even at 10 μg ml^{-1} of SLL-2 (Fig. 1c).

At these concentrations (10 or 100 μg ml^{-1}), the growth of CS-156 and JCUCS-1 (Fig. 1d, e)—as indicated by the increase of the *in vivo* chlorophyll *a* fluorescence—was not affected, whereas that of P083-2 gradually became inhibited, even at the lower concentration (Fig. 1f). At both 10 and 100 μg ml^{-1} SLL-2, growth slowed on day 4 relative to the control, and significantly ($P < 0.05$; Student's t test) smaller biomasses (*ca.* 50% and 60% of control, respectively) were observed at day 6. The effects of SLL-2 on the physiology of the *Symbiodinium* cells were completely inhibited in the presence of an inhibitor; *i.e.*, CS-156 cells were not arrested in the coccoid form when 0.2 *M* of melibiose, the most effective inhibitor of the hemagglutination of SLL-2 (5), was added to the culture. It should be noted that the other inhibitors of SLL-2 showed some toxicity to the culture at the effective concentrations. This result suggested that the property of the lectin to bind to the D-galactosyl moiety in the carbohydrate chain is required for its activity. Interestingly, however, the addition of a D-galactose-binding lectin from *Arachis hypogaea* (peanut) to three *Symbiodinium* strains did not show any coccoid-arresting activity even at higher concentrations (~300 μg ml^{-1}). Thus, the carbohydrate-binding property alone did not explain the unique actions of SLL-2 on the algal cells.

Similarly, we tested the effects of the lectin on three nonsymbiotic dinoflagellates (*Alexandrium minutum*, *Gymnodinium catenatum*, and *Prorocentrum micans*) and on a non-dinoflagellate control (the chlorophyte *Tetraselmis* sp.) (Fig. 3). The responses of these nonsymbiotic microalgae to SLL-2 differed from those observed for *Symbiodinium*. The addition of SLL-2 had no significant effect on either the motility or growth of *A. minutum* (Fig. 3a, e). The addition of SLL-2 (100 μg ml^{-1}) to cultures of *G. catenatum* and *P. micans* resulted in cell death after the cells inflated and burst within 24 h (Fig. 3b, c; Fig. 4b, d). Even at 10 μg ml^{-1}, a similar significant effect was observed on *G. catenatum*, but not on *P. micans*. Cells of *Tetraselmis* sp., the chlorophyte control, aggregated and formed cell clumps (Fig. 4f) with complete loss of cell motility and significant inhibition of growth after day 4, even at 10 μg ml^{-1} (*ca.* 60% inhibition on day 4; Fig. 3d, h).

In microalgae treated with SLL-2, immunochemical staining using the anti-SLL-2 antibody showed that the SLL-2 was localized on the surfaces of all *Symbiodinium* strains and other microalgae tested (Fig. 5). Although the cells of *G. catenatum* and *P. micans* burst, their debris were also clearly stained (Fig. 5c, d). These results indicate that the lectin binds to sites, probably to glycoproteins on the microalgal cell surface, in its mode of action.

The most intriguing aspect of these results is that the lectin affected the physiological condition of symbiotic algae, while either causing the deterioration of or having no effect on nonsymbiotic microalgal strains. These effects were distinct at the concentration level of 100 μg ml^{-1}. On the basis of the hemagglutination activity of the coelomic fluid obtained from fresh coral, we estimated the concentration of SLL-2 to be about 300 μg g^{-1} of the wet weight of *S. lochmodes*. We also found that the effective concentration of SLL-2 saturated at 100 μg ml^{-1} and the addition of 300 μg ml^{-1} did not show any toxicity to the *Symbio-*

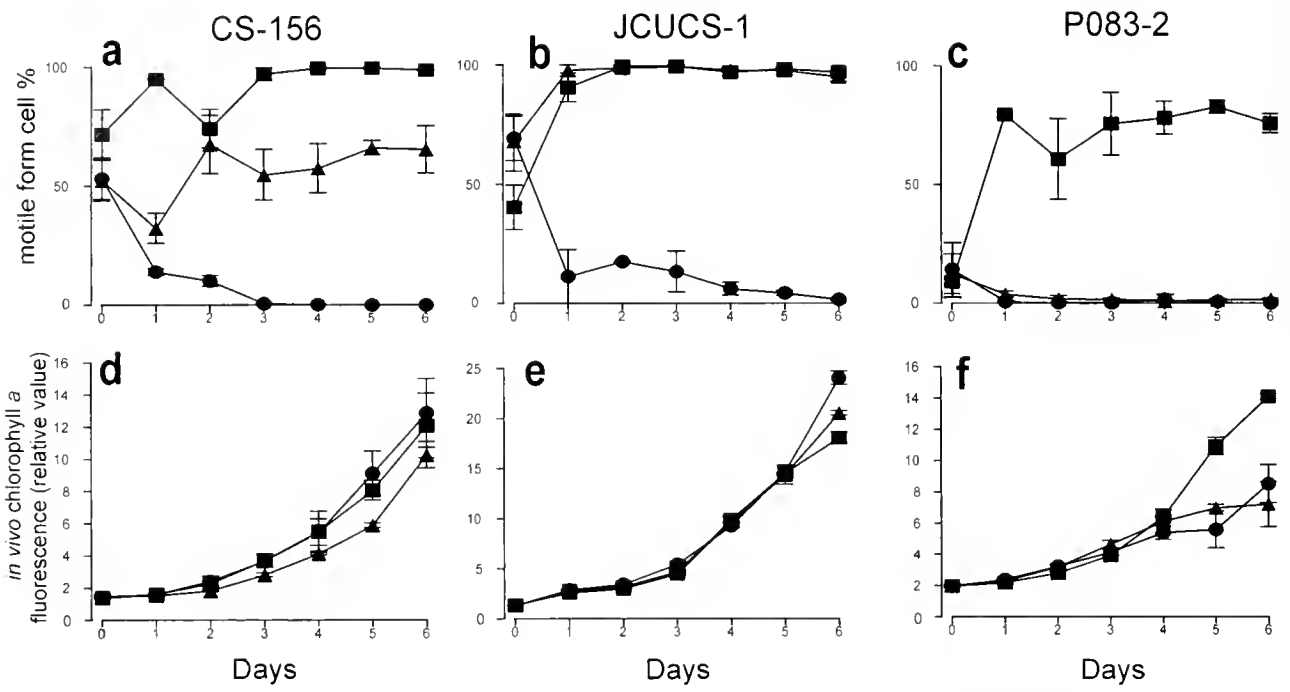

Figure 1. The percentage of motile-form cells (a–c) and growth (d–f) of three *Symbiodinium* strains (CS-156, JCUCS-1, and P083-2) in the presence of two concentrations of the carbohydrate-binding lectin SLL-2. Circles and triangles represent 100 and 10 μg ml^{-1} of SLL-2, respectively; squares are the control. Each data point represents the percentage of motile-form cells out of the total cells counted (>400) for each observation period (a–c). Cell growth was monitored by *in vivo* chlorophyll *a* fluorescence measurement (d–f). All data are given as the means ± standard deviation of triplicate wells. *Symbiodinium* strains P083-2 and JCUCS-1 were from culture stocks maintained at the Marine Biotechnology Institute (MBI), and CS-156 was obtained from the Commonwealth Scientific & Industrial Research Organization (CSIRO). The culture was spread on agar plates (IMK liquid medium, Wako pure chemical + 1.2 % agar) with a glass rod, then the *Symbiodinium* colonies, formed apart from bacterial colonies, were picked up with sterilized needle and transferred to sterilized liquid IMK medium. They were initially diluted (20,000 cells ml^{-1}) with the medium and transferred to 24-well flat-bottom plates (ultra-low protein binding; 3473, Costar). Following acclimation for 24 h (25 °C, 30 μmol photon m^{-2} s^{-1}, 12:12 light:dark cycle), *Symbiodinium* cells were confirmed to be in a diel motile phase (more than 70%) prior to SLL-2 addition. A solution (500 μl) of SLL-2 (4) (in 8 m*M* Tris-HCl prepared with 60% seawater, sterilized by 0.2 μm filtration, pH 7.6) was added to the culture to provide a final concentration of SLL-2 of 100 or 10 μg ml^{-1}. Control reactions were prepared by mixing equal volumes of the same seawater and buffer as above but in the absence of SLL-2. The swimming behavior and cell forms were observed under an inverted microscope (IX70, Olympus) daily between 9 and 10 AM (the period when the *Symbiodinium* strains used have the highest proportion of cells in the diel motile phase) for 6–7 days, starting right after the addition of SLL-2. Live images under magnifications of ×75 and ×300 were stored on a digital videotape recorder. The number of motile cells and non-motile cells (a total of more than 400 cells) in more than six observation fields (×75) of the images were counted. Cell growth in the wells was estimated by daily monitoring of *in vivo* chlorophyll *a* fluorescence (EX 485 ± 40 nm, EM 645 ± 40 nm) using a microplate fluorescence reader (FL600, Bio-tek). The first observation (day 0) was made within 1 h after the start of treatment. Note that upon the addition of both lectin (SLL-2) and control solutions, the shock of the treatment produced an initial decrease in the percentage of motile cells.

dinium cells. The results of this study provided some experimental evidence for the as-yet-unidentified ecological interaction between the microalgae and the coral. In our model, lectin stored in the nematocyst of the coral (5) is probably released when algal cells are introduced to the gastric cavity and the microalgae are then chemically selected by their varying responses to lectin; that is, the lectin is toxic to some nonsymbiotic algae—as in the cases of *G. catenatum*, *P. micans*, and *Tetraselmis* sp.—but others—as represented by *A. minutum* in this study—can sometimes escape unaffected. On the other hand, the lectin changes the physiology of *Symbiodinium*, creating conditions that may be favorable to the symbiosis between the algae and the coral.

Interestingly, our observation of the discrete effects of SLL-2 on different types of algae suggests that further selection may occur among the different clades of *Symbiodinium*. In gorgonians, infection by several clades of *Sym-*

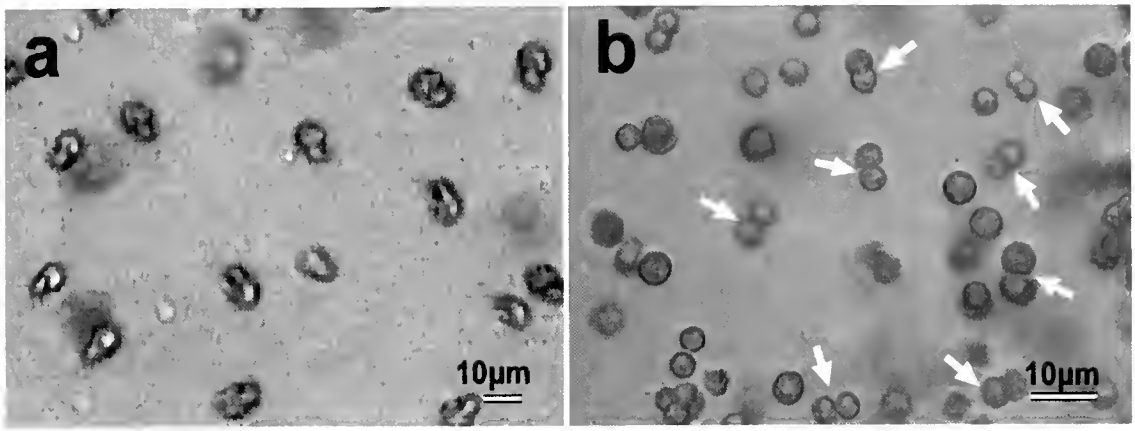

Figure 2. Light micrographs from the video-captured images of *Symbiodinium* sp. (strain CS-156) after SLL-2 treatment and in control wells. (a) Actively swimming CS-156 cells are in rapid motion and are blurred on this image (control). (b) CS-156 with SLL-2 treatment (day 3, 100 μg ml^{-1}) shows only coccoid-form cells and numerous dividing cells (arrows).

biodinium occurs at the onset of symbiosis; however, the population eventually converges into a single clade of algae (16). The strains of *Symbiodinium* (P083-2, JCUCS-1, and CS-156) used in the present experiments belong to different clades (A, B, and F, respectively) (17, 18). The actual *Symbiodinium* harbored in the coral could not be used due to the difficulty of culturing it; clade C, a ribotype of symbionts in *S. lochmodes* determined on the basis of its chloro-

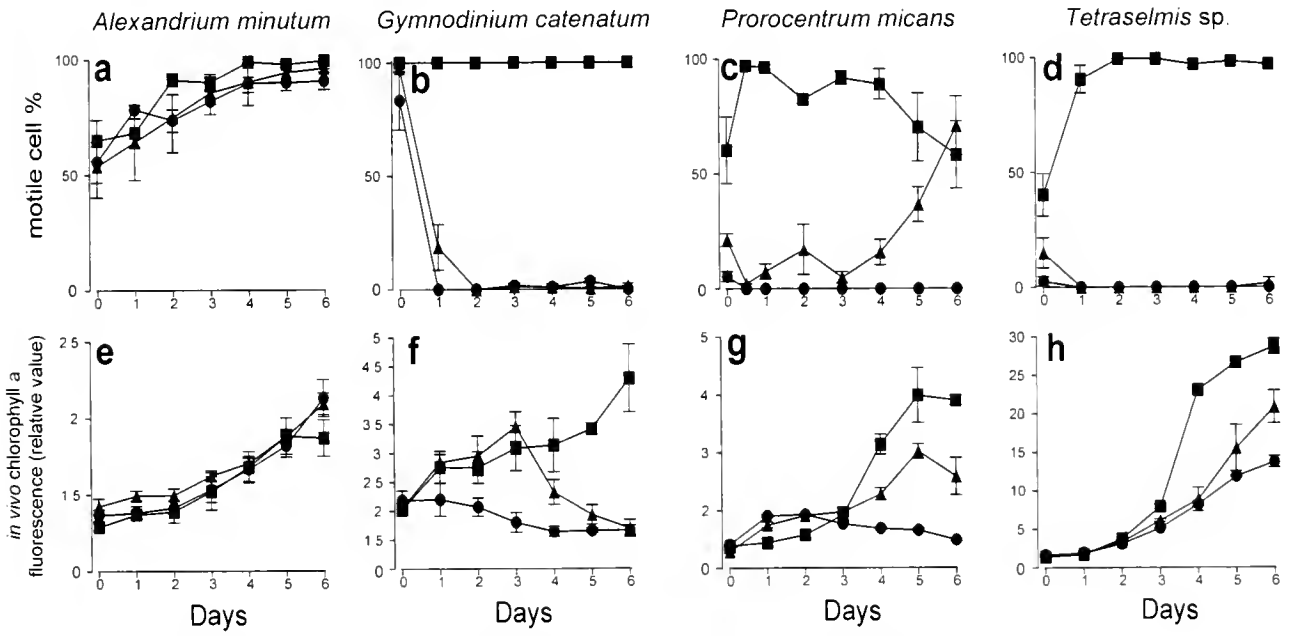

Figure 3. The percentage of motile cells (a–d) and the growth (e–h) of three nonsymbiotic dinoflagellates (*Alexandrium minutum*, *Gymnodinium catenatum*, and *Prorocentrum micans*) and a non-dinoflagellate chlorophyte (*Tetraselmis* sp.) in the presence of SLL-2. All experimental procedures were the same as those for *Symbiodinium* (Fig. 1), except for the initial cell concentrations: 2,000 cells ml^{-1} for the dinoflagellates and 20,000 cells ml^{-1} for *Tetraselmis* sp. Both *A. minutum* (Cu-AM1) and *Tetraselmis* sp. (Cu-Ch) were isolated and identified by Dr. L. Thaithaworn, Department of Marine Science, Chulalongkorn University, Thailand; *G. catenatum* (GC-27-1) and *P. micans* (P-A4) were isolated and identified by Dr. S. Sakamoto at the National Research Institute of Fisheries and Environment of Inland Sea, Japan. All the strains except *Tetraselmis* sp. and *P. micans* are axenic, and even in the nonaxenic cultures, no bacterial growth was apparent during the experiments.

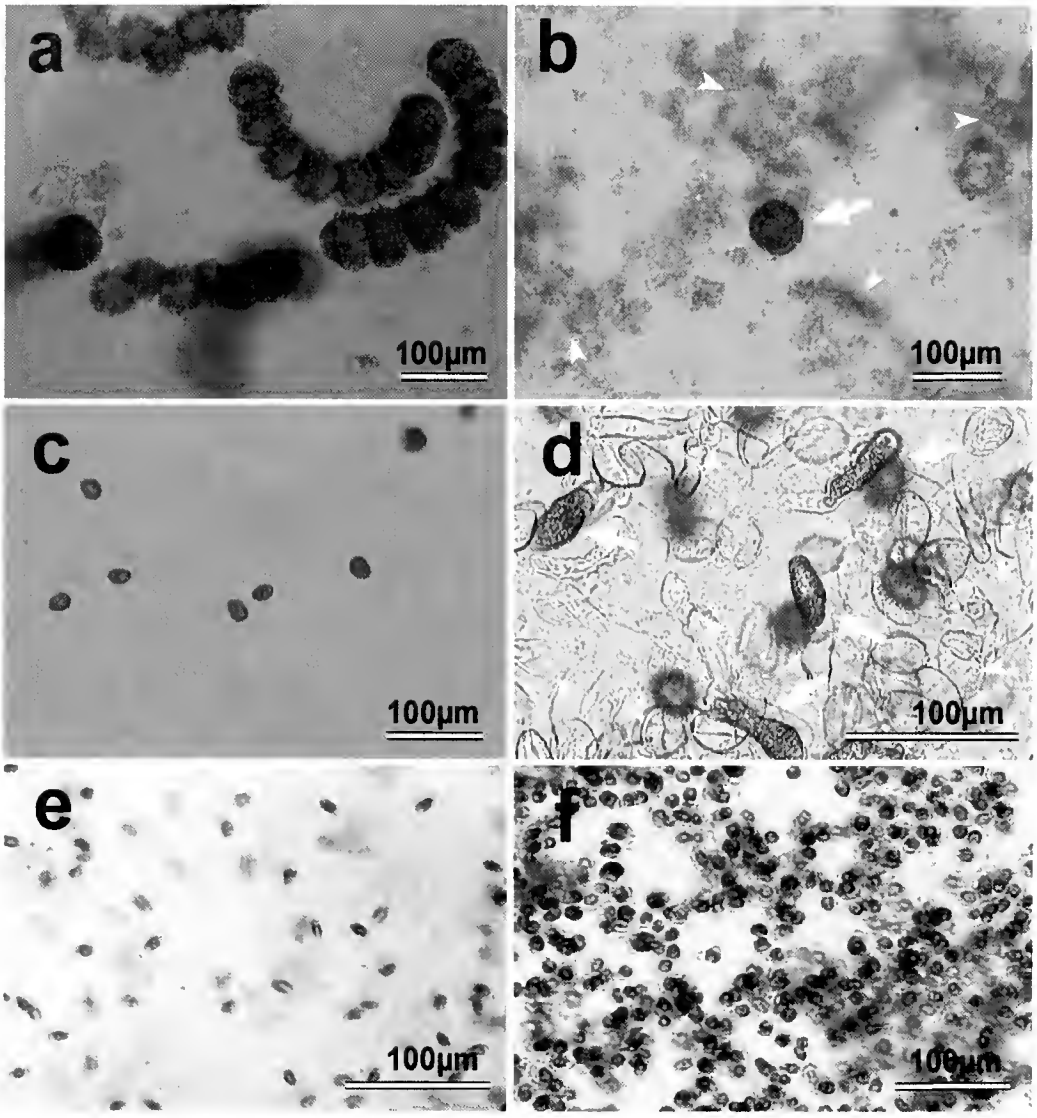

Figure 4. Light micrographs from the video-captured images of microalgae after SLL-2 treatment and in control wells. (a) *Gymnodinium catenatum* forming cell chains (control). (b) *G. catenatum* 24 h after SLL-2 (100 μg ml^{-1}) treatment showing a swollen cell (an arrow) and debris from destroyed cells (arrowheads). (c) Actively swimming *Prorocentrum micans* (control). (d) *P. micans* 24 h after SLL-2 (100 μg ml^{-1}) treatment showing cytoplasm ejected from the theca (arrows) and numerous empty thecae (arrowheads). (e) *Tetraselmis* sp. cells are in rapid motion and are blurred on this image (control). (f) *Tetraselmis* cells forming cell clumps without motility.

plast large subunit (23S) rDNA sequence (DDBJ Accession No. AB159231) (19), was not available. For these reasons, our experimental model is somewhat indirect for assessing the chemical recognition that actually occurs between the host and the algae. However, the facts that the responses of *Symbiodinium* to the lectin varied significantly among the strains used and that the clade of *Symbiodinium* in *S. lochmodes* was uniform strongly suggest that some selection analogous to our experiment had taken place in the coral-algae system. Therefore, further experiments using an actual *Symbiodinium* isolate of the coral or a culture of clade C will be of interest.

Of note, our results indicated that the action of SLL-2 toward *Symbiodinium* is mediated not only by carbohydrate-binding activity, but also by more specific but still unidentified mechanisms, since the peanut lectin that recognizes a D-galactosyl moiety such as SLL-2 was inert in our models.

Our finding of lectin-mediated chemical recognition and physiological modulation between symbiotic dinoflagellates and a coral is a novel one. Identifying the protein responsible for this process can illuminate physiological and possibly also evolutionary attributes of symbiosis, one of the coral reef's most important ecological aspects. Further investigation of the physiological and ecological aspects of

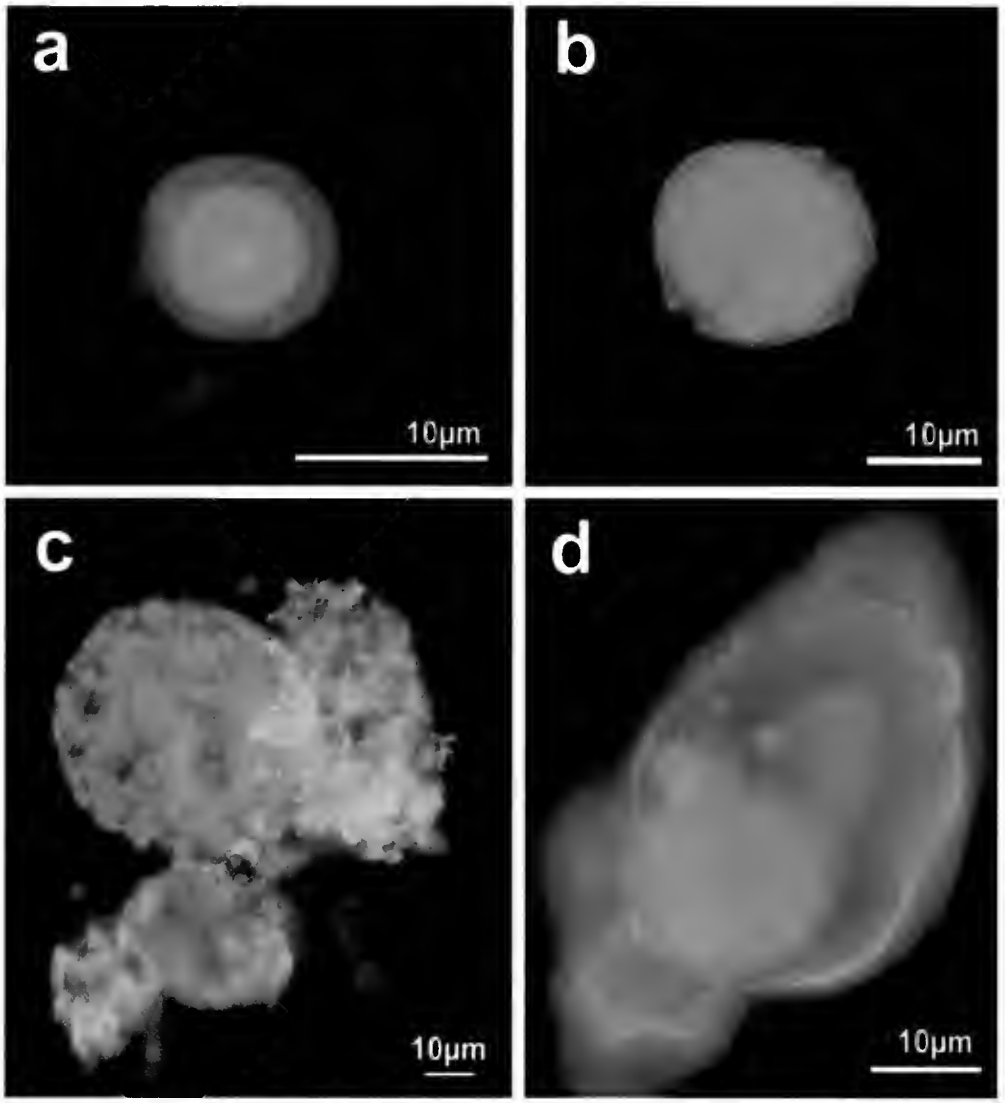

Figure 5. Fluorescent micrographs of immunostained cells at day 6 after treatment (100 μg ml^{-1}). Binding of anti-SLL-2 antibody is shown by green fluorescence; red fluorescence indicates the presence of chlorophyll *a* in the plastids. (a) *Symbiodinium* sp. (CS-156); (b) *Alexandrium minutum* (note: cell is not destroyed.); (c) destroyed cell of *Gymnodinium catenatum* with stained debris; and (d) burst cell of *Prorocentrum micans*. Immunostaining was conducted as follows: cells were harvested and washed several times by repeated centrifugation (1000 × *g*, 10 min) and resuspended in filtered seawater to remove unbound SLL-2. Then the cells were fixed in 4% paraformaldehyde in cacodylate buffer (0.1 *M* cacodylate/0.1 *M* sucrose, pH 7.6) for 4 h at 4 °C, and washed with the same buffer three times. Cells were then blocked with 2% bovine serum albumin (BSA) for 1 h, reacted with anti-SLL-2 antibody (5) diluted 1000 times with 20 m*M* Tris-HCl-buffer (pH 7.4) containing 0.2% BSA for 2 h at room temperature, and washed three times. Then the cells that reacted to the primary antibody were stained with fluorescein-isothiocyanate–labeled anti-rabbit IgG goat antibody (Funakoshi) diluted 1000 times with 20 m*M* Tris HCl buffer for 2 h at room temperature, and then washed three times with the same buffer. Observation was conducted under a fluorescent microscope (EX 455–490 nm, BS 500 nm, BH2-RFC, Olympus). The same immunostaining procedures were used on the cells in the control wells (without adding SLL-2), but no antibody bindings were observed.

these symbioses might allow us to better understand globally important ecological problems such as coral bleaching, which is triggered by the evacuation of zooxanthellae from the host.

Acknowledgments

The authors express their thanks to Mr. Saburo Hosaka, a chairman of the Establishment of Tropical Marine Ecological Research (ETMER), and the staff of Akajima Marine

Science Laboratory (AMSL) for access to their collection of specimens. Thanks are also due to Dr. Lirdwitayaprasit Thaithaworn, Chulalongkorn University, and Dr. Setsuko Sakamoto, National Research Institute of Fisheries and Environment of Inland Sea, for supplying cultures. This study is supported in part by a Study-In-Aid for Scientific Research (B) from the Ministry of Education, Culture, and Science, Japan to H.K. (80011964 and 15380145).

Literature cited

1. **Trench, R. K. 1987.** Dinoflagellates in non-parasitic symbioses. Pp. 530–570 in *The Biology of Dinoflagellates,* F. J. R. Taylor, ed. Blackwell, Oxford.
2. **Fitt, W. K., and R. K. Trench. 1983.** The relation of diel patterns of cell division to diel patterns of motility in the symbiotic dinoflagellate *Symbiodinium microadriaticum* Freudenthal in culture. *New Phytol.* **94:** 421–432.
3. **Yacobovitch, T., Y. Benayahu, and V. M. Weis. 2004.** Motility of zooxanthellae isolated from the Red Sea soft coral *Heteroxenia fuscescens* (Cnidaria). *J. Exp. Mar. Biol. Ecol.* **298:** 35–48.
4. **Trench, R. K. 1993.** Microalgal-invertebrate symbioses: a review. *Endocytobiosis Cell Res.* **9:** 135–175.
5. **Jimbo, M., T. Yanohara, K. Koike, K. Koike, R. Sakai, K. Muramoto, and H. Kamiya. 2000.** The D-galactose-binding lectin of the octocoral *Sinularia lochmodes:* characterization and possible relationship to the symbiotic dinoflagellates. *Comp. Biochem. Physiol. B* **125:** 227–236.
6. **Schwarz, J. A., V. M. Weis, and D. C. Potts. 2002.** Feeding behavior and acquisition of zooxanthellae by planula larvae of the sea anemone *Anthopleura elegantissima. Mar. Biol.* **140:** 471–478.
7. **Kinzie, R. A., III. 1974.** Experimental infection of aposymbiotic gorgonian polyps with zooxanthellae. *J. Exp. Mar. Biol. Ecol.* **15:** 335–345.
8. **Fitt, W. K. 1984.** The role of chemosensory behavior of *Symbiodinium microadriaticum,* intermediate hosts, and host behavior in the infection of coelenterates and molluscs with zooxanthellae. *Mar. Biol.* **81:** 9–17.
9. **Riggs, L. L. 1988.** Feeding behavior in *Aiptasia tagetes* (Duchassaing and Michelotti) planulae: a plausible mechanism for zooxanthellae infection of aposymbiotic planktotrophic planulae. *Caribb. J. Sci.* **24:** 201–206.
10. **Fitt, W. K., and R. K. Trench. 1983.** Endocytosis of the symbiotic dinoflagellate *Symbiodinium microadriaticum* Freudenthal by endodermal cells of the scyphistomae of *Cassiopeia xamachana* and resistance of the algae to host digestion. *J. Cell. Sci.* **64:** 195–212.
11. **Reynolds, W. S., J. A. Schwarz, and V. M. Weis. 2000.** Symbiosis-enhanced gene expression in cnidarian-algal associations: cloning and characterization of a cDNA, sym32, encoding a possible cell adhesion protein. *Comp. Biochem. Physiol. A* **126:** 33–44.
12. **Schwarz, J. A., and V. M. Weis. 2003.** Localization of a symbiosis-related protein, sym32, in the *Anthopleura elegantissima–Symbiodinium muscatinei* association. *Biol. Bull.* **205:** 339–350.
13. **Hirsch, A. M., M. R. Lum, and J. A. Downie. 2001.** What makes the rhizobia–legume symbiosis so special? *Plant Physiol.* **127:** 1484–1492.
14. **Müller, W. E., R. K. Zahn, B. Kurelec, C. Lucu, I. Müller, and G. Uhlenbruck. 1981.** Lectin, a possible basis for symbiosis between bacteria and sponges. *J. Bacteriol.* **145:** 548–558.
15. **Vasta, G. R. 1991.** The multiple biological roles of invertebrate lectins: their participation in nonself recognition mechanisms. Pp. 73–101 in *Phylogenesis of Immune Function,* G. W. War and N. Cohen, eds. CRC Press, Boca Raton, FL.
16. **Coffroth, M. A., S. R. Santos, and T. L. Goulet. 2001.** Early ontogenetic expression of specificity in a cnidarian–algal symbiosis. *Mar. Ecol. Prog. Ser.* **222:** 85–96.
17. **Carlos, A. A., B. K. Baillie, M. Kawachi, and T. Maruyama. 1999.** Phylogenetic position of *Symbiodinium* (Dinophyceae) isolates from tridacnids (Bivalvia), cardiids (Bivalvia), a sponge (Porifera), a soft coral (Anthozoa), and a free-living strain. *J. Phycol.* **35:** 1054–1062.
18. **LaJeunesse, T. C. 2001.** Investigating the biodiversity, ecology, and phylogeny of endosymbiotic dinoflagellates in the genus *Symbiodinium* using the ITS region: in search of a "species" level marker. *J. Phycol.* **37:** 866–880.
19. **Santos, S. R., D. J. Taylor, R. A. Kinzie, III, M. Hidaka, K. Sakai, and M. A. Coffroth. 2002.** Molecular phylogeny of symbiotic dinoflagellates inferred from partial chloroplast large subunit (23S)-rDNA sequences. *Mol. Phylogenet. Evol.* **23:** 97–111.

Reference: *Biol. Bull.* **207:** 87–92. (October 2004)

Phylogenetic Placement of "Zoochlorellae" (Chlorophyta), Algal Symbiont of the Temperate Sea Anemone *Anthopleura elegantissima*

LOUISE A. LEWIS[1,*] AND GISÈLE MULLER-PARKER[2]

[1] *University of Connecticut, Ecology and Evolutionary Biology, 75 North Eagleville Road, Storrs, Connecticut 06269; and* [2] *Western Washington University, Shannon Point Marine Center, Department of Biology, 1900 Shannon Point Road, Anacortes, Washington 98221*

Abstract. At northern latitudes the sea anemones *Anthopleura elegantissima* and its congener *A. xanthogrammica* contain unidentified green chlorophytes (zoochlorellae) in addition to dinophytes belonging to the genus *Symbiodinium*. This dual algal symbiosis, involving members of distinct algal phyla in one host, has been extensively studied from the perspective of the ecological and energetic consequences of hosting one symbiotic type over the other. However, the identity of the green algal symbiont has remained elusive. We determined the phylogenetic position of the marine zoochlorellae inhabiting *A. elegantissima* by comparing sequence data from two cellular compartments, the nuclear 18S ribosomal RNA gene region and the plastid-encoded *rbcL* gene. The results support the inclusion of these zoochlorellae in a clade of green algae that form symbioses with animal (*Anthopleura elegantissima*), fungal (the lichen genus *Nephroma*), and seed plant (*Ginkgo*) partners. This clade is distinct from the *Chlorella* symbionts of *Hydra*. The phylogenetic diversity of algal hosts observed in this clade indicates a predisposition for this group of algae to participate in symbioses. An integrative approach to the study of these algae, both within the host and in culture, should yield important clues about how algae become symbionts in other organisms.

Introduction

The sea anemone *Anthopleura elegantissima* (Brandt, 1835) is an important model organism for the study of cnidarian-algal symbioses because it contains the most phylogenetically diverse algal symbionts known for marine cnidarians. At least two dinoflagellates (zooxanthellae, *Symbiodinium californium* and *S. muscatinei*; LaJeunesse and Trench, 2000) and green algae (zoochlorellae, *Chlorella*-like green cells in the phylum Chlorophyta; Muscatine, 1971; O'Brien and Wyttenbach, 1980) are photosynthetic symbionts of these clonal anemones. Zoochlorellae in *A. elegantissima* are restricted to northern latitudes (> 43 °N; Secord and Augustine, 2000) and co-exist with one of the two zooxanthellae (*S. muscatinei*; LaJeunesse and Trench, 2000). Experimental studies have shown that the composition of algal partners in *Anthopleura* spp. is influenced by light and water temperature (O'Brien and Wyttenbach, 1980; Saunders and Muller-Parker, 1997). Field observations of anemones in different microhabitats and transplant experiments (Bates, 2000; Secord and Muller-Parker, 2004) support the role of low light and low temperature in influencing the occurrence of zoochlorellae in anemone hosts.

The ecological consequences of harboring different symbionts have been explored through recent investigations comparing *S. muscatinei* and zoochlorellae with respect to photosynthesis and carbon translocation (Engebretson and Muller-Parker, 1999; Verde and McCloskey, 1996, 2001, 2002), occurrence of UV-absorbing mycosporine-like amino acids (Shick *et al.*, 2002), and predation on the anemone host (Seavy and Muller-Parker, 2002, and references therein). These studies have not demonstrated any significant negative effects of hosting zoochlorellae, although Verde and McCloskey's carbon budgets show that, compared to zooxanthellae, zoochlorellae translocate much less carbon to the host because of their presumed high growth rate (Verde and McCloskey, 1996).

Received 7 April 2004; accepted 2 August 2004.

* To whom correspondence should be addressed. E-mail: louise.lewis@uconn.edu

Although the dinoflagellate symbionts of cnidarian hosts have been extensively investigated (Baker, 2003; LaJeunesse *et al.*, 2003), the common green symbiont harbored by *A. elegantissima* has yet to be phylogenetically identified. Previous pigment analyses have verified the status of the green symbiont as a member of the Chlorophyta (Muscatine, 1971). Ultrastructural studies also indicated typical chlorophyte morphology. The cells have plastids with two surrounding membranes, abundant starch storage, and pyrenoids that are not penetrated by thylakoids. This coccoid green alga is very small—about 6–10 μm in diameter (O'Brien, 1978; Verde and McCloskey, 1996)—and the cells divide in two. It was presumed to be a species of marine *Chlorella*, but attempts to identify it have been hampered by the inability to culture isolates from the anemone host (pers. obs., G. Muller-Parker).

Our goal was to obtain sequence data that would identify the green symbiont found in *A. elegantissima*. As the most common algal symbionts in animals in freshwater associations (sponges, hydra) are members of the genus *Chlorella* (Reisser and Widowski, 1992), we were particularly interested in determining the phylogenetic relatedness of both freshwater and marine symbiotic green algae, universally called zoochlorellae. However, given the paraphyly of *Chlorella* (Huss and Sogin, 1990; Huss *et al.*, 1999), the identity of green anemone symbionts is uncertain.

Materials and Methods

Cell isolation

Zoochlorellate (green) specimens of *Anthopleura elegantissima* were collected on 25 July 2003, during low tide, from a rock wall (+0.65 m above mean lower low water [MLLW]) at Alexander Beach, Fidalgo Island, Washington (48° 29′ 37″ N, 122° 40′ 52″ W). Anemones were collected randomly from separate locations on the rock wall to avoid possible selection of clonemates. Specimens were transported to Western Washington University's Shannon Point Marine Center and maintained in a flow-through natural seawater table for a month. The anemones were fed once a week with freshly hatched brine shrimp nauplii. They were last fed 5 days before zoochlorellae were isolated from five small green anemones selected randomly from the stock maintained in the seawater table. The anemones were cleaned of any adhering debris by wiping their external surfaces with tissues and rinsing them thoroughly in filtered (>0.5 μm) seawater. The five anemones were chopped into pieces with a razor blade, and the pieces were combined into one sample. The sample was homogenized in cold filtered seawater by using a motorized pestle and 60-ml glass tissue homogenizer. The anemone homogenate was distributed into four 15-ml centrifuge tubes and centrifuged at 1500 *g* for 5 min to separate the algae (pellet) from the animal (supernatant) parts of the anemone. The algal pellets were resuspended in filtered seawater and cleaned of remaining animal tissue by recentrifugation in additional washes of filtered seawater. After three rinses, the four algal pellets were combined into one 50-ml sample that was passed through a 30-μm Nitex mesh screen to remove animal clumps. The screened sample was centrifuged to concentrate the algae, and subsamples (~4.3×10^6 zoochlorellae, determined by hemacytometer counts) were placed into 1.5-ml microfuge tubes. The tubes were centrifuged to pellet the zoochlorellae, and the samples were lyophilized overnight using a VirTis Freezemobile 5 SL.

DNA extraction, PCR amplification, and sequencing

Genomic DNA was extracted from the lyophilized algal cells by using a modified CTAB (cetyltrimethylammonium bromide) extraction that included grinding the algal cells in the presence of sterile sand, following Shoup and Lewis (2003). The *rbcL* region was amplified in two separate reactions with primers M34 and M740r and M636 and M1390r (Lewis *et al.*, 1997), and these fragments were sequenced directly using amplification and internal primers. Double-stranded polymerase chain reaction (PCR) products were sequenced in 10-μl volumes with the PRISM system (Applied Biosystems, Inc.) using the manufacturer's directions. Chromatograms from individual sequencing runs were trimmed, then assembled into consensus sequences in Sequencher (GeneCodes Corp., Inc.). Most (96%) of the reported base calls were verified with sequencing reactions in both the forward and reverse orientations; the remaining nucleotides were verified from three independent sequencing reactions in the same orientation. The resulting *rbcL* fragment was 1252 nucleotides in length.

The 18S region was PCR amplified with primers 284F and 1081R (Phillips and Fawley, 2000), resulting in an 802-nucleotide fragment. Because of the presence of a mixture of animal and algal DNA in the extraction, purified PCR fragments were cloned using the TOPO TA cloning kit (Invitrogen) following the manufacturer's instructions. Ten colonies containing inserts were harvested. The presence of inserts of the predicted size was verified using PCR amplification with the M13 forward and reverse primers. The resulting PCR products were sequenced using 18S primers, yielding two clones containing algal PCR products.

The 18S and *rbcL* consensus sequences were subjected to BLAST searches (Altschul *et al.*, 1990) to screen for contaminant sequences prior to phylogenetic analyses. The 18S and *rbcL* sequences from the *A. elegantissima* green symbiont were deposited in Genbank under the numbers AY577786 and AY577787.

Phylogenetic analyses

To identify the closest matching sequences for inclusion in the phylogenetic analyses, the 18S and *rbcL* sequences

from the *A. elegantissima* green symbiont were compared to published sequences in NCBI using BLAST searches (Altschul *et al.*, 1990). These trebouxiophycean sequences and additional sequences from members of the class Trebouxiophyceae were included in the two alignments to better determine the phylogenetic placement of the symbiont. Available 18S sequences from other symbiotic green algae were also included. One of these included a partial (592-nucleotide) sequence of *Coccomyxa glaronensis*. Three species from the Chlorophyceae were used as a sister group to the Trebouxiophyceae. Foraminifera are known to contain green algal symbionts in the genus *Chlamydomonas* (Chlorophyceae); however, representative sequences from these taxa were not included in our analysis because they were characterized with ITS rDNA sequence data (Pawlowski *et al.*, 2001). Unlike the 18S alignment, the *rbcL* alignment contained many fewer sequences because of limited availability of green algal *rbcL* data in the literature, but it included sequences from the Ulvophyceae, Chlorophyceae, and Trebouxiophyceae. Genbank accession numbers from additional algal taxa are indicated by the species names in Figures 1 and 2. The final 18S alignment consisted of a total of 1774 characters, 112 of which were excluded from the analysis because they could not be aligned with certainty. Of the remaining 1662 characters, 191 were parsimony-informative. The final *rbcL* alignment contained 14 taxa and 1387 nucleotides, which included 429 parsimony-informative sites. The alignments will be available from TreeBASE (www.treebase.org).

Prior to phylogenetic analysis, each data set was analyzed using MODELTEST (Posada and Crandall, 1998). The favored substitution model for the 18S data was determined to be TIM + I + Γ. Parameter values were set as follows: relative base frequencies = (π_A = 0.2567, π_C = 0.2147, π_G = 0.2783, π_T = 0.2503), relative rate matrix = (r_{AC} = 1.0000, r_{AG} = 2.6862, r_{AT} = 1.2968, r_{CG} = 1.2968, r_{CT} = 6.1421, r_{GT} = 1.0), gamma shape = 0.6528, and proportion of invariant sites = 0.6168. The GTR + I + Γ model was determined to be best for the *rbcL* data set. Maximum likelihood parameter values were relative base frequencies = (π_A = 0.2608, π_C = 0.1644, π_G = 0.2374, π_T = 0.3374), relative rate matrix = (r_{AC} = 0.7657, r_{AG} = 2.3752, r_{AT} = 6.2564, r_{CG} = 1.1691, r_{CT} = 8.7699, r_{GT} = 1.0), gamma shape = 2.8267, and proportion of invariant sites = 0.5136.

All other portions of the phylogenetic analyses were performed using PAUP* 4.b.10 (Swofford, 2002) for UNIX. Maximum likelihood (ML) analysis used heuristic searches with 10 random additions of taxa, each followed by TBR branch swapping. Bootstrap analysis (Felsenstein, 1985) included 100 replicates, with a single random addition of taxa for each replicate, under the same model as was used for the heuristic searches. The maximum parsimony (MP) analysis included heuristic searches with 1000 random additions of taxa, followed by TBR branch swapping. Characters were given equal weight and were unordered. Bootstrap analysis included 10,000 replicates, with a single random addition of taxa per replicate.

Results

As discussed by Huss *et al.* (1999), many evolutionarily distinct lineages of small autosporic coccoid green algae are attributed to the genus *Chlorella*. While the green symbiont from *Anthopleura elegantissima* is phenotypically similar to *Chlorella* (Muscatine, 1971; O'Brien, 1978; Verde and McCloskey, 1996), it is not within the clade of *Chlorella sensu stricto* (Huss *et al.*, 1999). Using 18S data, the single ML tree (lnL score = −6641.10989) obtained (Fig. 1) indicated that the anemone alga is a member of the Trebouxiophyceae, and is in a lineage that contains other symbionts such as the isolate of *Coccomyxa glaronensis* obtained from the lichen *Nephroma* (Peltigerales) (Lohtander *et al.*, 2003), and the small green coccoids that are endophytic in the gametophytic tissues of *Ginkgo biloba* (Tremouillaux-Guiller *et al.*, 2002). The anemone alga is also distinct from species of *Trebouxia*, the most common genus of green photobionts in lichens (Friedl and Büdel, 1996), and another lichen symbiont in the genus *Myrmecia*. The MP analysis of 18S data resulted in 16 optimal trees (tree length = 770, CI = 0.5714). The strict consensus of these trees (not shown) differed from the ML tree in collapsing the weakly supported basal nodes in the ML tree (those indicated by circles) into a basal polytomy. However, the position of the *A. elegantissima* symbiont did not change; it was placed as before in a clade with *Coccomyxa* and *Paradoxia*, distinct from *Chlorella* and the *Hydra* symbionts.

Because the sequences of *Coccomyxa glaronensis* and those from the symbiont of *A. elegantissima* were partial 18S sequences, we also performed an MP analysis on the sites representing complete overlap of all sequences in the data set. This region corresponded to sites 264–618 in the full 18S alignment, for a total of 355 characters and 39 parsimony-informative sites. Heuristic searches, performed as for the full data set, produced 242 optimal trees (tree length = 102, CI = 0.7600). A strict consensus of these trees (not shown) was less resolved overall than that of the full data set. However, the zoochlorellae sequence grouped with sequences from *Paradoxia*, *Coccomyxa glaronensis*, and the *Ginkgo* endophytes, with a bootstrap value of 89.

Analyses of the *rbcL* data also place the green symbiont within the class Trebouxiophyceae, but separated from *Chlorella sensu stricto*. The single optimal ML tree (Fig. 2) had a lnL score of −7842.45399. These data were also analyzed using MP (not shown), which resulted in a single best tree (tree length = 1454, CI = 0.4986). This tree was identical to the ML tree except for the placement of the anemone symbiont near the base of the trebouxiophycean

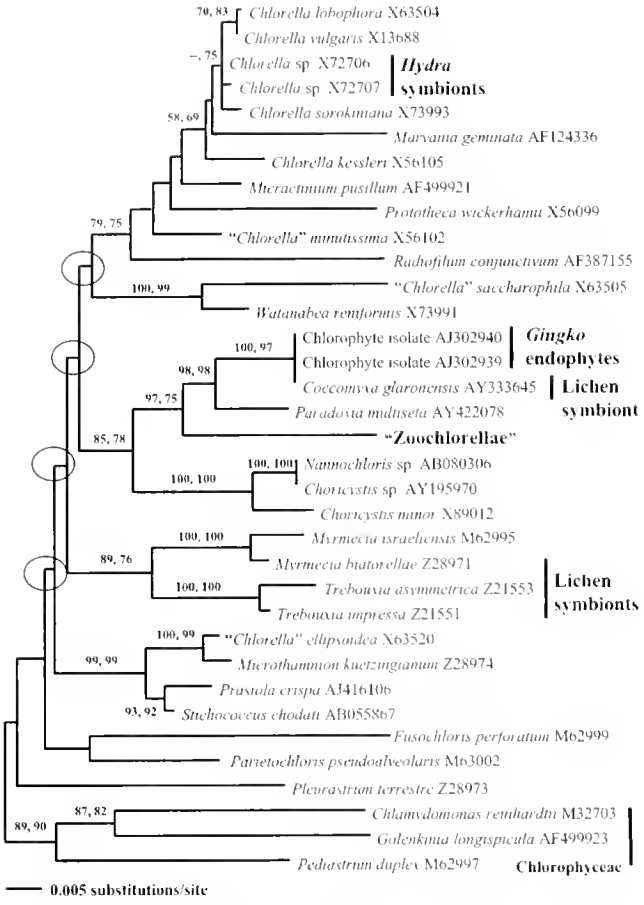

Figure 1. Phylogenetic tree obtained from a maximum likelihood analysis of 18S ribosomal RNA gene sequence from the green symbiont ("Zoochlorellae") of *Anthopleura elegantissima* and 34 additional green algae. With the exception of three sequences from members of the Chlorophyceae (indicated at base of tree by vertical bar), all of the sequences shown are from members of the Trebouxiophyceae. The positions of *Hydra* and lichen symbionts, and two *Ginkgo* endophytes, are also indicated. These sequences are from taxa that were isolated directly from their animal, plant, or fungal hosts. The nodes indicated by circles are those that collapse in the maximum parsimony analysis, leading to a basal polytomy. Numbers associated with nodes on the tree indicate maximum likelihood and maximum parsimony bootstrap proportions (out of 100 and 1000 replicates, respectively). Scale bar indicates the expected number of substitutions per site.

taxa, between *Prasiola* and a clade including the remainder of the Trebouxiophyceae and Chlorophyceae (indicated on Fig. 2). It is worthwhile emphasizing that there are currently a very limited number of published *rbcL* sequences of taxa in the Trebouxiophyceae; therefore, the placement of the "zoochlorellae" *rbcL* sequence is not close to any other taxa.

Discussion

Phylogenetic analysis of the nuclear-encoded 18S rDNA and plastid-encoded *rbcL* gene sequence data indicates that the green algal symbiont ("zoochlorellae") of *Anthopleura elegantissima* obtained from our sampling is a member of the Trebouxiophyceae (Chlorophyta), a diverse lineage of mainly coccoid green algae that has free-living and symbiotic members. The "zoochlorellae" 18S sequence forms a well-supported clade with those obtained from the lichen symbiont *Coccomyxa glaronensis*, the small green endophytes of *Ginkgo biloba* (Tremouillaux-Guiller *et al.*, 2002), and with the sequence from *Paradoxia*, a free-living alga (Fig. 1). This clade is also related to very small free-living taxa such as *Nannochloris*. The anemone alga is distinct from species of *Trebouxia*, the most common genus of green photobionts in lichens (Friedl and Büdel, 1996), and another lichen symbiont in the genus *Myrmecia*. Although the sequences of *Paradoxia* and *Coccomyxa* are the closest to that of "zoochlorellae" on the 18S phylogenetic tree, these sequences are quite distinct. The corrected distances between the 18S sequences of "zoochlorellae" and *Coccomyxa* and *Paradoxia* are 0.01907 and 0.03933, respectively. These values are closer to the range observed within orders, such as between *Myrmecia* and *Trebouxia* in the Trebouxiales, than for congeners of *Trebouxia* or *Chlorella* (data not shown).

The phylogenetic placement of zoochlorellae from *A.*

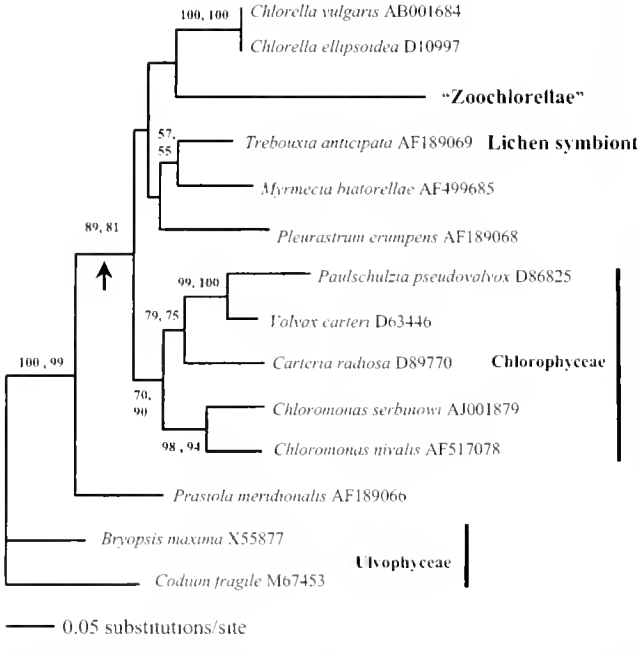

Figure 2. Phylogenetic tree obtained from a maximum likelihood analysis of *rbcL* data from the *Anthopleura elegantissima* green algal symbiont ("Zoochlorellae"), and published sequences from other members of the Trebouxiophyceae. Representative sequences of chlorophyceaen and ulvophyceaen algae were also included, as indicated by the vertical bars. One sequence of a green alga isolated from a lichen host is noted. The node indicated by an arrow shows the placement of the anemone symbiont in the maximum parsimony analysis. Numbers associated with nodes on the tree indicate maximum likelihood and maximum parsimony bootstrap proportions (out of 100 and 1000 replicates, respectively). Scale bar indicates the expected number of substitutions per site.

elegantissima in the same clade as a parasitic species of *Coccomyxa* (Fig. 1) is of particular ecological interest. Are zoochlorellae from *A. elegantissima* related to unicellular green algae that parasitize other marine animals? Algae are known to infect the epidermis of sea stars (Mortensen and Rosenvinge, 1910, 1933; pers. comm., R. Norris; all three cited in Stevenson, 1972). More recently, green algae from bivalve molluscs (mussels and scallops) have been identified as *Coccomyxa parasitica* (Stevenson and South, 1974; Gray *et al.*, 1999). However, the identification of this alga and of those that parasitize sea stars needs to be verified with molecular data, given the polyphyly of many phenotypically similar coccoid green algae (*e.g.*, Huss and Sogin, 1990; Lewis *et al.*, 1992; Potter *et al.*, 1997). In the echinoderms and molluscs, algal infection leads to tissue necrosis, loss of reproductive output, and eventual death. In all hosts, zoochlorellae maintain their photosynthetic pigments and, presumably, the ability to photosynthesize. In scallops, the algae are concentrated near shell margins where exposure to light is most likely (Stevenson, 1972). Muscatine (1971) raised the possibility that zoochlorellae are attempting to parasitize anemones and are tolerated because these hosts are capable of regulating algal populations by expelling excess algae. Perhaps the zoochlorellae in *Anthopleura* spp. are opportunistic symbionts, preempting space under conditions that promote their growth in anemones that form symbiotic associations with zooxanthellae. If so, this symbiosis may be fairly recent compared to that with zooxanthellae. Zoochlorellae persist in anemones under conditions that allow them to grow more rapidly than zooxanthellae. However, we do not know how these algae interact with each other and affect each other's growth rates under different environmental conditions. It will be difficult to advance our understanding of these interactions until we successfully culture both symbionts.

In 1881, Brandt introduced the term zoochlorella to describe the algae in freshwater hosts, including hydras, sponges and protists (Sapp, 1994). Since then, the term has been extended to include all green unicellular algae that inhabit animals. This term has no taxonomic value, as clearly the *Chlorella* symbionts of *Hydra* are phylogenetically distinct from the anemone symbiont (Fig. 1), and the genus *Chlorella* is now understood to be polyphyletic (Huss and Sogin, 1990; Huss *et al.*, 1999). Phylogenetic analyses using sequence data have indicated that green algae classified as *Chlorella* based on light microscopic features can be separated into many lineages within both the Chlorophyceae and Trebouxiophyceae. In fact, there are at least eight independent lineages that contain taxa previously classified as *Chlorella* (Huss *et al.*, 1999). *Chlorella sensu stricto* includes *C. vulgaris*, *C. lobophora*, *C. sorokiniana*, and *C. kessleri* (Trebouxiophyceae) and can be distinguished from other *Chlorella*-like taxa on the basis of its glucosamine-containing cell walls, absence of carotenoids, and pyrenoids with thylakoid penetrations (Huss *et al.*, 1999).

We do not know if multiple strains or species of morphologically similar but genetically different zoochlorellae are distributed along a latitudinal gradient within their host's range, as are the two species of *Symbiodinium*. Our cloning showed only one kind of green alga from the five pooled anemones. Although we attempted to sample individuals randomly at the field site, we do not know if the five anemone hosts were genetically related (members of the same clone) and if host genetics influences the type of algal symbiont. Future studies should compare the genetic composition of populations of zoochlorellae obtained from *A. elegantissima* and from *A. xanthogrammica* at other locations, especially at the southern and northern limits of distribution of the algae. Such comparisons would be useful to determine whether the biogeographic trends observed among dinophyte symbionts of cnidarians (Baker, 2003; LaJeunesse *et al.*, 2003) apply to symbiotic algae in other phyla. If, as we predict, different genotypes of zoochlorellae are distributed within the broad latitudinal range of their hosts, the nature of the symbiotic interactions between zoochlorellae, zooxanthellae, and the animal host, and the abilities of each partner to adapt to environmental change may differ according to geographic location.

The phylogenetic diversity of algal hosts observed in the trebouxiophycean clade containing the anemone symbiont, as illustrated in Figure 1, may indicate an inherited ability of this group of algae to participate in symbioses, making them good targets for the study of the initial establishment of a symbiotic association, host specificity, and nutritional interactions between the host and symbiont. For example, these algae may be predisposed to heterotrophy and low light conditions and able to survive long periods in the dark, and their free-living forms may differ in their growth and morphology. An integrative approach to the study of these algae, both within the host and in culture, should yield insight into the process of how algae become symbionts in other organisms.

Acknowledgments

We thank S. Olm for technical assistance and P. Lewis for critically reading the manuscript. This work was supported in part by National Aeronautics and Space Administration EXB02-0042-0054 to LAL.

Literature Cited

Altschul, S. F., W. Gish, W. Miller, E. W. Myers, and D. J. Lipman. 1990. Basic local alignment search tool. *J. Mol. Biol.* **215:** 403–410.

Baker, A. C. 2003. Flexibility and specificity in coral–algal symbiosis: diversity, ecology, and biogeography of *Symbiodinium*. *Annu. Rev. Ecol. Evol. Syst.* **34:** 661–689.

Bates, A. 2000. The intertidal distribution of two algal symbionts hosted

by *Anthopleura xanthogrammica* (Brandt 1835). *J. Exp. Mar. Biol. Ecol.* **249:** 249–262.

Engebretson, H. P., and G. Muller-Parker. 1999. Translocation of photosynthetic carbon from two algal symbionts to the sea anemone *Anthopleura elegantissima*. *Biol. Bull.* **197:** 72–81.

Felsenstein, J. 1985. Confidence limits on phylogenies: an approach using the bootstrap. *Evolution* **39:** 783–791.

Friedl, T., and B. Büdel. 1996. Photobionts. Pp. 8–23 in *Lichen Biology*, T. H. Nash, ed. Cambridge University Press, Cambridge.

Gray, A. P., I. A. N. Lucas, R. Seed, and C. A. Richardson. 1999. *Mytilus edulis chilensis* infested with *Coccomyxa parasitica* (Chlorococcales, Coccomyxaceae). *J. Molluscan Stud.* **65:** 289–294.

Huss, V. A. R., and M. L. Sogin. 1990. Phylogenetic position of some *Chlorella* species within the Chlorococcales based upon complete small-subunit ribosomal RNA sequences. *J. Mol. Evol.* **31:** 432–442.

Huss, V. A. R., C. Frank, E. C. Hartmann, M. Hirmer, A. Kloboucek, B. M. Seidel, P. Wenzeler, and E. Kessler. 1999. Biochemical taxonomy and molecular phylogeny of the genus *Chlorella* sensu lato (Chlorophyta). *J. Phycol.* **35:** 587–598.

LaJeunesse, T. C., and R. K. Trench. 2000. Biogeography of two species of *Symbiodinium* (Freudenthal) inhabiting the intertidal sea anemone *Anthopleura elegantissima* (Brandt). *Biol. Bull.* **199:** 126–134.

LaJeunesse, T. C., W. K. W. Loh, R. van Woesik, O. Hoegh-Guldberg, G. W. Schmidt, and W. K. Fitt. 2003. Low symbiont diversity in southern Great Barrier Reef corals, relative to those of the Caribbean. *Limnol. Oceanogr.* **48:** 2046–2054.

Lewis, L. A., L. W. Wilcox, P. A. Fuerst, and G. L. Floyd. 1992. Concordance of molecular and ultrastructural data in the study of zoosporic chlorococcalean green algae. *J. Phycol.* **28:** 375–380.

Lewis, L. A., B. D. Misher, and R. Vilgalys. 1997. Phylogenetic relationships of the liverworts (Hepaticae), a basal embryophyte lineage, inferred from nucleotide sequence data of the chloroplast gene *rbc*L. *Mol. Phylogenet. Evol.* **7:** 377–393.

Lohtander, K., I. Oksanen, and J. Rikkinen. 2003. Genetic diversity of green algal and cyanobacterial photobionts in *Nephroma* (Peltigerales). *Lichenologist* **35:** 325–339.

Muscatine, L. 1971. Experiments on green algae coexistent with zooxanthellae in sea anemones. *Pac. Sci.* **25:** 13–21.

O'Brien, T. L. 1978. An ultrastructural study of zoochlorellae in a marine coelenterate. *Trans. Am. Microsc. Soc.* **97:** 320–329.

O'Brien, T. L., and C. R. Wyttenbach. 1980. Some effects of temperature on the symbiotic association between zoochlorellae (Chlorophyceae) and the sea anemone *Anthopleura xanthogrammica*. *Trans. Am. Microsc. Soc.* **99:** 221–225.

Pawlowski, J., M. Holzmann, J. F. Fahrni, and P. Hallock. 2001. Molecular identification of algal endosymbionts in large miliolid foraminifera: 1. chlorophytes. *J. Eukaryot. Microbiol.* **48:** 362–367.

Phillips, K., and M. W. Fawley. 2000. Diversity of coccoid algae in shallow lakes during winter. *Phycologia* **39:** 498–506.

Posada, D., and K. A. Crandall. 1998. MODEL TEST: testing the model of DNA substitution. *Bioinformatics* **14:** 817–818.

Potter, D., T. C. LaJeunesse, G. W. Saunders, and R. A. Andersen. 1997. Convergent evolution masks extensive biodiversity among marine coccoid picoplankton. *Biodivers. Conserv.* **6:** 99–107.

Reisser, W., and M. Widowski. 1992. Taxonomy of eukaryotic algae endosymbiotic in freshwater associations. Pp. 21–40 in *Algae and Symbioses: Plants, Animals, Fungi, Viruses, Interactions Explored*, W. Reisser, ed. Biopress, Bristol, England.

Sapp, J. 1994. *Evolution by Association: A History of Symbiosis*. Oxford Univ. Press, New York.

Saunders, B., and G. Muller-Parker. 1997. The effects of temperature and light on two algal populations in the temperate sea anemone *Anthopleura elegantissima* (Brandt, 1835). *J. Exp. Mar. Biol. Ecol.* **211:** 213–224.

Seavy, B. E., and G. Muller-Parker. 2002. Chemosensory and feeding responses of the nudibranch *Aeolidia papillosa* to the symbiotic sea anemone *Anthopleura elegantissima*. *Invertebr. Biol.* **121:** 115–125.

Secord, D., and L. Augustine. 2000. Biogeography and microhabitat variation in temperate algal–invertebrate symbioses: zooxanthellae and zoochlorellae in two Pacific intertidal sea anemones, *Anthopleura elegantissima* and *A. xanthogrammica*. *Invertebr. Biol.* **119:** 139–146.

Secord, D., and G. Muller-Parker. 2004. Symbiont distribution along a light gradient within an intertidal cave. *Limnol. Oceanogr.* (In press).

Shick, J. M., W. C. Dunlap, J. S. Pearse, and V. B. Pearse. 2002. Mycosporine-like amino acid content in four species of sea anemones in the genus *Anthopleura* reflects phylogenetic but not environmental or symbiotic relationships. *Biol. Bull.* **203:** 315–330.

Shoup, S., and L. A. Lewis. 2003. Polyphyletic origin of parallel basal bodies in swimming cells of chlorophycean green algae (Chlorophyta). *J. Phycol.* **39:** 789–796.

Stevenson, R. N. 1972. *In vivo* and *in vitro* studies on an endozoic alga from the giant scallop, *Placopecten magellanicus* (Gmelin). M.S. thesis, Memorial University, St. John's, Newfoundland, Canada. 130 pp.

Stevenson, R. N., and G. R. South. 1974. *Coccomyxa parasitica* (Coccomyxaceae; Chlorococcales), a parasite of giant scallops in Newfoundland. *Br. Phycol. J.* **9:** 319–329.

Swofford, D. L. 2002. *PAUP*. Phylogenetic Analysis Using Parsimony* (*and Other Methods). Ver. 4. Sinauer Associates, Sunderland, MA.

Tremouillaux-Guiller, J., T. Rohr, R. Rohr, and V. A. R. Huss. 2002. Discovery of an endophytic alga in *Ginkgo biloba*. *Am. J. Bot.* **89:** 727–733.

Verde, E. A., and L. R. McCloskey. 1996. Photosynthesis and respiration of two species of algal symbionts in the anemone *Anthopleura elegantissima* (Brandt, 1835) (Cnidaria: Anthozoa). *J. Exp. Mar. Biol. Ecol.* **195:** 187–202.

Verde, E. A., and L. R. McCloskey. 2001. A comparative analysis of the photobiology of zooxanthellae and zoochlorellae symbiotic with the temperate clonal anemone *Anthopleura elegantissima* (Brandt). I. Effect of temperature. *Mar. Biol.* **138:** 477–489.

Verde, E. A., and L. R. McCloskey. 2002. A comparative analysis of the photobiology of zooxanthellae and zoochlorellae symbiotic with the temperate clonal anemone *Anthopleura elegantissima* (Brandt). II. Effect of light intensity. *Mar. Biol.* **141:** 225–239.

Reference: *Biol. Bull.* **207:** 93–102. (October 2004)

Patterns in Early Embryonic Motility: Effects of Size and Environmental Temperature on Vertical Velocities of Sinking and Swimming Echinoid Blastulae

KATHRYN McDONALD*

Friday Harbor Laboratories and Department of Biology, University of Washington, 620 University Road, Friday Harbor, Washington 98250-9299

Abstract. Early embryonic swimming is widespread among marine invertebrates, but quantitative information about swimming behaviors is scarce. Swimming may affect encounters with predators, positioning in the water column, and nutrient absorption. Measured rates and patterns of swimming and sinking for blastulae of four eastern Pacific echinoid species show that sinking speeds equal or exceed swimming speeds. Swimming speed scaled negatively with embryo size, though sinking speed did not scale with size. Analysis of swimming paths of *Strongylocentrotus franciscanus* revealed a temperature dependency in swimming pattern that affected speed of upward movement. Sinking speeds were significantly greater at 10 °C than at 14 °C for blastulae of all four species examined. In *Dendraster excentricus*, killing the blastulae annulled this temperature effect, indicating an active density regulation by these embryos. Finally, measurements of particle velocities around sinking and swimming *D. excentricus* blastulae show that swimming creates a more localized disturbance than sinking. Embryonic swimming may therefore decrease rather than increase encounters with pelagic predators. Results from subsequent experiments in which embryos were reared in low-oxygen environments suggest that any oxygen-absorption advantages of swimming have little, if any, effect on the development of *D. excentricus* embryos.

Introduction

The embryos of some benthic marine invertebrates develop singly in the plankton; others develop in benthic masses. While modes of embryogenesis vary, planktonic embryos of diverse taxa demonstrate early swimming ability. Solitary embryos of many species begin swimming hours prior to gastrulation. Embryos encased in egg masses may begin rotating within their capsules long before hatching. While even closely related species may differ in the timing of first swimming, positive correlations between time to first swimming and factors including egg size and time to first cleavage can account for much of the variability observed in age or stage at first swimming (Staver and Strathmann, 2002).

The ubiquity of early swimming among pelagic invertebrate embryos raises questions about its evolution and ecological consequences. The functional morphology of many invertebrate larval forms has been extensively explored; embryos are worthy of similar scrutiny, given that the survivorship of early stages has direct consequences for the viability of any developmental strategy. Interactions with predators, positioning in the water column, and uptake of dissolved nutrients are a few of the areas in which swimming could affect embryonic survival.

It has occasionally been demonstrated, and more frequently assumed, that larvae are more vulnerable to predation at early developmental stages in consequence of their smaller size and limited maneuverability (Pennington and Chia, 1984; Rumrill *et al.*, 1985; Pennington *et al.*, 1986; Rumrill, 1990). Non-swimming embryos might be still more vulnerable. In theory, flow-field differences between swimming and sinking particles produce different signals in the water column; ciliary swimming creates a steeper velocity gradient and therefore a more localized disturbance (Vogel, 1994). Sinking embryos might be more readily detectable by ambush predators. Conversely, swimming could increase encounter rates between predators and prey in a given volume of water (Gerritsen and Strickler, 1977;

Received 20 November 2003; accepted 6 July 2004.
* E-mail: kamcdon@u.washington.edu

Kiørboe and Saiz, 1995). Studies of interactions between planktonic predators and their prey (largely with copepods) have examined prey organisms with escape responses to predator proximity (Yen, 1988; Yen and Strickler, 1996; Kiørboe *et al.*, 1999); early embryos possess no such elaborate behaviors. But because the swimming capabilities of larvae play a large role in their ability to evade capture, we can also speculate that predators of embryos might experience more difficulty in handling swimming rather than non-swimming embryos.

A second hypothesis is that swimming enables a vertical migration into the water-column. Laboratory studies in still water indicate that most solitary embryos swim upward. Benthic development is associated with greater parental investment in embryos, in the form of gel layers, extra-embryonic capsules, and parental care (Pechenik, 1979; Strathmann, 1985; Lee and Strathmann, 1998; Bolton *et al.*, 2000). The perils implied by such protection suggest one advantage of vertical migration by solitary embryos. Still, the effectiveness of upward swimming must depend in large part upon the turbulence regimes embryos encounter (Metaxas, 2001). There is no cause to assume that the net upward movement of pelagic early swimming stages differs from that of pre-swimming stages in a mixed water column.

Developing sea urchin embryos consume oxygen at a near-constant rate during the early blastula stage (Yanagisawa, 1975; Isono and Yasumasu, 1968). At particle sizes characteristic of many invertebrate embryos (diameter 50–250 μm), oxygen absorption could be significantly increased through the changes in near-field flow brought about by swimming, as compared with passive sinking (Berg and Purcell, 1977). One hypothesis is that swimming enhances uptake of oxygen or other dissolved nutrients sufficiently to accelerate embryonic growth, thus increasing survivorship of embryos. Oxygen limitations for non-swimming embryos could impose a selective pressure on the timing of swimming in marine invertebrate embryogenesis.

Few published data are available on embryonic swimming abilities and behaviors. To explore the potential significance of early swimming to embryonic survival, it is necessary to know how physical characteristics of embryos (such as size and ciliation pattern) affect swimming, and how responsive swimming behaviors are to changes in environmental conditions. Even well-mixed water columns have some temperature and salinity structure, which could affect embryo distributions by altering swimming performance. Effects of swimming on nutrient or dissolved-gas uptake and on predator encounter rate are likely to depend upon speeds and patterns of embryonic swimming (Berg and Purcell, 1977; Rubinstein and Koehl, 1977; Shimeta and Jumars, 1991; Kiørboe and Saiz, 1995).

In a laboratory study, I have quantified sinking and swimming speeds of early blastulae from four echinoid species whose similar early development makes them a natural experimental system for investigating swimming behavior. Embryos of the sand dollar *Dendraster excentricus* (Eschscholtz, 1831) and the urchins *Strongylocentrotus droebachiensis* (Mueller, 1776), *S. franciscanus* (Agassiz, 1863), and *S. purpuratus* (Stimpson, 1857) develop to the blastula stage enclosed in a fertilization envelope. These species form coeloblastulae composed of monociliated cells. Blastulae begin rotating within the envelope prior to hatching, and upward swimming commences shortly after hatching. Upward orientation is passive and defined by the animal-vegetal axis. Although all embryos rotate as they swim, the angle of inclination from the vertical along the *A-V* axis varies within and among species. Under the conditions of this study, the blastulae of *D. excentricus* and *S. purpuratus* demonstrated little to no inclination of the *A-V* axis, whereas those of *S. droebachiensis* and *S. franciscanus* demonstrated a more noticeable inclination.

The objectives were to determine how swimming and sinking scale with size, if at all; how sinking speeds compare with swimming speeds; and whether these rates of movement are sensitive to changes in environmental temperature. In each species, recently hatched blastulae were the swimmers and unhatched blastulae the sinking embryos. The comparisons made are therefore akin to comparisons between swimming embryos and embryos in which hatching has been deferred to a later stage, rather than embryos that never develop ciliation.

Two extensions of this study are also presented. To test the hypothesis that swimming produces a more restricted signal to predators, I quantified flow characteristics around sinking (pre-hatching) and swimming embryos of *D. excentricus*. To evaluate the hypothesis that swimming rescues embryos from oxygen-limited conditions, the negative effects of lowered oxygen on embryogenesis must be demonstrated. Swimming could provide embryos with a diffusive advantage that they never need. For this reason, I examined the effects of decreased ambient oxygen on the growth and development of *D. excentricus* embryos.

Materials and Methods

Adult urchins (*Strongylocentrotus droebachiensis, S. purpuratus,* and *S. franciscanus*) and sand dollars (*Dendraster excentricus*) were collected and subsequently held at the Friday Harbor Laboratories, San Juan Island, Washington. Spawning was induced in ripe adults by injection of 0.53 *M* KCl. Embryos were reared on sea tables at temperatures of about 9.5°–12 °C until they were used in experiments. One to two hours prior to hatching, "sinking" (pre-hatching) embryos were taken from culture dishes and placed in syringes. If still present, jelly coats were removed by filtering embryos through Nitex mesh. Similarly, swimming embryos were taken from culture dishes between 1 and 2 h after hatching. Syringes were then incubated in

water baths for 10–15 min so that embryos could acclimate to the temperature within each experimental chamber.

Each chamber used to measure sinking and swimming rates consisted of a rectangular glass box nested within a rectangular plastic jacket (Fig. 1). Water from a temperature-controlled bath was recirculated through the jacket to bring the temperature within the inner chamber to either 10 °C or 14 °C. The inner chamber (outside dimensions: 12 cm high × 5.2 cm wide × 2.5 cm deep) was large enough to preclude wall effects in the central 0.8 cm of the box's depth. (The extent of wall effects on moving embryos was separately determined: see Discussion and Fig. 9.) A Sony video camera with a C-mounted macro lens (Canon, 55 mm/1:2.8) was focused on the center of the chamber and recorded the paths of embryos moving through its field of view. Sinking embryos were introduced into the top of the inner chamber *via* a standing glass tube: as they sank through the tube, they separated and then fell individually at terminal velocity past the camera. Swimming embryos were introduced *via* an L-shaped glass tube resting on the bottom of the chamber. A scale attached to the back of the inner chamber allowed for calibration of the recorded images.

After recordings were completed, vertical swimming speeds (and in some instances, swimming patterns) were quantified for individual embryos. Only isolated embryos swimming or falling past the camera were used in these measurements. Recordings at 10 °C and 14 °C were made simultaneously, with parallel apparatus and the same culture of embryos.

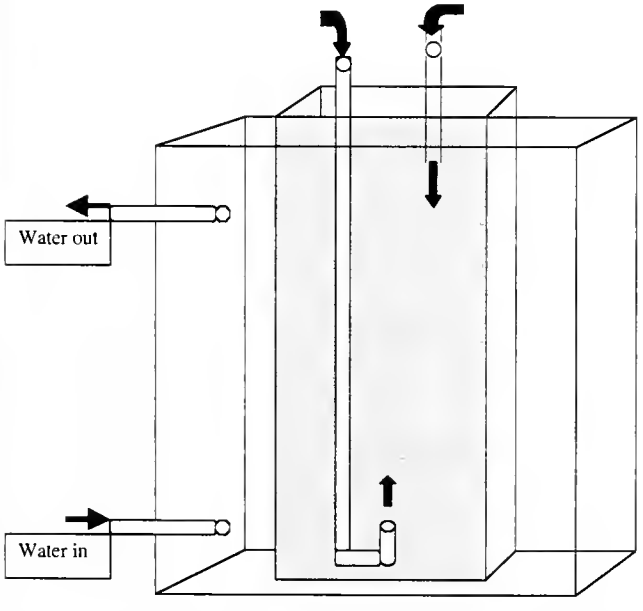

Figure 1. Diagram of experimental chamber used to measure rates of embryonic sinking and swimming. The chamber nested within a recirculating water bath that maintained seawater in the chamber at 10 °C or 14 °C. Blastulae were introduced to the chamber *via* syringe and glass tube.

To quantify flow-field characteristics of sinking and swimming *D. excentricus* embryos, a small chamber was built to fit on the stage of a horizontally mounted microscope. The chamber consisted of a 2-cm plastic petri dish, glued closed and inserted into a small acrylic plastic frame cut to size. Two small holes were drilled into one face of the dish. The circular chamber was filled with seawater and a suspension of 4.7-μm polystyrene divinylbenzene beads (Duke Scientific). The chamber was mounted on the microscope stage, and individual embryos were then gently introduced to its interior *via* a "slide" made of plastic tubing and one of the holes. Embryos moving in the bead suspension were tracked and video-recorded as they sank or swam, precluding repeated recordings of any individual. Video clips of bead movement around sinking and swimming embryos were then analyzed using ImageJ software (ver. 1.32 for Macintosh; available at http://rsb.info.nih.gov/ij/). Bead velocity could be determined frame by frame, yielding velocity profiles around sinking and swimming embryos.

Dendraster embryos were reared in three different oxygen environments to determine the sensitivity of embryonic growth and development to oxygen deprivation. Nitrogen gas was bubbled into two small tanks immersed in the same table of running seawater; rates of bubbling were adjusted to achieve stable (over a 36–48-h period) oxygen saturations of 6%–10% in the lowest oxygen treatment and 20%–25% in the intermediate oxygen treatment. Air bubbled into a third tank produced an oxygen saturation of 63%–69%. Embryos from a single culture were introduced to a mesh-sided container in each tank within an hour after insemination. Treatment containers were not mechanically stirred. A digital oxygen meter enabled frequent monitoring of oxygen levels within containers. At nine intervals throughout early development (16–45 h at 12°–13 °C; pre-hatching until prism stage), embryos were removed from each treatment and their images captured with a video microscope for later analysis. Data obtained for embryos included three measures of size as well as stage information (*e.g.*, whether embryos were rotating or nonrotating, hatched or unhatched), and abnormality rates.

Results

Blastula sizes for the four species examined are listed in Table 1. Post hoc Tukey HSD tests for between-species comparisons of sinking and swimming are summarized in Table 2.

Embryonic sinking speeds did not scale with size. At 10 °C, the smallest embryos (*Strongylocentrotus purpuratus*) sank significantly faster than the largest (*S. droebachiensis*), and at 14 °C, embryos of the three strongylocentrotid species sank at statistically indistinguishable rates (Table 2). These results indicate density differences among embryos of the four species examined. *S. purpuratus* embryos had

Table 1

Embryo size and calculated density

Species	Mean unhatched blastula diameter (μm) with fertilization envelope (n = 10)	Calculated density (kg m^{-3})*
Dendraster excentricus	159.8	$1.063 \times 10^3 \pm 0.007 \times 10^3$
Strongylocentrotus purpuratus	104.9	$1.120 \times 10^3 \pm 0.023 \times 10^3$
S. franciscanus	170.2	$1.072 \times 10^3 \pm 0.012 \times 10^3$
S. droebachiensis	211.7	$1.049 \times 10^3 \pm 0.003 \times 10^3$

* Calculations made using mean sinking rates of embryos at 10 °C; for seawater at 10 °C, $\mu = 1.391 \times 10^{-3}$ kg m^{-1}s^{-1}, $\rho = 1.024 \times 10^3$ kg m^{-3} at salinity of 30 ppt; note that unhatched embryos of these 4 species fill their fertilization envelopes to similar extents (65.3%–68.8% of total volume).

the greatest calculated density, followed by *S. franciscanus*, *Dendraster excentricus*, and *S. droebachiensis* (Table 1).

There was a strong negative correlation between swimming rate and embryo size (Fig. 2). This was true at both temperatures, so graphical data from only the 10 °C trials are shown. Sinking rates were significantly greater than swimming rates for three of the four species examined (Student's t tests, $P < 0.001$ in each case); the exception was *S. purpuratus*, whose embryos sank and swam at statistically indistinguishable rates (t test, $P = 0.45$) (Fig. 3). Again, this relationship holds true at both temperatures.

Effects of temperature on embryonic swimming rate varied by species, with one species (*D. excentricus*) swimming significantly more rapidly at 14 °C, and another (*S. franciscanus*) swimming more rapidly at 10 °C (t tests: $P < 0.01$, $P = 0.05$ respectively) (Fig. 4A). At 14 °C, *S. droebachiensis* embryos could seldom swim upward for more than a few millimeters at one time, resulting in a small sample size. Embryonic sinking rates were also sensitive to temperature. Unhatched blastulae of each species sank significantly more rapidly at 10 °C than at 14 °C (t tests: $P \leq 0.01$ for each comparison) (Fig. 4B). When unhatched *D. excentricus* blastulae were killed with 3 μM 2,4-dinitrophe-

Table 2

Between-species comparisons of sinking and swimming rates at 10° and 14 °C for Strongylocentrotus franciscanus, S. purpuratus, S. droebachiensis, *and* Dendraster excentricus

10°	Fastest			Slowest
Sinking				
Species	*S. franciscanus*	*S. purpuratus*	*S. droebachiensis*	*D. excentricus*
n	31	29	38	70
Mean (mm/s) ± SD	0.522 ± 0.1315	0.448 ± 0.1057	0.390 ± 0.0449	0.365 ± 0.0702
Swimming				
Species	*S. purpuratus*	*D. excentricus*	*S. franciscanus*	*S. droebachiensis*
n	30	80	50	32
Mean (mm/s) ± SD	0.426 ± 0.1145	0.218 ± 0.0160	0.189 ± 0.0597	0.150 ± 0.0383
14°	Fastest			Slowest
Sinking				
Species	*S. franciscanus*	*S. purpuratus*	*S. droebachiensis*	*D. excentricus*
n	39	32	53	78
Mean (mm/s) ± SD	0.416 ± 0.0690	0.384 ± 0.0861	0.369 ± 0.0260	0.307 ± 0.1080
Swimming				
Species	*S. purpuratus*	*D. excentricus*	*S. franciscanus*	*S. droebachiensis*
n	37	53	56	19
Mean (mm/s) ± SD	0.411 ± 0.1065	0.264 ± 0.0641	0.158 ± 0.0820	0.133 ± 0.0335

Results of Tukey HSD test after ANOVA (SYSTAT program). H_0: no effect of species on rate of embryo movement (swimming or sinking). All ANOVA tests rejected H_0 at $P < 0.001$: (10°, sinking: $F = 26.474$; 10°, swimming: $F = 141.229$; 14°, sinking: $F = 19.414$; 14°, swimming: $F = 81.476$).

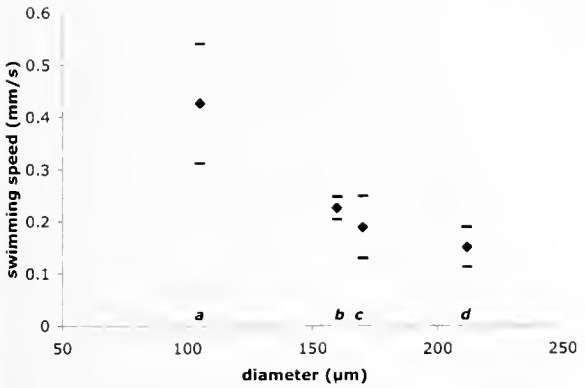

Figure 2. Mean swimming rates for blastulae at 10 °C. Bars show one standard deviation about the mean. **a** = *Strongylocentrotus purpuratus* (n = 30), **b** = *Dendraster excentricus* (n = 80), **c** = *S. franciscanus* (n = 50), **d** = *S. droebachiensis* (n = 32)

nol, a metabolic inhibitor (Flickinger, 1972), this temperature effect was negated.

A closer examination of the swimming pattern of *S. franciscanus* at the two temperatures revealed that the decrease in swimming rate at 14 °C was proximally caused by a change in swimming pattern. The radius of the helical path followed by swimming embryos was most frequently 1 embryo diameter or less, making accurate measurement of radii difficult, but helical period could vary widely among individuals. For ease of data extraction, I measured the period length (Fig. 5A). As temperature increased, the distribution of period frequencies shifted (Kolmogorov-Smirnov test for discrete data, significant difference at $\alpha < 0.001$) such that, on average, embryos at 14 °C were following paths with greater period (Fig. 5B). This had the effect of increasing the distance traveled between two vertical points, slowing their rate of ascent.

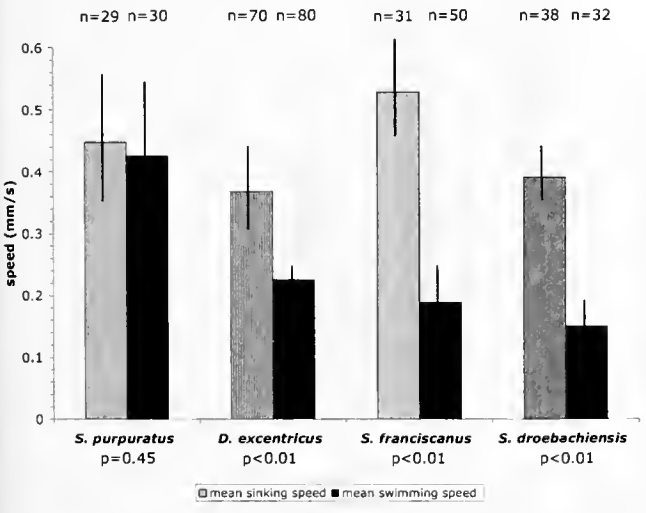

Figure 3. Comparison of sinking rates with swimming rates at 10 °C. P values for two-tailed t tests shown for each within-species comparison.

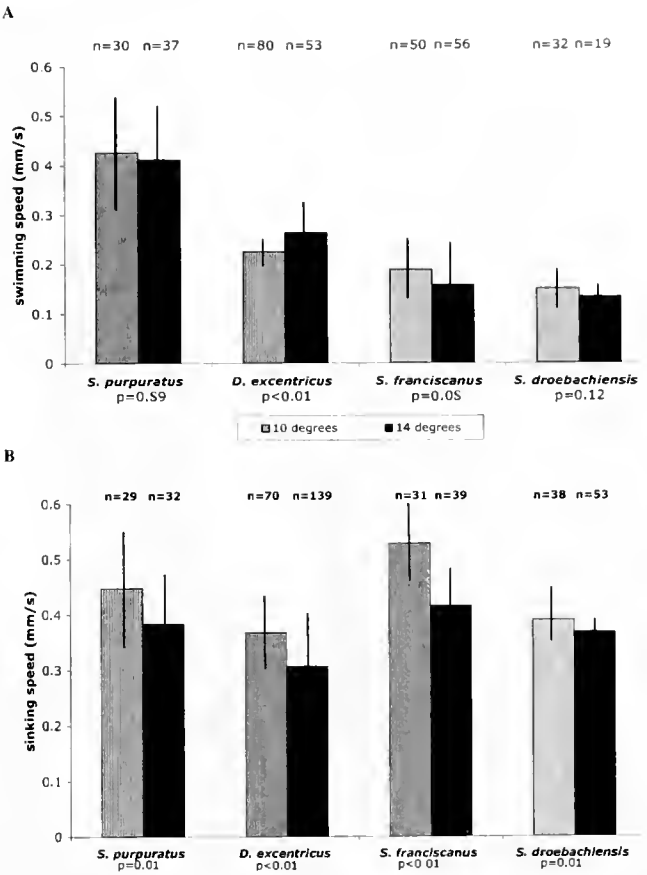

Figure 4. Sinking and swimming rates at two temperatures: light stippling indicates 10 °C; dark stippling indicates 14 °C. **(A)** Comparison of swimming rates at 10 °C and 14 °C. P values for two-tailed t tests shown for each within-species comparison. **(B)** Comparison of sinking rates at 10 °C and 14 °C. P values for two-tailed t tests shown for each within-species comparison.

High particle velocities around sinking and swimming *D. excentricus* embryos are shown in Figure 6. Swimming embryos produced a steep velocity gradient: maximum particle speed diminished rapidly with distance from the embryo surface. Sinking embryos produced a gentler velocity gradient that disturbed the water column at a greater distance from the moving embryo.

Oxygen deprivation had few significant effects on embryo development when embryos were reared in low-oxygen environments from the time of fertilization. A randomized blocked ANOVA (SYSTAT 9.0, Systat Software Inc.) showed significant effects of sample time on embryo length parallel to the animal-vegetal axis (df = 4, F = 3.515, P = 0.013), but no effects of oxygen treatment (df = 2, F = 0.612, P = 0.546) (Fig. 7A). The same ANOVA model showed significant effects of oxygen treatment on length perpendicular to the animal-vegetal axis (df = 2, F = 3.863, P = 0.024; Fig. 7B), but the spread of mean values (aver-

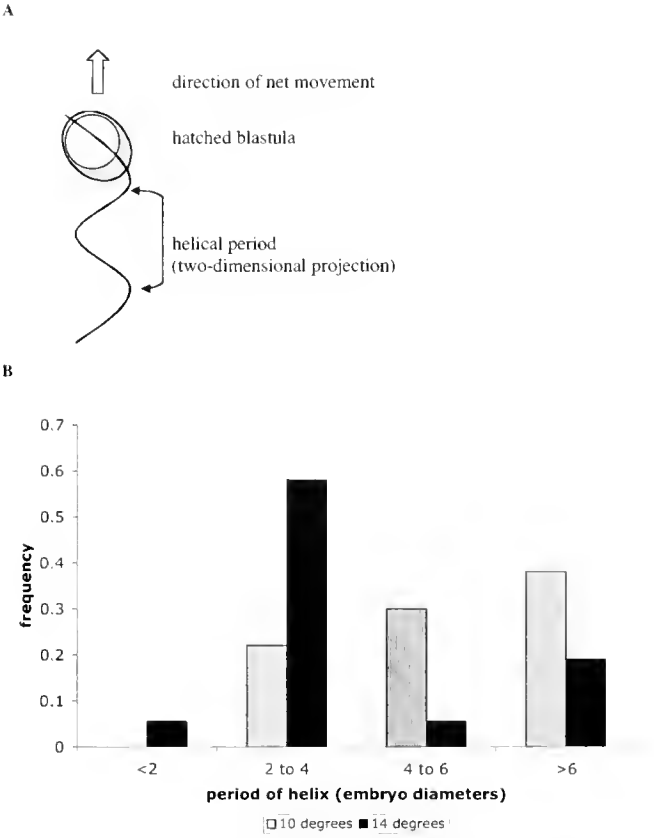

Figure 5. Illustration of variability in upward helical swimming paths of *Strongylocentrotus franciscanus* blastulae. **(A)** Two-dimensional schematic projection of the helical swimming pattern. **(B)** Distribution of helical periods among swimming blastulae at 10 °C and 14 °C. Kolmogorov-Smirnov test for discrete data, significant at $\alpha < 0.001$.

aged over all time segments for each treatment) encompassed a range of only 5 μm.

Some aspects of developmental timing demonstrated oxygen sensitivity. The frequency with which embryos were seen to rotate during the first three sampling times (prior to hatching) varied significantly by oxygen treatment, with sensitivity beginning at the intermediate oxygen level, or 20%–25% saturation (Fig. 8). The timing of vegetal plate buckling was accelerated by 2–3 h in the high oxygen treatment, as compared with the intermediate oxygen treatment (chi-square test, $P < 0.05$). At the sampling time 38 h post-fertilization, the three treatments varied significantly in the distribution of stages present: high-oxygen embryos were all prisms, while some low-oxygen embryos had not yet begun gastrulating. At this particular sampling time, each oxygen treatment showed a statistically distinct distribution of developmental stages (chi-square tests, $P < 0.001$ for each pairwise comparison).

Discussion

Embryo size and swimming speed

Stokes' law states that drag increases linearly with spheroid radius and speed of movement when Reynolds numbers are below unity. Terminal velocity at low Reynolds numbers, however, scales with the square of radius, since volume (and therefore mass) grows more rapidly than drag with increasing radius. Reynolds numbers calculated for the blastulae in this study were in the range of 0.02–0.06. If embryos are of equal density, their terminal velocities should scale positively with embryo size. This was not the

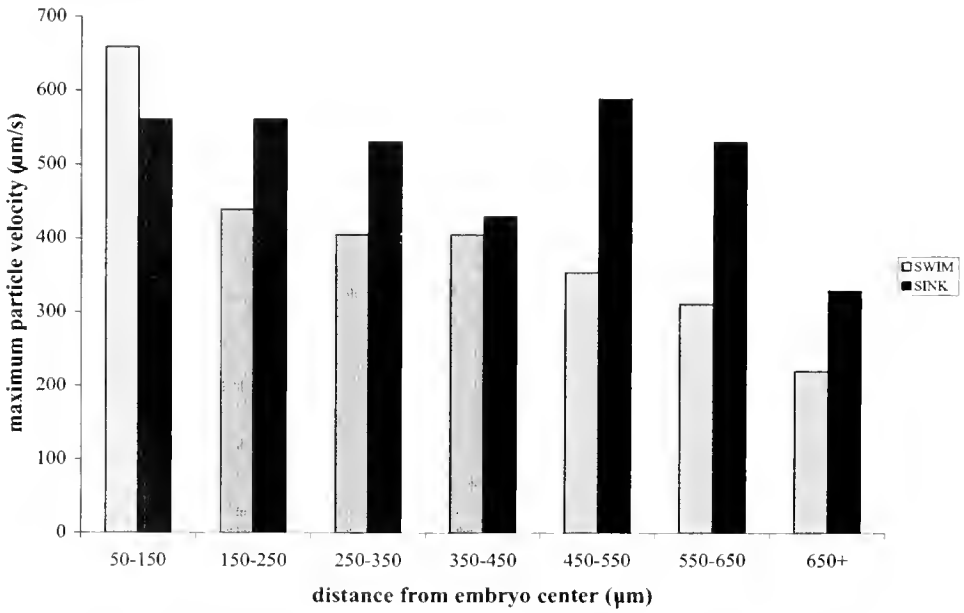

Figure 6. Maximum particle velocity around sinking and swimming *Dendraster excentricus* embryos as a function of distance from the embryo center. Outliers (defined as particles in each distance bin moving ≥50 μm/s faster than the next fastest particle) were removed.

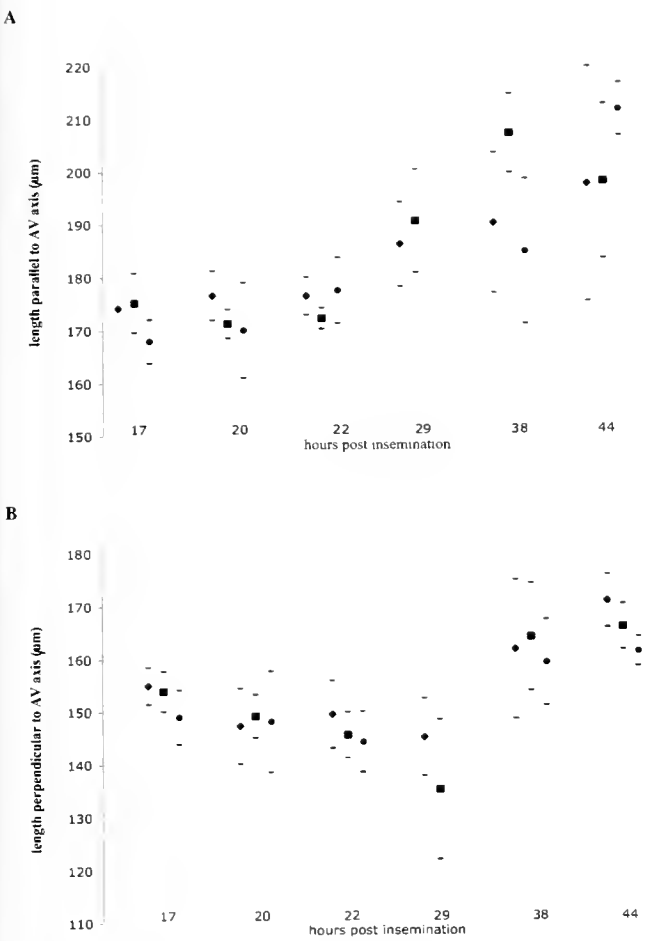

Figure 7. Expansion of *Dendraster excentricus* embryos in three oxygen-depleted environments. **(A)** Expansion along the animal-vegetal axis. **(B)** Expansion perpendicular to the animal-vegetal axis. Solid shapes indicate mean lengths in μm with corresponding SD bars. Solid diamond = high oxygen treatment (63%–69% saturation); solid square = intermediate oxygen treatment (20%–25% saturation); solid circle = low oxygen treatment (5%–9% saturation). One sampling interval (29 h post insem.) was missed for the low oxygen treatment. Note that sampling intervals are arranged categorically, not to scale.

case for embryos of the four species examined here, which indicates differences in interspecific density. Calculated densities are reported in Table 1.

While forces of drag and thrust acting on ciliated swimming embryos cannot be simply modeled using Stokes' law, some of the same relationships can guide our thinking about the factors influencing swimming speed. If, for instance, embryos of these species had about the same density and similar thrust-generating capacity—if they had roughly the same number of cells and hence cilia at hatching—then the strong negative scaling of speed with size could be due mainly to drag effects. However, there is evidence that smaller embryos can achieve greater upward velocity than their larger congeners with less investment in thrust. Kohtaro Tanaka (University of Washington; pers. comm.) found that *Dendraster excentricus* blastulae have 1200–1500 cells at hatching, while Hinegardner (1967) found approximately 350 cells for *Strongylocentrotus purpuratus*.

In other discussions of the tradeoff between embryo size and survivorship in invertebrates, small egg size is usually considered a liability for planktonic embryos. Small size may increase the number of predators capable of ingesting an embryo (Hansen *et al.*, 1994). Also, small planktotrophic embryos may need to spend more time feeding before they are capable of metamorphosis, extending their period of high mortality risk in the plankton (Vance, 1973; Strathmann, 1985; Sinervo and McEdward, 1988; Rumrill, 1990), though size-advantage hypotheses for early embryos are not strongly supported by data. The observed relationship between swimming speed and embryo size suggests one possible advantage of small egg size from the embryo's perspective. Since only four closely related species were used in establishing this relationship, a wider sampling of embryonic swimming rates would be useful.

Effects of temperature on motility

The increased sinking rates of pre-hatching blastulae at 10 °C as compared with 14 °C had implications for embryonic density. Because the viscosity of seawater increases with decreasing temperature, I expected to observe a slight increase in sinking rate with the 4 °C increase in temperature. The uniformity of the result (significant for all four species) suggested a previously unsuspected active density regulation by these unhatched blastulae. Because killed embryos at both temperatures reverted to sinking rates statistically similar to those of living embryos at 14 °C, it seems that the regulatory mechanism is acting at the lower

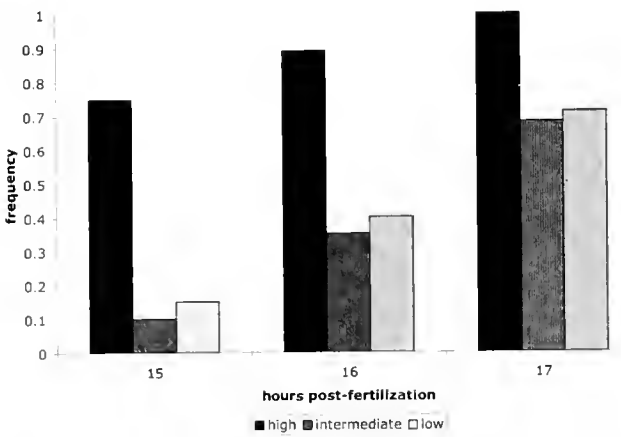

Figure 8. Frequency of occurrence of rotation in unhatched embryos reared in three oxygen environments. Embryos were scored as rotating or non-rotating. Chi-square tests distinguish between the high oxygen treatment as compared with low and intermediate treatments ($P < 0.01$ for each pairwise comparison), whereas the low and intermediate treatments are indistinguishable at any time point ($P > 0.05$).

rather than the higher temperature. It was expected that a metabolic inhibitor (2,4-dinitrophenol) would kill embryos without affecting their permeability, and the sinking speeds measured for killed embryos appear to support this assumption.

Tracking the sinking speeds of *D. excentricus* blastulae during development indicates that density regulation is occurring as early as the 7th cleavage, when the blastocoel begins to take shape (about the same time intercellular junctions are forming; Okazaki, 1975). Further investigation is needed to ascertain whether the regulation truly coincides with blastocoel formation.

Density regulatory mechanisms might be a complicating factor in comparisons of swimming rates between species. Some of the temperature sensitivity observed in embryonic swimming behavior could result from this regulatory activity. However, observations of *Strongylocentrotus franciscanus* swimming embryos indicate that, in their case, the temperature sensitivity is mediated at least in part by a change in swimming pattern. The decrease in upward velocity with increased temperature could be a useful physiological response in embryos entering a region where temperatures are higher than optimal for normal development.

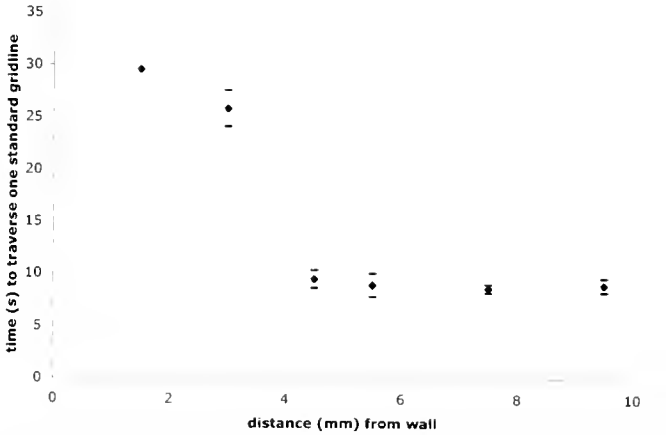

Figure 9. *Strongylocentrotus droebachiensis* blastulae sinking (14 °C) at various distances from the forward wall of the chamber depicted in Fig. 1. A camera lens was focused at different depths to track sinking rates and their sensitivity to wall proximity. The total inside depth of the chamber (19 mm) proved more than sufficient to allow measurement of speed of movement without the interference of wall effects. Embryos within about 4 mm of the chamber wall exhibited slowed sinking. Sinking speeds of embryos within 5 mm of the chamber center appeared stable. All sinking and swimming measurements reported in this study were taken from embryos passing within 2 mm of the chamber center.

Vertical speeds and velocity profiles

Measured sinking speeds for pre-hatching blastulae were, with one exception, significantly greater than speeds of upward swimming. This was surprising, as Mogami *et al.* (1988) found that *Hemicentrotus pulcherrimus* gastrulae swam about 3 times faster than they sank. The sinking rates reported by those authors are markedly lower than the results reported here for earlier embryonic stages. They employed a viewing chamber of 0.5-mm thickness, whereas I found measurable wall effects on sinking rates when embryos fell within 3–4 mm of a wall (Fig. 9). By restricting observations to the central 4 mm of the 19-mm chamber, wall effects were minimized. Also, these two studies define sinking embryos differently. Mogami *et al.* treated larvae with KCN to measure passive sinking rates at the same stages for which swimming rates were quantified. I have focused on slightly earlier developmental stages to achieve a similar comparison between vertical translation rates of hatched and unhatched embryos. These results demonstrate that non-swimming embryos of four echinoid species move through the water column at about the same speed as newly hatched swimmers.

If swimmers do not move more rapidly than non-swimmers, then the hypothesis that they are at a disadvantage because of increased encounters with certain types of predators (Gerritsen and Strickler, 1977; Greene, 1986) may be invalid. Effects of embryo speed on capture by predators probably vary, but studies with copepods indicated that increased prey velocity reduced the likelihood of post-encounter capture of ciliates whose volumes were similar to those of the embryos in this study (Jonsson and Tiselius, 1990). Rapidly sinking embryos might be as difficult for predators to capture as swimmers, though sinkers lack the helical motion and steeper velocity gradient characteristic of swimmers, with possible consequences for their vulnerability to detection and capture. Likewise, sinkers might not experience a marked disadvantage in terms of oxygen or dissolved-nutrient absorption.

The flow-field profiles of sinking and swimming *D. excentricus* blastulae demonstrate that flow characteristics differ even if actual rates of movement are more similar than previously suspected. As predicted, sinking embryos disturb the surrounding water column at a greater distance than do swimming embryos, which create steeper velocity gradients in the surrounding fluid. Natural turbulence can interfere with the ability of ambush predators to detect even short-range signals (Saiz *et al.*, 1992; Saiz and Kiorboe, 1995). Under conditions of low turbulent energy, however, ciliary activity may dampen water-column disturbance around moving embryos.

Swimming and oxygen stress

The steeper velocity gradient around swimming *D. excentricus* blastulae also has implications for the absorption of dissolved nutrients. Even if unhatched embryos sink at least as quickly as they are capable of swimming at hatching, the near-field velocity profile created by ciliary activity in swimming embryos could still provide swimmers with

greater nutrient and dissolved-gas flux. It is debatable whether early embryos gain anything from this flux increase. Some early embryos have been observed to transport dissolved organic molecules from the environment (Manahan, 1983; Shilling and Bosch, 1994), but the importance of such transport for embryonic growth and development has yet to be broadly established. Oxygen-sensitive phases in early urchin embryogenesis probably correspond to periods when metabolic demands are increasing. Older studies indicate that oxygen consumption in urchins increases during cleavage and plateaus briefly during the early blastula stage (summarized in Yanagisawa, 1975), whereas recent work with *Hemicentrotus pulcherrimus* shows respiratory rates that are nearly constant until hatching, after which time oxygen consumption increases continuously through gastrulation (Fujiwara *et al.*, 2000).

Rearing *D. excentricus* embryos in environments at 20%–25% and 5%–9% oxygen saturation demonstrated the impressive tolerance of these embryos for reduced-oxygen conditions. Changes in embryo size were similar across treatments, and although some delays in developmental timing resulted from low ambient oxygen, these delays were only 2–3 h. Oxygen availability was never so low that the development of hatched, swimming embryos prior to gastrulation was dramatically slowed or arrested, and size was unaffected; this suggests that swimming would rescue early planktonic embryos from hypoxia only when natural conditions were extreme.

Conclusions

The benefits of early swimming may include ecological and physiological effects that promote embryo survivorship. The results of this study indicate several potential advantages of swimming. Measured sinking speeds were in most cases greater than upward swimming speeds, so swimming could decrease encounters with predators. The flow-field characteristics around swimming embryos were also distinct from those of sinking embryos, which may further reduce detection or successful handling by predators. Embryo swimming speed scaled negatively with size in a still-water laboratory environment, indicating a possible advantage of small size for planktonic embryos. This speed-size scaling also raises the question of turbulence effects on swimming ability. The capacity of embryos to reorient themselves after being turned is a component of swimming behavior not explored in this study, but it is likely to be as important as upward swimming rate in determining embryo progress through turbulence. The tolerance of *Dendraster excentricus* embryos for low-oxygen conditions suggests that swimming may not be crucial for ensuring oxygen delivery to developing embryos, except in unusually hypoxic environments. Finally, the unexpected results indicating density regulation in unhatched blastulae of all four species examined are intriguing and deserve closer scrutiny for both pre-swimming and swimming stages.

Acknowledgments

I thank R.R. Strathmann for his advice and guidance. T. Daniel, J. Ruesink, D. Grünbaum, M.W. Jacobs, K.M. Sherrard, and B. Pernet offered valuable suggestions during the course of this work. Comments from two anonymous reviewers greatly improved the manuscript. This research was supported by National Science Foundation grants IBN-0113603 and OCE-0217304, a Wainwright fellowship from the Friday Harbor Laboratories, and a fellowship from Achievement Rewards for College Scientists (Seattle, WA, chapter).

Literature Cited

Berg, H. C., and E. M. Purcell. 1977. Physics of chemoreception. *Biophys. J.* **20:** 193–219.

Bolton, T. F., F. I. M. Thomas, and C. N. Leonard. 2000. Maternal energy investment in eggs and jelly coats surrounding eggs of the echinoid *Arbacia punctulata*. *Biol. Bull.* **199:** 1–5.

Flickinger, C. J. 1972. Influence of inhibitors of energy metabolism on the formation of Golgi bodies in amoebae. *Exp. Cell Res.* **73:** 154–160.

Fujiwara, A., Y. Kamata, K. Asami, and I. Yasumasu. 2000. Relationship between ATP level and respiratory rate in sea urchin embryos. *Dev. Growth Differ.* **42:** 155–165.

Gerritsen, J., and J. R. Strickler. 1977. Encounter probability and community structure in zooplankton: a mathematical model. *J. Fish. Res. Board Can.* **34:** 73–82.

Greene, C. H. 1986. Patterns of prey selection: implications of predator foraging tactics. *Am. Nat.* **128(6):** 824–839.

Hansen, B., P. K. Bjørnsen, and P. J. Hansen. 1994. The size ratio between planktonic predators and their prey. *Limnol. Oceanogr.* **39(2):** 395–403.

Hinegardner, R. T. 1967. Echinoderms. Pp. 139–155 in *Methods in Developmental Biology*, F. J. Wilt and N. K. Wessels, eds. Crowell-Collier, New York.

Isono, N., and I. Yasumasu. 1968. Pathways of carbohydrate breakdown in sea urchin eggs. *Exp. Cell Res.* **50:** 616–626.

Jonsson, P. R., and P. Tiselius. 1990. Feeding behaviour, prey detection and capture efficiency of the copepod *Acartia tonsa* feeding on planktonic ciliates. *Mar. Ecol. Prog. Ser.* **60:** 35–44.

Kiørboe, T., and E. Saiz. 1995. Planktivorous feeding in calm and turbulent environments, with emphasis on copepods. *Mar. Ecol. Prog. Ser.* **122:** 147–158.

Kiørboe, T., E. Saiz, and A. W. Visser. 1999. Predator and prey perception in copepods due to hydrodynamical signals. *Mar. Ecol. Prog. Ser.* **179:** 97–111.

Lee, C. E., and R. R. Strathmann. 1998. Scaling of gelatinous clutches: effects of siblings' competition for oxygen on clutch size and parental investment per offspring. *Am. Nat.* **151:** 293–310.

Manahan, D. T. 1983. The uptake of dissolved glycine following fertilization of oyster eggs. (*Crassostrea gigas* Thunberg). *J. Exp. Mar. Biol. Ecol.* **68:** 53–58.

Metaxas, A. 2001. Behaviour in flow: perspectives on the distribution and dispersion of meroplanktonic larvae in the water column. *Can. J. Fish. Aquat. Sci.* **58:** 86–98.

Mogami, Y., C. Oobayashi, T. Yamaguchi, Y. Ogiso, and S. Baba. 1988. Negative geotaxis in sea urchin larvae: a possible role of

mechanoreception in the late stages of development. *J. Exp. Biol.* **137:** 141–156.

Okazaki, K. 1975. Normal development to metamorphosis. Pp. 177–232 in *The Sea Urchin Embryo: Biochemistry and Morphogenesis,* G. Czihak, ed. Springer-Verlag, Berlin.

Pechenik, J. A. 1979. Role of encapsulation in invertebrate life histories. *Am. Nat.* **114:** 859–870.

Pennington, J. T., and F.-S. Chia. 1984. Morphological and behavioral defenses of trochophore larvae of *Sabellaria cementarium* (Polychaeta) against four planktonic predators. *Biol. Bull.* **167:** 168–175.

Pennington, J. T., S. S. Rumrill, and F.-S. Chia. 1986. Stage-specific predation upon embryos and larvae of the Pacific sand dollar, *Dendraster excentricus,* by 11 species of common zooplanktonic predators. *Bull. Mar. Sci.* **39(2):** 234–240.

Rubinstein, D. I., and M. A. R. Koehl. 1977. The mechanisms of filter-feeding: some theoretical considerations. *Am. Nat.* **111:** 981–994.

Rumrill, S. S. 1990. Natural mortality of marine larvae. *Ophelia* **32:** 163–198.

Rumrill, S. S., J. T. Pennington, and F.-S. Chia. 1985. Differential susceptibility of marine invertebrate larvae: laboratory predation of sand dollar, *Dendraster excentricus* (Eschscholtz), embryos and larvae by zoeae of the red crab, *Cancer productus* Randall. *J. Exp. Mar. Biol. Ecol.* **90:** 193–208.

Saiz, E., and T. Kiørboe. 1995. Predatory and suspension feeding of the copepod *Acartia tonsa* in turbulent environments. *Mar. Ecol. Prog. Ser.* **122:** 147–158.

Saiz, E., M. Alcaraz, and G. A. Paffenhofer. 1992. Effects of small-scale turbulence on feeding rate and gross-growth efficiency of three *Acartia* species (Copepoda: Calanoida). *J. Plankton Res.* **14:** 1085–1097.

Shilling, F. M., and I. Bosch. 1994. 'Pre-feeding' embryos of Antarctic and temperate echinoderms use dissolved organic material for growth and metabolic needs. *Mar. Ecol. Prog. Ser.* **109:** 173–181.

Shimeta, J., and P. A. Jumars. 1991. Physical mechanisms and rates of particle capture by suspension-feeders. *Oceanogr. Mar. Biol. Annu. Rev.* **29:** 191–257.

Sinervo, B., and L. R. McEdward. 1988. Developmental consequences of an evolutionary change in egg size: an experimental test. *Evolution* **42(5):** 885–899.

Staver, J. M., and R. R. Strathmann. 2002. Evolution of fast development of planktonic embryos to early swimming. *Biol. Bull.* **203:** 58–69.

Strathmann, R. R. 1985. Feeding and non-feeding larval development and life-history evolution in marine invertebrates. *Annu. Rev. Ecol. Syst.* **16:** 339–361.

Vance, R. R. 1973. On reproductive strategies in benthic marine invertebrates. *Am. Nat.* **107:** 339–352.

Vogel, S., 1994. *Life in Moving Fluids: The Physical Biology of Flow,* 2nd ed. Princeton University Press, Princeton.

Yanagisawa, T. 1975. Respiration and energy metabolism. Pp. 510–549 in *The Sea Urchin Embryo: Biochemistry and Morphogenesis,* G. Czihak, ed. Springer-Verlag, Berlin.

Yen, J. 1988. Directionality and swimming speeds in predator-prey and male-female interactions of *Euchaeta rimana,* a subtropical marine copepod. *Bull. Mar. Sci.* **43:** 395–403.

Yen, J., and J. R. Strickler. 1996. Advertisement and concealment in the plankton: What makes a copepod hydrodynamically conspicuous? *Invertebr. Biol.* **115:** 191–205.

Reference: *Biol. Bull.* **207:** 103–115. (October 2004)

A Waterborne Behavioral Cue for the Actinotroch Larva of *Phoronis pallida* (Phoronida) Produced by *Upogebia pugettensis* (Decapoda: Thalassinidea)

SCOTT SANTAGATA*

Allan Hancock Foundation, University of Southern California, 3616 Trousdale Parkway, Los Angeles, California 90089

Abstract. *Phoronis pallida* (Phoronida) occurs as a commensal within the burrow of *Upogebia pugettensis* (Decapoda: Thalassinidea). *Upogebia*-conditioned seawater (UCSW) induced an exploratory swimming behavior in competent larvae of *P. pallida* in a dosage-dependent manner. This behavior included a significant increase in swimming speed that was directed downward, along with the repeated probing of the bottom with the sensory portion of the oral hood. The waterborne cue from the shrimp was present in the gut effluent, and the swimming behavior was not the result of the elevated ammonia concentration. Molecular weight separation of the UCSW estimated that the cue was between 10 and 50 kDa. Enzymatic treatments showed that the cue's activity could be eliminated by arginase and significantly reduced by lipase. Competent larvae were also induced to metamorphose when exposed to 20 m*M* CsCl for 30 min. Larvae did not respond to CsCl when cultured about 4 weeks past the onset of competence. Compared with actinotroch larvae of other phoronid species, *P. pallida* larvae exhibit greater behavioral specificity and neuronal differences within the hood sense organ. These anatomical and behavioral differences may have been maintained through a coevolutionary process among *P. pallida* and species of thalassinid shrimps that share *Upogebia* life-history characteristics.

Received 15 March 2004; accepted 20 July 2004.

* Current address: Smithsonian Marine Station, 701 Seaway Drive, Fort Pierce, FL 34949. E-mail: santagata@sms.si.edu

Abbreviations: FSW, filtered seawater; NCSW, *Neotrypaea*-conditioned seawater; UCSW, *Upogebia*-conditioned seawater.

Introduction

Many marine invertebrates produce larvae that spend hours to months in the plankton before becoming competent to respond to environmental signals emanating from the adult habitat (Pawlik, 1992; Rittschof *et al.*, 1998). These signals include a variety of physical and chemical cues. Investigations into chemical cues have focused mainly on those that induce metamorphosis. Such chemical cues may be waterborne or bound to the substratum. Some metamorphic cues are produced by conspecifics (Pearce and Scheibling, 1990; Zimmer-Faust and Tamburri, 1994; Matsumura *et al.*, 1998), prey species of the adult (Hadfield and Pennington, 1990; Lambert *et al.*, 1997; Krug and Manzi, 1999), or by bacterial and algal species associated with the substratum (Morse and Morse, 1991; Leitz and Wagner, 1993).

Larval recruitment has sometimes been described as a passive process dependent upon hydrodynamic forces (Harvey *et al.*, 1995), but increasing evidence suggests that the adult distribution of marine invertebrates can be influenced by larval behaviors (Gross *et al.*, 1992; Eckman *et al.*, 1994; Kingsford *et al.*, 2002). Some waterborne chemical cues emanating from the adult habitat induce changes in the swimming behavior and orientation of competent larvae before metamorphosis (Zimmer-Faust and Tamburri, 1994; Tamburri *et al.*, 1996). Although settlement behaviors have often been associated with the cessation of larval swimming (Rodriguez *et al.*, 1995; Zhao and Qian, 2002), other accounts describe settlement behavior that includes active habitat exploration before metamorphosis. Waterborne cues that induce exploratory behaviors are particularly influential in low-flow estuarine habitats during slack tide or periods of moderate flow (Krug and Zimmer, 2000; Browne and Zim-

mer, 2001; Fingerut *et al.*, 2003; Forward *et al.*, 2003). Some of these chemical cues are low-molecular-weight peptides with either arginine or lysine at their carboxy terminus. These small peptides are present in the effluent of invertebrates and produced as the result of invertebrate secretion, metabolism, and digestion (Rittschof, 1993; Browne *et al.*, 1998).

A diverse community of invertebrates inhabits the mud flats along the Pacific coast of the United States. A dominant feature of these habitats is the network of burrows created by the marine worms *Chaetopterus variopedatus* and *Urechis caupo*, and thalassinid shrimps such as *Neotrypaea californiensis* and *Upogebia pugettensis* (Ricketts *et al.*, 1985; Manning and Felder, 1991). These taxa are also known for the commensal symbionts that inhabit their burrows (Ricketts *et al.*, 1985). *U. pugettensis* has at least 15 documented commensal species associated with it, 7 of which are obligate relationships. Fewer commensals and obligate relationships are documented for each of the other three burrowing invertebrates (Haig and Abbott, 1980; Ricketts *et al.*, 1985; Hornig *et al.*, 1989). Studies of echinoderms and their symbiotic polychaetes have found that chemical cues from the host are recognized by the symbionts (Wagner *et al.*, 1979), and stimuli produced by the hosts probably attract particular commensal species at either the larval or the adult stage.

The Phoronida comprises at least 10 recognized species and a larval form known as the actinotroch (Emig, 1974, 1982). Species of phoronid are also noted for their wide geographical distributions and often occur in conspecific aggregations (Emig, 1982; Zimmer, 1991). Along the Pacific coast of the United States, adults of *Phoronis pallida* (Fig. 1A) are found embedded in the burrow wall of *Upogebia pugettensis* (Fig. 1B; also see Thompson, 1972). *U. pugettensis* incorporates mucus from its hindgut gland into the walls of its burrows (Fig. 1C). Thompson (1972) demonstrated that this mucus was composed of mucopolysaccharides that exhibit neutral, nonsulfated acid, weak-acid, and weak-acid-sulfated properties. This secretion binds the surrounding sediments and acts as a lubricant. Secretions from the hindgut gland and other properties of *U. pugettensis* may act as cues that enhance the recruitment success of competent *P. pallida* larvae.

This study investigated the behavior and metamorphosis of *Phoronis pallida* [(Schneider, 1862) Silén, 1952] larvae in response to possible cue sources from its adult habitat. Enzymatic treatments and molecular-weight separations were used to test whether behavioral cues for *P. pallida* larvae shared molecular properties with larval chemical cues from other marine invertebrates. These data are compared to treatments with compounds that artificially induce behavioral changes and metamorphosis in the actinotroch larvae of other phoronid species (Herrmann, 1979, 1995).

A waterborne cue produced in the effluent of *Upogebia pugettensis* (Dana, 1852) induced competent larvae of *P. pallida* to swim faster in a downward direction and to repeatedly probe the bottom with the sensory portion of the oral hood. The induced behavior was dosage-dependent, and the activity of the cue was eliminated by treatment with arginase. The molecular weight of the cue was estimated to be between 10 and 50 kDa, indicating that the cue was not strictly a small peptide. Competent larvae were artificially induced to metamorphose when exposed to 20 m*M* CsCl for 30 min; however, no naturally occurring substrate or compound was found that induced natural metamorphosis. Although the exploratory behavior of *P. pallida* larvae differed slightly from reversible "settlement" behaviors described for veliger larvae (Chia and Koss, 1988), evidence suggests that active swimming behaviors ("dive-bombing") aid larvae in finding suitable metamorphic sites when in the bottom boundary layer (Finelli and Wethey, 2003). Compared with actinotroch larvae of other phoronid species, *P. pallida* larvae exhibit greater behavioral specificity and neuronal differences within the hood sense organ (Santagata, 2002). These anatomical and behavioral differences may have been maintained through a coevolutionary process among *P. pallida* and species of thalassinid shrimps that share life-history characteristics with *Upogebia*.

Materials and Methods

Collection of adults and culture of larvae

Phoronis pallida adults were collected in the summers of 1997, 1998, and 1999 from Bodega Bay (CA), Coos Bay (OR), and False Bay (WA). *P. pallida* was most often observed in the middle part of the Y-shaped burrow of *Upogebia pugettensis*. The best way to maximize the number of phoronids collected was to extract this portion of the shrimp's burrow by hand and sieve the sediment through a 1-mm screen. More than 50 phoronids per burrow have been observed in particular sites (Coos Bay, OR). Collection data supported the observations of Thompson (1972) that *P. pallida* is an obligate commensal with *U. pugettensis* but not with species of *Neotrypaea* at these study sites. Reproductive individuals of *P. pallida* (found May–October) are simultaneous hermaphrodites and may contain thousands of fertilized primary oocytes in the trunk coelom. Fertilized eggs are extruded through the nephridiopores into the burrow space, from which they are expelled to complete their development in the water column. Competent larvae were reared in the laboratory as described previously (Santagata, 2004).

Initial observations on the responses of larval stages to possible cues were made at the University of Southern California with larvae reared from adults collected from all field sites. Competent larvae are 450–550 μm in total length; they possess 10 tentacles and a single (red) corpuscle mass (Fig. 1D). Only this larval stage reared from

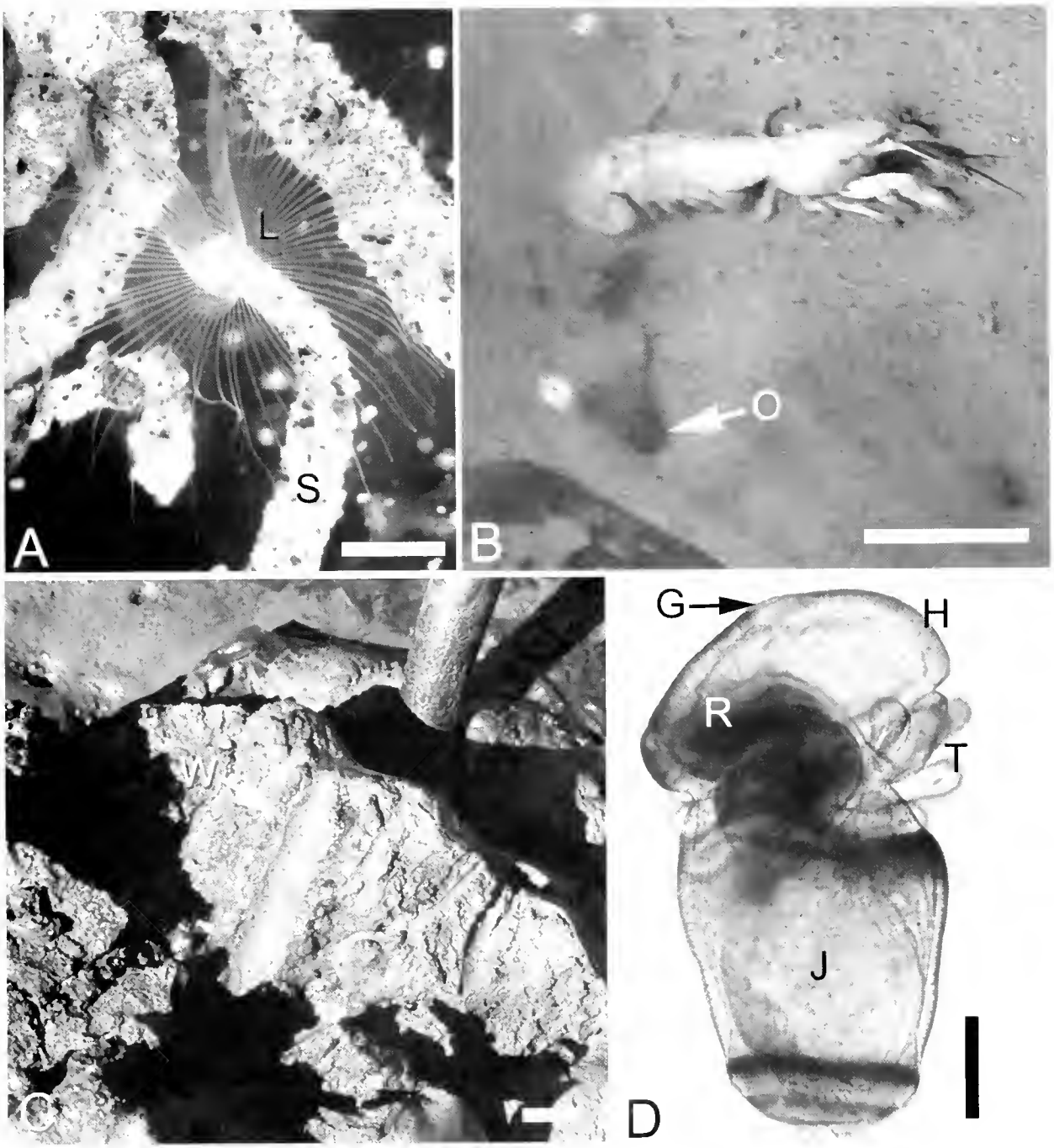

Figure 1. *Phoronis pallida* and *Upogebia pugettensis* from the populations at False Bay, San Juan Island, Washington. (A) Adult *P. pallida* with the lophophore (L) extended from its distinctive bent sand tube (S). (B) Adult shrimp of *U. pugettensis* extracted from its burrow. Note the opening to another *Upogebia* burrow (O). (C) Incurrent section of the burrow wall (W) of *Upogebia*. (D) Competent larva of *P. pallida* with a thickened hood (H) that includes the apical ganglion (G). Competent larvae also have a red corpuscle mass (R), 10 tentacles (T), and a differentiated juvenile trunk sac (J). Photograph in (D) reprinted with permission of Blackwell Publishing (Santagata, 2002). Scale bars: 2 mm (A), 5 cm (B and C), and 100 μm (D).

adults collected from False Bay, Washington, was included for subsequent experiments carried out at Friday Harbor Laboratories, Washington.

Cue preparation and experimental assays

Upogebia-conditioned seawater (UCSW) was prepared by placing two adult shrimp (each about 10 cm in length) in 2 l of aerated, 0.22-μm-filtered seawater (FSW) for 2 h at 15 °C. The shrimp were then removed, and the solution was refiltered (0.22 μm). *Neotrypaea californiensis*-conditioned seawater was prepared in the same manner. The hindgut gland of one specimen of *U. pugettensis* was dissected out, and aqueous extracts were prepared in 5 ml of FSW using a mortar and pestle. The gut of another specimen was also dissected out and bisected sagittally. Aerobic bacteria were isolated from the gut tissue with a sterilized loop and cultured on a marine agar medium (80% FSW, 20% distilled water, 5 g peptone, 1 g yeast extract, and 15 g agar/l). Three morphologically different colonies from these plates were cultured individually in liquid medium (same as above minus the agar) in sterile test tubes for a day at 37 °C. One culture was inoculated with all three bacterial types. These cultures were spun down and resuspended in the same volume of FSW. Phoronid larvae were exposed to 1:10 dilutions of bacteria in FSW and aqueous extracts of the hindgut gland. Pieces of the carapace, gut tissue, and burrow walls of *U. pugettensis* were also tested as other possible cue sources with behavioral and metamorphic activity.

Assays were carried out within sterile, 6-well cell culture plates (BD Biosciences) with replicates of 5 or 10 larvae per well. Competent larvae of *Phoronis pallida* were removed from their culture vessels and placed in FSW for 2 h before use. Initial observations of the behavior demonstrated by competent larvae exposed to UCSW were that larvae swam faster in a downward direction and also probed the bottom with the apical portion of the oral hood. Larvae often spun around several times in one spot on the bottom before swimming away to probe other sites. This characteristic exploratory behavior was also described for competent actinotrochs of *Phoronis muelleri* (Silén, 1954) before the onset of metamorphosis. These behavioral traits were used as the criterion for whether a larva exhibited the swimming behavior within a given treatment. For a cue to be effective in flow, it should induce behavioral changes rapidly (Zimmer-Faust and Tamburri, 1994); therefore the total number of larvae exhibiting this behavior was counted within a 3-min interval. The minimum dosage of UCSW required to induce the majority of larvae to exhibit the swimming behavior was determined with a dilution range from 10 to 500. The relationship between dosage ($\log_{10}$-transformed) and percent of larvae behaviorally induced (arcsine-transformed) was determined with a linear regression. This was compared to the artificial induction of larval swimming behaviors with elevated concentrations of ammonium chloride in FSW. Samples of UCSW solution were frozen and measured for total ammonia at the chemistry laboratory at the University of Washington's School of Oceanography.

Motion analysis of larval behavior

Horizontal swimming speeds over the bottom were estimated with point-to-point estimates from videotaped images of larvae in UCSW or FSW. Video images were gathered with a dissecting microscope and a Hitachi KP-C500 color CCD camera. Individual frames were captured from this videotape with a LG-3 frame grabber card (Scion Corporation) and processed with NIH Image software. Downward swimming velocities of larvae were measured with a 2-D motion analysis system (Motion Analysis Corp. model VP 110 and Expert Vision software, ver. 3.2) interfaced with a Sun Microsystems SPARC IPC computer workstation. Larvae were transferred to the top of a chamber (10 cm in width, 20 cm in length, and 31 cm in height) containing either FSW or a 1:10 dilution of UCSW. Trials were run at 16–18 °C. Larvae were not phototactic, and illumination was provided with a fiber optic light that pointed down the center of the chamber. Only larvae that remained within the cone-shaped illumination field could be visualized, eliminating larvae that traveled too close to the walls of the chamber. Larvae usually stayed within the light field for 30–90 s, and videotaped images of larval paths were sampled at 1–10 frames per s. The centroids of the raw paths were calculated; the resulting paths were edited for erroneous spurs, uniformly smoothed, and analyzed for their speed and trajectories.

Molecular weight of the behavioral cue

The molecular weight of the behavioral cue in UCSW was estimated with Millipore Centriplus concentrators with membrane cutoffs at 3, 10, 50, and 100 kDa. The concentrators were spun at 3000 *g* for the maximum time designated by the manufacturer. Once the concentrate was collected, it was diluted to its original concentration with FSW. Experimental trials were run as previously described with both the concentrate and filtrate at a 1:10 dilution. Positive controls consisted of recovery of the behavioral response by adding a 1:10 dilution of raw UCSW to all experimental trials after each treatment had been scored.

Enzymatic treatments of UCSW

To gain information about the chemical nature of the cue, UCSW was treated with various enzymes (see Table 2) according to the methods of Zimmer-Faust and Tamburri (1994), with some modifications. Concentrations of 2–4 units of enzyme per milliliter of UCSW were used, and incubations were at the optimum pH and temperature for

each enzyme for 30 min. Each solution of UCSW and enzyme was readjusted to 25 °C and a pH of 8.0 before being applied to the larvae (1:10 dilution). After swimming behavior in the enzymatic treatments was scored, untreated UCSW was added to each chamber at a dilution of 1:10 as a recovery-positive control to measure how many larvae within the enzymatic trials were capable of responding to raw UCSW. This also controlled for the unlikely possibility that the small amount of residual enzyme in these trials could have prevented the larvae from responding to UCSW. Incubations at these conditions of temperature and pH without enzyme have been shown to have no negative effects on the settlement cues of oysters (Zimmer-Faust and Tamburri, 1994). For these reasons, only the most extreme incubation conditions were tested for reducing the activity of UCSW without any enzyme (pH 5.0 or 9.5 at 37 °C for 30 min). One other remote possibility is that a particular enzyme might have the same effect on larval swimming behavior as UCSW. This would produce a false negative result even though the same enzyme might have degraded the activity of UCSW. Since there is no absolute way of knowing why a particular enzyme treatment did not work, this was not controlled for during these experiments. Enzyme treatments yield information only when they degrade the activity of the cue; when they do not have this effect, no information can be inferred about the chemical nature of the cue. Enzymatic treatments are only a rough guide about what the chemical nature of the behavioral cue might be rather than what it is not. Percentages of larvae exhibiting the swimming behavior in each treatment were arcsine-transformed before a one-way analysis of variance.

Artificial induction of metamorphosis

Metamorphosis was artificially induced by exposing larvae to 10–30 m*M* concentrations (in FSW) of either KCl or CsCl for no longer than 1 h. If a larva everted the trunk sac, it was immediately removed to FSW, and subsequent metamorphosis was observed through a dissecting microscope. Metamorphic stages were scored according to the following criteria, documented previously in Santagata (2002): stage one—partial histolysis of hood, telotrochal cells, and the larval portion of the tentacles; stage two—complete histolysis of larval tissues and partial eversion of the juvenile trunk sac; stage three—larval gut pulled inside the juvenile trunk sac, but portions of the larval trunk epithelium not completely pulled into the juvenile body; stage four—all previous events plus the larval trunk epithelium completely pulled into the juvenile body. All four stages could be completed within 2 h. A functional juvenile lophophore and circulatory system develops 2 days post-metamorphosis (Santagata, 2002). Most stage three and all stage four metamorphic types metamorphosed successfully, resulting in an anatomically complete juvenile.

Results

Behavioral cues

Live individuals of *Upogebia pugettensis*, dissected gut regions, burrow walls, and UCSW all induced the same behavioral response in larvae of *Phoronis pallida*, but did not induce metamorphosis (Table 1). Competent larvae exposed to both live specimens and freshly collected burrow walls also failed to induce metamorphosis (15 larvae exposed for 2 days). Aqueous extracts of the hindgut gland at a 1:10 dilution did not induce a behavioral response or metamorphosis. The three different bacterial colonies isolated from the gut of *U. pugettensis* did not induce any behavioral response; however most of these larvae did respond to UCSW (58% ± 17% SD). *Neotrypaea*-conditioned seawater (NCSW) produced inconsistent results. In six trials, no larvae responded to NCSW at a 1:10 dilution. Three of these larvae did respond behaviorally when exposed to full-strength NCSW, but did so after the 3-min period had elapsed. These same larvae did respond behaviorally to UCSW at a 1:10 dilution (35% ± 19 SD).

Since UCSW was the cue source with the most activity, all further experiments focused on characterizing it. Behavioral response to UCSW was correlated with the development of a 10th pair of larval tentacle buds and a red corpuscle mass. Development in culture is non-synchronous (Santagata, 2004), but the earliest development of these morphological traits and behavioral response to UCSW usually occurred between 30 and 35 days. Competent larvae responded to UCSW in a dosage-dependent manner (Fig. 2). Ten to thirty percent of larvae exhibited the swimming

Table 1

Effect of different possible cue sources for behavioral and metamorphic activity of competent larvae of Phoronis pallida

Cue source*	*S/n*
UCSW	5/5
Burrow walls	5/5
Upogebia gut tissue	5/5
Upogebia carapace	0/5
Upogebia gut bacteria	
Yellow bacteria	0/10
Orange bacteria	0/10
White bacteria	0/10
Bacterial mixture	0/10
Upogebia hindgut gland extract	0/30
NCSW 1:10†	0/60

None of these cue sources induced metamorphosis. Values are the number of larvae that exhibited the swimming behavior (*S*) out of the total number of larvae (*n*) in the treatment.

* UCSW and NCSW are, respectively, seawater conditioned with *Upogebia* and seawater conditioned with *Neotrypaea*.

† Three of these larvae did exhibit the swimming behavior when exposed to full-strength NCSW.

behavior in the presence of UCSW diluted as much as 1:500. However, most larvae exhibited the swimming behavior if exposed to a 1:10 dilution of UCSW. Most of the variation in the percentage of larvae that were behaviorally induced was explained by the dosage of UCSW ($r^2 = 0.84$).

I tested the responses of *Phoronis pallida* larvae to ammonium, which can induce settlement in oyster larvae (Coon *et al.*, 1990). The larvae responded behaviorally to very high levels of ammonium (10 m*M*; Fig. 3). However, UCSW contains only 5–7 μM of total ammonia, and levels during the experimental trials (1:10 dilution) were between 0.5 and 0.7 μM. According to the dosage-dependent response to ammonium chloride (Fig. 3), this concentration would be insufficient to elicit the same behavioral response.

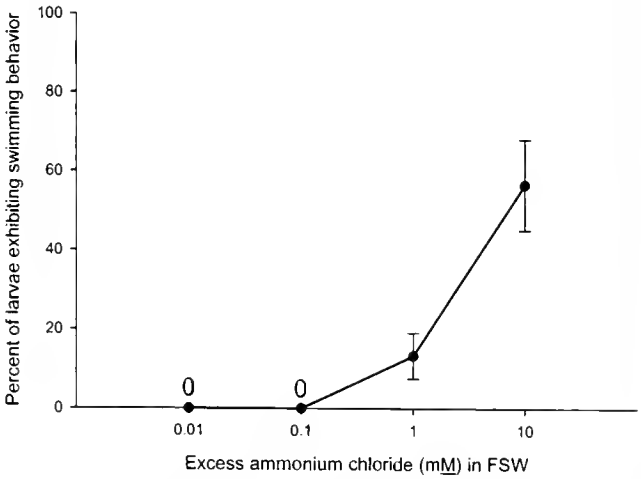

Figure 3. Behavioral response of *Phoronis pallida* larvae to increased concentration of ammonium chloride. Error bars equal one standard deviation from the mean and were calculated from 3 replicates of 10 larvae per treatment.

Motion analysis

Average swimming velocities were 1.25 mm/s for larvae in FSW and 3.92 mm/s for larvae in UCSW. The maximum speed for most larvae exposed to UCSW was about 5.5 mm/s, but a few larvae reached speeds of 7 mm/s. A one-way analysis of variance between the two treatments shows a significant difference (Fig. 4, df = 43, *F*-ratio = 68.3, $P < 0.0001$). Once larvae reached the substratum, the increased swimming speed was maintained between probing sites (horizontal speeds, see Fig. 4, df = 62, *F*-ratio = 308, $P < 0.0001$). Overall, larvae in FSW swam more slowly and hovered at the top of the water column, and larvae in UCSW swam faster toward the bottom and probed the substrate (Fig. 5).

Molecular weight separation and enzymatic treatments of UCSW

The activity of UCSW fractions above 10 kDa (*F*-ratio = 1.1, $P > 0.34$) and below 50 kDa ($F = 0.73$, $P > 0.44$) was equal to that of untreated UCSW. The below 10-kDa and above 50-kDa fractions (*F*-ratio = 89.3, $P \leq 0.001$ and $F = 400$, $P < 0.001$, respectively) did not induce any changes in larval behavior, but these larvae did respond to raw UCSW (Fig. 6).

The most extreme enzymatic incubation conditions (5.0 and 9.5 at 37 °C for 30 m) had no effect on the activity of UCSW (7 of 10 and 8 of 10 larvae were induced, respec-

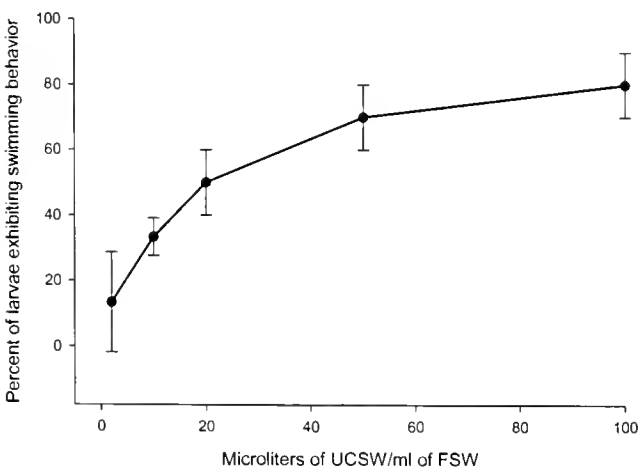

Figure 2. Dosage-dependent behavioral response of *Phoronis pallida* larvae to *Upogebia*-conditioned seawater (UCSW). Error bars equal one standard deviation from the mean and were calculated from 3 replicates of 10 larvae per treatment.

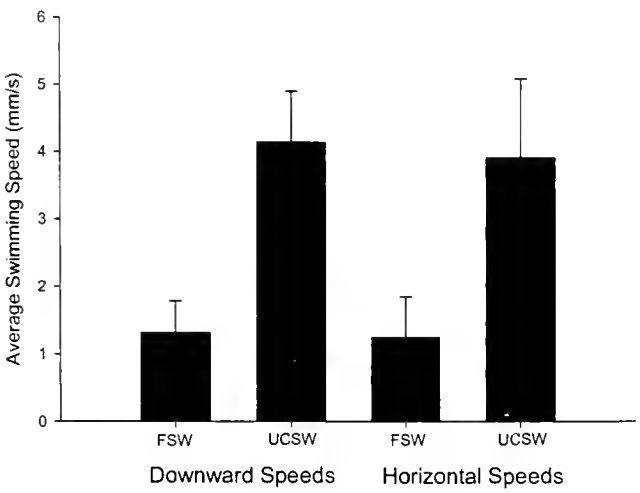

Figure 4. The average downward and horizontal swimming speeds of *Phoronis pallida* larvae in filtered seawater (FSW) and *Upogebia*-conditioned seawater. Error bars equal one standard deviation from the mean and were calculated from 30 paths per treatment.

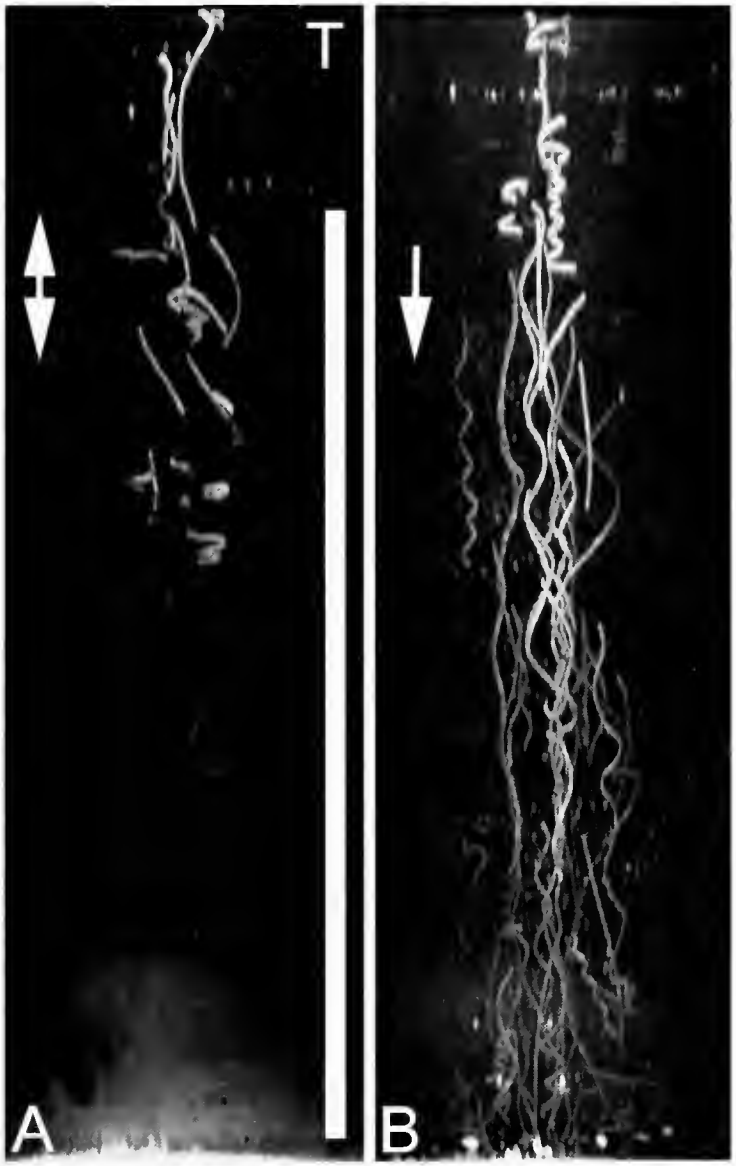

Figure 5. Time-lapse projections of larval behavior of *Phoronis pallida* in filtered seawater (FSW) and *Upogebia*-conditioned seawater (UCSW). Larval swimming was videotaped for 30 s. Video images were captured with fMovie 3.03, sampled at 10 frames/s, and exported as a stack of TIFF files. Time-lapse projections of these images were made with Image J 1.32 (Wayne Rasband, NtH). (A) Larval behavior in FSW. Larvae tended to hover at the top (T) of the chamber. (B) Larval behavior in UCSW. Larvae increased their swimming speed and swam down to the bottom of the chamber. Vertical scale bar is 20 cm.

tively). However, the arginase treatments consistently and completely eliminated the activity of the UCSW (Table 2, one-way ANOVA, df = 28, F-ratio = 63.9, $P < 0.001$). Lipase treatments also significantly reduced the activity of the UCSW, but about 13% of the larvae in this treatment exhibited the swimming behavior (one-way ANOVA, df = 34, $F = 27.9$, $P < 0.001$). Arginase specifically converts arginine to ornithine and requires that arginine be at the C-terminal position (Greenberg, 1960). Carboxypeptidase B should be able to cleave a C-terminal arginine, but this treatment yielded only minor (albeit statistically significant, $F = 5.4$, $P < 0.05$) negative effects on the activity of UCSW. Minor negative effects were also observed with the sulfatase treatments ($F = 17.8$ and $P < 0.01$). Since about half of the larvae in each of the carboxypeptidase B and sulfatase treatments were still able to exhibit the swimming behavior, differences between these treatments and UCSW were judged nonsignificant. Carboxypeptidase P and prolidase treatments were tested in an attempt to overcome possible steric hindrances to carboxypeptidase B. Neither of

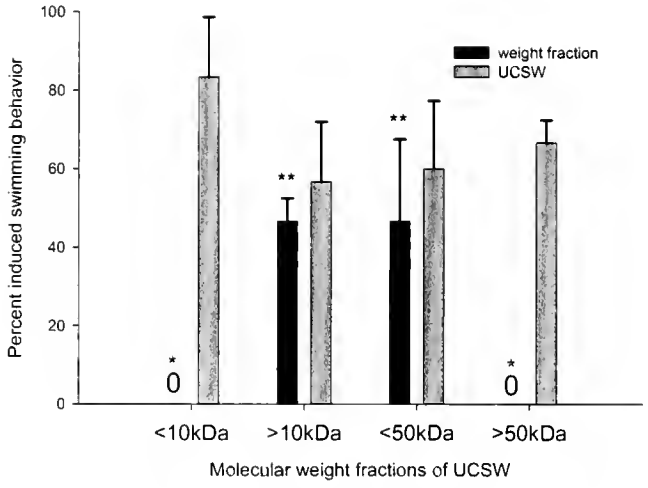

Figure 6. Results of the molecular weight fractions of *Upogebia*-conditioned seawater (UCSW) on the behavior of *Phoronis pallida* larvae. Error bars equal one standard deviation from the mean and were calculated from 3 replicates of 10 larvae per treatment. * Denotes where $P < 0.001$; ** denotes where $P > 0.34$.

these enzymatic treatments significantly reduced the activity of UCSW (Table 2).

Metamorphic induction with CsCl and KCl

The threshold concentration of cesium chloride that induced metamorphosis was approximately 10 m*M*, with an optimum effect at 20–25 m*M* (Table 3). CsCl at higher concentrations was toxic to larvae, and the minimum optimal exposure (20 m*M*) was chosen for all other experiments. Behavioral response to CsCl was immediate, and larvae that everted the trunk sac did so 15–30 min after initial exposure. The number of metamorphic stages produced with CsCl through developmental time for a single larval culture is summarized in Table 4. At 5 weeks, CsCl induced predominantly early stages of metamorphosis. Most viable juveniles were produced between weeks 6 and 7. At week 9, these experiments resulted primarily in arrested metamorphic stages. By day 71, larvae were not able to complete any stage of metamorphosis when exposed to CsCl. Post-competent larvae also stopped feeding. In general, the development of metamorphic competence within culture is non-synchronous (data from 14 cultures, see Santagata, 2004), but viable juveniles resulted more often between weeks 5 and 9 under these culture conditions. Potassium chloride was toxic to larvae at concentrations from 10 to 30 m*M*, and these treatments did not induce muscle contractions or any stage of metamorphosis.

Table 2

Effect of enzymatic treatments of Upogebia*-conditioned seawater on the swimming behavior of* Phoronis pallida *larvae*

Enzyme	Replicates†	Percent ± SD of larvae induced to swim‡	
		In enzyme-treated UCSW	After raw UCSW added
Arginase	**15**	**0 ± 0***	**64.0 ± 24.7**
Carboxypeptidase B	9	43.3 ± 18.0**	61.1 ± 16.2
Carboxypeptidase P	6	66.7 ± 12.1***	76.7 ± 8.1
Carboxypeptidase Y	3	63.3 ± 5.8***	73.3 ± 5.8
Leucine aminopeptidase	6	46.7 ± 21.6***	66.7 ± 12.1
Prolidase	3	66.7 ± 11.5***	76.7 ± 11.6
Lipase	**18**	**13.3 ± 13.7***	**56.1 ± 23.8**
Sulfatase	6	51.7 ± 9.8**	75 ± 8.4
Amylase and Maltase	3	63.3 ± 20.8***	63.3 ± 20.8
Lysozyme	6	70 ± 8.9***	73.3 ± 10.3

† Each replicate consisted of 10 larvae.

‡ UCSW, seawater conditioned with *Upogebia*. Statistically significant results are in bold type. Probability values are indicated as follows: * $P < 0.001$; ** $0.001 < P < 0.05$; *** $P > 0.05$.

Table 3

Effect of cesium chloride on metamorphosis of Phoronis pallida *larvae*

Concentration of CsCl in filtered seawater (in m*M*)	*n*	No metamorphosis	Stage			
			One	Two	Three	Four
5	15	15	0	0	0	0
10	29	23	2	1	2	1
15	27	15	3	3	6	0
20	**30**	**2**	**12**	**6**	**10**	**0**
25	**30**	**3**	**10**	**9**	**7**	**1**
30	31	12	12	5	2	0

The total number of larvae per treatment (N) is apportioned into metamorphic stages.

Table 4

*Effect of 20 m*M *CsCl on ten-tentacle larvae of* Phoronis pallida *through developmental time*

Age (days)	*n*	No metamorphosis	Stage		
			One	Two	Three and four
35 and 37	15	1	12	1	1
41 and 43	28	6	6	6	10
48, 49, and 50	33	3	8	6	16
63	20	5	14	0	1
68 and 69	14	2	9	1	2

Some close time points and metamorphic stages were pooled for convenience. *n* is the total number of larvae in each experiment.

Discussion

Behavioral responses to UCSW

In response to UCSW (seawater conditioned with the thalassinid shrimp *Upogebia pugettensis*), competent larvae of *Phoronis pallida* exhibited an exploratory behavior in a dosage-dependent manner. Larvae exhibiting this behavior swam fast and changed direction toward the bottom. Once in contact with the bottom, the larvae stopped for brief periods and probed the substratum with the apical ganglion (apical sense organ) and hood sense organ. Induced swimming behaviors of *P. pallida* larvae differ slightly from reversible "settlement" behaviors described for the veliger larvae of the nudibranch *Onchidoris bilamellata* (Chia and Koss, 1988). After reaching the bottom, *O. bilamellata* larvae crawl for up to 30 min unless they contact a barnacle (natural metamorphic cue). Some behavioral differences between veligers and actinotrochs are likely due to the functional morphology of their sensory and swimming structures. However, *P. pallida* larvae may also have maintained their increased swimming speeds between probing sites because of habitat differences. Barnacle habitats are large exposed surfaces, so when *O. bilamellata* larvae reach the bottom they are likely to be near a suitable place to metamorphose. In contrast, when the larvae of *P. pallida* reach the bottom, they must still get inside a burrow of *Upogebia*. Although pumping of the shrimp's pleopods may facilitate this event, *P. pallida* larvae may increase their chances of being swept into a burrow by maintaining their swimming speed between probing sites. Despite obvious differences in morphology, larval "settlement" behaviors similar to that of *P. pallida* have been described for oyster veligers (Finelli and Wethey, 2003). The dive bombing described for oyster veligers may aid the larvae in finding suitable metamorphic sites once in the bottom boundary layer (Finelli and Wethey, 2003), and it may represent a convergent behavioral response to waterborne cues among disparate larval forms.

Analysis of UCSW

Some naturally occurring settlement and metamorphic cues have been described as low-molecular-weight compounds (Hadfield and Pennington, 1990; Zimmer-Faust and Tamburri, 1994). Other studies have shown that larvae respond to insoluble, high-molecular-weight compounds that have smaller soluble components (Morse and Morse, 1991; Matsumura *et al.*, 1998; Krug and Manzi, 1999). In these latter studies, the cue was found to be a type of carbohydrate or protein. In this study, the stable waterborne cue was of high molecular weight with properties of both long-chain fatty acids and peptides.

Waterborne cues with lipid properties have been shown to act as phagostimulants and metamorphic inducers in marine invertebrates. Unsaturated fatty acids from macroalgae that have been esterified into glycerolipids induce feeding in one species of abalone (Ando *et al.*, 1997). Similar chemical cues from the kelp *Egregia* also act as a feeding stimulant to a trochid snail (Wakefield and Murray, 1998). Glycoglycerolipids isolated from green algae induce metamorphosis in a sea urchin (Takahashi *et al.*, 2002). The role of free fatty acids as chemical cues to larval settlement remains ambiguous. In species where free fatty acids have been implicated, it is not clear whether these compounds were extraction contaminants or acted as secondary cell-signaling messengers (for review of these analyses and discussions, see Pawlik, 1990; Jensen *et al.*, 1990; Leitz, 1993; Kitamura *et al.*, 1994). Resolving the lipid-like properties of the behavioral cue in UCSW will require finer chemical analyses.

The complete degradation of the activity of UCSW by arginase points to an important peptide component. Removal of all low-molecular-weight compounds (less than 10 kDa) did not significantly reduce the activity of the UCSW. This suggests that the peptide component of the waterborne cue was bound to the lipid component. Taken together, the evidence is consistent with the cue having glycerolipid or peptidoglycan-like properties. However, the minor negative effect of the sulfatase treatments suggests other possibilities, such as a resemblance to the sugars produced by diatoms (Zimmer and Tamburri, 1994). Besides algae, another possible source of these compounds is the species-specific types of bacterial symbionts in the gut of thalassinids (Harris, 1993; Pinn *et al.*, 1999). At least two species of *Upogebia* enrich their burrow walls with organic matter, which serves as a good niche for bacterial colonization (Thompson, 1972; Kinoshita *et al.*, 2003). Bacterial cell walls are a source of peptidoglycan-like molecules, and some produced by gram-negative bacteria are particularly resistant to degradation in marine environments (Jorgensen *et al.*, 2003). These factors would make the settlement cues associated with the effluent and burrows of *Upogebia* distinct from those of other co-occurring thalassinids or any other species in the mudflat.

Natural and artificial induction of metamorphosis

Herrmann (1979, 1995) documented that the larvae of *Phoronis muelleri* and *P. psammophila* are naturally induced to metamorphose with gram-positive and gram-negative bacteria isolated from sediments found in the adult habitat. The threshold concentration of bacterial cues necessary to induce metamorphosis also decreased during the competency period (Herrmann, 1995). If the competency period is prolonged, competent larvae of *P. muelleri* and *P. psammophila* will eventually (spontaneously) metamorphose, but this often results in what Herrmann described as aberrant metamorphosis. Although not rigorously tested,

Herrmann's metamorphic models support the hypothesis that metamorphic specificity decreases with larval age. However, Toonen and Pawlik (2001a) found no support for the "desperate larva hypothesis" during the prolonged planktotrophic period of *Hydroides dianthus* larvae. I found the behavioral and metamorphic cues for *P. pallida* to be more specific than for other species of phoronids, and I never observed spontaneous metamorphosis in culture. Unfortunately, a naturally occurring metamorphic inducer has not been found for *P. pallida*, but the CsCl experiments suggest a competency period of about 4 weeks. Estimates of competency periods with natural and artificial inducers can yield different temporal patterns (Pechenik *et al.*, 1995). Furthermore, the onset and duration of metamorphic competence is also affected by food availability (Pechenik *et al.*, 1996). For these reasons, measurements of the competency period of *P. pallida* larvae are only a rough estimate under these culture conditions (see Santagata, 2004). Loss of the behavioral and morphogenetic abilities gained at metamorphic competence has been found in other planktotrophic larval types after similar competency periods (Avila, 1998; Toonen and Pawlik, 2001a). Behavioral specificity during metamorphic competence clearly has some life-history-specific, species-specific, and polymorphism-specific trends (Krug, 1998; Hadfield *et al.*, 2001; Toonen and Pawlik, 2001b). Overall, data contained here and in Santagata (2004) are more consistent with the findings of Toonen and Pawlik (2001a). This may represent a functional convergence in life-history traits among planktotrophic larvae that exhibit specific settlement preferences.

Consistent with the data from *Phoronis muelleri* and *P. psammophila* (Herrmann, 1979, 1995), excess Cs^+ but not K^+ induced metamorphosis in the competent larvae of *P. pallida*. Evidence suggests that excess Cs^+ and NH_4^+ induces larval metamorphosis by increasing levels of intracellular NH_4^+, which in turn binds more methyl groups, which reduces the levels of S-adenosylmethionine (Berking, 1988; Berking and Herrmann, 1990). Interestingly, excess Cs^+ induced both the swimming behavior and metamorphosis, but excess NH_4^+ induced only the exploratory behavior. Metamorphic induction by excess Cs^+ and not K^+ or NH_4^+ may be indicative of signal transduction mechanisms that normally inhibit metamorphosis unless they are overwhelmed by external excitatory stimuli (Pires *et al.*, 2000; Leise *et al.*, 2001; Pechenik *et al.*, 2002; Katsukura *et al.*, 2003). This type of system would be advantageous for larvae that require specific behavioral and metamorphic cues.

Hood sense organ and behavioral specificity

Metamorphic competence in actinotrochs is defined by the differentiation of the juvenile neuromuscular system, development of the hood sense organ, and development of neuronal connections between the larval and juvenile neuromuscular systems (Santagata, 2002). At least four phoronid species have serotonergic sensory neurons in their hood sense organs and are capable of spontaneous metamorphosis when collected from the plankton (Santagata and Zimmer, 2002). *Phoronis pallida* is different from these species in at least two ways: the sensory neurons in the hood sense organ are not serotonergic (Santagata, 2002); and spontaneous metamorphosis does not occur in culture during the competency period (Santagata, 2004). Developmental modifications of chemosensory circuits have been correlated with behavioral specificity in the nematode *Caenorhabditis elegans* (Melkman and Sengupta, 2004). Compared with the actinotroch larvae of other phoronid species, the larvae of *P. pallida* have greater behavioral and metamorphic specificity that corresponds with modifications of the neuronal cell types within the hood sense organ.

Thalassinid life-history characteristics

Pacific and Atlantic populations of *Phoronis pallida* exhibit differences in adult habitat. Atlantic populations occur in soft sediments along with species of thalassinid shrimps, but have not been found as commensals within thalassinid burrows (Viéitez and Emig, 1979; Silén, 1952). Hawaiian populations of *P. pallida* occur in sandy substrates with no mention of an association with thalassinids (Bailey-Brock and Emig, 2000). Although the distributions of *P. pallida* and *Callianassa limosa* are similar in Port Phillip Bay, Australia (Poore, 1975; Emig *et al.*, 1977), the only other species of thalassinid that definitively contains *P. pallida* as a commensal within its burrow is *Upogebia major* (see fig. 1C in Kinoshita, 2002), which occurs in Tokyo Bay, Japan. *U. major* produces a burrow similar to that of *U. pugettensis*, and the two species share several behavioral traits (Kinoshita *et al.*, 2003). Whether distant populations of *P. pallida* that occur in different adult habitats represents cryptic speciation remains to be tested.

Differences in abundance, feeding behavior, and physiology may also account for the diversity of commensal species found with species of *Upogebia* rather than with other thalassinid shrimps. *U. pugettensis* and *U. major* each occur in a mean density of 40 shrimp per square meter, with occasional abundances greater than 100 shrimp per square meter (Swinbanks and Luternauer, 1987; Dumbauld *et al.*, 2001; Kinoshita *et al.*, 2003). Abundances in these ranges would provide a suitable settlement target for recruiting commensal species. Species of *Upogebia* are primarily herbivorous suspension feeders that occasionally engage in deposit feeding, whereas most other genera of thalassinids depend more on deposit feeding or omnivorous scavenging (Griffis and Suchanek, 1991; Nickell and Atkinson, 1995; Coelho *et al.*, 2000). The greater reliance upon suspension feeding may increase the recruitment success of symbiont

larvae to *Upogebia* burrows. *U. pugettensis* is also less resistant to anoxia and reduced salinity than co-occurring species of *Neotrypaea* (Thompson and Pritchard, 1969; Torres *et al.*, 1977; Swinbanks and Murray, 1981; Swinbanks and Luternauer, 1987; Astall *et al.*, 1997), and thus it is limited to more environmentally stable habitats. Habitat stability may contribute to greater survivorship among commensal species that associate with thalassinid shrimps that have *Upogebia* life-history characteristics.

Acknowledgments

I thank D. Bottjer, S. Bottjer, R. Emlet, J. Fingerut, J. Fuhrman, M. E. Rice, J. Riffell, R. R. Strathmann, R. K. Zimmer, C.A. Zimmer, R. L. Zimmer, and the staff of Friday Harbor Laboratories. R. K. Zimmer at the University of California–Los Angeles graciously provided access to the motion analysis equipment. Two anonymous reviewers and C. Derby provided constructive criticism of the paper. This paper is based in part on a thesis submitted by the author towards partial fulfillment of the doctoral degree requirements at the University of Southern California. This project was supported by grants from the American Museum of Natural History and the Wrigley Institute for Environmental Studies.

Literature Cited

Ando, Y., J. Nakamura, and T. Ota. 1997. Phagostimulant activity of phosphatidylcholine molecular species for young abalone *Haliotis discus hannai*. *Fish. Sci.* **63:** 1048–1049.

Astall, C. M., A. C. Taylor, and R. J. A. Atkinson. 1997. Behavioural and physiological implications of a burrow-dwelling lifestyle for two species of upogebiid mud-shrimp (Crustacea: Thalassinidea). *Estuar. Coast. Shelf Sci.* **44:** 155–168.

Avila, C. 1998. Competence and metamorphosis in the long-term planktotrophic larvae of the nudibranch mollusc *Hermissenda crassicornis* (Eschscholtz, 1831). *J. Exp. Mar. Biol. Ecol.* **231:** 81–117.

Bailey-Brock, J. H., and C. C. Emig. 2000. Hawaiian Phoronida (Lophophorata) and their distribution in the Pacific region. *Pac. Sci.* **54:** 119–126.

Berking, S. 1988. Ammonia tetraethylammonium barium and amiloride induce metamorphosis in the marine hydroid *Hydractinia*. *Roux's Arch. Dev. Biol.* **197:** 1–9.

Berking, S., and K. Herrmann. 1990. Dicapryloylglycerol and ammonium ions induce metamorphosis of ascidian larvae. *Roux's Arch. Dev. Biol.* **198:** 430–432.

Browne, K. A., and R. K. Zimmer. 2001. Controlled field release of a waterborne chemical signal stimulates planktonic larvae to settle. *Biol. Bull.* **200:** 87–91.

Browne, K. A., M. N. Tamburri, and R. K. Zimmer-Faust. 1998. Modelling quantitative structure-activity relationships between animal behavior and environmental signal molecules. *J. Exp. Biol.* **201:** 245–258.

Chia, F. S., and R. Koss. 1988. Induction of settlement and metamorphosis of the veliger larvae of the nudibranch *Onchidoris bilamellata*: *Int. J. Invertebr. Rep.* **14:** 53–70.

Coelho, V. R., R. A. Cooper, and S. D. Rodrigues. 2000. Burrow morphology and behavior of the mud shrimp *Upogebia omissa* (Decapoda: Thalassinidea: Upogebiidae). *Mar. Ecol. Prog. Ser.* **200:** 229–240.

Coon, S. L., M. Walch, W. K. Fitt, R. M. Weiner, and D. B. Bonar. 1990. Ammonia induces settlement behavior in oyster larvae. *Biol. Bull.* **179:** 297–303.

Dana, J. D. 1852. Macroura. Conspectus crustaceorum & conspectus of the Crustacea of the exploring expedition under Capt. C. Wilkes, U.S.N. *Proc. Acad. Nat. Sci. Phila.* **6:** 10–28.

Dumbauld, B. R., K. M. Brooks, and M. H. Posey. 2001. Response of an estuarine benthic community to application of the pesticide carbaryl and cultivation of Pacific oysters (*Crassostrea gigas*) in Willapa Bay, Washington. *Mar. Pollut. Bull.* **42:** 826–844.

Eckman, J. E., F. E. Werner, and T. F. Gross. 1994. Modeling some effects of behavior on larval settlement in a turbulent boundary layer. *Deep-Sea Res. II Top. Stud. Oceanogr.* **41:** 185–208.

Emig, C. C. 1974. The systematics and evolution of the phylum Phoronida. *Z. Zool. Syst. Evolutionsforsch.* **12:** 128–151.

Emig, C. C. 1982. The biology of Phoronida. *Adv. Mar. Biol.* **19:** 1–89.

Emig, C. C., D. F. Boesch, and S. Rainer. 1977. Phoronida from Australia. *Rec. Aust. Mus.* **30:** 455–474.

Finelli, C. M., and D. S. Wethey. 2003. Behavior of oyster (*Crassostrea virginica*) larvae in flume boundary layer flows. *Mar. Biol.* **143:** 703–711.

Fingerut, J. T., C. A. Zimmer, and R. K. Zimmer. 2003. Larval swimming overpowers turbulent mixing and facilitates transmission of a marine parasite. *Ecology* **84:** 2502–2515.

Forward, R. B., Jr., R. A. Tankersley, K. A. Smith, and J. M. Welch. 2003. Effects of chemical cues on orientation of blue crab, *Callinectes sapidus*, megalopae in flow: implications for location of nursery areas. *Mar. Biol.* **142:** 747–756.

Greenberg, D. M. 1960. Arginase. Pp. 257–267 in *The Enzymes, Vol. 4*, P. D. Boyer, H. Lardy, and K. Myrback, eds. Academic Press, New York.

Griffis, R. B., and T. H. Suchanek. 1991. A model of burrow architecture and trophic modes in thalassinidean shrimp (Decapoda, Thalassinidea). *Mar. Ecol. Prog. Ser.* **79:** 171–183.

Gross, T. F., F. E. Werner, and J. E. Eckman. 1992. Numerical modeling of larval settlement in turbulent bottom boundary layers. *J. Mar. Res.* **50:** 611–642.

Hadfield, M. G., and J. T. Pennington. 1990. Nature of the metamorphic signal and its internal transduction in larvae of the nudibranch *Phestilla sibogae*. *Bull. Mar. Sci.* **46:** 455–464.

Hadfield, M. G., E. J. Carpizo-Ituarte, K. del Carmen, and B. T. Nedved. 2001. Metamorphic competence, a major adaptive convergence in marine invertebrate larvae. *Am. Zool.* **41:** 1123–1131.

Haig, J., and D. P. Abbot. 1980. Macrura and Anomura: the ghost shrimps, hermit crabs, and allies. Pp. 577–593 in *Intertidal Invertebrates of California*, R. H. Morris, D. P. Abbott, and E. C. Haderlie, eds. Stanford University Press, Stanford, CA.

Harris, J. M. 1993. Widespread occurrence of extensive epimural rod bacteria in the hindguts of marine Thalassinidae and Brachyura (Crustacea, Decapoda). *Mar. Biol.* **116:** 615–629.

Harvey, M., E. Bourget, and R. G. Ingram. 1995. Experimental evidence of passive accumulation of marine bivalve larvae on filamentous epibenthic structures. *Limnol. Oceanogr.* **40:** 94–104.

Herrmann, K. 1979. Larval development and metamorphosis of *Phoronis psammophila* (Phoronida, Tentaculata). *Helgol. Wiss. Meeresunters.* **32:** 550–581.

Herrmann, K. 1995. Induction and regulation of metamorphosis in planktonic larvae—*Phoronis muelleri* (Tentaculata) as archetype. *Helgol. Meeresunters.* **49:** 255–281.

Hornig, S., A. Sterling, and S. D. Smith. 1989. Species profiles: life histories and environmental requirements of coastal fishes and inver-

tebrates (Pacific Northwest, U.S.A.) ghost shrimp and blue mud shrimp. *US Fish Wildl. Serv. Biol. Rep.* **82:** 1–14.

Jensen, R. A., D. E. Morse, R. L. Petty, and N. Hooker. 1990. Artificial induction of larval metamorphosis by free fatty acids. *Mar. Ecol. Prog. Ser.* **67:** 55–71.

Jorgensen, N. O. G., R. Stepanaukas, A. G. U. Pedersen, M. Hansen, and O. Nybroe. 2003. Occurrence and degradation of peptidoglycan in aquatic environments. *FEMS Microbiol. Ecol.* **46:** 269–280.

Katsukura, Y., C. N. David, C. J. P. Grimmelikhuijzen, and T. Sugiyama. 2003. Inhibition of metamorphosis by RFamide neuropeptides in planula larvae of *Hydractinia echinata*. *Dev. Genes Evol.* **213:** 579–586.

Kingsford, M. J., J. M. Leis, A. Shanks, K. C. Lindeman, S. G. Morgan, and J. Pineda. 2002. Sensory environments, larval abilities, and local self-recruitment. *Bull. Mar. Sci.* **70:** 309–340.

Kinoshita, K. S. 2002. Burrow structure of the mud shrimp *Upogebia major* (Decapoda: Thalassinidea: Upogebiidae). *J. Crustac. Biol.* **22:** 474–480.

Kinoshita, K., M. Wada, K. Kogure, and T. Furota. 2003. Mud shrimp burrows as dynamic traps and processors of tidal-flat materials. *Mar. Ecol. Prog. Ser.* **247:** 159–164.

Kitamura, H., S. Kitahara, and H. B. Koh. 1994. Induction of larval settlement and metamorphosis in the sea urchins *Pseudocentrotus depressus* and *Anthocidaris crassispina* by fatty acids. *Fish. Sci.* **60:** 311–313.

Krug, P. J. 1998. Poecilogony in an estuarine opisthobranch: planktotrophy, lecithotrophy, and mixed clutches in a population of the ascoglossan *Alderia modesta*. *Mar. Biol.* **132:** 483–494.

Krug, P. J., and A. E. Manzi. 1999. Waterborne and surface-associated carbohydrates as settlement cues for larvae of the specialist marine herbivore *Alderia modesta*. *Biol. Bull.* **197:** 94–103.

Krug, P. J., and R. K. Zimmer. 2000. Larval settlement: chemical markers for tracing production, transport, and distribution of a waterborne cue. *Mar. Ecol. Prog. Ser.* **207:** 283–296.

Lambert, W. J., C. D. Todd, and J. D. Hardege. 1997. Partial characterization and biological activity of a metamorphic inducer of the dorid nudibranch *Adalaria proxima* (Gastropoda: Nudibranchia). *Invertebr. Biol.* **116:** 71–81.

Leise, E. M., K. Thavaradhara, N. R. Durham, and B. E. Turner. 2001. Serotonin and nitric oxide regulate metamorphosis in the marine snail *Ilyanassa obsoleta*. *Am. Zool.* **41:** 258–267.

Leitz, T. 1993. Biochemical and cytological bases of metamorphosis in *Hydractinia echinata*. *Mar. Biol.* **116:** 559–564.

Leitz, T., and T. Wagner. 1993. The marine bacterium *Alteromonas espejiana* induces metamorphosis of the hydroid *Hydractinia echinata*. *Mar. Biol.* **115:** 173–178.

Manning, R. B., and D. L. Felder. 1991. Revision of the American Callianassidae (Crustacea, Decapoda, Thalassinidea). *Proc. Biol. Soc. Wash.* **104:** 764–792.

Matsumura, K., M. Nagano, and N. Fusetani. 1998. Purification of a larval settlement-inducing protein complex (SIPC) of the barnacle, *Balanus amphitrite*. *J. Exp. Zool.* **281:** 12–20.

Melkman, T., and P. Sengupta. 2004. The worm's sense of smell: development of functional diversity in the chemosensory system of *Caenorhabditis elegans*. *Dev. Biol.* **265:** 302–319.

Morse, D. E., and A. N. C. Morse. 1991. Enzymatic characterization of the morphogen recognized by *Agaricia humilis* (scleractinian coral) larvae. *Biol. Bull.* **181:** 104–122.

Nickell, L. A., and R. J. A. Atkinson. 1995. Functional morphology of burrows and trophic modes of three thalassinidean shrimp species, and a new approach to the classification of thalassinidean burrow morphology. *Mar. Ecol. Prog. Ser.* **128:** 181–197.

Pawlik, J. R. 1990. Natural and artificial induction of metamorphosis of *Phragmatopoma lapidosa-californica* (Polychaeta: Sabellariidae) with a critical look at the effects of bioactive compounds on marine invertebrate larvae. *Bull. Mar. Sci.* **46:** 512–536.

Pawlik, J. R. 1992. Chemical ecology of the settlement of benthic marine invertebrates. *Oceanogr. Mar. Biol.* **30:** 273–335.

Pearce, C. M., and R. E. Scheibling. 1990. Induction of settlement and metamorphosis in the sand dollar *Echinarachnius parma*: evidence for an adult-associated factor. *Mar. Biol.* **107:** 363–369.

Pechenik, J. A., M. G. Hadfield, and L. S. Eyster. 1995. Assessing whether larvae of the opisthobranch gastropod *Phestilla sibogae* Bergh become responsive to three chemical cues at the same age. *J. Exp. Mar. Biol. Ecol.* **191:** 1–17.

Pechenik, J. A., M. S. Estrella, and K. Hammer. 1996. Food limitation stimulates metamorphosis of competent larvae and alters postmetamorphic growth rate in the marine prosobranch gastropod *Crepidula fornicata*. *Mar. Biol.* **127:** 267–275.

Pechenik, J. A., W. Li, and D. E. Cochrane. 2002. Timing is everything: The effects of putative dopamine antagonists on metamorphosis vary with larval age and experimental duration in the prosobranch gastropod *Crepidula fornicata*. *Biol. Bull.* **202:** 137–147.

Pinn, E. H., L. A. Nickell, A. Rogerson, and R. J. A. Atkinson. 1999. Comparison of gut morphology and gut microflora of seven species of mud shrimp (Crustacea: Decapoda: Thalassinidea). *Mar. Biol.* **133:** 103–114.

Pires, A., R. P. Croll, and M. G. Hadfield. 2000. Catecholamines modulate metamorphosis in the opisthobranch gastropod *Phestilla sibogae*. *Biol. Bull.* **198:** 319–331.

Poore, G. C. B. 1975. Systematics and distribution of *Callianassa* (Crustacea, Decapoda, Macrura) from Port Phillip Bay, Australia, with descriptions of 2 new species. *Pac. Sci.* **29:** 197–209.

Ricketts, E. F., J. Calvin, and J. W. Hedgpeth. 1985. *Between Pacific Tides*, 5th ed., revised by D. W. Phillips. Stanford University Press, Stanford, CA.

Rittschof, D. 1993. Body odors and neutral-basic peptide mimics: a review of responses by marine organisms. *Am. Zool.* **33:** 487–493.

Rittschof, D., R. B. Forward, G. Cannon, J. M. Welch, M. McClary, E. R. Holm, A. S. Clare, S. Conova, L. M. McKelvey, P. Bryan, and C. L. Van Dover. 1998. Cues and context: larval responses to physical and chemical cues. *Biofouling* **12:** 31–44.

Rodriguez, S. R., C. Riquelme, E. O. Campos, P. Chavez, E. Brandan, and N. C. Inestrosa. 1995. Behavioral responses of *Concholepas concholepas* (Bruguière, 1789) larvae to natural and artificial settlement cues and microbial films. *Biol. Bull.* **189:** 272–279.

Santagata, S. 2002. Structure and metamorphic remodeling of the larval nervous system and musculature of *Phoronis pallida* (Phoronida). *Evol. Dev.* **4:** 28–42.

Santagata, S. 2004. The larval development of *Phoronis pallida* (Phoronida): implications for morphological convergence and divergence among larval body plans. *J. Morphol.* **259:** 347–358.

Santagata, S., and R. L. Zimmer. 2002. Comparison of the neuromuscular systems among actinotroch larvae: systematic and evolutionary implications. *Evol. Dev.* **4:** 43–54.

Schneider, A. 1862. Über die Metamorphose der *Actinotrocha branchiata*. *Arch. Anat. Physiol.* 47–65.

Silén, L. 1952. Researches on Phoronida of the Gullmar Fiord area (West coast of Sweden). *Ark. Zool.* **4:** 95–140.

Silén, L. 1954. Developmental biology of the Phoronidea of the Gullmar Fiord area (west coast of Sweden). *Acta Zool. (Stockh.)* **35:** 215–257.

Swinbanks, D. D., and J. L. Luternauer. 1987. Burrow distribution of thalassinidean shrimp on a Fraser Delta tidal flat, British Columbia. *J. Paleontol.* **61:** 315–332.

Swinbanks, D. D., and J. W. Murray. 1981. Biosedimentological zonation of Boundary Bay tidal flats, Fraser River Delta, British Columbia. *Sedimentology* **28:** 201–237.

Takahashi, Y., K. Itoh, M. Ishii, M. Suzuki, and Y. Itabashi. 2002.

Induction of larval settlement and metamorphosis of the sea urchin *Strongylocentrotus intermedius* by glycoglycerolipids from the green alga *Ulvella lens*. *Mar. Biol.* **140:** 763–771.

Tamburri, M. N., C. M. Finelli, D. S. Wethey, and R. K. Zimmer-Faust. 1996. Chemical induction of larval settlement behavior in flow. *Biol. Bull.* **191:** 367–373.

Thompson, R. K. 1972. Functional morphology of the hindgut gland of *Upogebia pugettensis* (Crustacea, Thalassinidea) and its role in burrow construction. Ph.D. dissertation, University of California, Berkeley, 202 pp.

Thompson, L. C., and A. W. Pritchard. 1969. Osmoregulatory capacities of *Callianassa* and *Upogebia* (Crustacea: Thalassinidea). *Biol. Bull.* **136:** 114–129.

Toonen, R. J., and J. R. Pawlik. 2001a. Settlement of the gregarious tube worm *Hydroides dianthus* (Polychaeta: Serpulidae). II. Testing the desperate larva hypothesis. *Mar. Ecol. Prog. Ser.* **224:** 115–131.

Toonen, R. J., and J. R. Pawlik. 2001b. Foundations of gregariousness: a dispersal polymorphism among the planktonic larvae of a marine invertebrate. *Evolution* **55:** 2439–2454.

Torres, J. J., D. L. Gluck, and J. J. Childress. 1977. Activity and physiological significance of the pleopods in the respiration of *Callianassa californiensis* (Dana) (Crustacea: Thalassinidea). *Biol. Bull.* **152:** 134–146.

Viéitez, J. M., and C. C. Emig. 1979. Presence of *Phoronis pallida* (Schneider, 1862) (Phoronida Lophophorata) on the Atlantic coast of Spain. *Tethys* **9:** 91–92.

Wagner, R. H., D. W. Phillips, J. D. Standing, and C. Hand. 1979. Commensalism or mutualism: attraction of a sea star towards its symbiotic polychaete. *J. Exp. Mar. Biol. Ecol.* **39:** 205–210.

Wakefield, R. L., and S. N. Murray. 1998. Factors influencing food choice by the seaweed-eating marine snail *Norrisia norrisi* (Trochidae). *Mar. Biol.* **130:** 631–642.

Zhao, B., and P. Y. Qian. 2002. Larval settlement and metamorphosis in the slipper limpet *Crepidula onyx* (Sowerby) in response to conspecific cues and the cues from biofilm. *J. Exp. Mar. Biol. Ecol.* **269:** 39–51.

Zimmer, R. L. 1991. Phoronida. Pp. 1–45 in *Reproduction of Marine Invertebrates, Vol. 6, Echinoderms and Lophophorates*, A. C. Giese, J. S. Pearse, and V. B. Pearse, eds. The Boxwood Press, Pacific Grove, CA.

Zimmer-Faust, R. K., and M. N. Tamburri. 1994. Chemical identity and ecological implications of a waterborne, larval settlement cue. *Limnol. Oceanogr.* **39:** 1075–1087.

Reference: *Biol. Bull.* **207:** 116–129. (October 2004)

Microscaling: Why Larger Anemones Have Longer Cnidae

LISBETH FRANCIS

Shannon Point Marine Center, Western Washington University, 1700 Shannon Point Rd., Anacortes, Washington 98221-4042

Abstract. Scaling analysis provides a quantitative method for describing and comparing how qualities of organisms vary as a function of body size. However, cell level phenomena have been notoriously hard to analyze because animal cells and organelles have such irregular shapes. The intracellular cnidae make good models of scaling at the cell level because they are durable and easy to image and measure. The mean length of unfired tentacle cnidae (spirocysts) varies continuously, and reversibly, with body size for three macrophagous anemone species. Significant differences in spirocyst shape and size relative to body mass are related to differences in tissue functions and species ecologies, strongly suggesting that cnida size, shape, and scaling patterns respond to natural selection. Cnida scaling patterns can be treated as features of cnidarian life histories. Spirocyst scaling exponents (slopes of log cnida dimension *vs.* log body weight) are similar to each other (0.05–0.09) and to reported values for animal somatic cells (0.017–0.17), but are much smaller than reported values for anemone basal diameters (0.30–0.38). I propose, here, a general, mechanical explanation for microscaling of structural secretory cells and their secretions, including the cnidae. Larger bodies require thicker, pliant sheets of sluggishly respiring extracellular support materials such as mesoglea and basement membrane. Thicker mesoglea can support larger, taller epithelial cells, which in turn provide additional maintenance services for these progressively thicker acellular layers. Ultimately, larger, taller cells can secrete and support larger, longer cnidae.

Received 31 July 2003; accepted 7 July 2004.

Abbreviations: b, slope of the log-log plot; OLS, ordinary least squares regression estimate of line fit; RMA, reduced major axis estimate of line fit; 95% CI, 95% confidence intervals (for slope and intercept estimates); %SEE, percent standard error of estimate.

Introduction

Although many organisms exhibit a wide range of adult body sizes, remarkably little is known about how cell size or organelle size varies (scales) with body size, or about the adaptive significance of such variation. Cnidae—structurally and functionally unique organelles of cnidarians (Mariscal, 1984) that include spirocysts, nematocysts, and ptychocysts—are particularly tractable for studying such microscaling because they have comparatively simple shapes and are much easier to image and to measure than entire cells and organelles. Cnidae are distinctive and morphologically variable microtools composed of a durable cartilage-like material (Blanquet, 1988) secreted inside a single cell. Mechanically, they are pressurized capsules with an attached eversible tubule that is inverted inside the capsule before firing. Either the capsule or its tubule may be filled with toxins, irritants, or adhesives that are released when the tubule everts during firing.

In spite of many quantitative studies of cnida size (Stephenson, 1929; Chintiroglou, 1996; Chintiroglou and Simsiridou, 1997; Chintiroglou *et al.*, 1996, 1997; Chintiroglou and Karalis, 2000; Zamponi and Acuña, 1991; Acuña and Zamponi, 1997; Williams, 1996, 1998, 2000), changes in cnida size with body size appear to have been overlooked or discounted; and no studies have been conducted on cnida scaling *per se*. In the taxonomic literature, tissue-specific size ranges for each cnida population have been treated as species-specific characters (discussed in Fautin, 1988), although a possible relationship between developmental stage or polyp size and cnida size has occasionally been noted (Cutress, 1955; Sebens and Laakso, 1978; Fautin *et al.*, 1989; Ryland *et al.*, 2004).

Sea anemones (order Actiniaria) make good subjects for a scaling study for four reasons. First, body size, rather than age, appears to be the most critical determinant of the life

history in this group. Second, growth is reversible: under favorable conditions anemones grow and under unfavorable conditions they shrink, so size and age are essentially decoupled (review in Shick, 1991). Third, in clonal species that aggregate (*e.g., Anthopleura elegantissima;* Francis, 1973a), a full range of stages may occur simultaneously, providing a morphologically diverse array of individuals cloned from the same zygote (Francis, 1976). Finally, among anthozoans, sea anemones have evolved the greatest variety both of cnidae and of polyps, with the highest level of regional specialization (*i.e.,* different sizes and types of cnidae in different parts of the body), resulting in substantial between-species variability (Schmidt, 1974; Weill, 1934 a, b). This variation within and among species allows strong comparative tests relating cnida scaling to species habitats and tissue functions.

I chose spirocysts for this first study of cnida microscaling for several reasons. First, spirocysts are easy to recognize. Second, they are an abundant, widespread, unique, and probably monophyletic cnida type, showing little evolutionary divergence in form within the Hexacorallia (Schmidt, 1974) and no major morphological differences among the actiniarian anemones (Rifkin, 1991). Third, in members of the genus *Anthopleura,* spirocysts occur in two tissues that have quite different functions: tentacles that are used mainly in feeding, and acrorhagi that are specialized, inducible structures (Francis, 1976) used only in territorial battles (Francis, 1973b), most often with other anemones (Francis, 1985). Finally, Williams (1996, 1998, 2000), who developed a standardized protocol for sampling, reporting, and testing cnida size variation, has confirmed that spirocysts from *Metridium* showed higher than usual coefficients of variation (Williams, 2000), validating a general impression that within-sample variability is higher for spirocysts than for other cnidae.

Here I describe scaling of one adhesive cnida type (spirocysts) from two different tissues (ectoderm of the feeding tentacles and acrorhagi) of two sympatric anemones that have contrasting diets, growth forms, and social structures. *Anthopleura elegantissima* (Brandt, 1835) dominates large areas of the mid-intertidal on rocky shores by replicating asexually to form dense, segregated clonal groups (Francis, 1973a). It uses the inducible acrorhagi to attack and repel all other anemones except clonemates (Francis, 1973b). While *A. elegantissima* eats primarily plankton, invertebrate larvae, and smaller intertidal invertebrates, *Anthopleura xanthogrammica* (Brandt, 1835) commonly eats larger intertidal invertebrates, including dislodged mussels and barnacles (Sebens, 1981a). *A. xanthogrammica* develops larger polyps than *A. elegantissima* (Sebens, 1981b), does not replicate asexually, and exhibits less aggression against conspecifics (Sebens, 1984). Data for the tentacle spirocysts of *Tealia crassicornis* (Mueller, 1776) (a closely related aclonal species without acrorhagi), are included for contrast, because this species captures larger and more active prey—including moderate-size crabs, snails, and mussels (Sebens and Laakso, 1978)—than is typical for species of *Anthopleura.*

Finally, I found differences in spirocyst size among tissues and species to be consistent with apparent differences in the selective regimes; however, increase in spirocyst size with body size was similar for all populations, with scaling exponents similar to those reported for cell size variation within and among animal species (Munro, 1969; Munro and Gray, 1969; Maldonado *et al.,* 1974; Peters, 1983; Calder, 1984; Stevenson *et al.,* 1995). To account for these unusually small scaling exponents, I introduce a possible mechanical explanation for microscaling at the cellular level. Cnida scaling (and the scaling of cellular secretions, generally) may typically reflect the underlying phenomenon of cell scaling.

Materials and Methods

Specimen collection and handling

Specimens of *Anthopleura elegantissima* were from Eagle Point and Eagle Cove, San Juan Island, Washington (48°28′N, 123°03′W). *A. xanthogrammica* specimens were all from Charleston, Oregon (43°20′N, 124°20′W); and specimens of *Tealia crassicornis* were from Anacortes (48°00′N, 131°01′W), and San Juan Island, Washington. Anemones were weighed alive by first removing any clinging debris, and then blotting them firmly to cause contraction and to remove all expressed moisture. This method is non-destructive and provides a practical basis for comparing the sizes of soft-bodied animals such as anemones. Daily measurements of 11 individuals (*A. elegantissima*) over a 3-day period indicated that wet weights were reproducible within ± 3%.

Within 2 weeks of collection, most animals were either examined alive, or preserved in 10% formalin after first anesthetizing them in seawater by adding an equal volume of magnesium sulfate solution (7.5% by weight of common Epsom salts).

Anemone selection

To determine whether average size of the tentacle spirocysts is a function of body size for the clonal aggregating anemone, *A. elegantissima,* I collected individuals spanning the range of sizes found within a clonal aggregation at Eagle Cove, Washington. Recently divided animals with obvious fission scars were always excluded. To compare the scaling of acrorhagial and tentacle spirocysts, I collected one or two individuals with well-developed acrorhagi from seven separate clusters of *A. elegantissima* in densely populated tidepools at Eagle Point, Washington.

To compare scaling patterns for aclonal species, I also

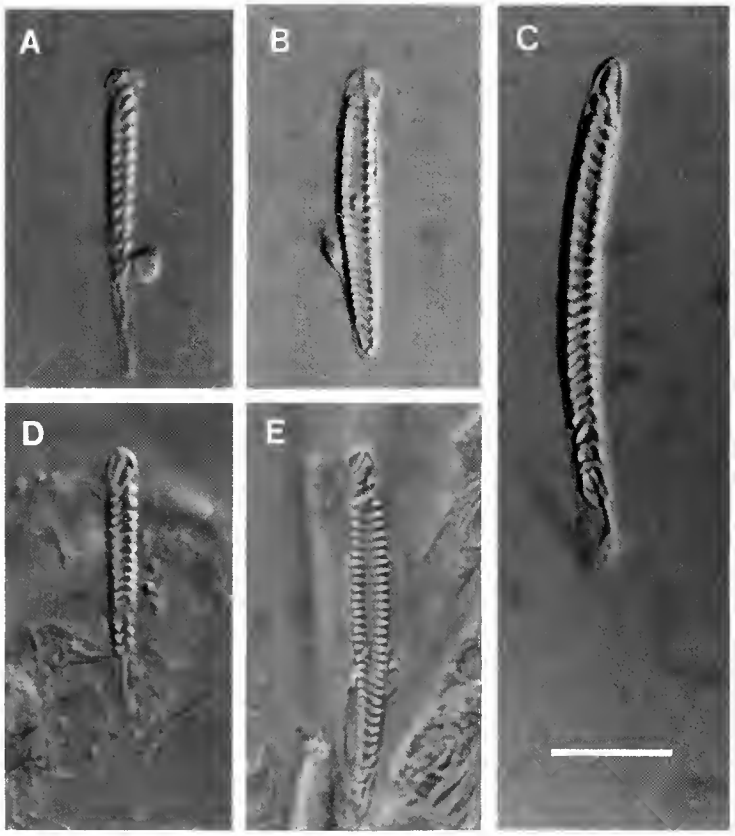

Figure 1. Comparison of average-sized spirocysts from three anemone species for specimens of the same size. In the living animals, the tubule end of the unfired spirocyst capsule (pointing upward in these photographs) presses tightly against the external cell membrane, so that the everting tubule is directed outward and away from the anemone during firing. Tentacle spirocysts are from *Anthopleura xanthogrammica* (**A**), *Anthopleura elegantissima* (**B**), and *Tealia crassicornis* (**C**). Acrorhagial spirocysts are from the same specimens of *A. xanthogrammica* (**D**) and *A. elegantissima* (**E**). Photographs were taken using differential interference contrast at 1000× (oil immersion). Each anemone weighed approximately 10 g. Scale bar 10 μm.

collected individuals of *Anthopleura xanthogrammica* and *Tealia crassicornis* (another sympatric, actonal species). Specimens of *A. xanthogrammica* were selected to span the size range from within a single population that included very small juveniles. Specimens of *T. crassicornis* included freshly collected individuals from Anacortes, Washington (Shannon Point Marine Center [SPMC]) and a few very large individuals that had been kept in the laboratory for some years (at SPMC, Anacortes, WA, and the University of Washington Laboratories, Friday Harbor, WA).

Tissue selection

One medium-to-large tentacle was taken from each individual anemone. To reduce variability (Robson, 1988), I consistently examined only the proximal one-third of the largest tentacle for the size-graded series of anemones from a single clone. Acrorhagial tissue from the *Anthopleura* species was obtained from the white tip that contains specialized cnidae used only in aggressive interactions with other anthozoans.

Spirocyst identification and measurement

Unfired spirocysts are easy to recognize in squash preparations of either fresh or preserved tissue. The capsule wall is unusually transparent, and the crystalline material inside the inverted tubule produces very strong birefringence. Under interference contrast illumination, spirocysts look like glowing tapered springs that have been squashed slightly in their transparent capsule sacks (Fig. 1). I prepared smears by macerating a sample of tissue mechanically in a drop of seawater and pressing this suspension into a thin layer between a slide and coverslip. Spirocysts were identified using a light microscope at 1000× (oil immersion) and measured to the nearest 0.1 μm using a computer-linked video camera (image analysis) system. Data on spirocyst sizes were collected systematically by scanning each slide

(as described in Williams, 1996) and measuring maximum lengths and widths (method of Hand, 1954) of the first 20 clearly visible, intact, and unfired capsules with their long axes parallel to the plane of the slide. Duplicated measurements using 20 video images indicated that spirocyst dimensions were reproducible within ± 1% (lengths) and ± 4% (widths).

Data analyses

For these data, no single refined and appropriate statistic exists for description and hypothesis testing, so different analyses were used for different purposes. Here I apply a series of generally conservative and robust statistics to describe and compare data on cnida size as a function of polyp size.

Mean capsule dimensions and their standard errors were calculated for systematic samples of 20 measurements from each tissue, which provided a good estimate of the true means (Williams, 1998). Subsequent analysis of variation in these means, rather than the raw data, offers better resolution for detecting real, between-sample differences, especially where levels of within-sample variability are very high, as they are here.

The nonparametric Spearman rank sum correlation (one-tailed test) was used to determine *P*-values for correlations between mean capsule dimensions and polyp wet weights (Zar, 1984), with groupwise error (asterisks) determined using the sequential Bonferroni adjustment (Jaccard and Wan, 1996).

Graphs were constructed using a linear scale on the *Y*-axis and log scale (for wet weight) on the *X*-axis (Longley, 1984) to eliminate the perceptual bias of the traditional log-log plot typically used in scaling studies (Smith, 1984). To compute scaling exponents, anemone wet weights and mean dimensions of the spirocyst capsules were transformed to common logarithms (base 10) for analysis.

Model II regression—slopes (scaling exponents) and intercepts for log-log plots. Since specimens were deliberately selected to span the existing size range of the anemones, the wet weights (and their logs) are not normally distributed. Furthermore, all of the variables are measured with error; and measurement error for the *X* and *Y* variables is similar (± 3% for wet weights and ±1%–4% for cnida dimensions). Thus these data do not meet the assumptions for Model I regression analysis (McArdle, 1988), nor for associated parametric methods such as ANOVA, ANCOVA, and multivariate analysis. For *R* values less than 0.9, the ordinary least squares (OLS) method typically underestimates the scaling exponent; and for R greater than 0.9, predictions of the Model I and Model II regressions converge (McArdle, 1988; LaBarbera, 1989).

Model II regression is appropriate for describing "functional relationships" such as these (Sokal and Rohlf, 1981; Rayner, 1985). Hence, to determine scaling exponents (slope of the log-log plot), lines were fitted to the log-transformed data using the reduced major axis (RMA) method, also known as the geometric mean regression, probably the most robust method for determining the slope for morphometric data of this kind (McArdle, 1988; LaBarbera, 1989). In addition to being scale-independent, the RMA estimate of the slope (b_{RMA}) is rotation-invariant (Smith, 1984; Rayner, 1985) and easily calculated from the OLS estimate of the slope (b_{OLS}) and *R*, the Pearson product moment correlation ($b_{RMA} = b_{OLS}/R$). The asymmetrical 95% confidence intervals (95% CIs) for the slopes were estimated using bootstrapping (10,000 iterations; SYSTAT, 1998, version 9; SPSS Inc., Evanston, IL). None of the conclusions in this study were sensitive to the choice of regression models.

Goodness of fit and standard error of estimate (SEE). The Pearson product moment correlation (*R*) is affected by the slope of the line and the range of values of both variables, and thus is a biased measure of the goodness of fit (Smith, 1984). Since *R* decreases as the slope of the line decreases, this is particularly problematic where the slopes are quite small, as they are here. As a measure of the strength of association, Smith (1984) recommended reporting the standard error of estimate (the standard deviation of residuals which is sometimes called "standard error of regression"), expressed as a percent of the mean *Y* value, for ease of interpretation. For log data, percent standard error of estimate can be calculated as follows:

$$\%\text{SEE} = \text{Antilog}(2 + \text{SEE as a log}) - 100$$

(Smith, 1984). Because the variances of RMA and OLS estimators are identical to the third significant digit (McArdle, 1988), I report *R* and SEE values based on OLS regression calculations.

Significance of between-sample differences. Comparisons between tissues and species were *a priori* tests of initial hypotheses, and were based on paired samples from the same individuals or from weight-paired individuals of different species. Paired student's *t*-tests (Sokal and Rohlf, 1981) were used to test for significant differences in the dimensions of tentacle and acrorhagial spirocysts from the same specimens. Between-species differences in capsule size were tested similarly by pairing polyps by weight (Zar, 1984) and testing for significant differences in spirocyst capsule dimensions and in polyp wet weights (weight differences never significant, here). The paired *t*-test assumes only that the differences (and not the variables themselves) are normally distributed (Zar, 1984). This method provides several advantages over simply comparing *Y*-intercepts us-

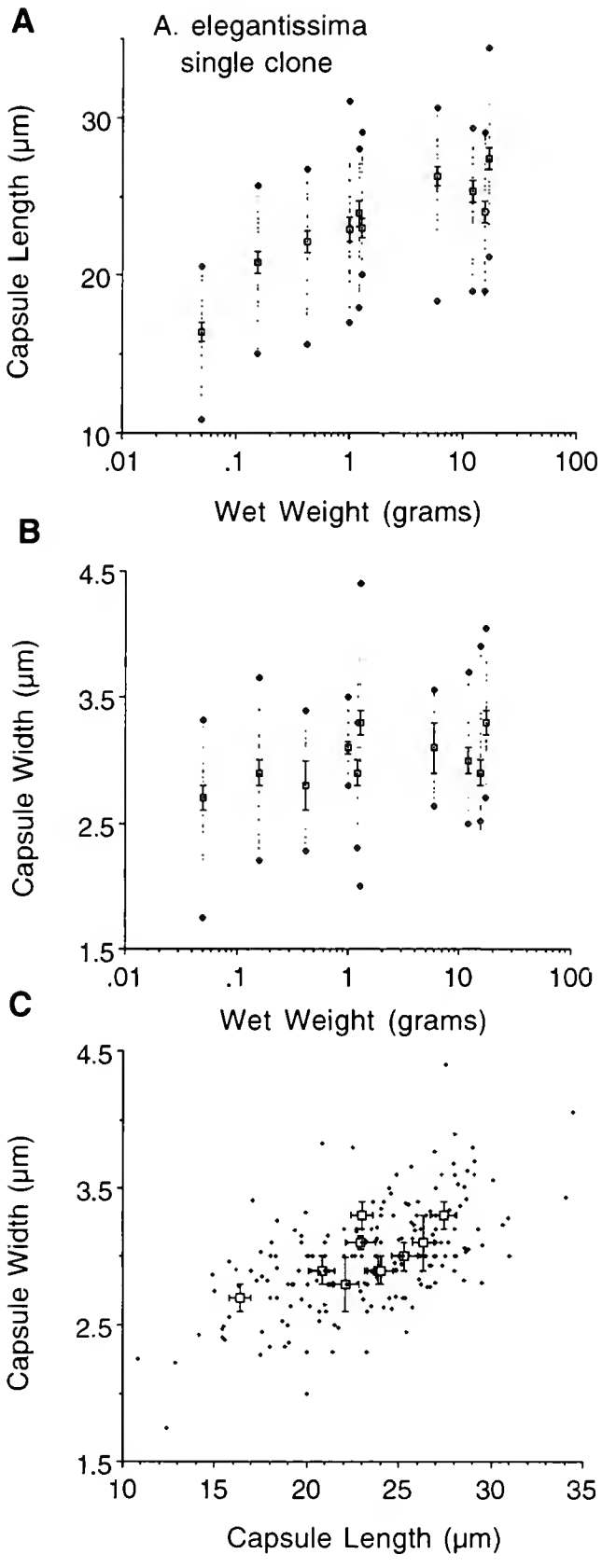

ing estimated 95% confidence intervals. (1) Conclusions are based on direct comparison of the data and are thus independent of assumptions used in calculating the best fit line and its confidence intervals. (2) Assessment is based on consistency across the overlapping range of body sizes, rather than on predicted differences for one arbitrary body size. (3) Providing *P*-values allows correction for groupwise error.

Scaling exponents were considered to be significantly different if one lay outside the 95% confidence interval for the other. Where scaling exponents do not differ significantly, line elevations may be compared similarly using the 95% CIs for the *Y*-intercepts (Hess, 1993).

Results

Average capsule length of the tentacle spirocysts increased continuously and significantly with increasing polyp size in all three macrophagous anemone species (Figs. 2A–5A; Table 1). Over the size ranges sampled, capsule lengths increased 22%–67%. Smaller increases in the capsule widths (0%–22%) generally were not significant at these sample sizes (Figs. 3B–5B, Table 2). The same patterns were apparent within a single clone of *Anthopleura elegantissima* (Fig. 2) where among-sample variation was minimized, and the increase in capsule width reached significance.

Scaling of tentacle spirocysts

Although the size of the tentacle spirocysts increased with body size in all cases, the spirocysts exhibited strong negative allometry. That is, scaling exponents for mean capsule length (0.052–0.086) and mean capsule width (0.021–0.039) were significantly smaller than the 0.33 predicted for proportional growth (= isometry for dimension length as a function of dimension mass), and smaller than reported scaling exponents for anemone basal diameters (0.30–0.38; Sebens, 1981a) (95% confidence intervals; Tables 1, 2).

Scaling of acrorhagial spirocysts from Anthopleura

For the genetically diverse sample of *A. elegantissima*, both capsule width and capsule length of the acrorhagial spirocysts increased significantly with increasing body

Figure 2. Increase in the size and aspect ratio of tentacle spirocysts as a function of body size within a single clone of the sea anemone *Anthopleura elegantissima*. Data are mean capsule dimensions (open squares), plus or minus their standard errors (bars), for 20 undischarged tentacle spirocysts (dots or small crosses) from each of 10 individuals from this clone. Polyp ranges are shown as open diamonds. Mean capsule length (**A**) and width (**B**) are shown as functions of anemone wet weight. Widths of the individual capsules (**C**) are shown as a function of individual capsule length for the pooled sample of 200 spirocysts from these 10 anemones.

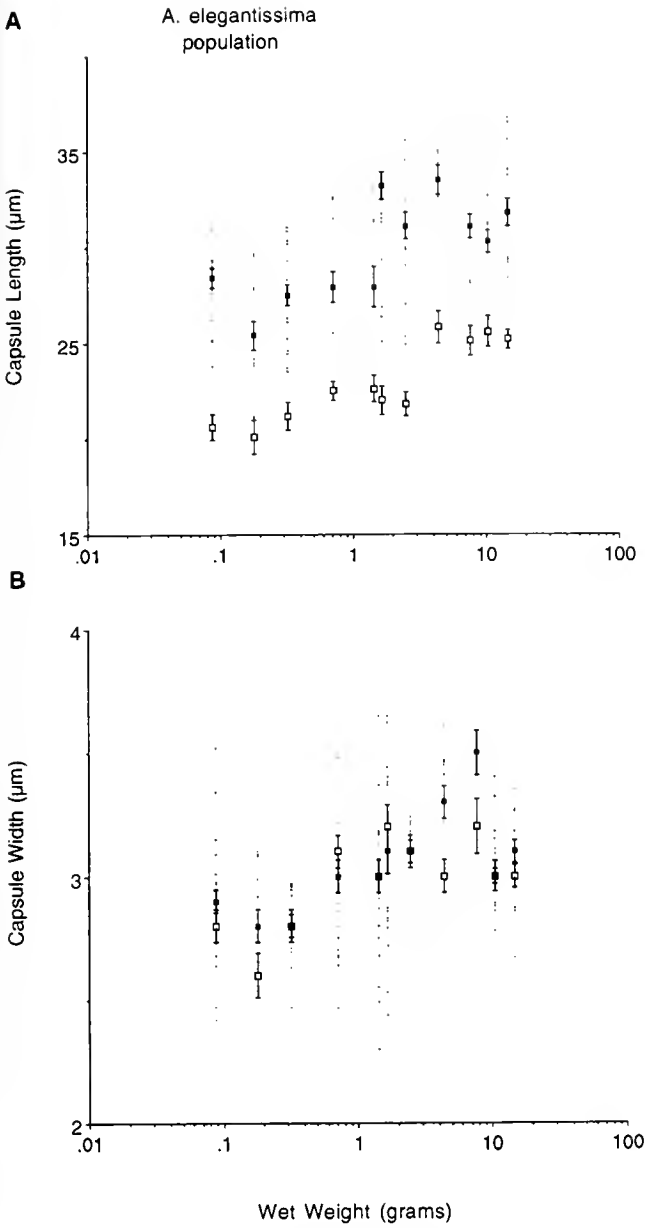

Figure 3. Length and width of acrorhagial spirocysts (solid squares) and tentacle spirocysts (open squares) from a genetically diverse sample of the clonal anemone *Anthopleura elegantissima.* Data are means, plus or minus their standard errors (bars), for 20 undischarged spirocysts (dots for tentacle spirocysts only) from each of the two tissue samples taken from individuals with well-developed acrorhagi (n = 11 individuals from 8 different clones). Average capsule lengths (**A**) and widths (**B**) are shown as functions of body size, for tentacle spirocysts and acrorhagial spirocysts from the same anemones.

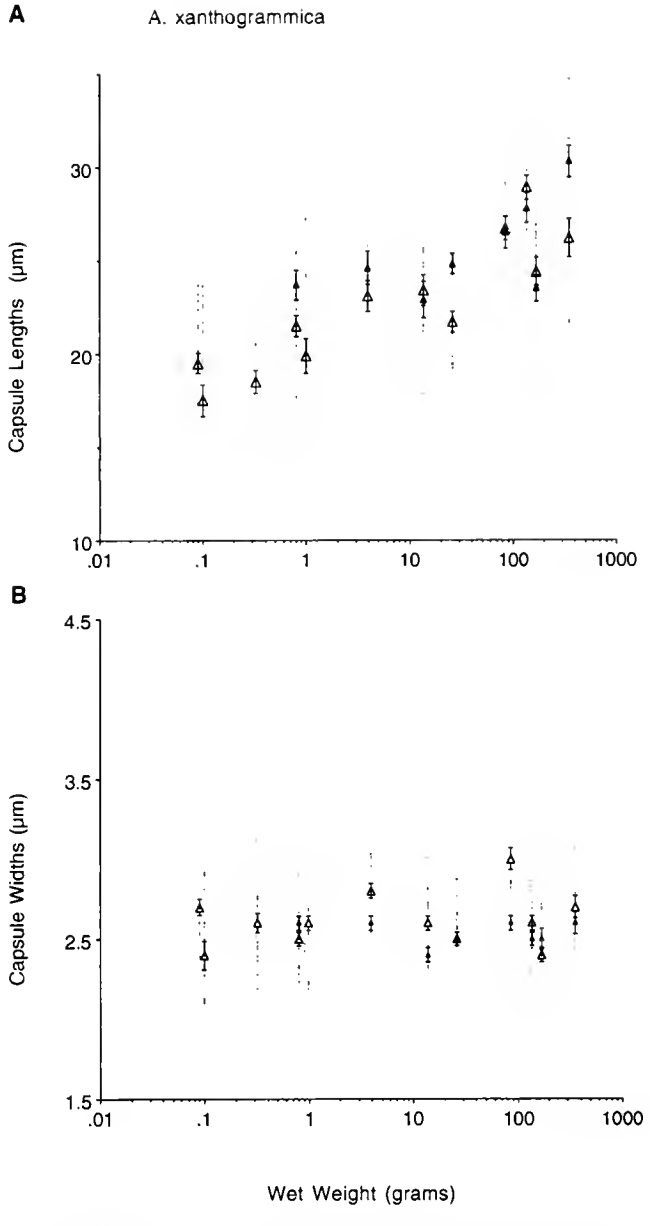

Figure 4. Length and width of acrorhagial spirocysts (solid triangles) and tentacle spirocysts (open triangles) of the aclonal anemone *Anthopleura xanthogrammica.* Data are means, plus or minus their standard errors (bars), for 20 undischarged spirocysts (dots for acrorhagial spirocysts only) from each of the two tissue samples taken from the same individuals. Because specimens of *A. xanthogrammica* smaller than 0.8 g wet weight consistently lack acrorhagi, there are more samples of tentacle spirocysts (n = 12 polyps) than of acrorhagial spirocysts (n = 8 polyps). Average capsule length (**A**) and width (**B**) are shown as functions of body size, for tentacle spirocysts and acrorhagial spirocysts from the same anemones.

weight (Tables 1, 2; Fig. 3). In contrast, for the non-clonal anemone *A. xanthogrammica,* neither width nor length of the acrorhagial spirocysts was significantly correlated with body size (Tables 1, 2). However, the consistent absence of acrorhagi in very small individuals reduced the size range of this sample (n = 8 individuals with acrorhagi; Fig. 4).

Variation in capsule shape

In all six spirocyst populations (three from *A. elegantissima,* two from *A. xanthogrammica,* and one from *Tealia crassicornis*), scaling exponents for capsule width (Table 2)

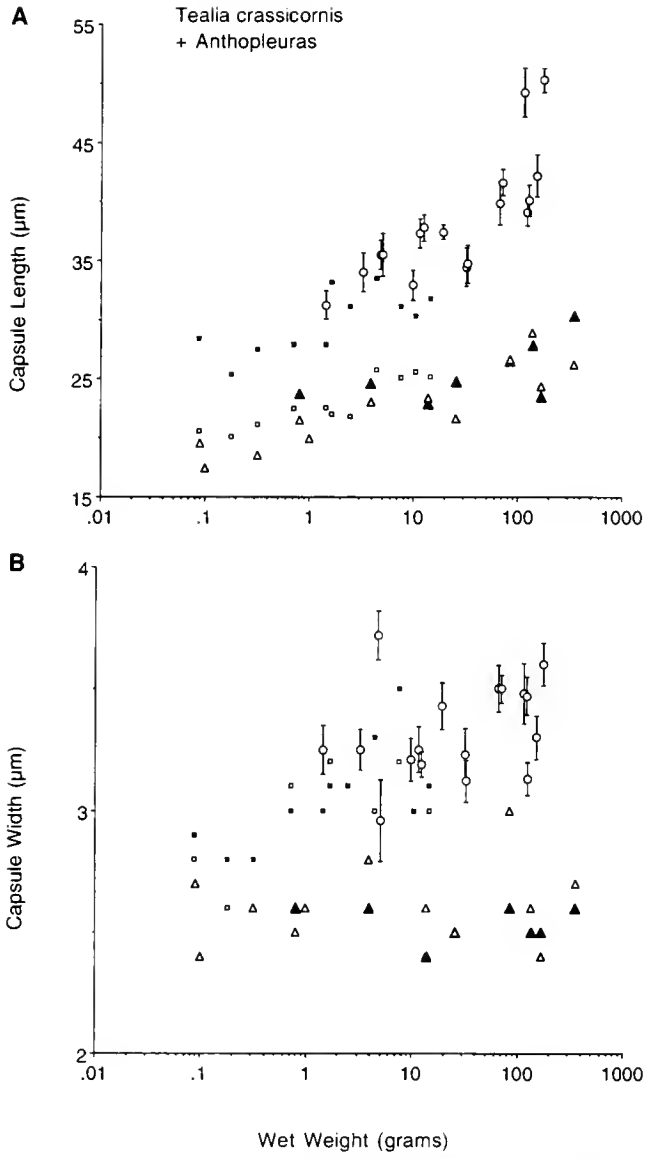

Figure 5. Scaling of tentacle spirocysts from *Tealia crassicornis* (circles), compared with scaling of tentacle and acrorhagial spirocysts from *Anthopleura elegantissima* (squares) and *A. xanthogrammica* (triangles). New data for *T. crassicornis* are means, plus or minus their standard errors (bars), for 20 spirocyst capsules from each sample. Average capsule length (**A**) and capsule width (**B**) are shown as functions of body size for tentacle spirocysts from *T. crassicornis* (means and their standard errors), with comparative data for tentacle spirocysts (open symbols) and acrorhagial spirocysts (filled symbols) from *A. xanthogrammica* and the genetically diverse sample of *A. elegantissima*. For clarity, the data for the two *Anthopleura* species from previous figures (Figs. 3, 4), are shown here without error bars.

were smaller than those for capsule length (Table 1). Except for the *A. elegantissima* acrorhagi, these differences were all significant statistically (*i.e.*, predicted exponents for capsule width were outside the 95% confidence intervals for capsule length exponents). Thus capsule aspect ratios increased consistently with capsule size in both tissues and for all three anemone species.

This shape variation was also apparent within the *A. elegantissima* clone: the scaling exponent for log individual capsule width as a function of log capsule length (Table 2; Fig. 2C) was 0.66, which was significantly smaller than the theoretical value of 1.0 predicted for proportional (isometric) scaling (95% confidence intervals; Table 2).

Differences in scaling exponents between tissues and species

Scaling exponents for capsule length did not differ significantly between the two *Anthopleura* species, for either tentacle or acrorhagial spirocysts (slopes all lay within each others' 95% confidence intervals, Table 1). Although the tentacle spirocysts from *T. crassicornis* showed a slightly higher scaling exponent than tentacle spirocysts from the genetically diverse samples of *A. elegantissima* and *A. xanthogrammica*, this exponent was not significantly higher than that of the *A. elegantissima* clone (Table 1). Furthermore, the higher scaling exponent of *T. crassicornis* was heavily influenced by two of the largest individuals (see Fig. 5A).

By contrast, the scaling exponents for capsule width were significantly lower for spirocysts from *A. xanthogrammica* tentacles and acrorhagi than for the other two anemones, whose capsule width exponents were indistinguishable from each other.

Spirocyst size: significant differences between tissues and species

Consistent differences in mean capsule size are clearly apparent from the combined semilog plot of polyp means (Fig. 5), and from photographs (Fig. 1) of average-sized spirocytes taken from specimens of the same size (10 g wet weight). Tentacle spirocysts from the genetically diverse sample of *A. elegantissima* were significantly shorter (paired *t*-test, $P < 0.001$*), but not narrower ($P < 0.2$), than their own acrorhagial spirocysts, and were both shorter and narrower than the tentacle spirocysts from *T. crassicornis* ($P < 0.05$*). Both tentacle and acrorhagial spirocysts from *A. xanthogrammica* were significantly shorter and narrower ($P < 0.05$*) than the intermediate-sized tentacle spirocysts of *A. elegantissima*.

Discussion

Cnida scaling is described here for the first time. Of the possible questions about this newly described phenomenon, here are a few that I find particularly compelling. Are cnida scaling and allometry real, characterizable, and distinctive kinds of intraspecific variability? Are such patterns rare, common or universal among cnidae? What effects might

Table 1

Spirocyst capsule length vs. *anemone size: scaling exponents and constants for three anemone species, from reduced major axis regression equations*

Species Tissue (n)§	Scaling exponent† (95% CI)	Intercept† (95% CI)	$\bar{X}$, $\bar{Y}$‡	R¶ (%SEE)	P#
Log mean spirocyst capsule length in μm (Y) vs. log anemone wet weight in grams (X) (see Figs. 2A–5A for data)					
Anthopleura elegantissima, single clone					
Tentacles (10 anemones)	0.072 (0.041–0.092)	22.4 (22.1–22.6)	0.1998, 1.362	0.897 (7.0%)	<0.0005***
A. elegantissima, genetically diverse sample					
Tentacles (11)	0.053 (0.043–0.072)	22.3 (22.1–22.5)	0.185, 1.359	0.920 (4.1%)	<0.0005**
Acrorhagi (11)	0.049 (0.033–0.079)	29.1 (28.7–29.3)	0.185, 1.474	0.791 (6.6%)	<0.025*
Anthopleura xanthogrammica					
Tentacles (12)	0.052 (0.039–0.065)	20.4 (19.9–20.8)	0.780, 1.349	0.908 (7.1%)	<0.0005**
Acrorhagi (8)	0.046 (0.022–0.091)	23.0 (18.6–23.6)	1.485, 1.405	0.632 (8.3%)	<0.05
Tealia crassicornis					
Tentacles (17)	0.086 (0.054–0.121)	28.8 (27.7–32.0)	1.402, 1.581	0.806 (8.3%)	<0.0005***

§ Number of anemones sampled (20 capsules per sample).

† Slope and detransformed Y-intercept (μm) with 95% confidence intervals.

‡ Mean values of (log X) and (log Y).

¶ Pearson's product-moment correlation coefficient (R) and percent standard error of estimate (%SEE).

P-value calculated for Spearman rank correlation with groupwise significance after sequential Bonferroni adjustment, where * = $P < 0.05$, ** = $P < 0.01$, *** = $P < 0.001$.

cnida scaling and allometry have on the structure, function, development, and evolution of cnidae and anemones? And most intriguing to me, what *causes* cnida scaling? Proximally, how might gross body size influence the size and shape of these intracellular microtools; and ultimately, are these patterns likely to be advantageous?

Intraspecific variation in cnida size

First and most importantly, cnida scaling is real: larger *Anthopleura* and *Tealia* do produce larger spirocysts. Furthermore, a reexamination of published data suggests that cnida scaling is actually widespread among anemones (Table 3). Of the 39 studied populations, 25 show positive correlations between *cnida length* and polyp size, and 3 of 13 show positive correlations between *cnida width* and polyp size. Curiously, rather than characterizing and explaining between-sample variability, previous studies have focused exclusively on defining invariant characters for species description and phylogeny (Stephenson, 1929; Weill, 1934a, b; Carlgren, 1949; Williams, 1996, 1998, 2000; Chintiroglou, 1996; Chintiroglou *et al.*, 1996, 1997; Chintiroglou and Simsiridou, 1997; Chintiroglou and Karalis, 2000). In this search for stable taxonomic characters, cnida scaling and other examples of intraspecific variability have typically been dismissed as inconvenient or unworkable (but see Ryland *et al.*, 2004). Although cnida scaling appears widespread among anemones, I am not aware of comparable information for other cnidarians.

Second, cnida size varies continuously. No size classes exist within individual samples (Figs. 2–4), or within the pooled sample from a single clone (Fig. 2C).

Variation in cnida shape with increasing cnida size

Multiple lines of evidence indicate that cnida shape changes with cnida size. This is particularly apparent from the combined sample of 200 tentacle spirocysts from 10 clonemates of *A. elegantissima* (Fig. 2C, Table 2). The width of individual capsules did increase as a function of capsule length; but the scaling exponent of 0.66 was significantly less than the scaling exponent of 1.0 expected for isometry ($P < 0.001$). In all tissues, all species, and all cnida types examined, cnida length increased more dramatically with increasing anemone size than did capsule width; the single exception being the acontial b-mastigophores from *Sagartia elegans* (data from Stephenson, 1929; Kramer and Francis, 2004; this study, Fig. 5, Tables 1–3). Size-range data in species descriptions show the same pattern. For 39 distinctive cnida populations from *A. elegantissima*, *T. crassicornis*, and *A. xanthogrammica*, the average percent difference between reported minimum and

Table 2

Spirocyst capsule width vs. anemone size or capsule length: scaling factors and constants for three anemone species, from reduced major axis regression equations

Species Tissue (n)§	Scaling exponent† (95% CI)	Intercept† (95% CI)	$\bar{X}$, $\bar{Y}$‡	R¶ (%SEE)	P#
a) Log mean spirocyst capsule width in μm (Y) vs. log anemone wet weight in grams (X) (see Figs. 2B–5B for data)					
Anthopleura elegantissima, single clone					
Tentacles (n_A = 10 anemones)	0.032 (0.021–0.048)	2.96 (2.93–2.976)	0.1998, 0.476	0.587 (5.9%)	<0.05*
A. elegantissima, genetically diverse sample					
Tentacles (n_A = 11)	0.036 (0.022–0.056)	2.94 (2.91–2.948)	0.185, 0.474	0.780 (5.1%)	<0.1
Acrorhagi (n_A = 11)	0.038 (0.020–0.061)	3.00 (2.97–3.02)	0.185, 0.484	0.783 (5.1%)	<0.01*
Anthopleura xanthogrammica					
Tentacles (n_A = 12)	0.021 (0.012–0.033)	2.51 (2.46–2.56)	0.780, 0.417	0.202 (6.8%)	>0.5
Acrorhagi (n_A = 8)	0.014 (0.007–0.028)	2.42 (2.31–2.481)	1.485, 0.404	0.126 (3.2%)	>0.5
Tealia crassicornis					
Tentacles (n_A = 17)	0.039 (0.025–0.056)	2.93 (2.77–3.07)	1.402, 0.521	0.312 (6.0%)	<0.25
b) Log individual capsule width in μm (Y) vs. log individual capsule length in μm (X) (see Figs. 2C for data)					
A. elegantissima, single clone					
Tentacles (n_c = 200 capsules)	0.661 (0.583–0.746)	0.375 (0.287–0.48)	1.3601, 0.474	0.60 (10.9%)	<0.0005**

§ (n_A) = number of anemones sampled (20 capsules per sample); (n_c) = number of individual spirocyst capsules.

† Slope and detransformed Y-intercept (μm) with 95% confidence intervals.

‡ Mean values of (log X) and (log Y).

¶ Pearson's product-moment correlation coefficient (R) and percent standard error of estimate (%SEE).

P-value calculated for Spearman rank correlation with groupwise significance after sequential Bonferroni adjustment, where * = $P < 0.05$, ** = $P < 0.01$, *** = $P < 0.001$.

maximum capsule dimensions was 56% for capsule widths and 102% for capsule lengths (data from Hand, 1955). Larger cnidae typically become disproportionately longer, regardless of cnida type, tissue, or species.

Taxonomic implications of intraspecific variation in cnida size and shape

Because cnida size and shape commonly change with body size within anemone species, their value as taxonomic characters is much reduced (Williams, 1996, 1998, 2000). Although taxonomists have acknowledged that intraspecific variability can be problematic (review by Fautin, 1988), cnida size ranges have typically been used in species descriptions, rather than mean cnida dimensions (± SD) for each specimen, because this saves time and space. I strongly recommend including specimen wet weights in all future work, and wherever possible, also including mean capsule dimensions (± SD) for a 1-g specimen, as a basis for quantitative comparisons between populations and species. For more detailed comparative work, cnida scaling exponents and the Y-intercepts (predicted capsule dimensions for a 1-g specimen) provide distinctive characters that may be particularly valuable for separating cryptic species (*e.g.*, *Metridium senile* and *M. farcimen*, Kramer and Francis, 2004).

Evolutionary significance of larger acrorhagial spirocysts in A. elegantissima

Increasing localization and specialization of cnidae is a common evolutionary trend among sea anemones (Schmidt, 1974). Specialization through enlargement of the acrorhagial spirocysts in *A. elegantissima* (this study) and its sibling species, *A. sola* (Pearse and Francis, 2000), appears to be an example of this pattern. Acrorhagial and tentacle spirocysts are the same size (and relatively small) in *A. xanthogrammica* (this study) and also in the more distantly related *A. artemisia* (Hand, 1965), which belongs to a different branch of the genus (Geller and Walton, 2001). Larger acrorhagial spirocysts may be a shared derived character linking the sibling species pair *A. elegantissima* (this study) and *A. sola*, and distinguishing them from the closely related *A. xanthogrammica*.

Table 3

Correlation of cnida dimensions with body size for 39 cnida populations from 9 anemone species

Anemone species	Sample size§ $n \times N$	Correlated†		Data source
		Capsule length	Capsule width	
Anthopleura elegantissima	20 × 11	2/2	1/2	Francis, this study
Anthopleura xanthogrammica	20 × 12	1/1	0/1	Francis, this study
	20 × 08	0/1	0/1	
Actinia equina mediterranea				
form I	40 × 20	6/7	—	Chintiroglou and Simsiridou, 1997
form II	40 × 20	3/7	—	Chintiroglou *et al.*, 1997
Cereus pedunculatus	30 × 07	1/2	1/2	Stephenson, 1929 (calculations here)
Edwardsia claparedii	40 × 10	4/8	—	Chintiroglou, 1996
Metridium senile	20 × 08	4/4	0/2	Kramer and Francis, 2004
Metridium farcimen	20 × 10	1/2	—	Kramer and Francis, 2004
	20 × 21	1/1	0/1	
	20 × 27	1/1	1/1	
Sagartia elegans	30 × 12	0/2	0/2	Stephenson, 1929 (calculations here)
Tealia crassicornis	20 × 17	1/1	0/1	Francis, this study‡
Totals	5120 capsules	25/39 correlated	3/13 correlated	

§ Number of cnidae per sample (n) times the number of polyps sampled (N).

† Correlated capsule lengths and capsule widths = proportion of cnida populations with significant positive correlation between capsule dimension and polyp size (*e.g.*, 5/8 = 5 correlated and 3 not significantly correlated).

‡ With assistance from Paul Mages.

Functional significance of cnida size and shape

Within the functional limits of a given design, cnida effectiveness may commonly increase with cnida size (see Purcell, 1984). The cnidae are extraordinarily complex collagenous, intracellular secretions serving a wide range of general and specialized functions. They are numerous, costly, and discarded after a single use, puncturing the enclosing cell in the process. Thus their production and use must entail considerable investment by the animals. Larger capsules can carry larger payloads of tubules, spines, barbs, venoms, or glues. Furthermore, fewer cnidocytes are sacrificed during the firing of a few large spirocytes than by firing many small ones. Consequently larger cnidae probably contribute to other advantages of large body size in anemones, including advantage in competition, escape in size from predation, and ability to handle larger prey (Francis, 1979; Sebens, 1983, 1987; Kramer and Francis, 2004).

Variation in cnida shape may also impact function. Based on mechanical analysis of pressure vessel geometry, larger cnidae may typically become more elongate, rather than stouter, because of the impact of capsule width on wall stress. Local tension in the walls of a pressurized cylinder increases in proportion to the diameter and is unaffected by the length (Alexander, 1983, p. 153). For the cnidae, this means that wider capsules with the same internal pressure will experience more distortion in the walls, and presumably also more distortion of the catch/latch mechanism, and therefore greater risk of wasteful spontaneous firing. Increasing cnida size beyond the point of spontaneous firing would require a change in cnida design (*e.g.*, thicker cnida walls or a different latch design). This may be one reason that capsule widths increase relatively slowly as cnida size increases with anemone size.

The more elongate shape of larger cnidae may also be important for rapid influx of water during cnida firing (Thomason, 1988). Increase in cnida size without shape change (capsule isometry) would reduce the surface-to-volume ratio (S/V), causing more delayed firing in larger cnidae. The short, narrow spirocysts of *A. xanthogrammica* should be the fastest in this group, both because of their relatively high S/V ratios and because the relatively shorter tubule in these small spirocysts (Fig. 1A, D) should complete eversion more quickly than the longer tubules in the larger spirocysts of *A. elegantissima* and *T. crassicornis* (Fig. 1B, C, E).

Adaptive significance of cnida size, shape, and scaling

Differences in cnida size are likely to be adaptive. For example, relatively higher investment in competitive interference was predicted for clonal than for non-clonal anemones (Francis, 1988), which is reflected in the relatively larger acrorhagial spirocysts of *A. elegantissima* (this study). As another example, larger defensive nematocysts in the acontia of *Metridium farcimen* reflect the relatively higher predator densities in its subtidal habitat, by comparison with the smaller acontial nematocysts associated with the shallower habitat of *M. senile* (Kramer and Francis, 2004).

Differences in cnida shape (Fig. 1) are also likely to be

advantageous. For example, having short, narrow tentacle spirocysts that complete their firing very rapidly may be particularly advantageous for *A. xanthogrammica* (Fig. 1A), which captures loose mussels in wave-exposed areas (Sebens, 1981a, 1983) of high velocities and rapid accelerations (Denny *et al.*, 1985). A more delayed response by the wider and longer tentacle spirocysts of *A. elegantissima* (Fig. 1B) may be adequate for capturing smaller, lighter prey (Sebens, 1981a), and should be more economical in terms of cell (spirocyte) loss during firing. On the lower shore, *T. crassicornis* has very long and wide tentacle spirocysts (Fig. 1C) whose higher payload volumes are perhaps more important than a very rapid response time for capturing and holding crabs (Sebens and Laakso, 1978), which although powerful, are not fast-moving.

Cnida scaling may also be adaptive. For example, if larger spirocysts with their larger payloads permit greater adhesion to prey, then larger tentacle cnidae may yield increased capture success with larger prey. Both cnida size (this study) and prey size increase with body size for *A. xanthogrammica* (Sebens, 1981a) and for *A. elegantissima* (Spearman rank correlation for anemone size class *vs.* average prey size, two-tailed test, $r_s = 0.762$, $P < 0.05$; calculated using data from Sebens, 1981a). This connection between prey and cnida scaling is also supported by contrasting data for two planktivorous *Metridium* species, where prey size does not increase with body size (Sebens, 1981a). For *M. farcimen* and *M. senile*, the length of tentacle cnidae increases more slowly with body size (scaling exponents, 0.008–0.03, Kramer and Francis, 2004) than for macrophagous *Anthopleura* and *Tealia* species (scaling exponents, 0.052–0.086, this study). Thus cnida scaling patterns can be treated as features of cnidarian life histories.

Structural implications of cnida size and shape

From a design standpoint, providing space and support for needle-like cnidae and assuring the stability of surrounding soft tissues could be problematic, especially during cnida firing. Anemones have the greatest variety of cnidae in the class Anthozoa (Schmidt, 1974), which differs from Scyphozoa and Hydrozoa in having elongate, rather than ovoid or spherical, cnidae (Mariscal, 1984). Like the cnidae that they support, the epithelial cells in anemones are unusually tall and thin, secreting and supported by an unusually fibrous and structured mesoglea which almost qualifies as connective tissue (Hyman, 1940; Chapman, 1966; Gosline, 1971; Koehl, 1977).

At the outer limits of stability, very dense arrays of very long cnidae in defensive structures (*e.g.*, capsule lengths ≅ 90 μm for *Metridium* acontial amastigophores and *Anthopleura* acrorhagial holotrichs; Hand, 1955) actually *do* cause local tissue disintegration during firing (Äbel, 1954; Francis, 1973b, Kramer and Francis, 2004). Maximum size of these cnidae may be limited by tissue thickness, or by any tendency to disrupt tissues during regular cycles of extreme body elongation and contraction (illustrations in Shick, 1991).

In contrast, cnidae in the feeding tentacles are less densely arrayed and smaller (capsule lengths ≅ 20–30 μm for *Tealia* and *Anthopleura;* Hand, 1955), and are not likely to disrupt the tissue during ordinary body movements. However, since tentacle cnidae are used frequently in numerous prey capture events, any tissue disruption during cnida firing will interfere with further prey capture, thereby favoring tissue stability in the feeding tentacles also. In both situations, cnida size is likely to be constrained more narrowly in smaller specimens with thinner tissues and less structural support.

Possible causes of cnida scaling

Cnida scaling could arise through natural selection where size-limiting factors apply more strongly to small animals. Limiting factors that may become progressively less restrictive with increasing body size include physiological and ecological factors such as the food and energy flux (Sebens, 1981a), as well as morphological factors such as tissue and mesoglea strength and stability (Shick, 1991), and physical limitations of space such as tissue thickness (Shick, 1991) and cell size (Peters, 1983; Calder, 1984; Stevenson *et al.*, 1995).

Since the thickness of both the mesoglea and the inner and outer epithelial layers of the anemone body typically does increase with body size (Shick, 1991), larger anemones should be able to accommodate and support larger cnidae. While this may explain scaling of exceptionally long cnidae that are at or near the limits of tissue tolerance (*e.g.*, capsule length of acrorhagial holotrichs ≅ 90 μm; Hand, 1955), it would not explain scaling of the much smaller acrorhagial spirocysts interspersed among them (capsule lengths ≅ 30μ, this study). Clearly, then, not all instances of cnida scaling are due to gradual release of the more rigorous spatial and support constraints on smaller individuals.

In fact, no one of these factors can explain all the available data. If increase in cnida size were purely a function of higher energy availability in larger specimens, then cnida size should increase similarly with body size in all the tissues of a species. In fact, scaling exponents for the tentacle cnidae are typically significantly smaller than for the acontial cnidae in both *Metridium senile* and *M. farcimen* (Kramer and Francis, 2004). Since scaling exponents may vary between tissues as well as between species, cnida size clearly is not controlled uniformly by size-related differences in the energy budget of the whole animal.

Cnida scaling also occurs where there is no obvious selective advantage based on functional differences between larger and smaller individuals. Although prey size *does not*

increase with body size for *Metridium* (Sebens, 1981a), larger individuals *do* have longer tentacle cnidae (Kramer and Francis, 2004), although these scaling exponents are unusually small (0.018–0.03, as compared with 0.052–0.072 for *Anthopleura* tentacle spirocysts, and 0.035–0.051 for *Metridium* acontial nematocysts). Thus larger tentacle cnidae in larger individuals cannot always be explained as aiding in the capture of larger prey.

Developmental significance of cnida size differences

Cnida scaling may be caused proximally by cell scaling. In *Hydra*, cnida size is related to cell size, which declines with the number of divisions that an interstitial cell undergoes before differentiation. More divisions result in more and smaller cnidocytes, which produce smaller cnidae (Lehn, 1951). This may also be true for anemones, where otherwise continuous cnida populations often include an occasional double-sized or half-sized capsule (Cutress, 1955; Daphne Fautin, University of Kansas, pers. comm.), perhaps produced by one division more or less than the usual for that interstitial cell line.

A direct relationship between cell size and the size of secreted structures may actually be rather common. In *Drosophila*, local polyploidy in bristle-secreting cells results in larger cells that secrete larger bristles (Adler *et al.*, 2000); and in the roundworm *Caenorhabditis elegans*, a mutation that produces adult dwarfing has been traced to miniaturization of a cell line that contributes to the size of the cuticle-secreting and syncytial hypodermis (Knight *et al.*, 2002).

If cell size determines cnida size, then cnida scaling presumably implies cell scaling. That is, the observation that larger anemones have larger cnidae implies that the size of the cnidocytes also varies continuously, and reversibly, as a function of anemone body size.

Implications for cell and organelle scaling

While growth typically involves changes in body proportions, the fact that this also occurs at the cellular and subcellular level may be surprising (Brown and West, 2000). Order-of-magnitude agreement between cnida scaling exponents (0.018–0.086; this study; Stephenson, 1929; Kramer and Francis, 2004) and cell scaling exponents (0.017–0.17; Peters, 1983; Calder, 1984; Stevenson *et al.*, 1995) suggests that cnida scaling may reflect a wider pattern of cell scaling.

Based on these accurate cnida measurements, a power law for cnidae and cells may be closer to 1/10 than to the well-known 2/3–3/4 power law for gross morphological and physiological functions. Measured scaling exponents for the lengths (b_L = 0.052–0.086) and widths (b_W = 0.021–0.039) of unfired cnidae can be used to estimate scaling exponents for cnida surface areas ($b_{SA} = b_L + b_W$ = 0.073–0.125) and volumes ($b_V = b_L + 2b_W$ = 0.094–0.164) as functions of body mass. Thus cnida functions that depend on capsule surface area or volume should have exponents between 0.073 and 0.164, quite different from the 0.67–0.75 exponents reported for gross body functions (Peters, 1983; Calder, 1984; Schmidt-Nielsen, 1984; Niklas, 1994).

As a general explanation for the scaling of epithelial secretory cells and their structural products (such as extracellular mesoglea and basement membrane), I suggest that larger, taller epithelial cells can supply more structural material per unit attachment area for building and maintaining thicker sheets of pliant, extracellular support materials to resist the increased wall stresses in larger, stouter pressurized cylinders of all kinds—including worms, blood vessels, and guts, as well as sea anemones (Francis, unpubl. obs.). The scaling of cnidocytes and their intracellular cnidae can be considered a special, restricted case of this more general phenomenon, since cnidae cannot be larger than the cells enclosing them.

Acknowledgments

Data for *Tealia crassicornis* were collected with Paul Mages with support of REU funding (NSF 0097190). Andrew Kramer wrote the algorithm and ran the bootstrapping program. For able assistance, I thank Antonia Crease, students Deanna Wynn, Cliff Hollins, and Paul Mages (NSF 9729816 and NSF9731144), and volunteers Deborah S. Frazee, Margaret Longley, Misa Peterman, Carley Reiter, Keith Tuley, and Richard Wills; for office space, Anne H. Pope; for helpful discussion and editing, Michael LaBarbera, A. Richard Palmer, Alison and Roger Longley, and Garry Odell; for access to facilities, the directors, staff, and colleagues at Shannon Point Marine Center (Western Washington Univ.), Long Marine Laboratory (Univ. of California, Santa Cruz), and Oregon Institute of Marine Biology (Univ. of Oregon); and for the image analysis system at Shannon Point, the NSF Instrumentation and Laboratory Improvement Program and Texaco Foundation. The anemones themselves and the beautiful work of T. A. Stephenson provided wonderful inspiration. Without such support, the work would not have been possible.

Literature Cited

Äbel, E. F. 1954. Ein Beitrag zur Giftwirking der Actinien und Function der Randsäckchen. *Zool. Anz.* **153:** 259–268.

Acuña, F. H., and M. O. Zamponi. 1997. The use of cnidocysts for ecological races identification from sea anemones populations (Anthozoa, Actiniidae). *Iheringia Ser. Zool.* **82:** 9–18.

Adler, P. N., J. C. Liu, and J. Charlton. 2000. Cell size and the morphogenesis of wing hairs in *Drosophila*. *Genesis* **28:** 82–91.

Alexander, R. McN. 1983. *Animal Mechanics*, 2nd ed. Blackwell Scientific, Oxford.

Blanquet, R. S. 1988. The chemistry of cnidae. Pp. 407–425 in *The*

Biology of Nematocysts, D. A. Hessinger and H. Lenhoff, eds. Academic Press, San Diego, CA.

Brown, J. H., and G. B. West, eds. 2000. *Scaling in Biology*. Oxford Univ. Press, New York.

Calder, W. A. III. 1984. *Size, Function, and Life History*. Harvard Univ. Press, Cambridge, MA.

Carlgren, O. 1949. A survey of the Ptychodactiaria, Corallimorpharia and Actiniaria. *K. Sven. Vetenskapsakad. Handl.* **1:** 1–121.

Chapman, G. 1966. The structure and functions of the mesoglea. Pp. 147–168 in *The Cnidaria and Their Evolution*, W. J. Rees, ed. *Symp. Zool. Soc. Lond.* No. 16.

Chintiroglou, C. C. 1996. Biometric study of *Edwardsia claparedii* (Panceri) cnidome (Actiniaria: Anthozoa). *Belg. J. Zool.* **126:** 177–180.

Chintiroglou, C. C., and P. Karalis. 2000. Biometric investigations on the cnidae of the Aegean colour morphs of *Anemonia viridis*. *J. Mar. Biol. Assoc. UK* **80:** 543–544.

Chintiroglou, C. C., and M. Simsiridou. 1997. Biometric investigations on the cnidae of the sea anemone *Actinia equina mediterranea* Form 1 *sensu* Schmidt, 1972. *Isr. J. Zool.* **43:** 5–11.

Chintiroglou, C. C., D. Doumenc, J. Le Renard, A. Foubert, and Ph. Kolyva-Machaira. 1996. Classification of cnidarian nematocysts using multivariate and digital image analysis. *Bios (Macedonia, Greece)* **4:** 123–135.

Chintiroglou, C. C., I. Christou, and M. Simsiridou. 1997. Biometric investigations on the cnidae of Aegean color morphs of *Actinia equina mediterranea sensu* Schmidt, 1972. *Isr. J. Zool.* **43:** 377–384.

Cutress, C. H. 1955. An interpretation of structure and distribution of cnidae in Anthozoa. *Syst. Zool.* **4:** 120–137.

Denny, M. W., T. L. Daniel, and M. A. R. Koehl. 1985. Mechanical limits to size in wave-swept organisms. *Ecol. Monogr.* **55:** 69–102.

Fautin, D. G. 1988. Importance of nematocysts to actinian taxonomy. Pp. 487–500 in *The Biology of Nematocysts*, D. A. Hessinger and H. M. Lenhoff, eds. Academic Press, San Diego, CA.

Fautin, D. G., A. Bucklin, and C. Hand. 1989. Systematics of sea anemones belonging to the genus *Metridium* (Coelenterata: Actiniaria), with a description of *M. giganteum* new species. *Wasmann J. Biol.* **47:** 77–85.

Francis, L. 1973a. Clone specific segregation in the sea anemone *Anthopleura elegantissima*. *Biol. Bull.* **144:** 64–72.

Francis, L. 1973b. Intraspecific aggression and its effect on the distribution of *Anthopleura elegantissima* and some related sea anemones. *Biol. Bull.* **144:** 73–92.

Francis, L. 1976. Social organization within clones of the sea anemone *Anthopleura elegantissima*. *Biol. Bull.* **150:** 361–376.

Francis, L. 1979. Contrast between solitary and clonal lifestyles in the sea anemone *Anthopleura elegantissima*. *Am. Zool.* **19:** 669–681.

Francis, L. 1985. The ecology and evolution of aggression among sea anemones (Actiniaria). *Natl. Geogr. Res.* **21:** 167–173.

Francis, L. 1988. Cloning and aggression among sea anemones (Coelenterata: Actiniaria) of the rocky shore. *Biol. Bull.* **174:** 241–253.

Geller, J. B., and E. D. Walton. 2001. Breaking up and getting together: evolution of symbiosis and cloning by fission in sea anemones (Genus *Anthopleura*). *Evolution* **55:** 1781–1794.

Gosline, J. M. 1971. Structure and composition of mesogloea in *Metridium*. *J. Exp. Biol.* **55:** 763–774.

Hand, C. 1954. The sea anemones of central California part I. The corallimorpharian and athenarian anemones. *Wasmann J. Biol.* **12:** 345–375.

Hand, C. 1955. The sea anemones of central California part III. The acontiarian anemones. *Wasmann J. Biol.* **13:** 189–251.

Hess, H. C. 1993. The evolution of parental care in brooding spirorbid polychaetes: the effect of scaling constraints. *Am. Nat.* **141:** 577–596.

Hyman, L. H. 1940. *The Invertebrates: Protozoa Through Ctenophora*. McGraw-Hill, New York.

Jaccard, H., and C. K. Wan. 1996. *LISREL Approaches to Interaction Effects in Multiple Regression*. Sage Publications, Thousand Oaks, CA.

Knight, C. G., M. N. Patel, R. B. R. Azevedo, and A. M. Leroi. 2002. A novel mode of ecdysozoan growth in *Caenorhabditis elegans*. *Evol. Dev.* **4**(1): 16–27.

Koehl, M. A. R. 1977. Mechanical diversity of connective tissue of the body wall of sea anemones. *J. Exp. Biol.* **69:** 107–125.

Kramer, A., and L. Francis. 2004. Predation resistance and nematocyst scaling for *Metridium senile* and *M. farcimen*. *Biol. Bull.* **207:** 130–140.

LaBarbera, M. 1989. Analyzing body size as a factor in ecology and evolution. *Annu. Rev. Ecol. Syst.* **20:** 97–117.

Lehn, H. 1951. Teilungsfolgen und Determination von I-Zellen für die Cnidenbildung bei *Hydra*. *Z. Naturforsch.* **6b:** 388–391.

Longley, R. D. 1984. Axon surface infolding and axon size can be quantitatively related in gastropod molluscs. *J. Exp. Biol.* **108:** 163–177.

Maldonado, R. H., C. San Jose, and B. Martinoya. 1974. Cell size and body weight in some homeotherms and poikilotherms. *Acta Physiol. Latinoam.* **24:** 328–335.

Mariscal, R. N. 1984. Cnidaria: cnidae. Pp. 57–68 in *Biology of the Integument, Vol. 1, Invertebrates*. J. Bereiter-Hahn, A. G. Maltolsy, and K. S. Richards, eds. Springer-Verlag, Berlin.

McArdle, B. H. 1988. The structural relationship: regression in biology. *Can. J. Zool.* **66:** 2329–2339.

Munro, H. N. 1969. Evolution of protein metabolism in mammals. Pp. 133–182 in *Mammalian Protein Metabolism*, Vol. 3. H. N. Munro, ed. Academic Press, New York.

Munro, H. N., and J. A. M. Gray. 1969. The nucleic acid content of skeletal muscle and liver in mammals of different body size. *Comp. Biochem. Physiol.* **28:** 897–905.

Niklas, K. J. 1994. *Plant Allometry: The Scaling of Form and Process*. Univ. of Chicago Press, Chicago.

Pearse, V. B., and L. Francis. 2000. *Anthopleura sola*, a new species, solitary sibling species to the aggregating sea anemone, *A. elegantissima* (Cnidaria: Anthozoa: Actiniaria: Actiniidae). *Proc. Biol. Soc. Wash.* **113:** 596–608.

Peters, R. H. 1983. *The Ecological Implications of Body Size*. Cambridge Univ. Press, New York.

Purcell, J. E. 1984. The functions of nematocysts in prey capture by epipelagic siphonophores (Coelenterata, Hydrozoa). *Biol. Bull.* **166:** 310–327.

Rayner, J. M. V. 1985. Linear relations in biomechanics: the statistics of scaling functions. *J. Zool. Lond. A* **206:** 415–439.

Rifkin, J. F. 1991. A study of the spirocytes from the Ceriantharia and Actiniaria (Cnidaria, Anthozoa). *Cell Tissue Res.* **266:** 365–373.

Robson, E. A. 1988. Problems of supply and demand for cnidae in Anthozoa. Pp. 179–207 in *The Biology of Nematocysts*, D. A. Hessinger and H. M. Lenhoff, eds. Academic Press, San Diego, CA.

Ryland, J. S., M. M. Brasseur, and J. E. Lancaster. 2004. Use of cnidae in taxonomy: implications for a study of *Acrozoanthus australiae* (Hexacorallia, Zoanthidae). *J. Nat. Hist.* **38:** 1193–1223.

Schmidt, H. 1974. On evolution in the Anthozoa. *Proc. 2nd Int. Coral Reef Symp.* **1:** 533–560.

Schmidt-Nielsen, K. 1984. *Scaling—Why is Animal Size So Important?* Cambridge University Press, Cambridge, MA.

Sebens, K. P. 1981a. The allometry of feeding, energetics, and body size in three sea anemone species. *Biol. Bull.* **161:** 152–171.

Sebens, K. P. 1981b. Reproductive ecology of the intertidal sea anemones *Anthopleura xanthogrammica* (Brandt) and *Anthopleura elegantissima* (Brandt) body size, habitat and sexual reproduction. *J. Exp. Mar. Biol. Ecol.* **54:** 225–250.

Sebens, K. P. 1983. Population dynamics and habitat suitability of the

intertidal sea anemones *Anthopleura elegantissima* and *A. xanthogrammica*. *Ecol. Monogr.* **53:** 405–433.

Sebens, K. P. 1984. Agonistic behavior in the intertidal sea anemone *Anthopleura xanthogrammica*. *Biol. Bull.* **166:** 457–472.

Sebens, K. P. 1987. The ecology of indeterminate growth in animals. *Annu. Rev. Ecol. Syst.* **18:** 371–407.

Sebens, K. P., and G. Laakso. 1978. The genus *Tealia* (Anthozoa: Actiniaria) in the waters of the San Juan Archipelago and the Olympic Peninsula. *Wasmann J. Biol.* **35:** 152–168.

Shick, J. M. 1991. *A Functional Biology of Sea Anemones*. Chapman and Hall, London.

Smith, R. J. 1984. Allometric scaling in comparative biology: problems of concept and method. *Am. J. Physiol.* **246:** R152–R160.

Sokal, R. R., and F. J. Rohlf. 1981. *Biometry: The Principles and Practice of Statistics in Biological Research*, 2nd ed. W. H. Freeman, New York.

Stephenson, T. A. 1929. On the nematocysts of sea anemones. *J. Mar. Biol. Assoc. UK* **16:** 173–201.

Stevenson, R. D., M. F. Hill, and P. J. Bryant. 1995. Organ and cell allometry in Hawaiian *Drosophila*: how to make a big fly. *Proc. R. Soc. Lond. B* **259:** 105–110.

Thomason, J. C. 1988. The allometry of nematocysts. Pp. 575–588 in *The Biology of Nematocysts*, D. A. Hessinger and H. M. Lenhoff, eds. Academic Press, San Diego, CA.

Weill, R. 1934a. Contribution à l'étude des cnidaires et de leurs nématocystes, vol. I, recherches sur les nématocystes (morphologie - physiologie - development). *Trav. Sta. Zool. Wimereux* **10:** 1–347.

Weill, R. 1934b. Contribution à l'étude des cnidaires et de leurs nématocystes, vol. II, valeur taxonomique du cnidome. *Trav. Sta. Zool. Wimereux* **11:** 349–701.

Williams, R. B. 1996. Measurements of cnidae from sea anemones (Cnidaria: Actiniaria): statistical parameters and taxonomic relevance. *Sci. Mar.* **60:** 339–351.

Williams, R. B. 1998. Measurements of cnidae from sea anemones (Cnidaria: Actiniaria) II: further studies of differences amongst sample means and their taxonomic relevance. *Sci. Mar.* **62:** 361–372.

Williams, R. B. 2000. Measurements of cnidae from sea anemones (Cnidaria: Actiniaria) III: ranges and other measures of statistical dispersion, their interrelations and taxonomic relevance. *Sci. Mar.* **64**(1): 49–68.

Zamponi, O. M., and F. H. Acuña. 1991. La variabilidad de los cnidocistos y su importancia en la determinacion de clines. *Physis (B. Aires)* **49:** 7–18.

Zar, J. H. 1984. *Biostatistical Analysis*. Prentice-Hall, Englewood Cliffs, NJ.

Reference: *Biol. Bull.* **207:** 130–140. (October 2004)

Predation Resistance and Nematocyst Scaling for *Metridium senile* and *M. farcimen*

ANDREW KRAMER[1] AND LISBETH FRANCIS[2,*]

[1] *Department of Fisheries and Wildlife, Michigan State University, East Lansing, Michigan 48824; and*
[2] *Shannon Point Marine Center, Western Washington University, 1700 Shannon Point Rd., Anacortes, Washington 98221-4042*

Abstract. Previous studies suggest that large body size reduces the risk of predation for acontiate sea anemones. For two species of *Metridium*, we found significant increases in the length of the acontial threads and in the mean lengths of the unfired acontial nematocyst capsules, with increasing body size. This supports the hypothesis that more damaging acontial defenses protect larger acontiate anemones from their predators. *Metridium* is planktivorous, and food size does not increase substantially with body size; so we expected smaller increases in nematocyst size for the feeding tentacles. In fact, scaling exponents were significantly smaller for the tentacle nematocysts than for acontial nematocysts of the same types in 3 out of 4 cases. This suggests that nematocyst scaling responds predictably to selection pressure. When specimens of the same size were compared, the non-clonal, subtidal species, *M. farcimen*, had significantly larger acontial nematocysts than did its clonal congener, *M. senile*, which lives at the upper tidal limits for major subtidal predators in the northeastern Pacific. Therefore, larger acontial nematocysts may be particularly advantageous where predation levels are high. These data demonstrate that closely related anemone species can be distinguished on the basis of ecologically and functionally relevant differences in nematocyst scaling.

Received 31 July 2003; accepted 6 July 2004.

* To whom correspondence should be addressed.

Abbreviations: a & b, intercept and slope of the log-log plot, OLS, ordinary least squares regression estimate of line fit; RMA, reduced-major axis estimate of line fit; 95% CI, ninety-five percent confidence intervals (for slope and intercept estimates); %SEE, percent standard error of estimate.

Introduction

Predation is one of the strongest evolutionary pressures on many organisms, favoring a diverse suite of adaptations that reduce predation risk (Curio, 1976; Vermeij, 1982; Sih, 1985, 1987; Bronmark and Miner, 1992). Larger body size often decreases vulnerability to predation (Paine, 1976; Tripet and Perrin, 1994; Arsenault and Himmelman, 1996; Lundvall *et al.*, 1999) because predators are physically unable to consume larger prey (Tripet and Perrin, 1994; Arsenault and Himmelman, 1996), or because larger prey are able to escape or to retaliate more effectively (Harris, 1986; Arsenault and Himmelman, 1996; Christensen, 1996; Lundvall *et al.*, 1999).

Acontiate sea anemones have specialized antipredator defenses. When attacked, the anemones contract and extrude many long, thread-like mesenterial filaments (the acontia) through the mouth and column wall (Hyman, 1940). The acontia are ciliated and motile, bearing densely packed tracts of large specialized nematocysts that fire on contact with predators. Damage from such contacts may dissuade a predator from continuing the attack (Harris, 1973; Edmunds *et al.*, 1976; Shick, 1991). The three types of nematocysts found in acontia (basitrichs, microbasic b-mastigophores, and microbasic amastigophores) are also found in the feeding tentacles; but the b-mastigophore and amastigophore found in the acontia are more than twice the size of the tentacle cnidae (Hand, 1956).

Three acontiate anemones in the genus *Metridium* co-occur in the Pacific Northwest. The two studied here, *M. senile* (Linnaeus, 1761) and *M. farcimen* (Tilesius, 1809), differ in growth form and habitat preference. *M. senile* is smaller, and predominantly intertidal in the Pacific Northwest. *M. senile* replicates asexually by pedal laceration, and usually occurs in large, genetically identical clonal groups

(Bucklin, 1987b). *M. farcimen* grows much larger; is found only in subtidal habitats (Fautin *et al.*, 1989); and does not replicate asexually, occurring as solitary individuals or as congregations of genetically distinct individuals (Bucklin, 1987a). Originally assumed to be an aclonal morph of *M. senile* (Hand, 1956), *M. farcimen* was shown through molecular analysis to be an independent species (Bucklin and Hedgecock, 1982) and its original name was reapplied by Fautin and Hand (2000). The third species, *M. exilis*, is a very small anemone that lives only in intertidal areas and forms clonal aggregations through binary fission (Hand, 1956).

Both laboratory studies and field observations suggest that *Metridium* becomes less vulnerable to predation with increasing body size. An important predator, the sea slug *Aeolidia papillosa*, shows a strong preference for small individuals of *M. senile* in choice experiments (Harris, 1976; Harris and Duffy, 1980). Furthermore, Harris (1973, 1991) found that *A. papillosa* is more likely to attack small individuals in an aggregation and, as a result, selects strongly for larger body size. Another key predator, the leather star *Dermasterias imbricata*, readily consumes small specimens of *M. senile* in the laboratory (Annett and Pierotti, 1984).

Body size of *Metridium* generally increases along a gradient from intertidal to subtidal habitats, mirroring an increase in density of both *A. papillosa* and leather stars. The presence of large individuals of *Metridium* sp. in the subtidal zone where predation pressure is more intense suggests a size refuge from predation (Annett and Pierotti, 1984; Harris, 1991).

Several possible explanations could account for the decreased vulnerability to predation of larger specimens of *Metridium*. Larger anemones may simply exceed the mechanical constraints of predator feeding mechanisms. This seems likely for the sea stars, which must settle on top of their prey (Annett and Pierotti, 1984). However, *A. papillosa* feeds by biting off pieces of the anemone in a manner not obviously limited by anemone size (Edmunds *et al.*, 1976).

If larger anemones have better defense mechanisms, this might contribute to the increased resistance of larger anemones to predation. Edmunds *et al.* (1974) found that anemone species that lack acontia were preferred over acontiate species by *A. papillosa*, suggesting that the acontia may provide effective defense against this predator. Harris (1973, 1986) reported that acontial defenses could dissuade *A. papillosa* from feeding and could even result in the death of the sea slug. He noted that this defense mechanism appeared to be related to the size of the anemone (Harris, 1986).

In a companion study, Francis (2004) shows how scaling analysis can be used to detect evolutionary changes in cnida size and shape by comparing homologous cnida populations from different anemone tissues and species. Here we look at the scaling of acontium length, acontium diameter, and mean capsule size of the two large acontial nematocysts (amastigophores and b-mastigophores). Strong positive correlation of any or all of these variables with body size would support the argument made by Harris (1986) that large anemones are less vulnerable to predation because they defend themselves more effectively against predators. In addition, because the larger-bodied, non-clonal species, *M. farcimen*, lives in deeper water where predators are more abundant, we also expected stronger antipredator defenses in *M. farcimen* than in the smaller-bodied and clonal *M. senile*.

In designing the scaling study, we predicted relatively rapid increase in the size of the large acontial nematocysts with increasing body size, due to ongoing directional selection caused by predation. By contrast, we expected relatively little increase in the size of these same two nematocyst types in the feeding tentacles. Because prey size does not increase significantly with body size for *Metridium* (Sebens, 1981), nematocysts involved primarily in food capture and handling should be subjected to stabilizing selection.

Materials and Methods

Specimen collection and handling

Between 15 June and 1 August 1999, we collected specimens of *Metridium farcimen* on the boat dock at Skyline Marina, Anacortes, Washington (48°30′N, 122°41′W) and specimens from a single *M. senile* clone on the Schwarz boat dock, Garrison Bay, on San Juan Island (48°35′N, 123°10′W). A clonal sample is ideal for isolating the effects of body size independent of genetic variation. Anemones were deliberately chosen to provide an even distribution of body sizes spanning the available size range. At Shannon Point Marine Center, Anacortes, Washington, the anemones attached to the tank or to glass bowls in a continuous-flow sea table, where they were fed pieces of frozen cod once or twice a week.

Body-size measurement

Within 2 weeks, we weighed the living anemones on a Mettler P1200 balance after blotting them to remove as much excess water as possible. Because these soft-bodied animals are continually changing shape by taking in and expelling large quantities of seawater, blotted wet weight provides a nondestructive basis for comparing polyp sizes that is more reliable than linear dimensions. For example, the diameter of the expanded oral disc can vary greatly with the degree of expansion of the anemone; and the relationship between oral disc size and tissue volume may vary considerably between species. Daily measurements of 10

individuals (*M. senile*) over a 3-day period indicated that wet weights were reproducible within ± 10%.

Nematocyst size measurement

Several extruded acontia or excised tentacles were fixed in 1–2 ml of 10% formalin to prevent nematocyst discharge. The tissues were disrupted using a glass tissue grinder to randomly mix and disperse the sample.

A drop of this nematocyst mixture was scanned systematically with non-overlapping fields (method of Williams, 1996), and maximum capsule lengths and widths of the first 20 each of the unfired b-mastigophore and amastigophore capsules were measured (method of Hand, 1954) using 400× magnification and a video image analysis system (Optimax software package). Means and their standard errors were calculated for each sample of 20 capsules. Duplicated measurements using 20 video images indicated that capsule dimensions were reproducible within ± 2% (length) and ± 5% (width).

Extended acontia measurement

To provide comparative estimates of acontial length for specimens of different size, we removed each anemone from the tank and held it upside down, which caused extrusion of the acontia. When the strand was fully extended under the pull of gravity, we measured the length from the oral sphincter to the most distal tip, which we called the extended acontia length.

To measure acontium diameter, we gently removed a single extruded acontial thread from each individual, placed it on a slide with a drop of seawater and coverslip, and measured the diameter (width) of an undamaged portion at 100×. Daily measurements of 10 individuals (*M. senile*) over a 3-day period indicated that acontium lengths and acontium diameters were reproducible within ± 31% and ± 13%, respectively.

Statistical analyses

Untransformed data were used to examine the relationship between body size and the other measurements obtained from each individual. For ease of interpretation, the graphs all use linear scale on the abscissa (mean nematocyst capsule dimensions, acontium diameter, and effective acontial length) and log scale on the ordinate (wet weight), as in Longley (1984) and Francis (2004). This makes it easier to display the standard errors of the means and to assess the magnitude and possible biological relevance of any between-sample differences (Smith, 1984).

Data were log-transformed (base 10) for statistical analyses, a common practice in scaling studies where the relationship is well represented by a power function (Huxley, 1932; Smith 1984) as would be predicted here by simple dimensional analysis (LaBarbera, 1989; Francis, 2004).

We calculated Spearman rank correlations for the relationship between anemone wet weight and each of the other metrics, using the NCSS software package, ver. 2000 (Hintze, 2001); and significance at $P = 0.05$ was determined using sequential Bonferroni adjustment within groups of related tests (Rice, 1989). A nonparametric test for correlation is most appropriate for determining the significance of these relationships because the wet weights are not normally distributed and there is error in both the dependent and independent variables. Thus the data do not meet the assumptions of ordinary least squares regression (OLS; Sokal and Rohlf, 1981; Rayner, 1985).

For describing functional relationships such as these, McArdle (1988) showed that reduced major axis regression (RMA) provides a more robust estimate of the slope (b_{RMA} = scaling exponent = $b_{OLS}/R = SD_Y/SD_X$) than does OLS, where values for Pearson's product moment correlation (R) are less than 0.9 and the error for X is more than one-third that of the Y variable (probably true, here). OLS consistently underestimates these slopes. Note, also, that OLS and RMA estimates converge as R increases, and that the variance and standard error are numerically the same for RMA and OLS estimators (McArdle, 1988). R and the percent standard error of estimate (%SEE; Smith, 1984) provide measures for goodness of fit.

RMA estimates and 95 percent confidence intervals (95% CIs) for the slopes and intercepts were generated by bootstrapping each data set 10,000 times using SYSTAT, ver. 9 (SPSS, 1998), selecting the median values to estimate slopes and intercepts, and selecting the 250th and 9750th values as the upper and lower 95% confidence values. Bootstrapping provides estimates without assumptions about data distribution, and these estimates agree to three decimal places with coefficients calculated directly from sample statistics.

Because the data do not meet the assumptions for a Model I ANOVA (or ANCOVA), we use the bootstrapped confidence intervals to compare slopes and intercepts (M. LaBarbera, Univ. of Chicago, pers. comm.). By definition, two slopes are significantly different at the 0.05 level if each mean is outside the 95% CI of the other; however, it is necessary to be aware of the possibility for multiple testing error (Hess, 1993).

Results

Scaling of acontia

Extended acontia length increased significantly with body size for both *Metridium* species (Fig. 1A, Table 1); and it increased more rapidly than would be predicted for isometric scaling (positive allometry). The predicted null value for isometric scaling of dimensions relative to mass (0.33) is

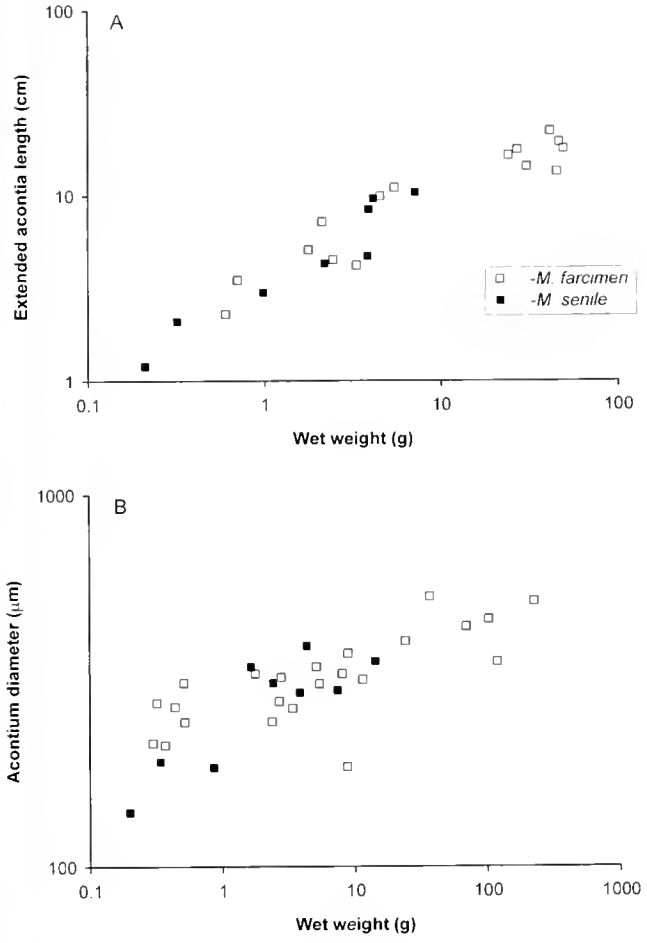

Figure 1. (A) Extended length and (B) thread diameter of the acontia *vs.* anemone wet weight. Data are a single measurement for each specimen. The scale for wet weight is logarithmic, and the scales for acontial dimensions are linear. Correlations with wet weight were all significant ($P < 0.05$ for groupwide error; Spearman rank correlation with sequential Bonferroni correction).

outside the 95% confidence intervals for both species (Table 1). An empirically measured scaling exponent for pedal disc diameter as a function of ash-free dry weight (mass) in *M. senile* (0.36) also lies outside the 95% CIs (Sebens, 1981).

By contrast, acontium diameter showed negative allometry; that is, increase in the diameter of the acontial threads with increasing body size was significantly less than the null prediction based on isometric scaling (Fig. 1B, Table 1). Positive correlation with body size was significant for *M. farcimen* but not for *M. senile*, after adjusting for multiple comparisons (Table 1).

Scaling of nematocyst capsules

For acontial nematocysts, mean lengths of the unfired nematocysts were significantly correlated with body weights for both nematocyst types and in both anemone species (Table 2). Scaling exponents for the four acontial nematocyst populations were not significantly different from one another (0.035 to 0.051; Fig. 2, Table 2). Again, the null expectation of isometry was rejected using 95% CIs. Nematocyst capsule lengths scale much more slowly than predicted based on the null scaling exponent (0.33).

By contrast, mean widths of the unfired capsules were not significantly correlated with body size for any of the acontial nematocysts (Fig. 3, Table 3).

For the tentacle nematocysts, mean length of the unfired capsules was significantly and positively correlated with body size for all cases except one. Change in capsule length was not correlated with body size for the tentacle b-mastigophores of *M. farcimen* (Fig. 2, Table 1).

Tissue differences in nematocyst scaling

Acontial nematocysts were consistently longer than tentacle nematocysts of the same type (Figs. 2 and 4), and scaling exponents were significantly higher for the acontial nematocysts in 3 cases out of 4 (Fig. 2; 95% CI, Table 2). The exception was *M. senile*, where 95% CIs for tentacle and acontial amastigophores overlapped (Fig. 2, Table 2).

Species differences

Scaling exponents were indistinguishable for homologous nematocyst populations from the two *Metridium* species (Table 2, overlapping 95% CIs for RMA estimates of the slopes for capsule length *vs.* wet weight). When specimens of the same size were compared (narrow allometry, *sensu* Smith, 1984), mean capsule length was always greater for *M. farcimen* than for *M. senile* (Fig. 2); and these differences in elevation were significant (Table 2, nonoverlapping 95% CIs for intercepts).

Discussion

Because predators prefer to eat smaller specimens of *Metridium*, Harris (1986) suggested that the effectiveness of specialized antipredator defenses may vary with anemone size. Our data support this hypothesis. The extended length and diameter of the acontial threads themselves and the capsule lengths of the large acontial nematocysts (b-mastigophores and amastigophores) were all positively correlated with body size.

Effectiveness of the acontia as predator deterrents presumably is related to the pain and damage caused to a potential predator and increases with the number and potency of nematocysts brought into contact with that predator. Thus, more acontial threads, longer acontia, more nematocysts, and larger acontial nematocysts should all improve deterrence.

Table 1

Acontium dimensions: scaling constants for Metridium farcimen *and* M. senile, *from reduced major axis regression equations*

Species (*n*)§	Scaling exponent† (95% CI)	Intercept† (95% CI)	$\bar{X}$, $\bar{Y}$‡	*R*¶ (%SEE)	*P*#
Log (effective acontia length, cm) (*Y*) *vs.* log (wet weight, g) (*X*)					
M. farcimen (15)	0.4498 (0.373–0.5165)	3.612 (3.148–4.233)	0.896, 0.961	0.94 (29%)	<0.0001*
M. senile (8)	0.5969 (0.4738–0.7993)	3.190 (2.872–3.401)	0.226, 0.639	0.96 (28%)	<0.0001*
Log (acontium diameter, mm) (*Y*) *vs.* log (wet weight, g) (*X*)					
M. farcimen (23)	0.1369 (0.1055–0.1788)	253.51 (236.59–266.69)	0.703, 2.500	0.75 (21%)	<0.0001*
M. senile (9)	0.2501 (0.1718–0.3493)	223.87 (209.41–236.05)	0.291, 2.423	0.86 (21%)	0.02

§ Number of anemones in the sample.

† Slope (scaling exponent, *b*) and intercept (*a*) of the RMA regression line (log (*Y*) = *b* * log (*X*) + log (*a*)); bootstrapped 95% confidence intervals (95% CI).

‡ $\bar{X}$ and $\bar{Y}$, mean values for log (*X*) and log (*Y*).

¶ Pearson correlation coefficient (*R*), and percent standard error of estimate (%SEE).

P value calculated in Spearman rank correlation.

* $P < 0.05$, groupwide error adjusted using a sequential Bonferroni adjustment.

Table 2

Nematocyst lengths: scaling constants for Metridium farcimen *and* M. senile, *from reduced major axis regression equations*

Nematocyst type: Species and tissue (*n*)§	Scaling exponent† (95% CI)	Intercept† (95% CI)	$\bar{X}$, $\bar{Y}$‡	*R*¶ (%SEE)	*P*#
Log (mean capsule length, nm) (*Y*) *vs.* log (wet weight, g) (*X*)					
b-mastigophore					
M. farcimen acontia (27)	0.0353 (0.0297–0.0408)	69.023 (68.234–69.823)	0.843, 1.869	0.88 (4%)	<0.0001*
M. farcimen tentacles (10)	0.0084 (0.0035–0.0169)	25.003 (24.660–25.235)	0.735, 1.405	0.11 (3%)	0.6
M. senile acontia (9)	0.0505 (0.033–0.0696)	60.117 (59.293–60.814)	0.291, 1.794	0.90 (2%)	0.0005*
M. senile tentacles (9)	0.0181 (0.0134–0.0224)	22.387 (22.336–22.454)	0.16, 1.353	0.92 (1%)	0.0065*
amastigophore					
M. farcimen acontia (21)	0.0431 (0.0362–0.0506)	71.614 (70.795–72.278)	0.575, 1.879	0.91 (3%)	<0.0001*
M. farcimen tentacles (10)	0.0112 (0.0075–0.0165)	27.861 (27.606–27.990)	0.735, 1.453	0.77 (2%)	0.0075*
M. senile acontia (9)	0.047 (0.0362–0.0651)	63.241 (62.373–63.680)	0.291, 1.814	0.95 (2%)	<0.0001*
M. senile tentacles (8)	0.0308 (0.0149–0.0529)	24.889 (24.604–25.177)	0.268, 1.405	0.75 (3%)	0.0053*

§ Number of anemones in the sample.

† Slope (scaling exponent, *b*) and intercept (*a*) of the RMA regression line (log (*Y*) = *b* * log (*X*) + log (*a*)); bootstrapped 95% confidence intervals (95% CI).

‡ $\bar{X}$ and $\bar{Y}$, mean values for log (*X*) and log (*Y*).

¶ Pearson correlation coefficient (*R*), and percent standard error of estimate (%SEE).

P value calculated in Spearman rank correlation.

* $P < 0.05$, groupwide error adjusted using a sequential Bonferroni adjustment.

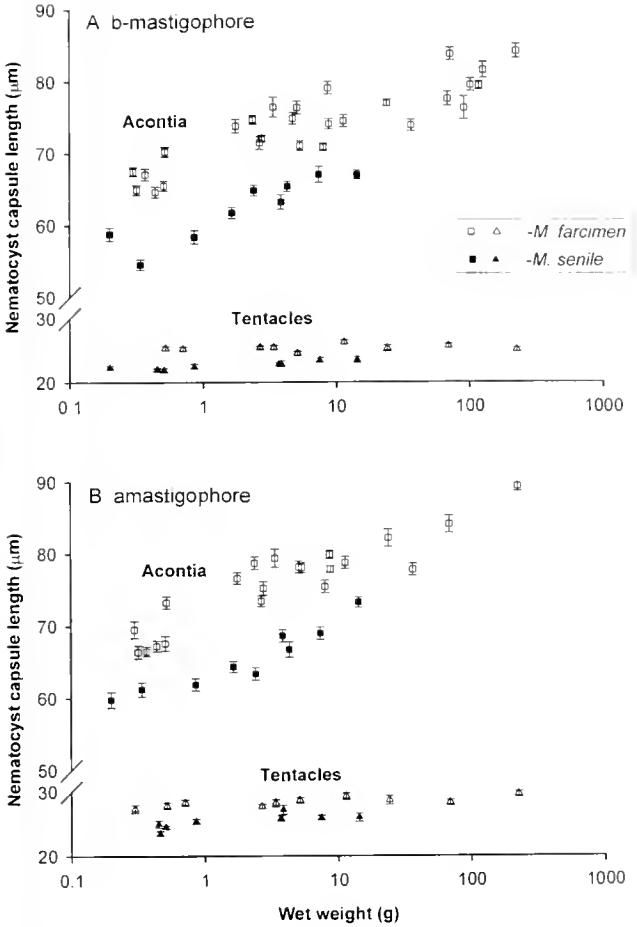

Figure 2. Mean length (± 1 SE) of unfired nematocyst capsules *vs.* anemone wet weight for (A) b-mastigophores and (B) amastigophores from the tentacles (triangles) and acontia (squares) of *Metridium farcimen* (unfilled shapes) and *M. senile* (filled shapes). Means and their standard errors are based on systematic samples of 20 unfired capsules from each tissue of each specimen. Correlations of each individual's mean capsule length with wet weight are significant for all acontial nematocysts and tentacle nematocysts except b-mastigophores from *M. farcimen* ($P < 0.05$ for groupwide error; Spearman rank correlation with sequential Bonferroni correction).

Larger anemones have more and bigger acontia than smaller conspecifics

Potential effectiveness of the acontia as deterrents should be a function of total nematocyst-bearing area, which is proportional to the diameter of each acontial thread, multiplied by the length of the thread, number of threads, and nematocyst density. Part of the increase in total nematocyst-bearing area as anemones grow occurs because the acontia connect to the inner edge of the mesenteries, and larger anemones have more mesenteries (Stephenson, 1928).

Larger anemones also have longer acontia (Fig. 1, Table 1) that can be extended farther, and thus are more likely to contact a predator. Longer acontia also carry more nematocysts and have more surface to wrap around a prospective predator. The length of the acontial threads increases more rapidly with body size (scaling exponents 0.45 and 0.60) than the null expectation (scaling exponent 0.33). This positively allometric relationship suggests that relatively rapid increase in acontial length with increasing body size (and increasing energy supply; Sebens, 1981) has been favored by natural selection in both *Metridium* species (Fig. 1A).

Acontium diameter, another factor in total nematocyst-bearing area, also increases with body size, but this relationship is negatively allometric. That is, as body size increases, acontium thickness increases less rapidly (Fig. 1B, scaling exponents 0.14–0.25) than external body dimensions such as foot diameter (0.36; Sebens, 1981) or the null expectation of isometry (0.33), and much less rapidly than acontium length (0.45 and 0.60). A less rapid increase in this aspect of acontial structure seems to favor deployment advantages over structural strength or maximum in-

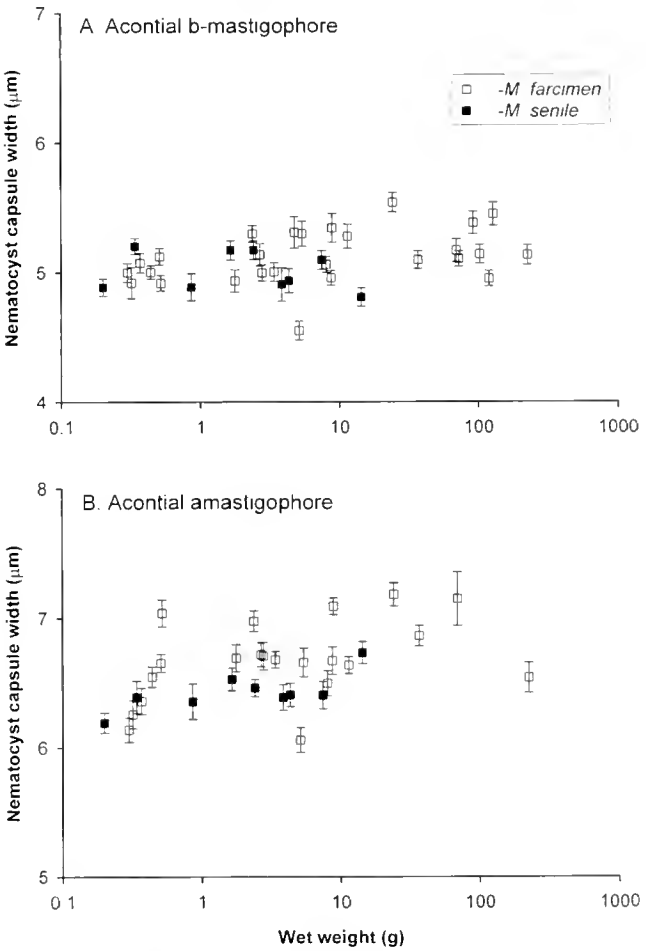

Figure 3. Mean width (± 1 SE) of unfired nematocyst capsules *vs.* anemone wet weight for acontial nematocysts. Correlations with wet weight are not significant for any of the populations ($P < 0.05$ for groupwide error; Spearman rank correlation with sequential Bonferroni correction).

Table 3

Nematocyst widths: scaling constants for Metridium farcimen *and* M. senile, *from reduced major axis regression equations*

Nematocyst type: Species and tissue (*n*)§	Scaling exponent† (95% CI)	Intercept† (95% CI)	$\bar{X}$, $\bar{Y}$‡	*R*¶ (%SEE)	*P*#
Log (mean capsule width, nm) (*Y*) *vs.* log (wet weight, g) (*X*)					
b-mastigophore					
M. farcimen acontia (27)	0.019 (0.0124–0.0286)	4.928 (4.837–4.991)	0.843, 0.709	0.37 (4%)	0.0158
M. senile acontia (9)	0.0216 (0.0138–0.0361)	4.933 (4.885–4.959)	0.291, 0.699	0.21 (3%)	0.61
amastigophore					
M. farcimen acontia (21)	0.0252 (0.0175–0.0363)	6.445 (6.350–6.510)	0.575, 0.824	0.41 (5%)	0.619
M. senile acontia (9)	0.0159 (0.0069–0.0231)	6.358 (6.327–6.396)	0.291, 0.808	0.73 (2%)	0.067

§ Number of anemones in the sample.

† Slope (scaling exponent, *b*) and intercept (*a*) of the RMA regression line ($\log(Y) = b * \log(X) + \log(a)$); bootstrapped 95% confidence intervals (95% CI).

‡ Mean values for log (*X*) and log (*Y*).

¶ Pearson correlation coefficient (*R*), and percent standard error of estimate (%SEE).

P value calculated in Spearman rank correlation.

* $P < 0.05$, groupwide error adjusted using a sequential Bonferroni adjustment.

crease in contact area. A relatively narrow acontial thread can be more flexible than a very thick thread, bending more readily with water currents and wrapping more easily around a predator's fine morphological features such as the cerata of a slug. While a relatively thin thread is likely to detach from the anemone more easily, the acontia appear to be disposable structures. Acontial nematocysts continue to fire after the acontial threads have become detached (pers. obs.).

Notably, only part of the acontial thread is nematocyst-bearing: the ciliated tract is dedicated to acontium mobility. It would be interesting to know whether these regions increase proportionally with increasing anemone size.

Size and potential effectiveness of acontial nematocysts increases consistently with body size

In the acontia, mean unfired capsule length of both nematocyst types increases as a function of wet weight, continuing to increase for the entire range of individuals sampled (Fig. 2). Capsule length is highly correlated with body size for both acontial nematocyst types in both *Metridium* species (Table 2). This increase in mean capsule lengths is substantial over the size ranges of anemones sampled and is likely to be biologically relevant. For this sample of *M. farcimen*, mean length of the acontial nematocyst capsules increases by 25%–29% for a 750-fold increase in body weight. For *M. senile*, a 70× increase in weight results in a 14%–23% increase in the mean length of the acontial nematocysts.

Longer nematocyst capsules can carry more toxin and a longer barbed tubule. The longer the barbed tubule, the more likely it is to succeed in penetrating the tissue of a prospective predator, and the deeper it can penetrate, increasing the potential for mechanical damage during penetration and deep damage by toxins.

Larger anemones do not have substantially wider acontial nematocysts. For *M. farcimen*, the actual increase in mean capsule width for the acontial b-mastigophores is only 2.6% for a 750-fold increase in body weight. For *M. senile*, there is no net increase in the mean width of the acontial nematocysts over the 70-fold increase in body size for this sample.

Differences between the two Metridium *species reinforce the case for a causal relationship linking predation pressure to anemone size and nematocyst size*

The acontial nematocysts of *M. farcimen* are consistently larger than those of *M. senile* for specimens of similar size across the entire range of overlapping body size (Fig. 2A). This can be seen as an extension of the pattern observed within each species individually.

Since *M. farcimen* is exclusively subtidal, it presumably is subjected to higher predation from subtidal predator species than is *M. senile*, especially at small body size. In the Pacific Northwest, *M. senile* lives primarily in the intertidal and on pilings, floats, and docks at protected sites where the threat of predation, especially by the leather star, probably is much less. If larger acontial nematocysts increase survival

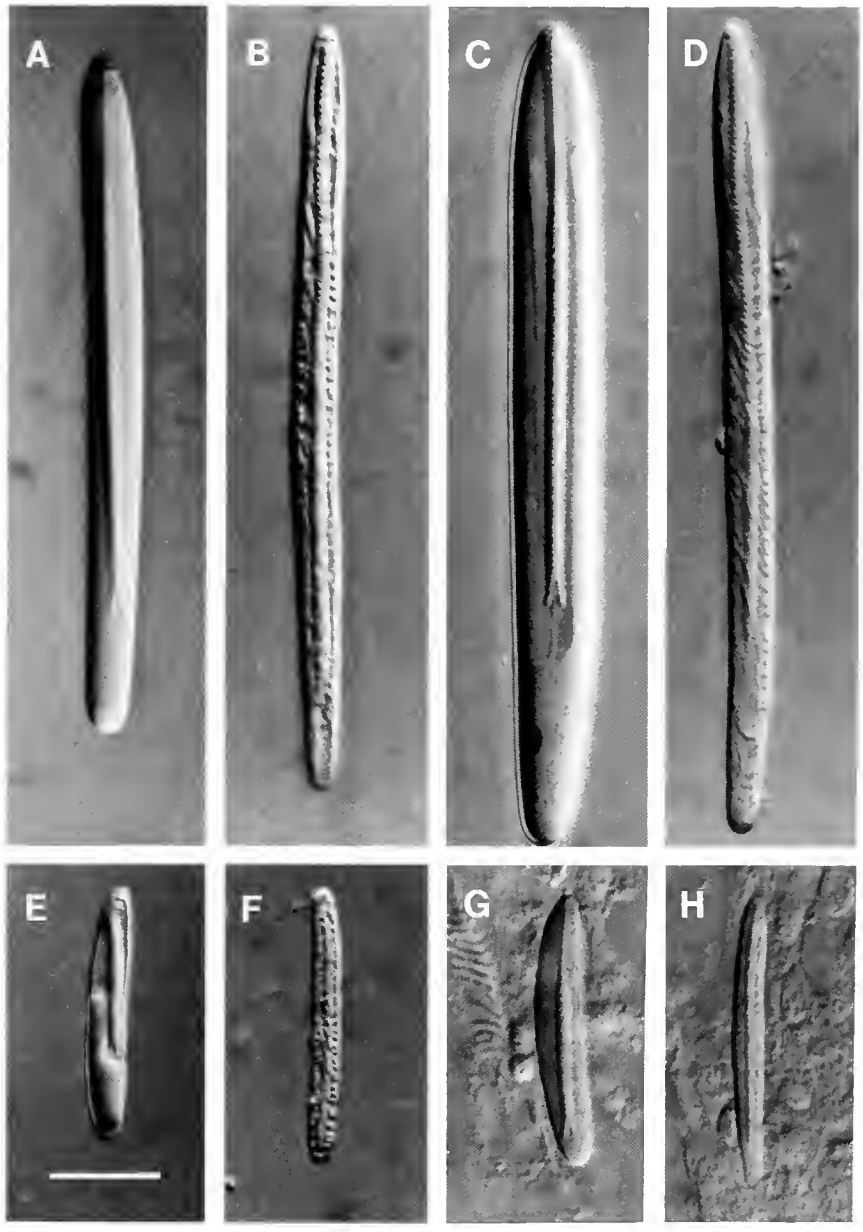

Figure 4. Microbasic b-mastigophores and microbasic amastigophores from the acontia and tentacles of two anemone species. Average-sized nematocysts were selected from 2.5-g specimens of *Metridium senile* (to the left; A, B, E, and F) and *M. farcimen* (to the right; C, D, G, and H). Acontial nematocysts (A, B, C, and D) are much larger than tentacle nematocysts from the same specimens (E, F, G, and H). Amastigophores (A, C, E, and G) are shown to the left of b-mastigophores (B, D, F, and H) from the same tissues. In life, the tubule end of the capsule (pointing upward in these photographs) is close to the outer cell surface of the acontial gastrodermis. Photographs were taken using differential interference contrast at 1000× (oil immersion). Scale bar: 10 μm.

and fitness in the presence of such predators, selection will usually be stronger for *M. farcimen* than for *M. senile*. This may explain why the acontial nematocysts of *M. farcimen* are larger than those of *M. senile*, for specimens of the same size. Sampling additional *M. senile* clones is necessary to determine whether the size difference is consistent across different habitats and genotypes.

We demonstrate for the first time that scaling studies using data on cnida size and anemone body size can be useful for distinguishing between closely related species, even when the size ranges for homologous cnida populations are overlapping. Fautin *et al.* (1989) stated that "nematocysts do not appear to differ consistently between the two [*M. farcimen* and *M. senile*], their size

Table 4

Lengths and widths of acontial nematocysts: scaling constants for Sagartia elegans *and* Cereus pedunculatus, *from reduced major axis regression equations, computed using data from Stephenson (1929)*

Nematocyst type: Species (n)§	Scaling exponent† (95% CI)	Intercept† (95% CI)	$\bar{X}$, $\bar{Y}$‡	R¶ (%SEE)	P#
Log (mean capsule length, nm) (Y) vs. log (body diameter^3, cm) (X)					
b-mastigophore					
S. elegans (12)	0.0463 (0.0202–0.0775)	29.992 (28.119–31.623)	0.902, 1.519	0.60	0.0074*
C. pedunculatus (7)	0.0361 (0.030–0.0447)	29.512 (29.309–29.717)	0.400, 1.485	0.95	0.0137
amastigophore					
S. elegans (12)	0.0568 (0.0243–0.1026)	47.863 (43.551–51.168)	0.902, 1.731	0.67	0.0061*
C. pedunculatus (7)	0.0569 (0.0423–0.0742)	35.318 (34.754–35.810)	0.400, 1.5706	0.95	0.0025*
Log (mean capsule width, nm) (Y) vs. log (body diameter^3, cm) (X)					
b-mastigophore					
S. elegans (12)	0.0629 (0.0242–0.1478)	2.941 (2.465–3.188)	0.902, 0.525	0.30	0.1397
C. pedunculatus (7)	0.0363 (0.0226–0.0507)	2.463 (2.430–2.493)	0.400, 0.460	0.82	0.0897
amastigophore					
S. elegans (12)	0.0465 (0.0269–0.0965)	4.761 (4.291–4.959)	0.902, 0.720	0.65	0.0213
C. pedunculatus (7)	0.0311 (0.0264–0.0358)	3.917 (3.899–3.933)	0.400, 0.605	0.98	0.0008*

§ Number of anemones in the sample.

† Slope (scaling exponent, b) and intercept (a) of the RMA regression line ($\log(Y) = b * \log(X) + \log(a)$); bootstrapped 95% confidence intervals (95% CI).

‡ Mean values for log (X) and log (Y).

¶ Pearson correlation coefficient (R), and percent standard error of estimate (%SEE).

P value calculated in Spearman rank correlation.

* $P < 0.05$, groupwide error adjusted using a sequential Bonferroni adjustment.

seemingly correlated more with size than species of the individual." In fact, when specimens of the same size are compared, there are large and significant differences in the mean sizes of the acontial nematocysts from the two *Metridium* species. The cnida size data for the *M. senile* clone are well outside the expected range of *M. farcimen* for all four nematocyst populations. Under any reasonable assumption about the position of the clonal data within the *M. senile* population data (based on the 95% CI for the intercept of the *M. farcimen* data on capsule length), *M. senile* has shorter mean nematocyst lengths for 4 out of 4 sampled cnida populations. Thus this is a robust result that we predict will be confirmed when a wider sample of genotypes from *M. senile* is examined.

Acontial nematocysts in other species scale similarly

Stephenson (1929, his tables I and II) reported mean lengths and widths for two nematocyst types, "penicilli" (probably amastigophores) and "spirulae" (probably b-mastigophores), from the acontia of *Sagartia elegans* (30 capsules per type for each of 12 specimens) and *Cereus pedunculatus* (30 capsules per type for each of 7 anemones—2 newly released, brooded young and 5 adults). Stephenson stated that his data showed no consistent relationship between body size and nematocyst size. In fact, mean cnida lengths are significantly correlated with body size for all four of his acontial cnida populations; and mean capsule widths are significantly correlated with body size for 1 of the 4 (Spearman rank correlation, our Table 4).

We also fit lines to the log-log plots of mean capsule dimension *versus* polyp diameter cubed. RMA slopes, intercepts, and R^2 values (Table 4) are very close to those reported here and by Francis (2004). Polyp diameters were cubed to make these plots dimensionally compatible with our data, and with most of the scaling literature, where body size typically is represented by a weight (Wt $\propto$ Vol. $\propto L^3$).

Natural selection can affect both nematocyst size and nematocyst scaling

Nematocyst size appears to vary in an adaptive manner among species and as a function of body size. This conclusion is based on differences in the sizes and scaling exponents for tentacle and acontial nematocysts of the same types from the two *Metridium* species (Figs. 2, 4; Table 2). These differences are linked to function-related differences in selection pressures. While feeding structures typically are subject to stabilizing selection, favoring optimal *cost-effectiveness*, structures used in antipredator defense are subject to directional selection, favoring *maximum affordable effect* (*cf.* energetic analysis of jumping *vs.* hovering; Alexander, 2000).

Metridium species are primarily filter feeders; and the size of captured prey is similar for anemones of different sizes, both in subtidal and in intertidal habitats (Purcell, 1977; Sebens, 1981; Sebens and Koehl, 1984). Hence there is little or no advantage to increased size in the tentacle nematocysts with increasing body size.

Actual increases in the mean size of tentacle nematocysts are relatively small. For *M. farcimen*, mean capsule lengths increase 0%–8% for a 750-fold increase in body weight; and for *M. senile*, capsule lengths increase 4%–6% for a 30- to 70-fold increase in body weight. Nonetheless, correlations with body size are significant in 3 cases out of the 4. There are at least three plausible explanations for this correlation, and they could act individually or in combination. (1) Food size, food type, or both may actually change somewhat with body size, favoring this slight increase in the size of some tentacle nematocyst types with increasing body size. (2) Scaling of the tentacle nematocysts may be advantageous in some context other than feeding. (3) Minimal scaling of these tentacle cnidae could also occur incidentally if the size of collagen-secreting cells typically does increase with body size (discussed by Francis, 2004).

For the acontial nematocysts, predation pressure favoring maximum affordable size is reflected in the larger size of the acontial nematocysts (Fig. 4) and the significantly larger RMA scaling exponents for acontial capsule lengths (0.035–0.051), as compared with the smaller scaling exponents (0.008–0.018) for the same nematocyst types in the tentacles (Fig. 2 and Table 2). There is one exception: for *M. senile*, the scaling exponents for capsule lengths of the acontial amastigophores (0.047) and the tentacle amastigophores (0.031) are not distinguishable at these sample sizes (Table 2).

Energy scaling analysis (Sebens, 1981) and mechanical analysis (Francis, 2004) both predict that larger anemones will be able to support larger defensive nematocysts: that is, the size of the maximum affordable and supportable defense structure should increase with body size. Sebens (1981) has shown that in some cases, larger anemone body size reflects higher net energy intake, suggesting that larger anemones may be able to afford relatively larger acontia and larger acontial nematocysts. Larger anemones also have thicker mesoglea (Shick, 1991; Francis, 2004), which can support a thicker attached layer of tissue and larger nematocysts (*i.e.*, larger acontia and acontial nematocysts, Figs. 1 and 2; Tables 1 and 2).

Significant differences in nematocyst scaling exponents have never before been reported. Both the larger size (Fig. 4) and larger scaling exponents of the acontial nematocysts, as compared with their tentacle homologs (Fig. 2), reflect the difference in selective regimes. This suggests both that nematocyst scaling is responsive to selection and that the size of acontial nematocysts plays an important role in antipredator defense.

Summary

The strong and consistent pattern of positive correlations between the size of defensive structures and body size for these two *Metridium* species supports the hypothesis that better acontial defenses provide a refuge from predation for larger acontiate anemones. These findings, combined with function-related differences between tissues and habitat-related differences between species, make a compelling argument for the value of larger acontial nematocysts in deterring potential predators. Differences in the scaling of tentacle and acontial nematocysts illustrate a novel pathway by which nematocysts may become specialized for particular functions.

Acknowledgments

Thanks to Richard Palmer, Mike LaBarbera, and an anonymous reviewer for valuable comments and suggestions. The work was supported in part by NSF 9731144, REU support through Western Washington University, Shannon Point Marine Center. For access to facilities and helpful discussion, we thank the directors, staff, and colleagues at SPMC (WWU); for the image analysis system at Shannon Point, we thank the NSF Instrumentation and Laboratory Improvement Program and Texaco Foundation. Without this support, the work would not have been possible.

Literature Cited

Alexander, R. McN. 2000. Hovering and jumping: contrasting problems in scaling. Pp. 37–50 in *Scaling in Biology*, J. H. Brown and G. B. West, eds. Oxford Univ. Press, New York.

Annett, C., and R. Pierotti. 1984. Foraging behavior and prey selection of the leather seastar *Dermasterias imbricata*. *Mar. Ecol. Prog. Ser.* **14:** 197–206.

Arsenault, D. J., and J. H. Himmelman. 1996. Size-related changes in vulnerability to predators and spatial refuge use by juvenile Iceland scallops *Chlamys islandica*. *Mar. Ecol. Prog. Ser.* **140:** 115–122.

Bronmark, C., and J. G. Miner. 1992. Predator-induced phenotypical change in body morphology in crucian carp. *Science* **258:** 1348–1350.

Bucklin, A. 1987a. Growth and asexual reproduction of the sea anemone *Metridium*: comparative laboratory studies of three species. *J. Exp. Mar. Biol. Ecol.* **110:**41–52.

Bucklin, A. 1987b. Adaptive advantages of patterns of growth and asexual reproduction of the sea anemone *Metridium senile* (L.) in intertidal and submerged populations. *J. Exp. Mar. Biol. Ecol.* **110:** 225–243.

Bucklin, A., and D. Hedgecock. 1982. Biochemical genetic evidence for a third species of *Metridium* (Coelenterata, Actiniaria). *Mar. Biol.* **66:** 1–7.

Christensen, B. 1996. Predator foraging capabilities and prey antipredator behaviours: pre- versus postcapture constraints on size-dependent predator-prey interactions. *Oikos* **76:** 368–380.

Curio, E. 1976. *The Ethology of Predation.* Springer-Verlag, New York.

Edmunds, M., G. W. Potts, R. C. Swinfen, and V. L. Waters. 1974. The feeding preferences of *Aeolidia papillosa* (L.) (Mollusca, Nudibranchia). *J. Mar. Biol. Assoc. UK* **54:** 939–947.

Edmunds, M., G. W. Potts, R. C. Swinfen, and V. L. Waters. 1976. Defensive behaviour of sea anemones in response to predation by the opisthobranch mollusc *Acolidia papillosa* (L.). *J. Mar. Biol. Assoc. UK* **56:** 65–83.

Fautin, D. G., and C. Hand. 2000. *Metridium farcimen*, the valid name of a common North Pacific sea anemone (Cnidaria: Actiniaria: Acontiaria). *Proc. Biol. Soc. Wash.* **113:** 1151–1161.

Fautin, D. G., A. Bucklin, and C. Hand. 1989. Systematics of sea anemones belonging to genus *Metridium* (Coelenterata: Actiniaria), with a description of *M. giganteum* new species. *Wasmann J. Biol.* **47:** 77–85.

Francis, L. 2004. Microscaling: why larger anemones have longer cnidae. *Biol Bull.* **207:** 116–129.

Hand, C. 1954. The sea anemones of central California part I The corallimorpharian and athenarian anemones. *Wasmann J. Biol.* **12:** 345–375.

Hand, C. 1956. The sea anemones of central California part III. The acontiarian anemones. *Wasmann J. Biol.* **13:** 189–251.

Harris, L. G. 1973. Nudibranch associations. Pp. 213–315 in *Current Topics in Comparative Pathobiology*, Vol. 2, T.C. Cheng, ed. Academic Press, New York.

Harris, L. G. 1976. Comparative ecological studies of the nudibranch *Aeolidia papillosa* and its anemone prey *Metridium senile* along the Atlantic and the Pacific coasts of the United States. *J. Molluscan Stud.* **42:** 301.

Harris, L. G. 1986. Size-selective predation in a sea anemone, nudibranch, and fish food chain. *Veliger* **29:** 38–47.

Harris, L. G. 1991. Comparative ecology of subtidal actiniarians from the coasts of California and the Gulf of Maine, USA. *Hydrobiologia* **216/217:** 271–278.

Harris, L. G., and S. J. Duffy. 1980. The influence of prey size on the preference hierarchy of the nudibranch *Aeolidia papillosa* (L.). *Am. Zool.* **20:** 1087 (abstract).

Hess, H. C. 1993. The evolution of parental care in brooding spirorbid polychaetes: the effect of scaling constraints. *Am. Nat.* **141:** 577–596.

Hintze, J. 2001. *NCSS and PASS* (software). Number Cruncher Statistical Systems, Kaysville, Utah.

Huxley, J. S. 1932. *The Problems of Relative Growth.* Methuen, London.

Hyman, L. H. 1940. *The Invertebrates: Protozoa Through Ctenophora.* McGraw-Hill, London.

LaBarbera, M. 1989. Analyzing body size as a factor in ecology and evolution. *Annu. Rev. Ecol. Syst.* **20:** 97–117.

Longley, R. D. 1984. Axon surface infolding and axon size can be quantitatively related in gastropod mollusks. *J. Exp. Biol.* **108:** 163–177.

Lundvall, D., R. Svanback, L. Persson, and P. Bystrom. 1999. Size-dependent predation in piscivores: interactions between predator foraging and prey avoidance abilities. *Can. J. Fish. Aquat. Sci.* **56:** 1285–1292.

McArdle, B. H. 1988. The structural relationship: regression in biology. *Can. J. Zool.* **66:** 2329–2339.

Paine, R. T. 1976. Size-limited predation: an observational and experimental approach with the *Mytilus-Piaster* interaction. *Ecology* **57:** 858–873.

Purcell, J. E. 1977. The diet of large and small individuals of the sea anemone *Metridium senile*. *Bull. S. C. Acad. Sci.* **76:** 168–172.

Rayner, J. M. V. 1985. Linear relations in biomechanics: the statistics of scaling functions. *J. Zool. (Lond.) A.* **206:** 415–439.

Rice, W. R. 1989. Analyzing tables of statistical tests. *Evolution* **43:** 223–225.

Sebens, K. P. 1981. The allometry of feeding, energetics, and body size in three sea anemone species. *Biol. Bull.* **161:** 152–171.

Sebens, K. P., and M. A. R. Koehl. 1984. Predation on zooplankton by the benthic anthozoans *Alcyonium siderium* (Alcyonacea) and *Metridium senile* (Actiniaria) in the New England subtidal. *Mar. Biol.* **81:** 255–271.

Shick, J. M. 1991. *A Functional Biology of Sea Anemones.* Chapman and Hall, London. 395 pp.

Sih, A. 1985. Evolution, predator avoidance, and unsuccessful predation. *Am. Nat.* **125:** 153–157.

Sih, A. 1987. Predators and prey lifestyles: an evolutionary overview. Pp. 203–224 in *Predation: Direct and Indirect Impacts on Aquatic Communities*, W. C. Kerfoot and A. Sih, eds. University Press of New England, Hanover, NH

Smith, R. J. 1984. Allometric scaling in comparative biology: problems of concept and method. *Am. J. Physiol.* **246:** R152–R160.

Sokal, R. R., and F. J. Rohlf. 1981. *Biometry: The Principles and Practices of Statistics in Biological Research*, 2nd ed. W. H. Freeman, New York.

Stephenson, T. A. 1928. *The British Sea Anemones*, Vol 1. The Ray Society, London.

Stephenson, T. A. 1929. On the nematocysts of sea anemones. *J. Mar. Biol. Assoc. UK* **16:** 173–201.

Tripet, F., and N. Perrin. 1994. Size-dependent predation by *Dugesia lugubris* (Turbellaria) on *Physa acuta* (Gastropoda): experiments and model. *Funct. Ecol.* **8:** 458–463.

Vermeij, G. A. 1982. Unsuccessful predation and evolution. *Am. Nat.* **120:** 701–720.

Williams, R. B. 1996. Measurements of cnidae from sea anemones (Cnidaria: Actiniaria): statistical parameters and taxonomic relevance. *Sci. Mar.* **60 (2–3):** 339–351.

Reference: *Biol. Bull.* **207:** 141–146. (October 2004)

Evidence for a Common Pattern of Peptidergic Innervation of Cnidocytes

PETER A. V. ANDERSON[1,2,*], LOUISE F. THOMPSON, AND CRAIG G. MONEYPENNY

Whitney Laboratory for Marine Bioscience and Departments of [1]Physiology and Functional Genomics, and [2]Neuroscience, University of Florida

Abstract. Tentacles from representatives of all four classes of the phylum Cnidaria were examined using antibodies against the neuropeptides FMRFamide and RFamide to reveal the organization of neurons and nerve nets associated with cnidocytes. The tentacles of all species examined contained FMRFamide- or RFamide-immunoreactive neurons, in varying densities. In representatives from the Scyphozoa, Hydrozoa, and Cubozoa, the FMRFamide-immunoreactive neurons formed plexuses at the base of the cnidocyte assemblages; in anthozoans, the absence of discrete assemblies of cnidocytes precluded visual co-localization of cnidocytes and immunoreactive neurons. In all four classes, immunoreactive sensory cells connected these peptidergic nerve nets to the surface of the tentacle. These findings suggest that members of all four cnidarian classes share a common organizational pattern, and it is proposed that this peptidergic innervation may be involved in the chemosensory regulation of cnidocyte discharge.

Introduction

Cnidocytes, the sting cells of members of the phylum Cnidaria, are used for a variety of functions, including food capture, locomotion, intra- and interspecific aggression, and defense. Cnidocyte discharge is very tightly regulated, presumably to minimize what is likely to be the considerable energetic cost of replacing very complex cells that can only be used once. Early studies (Parker and Van Alstyne, 1932; Pantin, 1942) developed the concept that cnidocytes functioned as independent effectors that required both chemical and mechanical stimuli for discharge, and that single cnidocytes bore receptors for both stimulus modalities. While there is considerable evidence to suggest that single cnidocytes do indeed bear both chemoreceptors (Thurm *et al.*, 1998) and mechanoreceptors (Brinkmann *et al.*, 1995; Thurm *et al.*, 1998) and can discharge in the absence of neurons (Aerne *et al.*, 1991), it is now generally accepted that they are not completely independent effectors. Instead, their discharge is thought to be regulated by a variety of intrinsic factors (Thurm *et al.*, 1998), including the state of satiation of the animal (Sandberg *et al.*, 1971; Smith *et al.*, 1974).

A variety of ultrastructural (for review, see Westfall, 2004) and histological (Anderson *et al.*, 1992; Golz, 1994) studies have reported on the association between nerves and cnidocytes, and it is now clear that cnidocytes are innervated by both sensory neurons and interneurons (Westfall, 2004). Ultrastructural studies of the innervation of cnidocytes in anemones (Anthozoa) have revealed the presence of a variety of types of synaptic vesicles, including both dense- and light-cored vesicles, suggesting the presence of a variety of transmitters, including Antho-RFamide peptides (Westfall, 2004). Here we expand on this understanding of the role of the peptidergic innervation of cnidocytes by demonstrating, in representatives of the three other cnidarian classes (Hydrozoa, Scyphozoa, and Cubozoa), a common pattern of peptidergic innervation of cnidocytes. This consists of a network or basket of peptidergic neurons that surrounds the base of clustered cnidocytes, together with a finite number of peptidergic sensory neurons that send processes to the surface of the tentacle.

Materials and Methods

Specimens of *Chrysaora quinquecirrha* (Desor, 1848) (Class Scyphozoa), *Physalia physalis* (Linnaeus, 1758), *Porpita porpita* (Linnaeus, 1758) *Cladonema* (sp.) (Class

Received 21 April 2004; accepted 2 August 2004.

* To whom correspondence should be addressed at Whitney Laboratory for Marine Bioscience, 9505 Ocean Shore Blvd., St. Augustine, Fl 32080. E-mail: paa@whitney.ufl.edu

Hydrozoa), *Chiropsalmus* (sp). (Class Cubozoa), and *Bunodosoma cavernata* (Bose, 1802) (Class Anthozoa) were collected in the vicinity of the Whitney Laboratory and maintained in running seawater at ambient temperatures. Pieces of tentacle or, in the case of *Cladonema*, small portions of colonies, were anesthetized in isotonic (0.37 *M*) $MgCl_2$ mixed 1:1 with seawater. Relaxed tentacles were then lightly stretched and pinned, using cactus spines (*Opuntia* sp.), onto a layer of Sylgard at the base of a petri dish. Individual polyps were excised from *Cladonema* colonies.

Excised tissue was then prepared for immunocytochemistry as described by Grimmelikhuijzen (1985). Briefly, tissues were fixed in 4% phosphate-buffered paraformaldehyde (pH 7.0) overnight at 4 °C, and rinsed (6 × 1 h) in phosphate-buffered saline containing 0.25% Triton X-100 (PBS-T). Samples were then incubated overnight at 4 °C in the presence of either an anti-FMRFamide antibody (Diasorin, Inc.) or an anti-RFamide antibody (146III provided by C. J. P. Grimmelikhuijzen, Univ. of Copenhagen) diluted 1:250 in PBS-T supplemented with 0.25% goat serum (PBS-T-G). After rinsing (4 × 1 h) with PBS-T, the samples were incubated overnight at 4 °C in secondary goat-anti-rabbit antibody conjugated to either FITC (Boehringer Mannheim) or Cy3 (Jackson Immunoresearch), diluted 1:150 with PBS-T-G. After a final round of rinsing, the samples were transferred to a drop of 90% glycerol in PBS containing 1 mg/ml o-phenylenediamine HCl on a microscope slide. The edges of the coverslip were then sealed with clear nail polish. Control samples were prepared in exactly the same manner, except that the secondary antibody was omitted. Samples were examined with either a Leica DMIRBE fluorescence microscope or a Leica laser scanning confocal microscope.

Results

In all the species examined, FMRFa-like immunostaining was present in the tentacles. In *Chrysaora*, *Cladonema*, *Physalia*, and *Porpita*, the staining was particularly dense with the anti-FMRFa antibody. In individual tentacles, immunoreactivity typically appeared as longitudinal arrays of neurons connected by transverse processes. In *Bunodosoma*, the anti-RFamide antibody staining was far more effective than anti-FMRFamide, and revealed a dense plexus of multipolar neurons throughout the ectoderm of the tentacles.

Equally common in all but *Aiptasia* were assemblies of immunoreactive neurons associated with cnidocytes. This organization was best illustrated in tentacles of *Chrysaora* (Fig. 1A), where cnidocytes clusters are more widely scattered than in the other species. In *Chrysaora*, immunoreactive nerve nets were associated with clusters of as few as

Figure 1. (A) Combined confocal fluorescence and Normarski image of part of a tentacle from *Chrysaora*. Note the green FMRFa-like immunoreactive nerve nets that are associated with each cluster of cnidocytes. (B) Combined laser scanning confocal/Normarski image of part of a tentacle from *Chrysaora*. Processes from the dense immunoreactive plexus at the base of the cnidocytes envelop (arrows) individual cnidocytes. Some cnidocysts display autofluorescence. (C) Laser scanning confocal image of a tentacle from *Chrysaora*. A presumed sensory neuron bearing a fine sensory process that projects into the external environment (yellow arrowhead) sends an axon to the dense immunoreactive plexus at the base of the cnidocytes. Note that several cnidocysts display autofluorescence. (D) Confocal image of a cnidosac from *Porpita*. Immunoreactive neurons (here stained red with Cy3) are present in the center of each sphere and connect the central plexus to the tentacle. Presumed sensory cells, with cell bodies at the surface of the cnidosacs and axons that connect to the central core of immunoreactivity, are evident (white arrows). Inset: Normarski photomicrograph of a single isolated cnidocyte from *Porpita* (same scale) showing the overall length of the cell. C, cnidocyst; CP, cytoplasmic processes; N, nucleus. (E) Higher magnification confocal image of the soma of a sensory cell (white arrow) in *Porpita* and its ciliary process (yellow arrowhead). (F) Confocal image of part of a cnidosac from *Physalia*. The cysts of the cnidocytes appear as unstained circles (asterisks). Note the presence of immunoreactive processes surrounding the cnidocytes, and a single cell that projects to the surface of the tentacle (arrow). (G) Combined laser-scanning confocal and Normarski image of the tip of a capitate tentacle of the hydroid *Cladonema*. Immunoreactivity is present in the ectoderm along the entire length of the tentacle, but is concentrated at the base of the cnidocytes. (H) Laser scanning confocal micrograph of the tip of a capitate tentacle of *Cladonema*, showing the presence of a dense immunoreactive plexus at the base of the cnidocytes, and a single immunoreactive process that extends to the surface of the tentacle (arrow). The cysts of the cnidocytes appear as unstained circles (asterisks). (I) A combined bright field/fluorescence image of part of a tentacle from *Chiropsalmus*. The cnidocytes are found in regularly spaced girdles that encircle the tentacles. Each ring of cnidocytes is associated with a dense array of immunoreactive (green-FITC) processes. At the edge of the tentacle it can be seen that these processes are located at the basal end of the cnidocytes. Threads from discharged cnidocysts (black arrow) show the location of the cnidocytes. (J) Fluorescence micrograph of part of a tentacle from *Chiropsalmus* showing a single immunoreactive cell (arrow) that projects to the surface of the tentacle, through the cnidocytes. (K) A laser scanning confocal image of part of a tentacle from the sea anemone *Bunodosoma*, showing a single immunoreactive sensory cell that projects to the surface of the tentacle. A single cilium from this cell (yellow arrowhead) projects into the mucus layer. This cell spans the width of the ectoderm of the tentacle, and connects with an immunoreactive nerve net located at the ectoderm-mesoglea interface.

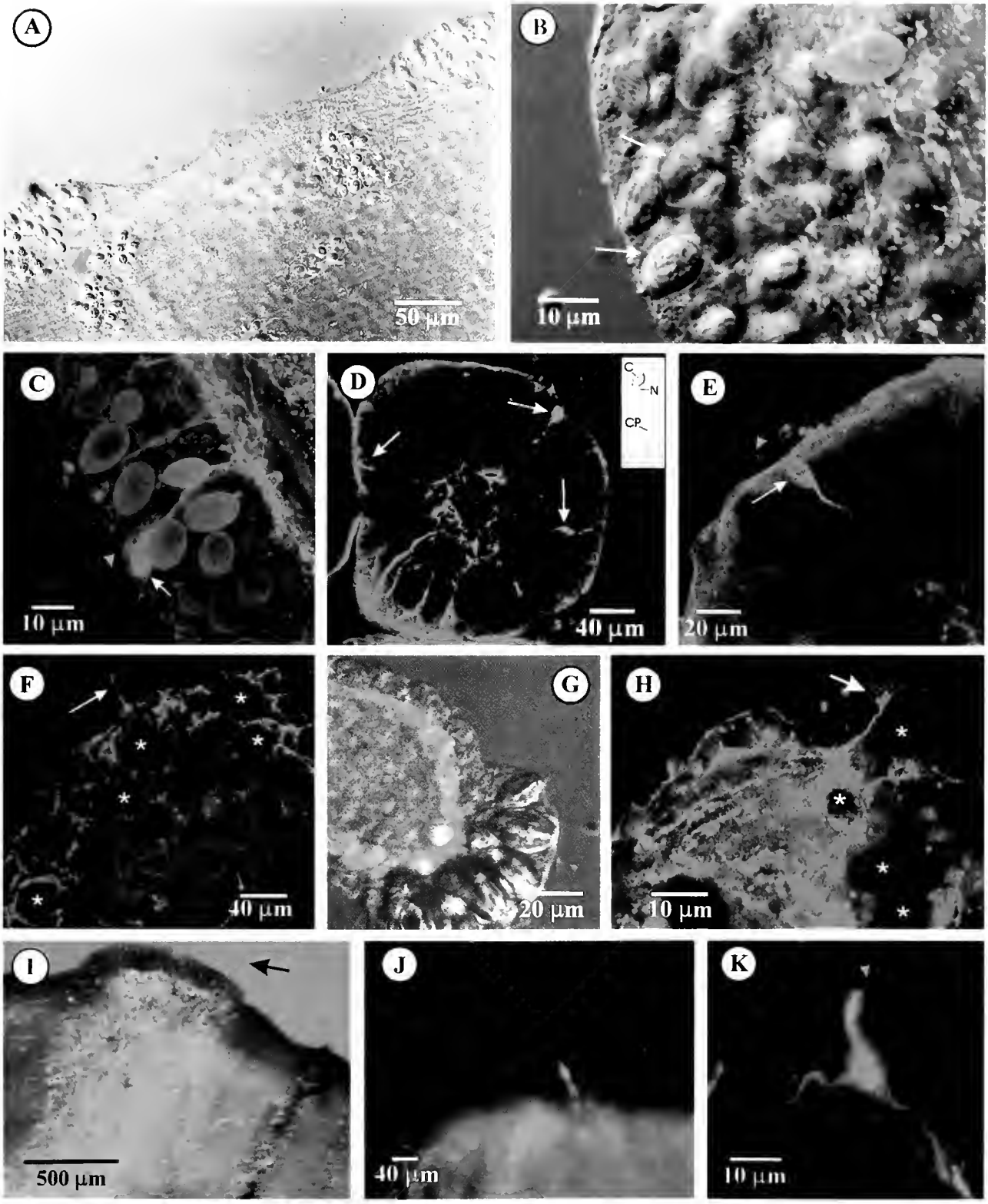
A
50 µm
B
10 µm
C
10 µm
D
C
N
CP
40 µm
E
20 µm
F
40 µm
G
20 µm
H
10 µm
I
500 µm
J
40 µm
K
10 µm

two or three cnidocytes as well as with the larger assemblies of cnidocytes. These assemblages of immunoreactive neurons had the appearance of baskets composed of immunoreactive neurons 1–2 μm in diameter. At higher power (Fig. 1B), the immunoreactive neurons in *Chrysaora* could be seen to be located primarily at the base of the cnidocytes. However, individual processes emerged from this dense plexus and partially enveloped individual cnidocytes (Fig. 1B).

Also evident in *Chrysaora* were individual immunoreactive neurons whose somata were located at the surface of tentacles and extended axons to the immunoreactive plexus at the base of the cnidocytes (Fig. 1C). A single fine process could occasionally be seen to emerge from the cell soma into the external medium (Fig. 1C). These cells had the typical appearance of sensory cells.

In the two siphonophore species examined, *Porpita* and *Physalia*, the tentacles bear large assemblies of cnidocytes, called cnidosacs, that appear as a line of hemispheres or spheres arranged along one edge of each tentacle. In a well-relaxed tentacle, this organization gives the appearance of a string of small blue beads. In *Porpita*, the cnidosacs almost form self-contained spheres that are attached to the tentacle through a small stalk (Fig. 1D). The central core of each cnidosac was inevitably filled with large numbers of immunoreactive processes that were connected to the shaft of the tentacle by additional immunoreactive neurons. Cnidocytes from *Porpita* are remarkably long, and much of their length is taken up by a long (80 μm), narrow, basally directed cytoplasmic projection (Fig. 1D, inset). Thus, although the immunoreactivity in *Porpita* was located in the central core of the cnidosac, its location was still ectodermal, around the base of the long cytoplasmic projections.

Several sensory neurons were observed to extend to the surface of each cnidosac (Fig. 1D, E). These cells had large ovoid somata (Fig. 1E), which were typically located near the surface of the tentacle; many had a single fine process that extended into the extracellular medium (Fig. 1E). Occasionally, cells that projected to the surface of the cnidosac had more centrally located somata (Fig. 1D). The cnidosacs in *Porpita* were small enough to be fully reconstructed from confocal optical slices and provided a measure of the overall density of sensory neurons. A typical cnidosac contained up to 6–7 sensory neurons.

In *Physalia*, the cnidosacs are more hemispherical and the ectoderm thinner than *Porpita*. When cnidosacs were viewed from the surface, a dense plexus of immunoreactivity surrounding the dark cores of the cnidocytes was apparent (Fig. 1F). When viewed tangentially, it could be seen that the immunoreactivity was largely restricted to the base of the ectoderm of the cnidosac, around the base of the cnidocytes (Fig. 1F), but that occasional neurons emerged from the plexus and extended to the surface of the tentacle (Fig. 1F).

In the case of the hydroid *Cladonema*, the FMRFa-like innervation of the tentacle was particularly evident. Immunoreactive processes located in what appeared to be the base of the ectoderm covered the entire tentacle (Fig. 1G). This nerve net was particularly dense, however, at the base of the capitate portion of the tentacle, immediately under the cluster of cnidocytes (Fig. 1G, H). This organization was very reminiscent of that in the two siphonophores and of that reported for another hydroid, *Coryne* (Golz, 1994). Once again, single neurons occasionally emerged from this plexus and extended through the cnidocytes to the surface of the tentacle (Fig. 1H).

In the cubomedusa *Chiropsalmus*, the bulk of tentacular cnidocytes exist in regular bands that encircle the entire tentacle (Fig. 1I). Once again, these cnidocyte bands were associated with a dense plexus of immunoreactive neurons that was located in the ectoderm of the tentacle, at the base of the cnidocytes (Fig. 1I). Single immunoreactive cells could be seen to emerge from this plexus to the surface (Fig. 1J).

The pattern of immunoreactivity in the anthozoan *Bunodosoma* differed markedly from that of the other species examined. As noted above, while the anti-FMRFamide antibody was only partially effective, the anti-RFamide antibody revealed a dense network of multipolar neurons located at the base of the ectoderm. When the edges of tentacles were viewed tangentially, single ciliated sensory cells were evident (Fig. 1K) and processes from these merged with the immunoreactive nerve net. The cilia of these sensory cells emerged from the surface of the tentacle, but seemed to extend no further than the mucus layer on the surface.

Discussion

Intracellular recordings from cnidocytes in the tentacles of *Physalia* (Purcell and Anderson, 1995) during applications of aqueous extracts of fish mucus are characterized by bursts of small depolarizing potentials. Similar activity is triggered in cnidocytes in the capitate tentacles of *Cladonema* by applications of an aqueous extract of *Artemia* (Price and Anderson, unpubl. data). In both cases, the activity is absent in tentacles that are bathed in a high-Mg^{2+}, low-Ca^{2+} seawater, implying that the depolarizing events are synaptic potentials. The fact that these events occur synchronously in closely apposed or adjacent cnidocytes (Purcell and Anderson, 1995) suggests that clustered cnidocytes receive a common synaptic input that is triggered by chemosensory stimulation of the tentacle.

The results presented here indicate that cnidocytes in both these species, together with representatives from at least two other cnidarian classes (Scyphozoa, Cubozoa) are innervated by neurons that are immunoreactive to antibodies against the peptide FMRFamide. Irrespective of the organi-

zation of the cnidocytes, be they in small planar clumps (*Chrysaora*), broad circumtentacular bands (*Chiropsalmus*), single capitate bulbs (*Cladonema*), or the linear arrangement of nearly cnidosacs found in *Physalia* and *Porpita*, a dense plexus of FMRFamide IR neurons is present around the base of the cnidocytes. The basal location of this plexus is best exemplified by *Porpita*, where the long cytoplasmic extension at the basal end of each cnidocyte creates a considerable separation between the cyst and the FMRFamide IR neurons. The basal location of this plexus is consistent with the site of neuro-cnidocyte synapses reported by other investigators (Holtmann and Thurm, 2001; Westfall, 2004), although there is evidence—in *Chrysaora* at least—that FMRFamide IR processes extend partway up the length of some cnidocytes, presumably forming synapses around the midpoint of the cell.

The sea anemone *Bunodosoma* may appear to be the exception to this pattern of peptidergic innervation. While the tentacles did contain a dense plexus of FMRFamide and RFamide immunoreactive neurons, it was not possible to discern any obvious association between these neurons and cnidocytes in the tentacles. EM studies of cnidocytes in the anemone *Aiptasia* (Westfall, 2004), on the other hand, have revealed the presence of RFamide immunoreactive dense-cored vesicles at neuro-cnidocyte synapses, suggesting that cnidocytes in anemones are indeed innervated by peptidergic neurons. The lack of a clear association between the immunoreactive nerve nets and cnidocytes may, therefore, simply be a consequence of the anemone's anatomy. In *Bunodosoma* and other anemone species, the ectoderm of the tentacles is filled, almost uniformly, with cnidocytes and, unlike the representatives of the other classes examined, there are no discontinuities in cnidocyte coverage that could be mapped to interruptions or breaks in the underlying peptidergic nerve net. Thus, the presence of a peptidergic nerve net over the entire tentacle could merely be a reflection of the uniform distribution of cnidocytes in the tentacles.

A consistent feature of the FMRFamide IR plexus in all species examined was the presence of what appear to be peptidergic sensory neurons that emerge from the plexus. Their classification as sensory neurons is based on the peripheral location of the cell body and the presence, in many of them, of a very fine process that extends into the external medium, criteria that are consistent with those used by other investigators (Saripalli and Westfall, 1996). Cells in the capitate tentacles of the hydroid *Coryne* and classified as sensory cells (Holtmann and Thurm, 2001) contain dense cored vesicles that are consistent with their being peptidergic. Although the sensory cells described here are relatively rare (a single 200-μm-diameter cnidosac in *Porpita* contains only 6–7), the average density is on the order of one sensory process per 8,000–10,000 μm^2 of cnidocyte-rich tentacle surface. However, because those sensory cells are afferent to a dense nerve net, or plexus, the result is that this organization has the potential to directly or indirectly activate a great many cnidocytes. It is not clear whether all cnidocytes in a cluster receive synaptic input directly. It is possible that only a finite number of cnidocytes are innervated but that the afferent input is conveyed to other cnidocytes through signaling systems such as nitric oxide (Salleo *et al.*, 1996; Colasanti *et al.*, 1997; Moroz *et al.*, 2004) or by way of gap junctions, which are very abundant in hydrozoans (Josephson and Schwab, 1979; Spencer, 1981) and may also be present in anthozoans (Germain and Anctil, 1996; Mire *et al.*, 2000). However, while agents that uncouple gap junctions affect the responses of hydrozoan (Price and Anderson, unpubl. data) and anthozoan (Mire *et al.*, 2000) cnidocytes, cnidocytes in the hydroid *Stauridiosarsia* (Brinkmann *et al.*, 1996) are not dye-coupled to one another or to adjacent cells, making the possible role of gap junctions equivocal.

It is not altogether surprising that these cnidocyte-specific plexuses were revealed using antibodies to FMRFamide. RFamide peptides are exceedingly common in the Cnidaria (for review, see Grimmelikhuijzen *et al.*, 2002). They have been isolated from representatives of all classes, with the exception of the Cubozoa where peptide studies have not yet been conducted; and they have been shown to be functionally important for development (Katsukura *et al.*, 2003) and physiological activity (McFarlane *et al.*, 1987, 1991). However, cnidarians do not possess FMRFamide *per se*, but rather a variety of other peptides that terminate in the sequence RFamide peptides. The fact that FMRFamide antibodies were only minimally effective in *Bunodosoma* while RFamide antibodies were effective may reflect this point, and suggests that the use of the antiRFamide antibody with the other species might reveal more details of the peptidergic innervation of the cnidocytes.

It must be stressed, however, that the presence of an RFamide-like innervation of cnidocytes does not preclude the involvement of other neurotransmitter pathways. While the evidence for other types of neurotransmitter in the phylum Cnidaria is not as conclusive as for peptides, evidence for other transmitters is growing (for review, see Anderson, 2004). In addition, some evidence (Kass-Simon and Scappaticci, 2004) suggests that glutamatergic pathways may also be involved in the regulation of *Hydra* cnidocytes, and that dopamine is involved in modulating the discharge of cnidocytes from *Corynidae* (Thurm *et al.*, 1998). Furthermore, the finding that the threshold for cnidocyte discharge is raised in satiated animals (Sandberg *et al.*, 1971; Smith *et al.*, 1974) suggests that regulatory pathways must be present—ones that somehow inhibit or down-regulate cnidocyte discharge.

As noted earlier, application of an extract of fish mucus to *Physalia* tentacles triggers bursts of electrical activity that can be recorded as synaptic events in single cnidocytes

(Purcell and Anderson, 1995). That synaptic input does not, however, evoke discharge of the impaled cnidocytes, or any adjacent ones. This suggests, therefore, that the synaptic activity may serve to somehow prime the cnidocyte in preparation for the subsequent mechanical stimulus that would indicate physical contact has been made with the source of the odorant. Given the organization of the cnidocyte-associated peptidergic nerve nets presented here and the presence of what appear to be peptidergic afferent sensory neurons, it is tempting to speculate that the synaptic activity that can be recorded from the cnidocytes of *Physalia* (Purcell and Anderson, 1995) and *Cladonema* (Price and Anderson, unpubl. data) arises, directly or indirectly, from these peptidergic nerve nets. While there is no direct physiological or pharmacological evidence that peptides are involved in the cnidocyte response, there is no evidence that peptides are not involved. Furthermore, electron microscopic immunocytochemistry has revealed the presence of RFamide peptides in the nerve terminals of neurocnidocyte synapses in anemones (Westfall, 2004). Thus, given their prevalent role in many aspects of cnidarian biology and their clear association with cnidocytes in all cnidarian classes, it would be surprising if neuropeptides were not actively involved in some aspect of the regulation of cnidocyte discharge.

Acknowledgments

Supported by NSF Grant IBN0110550. The authors are very grateful to Dr. Christelle Bouchard for comments on the manuscript, and to Dr. C. J. P. Grimmelikhuijzen for the RFamide antibody.

Literature Cited

Aerne, B. L., R. P. Stidwill, and P. Tardent. 1991. Nematocyst discharge in *Hydra* does not require the presence of nerve cells. *J. Exp. Zool.* **258:** 137–141.

Anderson, P. A. V. 2004. Cnidarian neurobiology: what does the future hold? *Hydrobiologia* (In press).

Anderson, P. A. V., A. Mooster, and C. J. P. Grimmelikhuijzen. 1992. The distribution of AnthoRF-amide-like immunoreactivity in scyphomedusae. *Cell Tissue Res.* **267:** 67–74.

Brinkmann, M., D. Oliver, and U. Thurm. 1995. Interaction of mechano- and chemosensory signals within the same sensory cell. *Pflug. Archiv. Eur. J. Physiol.* **429:** R153.

Brinkmann, M., D. Oliver, and U. Thurm. 1996. Mechanoelectric transduction in nematocytes of a hydropolyp (Corynidae). *J. Comp. Physiol. A* **178:** 125–138.

Colasanti, M., G. Venturini, A. Merante, G. Musci, and G. M. Lauro. 1997. Nitric oxide involvement in *Hydra vulgaris* very primitive olfactory-like system. *J. Neurosci.* **17:** 493–499.

Germain, G., and M. Anctil. 1996. Evidence for intercellular coupling and connexin-like protein in the luminescent endoderm of *Renilla koellikeri* (Cnidaria, Anthozoa). *Biol. Bull.* **191:** 353–366.

Golz, R. 1994. Occurrance and distribution of RFamide-positive neurons within the polyps of *Coryne* sp. (Hydrozoa, Corynidae). *Biol. Bull.* **186:** 115–123.

Grimmelikhuijzen, C. J. P. 1985. Antisera to the sequence Arg-Phe-amide visualize neuronal centralization in hydroid polyps. *Cell Tissue Res.* **241:** 171–182.

Grimmelikhuijzen, C. J. P., N. Williamson, and G. N. Hansen. 2002. Neuropeptides in cnidarians. *Can. J. Zool.* **80:** 1690–1702.

Holtmann, M., and U. Thurm. 2001. Mono- and oligo-vesicular synapses and their connectivity in a cnidarian sensory epithelium (*Coryne tubulosa*). *J. Comp. Neurol.* **432:** 537–549.

Josephson, R. K., and W. E. Schwab. 1979. Electrical properties of an excitable epithelium. *J. Gen. Physiol.* **74:** 213–236.

Kass-Simon, G., and A. A. Scappaticci. 2004. Glutamatergic and GABAergic control of the tentacle effector systems of *Hydra vulgaris*. *Hydrobiologia* (In press).

Katsukura Y., C. N. David, C. J. Grimmelikhuijzen, and T. Sugiyama. 2003. Inhibition of metamorphosis by RFamide neuropeptides in planula larvae of *Hydractinia echinata*. *Dev. Genes Evol.* **213:** 579–586.

McFarlane, I. D., D. Graff, and C. J. P. Grimmelikhuijzen. 1987. Excitatory actions of Antho-RFamide, an anthozoan neuropeptide, on muscles and conducting systems in the sea anemone *Calliactis parasitica*. *J. Exp. Biol.* **133:** 157–168.

McFarlane, I. D., P. A. V. Anderson, and C. J. P. Grimmelikhuijzen. 1991. Effects of three anthozoan neuropeptides, Antho-RWamide I and II and Antho-RFamide, on slow muscles from sea anemones. *J. Exp. Biol.* **156:** 419–431.

Mire, P., J. Nasse, and S. Venable-Thibodeaux. 2000. Gap junctional communication in the vibration-sensitive response of sea anemones. *Hear. Res.* **144:** 109–123.

Moroz, L. L., R. W. Meech, J. V. Sweedler, and G. O. Mackie. 2004. Nitric oxide regulates swimming in the jellyfish *Aglantha digitale*. *J. Comp. Neurol.* **472:** 26–36.

Pantin, C. A. F. 1942. The excitation of nematocysts. *J. Exp. Biol.* **19:** 294–310.

Parker, G. H., and M. A. Van Alstyne. 1932. The control and discharge of nematocysts especially in *Metridium* and *Physalia*. *J. Exp. Zool.* **16:** 329–344.

Purcell, J. E., and P. A. V. Anderson. 1995. Electrical responses to water-soluble components of fish mucus recorded from the cnidocytes of a fish predator, *Physalia physalis*. *Mar. Freshw. Behav. Physiol.* **26:** 149–162.

Salleo, A., G. Musci, P. F. A. Barra, and L. Calabrese. 1996. The discharge mechanism of acontial nematocytes involves the release of nitric oxide. *J. Exp. Biol.* **199:** 1261–1267.

Sandberg, D. M., P. Kanciruk, and R. N. Mariscal. 1971. Inhibition of nematocyst discharge correlated with feeding in a sea anemone, *Calliactis tricolor* (Leseur). *Nature* **232:** 263–264.

Saripalli, L. D., and J. A. Westfall. 1996. Classification of nerve cells dissociated from tentacles of the sea anemone *Calliactis parasitica*. *Biol. Bull.* **190:** 111–124.

Smith, S., J. Oshida, and H. Bode. 1974. Inhibition of nematocyst discharge in hydra fed to repletion. *Biol. Bull.* **147:** 186–202.

Spencer, A. N. 1981. The parameters and properties of a group of electrically coupled neurones in the central nervous system of a hydrozoan jellyfish. *J. Exp. Biol.* **93:** 33–50.

Thurm, U., M. Brinkmann, M. Holtmann, P. Lawonn, D. Oliver, and T. Sieger. 1998. Modulation of the output of a mechanosensory cell by chemosensory and synaptic inputs. Pp. 237–253 in *From Structure to Function in Sensory Systems*, C. Taddei-Ferretti, and C. Musio, eds. World Scientific Publishing, London.

Westfall, J. A. 2004. Neural pathways and innervation of cnidocytes in tentacles of sea anemones. *Hydrobiologia* (In press).

Abstracts of Papers Presented at THE GENERAL SCIENTIFIC MEETINGS OF THE MARINE BIOLOGICAL LABORATORY, Woods Hole, Massachusetts 9 and 10 August 2004

Program Chairs:
KAREN CRAWFORD, St. Mary's College of Maryland
KENNETH FOREMAN, Semester in Environmental Science, MBL
ROBERT GOULD, University of Illinois at Chicago
ROBERT PAUL MALCHOW, University of Illinois at Chicago

ABSTRACTS FROM THE 2004 GENERAL SCIENTIFIC MEETINGS OF THE MARINE BIOLOGICAL LABORATORY

Developmental Biology

Protein Chemistry, Molecular Biology, and Evolution

Bioinformatics

Microbiology, Pathology, and Immunology

Ecology and Population Biology

Reference: *Biol. Bull.* **207:** 151. (October 2004)

The MBL Awards for 2004

MBL Awards are given for the best paper presented at the General Scientific Meetings by a senior investigator, a junior investigator, a graduate student, and an undergraduate: additional papers are selected for Honorable Mention.

The five presentations selected for MBL Awards this year reflect the broad scope of science at the Laboratory. Among these reports we find that lipopolysaccharide, the prime cause of gram-negative bacterial toxicity, occurs in eukaryotes; that a long-term decrease in synaptic strength is induced by a transient suppression of NMDA receptor activity; that cis editing in a trypanosome is a model of guide-RNA structure and function; that a female lobster's sperm load affects her choice of a mate; and that enzyme activities can be used to assess the stimulatory effect of increased estuarine nitrogen on the growth of sea lettuce. This year's awardees are listed below with the title of their presentation and the page on which their abstract appears.

—The Editor
August 2004

Senior Investigator

- WINNER ..... Peter B. Armstrong
  with Margaret T. Armstrong, Steven M. Theg, Nikolai Braun, Norman Wainwright, and R. L. Pardy
  Histochemical evidence for lipopolysaccharide (endotoxin) in eukaryotes (p. 172)
- HONORABLE MENTION ..... Robert M. Gould
  with Hilary Morrison, Robert Campbell, and Edwin Gilland
  Evolution of myelin proteins (p. 168)

Junior Investigator

- WINNER ..... Robert C. Froemke
  with Dan Yang
  Transient NMDA receptor suppression induces long-lasting synaptic depression (p. 155)
- HONORABLE MENTION ..... Chuan-Chin Chiao
  with Emma J. Kelman and Roger T. Hanlon
  Disruptive body patterning of cuttlefish (*Sepia officinalis*) requires visual information on edges and brightness of objects on natural substrate backgrounds (p. 153)
- HONORABLE MENTION ..... James J. Tong
  Mitochondrial dynamics in synaptic plasticity in *Drosophila melanogaster* (p. 162)

Graduate Student

- WINNER ..... Daniel E. Golden
  with Stephen L. Hajduk
  Cis editing in *Trypanosoma brucei brucei* as a model for understanding guide-RNA structural and functional requirements (p. 169)
- HONORABLE MENTION ..... Omicron L. Ma
  with Sarah E. Webb and Andrew L. Miller
  Imaging patterns of Ca^{2+} transients during the blastula period in zebrafish embryos (p. 165)

Undergraduate

- WINNER ..... Patrick Flight
  with Gabriele Gerlach and Jelle Atema
  Sperm load impact on female courtship behavior in the American lobster (*Homarus americanus*) (p. 155)
- WINNER ..... Leanna R. Heffner
  with Mirta Teichberg, Sophia Fox, and Ivan Valiela
  Nitrate reductase and glutamine synthetase activity and growth in *Ulva lactuca* in Waquoit Bay: a time sequence of responses to differences in nitrogen supply (p. 175)
- HONORABLE MENTION ..... Clarissa A. Sabella
  with Ellen E. Faszewski, Jane C. Kaltenbach, William J. Kuhns, Max M. Burger, and Xavier Fernandez-Busquets
  Immunocytochemical detection of integrins α_3 and β_1 in allografts of the marine sponge, *Microciona prolifera* (p. 162)

Reference: *Biol. Bull.* **207:** 152. (October 2004)

Circadian Rhythms in *Limulus* Visual Sensitivity Compensate for Day-Night Changes in Light Intensity

E. Brown[1], J. Hitt[2], F. Dodge[2], and R. Barlow[2]
[1]University of Rochester, Rochester, New York
[2]SUNY Upstate Medical University, Syracuse, New York

At night a circadian clock transmits efferent optic nerve activity to the lateral eyes of *Limulus polyphemus*, increasing their sensitivity to light. The animal's use of vision to find mates at night suggests that the clock's effect on retinal sensitivity compensates for the nighttime decrease in ambient illumination. To test this possibility we recorded activity from optic nerve fibers *in situ* while the animal was exposed to day-night changes in illumination in its natural environment. Using a waterproof recording chamber we monitored the maintained activity of single or small clusters of optic nerve fibers. Placing an animal at a meter depth near the shoreline of Woods Hole, Massachusetts, enabled us to monitor optic nerve activity with a remote amplifier and recorder connected to the animal *via* a tether. A single optic nerve fiber typically responds to ambient daylight illumination at rates ranging from 4 to 14 impulses/s. In one experiment the steady-state firing rate was 4.7 ips in the early evening when the ambient intensity was 85 cd/m^2. At 8 p.m. the rate increased to 9.2 ips as the light intensity decreased to 0.054 cd/m^2. The rate was 11.8 ips under bright illumination the following day (22,000 cd/m^2) and dropped to 5.3 ips at 0.040 cd/m^2 that night. Similar results were recorded from animals that were placed in an aquarium next to a south-facing window in Woods Hole. The nearly 1,000,000-fold decrease in ambient illumination at night appears to be associated with only about a two-fold decrease in optic nerve response. We conclude that the circadian clock's input to the lateral eye nearly compensates for the diurnal changes in light intensity.

Supported by NSF, NEI, NIMH, RPB and the Lions of Central New York.

Reference: *Biol. Bull.* **207:** 152. (October 2004)

Circadian Rhythms in the Locomotor Activity of Juvenile Horseshoe Crabs

Mira Guo[1], Frederick Dodge[2], and Robert Barlow[2]
[1]Princeton University, Princeton, New Jersey
[2]SUNY Upstate Medical University, Syracuse, New York

The vision of horseshoe crabs, *Limulus polyphemus*, exhibits a remarkable circadian rhythm. Visual sensitivity increases at night in conjunction with an increase in mating activity. We investigated whether the animal exhibits other endogenous rhythms, and if so, whether they are coordinated with the rhythm of visual sensitivity. We found that juvenile animals exhibit a free-running, endogenous circadian rhythm in locomotor activity. Of animals tested, 10 out of 24 showed regular, cyclic locomotor activity when kept in constant conditions, both in constant light (n = 3) and in constant dark (n = 7). Using an automated, computerized video tracking system and existing circadian data analysis software, we found that cycles fell into two groups divided by period length. In the first group, periods varied from 12.3 h to 15.8 h (average = 13.7 h, standard deviation = 1.5 h); in the second, they varied from 23.1 h to 26.6 h (average = 25.0 h, standard deviation = 1.2 h). The locomotor activity of several animals with endogenous periods in the range of 24 h drifted over the course of 3 to 4 days. It is not clear whether the locomotor activity has a crepuscular component as well as a circadian one. We tested the effectiveness of brief light pulses to shift the phase of free-running activity rhythms. Exposing animals to a 2-h light pulse during their subjective night shifted the phases of 8 out of 12 animals by 0.4 h to 6.2 h. We conclude that juvenile horseshoe crabs possess cycles of locomotor activity. The rhythmic activity cycles free-run under constant conditions and can be shifted by light pulses. Both properties are indicative of endogenous biological oscillators. It remains to be determined whether the clock controlling circadian locomotor activity is linked with the clock modulating visual sensitivity.

Supported by NSF, NEI, NIMH, RPB and the Lions of Central New York.

Reference: *Biol. Bull.* **207:** 153. (October 2004)

Circadian Clock: Where Is It Located in the *Limulus* Brain?

T. Saito[1], K. Mori[2], and R. Barlow[1]
[1]SUNY Upstate Medical University, Syracuse, New York
[2]Tsukuba University, Tsukuba, Japan

At night a circadian clock in the brain of the horseshoe crab, *Limulus polyphemus,* transmits efferent optic nerve activity to the ventral, median, and lateral eyes. The efferent input increases the sensitivity of the lateral eyes, enabling the animals to find mates under dim nocturnal levels of illumination. We investigated the source of the clock-generated efferent optic nerve activity. A previous study reported that cell bodies of the efferent nerve fibers are located in the cheliceral ganglia, bilateral clusters of neurons at the lateral, posterior edges of the protocerebrum (Calman and Battelle, *Vis. Neurosci.* 6:481–495, 1991). The cells were identified by retrograde transport of Neurobiotin in optic nerve fibers. We report here that retrograde transport of cobalt plus nickel in the optic nerve fibers reveals neuronal cell bodies in the central body of the protocerebrum. The large U-shaped central body is posterior and medial to the primary visual centers, the lamina and medulla. Situated near the center of the protocerebrum, the bilateral clusters of neurons of the central body are linked by a connecting commissure. Retrograde transport reveals a small number of neurons (~15) consistent with electrophysiological recordings (R. Barlow, *J. Neurosci.* 3:856–870, 1983). We attempted to locate the source of clock-generated efferent activity by selective lesions. Lesioning the circumesophageal connectives, including the cheliceral ganglion, did not block the efferent activity, nor did lesions of the protocerebrum posterior to the central body and of the dorsal portion (~10%) of the central body. Efferent activity was abolished only by a deep lesion of the central body, that is, an ablation of the entire central body. We conclude that neurons in or below the central body are the sources of clock-generated efferent optic nerve activity. Attempts to record clock-like efferent activity from these neurons have not succeeded.

Support by NSF, NEI, NIMH, RPB and Lions of Central New York.

Reference: *Biol. Bull.* **207:** 153. (October 2004)

Disruptive Body Patterning of Cuttlefish (*Sepia officinalis*) Requires Visual Information on Edges and Brightness of Objects on Natural Substrate Backgrounds

Chuan-Chin Chiao[1,2], Emma J. Kelman[1,3], and Roger T. Hanlon[1]
[1]Marine Biological Laboratory, Woods Hole, Massachusetts
[2]National Tsing Hua University, Hsinchu, Taiwan
[3]University of Sussex, Brighton, United Kingdom

Cuttlefish (*Sepia officinalis*) show disruptive body patterns for camouflage on mixed light and dark gravel of appropriate size (equivalent to the area of the animal's own white square component on the dorsal mantle). However, the exact visual features that cuttlefish extract from natural substrates are largely unknown. We placed young cuttlefish (5–8 cm in mantle length) in a circular experimental arena (25 cm in diameter) and presented them with natural gravel and a picture of natural gravel. We established that the animals respond similarly to the three-dimensional natural gravel and to the two-dimensional pictures of natural gravel. We then applied a low-pass filter to remove the edges of the gravel and a high-pass filter to remove the overall brightness of the gravel on the pictures (*i.e.*, to enhance the edges of the gravel), and video-recorded the animals' resulting body patterns in response to these altered visual stimuli. Our results showed that disruptive body patterning of cuttlefish requires visual information on both the edges and the brightness of objects on natural substrate backgrounds. This indicates that the cuttlefish visual system must sample and process wide ranges of spatial frequency information from substrates to produce the appropriate body coloration for camouflage.

Reference: *Biol. Bull.* **207:** 154. (October 2004)

Visual Background Features That Elicit Mottled Body Patterns in Cuttlefish, *Sepia officinalis*

Alexandra Barbosa[1], Christopher F. Florio[1,2], Chuan-Chin Chiao[1,3], and Roger T. Hanlon[1]
[1]Marine Biological Laboratory, Woods Hole, Massachusetts
[2]Boston University Marine Program, Woods Hole, Massachusetts
[3]National Tsing Hua University, Hsinchu, Taiwan

Cuttlefish, *Sepia officinalis*, can produce a variety of body patterns for camouflage on natural substrates. Among these body patterns, the visual background cues for eliciting mottled patterns have not been studied systematically. The objective of this study was to determine the visual features that elicit mottled body patterns, which are characterized by light and dark splotches on the body. First, animals were presented with artificial substrates—black and white checkerboard squares of various sizes—to determine the area of the squares that would elicit mottled body patterns. Results indicate that checkerboard squares with an area of about 4%–12% of the area of the animal's white square (a light body patterning component in the dorsal mantle) elicited mottled body patterns in three test groups (10 animals of 1.65 cm mantle length (ML); 6 animals of 10 cm ML; 6 animals of 17 cm ML). Second, different ratios of black and white squares (of the appropriate size) were tested to determine whether a predominance of black *vs.* white had a stronger sensory influence on the resulting body pattern; *i.e.*, do the animals cue preferentially on the dark or light visual background objects? With 10 animals of 1.65 cm ML, three combinations worked similarly well: 1 white: 1 black; 1w:3b; and 3w:1b. The forward and reverse combinations of 1:15, 1:63 and 1:1023 did not elicit mottled body patterns consistently. Our conclusion is that a high frequency of light and dark small objects of similar proportions (1:1, 1:3, 3:1) in the visual background tends to elicit mottled body patterns. Future experiments are meant to determine the exact combinations of light and dark background objects and contrast ranges that are used by cuttlefish to produce adaptive coloration by means of mottled body patterns.

Reference: *Biol. Bull.* **207:** 154. (October 2004)

The Time Course of the Camouflage Response of Cuttlefish (*Sepia officinalis*)

Leib Litman[1] and Roger T. Hanlon[2]
[1]City University of New York, New York City, New York
[2]Marine Biological Laboratory, Woods Hole, Massachusetts

The camouflage changes of cuttlefish are thought to be instantaneous. In nature, cuttlefish have been observed (and videotaped) to blend into their surroundings almost as fast as they can move. However, this question has never been addressed experimentally. In an attempt to measure the speed of the camouflage response, we placed the cuttlefish on checkerboard and dark sand substrates, which are known from previous experiments to produce disruptive and uniform coloration, respectively; and we timed their camouflage responses. Unexpectedly, the animals did not produce camouflage immediately, but refined their body patterns over 3 to 5 minutes on average, sometimes taking up to an hour. One possibility for the slow responses in our experiment is that the cuttlefish are not as efficient on artificial substrates as they are on natural ones. Another possibility is that the instantaneous ability to camouflage in the wild is the result of the animal either (i) having had experience adapting to those substrates in the course of its life, or (ii) requiring certain visual stimuli during a critical period of early development. If so, the implication is that the sensory-motor camouflage response of cuttlefish is plastic to some extent and that the efficiency with which it is produced is, at least in part, a product of its life experience. While at this time the conclusion that the camouflage response of cuttlefish is experience- or critical-period-dependent remains speculative, this possibility is intriguing and should be pursued in future experiments.

Reference: *Biol. Bull.* **207:** 155. (October 2004)

Sperm Load Impact on Female Courtship Behavior in the American Lobster (*Homarus americanus*)

Patrick Flight[1], Gabriele Gerlach[2], and Jelle Atema[3]
[1]Duke University, Durham, North Carolina
[2]Marine Biological Laboratory, Woods Hole, Massachusetts
[3]Boston University Marine Program, Woods Hole, Massachusetts

During courtship, female lobsters (*Homarus americanus*) evaluate male pheromones to assess the quality of prospective mates. Females can store sperm for up to three years and use it to fertilize multiple egg clutches. We investigated whether the amount of sperm a female has stored impacts her mate choice, specifically, her preference for a dominant male. Females were classified based on the sperm load in their seminal receptacles. In a choice flume, they were then presented with the option of approaching the upstream shelter of either the dominant or subordinate member of an established male dominance pair. We measured three behavioral parameters: time spent attempting to enter each shelter, number of approaches to each male, and time spent within 30 cm of each shelter. We found that pre-molt females, who would lose any stored sperm during the molt, and females with little or no sperm spent significantly more time attempting to enter the shelter of the dominant male rather than that of the subordinate male; and they also averaged more approaches to the dominant. Conversely, females with high sperm loads were less interested in dominance. They typically spent more time attempting to enter the subordinate shelter and approached it more frequently, possibly in an attempt to evict the subordinate male. Time spent within 30 cm of the shelters was not different among females of all sperm levels. This study shows that molt state and stored sperm quantity affect a female's mate choice: pre-molt females and females with little or no stored sperm prefer the dominant over the subordinate male. This suggests that females have a mechanism to monitor their sperm load in addition to their molt state.

Reference: *Biol. Bull.* **207:** 155. (October 2004)

Transient NMDA Receptor Suppression Induces Long-Lasting Synaptic Depression

Robert C. Froemke[1,2] and Dan Yang[1]
[1]University of California, Berkeley, California
[2]Marine Biological Laboratory, Woods Hole, Massachusetts

At many synapses, the induction of long-term synaptic modification requires NMDA receptor activation and corresponding Ca^{2+} influx into the postsynaptic cell (Zucker, 1999). We report here that, for layer 2/3 pyramidal neurons, transient suppression of NMDA receptor activity induces a long-term decrease in synaptic strength. Whole-cell recordings were made from the soma or apical dendrite of layer 2/3 pyramidal cells in slices of rat visual cortex. EPSPs were evoked with small bipolar electrodes placed in layer 2/3 near the apical dendrite of the cell under study. These synapses are highly enriched for NMDA receptors (Salin and Bullier, 1995), and NMDA receptor potentials (NMDAR-EPSPs) were isolated with CNQX, picrotoxin, and 1.5 m*M* $[Mg^{2+}]_o$. We observed that pairing a single action potential (AP) with a subsequent NMDAR-EPSP led to an immediate reduction in the NMDAR-EPSP amplitude within a short time window (<100 ms), correlating with the time window for induction of spike-timing-dependent long-term depression (LTD) of EPSPs at these synapses. NMDAR-EPSP suppression and LTD have a similar pharmacological profile, and both are reduced or blocked by nimodipine, calcineurin inhibitory peptide, cyclosporin A, and internal BAPTA. Additionally, we found that long-lasting depression of synaptic strength could be induced in the absence of postsynaptic spiking by a temporary wash-in of either low doses of APV (2–4 μM) or an increase in $[Mg^{2+}]_o$ (6 m*M*). In contrast, temporary wash-in of 0 m*M* $[Mg^{2+}]_o$ produced a long-lasting enhancement of synaptic strength. These results suggest that the amount of NMDA receptor activation, and thus postsynaptic Ca^{2+} influx, is a critical determinant of sign and magnitude of long-term synaptic plasticity. For layer 2/3 synapses in particular, we propose a model in which basal synaptic transmission leads to an intermediate level of Ca^{2+} influx between the levels required for LTD or long-term potentiation.

RCF is supported by the Grass Foundation and the Howard Hughes Medical Institute. YD is supported by the National Eye Institute.

Reference: *Biol. Bull.* **207:** 156. (October 2004)

The Second Transmembrane Domain 7′ Position Influences Channel Kinetics in the Glycine αI Receptor

Eric B. Gonzales[1,2] and Glenn Dillon[1]
[1]University of North Texas Health Science Center at Fort Worth, Fort Worth, Texas
[2]Grass Fellow 2004, Marine Biological Laboratory, Woods Hole, Massachusetts

The cys-loop family of ligand-gated ion channels (LGICs) consists of the nicotinic acetylcholine, serotonin type-3 (5-HT3), glycine, and $GABA_A$ receptors and is responsible for mediating rapid neurotransmission in the CNS and PNS. Several amino acid residues of the second transmembrane domain (TM2) have been shown to influence gating kinetics in members of the cys-loop superfamily. Of these receptors, the 5-HT3A and glycine receptor can form homomeric receptors. The homomeric 5-HT3A receptors have significantly slower gating kinetics. Our lab has shown that the TM2 L7′T mutation in the TM2 domain alters gating of the 5-HT3A receptor. We hypothesize that the TM2 7′ residue influences channel gating in the homomeric glycine α1 receptor. To test this hypothesis, we have systematically mutated the 7′ residue to other amino acids to assess the properties required to alter gating. Wild type and mutant Gly α1 receptors were transiently expressed in HEK 293T cells and subsequently analyzed using the whole cell patch clamp recording technique. Concentration response profiles for these receptors were determined. Glycine sensitivity is altered in each of the mutant receptors tested, differing from the wild type 29.2 μM. The Gly EC_{50} for the T7′L and T7′A mutations, in μM, are 16.9 and 777, respectively. Using a rapid solution exchange system, the activation kinetics of these receptors are significantly slower at the glycine EC_{50} concentration. The T7′L mutation exhibits slower activation and deactivation than the wild-type receptor. These results demonstrate that the TM2 7′ residue is a critical determinant of channel gating kinetics in glycine receeptors and other cys-loop families of ion channels. Understanding how these receptors function will, in time, lead to the development of novel pharmacological therapeutics.

Reference: *Biol. Bull.* **207:** 156. (October 2004)

Local Synthesis of Presynaptic RNA in Squid Optic Lobe Slices

A. Giuditta[1], M. Eyman[1], C. Cefaliello[1], E. Ferrara[1], B.B. Kaplan[2], Z. Scotto Lavina[3], and R. De Stefano[1]
[1]University of Naples "Federico II", Naples, Italy
[2]NIMH, NIH, Bethesda, Maryland
[3]SISSA, Trieste, Italy

The use of squid model systems has greatly contributed to the demonstration that active systems of protein synthesis are present in axons and nerve terminals. Furthermore, experiments with isolated or perfused giant axons have shown that axoplasmic RNA may originate from periaxonal glial cells, thus confirming the concept that a local system of gene expression is endowed to axons. We are now presenting evidence that local RNA synthesis may also concern the large presynaptic terminals of retinal photoreceptors. These terminals contain conspicuous aggregates of polysomes and are responsible for essentially all the protein synthetic activity of optic lobe synaptosomes. In view of the retinal location of photoreceptor cell bodies, we decided to prepare synaptosomes from optic lobe slices incubated in artificial seawater containing [^{3}H]uridine. Under these conditions, any radiolabeled synaptosomal RNA could only originate from local sources. The radiolabeled TCA-precipitable product obtained from the incubated slices was sensitive to alkaline and RNase degradation, and its synthesis was inhibited by actinomycin D. Our data indicated that newly-synthesized RNA was present in the synaptosomal fraction in higher amounts than in the microsomal-cytosolic fraction. Its synaptosomal association was confirmed by experiments in which the incubated slices were exposed to a hypotonic medium that selectively disrupts synaptosomes. Under these conditions, essentially all radiolabeled RNA disappeared from the synaptosomal fraction. *In vitro* analyses supported the expected disruption of synaptosomes by showing a massive loss of synaptosomal protein synthesis induced by the hypotonic treatment. Sedimentation analyses on sucrose density gradients indicated that newly synthesized synaptosomal RNA is largely localized in light regions of the gradient, while sizable amounts sediment in gradient regions marked by ribosomal particles. Our data further support the view that axons and nerve terminals are endowed with a local gene expression system requiring the strict cooperation of glial cells.

Reference: *Biol. Bull.* **207:** 157. (October 2004)

Membrane Properties of Two Subtypes of Skate Bipolar Cells

Haohua Qian[1,2], *Richard L. Chappell*[1,3], *Stephen Redenti*[1,3], *and Harris Ripps*[1,2]
[1]*Marine Biological Laboratory, Woods Hole, Massachusetts*
[2]*University of Illinois at Chicago, College of Medicine, Chicago, Illinois*
[3]*Hunter College and The Graduate Center, CUNY, New York, New York*

Bipolar cells in the vertebrate retina are second order neurons that transmit visual information from rod and cone photoreceptors to the amacrine and ganglion cells of more proximal retinal layers. In most species, they consist typically of multiple subtypes that differ in their morphology, synaptic connections, and response properties. The individual subtypes of bipolar cell are thought to carry different aspects of the visual signal through the retina, and they often exhibit unique membrane properties and neurotransmitter receptors.

The skate retina presents an unusual situation. Unlike other vertebrate species, it contains only one class of photoreceptor, namely rods; and, thus far, only two morphologically and pharmacologically distinct subtypes of bipolar cell have been identified. The large-field bipolar cells, with extensive dendritic arbors, are glycine-insensitive, whereas the small-field bipolar cells, which have only one or two dendritic branches, are sensitive to glycine. In the present study, we explored further the membrane properties of these two subtypes of skate bipolar cell. Solitary bipolar cells were obtained by enzymatic and mechanical dissociation of the skate retina, and kept in modified L-15 medium for 1 to 3 days at 14 °C. Membrane currents, measured with whole-cell patch-clamp recording techniques, revealed that the two subtypes of bipolar cell exhibited different voltage-activated current responses. Both hyperpolarizing and depolarizing command voltages activated large membrane conductances on the small-field, glycine-sensitive bipolar cells. On the other hand, large-field (glycine-insensitive) bipolar cells were much less voltage sensitive. In addition, the inward currents activated by hyperpolarizing voltages displayed faster kinetics in small-field bipolar cells than those activated in large-field bipolar cells; and a clear difference was seen in the magnitude of the TEA-sensitive potassium currents present on the two cell types. In conclusion, two morphologically distinct subtypes of bipolar cell are seen in the all-rod skate retina, and they exhibit different voltage-activated current profiles and express different populations of neurotransmitter receptors.

Support: NIH Grant EY-12028 (HQ); Fight for Sight, PSC/CUNY Grant 66257-0035, and NCRR/NIH RCMI Award RR-03037 (RLC); and NIH Grant EY-06516 and RPB (HR).

Reference: *Biol. Bull.* **207:** 158. (October 2004)

Zinc Transport in Vertebrate Retina

Stephen Redenti[1] and Richard L. Chappell[1,2]
[1]The Graduate Center, CUNY, New York, New York
[2]Hunter College, CUNY, New York, New York

Zinc transporter-protein-3 (ZnT-3) has six transmembrane domains with a histidine-rich cytoplasmic loop responsible for mediating zinc transport. Studies of the central nervous system have localized ZnT-3 primarily to glutamatergic vesicles containing up to 300 μM zinc. We initially examined the distribution of the ZnT-3 protein in the light-adapted mouse retina using immunohistochemical techniques. The ZnT-3 protein was most concentrated in the region of the outer limiting membrane and photoreceptor inner segments, a mitochondrion-rich region where disk formation occurs. Strong labeling was also observed in the inner nuclear and ganglion cell layers. Weaker ZnT-3 reaction bands were present in the inner plexiform layer. In contrast, the outer nuclear layer and photoreceptor outer segments remained clear of ZnT-3 immunoreactivity. In general, ZnT-3 appeared to be localized in regions that have previously been found reactive for ionic zinc in light-adapted murine retinas.

In the present study, to verify cellular ZnT-3 localization, we isolated mouse retinal neurons and antibody-labeled for ZnT-3. With DAB labeling, Müller cell apical villi, soma, and endfeet exhibited ZnT-3 reactivity. Using FITC label and confocal analysis, ZnT-3 protein appeared to be localized throughout the Müller cell.

The dense labeling for ZnT-3 in the photoreceptor inner segment region has been puzzling since this is not a likely site for synaptic vesicles. It is, however, a location rich with the apical villi of Müller cells which may well account for this labeling. In fact, the Müller cell soma and endfeet are also present in other retinal layers reactive for ZnT-3, where they may also contribute to labeling observed. Based on these findings, it seems possible that Müller cells utilize ZnT-3 to regulate retinal zinc homeostasis.

Support: Fight for Sight, PSC/CUNY Grant 66257-0035, and NCRR/NIH RCMI Award RR-03037 (RLC).

Reference: *Biol. Bull.* **207:** 158–159. (October 2004)

Histidine Suppresses Zinc Modulation of Connexin Hemichannels Expressed in *Xenopus* Oocytes

Richard L. Chappell[1,2], Haohua Qian[1,3], Jane Zakevicius[1,3], and Harris Ripps[1,3]
[1]Marine Biological Laboratory, Woods Hole, Massachusetts
[2]Hunter College and The Graduate Center, CUNY, New York, New York
[3]University of Illinois College of Medicine, Chicago, Illinois

We showed previously that zinc modulates hemichannel currents of connexins (Cx35 and Cx38) expressed in *Xenopus* oocytes. In both cases the effects were biphasic; low concentrations of zinc enhanced, whereas higher concentrations decreased, current response magnitudes. The present study was designed to determine the effects of zinc on hemichannels formed by Cx26, a connexin expressed on dendrites of carp horizontal cells. In addition, we examined whether histidine, a zinc chelator, blocked the action of zinc or exerted a direct effect on Cx26 hemichannel currents.

Unlike results obtained with Cx35 or Cx38, the I-V curves of Cx26 hemichannels were constitutively open, gave large currents in response to both hyperpolarizing and depolarizing voltages, and had no evidence of outward rectification. Nevertheless, hemichannel currents mediated by Cx26 exhibited similar biphasic effects in response to increasing zinc concentrations, but with different sensitivities to zinc. Cx26 hemichannel currents were larger in 1 μM zinc than in control solutions, but progressively suppressed at higher concentrations. Current recovery after zinc application was very slow, taking up to 15 min following 1 mM zinc. Moreover, the zinc chelator histidine (1 mM) completely blocked the action of zinc (100 μM) but had no direct effect on hemichannel currents.

A recent hypothesis based on evidence from carp retina holds that currents through Cx26 hemichannels on horizontal cell dendritic processes serve to modulate calcium currents and related photoreceptor transmitter release *via* an ephaptic current within the synaptic region. The process is presumed to play a significant role in center-surround organization of distal neurons. We suggest that, if these channels were modulated by zinc as described here, the vesicular co-release of zinc and glutamate presumed to occur at the photoreceptor terminal could contribute to adaptive processes that involve the slow components of visual adaptation. Similar mechanisms involving zinc modulation of

hemichannels may be important elsewhere in the nervous system as well.

Support: Fight for Sight, PSC/CUNY Grant 66257-0035, and NCRR/NIH RCMI Award RR-03037 (RLC); NIH Grants EY-06516 (HR), EY-12028 (HQ), and RPB (HR).

Reference: *Biol. Bull.* **207:** 159. (October 2004)

Memory Enhancement by Bryostatin in *Hermissenda*

Andrew B. Scioletti[1], Alan M. Kuzirian[1], Herman T. Epstein[1], Thomas J. Nelson[2], and Daniel L. Alkon[2]

[1]Marine Biological Laboratory, Woods Hole, Massachusetts

[2]Blanchette Rockefeller Neuroscience Institute, Johns Hopkins University, Rockville, Maryland

Memory acquisition and information and behavioral recall are fundamental processes of great interest. Studies are being conducted in many model systems including marine molluscs like *Aplysia californica* and *Hermissenda crassicornis*.

Recently, the anti-cancer drug bryostatin has been found to enhance memory recall in rodent systems. Bryostatin is known to activate autophosphorylation of protein kinase-C (PKC), an enzyme implicated in memory formation. In *Hermissenda*, phosphorylated PKC activates calexcitin, a GTP/Ca^{2+}-binding protein that triggers calcium release from internal stores while concurrently inhibiting two voltage-dependent outward K^+ currents. The rise in internal Ca^{2+} coupled with a decrease in K^+ currents is putatively responsible for the enhanced long-lasting depolarization (LLD) shown in *Hermissenda* type B-cell photoreceptors to be associated with memory acquisition.

Hermissenda can be trained and tested using a Pavlovian conditioning regime of light (CS) paired with agitation (US) (paired training event, TE). Previous studies have shown that two TEs produced short-term memory (STM) lasting 7 min. Nine TEs produced long-term memory (LTM; present at 60 min and lasting one day) that ultimately led to consolidated LTM (CLTM; present at 220 min and lasting up to 6 days). In this study, experimental animals exposed to low bryostatin concentrations (0.1–0.25 ng/ml) and two TEs (that normally evoke only STM) demonstrated the enhanced memory stage of LTM. Both four and six TEs (that normally do not generate LTM) tested positively for CLTM with bryostatin added. Nine TEs coupled with bryostatin at a high concentration (1.0 ng/ml), however, down-regulated memory acquisition; and the animals exhibited no conditioned response with CS testing. These findings will help elucidate knowledge about memory acquisition, storage, and retrieval; contribute information that can be used to answer fundamental questions pertaining to education and more effective teaching methods; and mediate memory-related pathologies like Alzheimer's disease and other forms of dementia.

Reference: *Biol. Bull.* **207:** 160. (October 2004)

Marine Plants May Polarize Remote *Fucus* Eggs *via* Luminescence

Lionel F. Jaffe
Hopkins Marine Station, Pacific Grove, California and Marine Biological Laboratory, Woods Hole, Massachusetts

Fucus zygotes can be polarized—as shown by their later outgrowth directions—by many environmental influences. These include those exerted by all tested intertidal marine plants (including all of the main algal phyla as well as the flowering plant *Phyllospadix*) at distances of up to 5–10 mm away from a piece of the plant in a laboratory dish. Earlier studies inferred action *via* diffusing molecules. A reinvestigation indicates that such actions can be exerted *through* glass barriers and suggests action *via* luminescent and, perhaps, infrared signals. Since this polarizing influence is exerted by pieces of all tested plants, the infrared light signals might be emitted by luminescent bacteria growing in biofilms on the surfaces of all intertidal plants.

Reference: *Biol. Bull.* **207:** 160. (October 2004)
© 2004 Marine Biological Laboratory

Characterization of Anastral, Bipolar Spindle Development and Atypical Cytokinesis in Ammonia-Activated Sea Urchin Eggs

John H. Henson[1,2], Jessica E. Davis[2], Charles B. Shuster[1,3], Christopher A. Fried[1,2], and Calvin R. Simerly[4]
[1]Marine Biological Laboratory, Woods Hole, Massachusetts
[2]Dickinson College, Carlisle, Pennsylvania
[3]New Mexico State University, Las Cruces, New Mexico
[4]Magee Women's Research Institute, Pittsburgh, Pennsylvania

The mitotic apparatus (MA) of the early sea urchin embryo is often cited as the classic example of an aster-dominated MA that is organized *via* the introduction of a sperm-derived paternal centrosome. Previous studies have indicated that artificial activation of eggs can result in polymerization of microtubules associated with maternal centrosomal material, with the microtubule organization often taking the form of a monaster associated with condensed chromosomes. In the present study we have examined the generation of unusual bipolar spindle-like structures in eggs artificially activated with ammonia. Unfertilized sea urchin (*Lytechinus pictus*) eggs were activated by incubation in artificial seawater containing 15 m*M* ammonia chloride and fixed with cold methanol at the time appropriate for first division. The activated eggs were stained with antibodies against tubulin, actin, NuMA, centrosomal proteins, and the kinesin-like proteins Kif2, KRP_{110} and KRP_{170}, and stained cells were viewed on a laser-scanning confocal microscope. The majority of activated eggs demonstrated poorly organized microtubules and/or the presence of monasters, but a subset contained atypical bipolar spindle-like structures. These spindles were small, anastral, capable of anaphase-like chromosome segregation, and overall very reminiscent of meiotic spindles. The spindle matrix protein NuMA, the centrosomal protein 4D2, and the spindle motor proteins Kif2, KRP_{110} and KRP_{170} all localized to these structures. The ammonia-induced spindles were also observed in living eggs using polarization optics on an LC-PolScope (courtesy of Rudolf Oldenbourg and Grant Harris of the Marine Biological Laboratory). The activated eggs went on to attempt cytokinesis, which often involved unusual linear arrays of microtubules in the region of the developing cleavage furrow. These results suggest that microtubule motor and matrix proteins have the ability to organize a meiotic-like spindle in sea urchin eggs in the absence of the paternal centrosome.

Reference: *Biol. Bull.* **207:** 161. (October 2004)

Actin-Mediated Retrograde Flow in Sea Urchin Coelomocytes: Conversion From a Lamellipodial-Dominated to a Filopodial-Dominated Form

Christopher A. Fried[1,2], *Michelle Reina*[2], *and John H. Henson*[1,2]
[1]*Marine Biological Laboratory, Woods Hole, Massachusetts*
[2]*Dickinson College, Carlisle, Pennsylvania*

Sea urchin coelomocytes undergo extensive actin-based retrograde flow, mediated in part by the Arp2/3 complex-facilitated polymerization of a dendritic brushwork of actin filaments in a wide lamellipodium. In the present study we have experimented with changing this lamellipodial-based flow pattern into one that resembles the filopodial-dominated pattern present in neuronal growth cones. We have previously shown that the drug BDM displaces the Arp2/3 complex from the coelomocyte edge and results in a retraction of the actin dendritic meshwork. Digital video, fluorescence, and electron microscopy reveal that the edges of BDM-treated cells contain an array of unbranched, elongate, and tangentially oriented actin filaments that appear to be produced *de novo* from the cytoplasmic face of the plasma membrane. Ultrastructure of control cells suggests that these elongate filaments are present, but they are masked by the dense Arp2/3 complex-dependent brushwork. Application of cytochalasin D to BDM-treated cells halts the generation of these elongate filaments, implying that they are a product of an Arp2/3 complex-independent form of actin polymerization. Coelomocytes can be transformed from a lamellipodial to a filopodial state by hypotonic shock, and this treatment can result in the cessation of retrograde flow. Interestingly, combinations of BDM and hypotonic shock induce a growth-cone-like and filopodial-dominated form of actin-based retrograde flow in coelomocytes. Recent studies have suggested that growth cone motility is Apr2/3 complex-independent and Ena/VASP-dependent. Therefore, we hypothesize that the induction of growth-cone-like retrograde flow in coelomocytes results from BDM-based displacement of the Arp2/3 complex from the cell edge, combined with hypotonic shock stimulating Ena/VASP activity and/or inhibiting actin capping protein.

Reference: *Biol. Bull.* **207:** 161. (October 2004)
© 2004 Marine Biological Laboratory

Cell Division Dynamics of *Drosophila* Kc Cells Without Functional Mitotic Centrosomes

Yuki Kagawa[1], *Timothy L. Megraw*[2], *and Rudolf Oldenbourg*[1]
[1]*Marine Biological Laboratory, Woods Hole, Massachusetts*
[2]*University of Texas Southwestern Medical Center, Dallas, Texas*

We observed mitosis and cytokinesis of *Drosophila* Kc cells without functional mitotic centrosomes and compared our results to control cells to elucidate the roles of centrosomes in cell division dynamics. Using double-stranded RNA-mediated interference (RNAi), we suppressed the expression of centrosomin (Cnn), a core component of centrosomes. Cells without centrosomin can form a functional bipolar spindle and even develop to a complete organism (Megraw *et al.*, 2001). Here we used the LC-PolScope to observe the dynamics of the mitotic spindle in Kc cells during cell division. The LC-PolScope can detect birefringence of biological materials such as microtubules (MTs) in living cells without staining (Oldenbourg and Mei, 1995). During mitosis, the morphology and dynamics of the spindle in RNAi-treated cells were very similar to those in control cells, including our observations of chromosome segregation during anaphase. After anaphase, we found birefringent fibers between segregated sister chromatids in both RNAi-treated and control cells. In some RNAi-treated cells, we found that these birefringent fibers (probably microtubule bundles) are spread out to the inner surface of the cell; we didn't find such movement of birefringent fibers in the control cells. We speculate that this movement might be caused by the release of strain in the fibers. Our experimental findings indicate that the dynamics of the central spindle are changed in the RNAi-treated cells. We also found that most cells produce blebs on their surface during cell division in both RNAi-treated and control cells. We analyzed the rate of blebbing by using a time series of the complexity of the cell shape and found that there is little difference in the blebbing rate between the RNAi-treated and control cells.

This work is supported by the Japan Science and Technology Agency and the National Institutes of Health (EB002583).

Reference: *Biol. Bull.* **207:** 162. (October 2004)

Immunocytochemical Detection of Integrins α_3 and β_1 in Allografts of the Marine Sponge, *Microciona prolifera*

Clarissa A. Sabella[1], Ellen E. Faszewski[2], Jane C. Kaltenbach[1], William J. Kuhns[3], Max M. Burger[4], and Xavier Fernandez-Busquets[5]
[1]Mount Holyoke College, South Hadley, Massachusetts
[2]Wheelock College, Boston, Massachusetts
[3]Hospital for Sick Children, Toronto, Canada
[4]Friedrich Miescher Institute, Basel, Switzerland
[5]University of Barcelona, Barcelona, Spain

Integrins are a widely expressed family of cell surface adhesion receptors whose existence in sponges, the oldest extant Metazoan phylum, has been clearly established. In sponges, cell adhesion is mainly achieved through species-specific interactions of a type of proteoglycan molecule termed aggregation factor (AF). The deglycosylated AF protein in the marine sponge *Microciona prolifera* was cloned in our prior work and found to contain the integrin-binding motif RGD. In subsequent grafting experiments, we observed that antibodies raised against this protein detected a type of sponge stem cell, the archeocyte, that accumulated in the contact zone of allografts (between tissue from different individuals), but not of isografts (between genetically identical tissues). A similar distribution was observed for another type of sponge cell, the gray cell, which is specifically recognized by antibodies raised against the hyaluronan receptor CD44, also implicated in cellular adhesion. We also showed that immunoblots of *M. prolifera* cell membrane proteins revealed the presence of specific bands decorated by antibodies raised against mouse integrins α_3 and β_1. The purpose of the present work was to determine the distribution of α_3 and β_1 integrins in sponge grafts by means of immunocytochemical experiments. Double-staining experiments of allografts show colocalization of integrin and CD44 in the same cells concentrated at the zone of contact. Furthermore, epithelial pinacocytes do not express either integrin, but the internal core of the sponge (mesohyl) is abundant in cells that stain very strongly for α_3. The β_1 staining was much weaker but reached levels similar to those of α_3 if the tissue was desulfated prior to immunodetection. Since deglycosylated AF (archeocyte marker) will be more likely to have the RGD sequence exposed, we hypothesize that AF proteins expressed in archeocytes might interact with integrins expressed in gray cells in the initial stages of allogeneic recognition.

Funding was provided for Clarissa Sabella by HHMI (#71100-505003)

Reference: *Biol. Bull.* **207:** 162. (October 2004)
© 2004 Marine Biological Laboratory

Mitochondrial Dynamics in Synaptic Plasticity in *Drosophila melanogaster*

James Jiayuan Tong
Grass Fellow 2004, Marine Biological Laboratory, Woods Hole, Massachusetts
Center for Molecular and Mitochondrial Medicine and Genetics, University of California, Irvine, California

Mitochondria play a central role in a variety of cellular processes, including ATP generation by oxidative phosphorylation, production of toxic reactive oxygen species (ROS) as a by-product, robust regulation of calcium homeostasis inside the cell, and the initiation of apoptosis through the activation of the mitochondrial permeability transition pore (mtPTP). Genes that reduce ROS production and improve mitochondrial respiration extend the life span in *Drosophila* and mice. The pattern of mitochondrial motility underlies their essential role in providing ATP and regulating calcium homeostasis in the neuron, a functionally polarized and highly elongated cell. To identify the role of mitochondria in synaptic plasticity and memory, we studied mitochondrial dynamics in *Drosophila* 3rd instar larval motor axons and at neuromuscular junction synapses. Bidirectional and saltatory mitochondrial movements with variable stationary phases have been observed in motor axons using mito-GFP targeted to cytochrome *c* oxidase expressed in the fly nervous system, mitoTracker red, and TMRE. Adenine Nucleotide Translocator (ANT) mutant *sesB* showed reduced mitochondrial motility. Cell permeable cAMP analog, 8-bromo-cAMP (0.1 m*M* bath application), increased axonal mitochondrial movements and restored the mitochondrial motility in the *sesB* mutant. Neurofibromatosis-1 (NF1) expression, which extends the fly life span by 50% through cAMP/PKA/complex I signaling, showed an increased mitochondrial motility. At synapses, mitochondria "docked" at presynaptic boutons with occasional oscillatory movements. Genetic, pharmacological, and electrophysiological manipulations that alter synaptic functions are being explored to reveal the unique and essential role of mitochondria in synaptic plasticity. Photoactivating mito-GFP expressed in the neuroblastoma cell enables us to track single mitochondrial dynamics, including fusion and fission between mitochondria, and their interaction with the mitochondrial network in combination with the membrane potential indicator TMRE. A photoactivating mito-GFP construct is being constructed to monitor individual mitochondria and the mitochondrial network in synaptic plasticity and memory consolidation.

Reference: *Biol. Bull.* **207:** 163. (October 2004)

Role of Rab GTPases in Recruitment of Myosin-V to Vesicles of Squid Giant Axon

Sung Min You[1], Clarissa Cheney[2], Agnieszka Swiatecka-Urban[1], and George M. Langford[1]
[1]Dartmouth College, Hanover, New Hampshire
[2]Pomona College, Claremont, California

Myosin-V, an actin-based motor, is responsible for short-range axonal/dendritic transport in neurons. Recent studies have shown that Rab GTPases are required for the recruitment of myosin-V to vesicles. However, the Rab GTPase responsible for myosin-V recruitment to axoplasmic vesicles in the squid giant axon has not been determined, although our earlier data showed Rab GTPases are required for myosin-V-mediated vesicle transport. In this report, we provide additional evidence that Rab GTPases are required for the transport of axoplasmic vesicles in the squid giant axon. To study the role of Rab GTPases in myosin-V-mediated vesicle transport, a GST-labeled Rab-GDI was used in motility assays and affinity isolation experiments. A plasmid containing full-length cDNA for *Drosophila* GST-Rab-GDI (a gift from Dr. C. Cheney) was expressed in *E. coli*. The 75 kDa GST-tagged protein was purified on a GST affinity column and used in pull-down experiments with either clarified squid brain homogenates or FLAG-tagged Rab 11a transfected HEK cell lysates. Blots of the affinity isolated fractions were probed with either anti-Rab3a antibody or anti-Flag antibody. Motility assays using AVEC-DIC microscopy were performed with GST-Rab-GDI to determine whether vesicle transport in the squid giant axon is inhibited. Motile activity at 3.0 μM GST-Rab-GDI decreased from 36 $\pm$ 5 in the control assay to 15 $\pm$ 7 v/f/m. Therefore, GST-Rab-GDI inhibited vesicle transport by 58% at this concentration. At 8.0 μM GST-Rab-GDI, motile activity decreased by 88%. These data confirm that Rab activity is required for myosin-V-mediated vesicle transport in the axon. Although the Rab-GTPase responsible for Myosin-V-mediated axoplasmic vesicle transport was not identified, pull-down experiments using Rab-GDI provided potential candidate proteins. These data are consistent with published results showing that myosin-V is recruited to vesicles by Rab GTPases.

Supported by NSF Grant IBN-0131470, Dartmouth College Richter Grant, and MBL-Shifman Award to SMY.

Reference: *Biol. Bull.* **207:** 163. (October 2004)
© 2004 Marine Biological Laboratory

Isolation of the Myosin-V/Kinesin Heteromotor Complex by Sucrose Gradient Fractionation

John Paul Flores, Y. L. Lee, and George M. Langford
Dartmouth College, Hanover, New Hampshire

The molecular motors myosin-V and kinesin form a complex to transport vesicles within the neuron. Vesicles move long distances along microtubule tracks using kinesin motors and then switch to actin filaments for short distance movement using myosin-V motors. Affinity isolation of native kinesin with a glutathione S-transferase-tagged myosin-V globular tail fusion protein provided evidence that the two proteins can interact with one another to form a heteromotor complex. This complex provides a mechanism by which one motor can regulate the activity of the other, enabling vesicles to switch easily from one track to the other. Although the myosin-V/kinesin interaction has been shown, binding partners of the complex remain unknown. In this study, experiments were designed to isolate and identify proteins within the heteromotor complex from squid brain. Squid optic lobe extracts were loaded onto a 5%–30% linear sucrose gradient and spun at 200,000 *g* for 14 h. Fractions from the gradient were analyzed by SDS-PAGE and probed for the presence of myosin-V and kinesin *via* immunoblot. The peak fractions containing both motors of the complex were analyzed further by two-dimensional gel electrophoresis. The 2-D gels revealed approximately 50 protein spots between 30 and 66 kDa and isoelectric points in a pH range of 4–10. Approximately 10 spots in the peak fraction were enriched relative to the extract, and these proteins will be identified by N-terminal sequencing. No high molecular weight bands were visible on the blots in this pH range. Our previous studies have shown that enolase, α- and β-tubulin, and elongation factor 1β are myosin-V binding partners by affinity isolation. The sucrose density gradient fractionation provides an additional method to isolate binding partners of myosin-V.

Supported by NSF Grant IBN-0131470, Dartmouth College Richter Grant, and MBL-Shifman Award to JPF.

Reference: *Biol. Bull.* **207:** 164. (October 2004)

Identification of Novel Myosin-V Binding Partners by Immunoprecipitation and Column Chromatography

Carl J. DeSelm[1], R. Lu[2], C. M. Cheney[3], and George M. Langford[1]
[1]Dartmouth College, Hanover, New Hampshire
[2]Boston Biomedical Research Institute, Watertown, Massachusetts
[3]Pomona College, Claremont, California

Myosin-V, an actin-based motor, and kinesin, a microtubule-based motor, interact to form a "heteromotor" complex. The proteins that couple the heteromotor complex to neuronal vesicles have not been determined. The goal of this study is to identify novel binding partners of the myosin-V/kinesin heteromotor complex in the neuron.

To identify proteins involved in myosin-V/kinesin binding to neuronal cargo, we used a recombinant glutathione S-transferase-labeled globular tail domain of myosin-V (GST-GTD) in immunoprecipitation and column affinity chromatography experiments. Immunoprecipitations were performed using bacterially expressed GST-GTD incubated with clarified squid brain extract. Proteins bound to GST-GTD were separated by SDS-PAGE and individually sequenced. As a complementary method for isolating myosin-V binding partners, an affinity column was generated by attaching GST-GTD to a GSTrap column. Clarified squid brain was applied to the affinity column. After two washes, proteins bound to GST-GTD column were eluted, separated by 2-D gel electrophoresis, and sequenced.

The proteins identified by peptide sequence analysis as myosin-V binding partners in squid brain were elongation factor-β (EF-1β), enolase, and α- and β-tubulin. Although the functional significance of these interactions has yet to be determined, it is known that localization of elongation factor-1 to activated synapses is important for maintaining long-term potentiation. The translocation of EF-1β to the synapse may be myosin-V dependent. In addition, enolase, a glycolytic enzyme, diffuses across the cell membrane at high rates when the neuron is damaged. Myosin-V may be involved in transporting this enzyme to the cell cortex. The association of tubulin dimers in microtubules with the tail of myosin-V may provide a mechanism for linking the actin and microtubule cytoskeletons. Characterizing these interactions will be important in understanding novel roles of myosin-V in memory and in understanding the diversity of cargo transported by this molecular motor in neurons.

Supported by NSF Grant IBN-0131470 and NIH NS-040493.

Reference: *Biol. Bull.* **207:** 164. (October 2004)
© 2004 Marine Biological Laboratory

Anterograde Transport of Peptide-Conjugated Fluorescent Beads in the Squid Giant Axon Identifies a Zip-Code for the Synapse

Michael P. Conley[1,2], Marcus K. Jang[1,2], Joseph A. DeGiorgis[1,3], and Elaine L. Bearer[1,2]
[1]Marine Biological Laboratory, Woods Hole, Massachusetts
[2]Brown University, Providence, Rhode Island
[3]NIH, NINDS, Bethesda, Maryland

The giant axon of the squid has long served as a model system to study physiological events common to neuronal systems in many species and also active in most other eukaryotic cells. These physiological events include ion currents and vesicular transport. Endogenous transport vesicles move in the axon for up to six hours after dissection. Mid-size squid organelles 0.2–0.53 μm in diameter are transported in axoplasm at average velocities of 1.1 μm/s, whereas larger particles (>0.5 μm diameter), mostly mitochondria, move more slowly (0.2 μm/s). A major question in neurophysiology is how synaptic components are transported to the pre-synaptic terminal. The giant axon of the squid provides an assay for the molecular requirements of this transport that are highly conserved at the sequence level across species. The first microtubule-based motor, kinesin, was discovered in the squid axon and subsequently found in most other organisms. We are using the giant axon to uncover the molecular mechanisms of cargo/motor interactions. First, using GFP-labeled human herpes virus (HSV1) as a tool, we reconstituted HSV transport in both directions in the squid axon. Then we discovered that HSV particles moving in the anterograde direction are associated with cellular amyloid precursor protein (APP). Two summers ago we discovered that a peptide from the cytoplasmic C-terminus of APP (C-APP) is sufficient to move 100 nm beads in the axon towards the synapse at fast transport rates (0.9 μm/s), whereas uncoated negatively charged beads move rarely and slower (0.08 μm/s); and beads coated with other peptides do not move. This summer we are using multi-spectral imaging to observe many different colored beads simultaneously to screen a peptide library for transport activity in the giant axon. Thus the giant axon of the squid serves as a reliable assay to identify the molecular mechanisms of motor recruitment.

Supported by NINDS (E.L.B.).

Reference: *Biol. Bull.* **207:** 165. (October 2004)

Imaging Patterns of Ca^{2+} Transients During the Blastula Period in Zebrafish Embryos

Omicron L. Ma, Sarah E. Webb, and Andrew L. Miller
The Hong Kong University of Science and Technology, Hong Kong, People's Republic of China

It has been suggested that Ca^{2+} events occuring during the blastula period of zebrafish development might be involved in mediating the cell-to-cell adhesion between the enveloping layer (EVL) cells and/or might somehow play a role in dorsoventral patterning of the embryo. Using the Ca^{2+}-sensitive luminescent reporter, aequorin, and a custom-designed photon imaging microscope (PIM), we have started to re-investigate the patterns and possible functions of the blastula period Ca^{2+} transients. We have demonstrated that distinct Ca^{2+} transients occur throughout this period in small, localized cellular domains. When these transients were characterized with respect to time, they were found to occur with the highest frequency in a 75-minute window, from the 512-cell stage to about the sphere stage. A data analysis protocol was designed such that the imaged embryos were divided into quadrants "dorsal/ventral/left/right," and the Ca^{2+} transients from each quadrant were then quantified with respect to time. Analysis indicates that during the period of high Ca^{2+} transient frequency, a greater number of Ca^{2+} events occur in the "dorsal" quadrant of the embryo. In addition, using the fluorescent Ca^{2+} reporter Oregon Green 488 dextran (10 kDa) and two-photon confocal microscopy, we showed that the Ca^{2+} transients appear to be confined exclusively to the EVL. This suggests that this peridermal layer may play some as yet undescribed role in the signaling cascades that determine the developmental fate of the underlying embryonic deep cells. Furthermore, we demonstrated by transmission electron microscopy that the EVL cells, but not the deep cells, possess abundant mitochondria, which are asymmetrically distributed to the inner portion of the EVL cell that adjoins the underlying deep cell population.

Supported by RGC-CERG grants HKUST6106/01M, HKUST6214/02M and HKUST6279/03M.

Reference: *Biol. Bull.* **207:** 165. (October 2004)
© 2004 Marine Biological Laboratory

Role of Ca^{2+} Signaling During Early Pronephric Development in Zebrafish and *Xenopus* Embryos

Andrew L. Miller[1], Catherine Leclerc[2], Marc Moreau[2], and Sarah E. Webb[1]
[1]The Hong Kong University of Science and Technology, Hong Kong, People's Republic of China
[2]Centre de Biologie du Développement, Université Paul Sabatier, Toulouse, France

Recent studies from vertebrates have implicated a Ca^{2+}-dependent signaling pathway in normal kidney development, because the loss of function in either of two Ca^{2+}-related proteins is known to result in abnormal kidney development resulting in polycystic kidney disease. We have begun a study to image Ca^{2+} signaling during the formation of the pronephros (the functional embryonic kidney) in both intact zebrafish and *Xenopus laevis* embryos, as well as in *Xenopus* animal caps that are isolated at the blastula stage and induced to differentiate into pronephric tubules by incubation with retinoic acid (RA) and activin A (AA). By loading embryos with the Ca^{2+}-sensitive luminescent reporter, aequorin, and using a custom-designed photon-imaging microscope to continually visualize the Ca^{2+} signaling patterns, we are currently generating spatial and temporal maps of the Ca^{2+} signals that occur during pronephric formation in these two intact model systems, as well as in animal caps. Furthermore, we have begun to explore the requirement for, and the function of, these Ca^{2+} transients. We loaded intact *Xenopus* embryos with the caged calcium chelator, diazo-2, specifically into blastomeres that are known to develop into the pronephros. When the diazo-2 is uncaged at the earliest stages of pronephros development, the tubules that form are abnormal. In addition, tubulogenesis is inhibited in animal caps (incubated with RA and AA) that are treated with BAPTA. Furthermore, when intact zebrafish embryos are incubated with the L-type calcium channel blocker nifedipine for the first 60 hours of pronephros development, tubule formation is once again inhibited; and the ducts that develop are longer and narrower than the untreated controls. Our preliminary results thus support the proposal that Ca^{2+} signaling plays a crucial role in kidney formation and that zebrafish and *Xenopus* embryos provide suitable models to image Ca^{2+} dynamics during organogenesis.

Reference: *Biol. Bull.* **207:** 166. (October 2004)

MAP Kinase Expression Correlates With the Posterior Midline in Early Cleavage Stage Squid Embryos

Karen Crawford
Marine Biological Laboratory, Woods Hole, Massachusetts; and St. Mary's College of Maryland, Maryland

Classical experiments performed on gastropod embryos demonstrate that the D macromere plays a critical role in axial patterning as the founder cell of the dorsal lineage. Recently, MAP kinase (MAPK) signaling cascades in the gastropod *Ilyanassa obsoleta* have been linked to cell fate specification within the D macromere lineage and the micromeres of the A, B, and C quadrants (Lambert and Nagy, 2001). To determine whether a similar signaling mechanism is present in the long-finned squid, *Loligo pealei*, early cleavage stages and blastoderm stage embryos were studied by immunocytochemistry.

First cleavage bisects the squid embryo along its midline, while second cleavage separates the anterior and posterior regions. One- and two-cell stage embryos did not exhibit MAPK expression. Following second cleavage, MAPK was observed in the two posterior blastomeres. Expression was greatest along the first cleavage furrow or posterior midline, appearing more intensely in embryos fixed just prior to third cleavage. With third cleavage, MAPK was found exclusively within the two posterior midline macromeres. In living squid embryos, these cells undergo a delayed cleavage in comparison to the rest of the cells within the embryo. Departure from synchronous cleavage is characteristic of the D-lineage cells of gastropods. Just before sixth cleavage MAPK expression is restricted to the six central micromeres destined to form the shell gland primordia at the dorsal-most tip of the embryo. The D-lineage in gastropods also contributes early to the shell gland primordia. In later blastoderm stage embryos, MAPK expression is found in just two posterior cells; it fades while, with the onset of epiboly, an outer MAPK positive ring of cells begins to form. These results provide the first molecular support for the classic notion that squid possess mirror image A, B, C, and D quadrants organized along their first cleavage furrow, as described in *Cephalopoda*, by Adolf Naef in 1928.

Supported by a Faculty Development Grant and Aldom-Plansoen Distinguished Endowed Professorship in Contemporary Studies to K.C. from St. Mary's College of Maryland, and by Robert Baker (MBL and NYU).

Reference: *Biol. Bull.* **207:** 166. (October 2004)

Gill and Lung Rhythm in the Late-Stage Tadpole *Rana catesbeiana*

Mark H. Shalinsky and James Leiter
Dartmouth College, Hanover, New Hampshire

The late-stage tadpole, *Rana catesbeiana*, metamorphoses from an aquatic to a terrestrial animal, and during this period there are extreme changes in the respiratory system. Preliminary results show that there are differences in the electrical activity of the respiratory system between different late-stage tadpoles. Previous reports have shown that the massed neurogram activity from cranial nerves (CN) V, VII, IX, and X (trigeminal, facial, glossopharyngeal and vagus nerves respectively) and from spinal nerve (SN) II (analogous to CN XII, hypoglossal nerve in mammals) in the isolated tadpole brainstem generate neural bursts that correspond to the lung and gill ventilator activities generated in the intact specimens. In this study, recordings from CN VII and SN II were conducted to discern fictive lung from gill rhythms. Bath application of a μ-opioid agonist known to affect the respiratory rhythm in mammals differentially affected both the fictive gill and lung rhythms. Concurrently, an extracellular electrode was used to probe and isolate regions correlated with either fictive gill or lung rhythm (rostral to SN II and caudal to CN VIII). Once isolated, some populations showed sensitivity when the pH was changed from normocapnia (pH 7.8/1.5% CO_2) to hypercapnia (pH 7.2/5% CO_2). Finally, iontophoresis of Pontamine Sky Blue and subsequent sectioning of the tissue into 100 μm thick slices was used to identify the location of the extracellularly recorded population. This work will lead to a greater understanding of how the electrical circuitry and activity of a developing system (lung ventilaton) interacts with one that is already in place (gill ventilation).

The Grass Foundation supported this work through the Grass Fellowship Program.

Reference: *Biol. Bull.* **207:** 167. (October 2004)

Characterization of the Myostatin-Like Gene in *Argopecten irradians*

Adam Bissonnette[1] and Steven Roberts[2]
[1]Saint Anselm College, Manchester, New Hampshire
[2]Marine Biological Laboratory, Woods Hole, Massachusetts

The bay scallop, *Argopecten irradians*, is a marine bivalve with significant commercial and scientific importance, primarily as a result of the species' large adductor muscle. Recently, a myostatin-like transcript (sMSTN) has been isolated from this species. Myostatin is a member of the transforming growth factor β superfamily and has been shown to be an important negative regulator of muscle growth in several vertebrate species. To date, the function of the myostatin-like gene in invertebrates is undetermined. Therefore, the purpose of the present study was to further understand the role of this gene by 1) determining genomic structure of sMSTN and 2) quantifying the effects of treating bay scallops with a myostatin inhibitor (Myo-Blast: Cytodyne). To determine the genomic structure, a nested PCR-based genome-walking technique was performed. Briefly, oligonucleotide primers were designed corresponding to the 5′- and 3′-ends of sMSTN; and together with arbitrary primers (DW-ACP1, 2, 3, and 4 - SeeGene), two major PCR products were amplified (>1500 bp). The second approach was carried out on two groups of animals: experimentals and controls (n = 15, each). For three days, during two 2-hour treatment sessions per day, the two groups of animals were placed in containers containing non-flowing, but aerated, ambient seawater. Myo-Blast powder suspended in 250 ml of seawater was added to the experimental containers, while the controls received seawater only. After the three days of treatment, a differential display technique was used to identify the genes that had been regulated in the treated scallops, but not in the controls. Initial results indicate that a cyclin-T homologue in bay scallops is down-regulated in treated animals, suggesting possible differences in cell cycle activity between treated and control bay scallops. These results suggest that the MSTN gene has been conserved through evolution and could function *via* a molecular mechanism similar to that observed in mammals.

The work described here was supported by USDA grant 2003-35206-12834 (to SBR).

Reference: *Biol. Bull.* **207:** 167. (October 2004)

Use of the Split-Ubiquitin Two-Hybrid System to Identify Proteins Interacting With the Alzheimer Proteins APP and LRP

Rebecca Vitale and Joseph D. Buxbaum
Mount Sinai School of Medicine, New York, New York

Two proteins that have been strongly implicated in the pathology of Alzheimer's disease are the Alzheimer amyloid protein precursor (APP) and the LDL receptor-related protein (LRP). Both of these transmembrane proteins undergo cleavage in the intra-membranous domain by a presenilin/γ-secretase complex, releasing a cytoplasmic peptide. With APP this cleavage contributes to the release of the Aβ peptide, the peptide found in the extracellular plaques characteristic of Alzheimer's disease. LRP is a large (approximately 600 kDa) endocytic receptor with four clusters of ligand-binding repeats. The function of the cytoplasmic peptides cleaved from APP and LRP is still unclear. Notch is another transmembrane protein that undergoes cleavage in the intra-membranous domain by the presenilin/γ-secretase complex. The cytoplasmic peptide released from Notch goes to the nucleus where it interacts with an obligate binding partner from the CSL family of DNA-binding proteins to activate transcription. We are using a novel (split-ubiquitin) yeast two-hybrid approach, which allows for the use of transmembrane proteins as baits, to identify proteins interacting with the cytoplasmic domains of APP and LRP. Traditional yeast two-hybrid approaches have identified the FE65 family of proteins as APP-interacting proteins. Using the split-ubiquitin system, we confirmed that these proteins could be isolated from a mouse brain library as APP-interacting proteins. We are now characterizing additional clones from the APP and LRP screens to identify novel interacting proteins that may contribute to the function and/or processing of these proteins.

Reference: *Biol. Bull.* **207:** 168. (October 2004)

Evolution of Myelin Proteins

Robert M. Gould[1,2], Hilary Morrison[3], Robert Campbell[2], and Edwin Gilland[2]
[1]University of Illinois at Chicago
[2]Marine Biological Laboratory, Woods Hole, Massachusetts
[3]Bay Paul Center for Molecular Evolution, Marine Biological Laboratory, Woods Hole, Massachusetts

The myelinated nervous system arose in a common ancestor of all modern-day gnathostomes (jawed animals). Modern-day agnathans (jawless animals, *i.e.*, lamprey and hagfish) have nervous systems that contain large axons surrounded by glial cells, but no myelin. In order for myelination to evolve, both neurons and axons had to simultaneously develop appropriate communication pathways. Pathways from large axons were designed not only to attract glial cells, but also to induce them to form myelin internodes of appropriate size for the axon. The associating glial cells in turn need to signal neurons/axons to target ion channels and other proteins to specialized regions called nodes of Ranvier. The accumulation of ion channels at nodes of Ranvier is an essential feature of rapid saltatory nerve conduction.

With growing genomic and est databases, we felt that it would be possible to use structures of known myelination-associated proteins, both those expressed by glial cells and neurons, to identify homologues in animals that lack myelin. While there is a highly annotated and complete database from the sea squirt, *Ciona intestinalis*, <www.jgi.doe.gov/ciona>, there are very limited genomic and est sequences from species more closely related to myelination: amphioxus, lamprey, and hagfish. Hopefully, genomic sequencing projects involving these species will be available in the near future.

Protein sequence databases were generated for myelin basic protein, proteolipid protein/DM-20, protein zero, 2′, 3′-cyclic nucleotide phosphodiesterase (CNP) mal, and PMP22. Using protein sequences from human and fish homologues, we identified homologous proteins for DM-20 and PMP22 in *Ciona*.

This research was supported by an NSF grant to RMG.

Reference: *Biol. Bull.* **207:** 168. (October 2004)
© 2004 Marine Biological Laboratory

Genes Differentially Expressed in Growth Hormone Transgenic Salmon

Kristen M. Ettensohn[1,2], Peggy Biga[3], Christina Romano[1], Robert H. Devlin[4], and Steven B. Roberts[1]
[1]Marine Biological Laboratory, Woods Hole, Massachusetts
[2]Dartmouth College, Hanover, New Hampshire
[3]Great Lakes WATER Institute, Milwaukee, Wisconsin
[4]Fisheries and Oceans Canada, West Vancouver, British Columbia, Canada

Genes differentially expressed in liver and adipose tissue of growth hormone transgenic coho salmon, compared to wild-type controls, were identified using differential display (GeneFishing DEG System; SeeGene). Previous research has shown that these transgenic salmon grow at a significantly greater rate, with hyperplasia the primary factor influencing increased growth. Two genes identified with differential display include complement factor Bf-2 and methionine adenyltransferase. Complement factor Bf-2 was downregulated in transgenic liver tissue compared to the wild-type liver tissue. In several fish species, complement factor Bf-2 has been shown to activate the complement factor system *via* both alternative and classical pathways. Methionine adenyltransferase was up-regulated in transgenic adipose tissue compared to wild-type controls. Other researchers have shown that methionine adenyltransferase is associated with the stress responses. Quantitative real-time RT-PCR analysis (Brilliant SYBR Green QRT-PCR Master Mix Kit, 1-Step, Stratagene) in the Opticon Continuous Fluorescence Detection System (MJ Research Inc.) was used to verify differential expression. The combined data suggest that over-expression of growth hormone and/or faster growth rates observed in transgenic salmon influence liver and adipose gene expression.

Reference: *Biol. Bull.* **207:** 169. (October 2004)

Cis Editing in *Trypanosoma brucei brucei* as a Model for Understanding Guide-RNA Structural and Functional Requirements

Daniel E. Golden and Stephen L. Hajduk
Marine Biological Laboratory, Woods Hole, Massachusetts

RNA editing in trypanosomes is a unique post-transcriptional process which is responsible for correcting the coding sequences of many mitochondrial mRNAs. Uridines are specifically added or deleted from mRNA by an enzymatic cascade in which a pre-edited mRNA is specifically cleaved, uridines are added or removed, and the corrected mRNA is ligated. The process is directed by a class of small RNA molecules termed guide-RNAs (gRNAs). Guide-RNAs have a 5′ anchor sequence that base pairs with a section of the mRNA directly 3′ to the editing site, specifying the addition or deletion of uridines with its guiding sequence. The ability of this class of small non-coding RNAs to function correctly in the mitochondrion is an essential process for the survival of the parasite. Previous work has focused on the more common trans relationship of the mRNA and gRNA, but cytochrome oxidase subunit II (COII) mRNA contains its gRNA in the 3′UTR. Results detail how the COII 3′ UTR functions in a predicted and specific manner as a gRNA in cis. While the UTR is functionally indistinguishable from a gRNA, it does not retain all the attributes of a gRNA as traditionally described. The 3′ UTR of COII can correctly guide for uridine insertions at specific sites only when contained in cis to the pre-edited mRNA, not trans. Nevertheless the 3′ UTR shares some structural similarities with known gRNA structures, such as forming a secondary structure inconsistent with the lowest predicted energy structure. These similarities and differences have been exploited to define the minimum requirements of a functional gRNA. The goal is to better define the structural and biochemical properties of a gRNA in RNA editing and to address the origins of these unique molecules.

Reference: *Biol. Bull.* **207:** 169. (October 2004)

Initial Sequence and Protein Modeling Results of a Mitochondrial Genome Project on Understudied Invertebrate Phyla

Gillian E. Robbins[1,2], Gonzalo Giribet[3], Karin Kiontke[4], David H. Fitch[4], Jeffrey L. Boore[5], and Robert K. Campbell[1,2]
[1]Serono Reproductive Biology Institute, Rockland, Massachusetts
[2]Marine Biological Laboratory, Woods Hole, Massachusetts
[3]Harvard University, Cambridge, Massachusetts
[4]New York University, New York, New York
[5]DOE Joint Genome Institute, Walnut Creek, California

Mitochondria play an essential role in metabolism. Comprising its own circular DNA, the mitochondrial genome of metazoans typically encodes 2 rRNAs, 22 tRNAs, and 12 to 13 polypeptides. These polypeptides are responsible for the production of protein complexes in the inner mitochondrial membrane that facilitate the production of ATP. Based upon genomic similarities, eukaryotic mitochondria may have evolved from an alphaproteobacterium-like ancestor.

A mitochondrial genomics study was initiated using organisms from invertebrate phyla including Priapulida (*Halicryptus spinulosus*), Rotifera (*Encentrum tectipes*), Acanthocephala (*Echinorynchus gadi*), Gnathostomulida (*Gnathostomula peregrini*), Cycliophora (*Symbion pandora*), and Nematoda (*Oscheius tipulae* and *Rhabditoides regina*). Gene regions from cytochrome *c* oxidase I (*coxI*), cytochrome *b*, 12S rRNA and 16S rRNA were amplified and sequenced using universal primer pairs. Nested primers were then designed to amplify larger fragments of each mitochondrial genome. Nested PCR products (5–10 kb) were obtained from three organisms, which covered 50%–75% of the genomic mtDNA in highly purified form. These products will be subjected to shotgun sequencing. Further PCR studies of the remaining fragments, as well as those of other mitochondrial genomes, are ongoing.

Successful amplification of *coxI* sequences using LCO/HCO primers was achieved from all invertebrates studied. Cytochrome *c* oxidase, the terminal oxidase in the respiratory chain, reduces oxygen to water through electron and proton transfer. The PCR of the *coxI* from the rotifer (*E. tectipes*) sample yielded two divergent protein-coding sequences. BLAST analyses revealed one to be most closely related to other rotifer *coxI* sequences. The second sequence appears equally related to *coxI* genes from alphaproteobacteria (*e.g., Rickettsia*) and from various eukaryotes, suggesting that this gene and its associated genome could be in an interesting phylogenetic position.

Reference: *Biol. Bull.* **207:** 170. (October 2004)

Development of a Global Collaborative Taxonomic Name Service for the Location and Retrieval of Electronic Resources in Biology

David P. Remsen[1] and D. J. Patterson[2]
[1]MBLWHOI Library, Woods Hole, Massachusetts
[2]Marine Biological Laboratory, Woods Hole, Massachusetts

All information in biology is tied to the names of organisms, and names are placed in conceptual hierarchies referred to as biological classifications or taxonomies. These elements have been used as the basis of indexing and organizing biological information for over 250 years. The continued use of names and classifications to form the contemporary framework of biological metadata seems self-evident. This vision has been frustrated because scientific names are not fixed, stable, or unique, and because continuing evolutionary and taxonomic studies lead to changes in the potential metadata structure. As a result, 5% to 10% of scientific names become invalidated each decade. Thus, a single name is often not sufficient to locate and retrieve data resources from collections served by libraries, publishers, museums, and other providers of biological information resources. Contemporary information retrieval tools must address these issues if searches and indices used by information providers are to provide reliable access to information. We have developed a taxonomic name service that records and maps names and classifications and provides these data to remote systems and applications using standard exchange protocols. This system currently records and serves over 1.5 million unique biological names within over 50 classifications. Tests of client applications interfacing large data collections, particularly those with a historic component, reveal relevant data return increases ranging from 100% to 1000%. The Taxonomic Name Server architecture is divided into a set of layered subsystems that maximize the utility of the data and enable this system to form a collaborative infrastructure with other, independent global efforts to build a catalog of life.

Reference: *Biol. Bull.* **207:** 171. (October 2004)

Characterization of Bacteria Associated With Lobster Shell Disease

Phoenix Becker, Roxanna Smolowitz, Morgan Porter, Andrea Hsu, and Steven Roberts
Marine Biological Laboratory, Woods Hole, Massachusetts

Lobster shell disease is a condition that affects the outer three layers of a lobster's carapace and results in dramatic lesions of the exoskeleton. The causative agents of lobster shell disease are believed to consist of chitinoclastic bacteria. For the present study, bacteria associated with lobster shell disease in the New England region were identified, based on 16s rDNA sequences. American lobsters, *Homarus americanus*, with shell disease were collected from Rhode Island, Connecticut, Massachusetts, and Maine. Bacteria were isolated from lesions and individually cultured. Genomic DNA was extracted from the bacteria, and two primers were used (Fwd: 5′ AGA GTT TGA TCH TGG CTY AG 3′: Rev: 5′ ACG GNT ACC TTG TTA CGA CTT 3′) to amplify a segment (~1500 bp) of the 16s rDNA. Individual bands were cloned and sequenced at the Josephine Bay Paul Center of the Marine Biological Laboratory using the facility's protocols. Sequences were identified based on sequence homology using NCBI's BLAST server. A majority of the bacteria identified belonged to the *Cytophaga-Flavobacter* and Alpha proteobacteria groups. Other bacteria identified included members of the *Oceanobacillus*, *Staphylococcus*, and *Vibrio* genera. Results indicate that there could be specific geospatial distribution patterns for certain bacteria isolated. For example, most *Cellulophaga* species were found in Maine, and the *Oceanobacillus* species was detected in a Rhode Island lobster. These data suggest that bacterial species belonging to the *Cytophaga-Flavobacter* and Alpha proteobacteria groups are most likely the causative agents of lobster shell disease, because nearly all samples collected contained bacteria related to these groups.

Reference: *Biol. Bull.* **207:** 171. (October 2004)
© 2004 Marine Biological Laboratory

Diagnosis of *Edwardsiella tarda* Infection in Oyster Toadfish (*Opsanus tau*) Held at the Marine Resources Center

Shira Horenstein, Roxanna Smolowitz, Kevin Uhlinger, and Steven Roberts
Marine Biological Laboratory, Woods Hole, Massachusetts

Opsanus tau, the oyster toadfish, is an important laboratory animal used in neurophysiologic and diabetes research. Wild-caught and cultured fish are maintained year-round in tanks in the Marine Resources Center (MRC) at the Marine Biological Laboratory. *Edwardsiella tarda*, a member of the Enterobacteriaceae, was previously reported to cause severe disease in MRC toadfish, characterized by bacterial pericarditis and multifocal subacute necrosis in several organs. It continues to be an important disease in MRC toadfish. Currently, bacterial culture followed by biochemical profiling is the only method of *E. tarda* identification. Our objectives were to adapt a PCR-based method into a diagnostic test, to be used with blood and mucus, for identifying *E. tarda* in toadfish. Three populations were examined: cultured juveniles, wild-caught adults held for greater than three months, and new arrivals. Fish were randomly chosen from each group, anesthetized with MS-222, weighed, measured, and blood and surface mucus sampled. Genomic DNA was isolated from whole fish blood (DNeasy Kit—QIAGEN). Blood of new arrivals and cultured fish was analyzed for presence or absence of *E. tarda* using PCR methods that employed forward primer, Eta2-351 (5′-TAG GGA GGA AGG TGT GAA-3′) and *Edwardsiella* genus-specific reverse primer, Edwsp-780r (5′-CTC TAG CTT GCC AGT CTT-3′). No bacterial positive blood samples were found. Real-time PCR methods, usually more sensitive than PCR, were then used on both serially diluted *E. tarda* DNA and fish blood inoculated with serially diluted *E. tarda* culture. An assay was successfully developed utilizing the serially diluted *E. tarda* DNA. Future diagnostic screenings will include evaluating samples from the tank environment and processing the mucus. Developing a sensitive, reproducible assay for detecting *E. tarda* in blood and mucus will provide a more rapid and efficient diagnosis and treatment of infected fish.

Reference: *Biol. Bull.* **207:** 172. (October 2004)

Histochemical Evidence for Lipopolysaccharide (Endotoxin) in Eukaryotes

Peter B. Armstrong[1,2], *Margaret T. Armstrong*[1,2], *Steven M. Theg*[1], *Nikolai Braun*[1], *Norman Wainwright*[2], *and R. L. Pardy*[3]
[1]*University of California, Davis, California*
[2]*Marine Biological Laboratory, Woods Hole, Massachusetts*
[3]*University of Nebraska, Lincoln, Nebraska*

Lipopolysaccharide is a component of the outer membrane of gram-negative bacteria and is the principal mediator of gram-negative bacterial toxicity to animals. Toxicity is mediated by lipid A, the membrane-forming element of lipopolysaccharide. Although usually thought to be restricted to prokaryotes, recent evidence suggests the presence of lipopolysaccharide in certain eukaryotes. Glycolipids with all of the unique components of bacterial lipopolysaccharide, including the lipid A moiety, have been isolated from axenically-grown green algae; and the vascular plant *Arabidopsis thaliana* has been found to contain genes that encode all enzymes of the lipid A biosynthetic pathway. We used two lipid A binding agents to localize LPS in cells: LALF (*Limulus* antilipopolysaccharide factor), a 12 kDa protein from the secretory granules of the blood cells of the horseshoe crab; and polymyxin B, an antibiotic of fungal origin. LALF binding was detected with an antibody, and biodipy conjugated to polymyxin B was used to localize that agent. Our positive control, the gram-negative bacterium *Escherichia coli*, showed staining of the surface with both agents. We also found intense staining of the free-living alga *Chlorella* (strain NC64A—a green alga) and the related species *Prototheca* (strain 289—an achlorophylic, white alga that is an obligate heterotroph and is also an opportunistic pathogen of livestock and humans), and the commensal algae of *Paramecium bursaria* and *Chlorohydra viridissima*. Chloroplasts isolated from pea seedlings and chloroplasts of paraffin-sectioned pea seedling leaves stained with both staining agents. To minimize the possibility that the LPS found on algae and chloroplasts derives from bacteria-produced LPS that subsequently binds to the surfaces of these cells and organelles, we processed axenically grown algae and all specimens destined for paraffin embedding and sectioning with fixatives and other reagents prepared in LPS-free water (Sigma). Staining with LALF and biodipy-polymyxin B was intense. These results suggest that endogenously synthesized LPS is present at the surfaces of free-living and commensal green algae and is localized to the chloroplasts of vascular plants.

This research was supported by NSF Grant 0344360 to PBA.

Reference: *Biol. Bull.* **207:** 172. (October 2004)
© 2004 Marine Biological Laboratory

Blood Clotting in *Limulus* Immunity: Physiological Impairment of Clot-Entrapped Bacteria

Peter A. Bosniak[1] *and Peter B. Armstrong*[2]
[1]*Hunter College, New York City, New York*
[2]*University of California, Davis, California*

The fibrillar extracellular blood clot is presumed to function in hemostasis, wound healing, and immunity. In that latter regard, the clot immobilizes microbes invading through wounds to prevent their systemic dispersal in the host. In the American horseshoe crab, *Limulus polyphemus*, the clot has been shown to immobilize bacteria so effectively that bacteria embedded in the clot lack even thermal (Brownian) motion. Two processes can be imagined to account for immobilization: (1) bacteria within the clot are physically entrapped by an array of clot fibrils so dense as to prevent any motion, or (2) the bacteria adhere strongly to the clot fibrils so as to prevent motion. The role of bacterial adherence was examined by determining the extent to which free-swimming bacteria attach to the surface of a preformed clot. Blood clots were produced by collecting blood onto coverglasses immersed in 0.5 *M* NaCl in a petri dish. Blood cells attach to the coverglass, degranulate, and produce the extracellular clot as a layer above the attached cells. The clot-bearing coverslips were then mounted on a microscope slide in a simple perfusion chamber that allowed exchange of the bathing buffer and microscopic examination with oil immersion objectives. The marine bacterium *Vibrio alginolyticus*, an opportunistic pathogen of *Limulus*, was grown in suspension culture and used in the log phase of culture growth. Attachment to the surface of the clot was studied by focusing at the blood clot/buffer interface with a 100× oil immersion phase contrast objective; bacteria were then introduced into the observation chamber. *Vibrio* were observed to swim freely until contacting the clot surface, at which instant a majority attached to the surface of the clot and were immobilized. Some attached bacteria maintained the use of flagellae, as evidenced by rapid spinning around an attachment point, while others displayed an absence of any motion, including a loss of Brownian motion. Bacteria attach to the native clot and to clots extracted with 0.5% Triton X-100. Attachment is resistant to calcium chelation, 2 *M* NaCl, and 8 *M* urea. These results indicate that adherence to the clot is sufficient to produce bacterial immobilization and that physical entrapment is not required.

This research was supported by NSF Grant 0344360 (PBA) and a Howard Hughes Undergraduate Fellowship (PAB).

Reference: *Biol. Bull.* **207:** 173. (October 2004)

Spatial Distribution of Land Type in Regression Models of Pollutant Loading

Evan J. Fedorko[1], R. Gil Pontius, Jr.[1], Stephen P. Aldrich[2], Luc Claessens[3], Charles Hopkinson, Jr.[4], and Wilfred M. Wollheim[5]
[1]Clark University, Worcester, Massachusetts
[2]Michigan State, East Lansing, Michigan
[3]San Diego State, San Diego, California
[4]Marine Biological Laboratory, Woods Hole, Massachusetts
[5]University of New Hampshire, Durham, New Hampshire

We propose a method to improve landscape-pollution interaction regression models by including a variable that describes the spatial distribution of a land type with respect to the pattern of runoff within a drainage catchment. The proposed indicator is used as an independent variable to enhance the strength, as quantified by R^2 values, of regression relationships between empirical observations of in-stream pollutant concentrations and land type, by considering the spatial distribution of key land-type categories within the sample point's drainage area. We present an indicator that, when used in conjunction with a variable describing the proportion of the land type, adds a new dimension of explanatory power. We demonstrate the usefulness of this indicator by exploring the relationship between nitrate (NO_3^-) and land type within 40 drainage sub-catchments in the Ipswich River watershed, Massachusetts. Nutrient loads associated with non-point source pollution paths are related to land type within the drainage catchments of sample sites. Past studies have focused on the quantity of a particular land type within a sample point's drainage catchment. Quantifying the spatial distribution of key land-type categories in terms of location on a runoff surface improves our understanding of the relationship between sampled NO_3^- concentrations and land type. Regressions that employ the proportion of residential land type within catchments provide a fair fit ($R^2 = 0.67$). However, we find that a regression including a variable that indicates the spatial distribution of residential land improved the overall relationship between in-stream NO_3^- measurements and associated land type ($R^2 = 0.712$). We test the sensitivity of the results with respect to variations in the index definition in order to determine the conditions under which the spatial indicator variable is worthwhile.

Reference: *Biol. Bull.* **207:** 173. (October 2004)
© 2004 Marine Biological Laboratory

Estimating Groundwater-Derived Nitrogen Flux Into a Coastal Embayment: Salt Pond, Cape Cod, Massachusetts

Kayla Halloran[1], Matt Charette[2], Paul Henderson[2], Kevin Kroeger[2], Lindsey Ryckman[3], John Crusius[3], and Dirk Koopmans[3]
[1]Bucknell University, Lewisburg, Pennsylvania
[2]Woods Hole Oceanographic Institution, Woods Hole, Massachusetts
[3]United States Geological Survey, Woods Hole, Massachusetts

Submarine groundwater discharge (SGD) often contributes significant fluxes of nutrients to coastal waters and is an important vehicle for nitrogen transport. Salt Pond, a small eutrophic coastal embayment in Cape Cod, Massachusetts, is connected by a single outlet to the Nauset Marsh System and receives elevated anthropogenic nitrogen inputs associated with human development. A series of seepage meter deployments found that SGD was not related to tidal stage, suggesting that the groundwater hydraulic head is above the sea level at all times. The average SGD rate from seepage meters of 12 cm d^{-1} was comparable to a similar concurrent experiment, which employed radon as a tracer of SGD (4 cm d^{-1}). Groundwater sampling indicated that nitrate was transported conservatively through the aquifer, suggesting that little denitrification occurs during the mixing of fresh and salty groundwater. Using the seepage meter flow rates and average total dissolved nitrogen (TDN) concentrations in the groundwater, the SGD-derived TDN flux to the pond was 11.5 mmol m^{-2} day^{-1} (67% as nitrate, 30% as dissolved organic nitrogen, 3% as ammonium). Surface water sampling in the tidally flushed channel over a tidal cycle revealed that the Nauset Marsh is a net source of TDN to Salt Pond (12.7 mmol m^{-2} day^{-1}). Thus, Salt Pond is a net nitrogen sink, with a total of 24.2 mmol m^{-2} day^{-1} being retained by the system, most likely in the form of algal biomass and denitrification in the fine-grained organic rich sediments that characterize the deep basin.

Reference: *Biol. Bull.* **207:** 174. (October 2004)

Effect of Nutrient Enrichment and Salinity on Salt Marsh Invertebrates in the Plum Island Estuary

Jenn Kerry[1], Dorothy Boorse[1], and Robert Buchsbaum[2]
[1]Gordon College, Wenham, Massachusetts
[2]Massachusetts Audubon Society, Wenham, Massachusetts

Nutrient enrichment of tidal marshes accompanies landscape development and urbanization. Such enrichment can alter tidal marsh communities. As part of the Plum Island Long Term Ecological Research project, we investigated the impact of a sewage outfall in Greenwood Creek marsh, Ipswich, Massachusetts, on litter-inhabiting macroinvertebrates. Because the sewage outfall also introduced fresh water to the Greenwood marsh, we compared it to two reference marsh systems: one brackish and one marine. Mesh litterbags were filled with *Spartina patens* litter and placed in three vegetation zones [high marsh (*Spartina patens*), low marsh (*Spartina alterniflora*), and upland edge vegetation]. The stands of edge vegetation were of two types: *Typha angustifolia* in the brackish marsh and *Phragmites australis* in the sewage outfall marsh. Bags were incubated in each marsh system during two different two-week intervals, and after each interval, we collected and counted the invertebrates that had entered. We also compared the invertebrates caught in two types of litterbags (cloth and plastic mesh).

There were more individuals and more taxa in the brackish reference marsh than in the sewage outfall marsh, both of which had more individuals and taxa than the marine marsh. Greenwood Creek marsh had the highest nitrogen load of the three marshes, but the average salinity on the marsh was similar to the marine marsh. Fauna colonizing litterbags may be negatively affected by high salinity. This may have offset the expected increase in invertebrates due to nutrient loading in the Greenwood Creek marsh.

There were lower abundances of individuals in the *P. australis* edge vegetation zone than in any other vegetation zone, but there was no effect of vegetation on taxonomic richness. More individuals were collected during the second two-week experiment.

In the comparison between litterbag types, abundances of individuals and taxonomic richness were higher in the cloth mesh bags than in the plastic mesh bags. The plastic mesh bags had slightly smaller openings, and a large area was covered by a label through which fauna could not pass.

This work was supported by an NSF-REU (OCE 9726921). We are indebted to Kelsey Correa for field assistance and to the TIDE (NSF DEB 0213767) project for equipment.

Reference: *Biol. Bull.* **207:** 174. (October 2004)

Alkaline Phosphatase Activity in the Toxic Dinoflagellate *Karenia brevis*

Allison C. Craney[1], S. T. Haley, and S. T. Dyhrman[2]
[1]Mount Holyoke College, South Hadley, Massachusetts
[2]Woods Hole Oceanographic Institution, Woods Hole, Massachusetts

Over the past two decades, there has been an increase in both the occurrence and geographic extent of harmful algal blooms such as those of the toxic dinoflagellate *Karenia brevis*, further perpetuating threats to marine environments and to human health. *K. brevis* can cause neurotoxic shellfish poisoning (NSP) and respiratory irritation in humans. Blooms of *K. brevis* are common off the coast of Florida and seriously impact local economies when they occur. Despite its importance, little is known about how *K. brevis* acquires phosphorus, a nutrient critical to dinoflagellate nutrition. In this study, the enzyme alkaline phosphatase was examined. This is an enzyme that hydrolyzes organic phosphorus into a bioavailable form, typically after inorganic phosphate has been depleted. Axenic *K. brevis* CCMP 2281 cultures were grown in triplicate treatments of nutrient replete, low nitrogen (50 μM), and low phosphorus (1 μM) L1 medium. Alkaline phosphatase activity (APA) was assayed using both bulk and cell-specific (Enzyme Labeled Fluorescence) methods. Cell-specific assays suggested that APA in low phosphorus treatments was five-fold higher on average than the nutrient replete treatments, and almost four-fold higher than the low nitrogen treatments. Bulk assays corroborated a higher rate of APA in the low phosphorus treatments relative to the controls.

Reference: *Biol. Bull.* **207:** 175. (October 2004)

Nitrate Reductase and Glutamine Synthetase Activity and Growth in *Ulva lactuca* in Waquoit Bay: A Time Sequence of Responses to Differences in Nitrogen Supply

Leanna R. Heffner, Mirta Teichberg, Sophia Fox, and Ivan Valiela
Boston University Marine Program, Marine Biological Laboratory, Woods Hole, Massachusetts

Opportunistic macroalgae often bloom in waters receiving increased nitrogen inputs as a result of anthropogenic activity. To assess the growth of *Ulva lactuca*, a bloom-forming macroalga, to differences in nitrogen supply, we carried out cage incubations in two Cape Cod estuaries with different nitrogen loads, and enriched half of the algal fronds with nitrate. We measured the enzyme activities involved in nitrogen assimilation—nitrate reductase (NR) and glutamine synthetase (GS)—to assess nitrogen uptake in *Ulva* from the two estuaries for the different treatments. In addition, percent tissue nitrogen (N), stable isotopic signatures, and growth rates of the algae were measured. Nutrient analyses showed that nitrate concentrations were higher in the enriched cages than in the controls, and ammonium concentration did not vary between treatments. Over the course of the incubation, NR levels were significantly higher in algae from the high N-load estuary than from the low N-load estuary; and in both estuaries activity increased with nitrate enrichment. GS activity was similarly variable among all treatments. Percent tissue N in the enriched algae and algae from the high N-load estuary was higher than the controls and the algae from the low N load; and the isotopic signatures signaled a rapid turnover of nitrogen in the enriched algal fronds because they quickly incorporated the nitrate fertilizer into their tissue. After a 15-day incubation period, percent growth of *U. lactuca* in both estuaries was greater in the nitrate-enriched cages compared with the control cages. The growth observed in the enriched algae at the end of the incubation may be a response to increased NR activity, tissue N content, or both. These results corroborate observations that increased inputs of nitrate into estuarine waters rapidly stimulate growth of opportunistic macroalgae, such as *U. lactuca*, thus contributing to increasing occurrences of macroalgal blooms.

Reference: *Biol. Bull.* **207:** 175. (October 2004)

Life History Analysis of the Juvenile Horseshoe Crab in Pleasant Bay, Cape Cod

Sarah B. Cierpich[1], Sara P. Grady[2], and Ivan Valiela[2]
[1]University of Massachusetts, Amherst, Massachusetts
[2]Boston University Marine Program, Marine Biological Laboratory, Woods Hole, Massachusetts

Little is known about the early life history of the Atlantic horseshoe crab (*Limulus polyphemus*), and few studies have been done regarding its life history—specifically, first-year juvenile growth rate and mortality rate. Quadrat surveys were completed along transects perpendicular to the high-tide line in the intertidal zone of Pleasant Bay during low tide every semilunar period from mid-May through mid-August. The prosomal widths of the crabs were measured and recorded. The number of crabs found during the survey period increased, peaking in mid-July, indicating that peak spawning occurred in late June or early July. The spawning season for horseshoe crabs appears to have begun in mid to late March and appears to have ended in early August. The survey results also showed clear size differences between cohorts. An entire cohort was barely found during the survey, which suggests either impaired spawning or egg mortality due to weather conditions in late May. Growth and mortality rates declined with increasing juvenile crab size and age. This study provides information on the life history of juvenile horseshoe crabs, which can be useful in fisheries management and in the development of further life history studies of juvenile horseshoe crabs.

THE

BIOLOGICAL BULLETIN

2005 Subscription Form

Volumes 208-209, 6 issues

(Please print)

NAME: _____

INSTITUTION: _____

ADDRESS: _____

CITY: _____ STATE: _____ POSTAL CODE: _____

COUNTRY: _____ TELEPHONE: _____

FAX: _____ E-MAIL ADDRESS: _____

Please send me a 2005 subscription to *The Biological Bulletin* at the rate indicated below:

Price includes both print and online versions. All subscriptions run on the calendar year.

❒ Individual: $120.00 (6 ISSUES) ❒ Institutional: $360.00 (6 ISSUES)

❒ Individual: $70.00 (3 ISSUES) ❒ Institutional: $180.00 (3 ISSUES)

Check one: ❒ February, April, June or ❒ August, October, December

Please send me the following back issue(s): _____

❒ Individual: at $25.00 (PER ISSUE) ❒ Institutional: at $75.00 (PER ISSUE)

Delivery Options

❒ Surface Delivery (Surface delivery is included in the subscription price.)

❒ Air Delivery (Please add the correct amount to your payment.)

U.S. and Canada: $45.00 Mexico: $60.00 All other locations: $100.00

Payment Options

❒ Enclosed is my check or U.S. money order for $ _____

payable to Marine Biological Laboratory (with reference *The Biological Bulletin*)

❒ Please charge my ❒ VISA ❒ MasterCard ❒ Discover Card $ _____

Account No.: _____ Exp. Date: _____

Signature: _____ Date: _____

❒ Please send me an invoice. (Note: Payment must be received before subscription commences.)

Return this form with your check or credit information to:

Subscription Administrator, *The Biological Bulletin*
Marine Biological Laboratory, 7 MBL Street
Woods Hole, MA 02543 U.S.A.
Fax: 508-289-7922 • Tel: 508-289-7402 • E-mail: lreuter@mbl.edu

www.biolbull.org

Published by the Marine Biological Laboratory
Woods Hole, Massachusetts, 02543 U.S.A.

Director/Chief Executive Officer
Marine Biological Laboratory

The Marine Biological Laboratory (MBL), an international research and educational institution founded in 1888 and located in Woods Hole, Massachusetts, invites applications and nominations for the position of Director, who will serve as the institution's Chief Executive Officer.

The MBL is an international resource that provides a stimulating and productive research base for scientists in the areas of basic biology, biomedicine and environmental science. For more than a century, the Laboratory has prepared young biologists for leadership positions in research and teaching through its internationally recognized education programs. The MBL recently completed a visionary strategic plan that stresses interdisciplinary research and innovations in science education, the details of which are available at <http://www.mbl.edu/inside/what/planning/index.html>.

The Laboratory hosts a year-round staff of more than 290 scientists and support personnel, including 69 Ph.D.-level investigators working in more than 30 laboratories and research centers. During the summer months, an additional 1400 scientists and students from 300 institutions worldwide come to the MBL to conduct research and to train in modern techniques through intensive laboratory-based courses.

The Director reports to the Board of Trustees and oversees the scientific direction of the Laboratory, develops fundraising priorities, provides general supervision of the Laboratory, and controls the business of the Corporation. Candidates should have a strong record of scientific leadership, fundraising capability, and a demonstrated ability to form consensus among individuals with different perspectives and to lead them in achieving policy objectives.

It is anticipated that the appointment will commence July 1, 2006. The Marine Biological Laboratory is located in Woods Hole, MA, a village rich with scientific inquiry and discovery as well as one of the most beautiful locations on Cape Cod. Additional information about the MBL is available at <www.mbl.edu>.

Please send nominations or your letter of interest and resumé to:

MBL Director/CEO Search Committee
c/o Human Resources
Marine Biological Laboratory
7 MBL Street
Woods Hole, MA 02543

Review of applications will begin September 1, 2004, and continue until a successful applicant is identified.

The Marine Biological Laboratory is an Affirmative Action/Equal Employment Opportunity Employer

December 2004

THE BIOLOGICAL BULLETIN

Volume 207 • Number 3

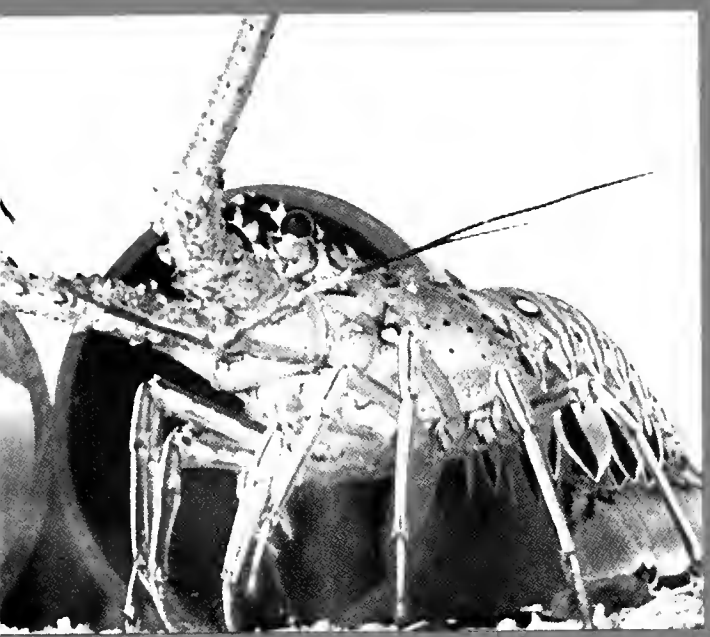

Published by the Marine Biological Laboratory

Woods Hole, Massachusetts

Introducing U1S2. New optics. New discoveries.

olympusamerica.com/microscopes 800-446-5967

OLYMPUS

Your Vision, Our Future

Cover

The Caribbean spiny lobster (*Panulirus argus*) shown on the cover in its experimental tank (upper left image) is displaying its typical food-search behavior. Its array of anterior thoracic limbs probes the substrate surface, and when a piece of food is contacted, it is picked up and transferred to the mouthparts, which, in crustaceans, comprise the anteriormost segmental appendages. A close-up image (lower left) shows the mouthparts manipulating a shucked mussel (the dark bushy structure is the byssus). The anteriormost of the mouthparts (the third maxillipeds) have a firm grip on the mussel, dimpling the yellow, pillowy surface of its exposed mantle; many of the setae at the tip of the appendages are in intimate contact with the prey's soft tissues. The scanning electron micrograph on the cover illustrates the clusters of simple setae found on the tip of the third maxilliped. The setae (diameter, 30–45 μm) are long, hollow cones of exoskeleton enclosing mechanosensory neurons.

In this issue of *The Biological Bulletin* (p. 195), Anders Garm, Charles Derby, and Jens Hoeg report on a morphological and physiological study of the mechanosensory neurons in the mouthpart setae of *P. argus*. Most important, they describe their test of the hypothesis that these sensory structures provide tactile information about the texture, shape, and movement of food items—information critical to the control of feeding behavior. The electrophysiological results show that the simple setae, which constitute the vast majority of the mouthpart setae, contain only one of two different types of mechanoreceptor neurons: displacement-sensitive neurons that respond to deflection of the entire shaft at its base, and bend-sensitive neurons that respond to bending of the distal portion of the setal shaft. This is the first experimental demonstration of bend-sensitive neurons in any arthropod sensory seta.

Together the two types of mechanosensory neurons seem to constitute a form of somatosensory system. This would suggest that the mechanosensory input to the central nervous system during feeding is more complex than previously thought and might underlie the flexibility of crustacean feeding behavior. Presumably, displacement-sensitivity provides information about the size, shape, and movement of prey and thus contributes to the manipulation of such food items. Input from bend-sensitive neurons also contributes to these perceptions; but in addition, it indicates the relative hardness of the prey, which will influence the decision about whether the food should be crushed or bitten by the mandibles.

The images of the spiny lobster and its mouthparts were taken from macro-video recordings. (The lobster is about 25 cm in length; its maxillipeds are 4 mm in diameter; and the gray tube behind it serves as a shelter.) The video images and the scanning electron micrograph were both made by Anders Garm (Lund University, Sweden), who also drafted the cover. The final cover design was prepared by Beth Liles (Marine Biological Laboratory, Woods Hole, Massachusetts).

THE
BIOLOGICAL BULLETIN
DECEMBER 2004

Published by
Marine Biological Laboratory
Woods Hole, Massachusetts

http://www.biolbull.org

Neurobiologist James L. Olds Named 10th Editor of *The Biological Bulletin*

After a search led by John Dowling, the President of the Marine Biological Laboratory (MBL) Corporation, the MBL is pleased to announce that James L. Olds has been appointed editor-in-chief of *The Biological Bulletin*, effective January 1, 2005. Olds will be the 10th editor of the journal, succeeding Michael J. Greenberg of the University of Florida's Whitney Laboratory, who has worked tirelessly on behalf of the journal for 15 years. Olds is the director of the Krasnow Institute for Advanced Study at George Mason University in Fairfax, Virginia, and has had close MBL ties since 1978. He will serve a five-year, renewable term at the *Bulletin*.

"Dr. Olds brings a wealth of experience in administration, scientific research, and publishing to his editorship," says William T. Speck, MBL director and CEO. "He will follow in the footsteps of one of the journal's most visionary and skilled editors, Mike Greenberg, to whom we owe a great debt of gratitude."

After graduating from Amherst College and obtaining his Ph.D. in neurosciences from the University of Michigan, Olds served as a staff fellow, project officer, and later senior staff fellow at the NINDS/NIH. He was Executive Director of the American Association of Anatomists from 1995 to 1998, where he oversaw the management of that society's journal, *The Anatomical Record*. He was appointed director of the Krasnow Institute in 1998.

Olds's long association with the MBL began after college, when he participated in the "Year in Science Program." He was elected to the MBL Corporation in 1991 and served on a special editorial board of the *Bulletin* in 1992. He was also a member of the MBL's computer advisory committee from 1991 through 2002.

An expert in the role nerve cells, or neurons, play in learning and memory, Olds's research is directed toward understanding and simulating the machinery that permits neurons and neuronal assemblies to store and recall memories, both under normal and diseased conditions. He uses cutting-edge computerized equipment to image and simulate the cells and aims to eventually develop techniques that will reveal the three-dimensional structure and maps of memory function in both animal and human brains in near real-time.

"I am delighted to be taking the helm of this wonderful journal at this time in its long history," says Olds. "I am most grateful to Mike Greenberg for his mentorship, his incredible dedication to quality science, and for leaving the MBL's flagship journal in such great shape. I am pleased that Mike has agreed to continue on with the *Bulletin* as a valued member of the editorial board."

Authors may now submit their papers to Dr. Olds, in care of the Editorial Office in Woods Hole.

CONTENTS

VOLUME 207, NO. 3: DECEMBER 2004

NOTICE

In 2005, articles published in *The Biological Bulletin* in prior years will be made available as PDF files, and **at no charge**, on the journal's HighWire web site. Similarly, JSTOR—a non-profit archive for scholarly journals—will add back issues of *The Biological Bulletin* to its Ecology and Botany Collection; the articles will be available through libraries that have bought subscriptions to JSTOR. Both the HighWire site and JSTOR will provide access to an unbroken run of *Bulletin* articles reaching back to Volume 1, issue 1 (*i.e.*, October 1899). Recent articles—defined, at present, as those published during the most recent 12-month period—will be accessible only to individuals with a subscription to the journal, through libraries with such a subscription, or, to non-subscribers, by paying per view of an article. The year of constrained access—a period reduced from two years only recently in response to the call for open access to journal articles—is mutable and will be reconsidered in consultation with the *Bulletin's* new editor, James L. Olds, in the coming year.

This expanded service will enhance scientific scholarship, not only by making this journal's valuable older articles more accessible, but also by making them more easily detectable by electronic search engines.

THE BIOLOGICAL BULLETIN

THE BIOLOGICAL BULLETIN is published six times a year by the Marine Biological Laboratory, 7 MBL Street, Woods Hole, Massachusetts 02543.

Subscriptions and similar matter should be addressed to Subscription Administrator, THE BIOLOGICAL BULLETIN, Marine Biological Laboratory, 7 MBL Street, Woods Hole, Massachusetts 02543. Subscription includes both print and online journals. Subscription per year (six issues, two volumes): $325 for libraries; $120 for individuals. Subscription per volume (three issues): $165 for libraries; $70 for individuals. Back and single issues (subject to availability): $75 for libraries; $25 for individuals.

Communications relative to manuscripts should be sent to James L. Olds, Editor-in-Chief, or Pamela Clapp Hinkle, Managing Editor, at the Marine Biological Laboratory, 7 MBL Street, Woods Hole, Massachusetts 02543. Telephone: (508) 289-7149. FAX: 508-289-7922. E-mail: pclapp@mbl.edu.

http://www.biolbull.org

THE BIOLOGICAL BULLETIN is indexed in bibliographic services including *Index Medicus* and MEDLINE, *Chemical Abstracts*, *Current Contents*, *Elsevier BIOBASE/Current Awareness in Biological Sciences*, and *Geo Abstracts*.

Printed on acid free paper,
effective with Volume 180, Issue 1, 1991.

POSTMASTER: Send address changes to THE BIOLOGICAL BULLETIN, Marine Biological Laboratory, 7 MBL Street, Woods Hole, MA 02543.

Periodicals postage paid at Woods Hole, MA, and additional mailing offices.
ISSN 0006-3185

INSTRUCTIONS TO AUTHORS

The Biological Bulletin accepts outstanding original research reports of general interest to biologists throughout the world. Papers are usually of intermediate length (10–40 manuscript pages). A limited number of solicited review papers may be accepted after formal review. A paper will usually appear within four months after its acceptance.

Very short, especially topical papers (less than 9 manuscript pages including tables, figures, and bibliography) will be published in a separate section entitled "Research Notes." A Research Note in *The Biological Bulletin* follows the format of similar notes in *Nature*. It should open with a summary paragraph of 150 to 200 words comprising the introduction and the conclusions. The rest of the text should continue on without subheadings, and there should be no more than 30 references. References should be referred to in the text by number, and listed in the Literature Cited section in the order that they appear in the text. Unlike references in *Nature*, references in the Research Notes section should conform in punctuation and arrangement to the style of recent issues of *The Biological Bulletin*. Materials and Methods should be incorporated into appropriate figure legends. See the article by Lee (October 2003, Vol. **205:** 99–101) for sample style. A Research Note will usually appear within two months after its acceptance.

The Editorial Board requests that regular manuscripts conform to the requirements set below; those manuscripts that do not conform will be returned to authors for correction before review.

1. ***Manuscripts.*** Manuscripts, including figures, should be submitted in quadruplicate, with the originals clearly marked. (Xerox copies of photographs are not acceptable for review purposes.) Please include an electronic copy of the text of the manuscript. Label the disk with the name of the first author and the name and version of the wordprocessing software used to create the file. If the file was not created in some version of Microsoft Word, save the text in rich text format (rtf). The submission letter accompanying the manuscript should include a telephone number, a FAX number, and (if possible) an E-mail address for the corresponding author. The original manuscript must be typed in no smaller than 12 pitch or 10 point, using double spacing (*including* figure legends, footnotes, bibliography, etc.) on one side of 16- or 20-lb. bond paper, 8 by 11 inches. Please, no right justification. Manuscripts should be proofread carefully and errors corrected legibly in black ink. Pages should be numbered consecutively. Margins on all sides should be at least 1 inch (2.5 cm). Manuscripts should conform to the *Council of Biology Editors Style Manual*, 5th Edition (Council of Biology Editors, 1983) and to American spelling. Unusual abbreviations should be kept to a minimum and should be spelled out on first reference as well as defined in a footnote on the title page. Manuscripts should be divided into the following components: Title page, Abstract (of no more than 200 words), Introduction, Materials and Methods, Results, Discussion, Acknowledgments, Literature Cited, Tables, and Figure Legends. In addition, authors should supply a list of words and phrases under which the article should be indexed.

2. ***Title page.*** The title page consists of a condensed title or running head of no more than 35 letters and spaces, the manuscript title, authors' names and appropriate addresses, and footnotes listing present addresses, acknowledgments or contribution numbers, and explanation of unusual abbreviations.

3. ***Figures.*** The dimensions of the printed page, 7 by 9 inches, should be kept in mind in preparing figures for publication. We recommend that figures be about 1 times the linear dimensions of the final printing desired, and that the ratio of the largest to the smallest letter or number and of the thickest to the thinnest line not exceed 1:1.5. Explanatory matter generally should be included in legends, although axes should always be identified on the illustration itself. Figures should be prepared for reproduction as either line cuts or halftones. Figures to be reproduced as line cuts should be unmounted glossy photographic reproductions or drawn in black ink on white paper, good-quality tracing cloth or plastic, or blue-lined coordinate paper. Those to be reproduced as halftones should be mounted on board, with both designating numbers or letters and scale bars affixed directly to the figures. All figures should be numbered in consecutive order, with no distinction between text and plate figures and cited, in order, in the text. The author's name and an arrow indicating orientation should appear on the reverse side of all figures.

Digital art: The Biological Bulletin will accept figures submitted in electronic form; however, digital art must conform to the following guidelines. Authors who create digital images are wholly responsible for the quality of their material, including color and halftone accuracy.

Format. Acceptable graphic formats are TIFF and EPS. Color submissions must be in EPS format, saved in CMKY mode.

Software. Preferred software is Adobe Illustrator or Adobe Photoshop for the Mac and Adobe Photoshop for Windows. Specific instructions for artwork created with various software programs are available on the Web at the Digital Art Information Site maintained by Cadmus Professional Communications at http://cpc.cadmus.com/da/

Resolution. The minimum requirements for resolution are 1200 DPI for line art and 300 for halftones.

Size. All digital artwork must be submitted at its actual printed size so that no scaling is necessary.

Multipanel figures. Figures consisting of individual parts (*e.g.*, panels A, B, C) must be assembled into final format and submitted as one file.

Hard copy. Files must be accompanied by hard copy for use in case the electronic version is unusable.

Disk identification. Disks must be clearly labeled with the following information: author name and manuscript number; format (PC or Macintosh); name and version of software used.

Color: The Biological Bulletin will publish color figures and plates, but must bill authors for the actual additional cost of printing in color. The process is expensive, so authors with more than one color image should—consistent with editorial concerns, especially citation of figures in order—combine them into a single plate to reduce the expense. On request, when supplied with a copy of a color illustration, the editorial staff will provide a pre-publication estimate of the printing cost.

4. ***Tables, footnotes, figure legends, etc.*** Authors should follow the style in a recent issue of *The Biological Bulletin* in preparing table headings, figure legends, and the like. Because of the high cost of setting tabular material in type, authors are asked to limit such material as much as possible. Tables, with their headings and footnotes, should be typed on separate sheets, numbered with consecutive Arabic numerals, and placed after the Literature Cited. Figure legends should contain enough information to make the figure intelligible separate from the text. Legends should be typed double spaced, with consecutive Arabic numbers, on a separate sheet at the end of the paper. Footnotes should be limited to authors' current addresses, acknowledgments or contribution numbers, and explanation of unusual abbreviations. All such footnotes should appear on the title page. Footnotes are not normally permitted in the body of the text.

5. ***Literature cited.*** In the text, literature should be cited by the Harvard system, with papers by more than two authors cited as Jones *et al.*, 1980. Personal communications and material in preparation or in press should be cited in the text only, with author's initials and institutions, unless the material has been formally accepted and a volume number can be supplied. The list of references following the text should be headed Literature Cited, and must be typed double spaced on separate pages, conforming in punctuation and arrangement to the style of recent issues of *The Biological Bulletin*. Citations should include complete titles and inclusive pagination. Journal abbreviations should normally follow those of the U. S. A. Standards Institute (USASI), as adopted by Biological Abstracts and Chemical Abstracts, with the minor differences set out below. The most generally useful list of biological journal titles is that published each year by Biological Abstracts (BIOSIS List of Serials; the most recent issue). Foreign authors, and others who are accustomed to using The World List of Scientific Periodicals, may find a booklet published by the Biological Council of the U.K. (obtainable from the Institute of Biology, 41 Queen's Gate, London, S.W.7, England, U.K.) useful, since it sets out the World List abbreviations for most biological journals with notes of the USASI abbreviations where these differ. Chemical Abstracts publishes quarterly supplements of additional abbreviations. The following points of reference style for The Biological Bulletin differ from USASI (or modified World List) usage:

A. Journal abbreviations, and book titles, all underlined (for *italics*)

B. All components of abbreviations with initial capitals (not as European usage in World List *e.g.*, *J. Cell. Comp. Physiol.* NOT *J. cell. comp. Physiol.*)

C. *All* abbreviated components must be followed by a period, whole word components *must not* (*i.e.*, *J. Cancer Res.*)

D. Space between all components (*e.g.*, *J. Cell. Comp. Physiol.*, not *J.Cell.Comp.Physiol.*)

E. Unusual words in journal titles should be spelled out in full, rather than employing new abbreviations invented by the author. For example, use *Rit Vísindafjélags Íslendinga* without abbreviation.

F. All single word journal titles in full (*e.g.*, *Veliger*, *Ecology*, *Brain*).

G. The order of abbreviated components should be the same as the word order of the complete title (*i.e., Proc.* and *Trans.* placed where they appear, not transposed as in some BIOLOGICAL ABSTRACTS listings).

H. A few well-known international journals in their preferred forms rather than WORLD LIST or USASI usage (*e.g., Nature, Science, Evolution* NOT *Nature, Lond., Science, N.Y.; Evolution, Lancaster, Pa.*)

6. ***Sequences.*** By the time a paper is sent to the press, all nucleotide or amino acid sequences and associated alignments should have been deposited in a generally accessible database (*e.g.*, GenBank, EMBL, SwissProt), and the sequence accession number should be provided.

7. ***Reprints, page proofs, and charges.*** Authors may purchase reprints in lots of 100. Forms for placing reprint orders are sent with page proofs. Reprints normally will be delivered about 2 to 3 months after the issue date. Authors will receive page proofs of articles shortly before publication. They will be charged the current cost of printers' time for corrections to these (other than corrections of printers' or editors' errors). Other than these charges for authors' alterations, *The Biological Bulletin* does not have page charges.

CONTENTS
for Volume 207

No. 1: August 2004

No. 2: October 2004

No. 3: December 2004

Reference: *Biol. Bull.* **207:** 177–182. (December 2004)

Composition of a One-Year-Old *Riftia pachyptila* Community Following a Clearance Experiment: Insight to Succession Patterns at Deep-Sea Hydrothermal Vents

B. GOVENAR[1,*], M. FREEMAN[1], D. C. BERGQUIST[1,†], G. A. JOHNSON[2], AND C. R. FISHER[1]

[1] *Department of Biology, 208 Mueller Laboratory, Pennsylvania State University, University Park, Pennsylvania 16802; and* [2] *University of North Carolina at Chapel Hill, Institute of Marine Sciences, Morehead City, North Carolina 28557*

In the basalt-hosted hydrothermal vent habitat around 9°50′N on the East Pacific Rise, the vestimentiferan tubeworms Tevnia jerichonana *and* Riftia pachyptila *(Polychaeta: Siboglinidae) commonly settle before the mussel* Bathymodiolus thermophilus *(Bivalvia: Mytilidae). We removed six aggregations of* R. pachyptila *and deployed mussels on the cleared sources of diffuse flow to test the effect of the* B. thermophilus *on the subsequent colonization by the tubeworms. None of the transplanted mussels persisted on the cleared sources of diffuse flow; however, aggregations of* R. pachyptila *grew in half of the clearances. We collected one of the aggregations of* R. pachyptila *along with the associated fauna for determination of relative abundance and biomass in this one-year-old community. This aggregation consisted of 647 specimens of* R. pachyptila *that hosted individuals of 24 species, including small individuals of* T. jerichonana *and* B. thermophilus. *The abundance of the associated fauna was numerically dominated by gastropods, and the biomass was dominated by the Alvinellid polychaete* Paralvinella grasslei.

Following an eruption, the vestimentiferan tubeworms *Tevnia jerichonana* and *Riftia pachyptila* (Polychaeta: Siboglinidae) quickly colonize the basalt-hosted hydrothermal vents around 9°50′N (East Pacific Rise) and soon grow to visually dominate these habitats (1, 2, 3). Colonization by the vent mussel *Bathymodiolus thermophilus* often follows shortly, and the mussels eventually overgrow the tubeworms at most sites (2, 4, 5). Both tubeworms and mussels harbor sulfur-oxidizing chemoautotrophic endosymbionts, which provide the bulk of their nutrition (6, 7). However, mussels have also maintained the ability to filter-feed (8), which apparently allows them to occupy a wider range of environmental conditions and better tolerate declining hydrothermal vent activity than the tubeworms (9). The mechanism of ecological succession in these hydrothermal vent habitats is not fully understood, but may be regulated by a combination of pre-settlement factors, such as the use of biogenic cues (3) and the response to geochemical changes (2), and post-settlement factors, such as physical overgrowth (4) and resource competition (5).

We conducted a manipulative experiment to test the hypothesis that the mussel *B. thermophilus* prevents further colonization of a vent by tubeworms. In May 1998, six aggregations of the giant tubeworm *R. pachyptila* were cleared from a site named Riftia Field (9°50.705′N 104°17.593′W). The original location and source of diffuse flow for each aggregation were marked and recorded on video. After the aggregations were cleared, the temperatures of the venting fluid were measured, using the low-temperature probe of the DSV *Alvin,* and ranged from 20–22 °C above ambient at the six locations. Then about 600 mussels were collected from a nearby site ("East Wall", 9°50.614′N 104° 17.509′W) and about 200 were deployed over each of three cleared sources of diffuse flow (treatments). Mussels were not deployed on the three other cleared areas (con-

Received 28 April 2004; accepted 4 October 2004.

* To whom correspondence should be addressed. E-mail: breea@psu.edu

† Present address: Department of Fisheries and Aquatic Sciences, University of Florida, Gainesville, FL 32653.

trols). One month later, a French expedition (HOPE98, *L'Atalante/Nautile*) to the same hydrothermal vent field reported that there were no mussels visible at Riftia Field (pers. obs., S. Hourdez, Station Biologique Roscoff). In April 1999, we confirmed that all but one of the mussels had disappeared without a trace, and found that aggregations of *R. pachyptila* had grown in three of the previously cleared diffuse flow sources. No disarticulated mussel shells were seen anywhere within this vent site, and it was not obvious whether the mussels had migrated or had been eaten. The single live mussel was observed attached to a syntactic foam marker, 50 cm above the ocean floor. In a mensurative experiment to examine the fate of the mussel deployment and the rate at which they left the area, another 200 mussels were deployed over one of the cleared (and still uncolonized) sources of diffuse flow and their movement was documented with a time-lapse camera. The temperature at this source (21 °C above ambient) had not changed significantly since the year before. After 17.5 h, the two-dimensional surface area covered by mussels increased by 32% as they began to move away from the deployment site. The fastest of the mussels moved at an average speed of 0.74 cm h^{-1} during the observation period. Why the adult mussels migrated away from the source of diffuse flow is unclear. Environmental conditions (*i.e.*, sulfide concentrations or temperature) may have prevented the adult mussels from staying within the site of deployment, although the same species lives in apparently similar microhabitats on the Galapagos Rift (9) and in this vent field (10).

In April 1999, aggregations visually dominated by *R. pachyptila* had grown over three of the six cleared sources of diffuse flow (two treatment patches and one control). There was no evidence of recolonization at the other three, although diffuse flow was still present at every site. The temperatures ranged from 21–30 °C above ambient at the sources of the diffuse flow. Considering the almost complete absence of adult mussels in 1999 and their motility, the absence of a treatment effect on the recolonization of *R. pachyptila* was not surprising. There was no *T. jerichonana* visible in video records of any of the recolonized patches, which is unexpected because this species is often an early colonist to the basalt substrate in this area and has been hypothesized to facilitate *R. pachyptila* colonization (1, 2, 3, 11). However, settlement of *R. pachyptila* has been previously documented on a variety of natural and artificial substrates without the prior establishment of *T. jerichonana* (2, 11, 12). In this experiment, the cleared patches had previously been colonized by *R. pachyptila* and were close to mature *R. pachyptila* aggregations, which may have facilitated conspecific settlement at this site. The apparent absence of mussels and *T. jerichonana*, along with the seemingly random settlement of *R. pachyptila* to some of the cleared sources of diffuse flow, provides additional evidence of the unpredictability of larval settlement around diffuse sources of hydrothermal flow.

At one of the recolonized patches, the base of the *R. pachyptila* tubes was tightly interconnected and centered directly above the venting source, which was confirmed during the previous year to be a single small hole (~ 3 cm in diameter). This aggregation of *R. pachyptila* was collected, intact, by its base, with the manipulator arm of *Alvin*, and placed into a sealed acrylic box for transport to the surface. Although some of the associated fauna were lost during the collection, review of the video record confirmed the pilot's report that very few individuals fell from the *R. pachyptila* aggregation as it was placed into the collection box. Over 600 individuals of *R. pachyptila* were collected in this sample, along with 24 other species (Table 1). All macrofaunal species (> 500 μm) were identified, enumerated, and weighed for determination of relative abundance and biomass in this one-year-old *R. pachyptila* community (Table 1).

Growth rates of *R. pachyptila* have been estimated from the length of the tubes (1, 2). However, individuals of this species can grow chitinous septa in the middle of their tubes, and they may inhabit only a portion of the total length of the tube (13, 14). Therefore, tube growth may not reliably reflect animal growth. In this collection of *R. pachyptila*, there was a strong negative relationship between the total length of the tube and the percentage of the tube occupied by the worm (Fig. 1). Some of the largest worms occupied only 20% of their tubes, and tubes greater than 60 cm were never more than 60% occupied. The tube of *R. pachyptila* serves to protect the soft tissue of the animal and also to place the gas-exchange organ (the plume) in the mixing zone of diffuse hydrothermal effluent and the ambient deep-ocean water. Tube shape and length will thus be affected by the position of an individual within an aggregation and the characteristics of the vent fluid flow to that aggregation. Therefore, we consider it unlikely that the relation shown in Figure 1 will hold for *R. pachyptila* in other microhabitats, because the lack of direct correlation between tube length and animal length is characteristic of this species (pers. obs., C.R. Fisher). A size frequency histogram, constructed from the mass (wet weight) of all of the *R. pachyptila* individuals in this aggregation, suggests that this species either exhibits extremely (and we suggest unbelievably) variable individual growth rates, or that recruitment occurred throughout the previous year and included very recent settlement of *R. pachyptila* (Fig. 2). About 45% of the worms in the aggregation were sexually mature (with a sex ratio of 1 male to 1.3 females), and 16% weighed less than 1 g (Fig. 2). In 1997, *R. pachyptila* populations at the same site (Riftia Field) were similarly skewed to the smallest individuals, and the sex ratio was also around 1 to 1 (12). Negative species interactions may contribute to high juvenile mortality, but the use of biogenic cues by adult *R. pachyptila* may

Table 1

Composition of the macrofaunal assemblage associated with an aggregation of Riftia pachyptila

Group	Species	Abundance	Relative abundance (%)	Biomass (g)	Relative biomass (%)
Symbiont-containing species					
Polychaeta	*Riftia pachyptila*	647	95.71	3252.94	99.99
	Tevnia jerichonona	23	3.40	0.14	<0.01
Bivalvia	*Bathymodiolus thermophilus*	6	0.89	0.23	0.01
All other species					
Polychaeta	*Paralvinella grasslei*	2583	10.74	65.46	59.11
	Paralvinella pandorae irlandei	211	0.88	0.09	0.08
	Amphisamytha galapagensis	397	1.65	0.05	0.04
	Hesiospina vestimentifera	11	0.05	0.03	0.02
	Nereis sandersi	2	0.01	0.27	0.24
	Galapagomystides arstata	211	0.88	1.22	1.10
	Branchinotogluma grasslei	14	0.06	0.09	0.08
	Branchinotogluma hessleri	6	0.02	0.02	0.02
	Branchinotogluma sandersi	2	0.01	0.04	0.04
	Branchiplicatus cupreus	1	<0.01	0.18	0.16
	Iphionella riseusis	1	<0.01	<0.01	<0.01
	Lepidonotopodium riftense	2	0.01	0.01	<0.01
	Levensteiniella kincaidi	1	<0.01	<0.01	<0.01
	Opisthotrochopodus alvinus	12	0.05	0.04	0.04
Gastropoda	*Cyathermia naticoides*	9757	40.58	13.94	12.59
	Gorgoleptis spiralis	8	0.03	<0.01	<0.01
	Lepetodrilus elevatus	7123	29.63	9.44	8.53
	Lepetodrilus pustulosus	1327	5.52	3.37	3.04
	Nodopelta spp.	142	0.59	0.71	0.64
	Rhynchopelta concentrica	2172	9.03	9.52	8.60
Crustacea	*Bythograea thermydron*	30	0.12	6.25	5.64
	Ventiella sulfuris	28	0.12	0.02	0.02
Total (symbiont-containing species)		676		3253.31	
Total (all other species)		24,041		110.74	
Total		24,717		3364.05	

The wet weight of *Riftia pachyptila* was estimated using methods described in Figure 2. The wet weight (frozen in preweighed bags), dry weight (dried for 12 h at 60 °C), and ash-free dry weight (combusted for 8 h at 500 °C) of a subset of the individuals was measured on a Mettler-Toledo (AG245) balance after returning to the laboratory. After all of the other species were identified to the lowest possible taxon, subsamples were dried and weighed following the above procedure to calculate the biomass in ash-free dry weight. Two species of dirivultid copepods were also collected with this aggregation; however, the abundance and biomass of these meiofaunal species were not included in this table, which describes the macrofaunal composition of the community (pers. comm., S. Ivaneneko, Moscow State University).

facilitate gregarious settlement and result in high population turnover (10, 12).

This collection of an intact *R. pachyptila* aggregation along with the associated fauna provided an opportunity to gain insight into the structure of a *R. pachyptila* community of a known age. After one year, this aggregation included 647 individuals of *R. pachyptila* weighing 3.25 kg (ash-free dry weight) (Table 1) and contributing 96.7% of the total community biomass. The surface area of the *R. pachyptila* tubes provided 4.75 m^2 of biogenic substrate available for colonization by other species. At least 24 macrofaunal species occupied the surfaces and interstitial spaces of the tubes, representing 13 families from phyla Annelida, Mollusca, and Arthropoda (Table 1). Colonization rates on the cleared sources of diffuse flow in this experiment were similar to those on basalt blocks that were embedded in vestimentiferan aggregations (10). However, the reassembly of the community was much faster after this clearance experiment than after an eruption and the creation of new hydrothermal vents. By the time *R. pachyptila* had formed dense aggregations (3.5 years post-eruption), the number of species observed was similar to the species richness in this one-year-old *R. pachyptila* aggregation (2).

The macrofaunal species of this community are primarily grazers and scavengers and do not rely on *R. pachyptila* as their primary source of nutrition (15, 16). The gastropods were the most abundant of the associated fauna, accounting for 85.4% of the total 24,041 individuals. The most common species were the snail *Cyathermia naticoides* (40.6%) and the limpets *Lepetodrilus elevatus* (29.6%) and *Rhyncopelta concentrica* (9.0%) (Table 1). Gastropods also dominate the abundance of communities associated with the

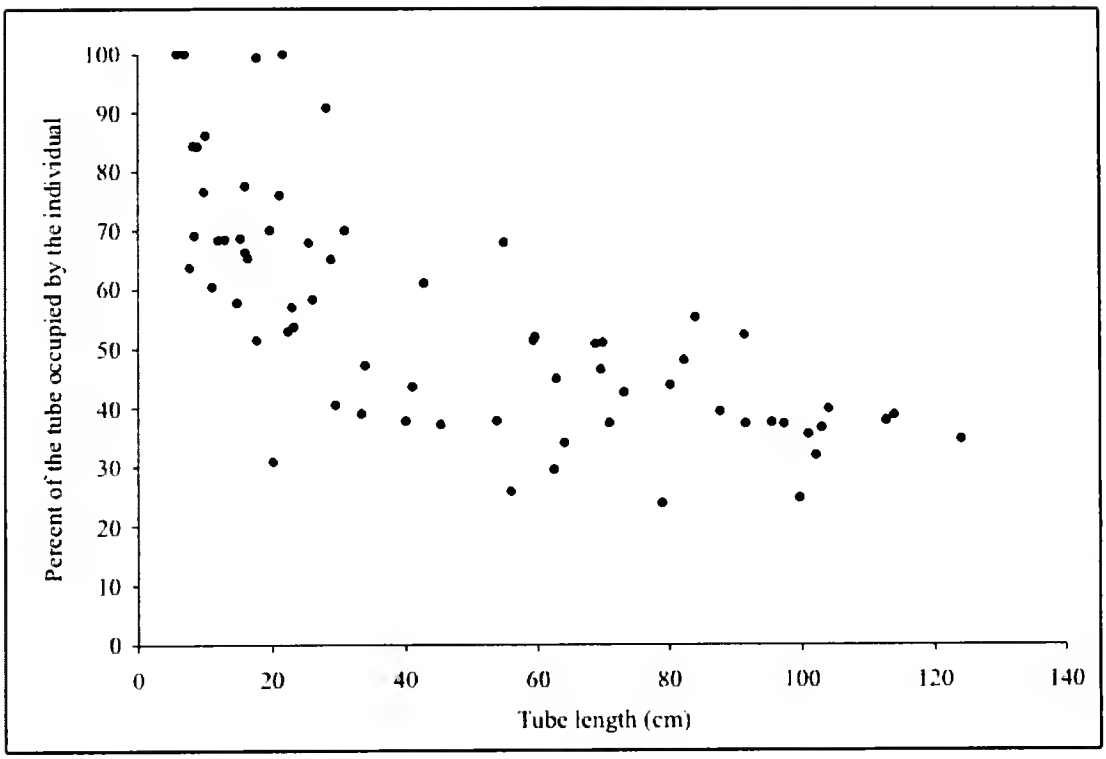

Figure 1. The percent of the *Riftia pachyptila* tube occupied by the individual worm decreases as the tube length increases. The occupied tube length was measured from the anterior opening of the tube to the first septum inside the tube.

vestimentiferan *Ridgeia piscesae* in the basalt-hosted hydrothermal vents at the Juan de Fuca Ridge in the northeast Pacific Ocean (17, 18), and *Lepetodrilus* spp. is often the dominant gastropod in a variety of vent habitats at the Juan de Fuca Ridge and the northern and southern East Pacific Rise (17, 18, 19, 20, 21, 22, 23). Although only accounting for 10.7% of the associated fauna abundance, the polychaete *Paralvinella grasslei* contributed the largest fraction (59.1%) of the associated fauna biomass (Table 1). In this *R. pachyptila* aggregation, the density of *P. grasslei* was considerably higher than on basalt blocks deployed for 13 months in a similar habitat at this vent field (10; unpubl. data, L. Mullineaux, Woods Hole Oceanographic Institution). *P. grasslei* lives in a thick mucous casing at the base of *R. pachyptila* tubes and may preferentially live in association with *R. pachyptila*. Among the species found attached to *R. pachyptila* tubes were small individuals of *T. jerichonana* (23 specimens, maximum tube length < 4 cm) and *B. thermophilus* (6 specimens, maximum shell length < 1.5 cm). The presence of the juvenile mussels is especially interesting in the context of the emigration of the adults transplanted to these sites. The adult mussels were deployed directly on the source of diffuse venting, which may have exceeded their tolerance range. The juvenile mussels may have settled in a more suitable habitat on the *R. pachyptila* tubes. Situated well above the venting source, the juvenile mussels would have been exposed to less concentrated hydrothermal flow, where the temperatures and the concentrations of reduced chemicals are lower and the oxygen concentration is higher than in fluids emanating from the basalt. In various marine environments, habitat created by foundation species can alter hydrodynamics, water chemistry, food availability, larval settlement, and biological interactions, in the addition to providing space for colonization and refuge from competitors and predators (24, for review). The data presented here suggest that *R. pachyptila* may modify the vent habitat to facilitate the colonization of other species. In this way, *R. pachyptila* seems to play an important role in the succession of species and the composition of the community in the diffuse-flow habitat of basalt-hosted hydrothermal vents at the East Pacific Rise.

Acknowledgments

We thank the captain, pilots, and crews of the R/V *Atlantis* and the DSV *Alvin* for their expertise and assistance in shipboard and submersible operations on the 1998 (AT 3-19) and 1999 (AT 3-33) cruises. We are also grateful to L. Mullineaux for her contribution to the improvement of this manuscript, to S. Ivanenko and S. Hourdez for their assistance with species identification, to Steve Rose and Eileen McTague for their assistance in the laboratory, and to the

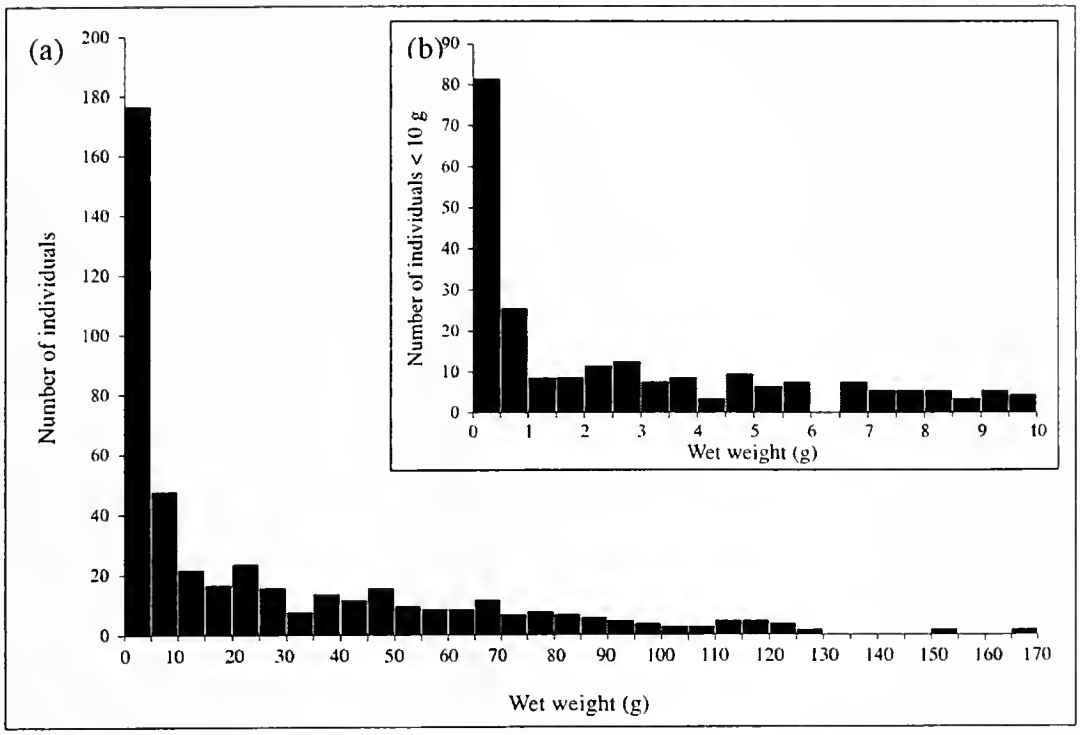

Figure 2. Histograms of the number of *Riftia pachyptila* individuals in 5-g size classes: (a) all individuals; (b) individuals weighing less than 10 g. At sea, wet weights of some individuals were estimated by volume displacement in a graduated cylinder and some individuals were frozen to be measured in the laboratory on a Mettler-Toledo (AG345) balance. The remaining individuals were preserved in 10% formalin, and the wet weights of a portion of these individuals were similarly estimated by volume displacement; the rest were measured on the balance. Wet weight was estimated by volume using linear regression (frozen: wet weight = 1.0256 (volume) + 0.1406, $r^2 = 0.995$, $P < 0.001$; preserved: wet weight = 0.8783 (volume) + 2.310., $r^2 = 0.986$, $P < 0.001$) (JMP, version 5.0, SAS).

Eberly College of Science, Pennsylvania State University, for the support of undergraduate participation in this project. This work was funded by the National Science Foundation grants OCE-9712808 (to CRF), OCE-9712233 (to L. Mullineaux), and OCE-9712809 (to C. Peterson).

Literature Cited

1. **Lutz, R. A., T. M. Shank, D. J. Fornari, R. M. Haymon, M. D. Lilley, K. L. Von Damm, and D. Desbruyeres. 1994.** Rapid growth at deep-sea vents. *Nature* **371:** 663–664.
2. **Shank, T. M., D. J. Fornari, K. L. Von Damm, M. D. Lilley, R. M. Haymon, and R. A. Lutz. 1998.** Temporal and spatial patterns of biological community development at nascent deep-sea hydrothermal vents (9°50′N, East Pacific Rise). *Deep-Sea Res. II* **45:** 465–515.
3. **Mullineaux, L. S., C. R. Fisher, C. H. Peterson, and S. W. Schaeffer. 2000.** Tubeworm succession at hydrothermal vents: use of biogenic cues to reduce habitat selection error? *Oecologia* **123:** 275–284.
4. **Hessler, R. R., W. M. Smithey, M. A. Boudrias, C. H. Keller, R. A. Lutz, and J. J. Childress. 1988.** Temporal change in megafauna at the Rose Garden hydrothermal vent (Galapagos Rift, eastern tropical Pacific). *Deep-Sea Res. A* **35:** 1681–1710.
5. **Johnson, K. S., J. J. Childress, C. L. Beehler, and C. M. Sakamoto. 1994.** Biogeochemistry of hydrothermal vent mussel communities—the deep-sea analog to the intertidal zone. *Deep-Sea Res. I* **41:** 993–1011.
6. **Fisher, C. R. 1990.** Chemoautotrophic and methanotrophic symbioses in marine invertebrates. *Rev. Aquat. Sci.* **2:** 399–436.
7. **Childress, J. J., and C. R. Fisher. 1992.** The biology of hydrothermal vent animals: physiology, biochemistry, and autotrophic symbioses. *Oceanogr. Mar. Biol. Annu. Rev.* **30:** 337–441.
8. **Page, H. M., A. Fiala-Medioni, C. R. Fisher, and J. J. Childress. 1991.** Experimental evidence for filter-feeding by the hydrothermal vent mussel, *Bathymodiolus thermophilus*. *Deep-Sea Res. A* **38:** 1455–1461.
9. **Fisher, C. R., J. J. Childress, A. J. Arp, J. M. Brooks, D. Distel, J. A. Favuzzi, H. Felbeck, R. Hessler, K. S. Johnson, M. C. Kennicutt, S. A. Macko, A. Newton, M. A. Powell, G. N. Somero, and T. Soto. 1988.** Microhabitat variation in the hydrothermal vent mussel *Bathymodiolus thermophilus* at Rose Garden vent on the Galapagos Rift. *Deep-Sea Res. A* **35:** 1769–1792.
10. **Mullineaux, L. S., C. H. Peterson, F. Micheli, and S. W. Mills. 2003.** Succession mechanism varies along a gradient in hydrothermal fluid flux at deep-sea vents. *Ecol. Monogr.* **73:** 523–542.
11. **Hunt, H. L., A. Metaxas, R. M. Jennings, K. M. Halanych, and L. S. Mullineaux. 2004.** Testing biological control of colonization by vestimentiferan tubeworms at deep-sea hydrothermal vents (East Pacific Rise, 9°50′N). *Deep-Sea Res. I* **51:** 225–234.
12. **Thiébaut, E., X. Huther, B. Shillito, D. Jollivet, and F. Gaill. 2002.**

Spatial and temporal variations of recruitment in the tube worm *Riftia pachyptila* on the East Pacific Rise (9°50′N and 13°N). *Mar. Ecol. Prog. Ser.* **234:** 147–157.

13. **Gaill, F., B. Shilito, F. Menard, G. Golfinet, and J. J. Childress. 1997.** The rate and process of tube production by the deep-sea hydrothermal vent tubeworm *Riftia pachyptila*. *Mar. Ecol. Prog. Ser.* **148:** 135–143.
14. **Ravaux, J., L. Chamoy, and B. Shillito. 2000.** Synthesis and maturation processes in the exoskeleton of the vent worm *Riftia pachyptila*. *Mar. Biol.* **136:** 505–512.
15. **Fisher, C. R., J. J. Childress, S. A. Macko, and J. M. Brooks. 1994.** Nutritional interactions in Galapagos Rift hydrothermal vent communities: inferences from stable carbon and nitrogen isotope analyses. *Mar. Ecol. Prog. Ser.* **103:** 45–55.
16. **Micheli, F., C. H. Peterson, L. S. Mullineaux, C. R. Fisher, S. W. Mills, G. Sancho, G. A. Johnson, and H. S. Lenihan. 2002.** Predation structures communities at deep-sea hydrothermal vents. *Ecol. Monogr.* **72:** 365–382.
17. **Tsurumi, M., and V. Tunnicliffe. 2001.** Characteristics of a hydrothermal vent assemblage on a volcanically active segment of Juan de Fuca Ridge, northeast Pacific. *Can. J. Fish. Aquat. Sci.* **58:** 530–542.
18. **Tsurumi, M., and V. Tunnicliffe. 2003.** Tubeworm-associated communities at hydrothermal vents on the Juan de Fuca Ridge, northeast Pacific. *Deep-Sea Res. I* **50:** 611–629.
19. **Sarrazin, J., V. Robigou, S. K. Juniper, and J. R. Delaney. 1997.** Biological and geological dynamics over four years on a high-temperature sulfide structure at the Juan de Fuca Ridge hydrothermal observatory. *Mar. Ecol. Prog. Ser.* **153:** 5–24.
20. **Sarrazin, J., and S. K. Juniper. 1999.** Biological characteristics of a hydrothermal edifice mosaic community. *Mar. Ecol. Prog. Ser.* **185:** 1–19.
21. **Govenar, B. W., D. C. Bergquist, I. A. Urcuyo, J. T. Eckner, and C. R. Fisher. 2002.** Three *Ridgeia piscesae* assemblages from a single Juan de Fuca sulphide edifice: structurally different and functionally similar. *Cah. Biol. Mar.* **43:** 247–252.
22. **Van Dover, C. L. 2002.** Community structure of mussel beds at deep-sea hydrothermal vents. *Mar. Ecol. Prog. Ser.* **230:** 137–158.
23. **Van Dover, C. L. 2003.** Variation in community structure within hydrothermal vent mussel beds of the East Pacific Rise. *Mar. Ecol. Prog. Ser.* **253:** 55–66.
24. **Bruno, J. F., and M. D. Bertness. 2001.** Habitat modification and facilitation in benthic marine communities. Pp. 201–218 in *Marine Community Ecology*. M. D. Bertness, S. D. Gaines, and M.E. Hay, eds. Sinauer Associates, Sunderland, MA.

Reference: *Biol. Bull.* **207:** 183–187. (December 2004)

Long-Term Consequences of Agonistic Interactions Between Socially Naïve Juvenile American Lobsters (*Homarus americanus*)

RACHEL L. RUTISHAUSER[1], ALO C. BASU[1], STUART I. CROMARTY[2], AND EDWARD A. KRAVITZ[1,*]

[1] *Harvard Medical School, Department of Neurobiology, 220 Longwood Avenue, Boston, Massachusetts 02115; and* [2] *Assumption College, Department of Natural Sciences, 500 Salisbury Street, Worcester, Massachusetts 01609-1296*

Agonistic behavior of decapod crustaceans occurs in the wild, is highly stereotypical, and is readily quantifiable. Here we explore the persistence of dominance relationships in socially naïve juvenile American lobsters (Homarus americanus) *by examining the time frame over which behavior changes as a result of previous fight experience. We paired opponents for three fights: initial; 1 hour later; and after 1, 4, or 7 days of separation. As reported in previous studies, the mean duration of encounters decreased when a dominance relationship had been established. After 1 day of separation, both duration and intensity of encounters remained significantly lower compared to the initial fight. At 4 days of separation, the duration of encounters was still significantly reduced, indicating that the behavior of socially naïve juvenile lobsters is influenced by fight experience for at least 4 days.*

Though aggression has been studied extensively, little is known about its underlying neural mechanisms. The purpose of the present study was to examine the persistence of behavioral effects of fighting experience in socially naïve juvenile lobsters (*Homarus americanus* Milne-Edwards, 1837), as a step toward investigating both the neural substrate and ethological relevance of such effects. In socially naïve juvenile lobsters, fighting behavior is highly stereotypical, easily evoked, and readily quantifiable (1). In the wild, fights are often short, as size asymmetries and previous experience play an important role in early decision-making (2, 3). In the laboratory, stable dominance relationships form readily between pairs of lobsters (1, 2, 4), and hierarchies form within groups (5, 6, 7, 8).

Previous studies have shown that subordinates tend to avoid engaging dominants (1, 3, 5, 6, 9), and if interactions do take place, their duration and intensity are reduced. Thus, with the formation of dominance relationships, fighting tapers off, and the duration and intensity of encounters can be used as measures of "willingness" to fight (1). Studies of adult, socially experienced lobsters indicate that recognition of a dominance relationship is retained for at least 1 day of separation after an initial fight (4). Pairs separated for 7 days showed variable results, and all animals seemed to have forgotten their initial dominance relationships after 14 days. Although the patterns of fighting behavior between pairs of experienced and pairs of socially naïve animals are similar, differences are apparent, for example, in the time taken to establish dominance and in the intensity of fighting. Karavanich and Atema (4) postulate that these differences may be due to shaping of the adult behavior by experience. Naïve lobsters exhibit more ritualized fighting, making it possible to quantify the behavior and to define the consequences of experience on the subsequent patterns of behavior (1).

We have characterized the conduct of pairs of socially naïve, juvenile animals over three 30-min fighting periods. The first fight served to establish the dominance relationship, the second (1 h later) was used to confirm that relationship, and the third (either 1, 4, or 7 days later) was used to determine how long the effects of the initial two fighting periods continued to influence subsequent fighting behavior. A preliminary report of these data has been published (10).

Juvenile lobsters, that had been isolated visually and physically, but not chemically, from the fourth post-larval

Received 9 July 2004; accepted 25 August 2004.

* To whom correspondence should be addressed: E-mail: edward_kravitz@hms.harvard.edu

stage were obtained from a rearing facility at the New England Aquarium, Boston, Massachusetts. Animals were weighed to determine their size (1.04–3.49 g) and were molt-staged based on exoskeletal flexibility. Only intermolt animals were used because agonistic behavior varies over the molt cycle (11, 12). After transport to a 15–16 °C room with a 12-h light/dark cycle at Harvard Medical School, lobsters were again visually and physically but not chemically isolated, and housed in perforated opaque containers in circulating artificial seawater (Marine Biotech, salinity 33 ppt). They were fed squid, shrimp, or fish three times a week. Animals were isolated in individual 9-l tanks the day before their first fights.

The following three experimental groups of lobsters were assembled randomly: animals separated for 1 day (7 pairs), animals separated for 4 days (7 pairs), and animals separated for 7 days (6 pairs). Within-pair differences in weight ranged from 9% to 29%. A one-way parametric analysis of variance (ANOVA) confirmed that the mean percent weight difference between individuals in a pair did not vary significantly between the three experimental groups ($P > 0.05$). Under these conditions, animals usually establish a hierarchical relationship during their first 30-min fighting period (1). Pairs were selected at random, paying no attention to gender because in animals of the early developmental stage used, claws are relatively undifferentiated between the sexes (8, 13, 14). Difference in claw size is a major factor conferring fighting advantage in adult male lobsters (6). Formation of a dominance relationship was determined based on consistent retreats in the first fight by one animal, and only pairs that exhibited a stable dominance relationship between the first and second fight were paired for a third fight.

The fights were set up in the following manner: two animals were removed from their isolation tanks; placed on either side of an opaque divider in a 38-l observation tank with a gravel-lined floor; and allowed to acclimate, with a charcoal filter running, for 30 min. The divider was removed for 30 min (Fight 1), replaced for 1 h, and removed again for 30 min (Fight 2), after which the opponents were returned to their isolation tanks. Pairs were separated for 1, 4, or 7 days, after which the animals were acclimated in the fight tank for 30 min, and then allowed to fight for 30 min (Fight 3). The filter in the observation tank was turned off whenever the divider was removed. Artificial seawater was changed and filtered between each pair, and all fights were videotaped using a Panasonic 3260 or PV-A208 video camera. Only physically intact animals were used, and these were not re-used after a series of three fights.

During fight periods, opponents came together, interacted, and then separated. Each such event was called an "encounter," and these occurred repeatedly during a fight. Each encounter was scored from the time two animals came within one body length of each other to when one or both broke off and they remained separated for at least 5 s. Measurements taken included encounter duration and maximum intensity level reached during the encounter (on a scale from 0 to 3; see (1)), which animal approached, and which animal retreated. Opponents were distinguished by their exoskeletal markings and coloring. Data were entered into FileMaker Pro and analyzed using Microsoft Excel or OriginLab 7.0.

We analyzed changes in the mean duration of individual encounters within 30-min fighting periods, as well as the summed duration of all encounters within 30-min fighting periods. For the analysis of fight intensity, we divided the intensity scale into two bins: level 0, when only one animal is engaged in offensive aggressive behavior; and levels 1–3, when both animals are engaged in offensive aggressive behavior. The percentage of encounters that reached a maximum intensity greater than 0 was then compared across fighting periods. Nonparametric Friedman ANOVAs were used to detect significant differences in encounter duration and intensity across the three fighting periods for each group, followed by *post hoc* Wilcoxon signed-rank tests for all three possible pairwise comparisons of fights within a group.

Figure 1 shows the durations of all encounters for the three groups of animals over all fights. The greatest variation in the duration of individual encounters occurs in about the first 15 encounters of the initial fight within each group (Fig. 1, left). As the initial fight progressed and dominance was established, the duration of individual encounters was reduced. To test whether fighting behavior changed significantly after different periods of separation, we used Friedman ANOVAs for within-group differences across Fights 1, 2, and 3 in the three groups of animals. The data for mean duration, summed encounter duration, and percent of encounters with maximum intensity greater than 0 are presented in Table 1 and are represented graphically in Figure 2.

The mean duration of encounters was significantly lower in the third fight when compared to the initial fight for animals separated for 1 day (ANOVA: $P < 0.025$; *post hoc* Fight 1 *vs.* 3: $P < 0.05$) and 4 days (ANOVA: $P < 0.025$; *post hoc* Fight 1 *vs.* 3: $P < 0.05$), but not 7 days (ANOVA: $P < 0.01$; *post hoc* Fight 1 *vs.* 3: $0.05 < P < 0.10$). The same trend is demonstrated with the summed duration data (Table 1). Thus, animals separated for 1 or 4 days fought less during their third fight than they did during their first fight. Apparent differences in encounter durations during Fight 1 between groups (i) could not be compared directly by Friedman ANOVA due to the different number of pairs fought in the group separated for 7 days ($n = 6$) and the other two groups ($n = 7$); and (ii) likely result from chance, as initial fights for all three experimental groups were conducted in parallel and animals were assigned to groups at random. The maximum intensity data yielded a consistent

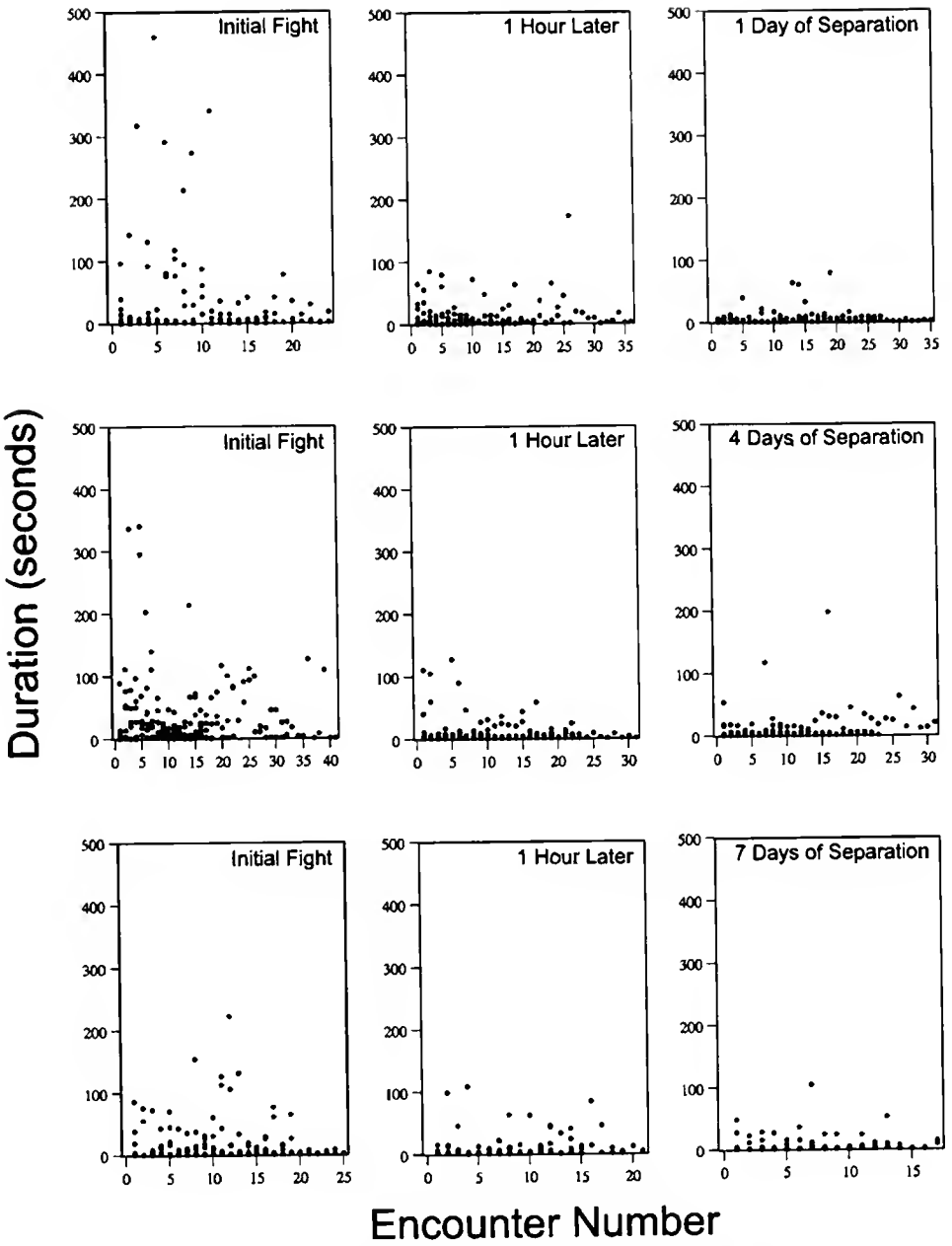

Figure 1. Scatter plots of encounter duration. Duration of encounter (in seconds) is plotted against the number of the corresponding encounter in chronological sequence. Each point represents an individual encounter. Data points for pairs of animals within the same experimental group were plotted together for each fight.

finding for pairs separated for 1 day (ANOVA: $P < 0.05$; *post hoc* Fight 1 *vs.* 3: $P < 0.05$); however, there is no significant difference for pairs separated for 4 or 7 days. No significant differences were found in the *post hoc* comparisons of Fight 2 to either Fight 1 or Fight 3 for any measurements within any group.

In many species, agonistic experience has long-lasting effects on the subsequent behavior of both winners and losers (15). Here, we focus on the persistence of such effects in pairs of socially naïve juvenile lobsters allowed to interact under controlled conditions. Our results show that two short, 30-min fights can exert significant long-lasting effects on the fighting behavior of socially naïve juvenile lobsters. Due to their extended duration, we refer to them as "memory" effects, although we have not addressed their underlying mechanisms—for example, whether these effects indicate a memory of hierarchical decisions made or are specific to the individual familiar opponent remains an open question.

Our results using juvenile animals have similarities to

Table 1

Comparison of Fight 1, Fight 2, and Fight 3

Days of separation	Fight 1	Fight 2	Fight 3	Friedman ANOVA	Wilcoxon signed-rank (Fight 1 *vs.* 3)
Mean Encounter Duration (seconds)					
1	47.09 (± 56.35)	13.74 (±9.67)	5.92 (± 2.63)	$P < 0.025$	$P < 0.05$
4	35.30 (± 19.54)	10.53 (± 7.70)	8.57 (± 8.12)	$P < 0.025$	$P < 0.05$
7	22.11 (± 13.68)	10.85 (± 9.46)	7.16 (± 7.58)	$P < 0.01$	$0.05 < P < 0.10$
Summed Encounter Duration (seconds)					
1	579.71 (± 177.812)	247.57 (± 70.06)	124.14 (±36.19)	$P < 0.05$	$P < 0.05$
4	811.29 (± 195.95)	219.71 (± 55.80)	204.00 (± 107.19)	$P < 0.005$	$P < 0.05$
7	443.83 (± 120.28)	189.33 (± 90.09)	111.83 (± 59.30)	$P < 0.01$	$0.05 < P < 0.10$
Percent of Encounters with Maximum Intensity > 0					
1	77.51 (± 10.44)	56.32 (± 25.75)	38.90 (± 23.02)	$P < 0.05$	$P < 0.05$
4	64.92 (± 32.58)	54.03 (± 27.37)	55.04 (± 30.47)	NSD	N/A
7	66.58 (± 20.87)	70.40 (± 16.11)	45.90 (± 34.29)	NSD	N/A

Mean encounter duration, summed encounter duration, and percent encounters with a maximum intensity > 0 (± standard deviation) for Fight 1 (initial), Fight 2 (1 hour later), and Fight 3 (1, 4, or 7 days later). NSD = No significant difference; N/A = not examined because Friedman ANOVA yielded no significant difference.

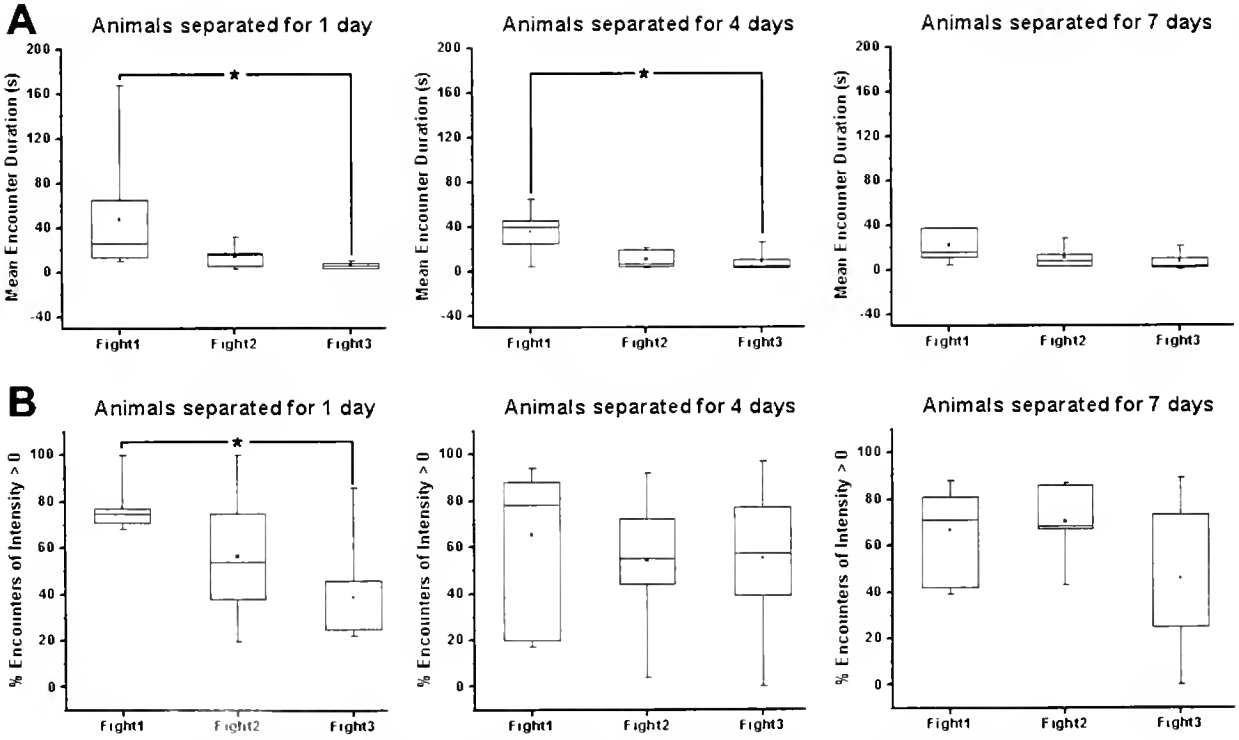

Figure 2. Mean duration of encounters and percent of encounters in which both animals are aggressive. Both mean duration of encounters (A) and the percent of encounters that reach a maximum intensity of level 1, 2, or 3 (B) are reduced in the third fight relative to the initial fight for animals separated for one day. There is also a reduction in mean encounter duration between Fight 1 and Fight 3 for animals separated for 4 days. Box plots range from 25th to 75th percentile of data, whiskers extend to minimum and maximum values, median value is indicated with a line, and mean with a dot. All values for pairs of animals assigned to the same group were pooled together for each fight within the group.

those reported in studies of adult socially experienced lobsters (4). In the latter studies, animals fought with decreased agonistic intensity against familiar opponents but not unfamiliar opponents 1 day after their initial fights. After 7 days, results were variable and differences were not statistically significant; after 14 days there was no evidence of any memory of status. Here, we have studied dominance recognition in socially naïve juvenile lobsters. These animals differ not only in age but also in social experience from wild-caught adult lobsters. In our experiments, they fought with their first and only opponent. This is a critical distinction, as the previous experience of adult lobsters likely influences their behavior in subsequent interactions. Our study did not address the issue of individual recognition.

Although a wide time range has been observed in the persistence of memory of social status in other species (15), two generalizations have emerged. The first is that memory of status lasts longer in losers of fights than in winners. This result has been suggested to indicate the greater importance of an animal knowing that it is a poor fighter for surviving future encounters in the wild. The second generalization is that animals that have fewer encounters in the wild remember the outcome of those encounters for longer periods of time. That is, to apply its past experiences adaptively, an animal with few encounters requires a longer memory.

Our study and others (4) indicate that lobsters retain memory of social status for a relatively long time. Field observations show that adult lobsters spend much of their lives isolated in shelters, encountering conspecifics largely when foraging for food (16, 17). Though these studies targeted specific sub-populations of lobsters, the relatively low frequency of agonistic encounters observed is consistent with the idea that lobsters should retain a relatively long memory of status. The agonistic behavior of juvenile lobsters in the field has yet to be studied. The duration of memory retention found in this study suggests that changes in gene expression might underlie these changes in behavior, since it is unlikely that purely second-messenger-mediated mechanisms would last for days. Our present results, however, yield no insights into the nature of the biological changes that might take place. What they do offer is information on the time window during which such changes should be sought.

Acknowledgments

We thank Mr. Jason Goldstein and Dr. Marianne Farrington for supplying us with juvenile animals from a rearing facility at the New England Aquarium, Dr. Margaret Bradley for advice and assistance pertaining to experimental setup and animal care in our laboratory at Harvard Medical School, and Dr. Mayumi Morimoto for statistical consultation. This research was supported by a grant from the National Science Foundation (IBN-0090730 to EAK).

Literature Cited

1. **Huber, R., and E. A. Kravitz. 1995.** A quantitative analysis of agonistic behavior in juvenile American lobsters (*Homarus americanus*). *Brain Behav. Evol.* **46:** 72–83.
2. **Scrivener, J. C. 1971.** Agonistic behavior of the American lobster, *Homarus americanus*. *Fish. Res. Board. Can, Tech. Rep.* **235:** 1–113.
3. **Atema, J., and J. S. Cobb. 1980.** Social behavior. Pp. 409–450 in *The Biology and Management of Lobsters*, Vol. 1, B. F. Philips, ed. Academic Press, New York.
4. **Karavanich, C., and J. Atema. 1998.** Individual recognition and memory in lobster dominance. *Anim. Behav.* **56:** 1553–1560.
5. **Stein, L., S. Jacobson, and J. Atema. 1975.** Behavior of lobsters (*Homarus americanus*) in a semi-natural environment at ambient temperatures and under thermal stress. *Woods Hole Oceanogr. Inst. Tech. Rep.* 75.
6. **Jacobson, S. M. 1977.** Agonistic behavior, dominance and territoriality in the American lobster, *Homarus americanus*. Ph.D. dissertation, Boston University, Boston, MA.
7. **Sastry, A. N., and R. E. Ehinger. 1980.** Dominance hierarchies among communally held juvenile lobsters, *Homarus americanus*. *Mar. Behav. Physiol.* **7:** 85–93.
8. **Atema, J., and R. Voight. 1995.** Behavior and sensory biology. Pp. 331–348 in *Biology of the Lobster Homarus americanus*, J. R. Factor, ed. Academic Press, San Diego.
9. **Karavanich, C., and J. Atema. 1998.** Olfactory recognition of urine signals in dominance fights between male lobster, *Homarus americanus*. *Behaviour* **135:** 719–730.
10. **Rutishauser, R. L., E. J. Wilkinson, A. E. Hower, A. Delago, S. I. Cromarty, R. Huber, B. S. Beltz, and E. A. Kravitz. 1999.** Agonistic behavior in lobsters: persistence of fight-induced changes in status and modulation by serotonin. Abstract Program No. 32.33. Society for Neuroscience, Miami, FL.
11. **Tamm, G. R., and J. S. Cobb. 1978.** Behavior and crustacean molt cycle—changes in aggression of *Homarus americanus*. *Science* **200:** 79–81.
12. **Cromarty, S. I., J. S. Cobb, and G. Kass-Simon. 1991.** Behavioral analysis of the escape response in the juvenile lobster *Homarus americanus* over the molt cycle. *J. Exp. Biol.* **158:** 565–581.
13. **Lang, F., C. K. Govind, W. J. Costello, and S. I. Greene. 1977.** Developmental neuroethology—changes in escape and defensive behavior during growth of lobster. *Science* **197:** 682–685.
14. **Govind, C. K. 1992.** Claw asymmetry in lobsters: case study in developmental neuroethology. *J. Neurobiol.* **23:** 1423–1445.
15. **Hsu, Y., and L. L. Wolf. 1999.** The winner and loser effect: integrating multiple experiences. *Anim. Behav.* **57:** 903–910.
16. **Karnofsky, E. B., J. Atema, and R. H. Elgin. 1989.** Field observations of social behavior, shelter use, and foraging in the lobster, *Homarus americanus*. *Biol. Bull.* **176:** 239–246.
17. **Karnofsky, E. B., J. Atema, and R. H. Elgin. 1989.** Natural dynamics of population structure and habitat use of the lobster, *Homarus americanus*, in a shallow cove. *Biol. Bull.* **176:** 247–256.

Reference: *Biol. Bull.* **207:** 188–190. (December 2004)

Histidine Suppresses Zinc Modulation of Connexin Hemichannels

RICHARD L. CHAPPELL[1,2,*], HAOHUA QIAN[1,3], JANE ZAKEVICIUS[1,3], AND HARRIS RIPPS[1,3]

[1] *Marine Biological Laboratory, Woods Hole, Massachusetts;* [2] *Hunter College and The Graduate Center, CUNY, New York, New York; and* [3] *University of Illinois at Chicago, College of Medicine, Chicago, Illinois*

Zinc has been shown to modulate hemichannel currents of connexins Cx35 and Cx38 in Xenopus *oocytes (1). In both cases the effects were biphasic;* i.e., *low concentrations of zinc enhanced, whereas higher concentrations decreased, the magnitudes of the voltage-activated hemichannel currents. The present study was designed to determine the effects of zinc on hemichannels formed by Cx26, a connexin reportedly expressed on dendrites of carp horizontal cells and implicated in a mechanism for photoreceptor feedback (2, 3, 4). In addition, we examined whether histidine, a zinc chelator, would block the action of zinc on Cx26 hemichannel currents, or would exert a direct effect on those currents.*

Methods for oocyte preparation and recording of connexin hemichannel currents followed procedures described previously (5). Briefly, Stage V–VI oocytes were removed from gravid female *Xenopus*, enzymatically dissociated and defolliculated, and then used to express human Cx26 connexin in the presence of an antisense oligomer to the endogenous oocyte connexin (Cx38). The oocytes were maintained in modified Barth's solution (MB) that contained [in m*M*]: NaCl [88], KCl [1], $NaHCO_3$ [2.3], *N*-2-hydroxyethylpiperazine-*N*′-2-ethanesulfonic acid (HEPES) [15], $Ca(NO_3)_2$) [0.33], $CaCl_2$ [0.41], and $MgSO_4$ [0.82]; pH 7.6. Voltage-activated membrane currents were recorded with a two-electrode voltage clamp. The two protocols we used gave equivalent results: (1) with the cell clamped at 0 mV, 10-s voltage steps were imposed from −50 mV to +50 mV in 10-mV increments, and (2) from the holding potential of 0 mV, currents were recorded in response to voltage ramps extending from −100 mV to +60 mV at a rate of 0.04 mV/ms.

Figure 1 compares a representative record from an oocyte expressing Cx26 with those obtained from an antisense-injected cell and one that was not injected but expressed Cx38, its endogenous connexin. Note the efficacy with which the antisense oligo suppressed the current mediated by Cx38, and the significantly greater membrane currents of Cx26 in response to both depolarizing and hyperpolarizing voltages.

Figure 2A shows current recordings from oocytes expressing human Cx26 in MB and after the addition of various concentrations of zinc. In MB, a voltage ramp from −100 mV to +60 mV elicited large currents at all potentials positive and negative to the reversal potential (−10 mV), suggesting that the hemichannels are constitutively open (5). In the presence of low (1 μM) concentrations of zinc, the magnitude of the currents through Cx26 hemichannels was substantially enhanced. Higher concentrations of zinc, however, decreased these currents in a dose-dependendant fashion such that 10 μM zinc reduced the hemichannel currents to the level seen in control MB solution, and 100 μM and 1 mM zinc further decreased the hemichannel currents. The bar graphs of Figure 2B, taken from the data in Figure 2A, illustrate the effects of zinc on Cx26 hemichannel currents recorded at +40 mV. Both the enhancement and inhibition by zinc of the Cx26 hemichannel current showed little voltage dependence. As shown in Figure 2C, the ratio of the membrane currents measured in zinc to those recorded in MB were virtually unchanged across the range of membrane voltage tested (from −100 mV to +60 mV) for both low concentrations (1 μM) and

Received 1 September 2004; accepted 7 October 2004.

* To whom correspondence should be addressed at Hunter College Biology Department, 695 Park Avenue, New York, NY 10021. E-mail rchappell@gc.cuny.edu

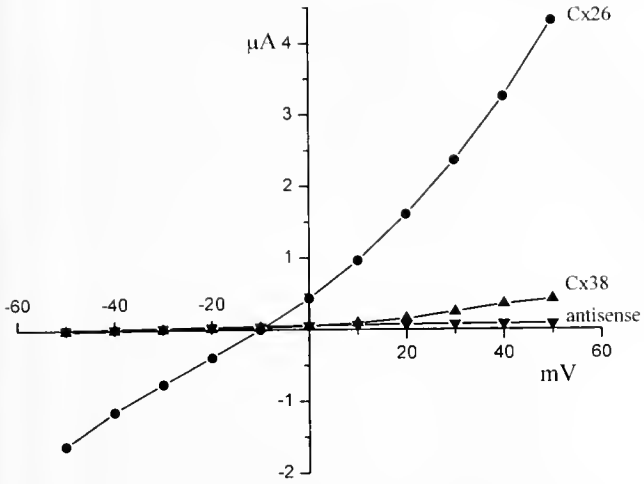

Figure 1. The I-V curves resulting from recordings of the nonjunctional membrane currents of *Xenopus* oocytes expressing Cx26, the endogenous Cx38, or an antisense oligomer to nucleotides within the coding region of Cx38.

high concentrations (100 μM) of zinc. However, recovery of Cx26 hemichannel currents following application of 1 mM zinc was extremely slow, requiring more than 15 min for the current to return to control level after the zinc was removed (Fig. 2D).

We found that 1 mM histidine, a zinc chelator, completely blocked the inhibitory effects of 100 μM zinc on Cx26 hemichannel currents. In the presence of 1 mM histidine, the voltage-activated currents obtained in 100 μM zinc were almost identical to those recorded in MB (Fig. 3A). In addition, we showed that 1 mM histidine alone had no direct effect on hemichannel currents. Averaged values from five cells exposed to the various experimental conditions are shown in Figure 3B.

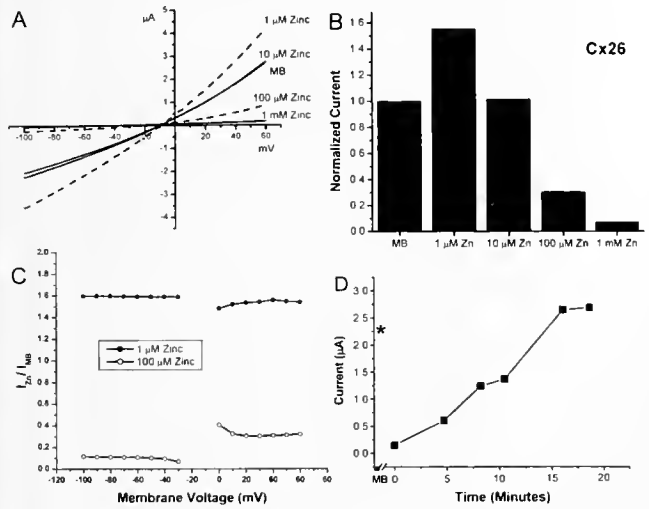

Figure 2. Zinc modulates hemichannels formed by Cx26 connexins expressed in *Xenopus* oocytes. (A) Voltage ramp recordings show greater current responses in 1 μM zinc than in control (MB) solution. The effect is biphasic, such that with higher concentrations, the currents are progressively suppressed in a dose-dependant fashion. (B) Dose-response relation for Cx26 hemichannel currents measured at +40 mV during the voltage ramp from −100 mV to +60 mV. (C) Ratios of membrane currents measured in zinc to those measured in MB (I_{Zn}/I_{MB}) are not a function of clamp voltage. (D) Current recovery following the application of 1 mM zinc was very slow, taking almost 15 min for full recovery to control levels (asterisk); the currents plotted here were measured at +50 mV.

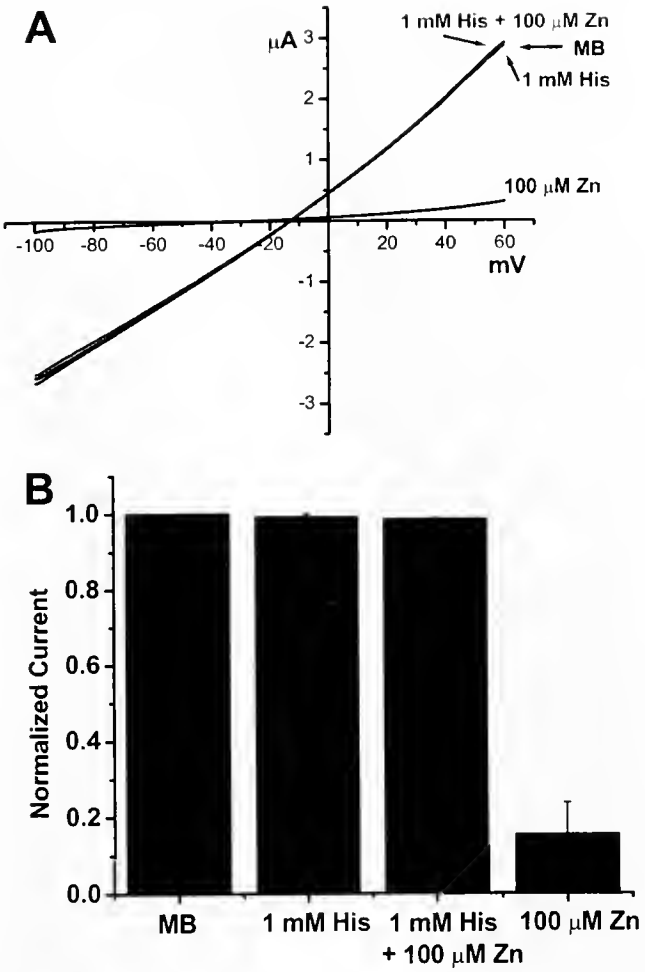

Figure 3. Histidine has no direct effect on Cx26 hemichannels. (A) 100 μM zinc, which had a profound effect on Cx26 hemichannel membrane currents, was completely ineffective in the presence of 1 mM histidine (His). When compared with currents elicited in the control MB solution, 1 mM histidine alone had no effect on the Cx26 hemichannel currents elicited by a voltage ramp from −100 to +60 mV. (B) Bar graphs showing normalized currents, recorded at +40 mV, for the four experimental conditions; error bars = ±S.E.M., n = 5.

The possible roles of hemichannels in the retina and elsewhere in the nervous system remain controversial. However, there is both histological and physiological evidence that Cx26 hemichannels on the horizontal cell dendrites that invaginate carp photoreceptor terminals participate in a feedback mechanism that regulates calcium entry and thereby affects transmitter release (3). Although similar

findings have been reported in turtle retina (4), studies of mouse retina suggest that murine horizontal cells lack Cx26 (6), and express Cx57 (7). Nevertheless, a study of horizontal cell–photoreceptor feedback in mouse retina using the hemichannel blocker carbenoxolone yielded data that were consistent with a model in which hemichannels modulate cone transmitter release by effectively opening more Ca^{2+} channels (8). In contrast, carbenoxolone was recently reported to reduce the amplitude of Ca^{2+} channel currents in isolated salamander cones, suggesting that carbenoxolone could be inhibiting Ca^{2+} channels directly (9).

The results reported here and in earlier studies on the zinc sensitivity of hemichannel currents led us to consider the zinc effects in the context of the hemichannel feedback mechanism of Kamermans *et al.* (3). In this connection, it is important to recall the pioneering study of Wu *et al.* (10), who showed histochemically the presence of a relatively high concentration of reactive zinc in the region of the photoreceptor terminals in salamander retina, and the fact that similar findings were obtained in the retinas of skate (11) and rat (12). The colocalization of zinc with glutamate in the photoreceptor terminals, and the results of electrophysiological experiments showing that zinc suppressed glutamate release by reducing calcium entry into the terminals (10), led the authors to suggest that zinc may serve as a gain-control mechanism at the first synapse of the visual system. Although the possibility remains that zinc exerts a direct effect on calcium channels, its effect on transmitter release may derive from its ability to modulate the hemichannel currents on horizontal cells at the photoreceptor synapse. On this view, raising the extracellular concentration of zinc ($> 10\ \mu M$) to suppress Cx26 hemichannel currents would be expected to reduce calcium entry in the photoreceptor terminals and thus reduce the release of its neurotransmitter, glutamate.

The present findings may have a direct bearing on the results of recent studies showing that 100–500 μM histidine significantly enhances the electroretinographic b-wave responses in the dark-adapted retinas of both skate and zebrafish (13, 14, 15). Glutamate release and, presumably, the co-release of zinc are maximal in darkness, and their rapid reduction by a light flash elicits a voltage response in second-order neurons that is proportional to the magnitude of the decrease in neurotransmitter. If zinc reduces the calcium-regulated release of glutamate through its action on hemichannels, its chelation by histidine would enhance glutamate release and produce the observed increase in the b-wave potential generated by second-order cells. Thus, if zinc is co-released with glutamate, as has been shown for some glutamatergic hippocampal cells (16), the presence of zinc within the photoreceptor synapse may serve to establish the basal level of transmitter release.

Acknowledgments

This work was supported in part by Fight for Sight, PSC/CUNY Grant 66257-0035, and NCRR/NIH RCMI Award RR-03037 (RLC); NIH Grants EY-06516 (HR), EY-14557 (HR), EY-12028 (HQ); and a Senior Research Investigator Award from Research to Prevent Blindness (HR).

Literature Cited

1. **Chappell, R. L., J. Zakevicius, and H. Ripps. 2003.** Zinc modulation of hemichannel currents in *Xenopus* oocytes. *Biol. Bull.* **205:** 209–211.
2. **Janssen-Bienhold, U., K. Schultz, A. Gellhaus, P. Schmidt, J. Ammermüller, and R. Weiler. 2001.** Identification and localization of connexin26 within the photoreceptor-horizontal synaptic complex. *Vis. Neurosci.* **18:** 169–178.
3. **Kamermans, M., I. Fahrenfort, K. Schultz, U. Janssen-Bienhold, T. Sjoerdsma, and R. Weiler. 2001.** Hemichannel-mediated inhibition in the outer retina. *Science* **292:** 1178–1180.
4. **Pottek, M., W. Hoppenstedt, U. Janssen-Bienhold, K. Schultz, I. Perlman, and R. Weiler. 2003.** Contribution of connexin26 to electrical feedback inhibition in the turtle retina. *J. Comp. Neurol.* **466:** 468–477.
5. **Ripps, H., H. Qian, and J. Zakevicius. 2004.** Properties of connexin26 hemichannels expressed in *Xenopus* oocytes. *Cell. Mol. Neurobiol.* **24:** 647–665.
6. **Deans, M. R., and D. L. Paul. 2001.** Mouse horizontal cells do not express connexin26 or connexin36. *Cell Commun. Adhes.* **8:** 361–366.
7. **Hombach, S., U. Janssen-Bienhold, G. Sohl, T. Schubert, H. Bussow, T. Ott, R. Weiler, and K. Willecke. 2004.** Functional expression of connexin57 in horizontal cells of the mouse retina. *Eur. J. Neurosci.* **19:** 2633–2640.
8. **Xia, Y., and S. Nawy. 2003.** The gap junction blockers carbenoxolone and 18β-glycerretinic acid antagonize cone-driven light responses in the mouse retina. *Vis. Neurosci.* **20:** 429–435.
9. **Vessey, J. P., M. R. Lalonde, H. A. Mizan, N. C. Welch, M. E. M. Kelly, and S. Barnes. 2004.** Carbenoxolone inhibition of voltage-gated Ca channels and synaptic transmission in the retina. *J. Neurophysiol.* **92:** 1252–1256.
10. **Wu, S. M., X. Qiao, J. L. Nobels, and X. L. Yang. 1993.** Localization and modulatory actions of zinc in vertebrate retina. *Vision Res.* **33:** 2611–2616.
11. **Qian, H., L. Li, R. L. Chappell, and H. Ripps. 1997.** GABA receptors of bipolar cells from the skate retina: actions of zinc on GABA-mediated membrane currents. *J Neurophysiol.* **78:** 2402–2412.
12. **Ugarte, M., and N. N. Osborne. 1999.** The localization of free zinc varies in rat photoreceptors during light and dark adaptation. *Exp. Eye Res.* **69:** 459–461.
13. **Rosenstein, F. J., and R. L. Chappell. 2003.** Endogenous zinc as a retinal neuromodulator: evidence from the skate (*Raja erinacea*). *Neurosci. Lett.* **345:** 81–84.
14. **Redenti, S., and R. L. Chappell. 2003.** Zinc chelation enhances the sensitivity of the ERG b-wave in dark-adapted skate retina. *Biol. Bull.* **205:** 213–214.
15. **Redenti, S., and R. L. Chappell. 2002.** Zinc chelation enhances the zebrafish retinal ERG b-wave. *Biol. Bull.* **203:** 200–202.
16. **Frederickson, C. J., and D. W. Moncrieff. 1994.** Zinc-containing neurons. *Biol. Signals* **3:** 127–139.

Reference: *Biol. Bull.* **207:** 191–194. (December 2004)

Potassium Currents Distinguish the Two Subtypes of Morphologically Distinct Skate Bipolar Cells

HAOHUA QIAN[1,2,*], RICHARD L. CHAPPELL[1,3], STEPHEN REDENTI[1,3], AND HARRIS RIPPS[1,2]

[1] *Marine Biological Laboratory, Woods Hole, Massachusetts;* [2] *University of Illinois at Chicago, College of Medicine, Chicago, Illinois; and* [3] *Hunter College and The Graduate Center, CUNY, New York, New York.*

Bipolar cells in the vertebrate retina are second-order neurons that convey visual information from photoreceptors to ganglion cells, the neurons that relay the message to the brain. Bipolar cells consist typically of multiple subtypes that differ in their morphology, synaptic connections, and response properties. The individual subtypes are thought to carry different aspects of the visual signal through the retina, and they often exhibit unique membrane properties and neurotransmitter receptors (1). In the all-rod skate retina, only two morphologically and pharmacologically distinct subtypes of bipolar cell have been identified thus far. The large-field bipolar cells, with extensive dendritic arbors, are glycine-insensitive, whereas the small-field bipolar cells, which have only one or two dendritic branches, are sensitive to glycine (2). In the present study, we explored further the membrane properties of these two subtypes of skate bipolar cell with emphasis on the voltage-sensitive potassium currents. Our results show that the cells exhibit different voltage-activated current profiles, suggesting that the signals they transmit contain different features of the visual scene.

Solitary bipolar cells were prepared from skate retina according to the published protocol (3), and were approved by the IACUCs of the University of Illinois College of Medicine and the Marine Biological Laboratory, Woods Hole, Massachusetts. Briefly, skates (*Raja erinacea*) were anesthetized in 0.02% MS222 and double pithed following cervical section; the eyes were then enucleated and hemisected. After removing most of the vitreous, the retina was gently peeled from the underlying tapetal region and incubated for 50 min in a modified culture medium containing 1.8 mg/ml papain (Calbiochem, La Jolla, CA) and 1 mg/ml L-cysteine. The tissue was dissociated by trituration through a sterile pipette, and groups of isolated neurons were kept at 14 °C for up to one week in culture dishes containing an elasmobranch Ringer solution comprising (in m*M*): NaCl (250), KCl (6), $MgCl_2$ (1), $CaCl_2$ (4), urea (360), glucose (10), and HEPES (5), titrated to pH 7.6 with NaOH. Whole-cell voltage clamp recordings were obtained from the cell bodies of individual bipolar cells using patch pipettes filled with a solution containing (in m*M*): KCl (204), EGTA (11), $CaCl_2$ (1), $MgCl_2$ (1), and HEPES (10), titrated to pH 7.6 with KOH. Subtypes of bipolar cells were identified by their morphological appearance and their differential responses to glycine (2).

Skate bipolar cells are readily identified in culture. They have a pear-shaped cell body, from which a prominent axon emerges. The length of the axon is quite variable, perhaps reflecting ON and OFF cell types (4) and variation in the retinal regions from which the cells originate. At its distal end, the cell body extends dendrites whose pattern aids in distinguishing the two subtypes. Figure 1 illustrates several examples of the two subtypes found in the skate retina. Large-field bipolar cells extend several prominent branches with extensive dendritic arbors that enable them to receive input from many photoreceptors (Fig. 1A). In contrast, small-field bipolar cells contain one, or at most two, branches extending from a large dendritic process (Fig. 1B). In our previous study we reported that small-field bipolar cells are responsive to glycine, whereas large-field bipolar cells are glycine-insensitive (2); we obtained similar results in the present study (data not shown).

Received 1 September 2004; accepted 7 October 2004.

* To whom correspondence should be addressed at Department of Ophthalmology and Visual Sciences, University of Illinois at Chicago, 1855 West Taylor Street, Chicago, Illinois 60612. E-mail: hqian@uic.edu

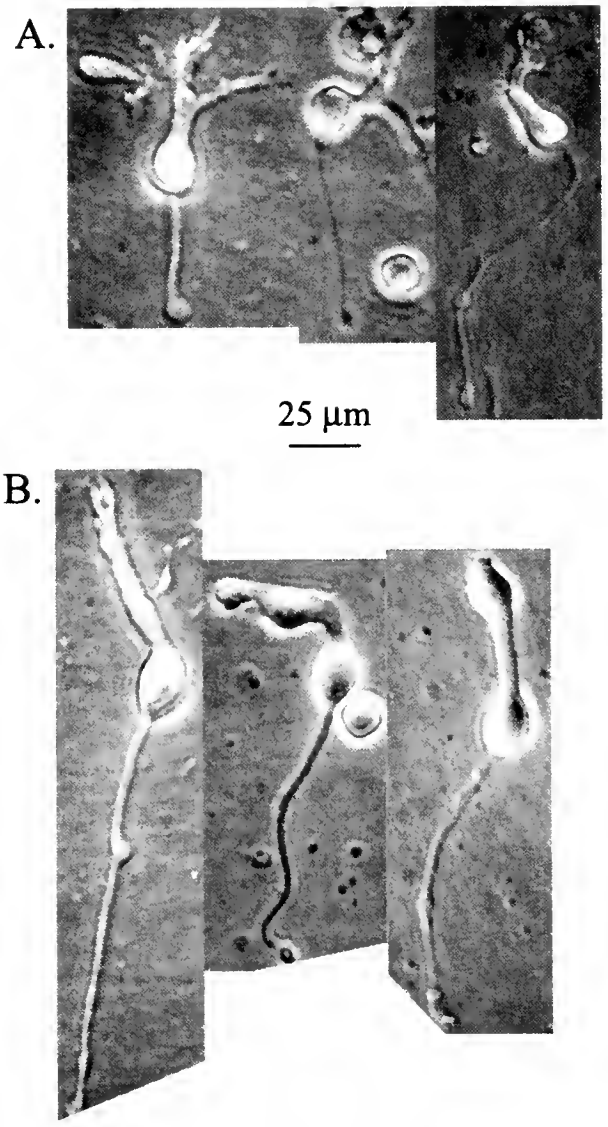

Figure 1. Examples of two morphological subtypes of bipolar cells isolated from skate retina. The two subtypes are distinguished by their dendritic pattern. (A) Large-field bipolar cells contain several small dendrites that arborize within the outer plexiform layer, and axons that extend downward to the inner plexiform layer of the retina. (B) Small-field bipolar cells have only one (or two) main dendrites.

Under whole-cell voltage clamp recording conditions, the small- and large-field bipolar cells exhibited different voltage-activated membrane currents. Figure 2A shows typical current recordings from cells held at −60 mV and stepped to membrane potentials from −120 to +60 mV in 20 mV steps (inset). At voltages positive or negative to the resting potential (−40 mV), small-field cells invariably gave rise to larger membrane currents than those of the large-field, glycine-insensitive cells. This is clearly evident in the averaged current-voltage relationships for small- and large-field cells shown in Figure 2B, in which the peak amplitudes are plotted as a function of transmembrane voltage. Note also that, although the I-V curves for both cell types display outward rectification, this is much more apparent in the recordings from small-field bipolar cells; *i.e.*, low-amplitude membrane currents were elicited at hyperpolarizing voltages between −120 and −40 mV, but as the magnitude of the depolarizing voltage steps increased from −20 mV to +60 mV, the outward current responses grew linearly at a rate of 17.5 pA/mV. Nevertheless, the outward currents elicited from both bipolar cell subtypes exhibit little time-dependence.

On the other hand, the inward currents induced in small- and large-field bipolar cells by hyperpolarizing voltage steps differed both in amplitude and time course. The differences in amplitude are clearly evident in the I-V relations shown in Figure 2B. In Figure 3, which compares the time courses of the inward currents, the inset shows the almost instantaneous response of the small-field bipolar cells,

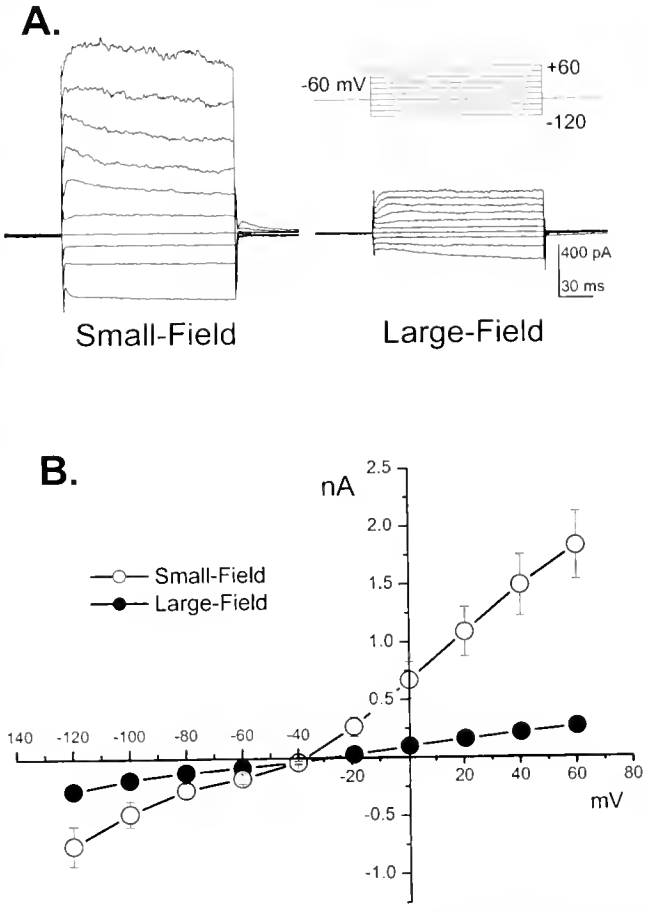

Figure 2. Voltage-activated membrane currents on small- and large-field bipolar cells. (A) Example of current traces elicited by the voltage protocol shown in the upper right-hand panel. (B) Averaged current-voltage relationship for small- and large-field bipolar cells. Data points represent the average of 8 (small-field) and 12 (large-field) experiments; error bars = ± SEM. Note that the error bars for large-field bipolar cells are within the size of the symbols.

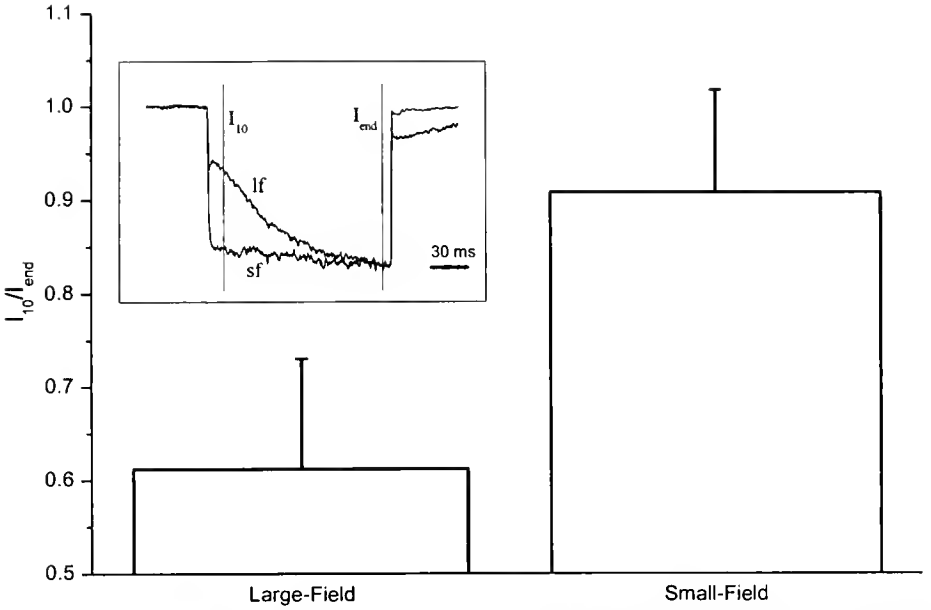

Figure 3. Comparison of the time course of the inward currents elicited by hyperpolarizing voltage steps from −60mV to −120mV for large-field and small-field bipolar cells. The inset shows typical responses from a small-field (sf) and a large-field (lf) cell and indicates the times (I_{10} and I_{end}) at which the measurements of the responses are made to calculate the ratios I_{10}/I_{end}, which are graphed. The current amplitudes have been normalized to their peak values; error bars = ± SEM for the 8 and 12 experiments of Fig. 2.

whereas an equivalent voltage step imposed on large-field bipolar cells elicited a slowly developing inward current. To quantitate the difference, we calculated the ratio of the current amplitude measured 10 ms after onset of the hyperpolarizing voltage step (I_{10}) to that measured at the end of voltage protocol (I_{end}) for voltage steps from −60 mV to −120 mV. For small-field bipolar cells, the ratio (I_{10}/I_{end}) was 0.91 ± 0.11 (n = 8), whereas for large-field bipolar cells, the ratio was 0.61 ± 0.12 (n = 12).

A large component of the outward current induced by

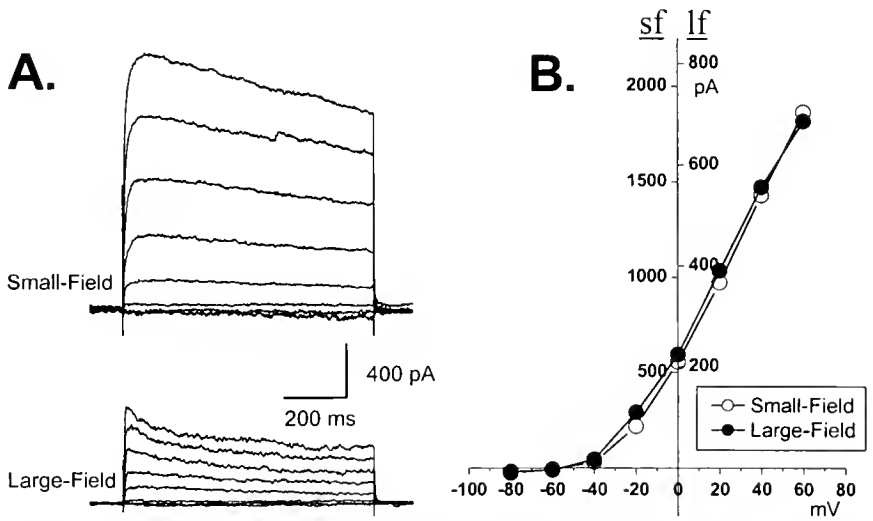

Figure 4. Comparison of the currents blocked by tetraethylammonium (TEA) in the two subtypes of skate bipolar cells. (A) The TEA-sensitive currents obtained by subtracting the membrane currents recorded in Ringer solution containing 20 m*M* TEA from the currents obtained in normal Ringer. (B) The I-V curves of the TEA-sensitive currents are equivalent for small- and large-field bipolar cells when they are adjusted to account for the different response amplitudes; sf = small-field, and lf = large-field bipolar cell.

depolarizing voltage was sensitive to tetraethylammonium (TEA). Figure 4A provides an example of the TEA-sensitive currents isolated from small- and large-field bipolar cells. They were obtained by subtracting the currents recorded in Ringer containing 20 m*M* TEA from the currents obtained from the same cell in normal Ringer. Although the amplitudes of the TEA-sensitive currents differ significantly, they display a similar voltage activation profile; *i.e.*, the I-V relationships are virtually identical after adjusting appropriately the scale of ordinates (Fig. 4B). The currents activate rapidly at depolarizing voltages ≥ -20 mV, they deactivate quickly after membrane repolarization, and the I-V relation appears to have a profile similar to that of the delayed rectifier (*e.g.*, the Kv3 channel family) observed in many other preparations (5, 6).

In conclusion, the two morphologically distinct subtypes of bipolar cell seen in the all-rod skate retina also exhibit different profiles of voltage-activated potassium current. In previous studies, we have shown that these two types of cell also express different populations of neurotransmitter receptors (2). In particular, small-field bipolar cells are glycine-sensitive, have a predominance of $GABA_A$ receptors, and give rise to large voltage-activated membrane currents. In contrast, the large-field bipolar cells do not respond to glycine, contain a larger proportion of $GABA_C$ receptors, and have small voltage-activated currents. The segregation of these properties into parallel pathways suggests that small-field bipolar cells are involved in the transmission of transient, high-intensity signals, whereas the large-field bipolar cells may be specialized for the transmission of sustained, low-intensity signals. Note that, in studies on the multitude of subtypes of bipolar cell in other vertebrate species, variations in voltage sensitivity (7, 8, 9), kinetic properties (10), and receptor types (11) have been shown to affect the strength of the visual signal and its temporal and spatial characteristics. If the two morphologically distinct subtypes of bipolar cell in skate represent the only types present, the all-rod skate retina could provide an advantageous preparation with which to correlate membrane properties with the physiological functions of the subtypes of bipolar cell.

Acknowledgments

This study was supported in part by NIH Grant EY-12028 (HQ); Fight for Sight, PSC/CUNY Grant 66257-0035, and NCRR/NIH RCMI Award RR-03037 (RLC); NIH Grant EY-06516 and a Senior Research Investigator Award from Research to Prevent Blindness (HR).

Literature Cited

1. **Wu, S. M., F. Gao, and B. R. Maple. 2000.** Functional architecture of synapses in the inner retina: segregation of visual signals by stratification of bipolar cell axon terminals. *J. Neurosci.* **20:** 4462–4470.
2. **Qian, H., H. Ripps, E. Schnette, and R. L. Chappell. 2001.** Responses of small- and large-field bipolar cells to GABA and glycine. *Brain Res.* **893:** 273–277.
3. **Qian, H., L. Li, R. L. Chappell, and H. Ripps. 1997.** GABA receptors of bipolar cells from the skate retina: actions of zinc on GABA-mediated membrane currents. *J. Neurophysiol.* **78:** 2402–2412.
4. **Schlemermeyer, E., and R. L. Chappell. 1996.** Immunocytochemical evidence for ON and OFF bipolar cells in the retina of the skate, *Raja erinacea*. *J. Neurocytol.* **125:** 625–635.
5. **Malchow, R. P., H. H. Qian, H. Ripps, and J. E. Dowling. 1990.** Structural and functional properties of two types of horizontal cell in the skate retina. *J. Gen. Physiol.* **95:** 177–198.
6. **Rudy, B., and C. J. McBain. 2001.** Kv3 channels: voltage-gated K^+ channels designed for high-frequency repetitive firing. *Trends Neurosci.* **24:** 517–526.
7. **Connaughton, V. P., and R. Nelson. 2000.** Axonal stratification patterns and glutamate-gated conductance mechanisms in zebrafish retinal bipolar cells. *J. Physiol.* **524:** 135–146.
8. **Hu, H. J., and Z. H. Pan. 2002.** Differential expression of K^+ currents in mammalian retinal bipolar cells. *Vis. Neurosci.* **19:** 163–173.
9. **Ma, Y. P., J. Cui, H. J. Hu, and Z. H. Pan. 2003.** Mammalian retinal bipolar cells express inwardly rectifying K^+ currents (I_{Kir}) with a different distribution than that of I_h. *J. Neurophysiol.* **90:** 3479–3489.
10. **Awatramani, G. B., and M. M. Slaughter. 2000.** Origin of transient and sustained responses in ganglion cells of the retina. *J. Neurosci.* **20:** 7087–7095.
11. **DeVries, S. H. 2000.** Bipolar cells use kainate and AMPA receptors to filter visual information into separate channels. *Neuron* **28:** 847–856.

Reference: *Biol. Bull.* **207:** 195–208. (December 2004)

Mechanosensory Neurons With Bend- and Osmo-sensitivity in Mouthpart Setae From the Spiny Lobster *Panulirus argus*

ANDERS GARM[1,*], CHARLES D. DERBY[2], AND JENS T. HØEG[1]

[1] *Zoological Institute, University of Copenhagen, Denmark; and* [2] *Department of Biology, Georgia State University, Atlanta, Georgia*

Abstract. The mouthparts of the spiny lobster *Panulirus argus* hold primarily two types of setae—simple setae and cuspidate setae. Mechanosensory neurons from these setae were examined by electrophysiological recordings. The population of simple setae contained two types of mechanosensory neurons: displacement-sensitive neurons, which responded to deflection at the setal base; and bend-sensitive neurons, which responded to bending of the setal shaft. Displacement-sensitive neurons, in general, responded phasically and only during actual displacement. Typically, their response changed with alteration of the direction, amplitude, and velocity/acceleration of the mechanical stimulus. Bend-sensitive neurons, in general, responded phaso-tonically and carried information on the direction and region of bending. This is the first experimental demonstration of bend sensitivity for arthropod setae. Cuspidate setae contain highly sensitive mechanosensory neurons; however, due to the rigid nature of these setae, whether they were bend sensitive or displacement sensitive could not be determined, and they were thus called "tactile neurons." Bend-sensitive neurons, but not displacement-sensitive neurons or tactile neurons, showed graded responses to changes in osmolarity. The osmosensitivity of these neurons could mediate behavioral responses to changes in the osmolarity of seawater or food.

Introduction

Because they are completely covered by an exoskeleton, crustaceans need specialized sensors to detect external stimuli. These specializations, called setae, are hollow, hairlike extensions of the cuticle that contain the dendrites of the sensory neurons. Individual setae of aquatic crustaceans are either mechanosensory, chemosensory, or bimodal (both mechanosensory and chemosensory), the latter being the most common type based on morphological evidence (Schmidt and Gnatzy, 1984; Derby, 1989; Schmidt, 1989; Cate and Derby, 2001, 2002a, 2002b; Garm *et al.*, 2003). Crustaceans have been shown to respond behaviorally to changes in the osmolarity of their surroundings (Jury *et al.*, 1994; Dufort *et al.*, 2001); while the sensory structures behind this behavior are unknown, there are indications that the setal mechanoreceptors may sense osmotic changes (Tazaki, 1975).

Unimodal mechanosensory setae are located on the dorsal side of the carapace and abdomen and on the antennae of many decapod crustaceans. They are typically plumose (featherlike) in shape, innervated by one to four mechanosensory neurons, and specialized for detecting waterborne vibrations (Wiese, 1976; Vedel and Clarac, 1976; Tautz *et al.*, 1981; Vedel, 1985). They are sensitive to displacement, being responsive to movements of the entire seta around the basal membranous region, and can respond to displacements as small as 0.01 degrees (Wiese, 1976). Moreover, they respond most strongly to displacement in one direction, usually perpendicular to the outgrowths of the seta. Equipped with fields of these setae, each with a different directionality, animals can obtain detailed information about the location of the source of the vibrations.

Bimodal setae with mechanosensitivity have been experimentally demonstrated for a variety of setal types on the pereiopods and antennae of decapods (Shelton and Laverack, 1970; Hatt and Bauer, 1980; Altner *et al.*, 1983; Cate and Derby, 2001, 2002a, 2002b; Schmidt *et al.*, 2003).

Received 18 February 2004; accepted 10 September 2004.

* To whom correspondence should be addressed at Department of Cell and Organism Biology, Lund University, Helgonavagen 3, 22362 Lund, Sweden. E-mail: anders.garm@cob.lu.se

These mechanosensory neurons are believed to be displacement-sensitive, but little is known about their sensory properties such as directionality or response to changes in velocity.

Decapod crustaceans are known to have flexible feeding behavior. They can change how their mouthparts are used in feeding, depending on the nature—especially the size—of the prey item (Greenwood, 1972; Caine, 1975a, 1975b; Gerlach *et al.*, 1976; Kunze and Anderson, 1979; Schembri, 1982; Hunt *et al.*, 1992; Johnston, 1999; Garm and Høeg, 2001; Garm *et al.*, 2003; Garm, 2004). Moreover, crustacean mouthparts are known to have a high density of setae with a great diversity in external morphology (Schembri, 1982; Stemhuis *et al.*, 1998; Garm and Høeg, 2000; Coelho *et al.*, 2000), and the sparse morphological evidence suggests that most are bimodal mechanoreceptors and chemoreceptors (Paffenhöfer and Loyd, 2000; Garm *et al.*, 2003). To modify their feeding behavior, therefore, crustaceans are likely to acquire tactile information about the texture and shape of food while it is being handled by the mouthparts. Most of this information probably comes from the setae on the maxillipeds, since these mouthparts perform most of the manipulation and orientation of prey items during handling.

In this study, we have tested the hypothesis that mechanosensory neurons in the mouthpart setae of decapod crustaceans provide tactile information important for controlling feeding behavior. We have used the Caribbean spiny lobster *Panulirus argus* (Latreille, 1804) because it is an established model animal for crustacean sensory biology (Derby, 2000; Derby *et al.*, 2001; Harrison *et al.*, 2001; Ache, 2002; McClintock and Xu, 2002), and because its setae are large and thereby accessible for experimental work. Our focus is on the mandibular palp, the medial rim of the basis of maxilla 1 and maxilliped 1, the propodus and dactylus of the endopod of maxilliped 2, and the dactylus of the endopod of maxilliped 3. These structures are often in direct contact with prey during food manipulation (Garm, 2004), and thus are likely to have sensory functions; moreover, they are of sufficient size for convenient experimental manipulation. We examined the sensitivity of these neurons to setal displacement (deflection at their insertion), setal bending (deflection along their shaft), and osmotic changes in the seawater around them.

Materials and Methods

Video recordings

Adult male and female spiny lobsters, *Panulirus argus*, with carapace lengths of 45–90 mm, were obtained from Bermuda and kept in a 300-l aquarium at Danmarks Akvarium in Copenhagen. The video recordings were made in 50-l aquaria. Both systems had running seawater at 24 °C. For the recordings, the animals were fed mussels, fish meat, krill, and squid. A SONY DXC 950P color (Y/C) 3CCD camera equipped with a Micronikkor 105-mm macro lens was placed outside the aquarium and enabled 5-μm resolution. Recordings were made on PAL super VHS. Light was obtained from a 120-W bulb. Representative images of mouthpart movements were captured with a time resolution of 20 ms (50 images/s) using the frame grabber card DVRaptor from Canopus; the images were imported into CorelDraw 10.0, with a resolution of 720 × 564 pixels.

Electrophysiology

Spiny lobsters, *Panulirus argus*, with carapace lengths of of 40–80 mm, were captured in the Florida Keys and maintained in two 400-l aquaria with artificial seawater (Instant Ocean, Aquarium Systems, Mentor, OH) at 23–28 °C, and fed shrimp and squid. Mouthparts examined in this study included the mandibular palp (n = 4), basis of maxilla 1 (n = 2), basis of maxilliped 1 (n = 6), endopod of maxilliped 2 (n = 10), and endopod of maxilliped 3 (n = 21). Between one and four neurons were studied per appendage. To gain access to the nerve bundles and artery of the various mouthparts, one of the appendages was ablated immediately before each experiment and dissected in cold lobster saline (gram/liter: 28 NaCl, 0.75 KCl, 3.4 $MgCl_2 \cdot 6H_2O$, 2.5 $CaCl_2 \cdot 2H_2O$, 3 Na_2SO_4, 0.3 glucose, 0.72 HEPES). For maxilliped 3, both the dactylus and propodus were removed from the endopod. The cuticle was removed from the propodus, and after the apodeme was cut at its insertion onto the dactylus, the muscle was gently removed with forceps. This dissection left behind only the principal artery flanked by the major nerve to the appendage. The artery and nerve bundle were separated from each other with a pair of fine tungsten needles, and the nerve was divided into four to six bundles. For the mandibular palp and endopod of maxilliped 2, the procedure was similar, although the endopod of maxilla 2 was cut at the merus-carpus joint, and the nerve in the carpus was used instead. For maxilla 1 and maxilliped 1, the basis was cut from the limb, and the cuticle was removed from the proximal half. In these limbs, only a small amount of muscle and connective tissue had to be removed to reveal the nerve and artery. When maxilla 1 or maxilliped 1 was used, the lobster was anesthetized on ice before dissection. Even though involved in food handling, the basis of maxilla 2 was not examined due to its small size.

After the dissection, the preparation was secured in a stimulating-recording chamber made of two petri dishes separated by a dental-wax barrier (Fig. 1A). The preparation was secured in the wax such that its two parts were bathed in different solutions. The distal part of the preparation, which housed undissected cuticle and setae, was situated in a stimulating dish that contained artificial seawater (gram/liter: 24.7 NaCl, 0.66 KCl, 4.7 $MgCl_2 \cdot 6H_2O$, 1.9

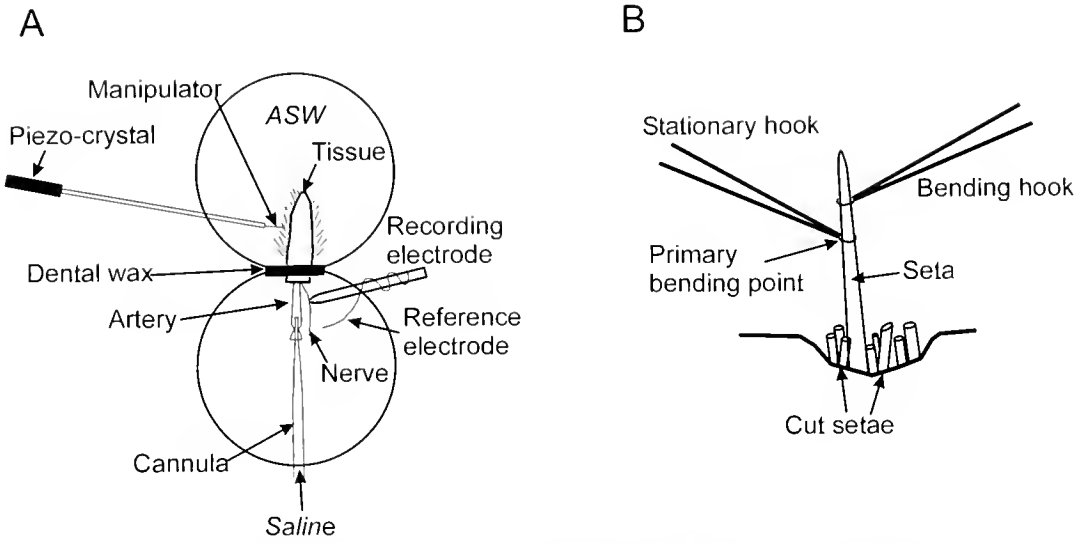

Figure 1. Experimental setup. (A) Schematic overview of the stimulating-recording chamber, showing how mechanical stimuli were applied with a piezoelectric-crystal-controlled probe. (B) Stimulation of a bend-sensitive cell. Neighboring setae were removed to allow space for stimulation of the seta innervated by the neuron of interest. This seta was bent around the attachment of a stationary hook. The bending hook was moved either by a piezoelectric crystal (see A) or by hand.

$CaCl_2 \cdot 2H_2O$, 6.3 $MgSO_4 \cdot 7H_2O$, 0.18 $NaHCO_3$); the proximal part, which contained the exposed nerve and artery, was situated in a recording dish that contained saline. After the wax barrier was sealed, the artery was cannulated and perfused with pressurized, oxygenated lobster saline at a rate of 0.4–1.1 ml/min (see Derby, 1995, for more details). The time from ablation of the mouthpart to perfusion was 10–15 min, and nerve recordings were initiated 15 min later.

Electrophysiological recordings were made *en passant* with fine-tipped extracellular suction electrodes (Derby, 1995). To determine whether the recording included mechanosensory neurons, a probe was used to brush the setae. If neural responses were detected, the seta innervated by the active neuron was identified by stimulating progressively smaller areas with the probe. The neighboring setae were then removed with a pair of scissors to ensure space for the micromanipulators and to ensure free movements of the seta of interest (Fig. 1B).

Two types of mechanical stimulation were presented—displacement and bending. Displacement is defined as moving the setae, with no apparent bending of the setal shaft itself, so that the angle between the base of the seta and the cuticle at its socket changes. Bending is defined as a deflection in the setal shaft, without any detectable displacement at its base. To examine displacement sensitivity, the seta was attached to a small tungsten hook, which in turn was connected to a piezoelectric crystal *via* an extension arm (Fig. 1A). Movement of the crystal was effected by applying 50–500 V, either in square or triangular pulses, using a wave generator amplified by a high-voltage DC amplifier. This provided movements ranging in amplitude from 0.12–1.2 mm measured with a micrometer scale bar. Simply attaching the hook to a simple seta resulted in no detectable alteration of the movements. To ensure that no force was applied in other than the direction of displacement, the hook moved freely along the setal shaft. This had the side effect that the angular velocity of the displacement was not constant, but declined within a single displacement following the equation: $\tan \alpha = D/L$, where α is the angle of displacement, D is the distance traveled by the hook, and L is the distance from the socket of the seta to the initial attachment point of the hook. This also meant that the two parameters, velocity and acceleration, could not be separated in our experiments. This coupling was enhanced by the failure of the hook to attain maximum velocity instantaneously; rather there was a period of acceleration, which was most significant when square signals were used. In effect the displacements started with a short period of acceleration to maximum velocity, then slowly decelerated until the direction reversed.

A change in the velocity/acceleration and amplitude of the stimulus was accomplished by changing the voltage and duration of the electrical signal from the wave generator. In these tests, triangular stimuli were used. When the velocity/acceleration sensitivity was tested, the amplitude was fixed at either 0.48 mm (200 V) or 0.72 mm (300 V), and stimulus duration was then varied using a stimulus frequency range of 1–10 Hz. When amplitude sensitivity was tested, the velocity/acceleration was fixed by using half the stimulation duration when doubling the voltage. Stimuli were presented

continuously for 15 s. Most displacement-sensitive neurons were also tested for bend sensitivity.

To examine bend sensitivity, one hook was situated at the place of desired bending, and the distal part was then moved to an angle of about 45° by either a handheld needle or a hook connected to a piezoelectric crystal (Fig. 1B). The neurons were also tested for their sensitivity to bending proximally relative to the holding point. All bend neurons were tested for displacement sensitivity by using maximum amplitude as described above.

When testing directionality, both displacement and bending were presented in four directions: distally (towards the tip of the appendage), proximally (away from the tip of the appendage), and medially and laterally (to the left and to the right of the appendage). Four displacement-sensitive and four bend-sensitive neurons were tested for the persistence of their response after the distal half of the seta was removed with a pair of scissors.

Because cuspidate setae and their reduced socket are very rigid, they could not be moved by the crystal, but only by a handheld needle. Thus, displacement and bending could not be reliably separated.

Sensitivity to changes in osmolarity was tested by placing the appendage in a tube with full-strength artificial seawater (*i.e.* 3.5%) flowing at 5 ml/min. The seawater was then exchanged with a 8-s pulse of either deionized water or a concentration series of artificial seawater from 1.75%–5.25% (*i.e.*, 50%–150% full-strength seawater) made by changing the concentration of NaCl. The concentration series was presented in steps first from 100% down to 50% and then from 100% up to 150%, with intertrial time intervals of 1 min. Three of each neuron type were also tested with deionized water for 5–15 min.

Each recording was made for 10 s with a sampling frequency of 56 kHz using Axoscope 9.0 software (Axon Instruments, Inc., Union City, CA). Spike sorting and quantification were performed using Datapac 2000 software (RUN Technologies, Mission Viejo, CA). All spikes for a given stimulation were used when analyzing both the number of spikes per stimulation and the interspike interval during a single stimulation.

Results

The results are summarized in Tables 1 and 2. Recordings were obtained from neurons innervating two types of setae—simple and cuspidate (Fig. 2A, B). None of the neurons showed any spontaneous activity. Simple setae contained neurons that appeared to belong to either of two categories (Tables 1 and 2, Fig. 3). The first were displacement-sensitive neurons that responded to deflection of the entire seta at its socket. The second were bend-sensitive neurons that responded to bending of the setal shaft; a few of these neurons also gave small responses when displaced, presumably because of slight concomitant bending upon being displaced. The video recordings showed that bending does occur during food manipulation (Fig. 2C, D; supplementary video clips can be viewed at <http://www.mbl.edu/BiologicalBulletin/VIDEO/BB.video.html>).

The cuspidate setae contained neurons sensitive to the slightest movements of the seta, but since these neurons could not be stimulated in a controlled manner, they are referred to as "tactile neurons."

Displacement-sensitive neurons

Displacement-sensitive neurons displayed phasic responses, spiking only during the actual setal displacement (Fig. 3A). None of the neurons responded to bending, and all of the neurons continued to respond to displacements after the distal half of their seta was removed. They were differentially sensitive to the direction, velocity, and amplitude of displacement, as described below.

Half of the displacement neurons (9 of 18 tested) showed directional sensitivity; in most cases, they responded much more strongly (*i.e.* with more spikes) to one of the four directions (Fig. 4). The "best" direction varied among the nine neurons, but distal and proximal displacement was most frequently the best direction. Only one neuron gave most spikes to lateral displacement, and no neuron responded most strongly to medial displacement. Some responded exclusively to displacement in one direction, but 7 of 9 neurons responded to two or more directions (Fig. 4). There was no significant difference between the number of

Table 1

Number of cells tested for each stimulation parameter or combination of parameters

Type	Dir[1]	Amp[2] + Vel[3] + Dir	Amp + Vel	Amp + Dir	Vel + Dir	Region[4]	Region + Dir
Displace	6	2	4	4	6	—	—
Bend	4	—	—	—	—	4	6

[1] Dir, Direction: Seta was bent or displaced in four directions (proximal, distal, medial, lateral).
[2] Amp, Aplitude: Seta was displaced with a series of amplitudes ranging from 0.2–1.2 mm.
[3] Vel, Velocity/Acceleration: Seta was displaced with a series of velocities/accelerations up to 12 mm/s.
[4] Region: Seta was bent at different regions along the shaft.

Table 2

Summary of sensitivity of mechanosensory neurons

Setae type	Location	Modality	# of Cells tested	Responding to deionized water	Responding after cut midways	Directional sensitivity[1]	Amplitude sensitivity[2]	Velocity sensitivity[3]	Region sensitivity[4]
Cuspidate	Mx1	"Tactile"	2						
	Mxp2	"Tactile"	4	0/1	1/1				
	Mxp3	"Tactile"	4	1*/1	1/1				
Simple	Mdp	Bend	2			2/2			1/2
		Displace	3	0/1		2/3	1/1	2/2	
	Mxp1	Bend	5		0/1	0/1			1/1
		Displace	3		1/1	1/2			1/1
	Mxp2	Bend	6	4/4	0/3	2/3			4/4
		Displace	6	0/3	2/2	1/3	1/1	3/3	
	Mxp3	Bend	12	7/7		2/4			2/3
		Displace	21	0/5	1/1	5/10	6/6	6/6	

Responses are given as *x*/*y*, where *x* out of *y* tested cells responded to changes in the given parameter.
[1] Cell produced more spikes when stimulated in some directions than others.
[2] Cell produced more spikes when stimulated with higher amplitudes.
[3] Cell produced shorter interspike intervals when stimulated at higher maximum velocity/acceleration.
[4] Cell produced more spikes when the seta was bent at certain regions along the shaft than others.
* Cell responded only after the distal half of seta was cut off.

spikes produced per displacement of nondirectional neurons and directional neurons when displaced in their "best" direction (Students *t*-test, $P > 0.2$).

Displacement neurons were also amplitude sensitive (Table 2, Fig. 5). Greater amplitudes of displacement caused more spiking activity. This relationship is highly linear, with a slope of about 5; that is, a log increase in stimulus amplitude causes a 5-fold increase in the number of spikes (Fig. 5A). The mean spike interval did not correlate with stimulus amplitude (Fig. 5B). The neurons had a high threshold, and the setae that they innervated had to be moved some distance before they responded. Although we did not precisely measure the amplitude or angle of displacement at threshold, we estimated from microscopy that it was 0.15–0.20 mm, equal to 4–6° for a 2-mm-long seta. The threshold amplitude did not seem to change with higher stimulus velocity.

Velocity/acceleration was a third parameter influencing the response of the displacement neurons (Fig. 6). Increasing the maximum velocity of displacement caused an increased response magnitude, reflected as a decrease in mean interspike interval in all 12 tested neurons. Since most neurons gave a constant number of spikes, the spike trains were shorter at higher velocities/accelerations. When the maximum velocity was doubled, the mean interspike interval declined by 39% ± 6% (SEM), $n = 12$. In a few cases, there was a significant linear correlation between the maximum velocity and the mean interspike interval (example given in Fig. 6). At low velocities, no spikes were produced when the seta returned to its original position, but at higher velocities, one spike was occasionally produced during the return to the resting position of the seta.

Displacement neurons did not respond to changes in the osmolarity of the medium around the setae (Table 2). They did not respond to pulses of deionized water, and when bathed in deionized water, they continued to respond normally to displacements for at least 15 min. In one neuron, the cuticle was removed by cutting the seta, first midway up the shaft and subsequently even more proximally, and this neuron continued to respond to displacements and showed no response to deionized water.

Bend-sensitive neurons

Bend-sensitive neurons generally gave phaso-tonic responses to bending of the setal shaft in that they continued to spike during bending sustained for many seconds (Fig. 3C). During such a prolonged period of bending, the neurons adapted to the stimulus and their firing frequency declined (Fig. 7). The rate of adaptation varied greatly, as indicated by the large standard error of the mean in firing rate over the various time intervals.

Of 10 bend neurons, 6 showed directional sensitivity (Table 2, Fig. 8). Like most of the directional displacement neurons, bend neurons did not respond exclusively to bending in one direction, but generally one direction produced a

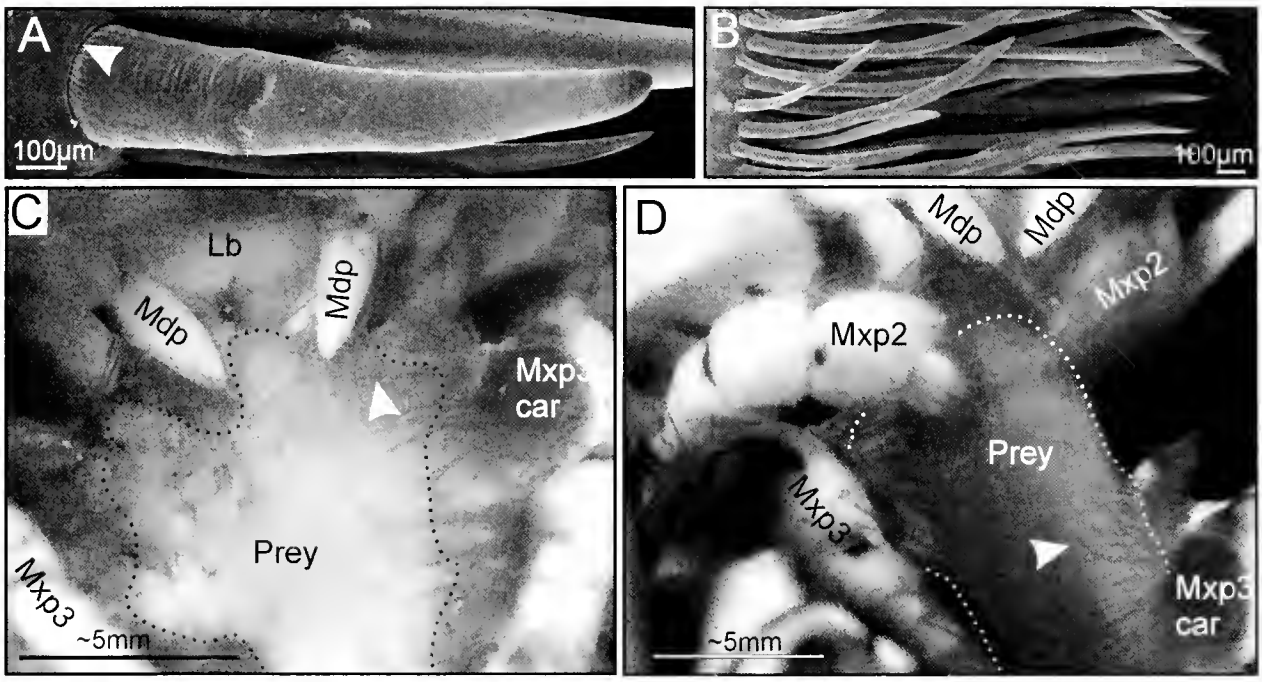

Figure 2. Morphology of the setae: scanning electron micrograph (SEM) and video images. (A) SEM image of a stout cuspidate seta from the endopod of maxilliped 2; the arrowhead indicates the very reduced socket of the seta. (B) SEM image of simple setae from the basis of maxilliped 1. (C, D) Video still images taken *ca.* 1 s apart showing a simple seta (arrowhead) that is from the carpus of maxilliped 3 (Mxp3 car) and bends during food manipulation. The seta is almost straight before prey contact (C) but bends in the distal half when contact is made (D). The broken line indicates the prey held by the mouthparts. car = carpus, Lb = labrum, Mdp = mandibular palp, Mxp2 = maxilliped 2, Mxp3 = maxilliped 3.

phaso-tonic high-frequency response, while other directions produced phasic responses and lower response rates (Fig. 8). Eight of the ten neurons tested responded unequally to bending at different regions in that they only responded to bending of the distal half of the seta (Fig. 9), but the experimental setup did not allow for precise location of the most sensitive region. Two neurons responded to bending anywhere along the setal shaft. None of the four tested neurons responded to bending after the distal half of the seta was removed.

Bend neurons were sensitive to changes in osmolarity (Fig. 10). All tested neurons (n = 11) responded with high-frequency spiking to pulses of deionized water. The response to bending did not change after stimulation with 8-s pulses of deionized water. Three neurons were kept in deionized water for a prolonged period, and they all stopped responding to the deionized water after 1–2 min. One neuron spiked constantly for 1.5 min before it stopped responding. These three neurons showed a profound reduction in responsiveness to bending before they stopped responding. None of the three neurons responded to bending after 5 min in deionized water, and none of them recovered after 30 min in full-strength seawater.

Bend neurons differed in their responses to the salinity treatments. Four bend neurons from maxilliped 3 were tested with a set of seawater stimuli at different osmolarities—1.75% to 5.25% salt concentration. (Full-strength seawater is 3.5%, so these range from 50% to 150% of normal seawater; Fig. 10B). One neuron responded most strongly to hyperosmotic stimuli (Fig. 10B, neuron 1); one neuron responded only to hyposmotic stimuli (Fig. 10, neuron 2); and two neurons responded in similar ways to hypo- and hyperosmotic stimuli (Fig. 10, neurons 3–4), but with different intensities. The response to changes in salinity showed a response latency of several seconds, even when the neurons were exposed to deionized water (Fig. 10A).

Tactile neurons from cuspidate setae

The 10 tactile neurons obtained from cuspidate setae were highly sensitive, responding to the slightest touch by the probe that caused no visible setal movement (Fig. 11A). Eight of the neurons gave phaso-tonic responses to prolonged displacement (Fig. 11B); these neurons tended to adapt similarly to bend neurons (Fig. 11C). Sensitivity to direction, amplitude, or velocity of mechanical stimulation was not examined because stimulation was necessarily performed by hand and therefore was not accurate enough for such quantification.

The tactile neurons were not sensitive to pulses of deion-

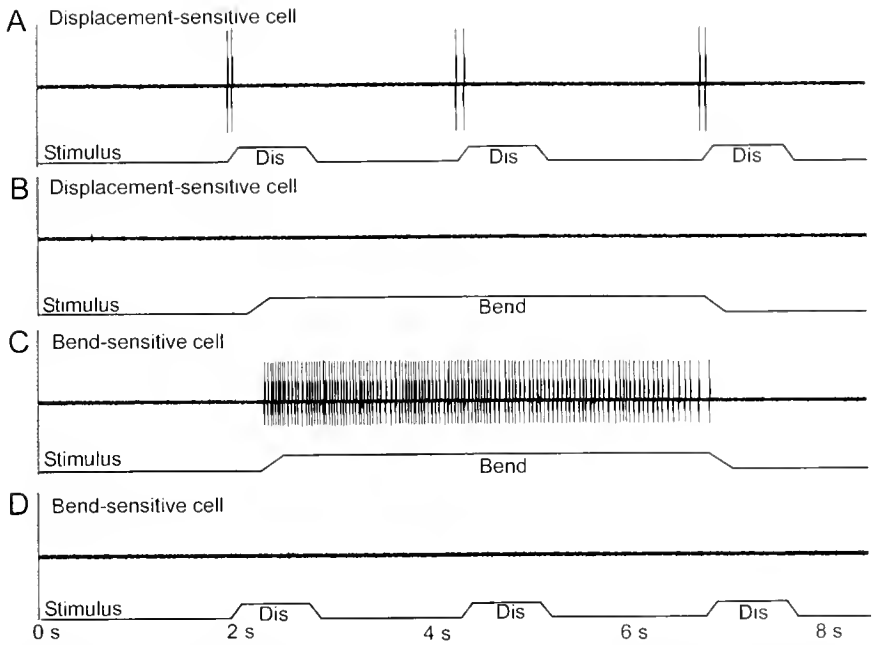

Figure 3. Typical response characteristics of the two types of mechanosensory neurons from simple setae. (A) and (B): A displacement-sensitive neuron. (A) The neuron responded phasically to a 1-s displacement. Note that the spikes occurred only during the displacement and not during the stationary state. (B) The neuron from A did not respond to prolonged bending. (C) and (D): A bend-sensitive neuron. (C) The neuron responded phaso-tonically during the entire 5 s of bending. (D) The neuron from C did not respond to displacement.

ized water. In one neuron, the cuticle was opened by cutting (with a pair of scissors) the seta at the midpoint along the setal shaft. This neuron continued to respond to tactile stimuli and began to respond to pulses of deionized water.

Discussion

Two types of mechanosensory neuron from the simple setae on the mouthparts of *Panulirus argus* were demonstrated in this study: displacement-sensitive neurons and bend-sensitive neurons. Furthermore, highly sensitive "tactile" neurons were found in the cuspidate setae. The identification of bend-sensitive neurons was one of our most significant findings; such neurons have not been previously demonstrated for any arthropod seta. Our results, taken together, clearly show that the mechanosensory input during feeding is more complex than previously believed (Altner *et al.*, 1983).

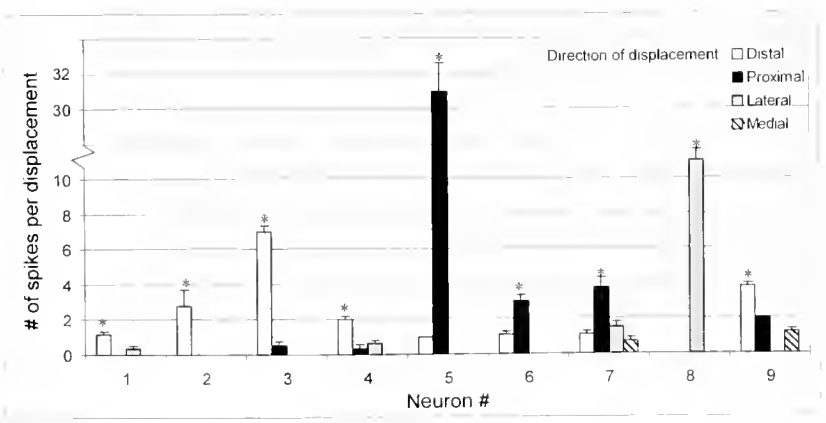

Figure 4. Directional sensitivity of nine displacement neurons. Only neurons 2 and 8 responded exclusively to displacement in one direction, but all nine neurons had a "best" direction that produced the most action potentials. The "best" directions tended to be proximal or distal. Responses marked with an asterisk are significantly larger than those to the other directions (ANOVA with Tukey's *post hoc* tests, $P < 0.05$). The directions are relative to the long axis of the limb. Values are means ± SEM, $n = 6–8$ (repeated stimulations of the same neuron).

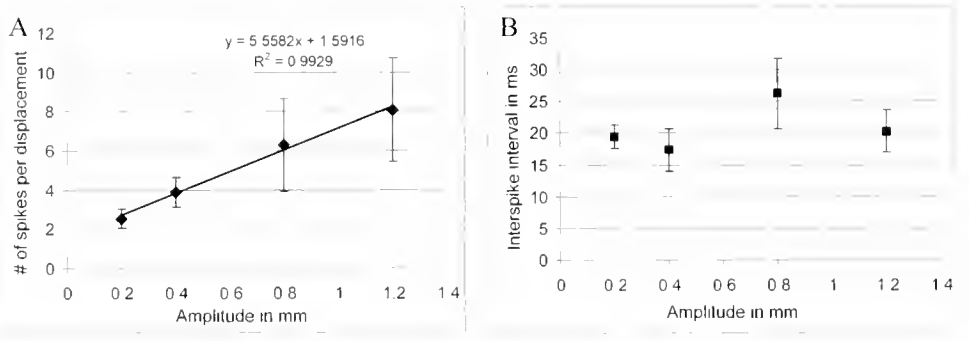

Figure 5. Amplitude sensitivity of displacement neurons. (A) Response of displacement neurons, in spikes per displacement, increased with stimulus amplitude. Note that the stimulus amplitude refers to the distance traveled by the manipulatory hook and that the distance traveled by any given part of the seta was not linear but followed a sine curve (see Materials and Methods for details). A best-fit regression line is drawn through the data points, and the regression equation and coefficient of determination (R^2) are shown above it. (B) The mean interspike interval was not influenced by changes in the stimulus amplitude. Values are means ± SEM, $n = 8$ (8 neurons were tested with each amplitude, but the value from each neuron was a mean of 10 stimulations).

Bend-sensitive neurons

Several observations support bend-sensitivity. First, most of the bend neurons did not respond to large displacements, and the few that did gave a very small response—much smaller than to bending. In addition, six out of eight neurons did not respond to bending of the proximal half of the seta, showing that distal distortion is needed to activate most of the bend neurons. Finally, none of the bend neurons responded after the distal part of the setal shaft was removed, whereas all the displacement neurons kept responding after the ablation. This again shows that the sensitive part of most of the bend neurons lies within the distal half of the seta. We therefore conclude that the division of the mechanosensory neurons into bend- and displacement-sensitive neurons is a real property and not a stimulation artifact.

This is the first demonstration of bend sensitivity among mechanosensory neurons in arthropod setae; only displacement sensitivity has been found in earlier studies (Wiese, 1976; Vedel and Clarac, 1976; Tazaki, 1977; Janse, 1980; Tautz *et al.*, 1981; Solon and Kass-Simon, 1981; Altner *et al.*, 1983; Vedel, 1985; Heinisch and Wiese, 1987; Crouau, 1995; Keil, 1998). Crouau (1989) suggested that the plumose setae from the antenna of the mysid *Antromysis juberthiei* are bend sensitive but with neurons responding to both bending and displacement; no experimental evidence was provided for this suggestion.

Simple setae are likely to bend during food handling by the mouthparts when prey is grasped and pressure is applied directly to the tip of the setae. The setae do bend during food

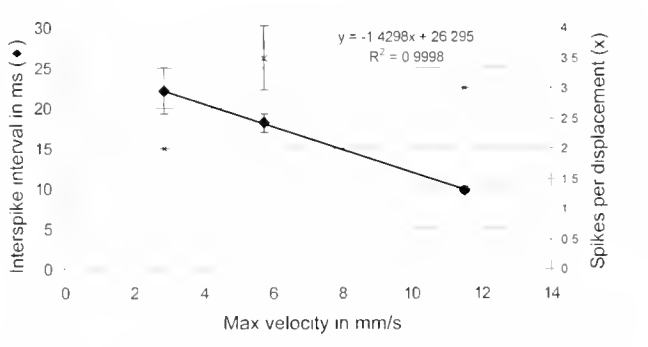

Figure 6. A displacement-sensitive neuron showed a decline in mean interspike interval with higher velocities (diamond symbols). The values are means ± SEM, $n = 10$. The line indicates the best-fit linear regression. The equation and coefficient of determination (R^2) are shown above the line. The number of spikes did not change with changes in velocity (X-shaped symbols). Note that the velocity is given for the manipulatory hook and that the angular velocity followed a sine curve (see Materials and Methods for details). The values refer to the maximum velocities of the seta.

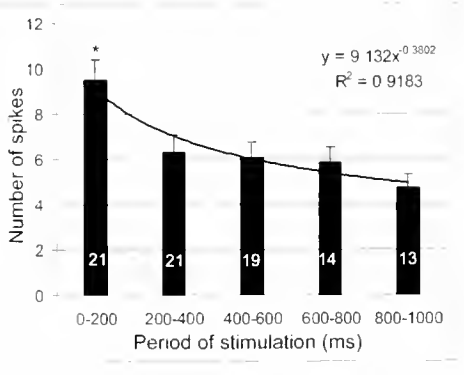

Figure 7. Adaptation of the phaso-tonic response of bend neurons. Values are means ± SEM; n is written in each bar. The reason for the decline in n values is that the neurons were stimulated for different periods. The asterisk indicates that the responses in the first period were significantly larger than the responses in the subsequent periods (ANOVA with Tukey's *post hoc* test, $P < 0.02$). All of the neurons displayed a slow adaptation to prolonged bending, seen as a decline in spiking frequency. The equation is the best-fit regression line, and R^2 is the coefficient of determination.

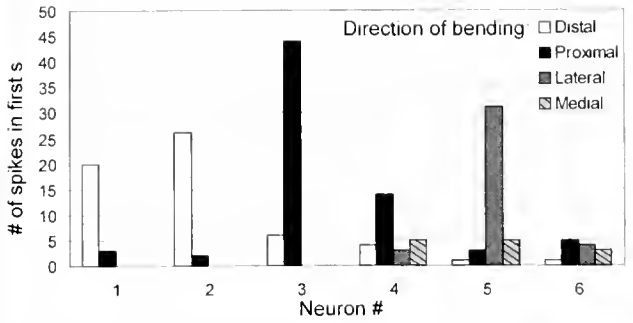

Figure 8. Six of ten tested bend neurons were directionally sensitive, responding with more spikes when bent in one direction than in others. The given direction of bending is relative to the long axis of the appendage. None of the six neurons responded exclusively to one direction of bending, but in general they showed a "best" direction. Neuron 6 was different in that it seemed to display a "worst" direction. No error bars are given since $n = 1$ for all recordings.

manipulation (Fig. 2), and this should activate the bend-sensitive neurons. As seen in video recordings, the distal part of the seta is most likely to bend during food manipulation, consistent with the fact that most bend neurons are only sensitive to bending distally (Fig. 9). Decapods in general have mandibles with separate areas for biting or crushing the prey (incisor and molar processes, respectively) (Lavalli and Factor, 1992; Garm and Høeg, 2001). Bend sensitivity, perhaps in coordination with proprioceptors, may provide animals with information on the hardness of the prey, affecting the decision about whether to crush or bite the prey item with the mandibles. The phaso-tonic response of bend neurons should ensure that the animals get information on the position of the object even when the prey is not moving or being moved. The directionality and region of sensitivity of bend neurons should give information on shape, texture, and location of the prey item, in addition to the stimulus direction and velocity information provided by displacement neurons (discussed below).

An interesting question is how the directional sensitivity of the bend neurons is enabled. It could be due either to the mechanical properties of the setal cuticle making bending more likely in one or more directions, or to the morphological arrangement of neurons inside the setal lumen. We did not examine the mechanical properties of the setae in any detail; but since the recorded responses are all to the same degree of bending (approximately 45°), stiffness of the setae cannot account for the observed directionality. We therefore believe that the arrangement of the outer dendritic segments is causing the directionality of some of the bend neurons. Normally the sensory cilia are arranged in a ciliary compartment enclosed by a dendritic sheath with no noticeable order or orientation, but this may be different for these

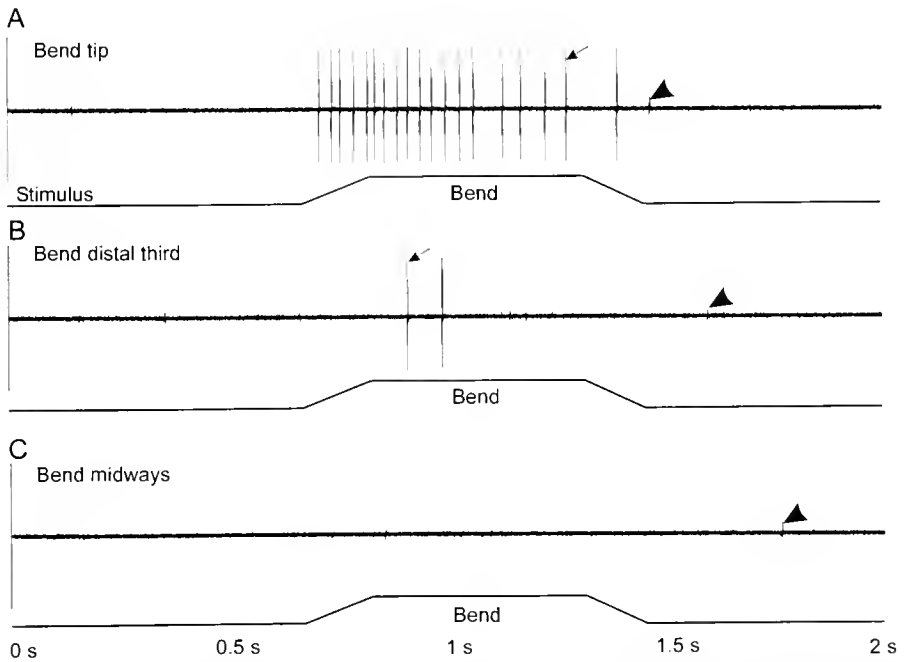

Figure 9. Responses from a bend neuron (arrow) to bending at different regions of the setal shaft. (A) When the seta was bent close to its tip, the neuron responded phaso-tonically throughout the entire period of bending. (B) When the seta was bent in the region about a third of the way from the tip, the neuron responded phasically with only two spikes. (C) This neuron, similar to five of the other bend neurons tested for region-sensitivity, did not respond to bending at the proximal half of the setal shaft. Arrowheads indicate responses from unidentified neurons.

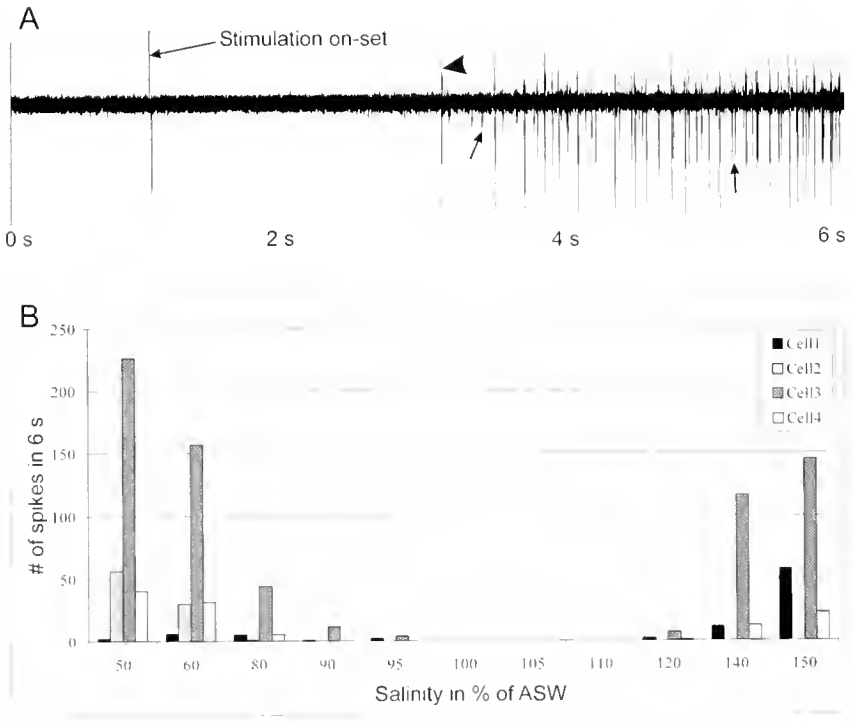

Figure 10. Bend neurons were sensitive to osmolarity. (A) Response to an 8-s pulse of deionized water. The response had a typical latency of a few seconds. (B) Response of four bend neurons to changes in osmolarity. Note that neuron 2 responded only to hypo-osmolarity, and neuron 1 mostly to hyper-osmolarity. The percentage given is relative to the response to full-strength seawater (3.5% salinity). The 6-s spike count started at the first spike.

directionally sensitive bend neurons. We must also ask how the ultrastructural arrangement ensures that most of the bend neurons were sensitive only to bending of the distal half of the seta. This might result from the transition zone between the inner and outer dendritic segment lying midway in the shaft, as it does for some aesthetase setae (Ache, 1982). Since the outer dendritic segment is assumed to be the receptive part (Schmidt and Gnatzy, 1984; Crouau, 1994, 2001), such an arrangement would make the proximal part of the seta insensitive.

Displacement-sensitive neurons

Except for the higher amplitude threshold, the physiological properties of displacement-sensitive neurons in simple setae on the mouthparts of *P. argus* are similar to many, though not all, previously described mechanosensors on other body parts from a variety of crustaceans. We show that the amplitude of displacement is encoded in the number of action potentials produced and the velocity/acceleration in the firing frequency. This is in good concordance with earlier findings for mechanosensory neurons from crustaceans (Wiese, 1976; Tautz *et al.*, 1981; Altner *et al.*, 1983; Derby, 1989; Fields *et al.*, 2002). The function of displacement-sensitive neurons has been suggested to be sensing vibrations and thereby detecting prey, predators, or conspecifics from a distance (Wiese, 1976; Tazaki, 1977; Tautz *et al.*, 1981; Masters *et al.*, 1982; Vedel, 1985). However, this is probably not the case for the displacement-sensitive neurons from mouthpart setae. These neurons are directly involved in coarse manipulation of food and are therefore more likely to collect tactile information about the food items. This means that their dynamic range should be biased towards high-amplitude stimulation, which correlates well with our results. For example, the angular sensitivity thresholds of 4–6° reported here are higher than previously reported thresholds from displacement neurons. Mechanosensory neurons from the plumose setae of other decapod crustaceans have thresholds down to 0.01° (Wiese, 1976), and there are indications of even lower thresholds in copepod antennae (Fields *et al.*, 2002). Mechanosensory neurons of insects and spiders also have lower thresholds than we report here (Keil, 1998; Barth and Höller, 1999; Cokl and Virant-Doberlet, 2003). This difference in thresholds again supports the functional difference between mouthpart setae and setae found on other structures believed to be specialized motion detectors.

The detailed response pattern of mouthpart displacement neurons probably adds significantly to the information gath-

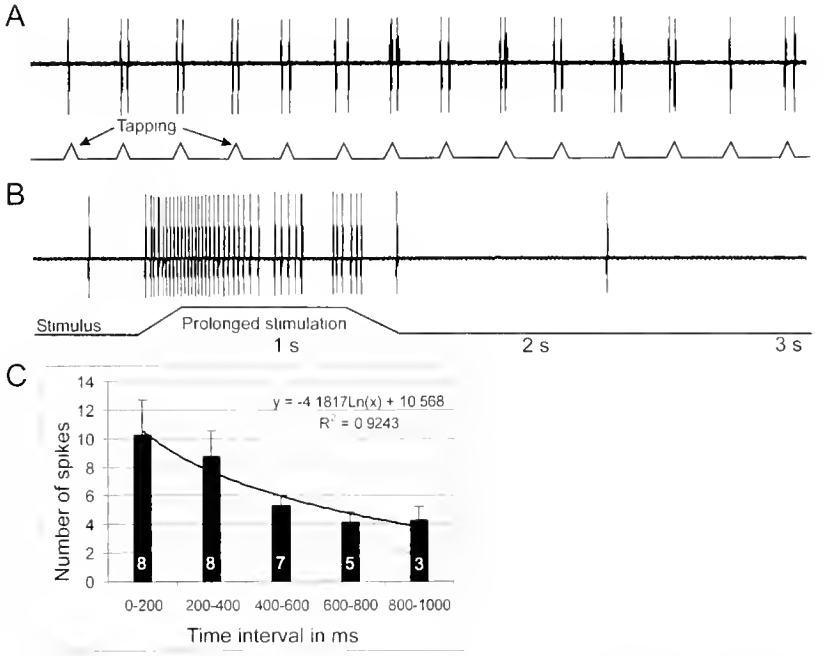

Figure 11. "Tactile" neurons from cuspidate setae. (A) Tapping the setae caused no visible movements of the seta, but produced one to two spikes per stimulation. (B) Example of phaso-tonic response to prolonged stimulation. (C) The phaso-tonic neurons from cuspidate setae tended to adapt slowly to prolonged stimulation, but the responses were not significantly different at the 0.05 significance level (ANOVA). The line is the best-fit regression; the line equation and coefficient of determination are shown. Values are means ± SEM; *n* is indicated in bars. The decline in *n* values is due to the neurons being stimulated for different periods.

ered about the prey items during feeding. If a living prey held by the mouthparts tries to escape, the directional sensitivity of the displacement neurons could indicate the direction of the movement. The amplitude- and velocity-sensitive neurons could give further detailed information about the movements of the prey.

Tactile neurons from cuspidate setae

Tactile neurons from cuspidate setae give phaso-tonic spiking responses, and they have very low response thresholds as indicated by their responsiveness to very small movements. This is not surprising since cuspidate setae have a much reduced socket and can hardly pivot in this socket (Vedel, 1985). Cuspidate setae are situated on the very distal or medial edge of the mouthparts and will therefore make the initial contact with prey. They are the setae most involved in the actual holding of the prey (Garm, 2004). Consequently, the tactile neurons could provide information about when contact is made, and possibly also about the texture of the prey, by correlating the amplitude of the displacement with information from internal proprioceptors. The responsiveness is similar to that described for mechanosensory neurons in cuspidate setae referred to as "spines" on antenna 2 of *Panulirus vulgaris* (Vedel, 1985).

Combined mechanosensory function of mouthpart setae

The array of mechanosensory input from the mouthpart setae described by our experiments could be viewed as a somatosensory system that provides detailed information about the shape, size, texture, position, and movements of prey items. The spatial resolution should also be considerable, since the setae are closely packed on most parts of the food-handling areas. The acquisition of such detailed information during food handling conflicts with an earlier suggestion about the amount of tactile information gathered during feeding. Mechanosensory neurons on the chelae of *Austropotamobius torrentium* were suggested to provide only crude information on the presence or absence of food (Altner *et al.*, 1983). On the other hand, behavioral studies of other decapods support the notion that detailed information is available to the animals. When squat lobsters (*Munida sarsi* and *M. tenuimana*) and shrimp (*Palaemon adspersus*) handle prey, the flexible and variable mouthpart movements are performed with high speed and precision (Garm and Høeg, 2001; Garm *et al.*, 2003). Such movements can only be performed with detailed somatosensory input.

Osmosensitivity of mouthpart mechanosensory neurons

Sensitivity to changes in osmolarity is known from behavioral experiments on some decapod crustaceans, such as

the clawed lobster *Homarus americanus* (Jury *et al.*, 1994; Dufort *et al.*, 2001). Moreover, both chemosensors (Derby, unpubl. data) and mechanosensors (Tazaki, 1975) of spiny lobsters can be sensitive to stimulus osmolarity. Schmidt (1989) also found osmosensitivity on the walking legs of *Carcinus maenas*, but did not show other modalities of these neurons. We have shown that bend-sensitive neurons respond to salinity changes, with some neurons responding only to hyposmotic stimuli, some mainly to hyperosmotic stimuli, and some to both. Differential responses such as these could be the underlying sensory mechanism for behavioral responses to osmotic stimuli. Similar bimodal properties have been reported from osmosensory and mechanosensory neurons in tactile setae of the antennae of the spiny lobster *Panulirus japonicus* (Tazaki, 1975). Interestingly, the bimodal neurons in *P. japonicus* were described as being sensitive to displacement, but the method of mechanical stimulation used by Tazaki (1975) was such that bending during displacement may have occurred.

Many interesting questions stem from the finding of bimodal neurons that are sensitive to both mechanical and osmotic stimulation. First, what is the primary modality of these neurons, and is the secondary modality merely noise in the animal's sensory input? Due to the diversity of the detailed bend response, we believe that the neurons are primary bend neurons. Since the osmoresponse is also complex and contains information about osmolarity, we find it likely that the neurons are truly bimodal and that they probably convey both types of information. The sensitivity of the bend neurons to osmolarity could mediate the observed behavioral responses to salinity changes, but such a sensory system would be much more effective in detecting salinity changes from a distance if it were situated on the long antenna 2, as also indicated by Tazaki (1975). Alternatively, mouthpart osmoreceptors might provide information about the chemical quality of prey items. *Panulirus argus*, like most decapods, is partly a scavenger, and the osmolarity of decaying prey changes due to metabolites produced by the actions of microorganisms and due to the breakdown and solubilization of insoluble macromolecules (R. Glud, Institute of Biology, University of Copenhagen; *pers. comm.*). But whether these processes will result in osmotic changes large enough for the neurons to detect is questionable. Furthermore, a latency of more than 2 s also seems to obscure the function, since the prey will often be at least partly ingested in this time frame. It is therefore not obvious to us what information may be conveyed by the osmosensitive neurons.

Bimodal receptor neurons are not common but have been found in molluses and crustaceans. Bimodal chemosensory and mechanosensory neurons have been found in the crayfish *Austropotamobius torrentium* and in the opisthobranch gastropod *Tritonia diomedea* (Audesirk and Audesirk, 1980; Hatt, 1986). In the case of *Tritonia*, bimodality is suggested to be due to peripheral synapses between unimodal afferents (Audesirk and Audesirk, 1980). The caudal photoreceptor of crayfish offers another example of bimodal sensory neurons responding to both mechanical and photostimuli; in this case the primary modality is believed to be photosensation (Pei *et al.*, 1996).

We are intrigued by the finding that only bend neurons respond to changes in osmolarity. One possible explanation is that the morphological arrangement of mechanosensory neurons in these setae is such that only bend neurons are exposed to the external environment. This idea is supported by the observation that after the cuspidate setae were amputated halfway up the shaft, the tactile neurons within them could be made to respond to deionized water. Morphological studies are needed to verify this hypothesis.

Acknowledgments

The authors thank Dr. Hank Trapido-Rosenthal (Bermuda Biological Station for Research) and the staff of the Florida Key Marine Laboratory for supplying lobsters, and Dr. Manfred Schmidt for critical comments on the manuscript. We are also grateful to Danmarks Akvarium, Copenhagen, for letting us maintain and observe the animals in their facilities. We thank James Newcomb (Georgia State University) for constructive comments and helpful discussions. This study was supported by the University of Copenhagen, the Danish Research Council, grant DC00312 from the National Institute on Deafness and other Communication Disorders, grant IBN-0077474 from the National Science Foundation, the Georgia Research Alliance, and the GSU Research Program Enhancement Fund. All experiments in this study comply with the "Principles of Animal Care," publication No. 86-23, revised 1985, of the National Institutes of Health, and with the laws of the United States of America.

Literature Cited

Ache, B. W. 1982. Chemoreception and thermoreception. Pp. 369–398 in *The Biology of Crustacea*, Vol. 3, H. L. Atwood and D. C. Sandeman, eds. Academic Press, New York.

Ache, B. W. 2002. Crustaceans as animal models for olfactory research. Pp. 189–199 in *Crustacean Experimental Systems in Neurobiology*, K. Wiese, ed. Springer-Verlag, New York.

Altner, I., H. Hatt, and H. Altner. 1983. Structural properties of bimodal chemo- and mechanosensitive setae on the pereiopod chelae of the crayfish, *Austropotamobius torrentium*. *Cell Tissue Res.* **228:** 357–374.

Audesirk, G., and T. Audesirk. 1980. Complex mechanoreceptors in *Tritonia diomedea*. I. Responses to mechanical and chemical stimuli. *J. Comp. Physiol. A* **141:** 101–110.

Barth, F. G., and A. Höller. 1999. Dynamics of arthropod filiform hairs. V. The response of spider trichobothria to natural stimuli. *Proc. R. Soc. Lond. B Biol. Sci.* **354:** 183–192.

Caine, E. A. 1975a. Feeding and mastication structures of selected Anomura (Crustacea). *J. Exp. Mar. Biol. Ecol.* **18:** 277–301.

Caine, E. A. 1975b. Feeding and mastication structures of six species of

crayfish genus *Procambarus* (Decapoda, Astacidae). *Forma Functio* **8:** 49–66.

Cate, H. S., and C. D. Derby, 2001. Morphology and distribution of setae on the antennules of the Caribbean spiny lobster *Panulirus argus* reveal new types of bimodal chemo-mechanosensilla. *Cell Tissue Res.* **304:** 439–454.

Cate, H. S., and C. D. Derby, 2002a. Hooded sensilla homologues: structural variations of a widely distributed bimodal chemo-mechanosensillum. *J. Comp. Neurol.* **444:** 345–357.

Cate, H. S., and C. D. Derby, 2002b. Ultrastructure and physiology of the hooded sensillum, a bimodal chemo-mechanosensillum of lobsters. *J. Comp. Neurol.* **442:** 293–307.

Coelho, V. R., A. B. Williams, and S. A. Rodrigues, 2000. Trophic strategies and functional morphology of feeding appendages, with emphasis on setae of *Upogebia omissa* and *Pomatogebia operculata* (Decapoda: Thalassinidea: Upogebiidae). *Zool. J. Linnean Soc.* **130:** 567–602.

Cokl, A., and M. Virant-Doberlet, 2003. Communication with substrate-borne signals in small plant-dwelling insects. *Annu. Rev. Entomol.* **48:** 29–52.

Crouau, Y. 1989. Feeding mechanisms of the Mysidacea. Pp. 153–172 in *Functional Morphology of Feeding and Grooming in Crustacea*, B. E. Felgenhauer, L. Watling, and A. B. Thistle, eds. AA Balkema, Rotterdam.

Crouau, Y. 1994. An unusual mechanosensitive cell in a crustacean exteroceptor. *Biol. Cell* **80:** 71–74.

Crouau, Y. 1995. Association in a crustacean sensory organ of two usually mutually exclusive mechanosensory cells. *Biol. Cell* **85:** 191–195.

Crouau, Y. 2001. Mechanosensitive cells of hexapods, crustaceans and myriopods setae: a comparison under phylogenetic aspects. *Ann. Soc. Entomol. Fr.* **37:** 233–242.

Derby, C. D. 1989. Physiology of sensory neurons in morphologically identified cuticular sensilla of crustaceans. Pp. 27–48 in *Functional Morphology of Feeding and Grooming in Crustacea*, B. E. Felgenhauer, L. Watling, and A. B. Thistle, eds. AA Balkema, Rotterdam.

Derby, C. D. 1995. Single unit electrophysiological recordings from crustacean chemoreceptor neurons. Pp. 241–250 in *Experimental Cell Biology of Taste and Olfaction. Current Techniques and Protocols*, A. I. Spielman and J. G. Brand, eds. CRC Press, New York.

Derby, C. D. 2000. Learning from spiny lobsters about chemosensory coding of mixtures. *Physiol. Behav.* **69:** 203–209.

Derby, C. D., P. Steullet, A. J. Horner, and H. S. Cate, 2001. The sensory basis of feeding behaviour in the Caribbean spiny lobster, *Panulirus argus*. *Mar. Freshw. Res.* **52:** 1339–1350.

Dufort, C. G., S. H. Jury, J. M. Newcomb, D. F. O'Grady, and W. H. Watson, 2001. Detection of salinity by the lobster, *Homarus americanus*. *Biol. Bull.* **201:** 424–434.

Fields, D. M., D. S. Shaeffer, and M. J. Weissburg, 2002. Mechanical and neural response from the mechanosensory hairs on the antennule of *Gaussia princeps*. *Mar. Ecol. Prog. Ser.* **227:** 173–186.

Garm, A. 2004. Mechanical functions of setae from the mouth apparatus of seven species of decapod crustaceans. *J. Morphol.* **260:** 85–100.

Garm, A., and J. T. Hoeg, 2000. Functional mouthpart morphology of the squat lobster *Munida sarsi*, with comparison to other anomurans. *Mar. Biol.* **137:** 123–138.

Garm, A., and J. T. Hoeg, 2001. Function and functional groupings of the complex mouth apparatus of the squat lobsters *Munida sarsi* Huus and *M. tenuimana* G. O. Sars (Crustacea: Decapoda). *Biol. Bull.* **200:** 281–297.

Garm, A., E. Hallberg, and J. T. Hoeg, 2003. Role of maxilla 2 and its setae during feeding in the shrimp *Palaemon adspersus* (Crustacea: Decapoda). *Biol. Bull.* **204:** 126–137.

Gerlach, S. A., D. K. Ekstrom, and P. B. Eckardt, 1976. Filter feeding in the hermit crab, *Pagurus bernhardus*. *Oecologia* **24:** 257–264.

Greenwood, J. G. 1972. The mouthparts and feeding behaviour of the species of hermit crabs. *J. Nat. Hist.* **6:** 325–337.

Harrison, P. J. II., H. S. Cate, P. Steullet, and C. D. Derby, 2001. Structural plasticity in the olfactory system of adult spiny lobsters: postembryonic development permits life-long growth, turnover, and regeneration. *Mar. Freshw. Res.* **52:** 1357–1365.

Hatt, H. 1986. Responses of a bimodal neuron (chemo- and vibration-sensitive) on the walking legs of the crayfish. *J. Comp. Physiol. A* **159:** 611–617.

Hatt, H., and U. Bauer, 1980. Single unit analysis of mechano- and chemosensitive neurons in the crayfish claw. *Neurosci. Lett.* **17:** 203–207.

Heinisch, P., and K. Wiese, 1987. Sensitivity to movement and vibration of water in the North Sea shrimp *Crangon crangon* (L.). *J. Crustac. Biol.* **7:** 401–413.

Hunt, M. J., H. Winsor, and C. G. Alexander, 1992. Feeding by the penaeid prawns: the role of the anterior mouthparts. *J. Exp. Mar. Biol. Ecol.* **160:** 33–46.

Janse, C. 1980. The function of the statolith-hair and free-hook-hair receptors in the statocyst of the crab, *Scylla serrata*. *J. Comp. Physiol. A* **137:** 51–62.

Johnston, D. J. 1999. Functional morphology of the mouthparts and alimentary tract of the slipper lobster *Thenus orientalis* (Decapoda: Scyllaridae). *Mar. Freshw. Res.* **50:** 213–223.

Jury, S. H., M. T. Kinnison, W. H. Howell, and W. H. Watson, 1994. The behavior of lobsters in response to reduced salinity. *J. Exp. Mar. Biol. Ecol.* **180:** 23–37.

Keil, T. A. 1998. The structure of integumental mechanoreceptors. Pp. 385–404 in *Insecta*, F. W. Harrison and M. E. Rice, eds. Wiley-Liss, New York.

Kunze, J., and D. Anderson, 1979. Functional morphology of the mouthparts and gastric mill in the hermit crabs *Clibanarius taenitua* (Milne Edwards), *Clibanarius virescens* (Krauss), *Paguristes squamonsus* McCulloch and *Dardanus setifer* (Milne-Edwards) (Anomura: Paguridea). *Aust. J. Mar. Freshwater Res.* **30:** 683–722.

Lavalli, K. L., and J. R. Factor, 1992. Functional morphology of the mouthparts of juvenile lobsters, *Homarus americanus* (Decapoda: Nephropidae), and comparison with the larval stages. *J. Crustac. Biol.* **12:** 467–510.

Masters, M., B. Aicher, J. Tautz, and H. Mark, 1982. A new type of water vibration receptor on the crayfish antenna. II. Model of receptor function. *J. Comp. Physiol. A* **149:** 409–422.

McClintock T. S., and F. Xu, 2002. Molecular physiology of G-proteins in olfactory transduction and CNS neurotransmission in the lobster. Pp. 359–366 in *The Crustacean Nervous System*, K. Wiese, eds. Springer-Verlag, Berlin.

Paffenhöfer, G. A., and P. A. Loyd, 2000. Ultrastructure of cephalic appendages setae of marine planktonic copepods. *Mar. Ecol. Prog. Ser.* **203:** 171–180.

Pei, X., L. A. Wilkens, and F. Moss, 1996. Light enhances hydrodynamic signaling in the multimodal caudal photoreceptor interneurons of the crayfish. *J. Neurophysiol.* **76:** 3002–3011.

Schembri, P. J. 1982. Functional morphology of the mouthparts and associated structures of *Pagurus rubricatus* (Crustacea: Decapoda: Anomura) with special reference to feeding and grooming. *Zoomorphology* **101:** 17–38.

Schmidt, M. 1989. The hair-peg organs of the shore crab, *Carcinus maenas* (Crustacea: Decapoda): ultrastructure and functional properties of sensilla sensitive to changes in seawater concentration. *Cell Tissue Res.* **257:** 609–621.

Schmidt, M., and W. Gnatzy, 1984. Are the funnel-canal organs the

'campaniform sensilla' of the shore crab *Carcinus maenas* (Decapoda: Crustacea)? II. Ultrastructure. *Cell Tissue Res.* **237:** 81–97.

Schmidt, M., U. Grünert, and C. D. Derby. 2003. Non-olfactory sensilla mediate chemically induced antennular grooming in the spiny lobster, *Panulirus argus*. *Soc. Neurosci. Abstr.* #595.5.

Shelton, R. G. J., and M. S. Laverack. 1970. Receptor hair structure and function in the lobster *Homarus gammarus* (L.). *J. Exp. Mar. Biol. Ecol.* **4:** 201–210.

Solon, M. H., and G. Kass-Simon. 1981. Mechanosensory activity of hair organs on the chelae of *Homarus americanus*. *Comp. Biochem. Physiol.* **68A:** 217–223.

Stemhuis, E. J., B. Danwe, and J. J. Videler. 1998. How to bite the dust: morphology, motion pattern and function of the feeding appendages of the deposit-feeding thalassinid shrimp *Callianassa subterranea*. *Mar. Biol.* **132:** 43–58.

Tautz, J., M. Masters, B. Aicher, and H. Mark. 1981. A new type of water vibration receptor on the crayfish antenna. *J. Comp. Physiol. A* **144:** 533–541.

Tazaki, K. 1975. Sensory units respond to osmotic stimuli in the antennae of the spiny lobster *Panulirus japonicus*. *Comp. Biochem. Physiol.* **51A:** 647–653.

Tazaki, K. 1977. Nervous responses from mechanosensory hairs on the antennal flagellum in the lobster *Homarus gammarus* (L.). *Mar. Behav. Physiol.* **5:** 1–18.

Vedel, J. P. 1985. Cuticular mechanoreception in the antennal flagellum of the rock lobster *Panulirus vulgaris*. *Comp. Biochem. Physiol.* **80A:** 151–158.

Vedel, J. P., and F. Clarac. 1976. Hydrodynamic sensitivity by cuticular organs in the rock lobster *Panulirus vulgaris*. Morphological and physiological aspects. *Mar. Behav. Physiol.* **3:** 235–251.

Wiese, K. 1976. Mechanoreceptors for near-field water displacement in crayfish. *J. Neurophysiol.* **39:** 816–833.

Reference: *Biol. Bull.* **207:** 209–216. (December 2004)

Physiological and Morphological Identification of Photosensitive Neurons in the Opisthosomal Ganglia of *Limulus polyphemus*

KAZUO MORI*, TAKEHIKO SAITO, AND TAKETERU KURAMOTO

Shimoda Marine Research Center, University of Tsukuba, Shimoda, Shizuoka, 415-0025, Japan

Abstract. The motor outputs of the isolated opisthosomal ventral nerve cord in *Limulus polyphemus* are modulated by light. We have identified the photosensitive neurons and examined their physiological and morphological properties using intracellular recording and staining techniques. We found that photosensitive neurons are present in each ganglion of the opisthosomal ventral nerve cord. These neurons often discharged action potentials spontaneously in the dark, and they increased the frequency of this discharge in the light. The mean latency (±SD) of the light-induced action potential was 2.2 ± 1.1 s. Cells responded in a graded fashion over a 2-log unit of light intensity. The peak spectral sensitivity was 425 nm or lower. The Lucifer-yellow-labeled photosensitive neurons had oval somata with mean (±SD) diameters of 102 ± 3 μm (long axis) and 75 ± 5 μm (short axis), and extended their axons to the contralateral region of the ventral nerve cord. The soma had no dendrites, and the axon had thin branches.

Introduction

Extra-retinal photoreceptors have been detected in the central nervous system of arthropods (for review, see Page, 1982). For example, photosensitive neurons have been found in the 6th abdominal ganglion of crayfish (Prosser, 1934; Kennedy, 1958, 1963; Bruno and Kennedy, 1962), in the abdominal ganglion and the brain of insects (Arikawa *et al.*, 1991; Ichikawa, 1991; Hariyama, 2000), in the brain of spiders (Yamashita and Tateda, 1981, 1983), and in the telson (Zwicky, 1968) and the metasomata of scorpions (Geethabali and Rao, 1973). Among these extra-retinal photoreceptors, the caudal photoreceptors in crayfish have been studied extensively because they are accessible for intracellular recording (Wilkens and Larimer, 1972, 1976; Kruszewska and Larimar, 1993) and because their activity can be correlated with the animal's behavior (Welsh, 1934; Edwards, 1984; Simon and Edwards, 1990).

The horseshoe crab, often referred to as a "living fossil," has proved useful for studying the phylogenetic development of arthropods. Because of its accessible eyes, the animal is also an admirable model for vision research: extensive studies have been performed on its lateral eyes (Hartline and Ratliff, 1957; Ratliff, 1974; Barlow *et al.*, 2001) and ventral photoreceptor (for review, see Dorlöchter and Stieve, 1997). Studies on extra-retinal photoreceptors in the central nervous system have, however, been limited (Snodderly, 1971).

Using extracellular recording techniques, we recently observed that motor outputs of the isolated opisthosomal ventral nerve cord of *Limulus* are modulated by direct light stimulation (Mori and Kuramoto, 2004). Encouraged by this finding, we used intracellular recording techniques to search for photosensitive neurons in isolated ganglia of opisthosomal ventral nerve cord and examined their physiological and morphological properties. The results indicate that photosensitive neurons are present in each ganglion of opisthosomal ventral nerve cord, and the peak of their spectral response is 425 nm or lower. The functional significance of the photosensitive neurons in the *Limulus* central nervous system is compared with those found in other arthropods.

Materials and Methods

Preparation

The horseshoe crabs (*Limulus polyphemus* (Linnaeus, 1758), both sexes, 17–21 cm in carapace width) were purchased from the Marine Resource Center (Marine Biological Laboratory, Woods Hole, MA). They were reared in the

Received 10 March 2004; accepted 24 August 2004.

* To whom correspondence should be addressed at Center for Vision Research, SUNY Upstate Medical University, 750 East Adams Street, Syracuse, NY 13210. E-mail: morik@upstate.edu

aquaria of Shimoda Marine Research Center (Shizuoka, Japan) under a natural light/dark cycle. The temperature in the aquaria ranged between 11 and 25 °C throughout the year.

For these experiments, an animal was inverted, and the gill plates together with the opisthosomal ventral nerve cord were dissected free from the animal. Under a stereomicroscope, a chain of 9th to 16th opisthosomal ganglia with intact dorsal and ventral nerves were freed from surrounding tissue. They were put into a petri dish filled with physiological saline solution and kept at 4 °C until used. In every experiment, a single ganglion was isolated from a chain of opisthosomal ganglia and mounted ventral side up on a silpot platform in an acrylic chamber ($3 \times 2 \times 0.7$ cm^3). The sheath of the ganglion and the connective tissue surrounding cell bodies were carefully removed. The preparation was perfused with saline solution saturated with air by bubbling. The saline solution contained (in m*M*) 530 NaCl, 10.7 KCl, 18.0 $CaCl_2$, 24.6 $MgCl_2$, 2.3 $NaHCO_3$, and 3 glucose; adjusted to pH 7.4. The temperature of the saline was maintained between 17 and 19 °C during the experiment.

Electrodes

For intracellular recordings from photosensitive neurons, micropipettes were made from glass capillary tubing (BF100-86-10, Sutter) using a Brown-Flaming micropipette puller (P-97, Sutter) and filled with 3 *M* KCl solution. The resistance of the electrodes was 20–30 MΩ. The electrode was connected to a DC amplifier (MEZ-8301, Nihon Kohden) through a high-impedance negative-capacitance preamplifier (JZ-101J, Nihon Kohden). For extracellular recording of segmental nerves, glass suction pipettes filled with saline were connected to an AC amplifier (AB621G, Nihon Kohden). For intracellular staining, the micropipettes were filled with 3% Lucifer yellow (Polyscience Inc.) in 100 m*M* LiCl (15–80 MΩ). All nerve signals were digitized (Digidata 1200B, Axon Inst.), saved on a computer, and analyzed with Axoscope software (version 9, Axon Instruments).

Light stimulus

The preparation was illuminated with a halogen lamp (300 W) through a heat-absorbing filter, lens, mechanical shutter, and mirror system. The intensity of light of 0.0 log units roughly corresponds to 1.5×10^{17} quanta/cm^2·s at the surface of the preparation and is attenuated with neutral-density filters between 0.0 and −3.0 log units. Monochromatic light (425, 450, 475, 500, 550, and 600 nm) was obtained by narrow-band interference filters (Optical Coatings Japan) in the light path. Neutral-density filters adjusted the quantal flux for each filter to 1.6×10^{14} quanta/cm^2·s.

Intracellular staining

Lucifer yellow was iontophoretically injected into physiologically examined cells with negative electrical currents of 5–15 nA at 2.5 Hz for 30–90 min. Ganglia containing stained cells were kept overnight at 4 °C and then fixed for 2 h in 4% paraformaldehyde in 0.1 mol/l phosphate buffered saline (PBS) at pH 7.4. After washing for 1.5 h in PBS and several minutes in distilled water, they were dehydrated in a graded ethanol series and cleared in methylsalicylate. The stained neurons in whole-mount preparations were observed with a fluorescence microscope (Optiphot, Nikon) and photographed with a digital camera (Coolpix 990, Nikon).

Results

Intracellular and extracellular recordings from isolated opisthosomal ganglia

Each opisthosomal ganglion contains a pair of segmental nerves (dorsal and ventral nerves) with the dorsal nerves lying anterior to the ventral nerves. The dorsal nerves innervate visceral organs such as the intestine and the heart, and the ventral nerves innervate the muscles of the gill plates (Patten and Redenbaugh, 1900; Carlson, 1905). A cluster of cell bodies is located at the base of each segmental nerve.

Using intracellular electrodes, we located photosensitive neurons in single isolated opisthosomal ganglia. We also recorded extracellularly from dorsal or ventral nerves to correlate the activity of motor neurons with the activity of photosensitive neurons. Figure 1 illustrates the extracellular discharge pattern of the right ventral nerves of the 9th ganglion (Fig. 1A) and the intracellular response of a photosensitive neuron in the cluster of cell bodies of the same ganglion (Fig. 1B). In darkness, a periodic burst discharge, corresponding to gill plate activity, was recorded extracellularly from ventral nerves, and spontaneous action poten-

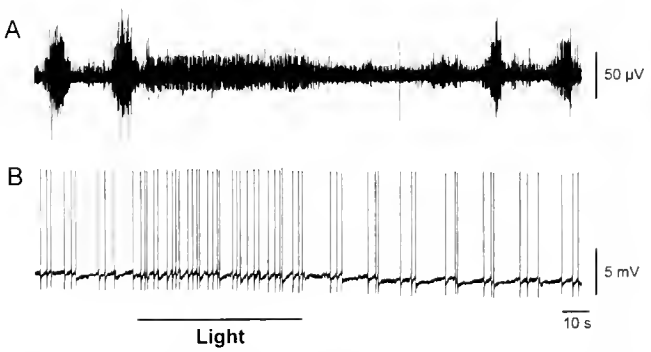

Figure 1. Simultaneous recordings of extracellular responses from the right ventral nerve in isolated 9th ganglion (A), and intracellular responses from a photosensitive neuron within a cluster of cell bodies in the same ganglion (B). In (A), illumination produced the inhibition of rhythmic burst activity and the appearance of sustained bursting. In (B), the frequency of action potentials increased by illumination.

tials with an irregular interval were recorded intracellularly from a single neuron. Illumination of the ganglion increased the frequency of action potentials and inhibited the periodic burst discharge of ventral nerves, producing a sustained discharge.

To determine whether the photosensitive neurons respond to light directly or through synapses, the preparation was treated with Co^{2+}, a blocker of chemical transmission. Figure 2 shows simultaneous recordings from the left ventral nerves of the 13th ganglion and a photosensitive neuron in the same ganglion before (A) and after (B) application of Co^{2+}. In the presence of 20 m*M* Co^{2+}, the periodic burst discharge was inhibited within 3 min, while the frequency of action potentials without illumination was not significantly changed. Illumination increased the frequency of action potentials (Fig. 2B), suggesting that this photosensitive neuron is a primary photoreceptor. The effects of Co^{2+} partially recovered after washout (not shown).

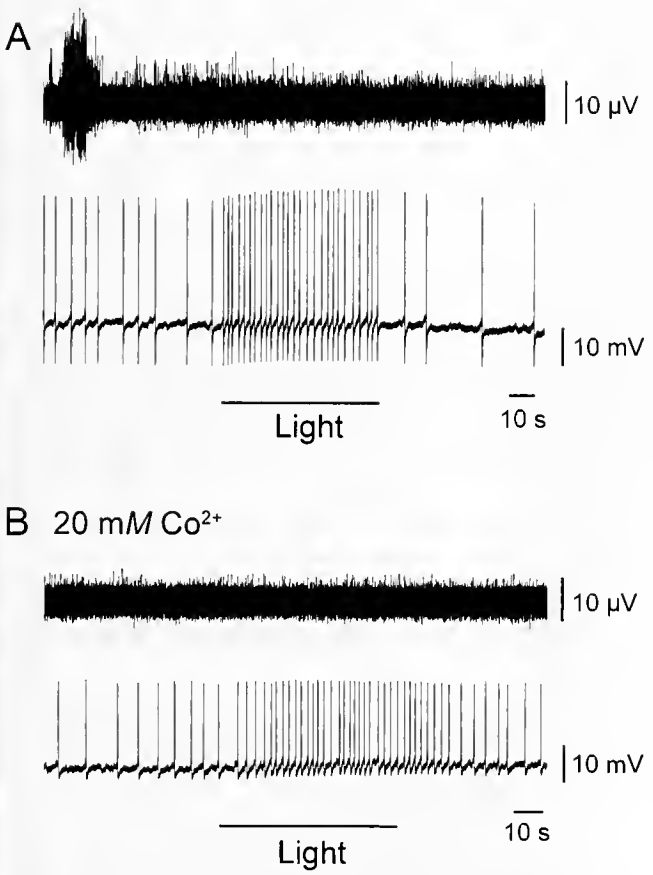

Figure 2. Effect of Co^{2+} on extracellular responses from the left ventral nerve in isolated 13th ganglion, and intracellular responses from a photosensitive neuron within a cluster of cell bodies in the same ganglion (A) before application of Co^{2+}; (B) 15 min after application of Co^{2+} (20 m*M*). Motor activity in the ventral nerve (upper trace) was reduced. The frequency of action potentials (lower trace) without illumination and the increase in the frequency of action potentials with illumination were not significantly changed in the presence of Co^{2+}.

Physiological properties of the photosensitive neurons

Photosensitive neurons are not abundant in isolated opisthosomal ganglia. Thus far, less than 2% of the neurons that we examined (20 out of 1050) exhibited photosensitivity. All 20 photosensitive neurons exhibited spontaneous action potentials in the dark and responded to light with an increase in the frequency of action potentials. The level of spontaneous activity and the response to light varied from cell to cell and, occasionally, during the course of experiment on the same cell. Three examples of photoresponses are shown in Figure 3. Responses just before and at the beginning of illumination (dotted line under each left trace) are shown on the right with an expanded time scale. Responses shown in Figure 3A and B were obtained from the same cell in the 12th ganglion. The cell had a resting potential of about −30 mV and exhibited few spontaneous action potentials in the dark within several minutes after penetration (Fig. 3A). In the course of the experiment, however, the frequency of action potentials gradually increased to about 1 impulse/s (ips) without a significant change in the membrane potential (Fig. 3B). After illumination, the membrane potential depolarized about 2 mV, and the frequency of action potentials increased to 2 ips. The latency of the response was 0.6 s in Figure 3A and 2 s in Figure 3B. The response in Figure 3C was recorded in the 15th ganglion. In the dark, the cell discharged an irregular spike frequency of about 0.1 ips. Light stimulation caused a slight depolarization of the membrane potential and increased the spike frequency to about 0.4 ips.

Figure 4 shows the effect of duration of light on a photosensitive neuron in the 12th ganglion. Light stimulation increased the frequency of action potentials from a rate of about 0.3 ips to 0.8 ips. The light-evoked response of 0.8 ips was independent of the stimulus duration up to 60 s, indicating minimal adaptation to the light stimulus. Photosensitive neurons did not exhibit substantial adaptation to light.

Photosensitive neurons have a graded response to light intensity. Figure 5 (A–F) shows responses recorded from a photosensitive neuron in the 9th ganglion to light of different intensities. The frequency of action potentials increased at light intensities greater than −2.0 log units, reaching a maximum of 0.9 ips at 0.0 log units. The number of action potentials to different light intensities was normalized to that evoked by the maximal light intensity (0.0 log units) and plotted against the log intensity of light for the three cells in Figure 5G. The data from the cell in Figure 5 (A–F) are illustrated by filled circles. The intensity-response curve indicates that the photosensitive neurons can convey information about light intensity over a 2-log unit.

Photosensitive neurons respond maximally to short wavelength illumination. Using different wavelengths of light, we examined the spectral response properties of five neurons. Figure 6 (A–D) shows a representative spectral response pattern of a photosensitive neuron in the 9th gan-

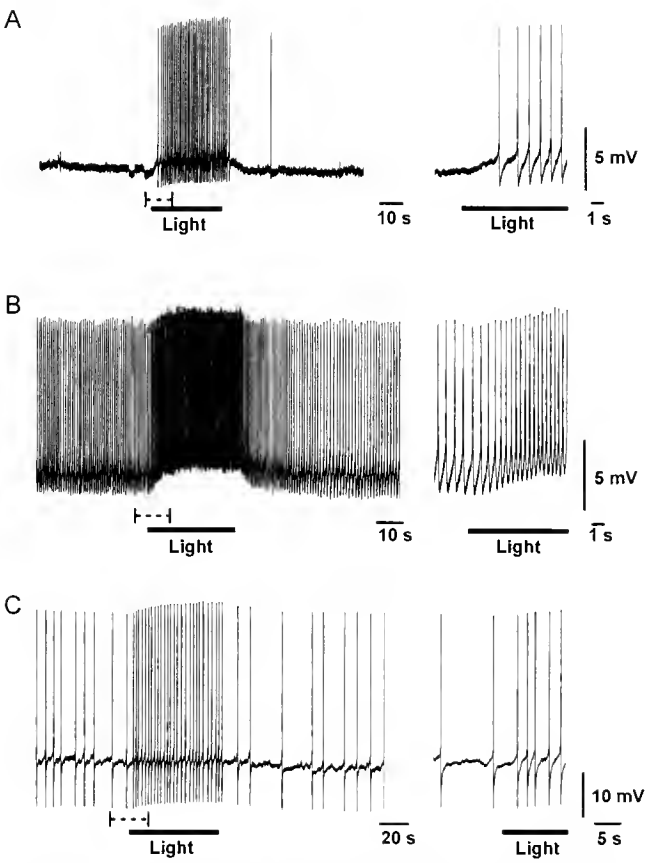

Figure 3. Three examples of the dark-adapted activity patterns and light responses of photosensitive neurons. (A and B) Responses from the same neuron in the cluster of cell bodies at the right dorsal nerve in an isolated 12th ganglion. In (A), the record was obtained 5 min after penetration. The cell was essentially quiescent in the dark. In (B), the record was obtained 80 min after the recording in (A). The frequency of action potentials in the dark increased without significant change in membrane potential. (C) Response from a neuron in the 15th ganglion. This neuron had a relatively low frequency of spontaneous action potentials with irregular spike intervals. All cells responded to light with an increase in the frequency of action potentials and a corresponding increase in the slope of the pacemaker potential, as seen in responses just before and at the beginning of illumination (dotted line under each left trace) and on the right with an expanded time scale.

glion. Monochromatic light of equal quantal flux but different wavelength was applied successively to the ganglion from 425 nm to 600 nm. The response increased slightly at 500 nm and became maximal at 425 nm. The number of action potentials at each wavelength was normalized with respect to the number of action potentials at 425 nm and plotted as a function of wavelength for five cells (Fig. 6E). The spectral-response curve suggests that photosensitive neurons are maximally sensitive at 425 nm or shorter wavelengths.

Morphological properties of the photosensitive neurons

All photosensitive neurons extend axons to the contralateral region of the ventral nerve cord, and most extend axons longitudinally in the cord. These morphological properties are based on observations of the Lucifer yellow (LY) that was iontophoretically injected into 12 photosensitive neurons after recording their electrical responses. Of 12 cells injected with LY, 6 were successfully stained. Figure 7 shows a photomicrograph of the cell in Figure 3A and B. The cell has an oval soma with a diameter of 103 μm (long axis) and no dendrites. A single axon extends toward the contralateral region without any branches, then turns, ascending in the connective toward the anterior ganglion (Figure 7, inset). Several thin branches are sparsely distributed along the axon within the 12th ganglion. Diagrams in Figure 8 show the 9th–16th opisthosomal ventral nerve cord with the recording sites of the 20 recorded photosensitive neurons marked by filled circles (Fig 8A) and 6 LY-stained photosensitive neurons (Fig. 8B). The diameter of the cell bodies ($n = 6$) was 102 ± 3 μm (long axis) and 75 ± 5 μm (short axis). Each cell extended its axon to the contralateral region. In five of the six cells, the axons ran along the longitudinal ventral nerve cord to either anterior or posterior connectives (Fig. 8B, circled A–D and F); the axon of the sixth cell was restricted in the ganglion (Fig. 8B, circled E).

Discussion

Extra-retinal photoreceptors that have been found in *Limulus* include ventral photoreceptors (Millecchia *et al.*,

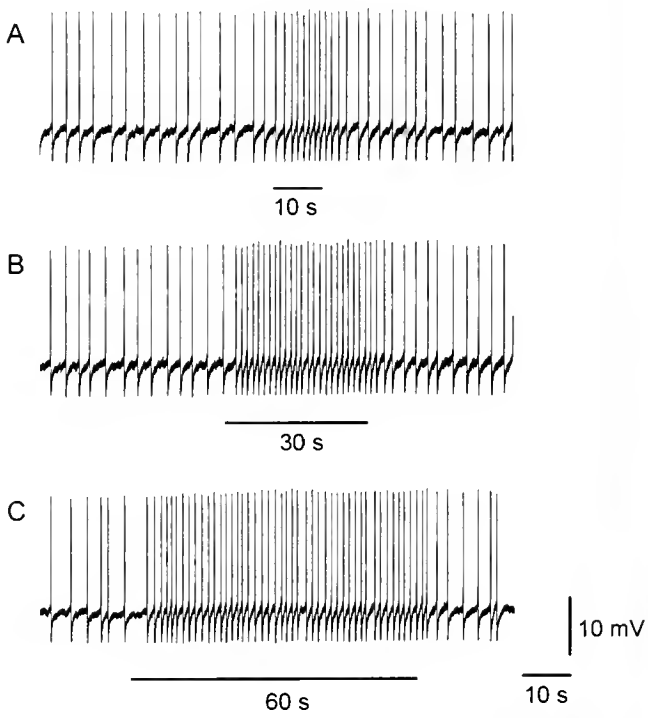

Figure 4. Effect of light of different duration on a photosensitive neuron within a cluster of cell bodies at the base of the right dorsal nerve of the 12th ganglion. An increase in the frequency of action potentials with illumination was maintained during illumination.

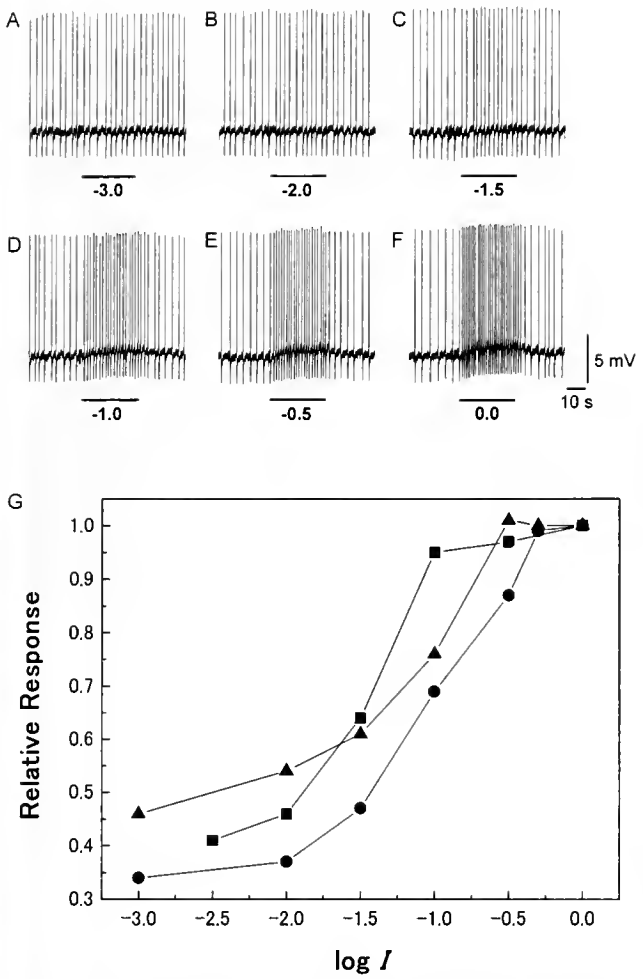

Figure 5. (A–F) Effect of light of different intensities on a photosensitive neuron within a cluster of cell bodies at the base of the left dorsal nerve of the 9th ganglion. Light stimuli between −3.0 and 0.0 log units were successively applied at intervals of several minutes. (G) The number of action potentials at each intensity of light was normalized with the number of action potentials at the maximum intensity of light and plotted against different intensities.

1966), photoreceptors adjacent to the optic ganglia (Snodderly, 1971), photoreceptors in the median optic nerves (Samie *et al.*, 1995), and photoreceptors in the telson (Hanna *et al.*, 1988). Here, we found new photosensitive neurons in the opisthosomal ventral nerve cord. These often exhibited spontaneous action potentials in the dark and an increase in the number of action potentials in light. The latency of the response to light was on the order of seconds. The frequency of action potentials was maintained during illumination and modulated by light intensity over a 2-log unit. The peak spectral response was at 425 nm or lower.

Are photosensitive neurons photoreceptors?

In *Limulus*, ventral photoreceptors and photoreceptor cells of the lateral and median eyes respond to light with a transient peak depolarization followed by a steady-state depolarization (Hartline *et al.*, 1952; Millecchia *et al.*, 1966; Nolte and Brown, 1972). On the other hand, the response of photosensitive neurons in the *Limulus* ventral nerve cord exhibits tonic discharges to light with little adaptation, which is similar to the response of the caudal crayfish photoreceptor (CPR) of the crayfish (Kennedy, 1958, 1963; Wilkens and Larimer, 1972). In the crayfish ventral nerve cord, primary photoreceptors are identified by at least two criteria: the production of a slow depolarization, with superimposed action potentials, upon illumination, and the

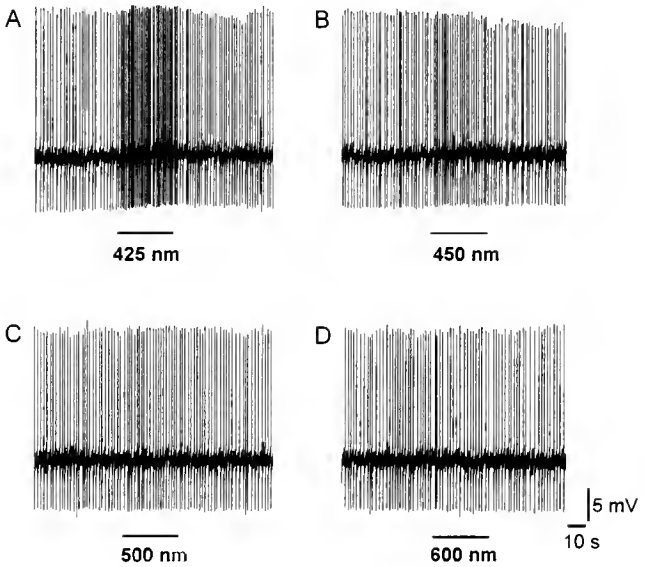

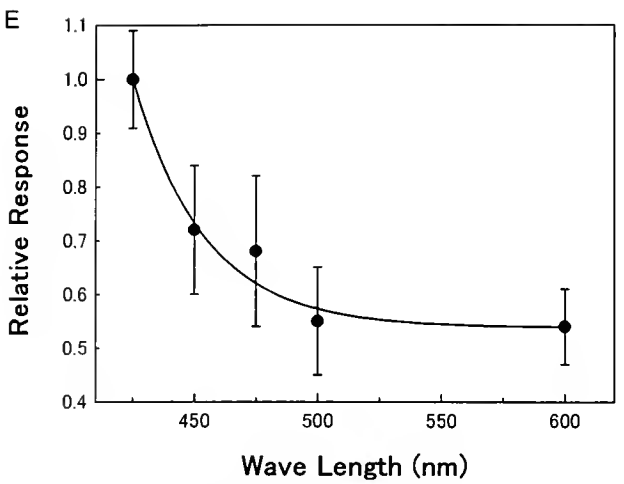

Figure 6. (A–D) Effect of light of different wavelengths on a photosensitive neuron within a cluster of cell bodies at the base of left dorsal nerve in the 9th ganglion. Monochromatic light with a duration of 30 s is shown below each record. Light stimuli were applied at intervals of several minutes. The maximum spectral response was seen at 425 nm. (E) The number of action potentials at each wavelength was normalized to the number of action potentials at 425 nm and plotted against different wavelengths. Values are mean (±SD).

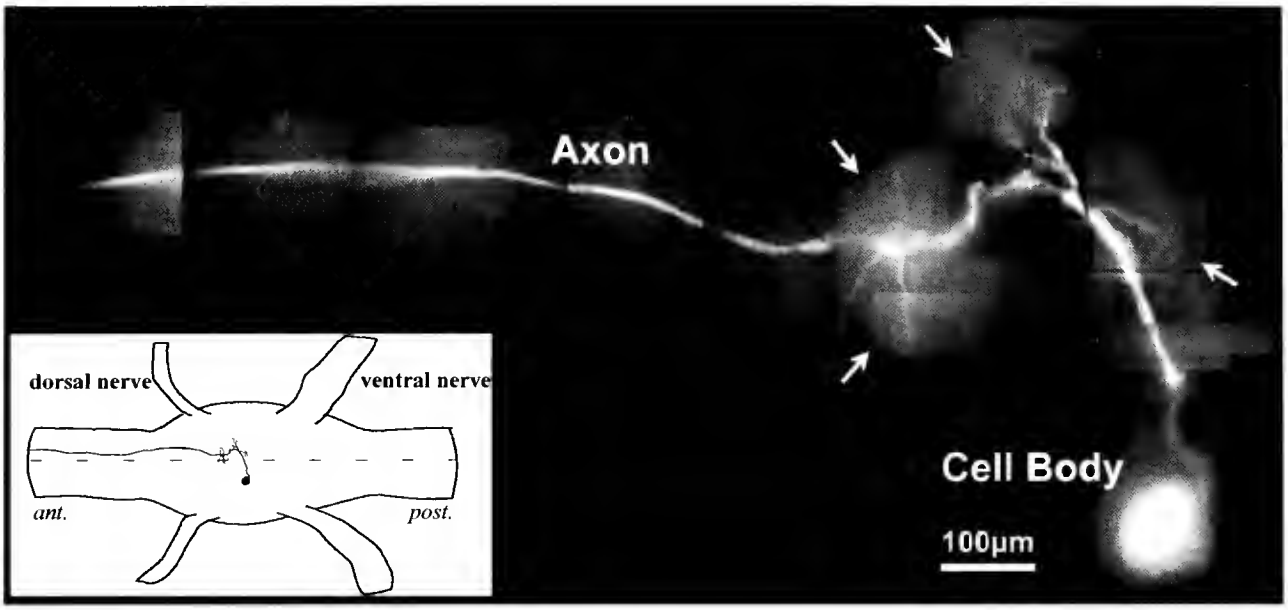

Figure 7. Ventral view of a Lucifer-yellow-injected photosensitive neuron in the 12th ganglion. The cell body (103 μm in diameter, long axis) extends an axon toward the contralateral region, where the axon turns sharply and ascends toward the 11th ganglion with some dendritic branches (arrows). Inset: a schematic drawing of the neuron in the ganglion.

resetting of the endogenous rhythm by interpolated antidromic impulses (Kennedy 1963). In the present study, many photosensitive neurons also responded to light with a slow depolarization and an increase in action potential frequency. Although we did not examine whether an antidromic pulse stimulation resets the spontaneous activity rhythm, the fact that, when chemical transmission was suppressed by Co^{2+}, photosensitive neurons did not lose spon-

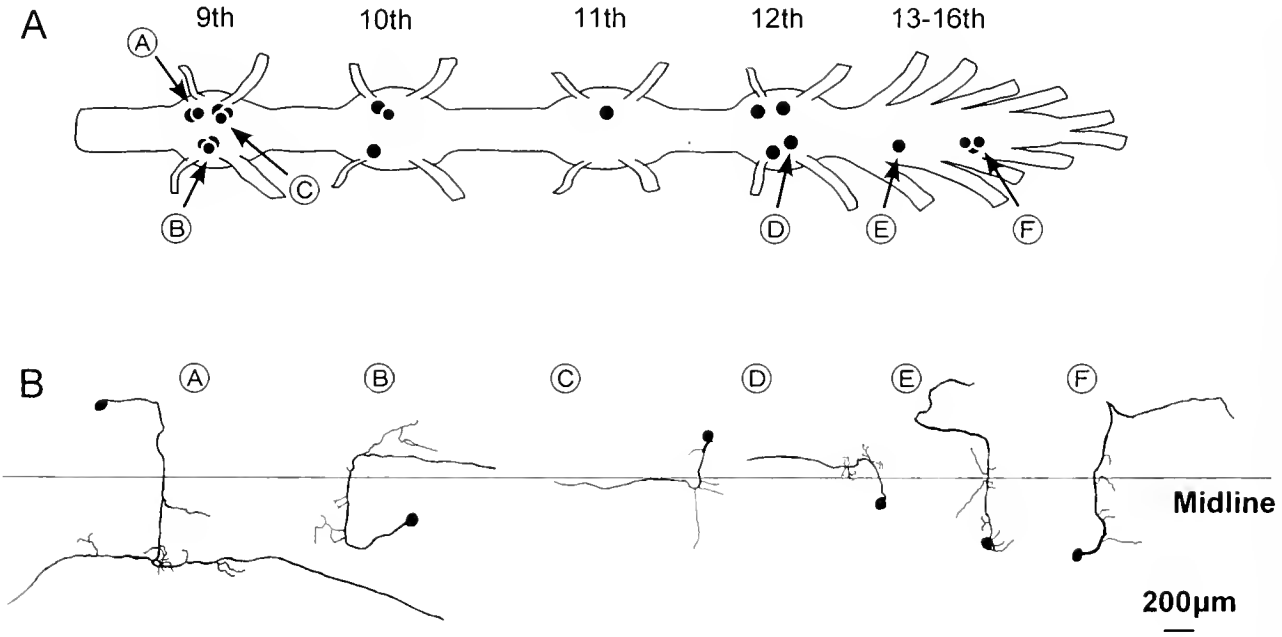

Figure 8. Ventral view of the opisthosomal ventral nerve cord (A), and the morphology of 6 Lucifer-yellow-labeled photosensitive neurons (B). In (A), filled circles indicate the location of somata of 20 photosensitive neurons that are examined physiologically. In (B), morphology of the labeled neurons is schematically illustrated. Circled letters in (B) correspond to those in (A). The midline of the opisthosomal ventral nerve cord is shown.

taneous action potentials in the dark and photosensitivity to light suggests that they are primary photoreceptors.

Comparison of extra-retinal photoreceptors in Limulus *and other arthropods*

From a phylogenetic point of view, it is important to point out similarities and differences in the extra-retinal photoreceptors of *Limulus* and other arthropods. Like *Limulus*, the scorpion is a chelicerate, and it shares a number of features in its structure and development with the horseshoe crab. It has been reported, using extracellular recording (Zwicky, 1968; Geethabali and Rao, 1973) and behavioral techniques (Zwicky, 1968, 1970), that the scorpion has extra-retinal photoreceptors in some abdominal ganglia, and that the peak spectral response is 568 nm with a secondary peak at 440 nm. A more detailed comparison between the extra-retinal photoreceptors of *Limulus* and the scorpion must await further analysis using intracellular recordings in scorpions. In the brain of spiders, extra-retinal photoreceptors with a peak spectral response at 420–440 nm have been detected using extracellular recording techniques (Yamashita and Tateda, 1981, 1983).

The photosensitive properties of *Limulus* neurons can be better compared to the caudal photoreceptor of the crayfish, which has been studied more extensively. The CPR in crayfish is composed of two bilaterally symmetrical neurons located in the 6th abdominal ganglion. Like those in *Limulus*, they exhibit spontaneous action potentials in the dark and a tonic increase in the frequency of action potentials in light (Prosser, 1934; Kennedy, 1963); but their peak spectral response is at 500 nm (Bruno and Kennedy, 1962; Larimer, 1966) rather than at 425 nm or lower. It is worth noting that the peak spectral response of extra-retinal photoreceptors in *Limulus* is similar to that in scorpion (the secondary peak) and spider, which are phylogenetically closer to the horseshoe crab.

The latency of the response in *Limulus* extra-retinal photoreceptors ranged from 0.5 to 5 s, with a mean ± SD value of 2.2 ± 1.1 s. Such a long latency has been also reported for CPR neurons (0.3–12 s, Kennedy, 1958). The large range of latencies may be partly due to measurement errors caused by a fluctuation in the intervals between spontaneous action potentials. Nevertheless, latencies on the order of seconds are significantly longer than those reported for lateral or ventral photoreceptors, which are on the order of milliseconds. A second messenger cascade has been suggested for the long response latency in crayfish CPR (Kruszewska and Larimer, 1993). The phototransduction mechanism remains unresolved for extra-retinal photosensitive neurons in *Limulus* ventral nerve cord.

Dye-injection experiments demonstrate that all somata of photosensitive neurons examined in *Limulus* extend an axon to the contralateral region, where it runs longitudinally along the opisthosomal ventral nerve cord in either or both directions. In crayfish, a pair of CPR interneurons also consists of a contralateral soma and ipsilateral axonal branches (Wilkens and Larimer, 1972). The axon of the CPR projects the length of the ventral nerve cord from the 6th ganglion to the brain (Simon and Edwards, 1990). In contrast, *Limulus* has photosensitive neurons in each ganglion of the ventral nerve cord. In one of six LY-stained cells, the axon was restricted to a single ganglion (Fig. 8B, circled E), whereas the other five cells extended their axons to anterior or posterior connectives (Fig. 8B, circled A–D and F). Therefore, it appears that they extend axons to more than one ganglion. Another morphological difference between the photoreceptor of the two species is the paucity of dendrites in *Limulus* relative to those in crayfish. Furthermore, in crayfish, these dendrites and not the cell body have been assumed to be photosensitive. The site of the light sensitivity of the photosensitive neurons in the opisthosomal ganglion of *Limulus* is not known.

Functional significance of extra-retinal photosensitive neurons

Extra-retinal photoreceptors in arthropods are often functionally associated with the entrainment of circadian rhythms (Yamashita and Tateda, 1981; Page, 1982). In crayfish, for example, circadian locomotor activity can be entrained by illumination of the brain (Page and Larimer, 1972). Furthermore, illumination of the CPR evokes leg movements (Welsh, 1934; Edwards, 1984; Simon and Edwards, 1990) and disrupts circadian locomotion (Fuentes-Pardo and Inclán-Rubio, 1987; Inclán-Rubio and Fuentes-Pardo, 1987). In scorpions, Zwicky (1968, 1970) has speculated that the negative phototaxis might be mediated by extra-retinal photoreceptors.

In the present and previous studies (Mori and Kuramoto, 2004), we have observed that illumination of isolated opisthosomal ganglia of the *Limulus* ventral nerve cord either inhibited or accelerated (or both) the activity of dorsal and ventral nerves. We suggest that light stimulation may modulate the activity of visceral organs and gill plates. In preliminary experiments, blue light from an LED embedded between the gill plates of a restrained animal accelerated the heart beat in some animals (data not shown). This result suggests that external light can reach the photosensitive neurons through the semitransparent skin of the intact animal and perhaps have a role in behaviors such as an animal righting itself. Photosensitive neurons may have an ever greater role in the behavior of juvenile horseshoe crabs because they are more transparent than adults. How environmental light modulates organ activities and animal behavior are subjects for future research.

Acknowledgments

We thank Dr. Robert B. Barlow (SUNY Upstate Medical University) for his critical reading of the manuscript and

comments. This research is a study of the Shimoda Marine Research Center (Contribution No. 700).

Literature Cited

Arikawa, K., K. Uchiumi, and E. Eguchi. 1991. Extraocular photoreceptors in the last abdominal ganglion of a swallowtail butterfly, *Papilio xuthus*. *Naturwissenschaften* **78:** 82–84.

Barlow, R. B., J. M. Hitt, and F. A. Dodge. 2001. *Limulus* vision in the marine environment. *Biol. Bull.* **200:** 169–176.

Bruno, M. S., and D. Kennedy. 1962. Spectral sensitivity of photoreceptor neurons in the sixth ganglion of the crayfish. *Comp. Biochem. Physiol.* **6:** 41–46.

Carlson, A. J. 1905. Comparative physiology of the invertebrate heart. I. The innervation of the heart. *Biol. Bull.* **8:** 123–169.

Dorlöchter, M., and H. Stieve. 1997. The *Limulus* ventral photoreceptor: light response and the role of calcium in a classic preparation. *Prog. Neurobiol.* **53:** 451–515.

Edwards, D. H., Jr. 1984. Crayfish extraretinal photoreception. I. Behavioural and motoneuronal responses to abdominal illumination. *J. Exp. Biol.* **109:** 291–306.

Fuentes-Pardo, B., and V. Inclán-Rubio. 1987. Caudal photoreceptors synchronize the circadian rhythms of crayfish. I. Synchronization of ERG and locomotor circadian rhythms. *Comp. Biochem. Physiol. A* **86:** 523–527.

Geethabali, and K. P. Rao. 1973. A metasomatic neural photoreceptor in the scorpion. *J. Exp. Biol.* **58:** 189–196.

Hanna, W. J. B., J. A. Horne, and G. H. Renninger. 1988. Circadian photoreceptor organs in *Limulus*. II. The telson. *J. Comp. Physiol. A* **162:** 133–140.

Hariyama, T. 2000. The brain as a photoreceptor: intracerebral ocelli in the firefly. *Naturwissenschaften* **87:** 327–330.

Hartline, H. K., and F. Ratliff. 1957. Inhibitory interaction of receptor units in the eye of *Limulus*. *J. Gen. Physiol.* **40:** 357–376.

Hartline, H. K., H. G. Wagner, and E. F. MacNichol, Jr. 1952. The peripheral origin of nervous activity in the visual system. *Cold Spring Harbor Symp. Quant. Biol.* **17:** 125–141.

Ichikawa, T. 1991. Brain photoreceptors in the pupal and adult butterfly: fate of the larval ocelli. *Zool. Sci.* **8:** 471–476.

Inclán-Rubio, V., and B. Fuentes-Pardo. 1987. Caudal photoreceptors synchronize the circadian rhythms of crayfish. II. Functional relationships between caudal and visual photoreceptors. *Comp. Biochem. Physiol. A* **86:** 529–536.

Kennedy, D. 1958. Responses from the crayfish caudal photoreceptor. *Am. J. Ophthalmol.* **46:** 19–26.

Kennedy, D. 1963. Physiology of photoreceptor neurons in the abdominal nerve cord of the crayfish. *J. Gen. Physiol.* **46:** 551–572.

Kruszewska, B., and J. L. Larimer. 1993. Specific second messengers activate the caudal photoreceptor of crayfish. *Brain Res.* **618:** 32–40.

Larimer, J. L. 1966. A functional caudal photoreceptor in blind cavernicolous crayfish. *Nature* **210:** 204–205.

Millecchia, R., J. Bradbury, and A. Mauro. 1966. Simple photoreceptors in *Limulus polyphemus*. *Science* **154:** 1199–1201.

Mori, K., and T. Kuramoto. 2004. Photosensitivity of the central nervous system of *Limulus polyphemus*. *Zool. Sci.* **21:** 731–737.

Nolte, J., and J. E. Brown. 1972. Electrophysiological properties of cells in the median ocellus of *Limulus*. *J. Gen. Physiol.* **59:** 167–185.

Page, T. L. 1982. Extraretinal photoreception in entrainment and photoperiodism in invertebrates. *Experientia* **38:** 1007–1013.

Page, T. L., and J. L. Larimer. 1972. Entrainment of the circadian locomotor activity rhythm in crayfish. *J. Comp. Physiol.* **78:** 107–120.

Patten, W., and W. A. Redenbaugh. 1900. Studies on *Limulus*. II. The nervous system of *Limulus polyphemus*, with observation upon the general anatomy. *J. Morphol.* **16:** 91–200.

Prosser, C. L. 1934. Action potentials in the nervous system of the crayfish. II. Responses to illumination of the eye and caudal ganglion. *J. Cell Comp. Physiol.* **4:** 363–377.

Ratliff, F., ed. 1974. *Studies on Excitation and Inhibition in the Retina. A Collection of Papers from the Laboratories of H. Keffer Hartline.* Chapman and Hall, London.

Samie, F. H., R. N. Jinks, W. W. Weiner, and S. C. Chamberlain. 1995. The morphology and physiology of a "mini-ommatidium" in the median optic nerve of *Limulus polyphemus*. *Vis. Neurosci.* **12:** 69–76.

Simon, T. W., and D. H. Edwards. 1990. Light-evoked walking in crayfish: behavioral and neuronal responses triggered by the caudal photoreceptor. *J. Comp. Physiol. A* **166:** 745–755.

Snodderly, M., Jr. 1971. Processing of visual inputs by brain of *Limulus*. *J. Neurophysiol.* **34:** 588–611.

Welsh, J. H. 1934. The caudal photoreceptor and responses of the crayfish to light. *J. Cell Comp. Physiol.* **4:** 379–388.

Wilkens, L. A., and J. L. Larimer. 1972. The CNS photoreceptor of crayfish: morphology and synaptic activity. *J. Comp. Physiol.* **80:** 389–407.

Wilkens, L. A., and J. L. Larimer. 1976. Photosensitivity in the sixth abdominal ganglion of decapod crustaceans: a comparative study. *J. Comp. Physiol. A* **106:** 69–75.

Yamashita, S., and H. Tateda. 1981. Efferent neural control in the eyes of orb weaving spiders. *J. Comp. Physiol. A* **143:** 477–483.

Yamashita, S., and H. Tateda. 1983. Cerebral photosensitive neurons in the orb weaving spiders, *Argiope bruennichii* and *A. amoena*. *J. Comp. Physiol. A* **150:** 467–472.

Zwicky, K. T. 1968. A light response in the tail of *Urodacus*, a scorpion. *Life Sci.* **7:** 257–262.

Zwicky, K. T. 1970. Behavioural aspects of the extraocular light sense of *Urodacus*, a scorpion. *Experientia* **26:** 747–748.

Reference: *Biol. Bull.* **207:** 217–224. (December 2004)

Passive Flow Through an Unstalked Intertidal Ascidian: Orientation and Morphology Enhance Suspension Feeding in *Pyura stolonifera*

N. A. KNOTT*, A. R. DAVIS, AND W. A. BUTTEMER

School of Biological Sciences, University of Wollongong, Wollongong NSW 2522, Australia

Abstract. Passive flow is believed to increase the gains and reduce the costs of active suspension feeding. We used a mixture of field and laboratory experiments to evaluate whether the unstalked intertidal ascidian *Pyura stolonifera* exploits passive flow. We predicted that its orientation to prevailing currents and the arrangement of its siphons would induce passive flow due to dynamic pressure at the inhalant siphon, as well as by the Bernoulli effect or viscous entrainment associated with different fluid velocities at each siphon, or by both mechanisms. The orientation of *P. stolonifera* at several locations along the Sydney-Illawarra coast (Australia) covering a wide range of wave exposures was nonrandom and revealed that the ascidians were consistently oriented with their inhalant siphons directed into the waves or backwash. Flume experiments using wax models demonstrated that the arrangement of the siphons could induce passive flow and that passive flow was greatest when the inhalant siphon was oriented into the flow. Field experiments using transplanted animals confirmed that such an orientation resulted in ascidians gaining food at greater rates, as measured by fecal production, than when oriented perpendicular to the wave direction. We conclude that *P. stolonifera* enhances suspension feeding by inducing passive flow and is, therefore, a facultatively active suspension feeder. Furthermore, we argue that it is likely that many other active suspension feeders utilize passive flow and, therefore, measurements of their clearance rates should be made under appropriate conditions of flow to gain ecologically relevant results.

Received 15 March 2004; accepted 8 August 2004.

* To whom correspondence should be addressed, at Department of Zoology, University of Melbourne, Victoria 3010, Australia. E-mail: nknott@unimelb.edu.au

Introduction

The gain and use of energy influence the fitness of all organisms (Townsend and Calow, 1981; Sibly and Calow, 1986). The net gain from feeding depends on how much food an animal consumes and assimilates minus the costs associated with the capture, digestion, and absorption of food, as well as the discarding of waste (Sibly, 1981; Townsend and Hughes, 1981; Sibly and Calow, 1986). For active suspension feeding invertebrates, there is the potential, by using external water movement, to increase the food consumed or reduce the costs of feeding, or both (Vogel and Bretz, 1972; Allanson *et al.*, 1992; Vogel, 1994). Active suspension feeders must pump water across their filtering structures to feed, which incurs a metabolic cost (Jørgensen, 1966; Wildish and Kristmanson, 1997). Passive flow induced by external water movement (Vogel, 1974) may, however, enable active suspension feeders to augment the flow of water through their filtering structures, hence increasing their feeding rate or reducing the energy required to move water actively, or both (Vogel and Bretz, 1972; Vogel, 1974, 1994; LaBarbera, 1977, 1984; Wildish and Kristmanson, 1997).

Active suspension feeders, such as solitary ascidians, could induce passive flow from external water movement in several ways (Vogel and Bretz, 1972; Vogel, 1974, 1994). The most obvious is by orienting the inhalant siphon into the flow and the exhalant siphon away from the flow. The resultant dynamic pressure on the inhalant siphon would force water through the ascidian (Vogel, 1974, 1994; Kott, 1989). The stalked ascidian *Styela montereyensis* has been shown to use dynamic pressure (Young and Braithwaite, 1980). The stalk of *S. montereyensis* enables it to orient its inhalant siphon into the prevailing current by the force of water movement alone. Ascidians without stalks have fixed

orientations and, as a result, induction of passive flow may be more constrained. Yet many marine habitats, both intertidal and subtidal, experience water movement that can be predictable in both direction and strength (Wainwright and Dillion, 1969; Denny, 1988). In such habitats, there is the potential for unstalked ascidians to use dynamic pressure for assisted feeding, but this has not yet been demonstrated. The Bernoulli effect and viscous entrainment (Day, 1974; Vogel, 1978, 1994; Kott, 1989) may also enable unstalked ascidians to induce passive flow from external water movement by positioning their exhalant siphons higher above the substratum than their inhalant siphons (Vogel, 1974, 1977; Allanson *et al.*, 1992).

Pyura stolonifera (Heller, 1978) is the common solitary ascidian found on intertidal rocky shores along the east coast of Australia (Kott, 1985). This unstalked ascidian has its inhalant siphon directed horizontally and its exhalant siphon higher and directed vertically (Fig. 1; Day, 1974; Kott, 1985). Furthermore, casual observations suggested that the inhalant siphons of these ascidians were usually directed into the oncoming waves. We predicted that this arrangement and orientation of the siphons would induce passive flow through the ascidian. To evaluate whether *P. stolonifera* induces passive flow from the movement of water over intertidal shores, we investigated four questions: (1) whether the ascidian was nonrandomly oriented, (2) whether the arrangement of the ascidian's siphons was capable of inducing passive flow, (3) whether the orientation of the ascidian affects the magnitude of passive flow, and (4) whether its orientation into the flow increases its feeding rate on the rocky shore.

Materials and Methods

Field orientation

We surveyed the orientation of *Pyura stolonifera* at six rocky shores covering a wide range of wave exposures and orientations along the Sydney-Illawarra coast (Fig. 2). The orientation of the ascidian, defined as the direction of the axis running from the exhalant to the inhalant siphon, was measured to the nearest 5° using a magnetic compass. At each shore, the *P. stolonifera* population was sampled representatively using at least five 1-m^2 quadrats positioned randomly along a 50-m transect laid out parallel to the shoreline within the population. In each quadrat, the orientation of all ascidians and the direction of the waves coming

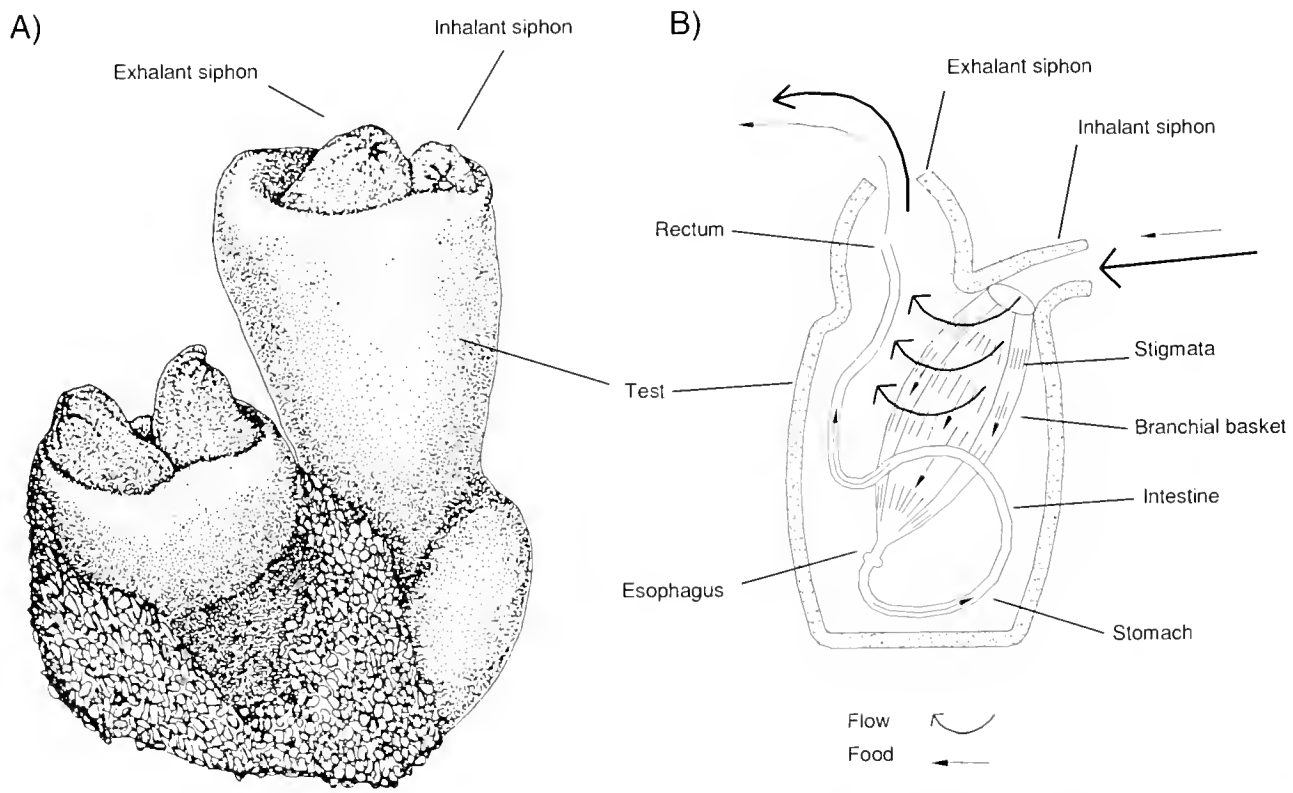

Figure 1. Morphology of the intertidal ascidian *Pyura stolonifera*. (A) Diagram of the external morphology of non-feeding animals with partially retracted siphons (reprinted with permission from P. Kott and Museum of Queensland Press; Kott, 1985). (B) Schematic diagram showing the internal structure of the ascidian and the pathways for water and food through the ascidian. The exhalant siphon is projected directly upwards, and the inhalant siphon is projected parallel to the substratum.

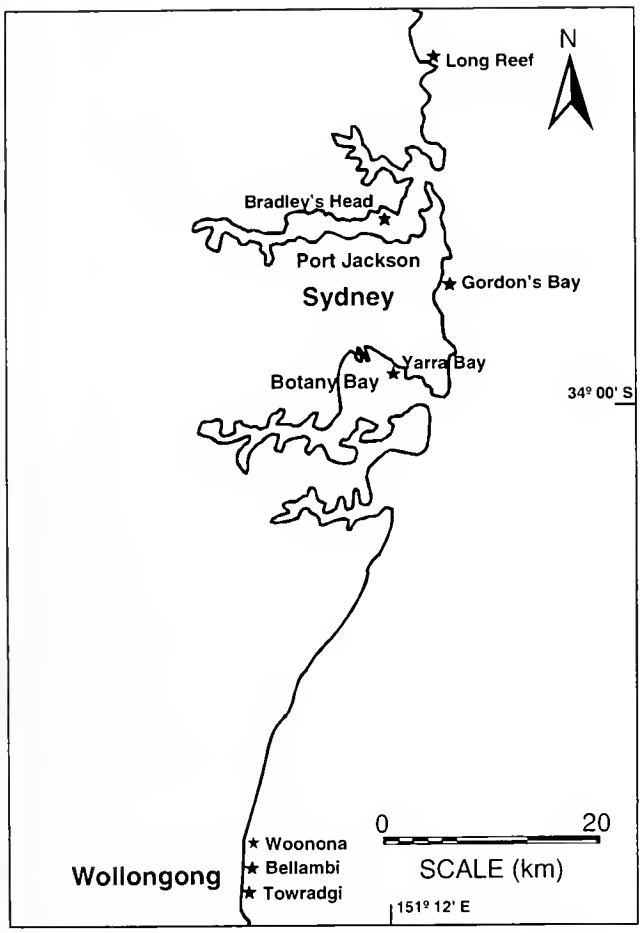

Figure 2. Study locations along the Sydney-Illawarra coast.

onto the shore at the time of sampling were measured. Because the direction of the waves varied along the transect, the measurements of the ascidians in each quadrat were standardized against the mean wave direction of the quadrats across the whole transect. The orientations of more than 240 individuals of *P. stolonifera* were measured at each shore.

Flume experiment

To evaluate whether the morphology of *P. stolonifera* could induce passive flow, we used a flume and functional wax models of the ascidian. This enabled us to simplify the investigation of the ascidian's potential to induce passive flow. Also, we used models instead of real animals because the models could not play any active role in producing flow.

Models were cast from five live ascidians that were selected haphazardly from populations at Bellambi and Woonona (Fig. 2) and covered a representative range of sizes (test height 3–10 cm; test diameter 4–7 cm). Models were hollow, microcrystalline wax castings from alginate molds of the ascidians. Inside each model, tubing (5-mm diameter) connected the inhalant opening to a reservoir (a 50-ml plastic bottle) and the reservoir to the exhalant siphon.

The reservoir was filled with blue food dye; we reasoned that, when the model was placed in the flume, any water movement through it would dilute the dye. The relationship between the dilution of the dye and the amount of water that moved through each model was calculated by passing set amounts of water (5–80 ml) through each model and spectrophotometrically measuring the absorbance of the reservoir contents after each run. This relationship proved to be very strong, with the coefficient of determination (r^2) for each model being greater than 0.995.

To evaluate whether the arrangement of the siphons of *P. stolonifera* was capable of exploiting passive flow, we tested the hypothesis that if the models were positioned within the directional flow of the flume, dye would escape from the exhalant siphon but not from the inhalant siphon. We also investigated whether the orientation of the ascidian influenced the magnitude of passive flow. We predicted that passive flow through the models would be greater when they were oriented with inhalant siphons into the flow (360°) than when oriented perpendicular to (90°) or away from (180°) the flow. The flow rate through each model was measured three separate times ($n = 3$) at each of these orientations. Replicate measurements were interspersed in terms of both models and orientations. Models were positioned in the flume for 5 min for each measurement.

The flow through the flume was laminar and reached free-stream velocity within 2 cm of the bottom and sides of the flume. The working section of the flume was 0.4 m deep, 0.3 m wide, and 3.5 m long, and along with the size of the models, satisfied the size requirements for flumes and experimental subjects set out by Nowell and Jumars (1987). The experiment was done at a mean flow speed of 15.2 cm s^{-1} with a standard deviation of 0.25 cm s^{-1}.

Field feeding experiment

We predicted that if passive flow enhances the feeding success of *P. stolonifera*, individuals oriented with their inhalant siphons into the waves would consume more food than those oriented perpendicular to the waves. To test this hypothesis, we positioned ascidians on the intertidal shore at Bellambi so that they were oriented into (360°) or perpendicular to (90°) the wave direction and measured their subsequent fecal production to infer their feeding rate (as described in Young and Braithwaite, 1980).

Ascidians used in this experiment were collected from the rocky shore at Bellambi (Fig. 2). Each animal had its exterior cleaned carefully and was then held in a laboratory seawater system for 72 h. Within this period, the ascidians evacuate more than 90% of their gut contents ($n = 5$; N. Knott, unpubl. data). Ascidians were attached to heavy steel

plates (3 × 25 × 50 cm) with epoxy resin (Epirez). Four ascidians were attached to each plate: two oriented into (360°) and two perpendicular to (90°) the wave direction. The epoxy was allowed to set for 12 h and, at the next low tide, the ascidians were returned to the rocky shore at Bellambi. After 24 h, the ascidians were brought back to the laboratory and removed from the plates. Their exteriors were washed and they were submerged in separate beakers containing filtered seawater. After 72 h, the ascidians were removed from the labeled beakers, and the water and feces from each beaker were filtered. The filter paper was dried at 70 °C for 1 h and weighed to calculate the dry mass of the feces to the nearest milligram. The ascidians themselves were removed from their tests and dried at 70 °C for 5 d to obtain their dry body mass to the nearest milligram. There was no relationship between the dry mass of the ascidians and their fecal production for either treatment, so fecal production was used as a measure of feeding rate independent of dry weight.

To evaluate whether any effects of orientation on the feeding rate of *P. stolonifera* were temporally consistent, the experiment was repeated. Both experiments initially had 12 replicate ascidians with each orientation (360° or 90°). In the first experiment, the mortality rate was high (42%), probably because the epoxy resin was set with the steel bases submerged in the laboratory seawater system. Rust particles from the steel plates made the water cloudy and possibly affected the ascidians. In the second experiment, the epoxy was set in open air for 12 h and few ascidians died (8% mortality rate).

Data analysis

The orientation of *P. stolonifera* populations was tested using Rayleigh's Z-test for nonrandomness (Batschelet, 1981; Zar, 1984). Data from the flume and feeding experiments were analyzed using analysis of variance. The experimental designs are provided in the table captions for each analysis of variance. In the feeding experiment, blocks were not included as a factor because of the loss of replicate ascidians, primarily in the first experiment. The normality and heterogeneity of variances were assessed for both the model and the feeding experiments by using box plots and plots of the residuals against means (Quinn and Keough, 2002).

Results

Field orientation

Across a range of wave-exposed rocky shores, the orientation of *Pyura stolonifera* was consistently nonrandom (Table 1). Furthermore, the mean orientation of the ascidian was closely associated with the estimated wave direction at each location (Table 1). That is, *P. stolonifera* tended to be oriented with its inhalant siphons directed into or away from the wave direction. This is illustrated by the circular frequency graphs of the orientation of *P. stolonifera* at two rocky shores (Fig. 3). At some locations, the ascidians had a unidirectional orientation, tending mainly to be oriented into the wave direction (*e.g.*, Long Reef, Fig. 3 and Table 1); at other locations, they had a bidirectional orientation, tending to be positioned into or away from the wave direction (*e.g.*, Towradgi, Fig. 3 and Table 1). The variability in the orientation of the ascidians differed substantially among locations (*r* values, Table 1): for example, variation was low at Long Reef, but high at Bellambi.

Flume experiment

The arrangement of the siphons of *P. stolonifera* induced passive flow. Dye streamed out of the exhalant siphon of

Table 1

Orientation of Pyura stolonifera *at six rocky intertidal shores of varying wave exposure along the Sydney-Illawarra coast*

Location	Wave exposure	Orientation		Wave direction[c]	r[d]	P[e]	Sample size
		Mean value[a]	Type[b]				
Long Reef	High	12 ± 7°	Uni	30°	0.670	<0.001	264
Towradgi	High	162 ± 18°	Bi	150°	0.283	<0.001	387
Bellambi	Moderate	36 ± 26°	Bi	20°	0.233	<0.001	247
Gordon's Bay	Moderate	183 ± 11°	Uni	170°	0.506	<0.001	410
Yarra Bay	Low	311 ± 8°	Uni	300°	0.611	<0.001	411
Bradley's Hd	Low	112 ± 19°	Uni	90°	0.289	<0.001	261

[a] Mean orientation of the populations ± the 95% confidence intervals. Calculated as per Zar (1984).

[b] Uni = unidirectional orientation; Bi = bidirectional orientation.

[c] Mean estimated wave direction along the sampled shoreline on the day of sampling.

[d] r is a measure of the variance of the orientation of the population (a value of 1 means that all individuals have the same orientation as the mean, whereas a value of 0 indicates that the population is uniformly distributed).

[e] P values from Rayleigh's Z test for random circular distribution (Zar, 1984).

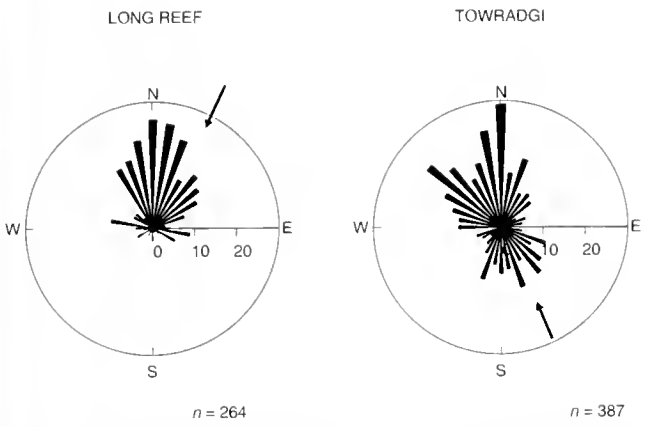

Figure 3. Circular frequency histograms of the orientation of *Pyura stolonifera* on two rocky intertidal shores. Arrows indicate the estimated wave direction at each shore on the day of sampling.

each model ascidian at all orientations (Fig. 4). Passive flow was, however, significantly greater through each model when oriented into the flow (360°) than when oriented perpendicular to the flow (90°) (Fig. 4; Table 2). Depending on the model, the difference in passive flow at these two orientations was 5- to 25-fold (Fig. 4). Some of the models showed relatively high rates of passive flow while oriented away from the flow (180°), but only one model, had significantly higher passive flow rates at this orientation than when oriented perpendicular to the flow (Table 2).

Field feeding experiment

Individuals of *P. stolonifera* oriented into the waves produced about twice as much fecal material as those oriented perpendicular to the waves, after being on the rocky shore for 24 h (Fig. 5; Table 3). This orientation effect was consistent even though the ascidians consumed less food in the first experiment than in the second (Fig. 5; Table 3).

Table 2

Analysis of variance of passive flow through model Pyura stolonifera *at three orientations in relation to the flow through the flume*

Source	SS	DF	MS	*F*	*P*
Model	14.83	4	3.71	17.3	0.0000
Orientation	37.85	2	18.93	21.7	0.0006
Model × Orientation	6.98	8	0.87	4.07	0.0022
Residual	6.42	30	0.21		
Pair-wise comparisons					
Model 1: 360 > 180 = 90			Model 4: 360 > 180 = 90		
Model 2: 360 > 180 = 90			Model 5: 360 > 180 = 90		
Model 3: 360 > 180 > 90					

Orientation was a fixed factor with three levels (360°, 90° and 180°), and Model was a random orthogonal factor with five levels ($n = 3$). The data were transformed to $\log_e x$ to normalize the data and reduce the differences among variances. SNK tests were used to detect differences between means.

Discussion

The unstalked ascidian *Pyura stolonifera* is a facultatively active suspension feeder (*sensu* LaBarbera, 1984) as it can actively pump water through its branchial basket by using its cilia, but its orientation and siphonal arrangement also induce passive flow. This conclusion is based on our results from laboratory and field experiments. First, on all rocky shores sampled, covering a large section of the Sydney-Illawarra coast (about 70 km) and a wide range of wave exposures, individuals of *P. stolonifera* were usually oriented into the waves. Second, our flume experiments demonstrated clearly that this orientation would maximize the

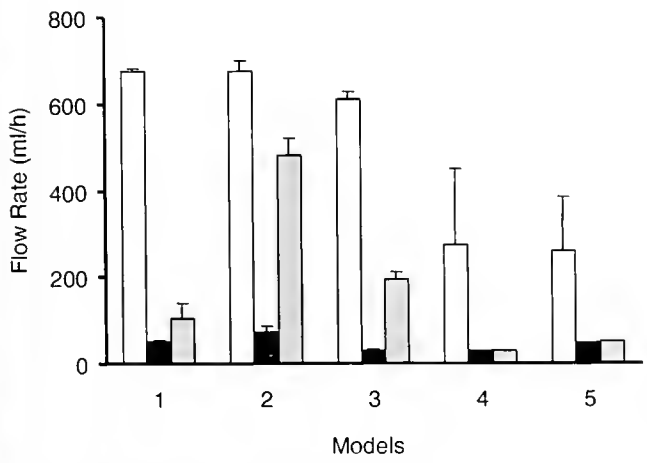

Figure 4. Passive flow (mean ± s.e.; $n = 3$) through model *Pyura stolonifera* at three orientations in relation to flow through the flume. □ 360°, ■ 90°, and ▨ 180°.

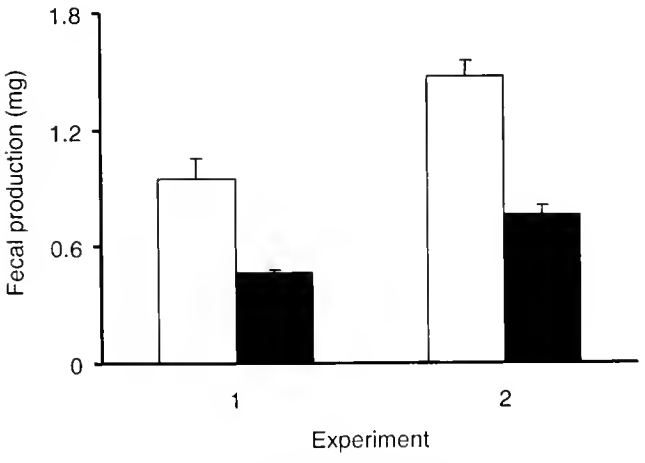

Figure 5. Fecal production (mean ± s.e.) of *Pyura stolonifera* after 24 h at two orientations in relation to wave direction. Experiment 1, $n = 7$; Experiment 2, $n = 10$. □ 360° and ■ 90°.

Table 3

Analysis of variance of the fecal production of Pyura stolonifera *over 24 hours at two orientations on a rocky intertidal shore*

Source	SS	DF	MS	*F*	*P*
Experiment	2.363	1	2.363	10.242	0.003
Orientation	2.901	1	2.901	13.386[a]	0.001
Exp × Or	0.000	1	0.000[a]	0.000	1.000
Residual	6.923	30	0.231[a]		

Experiment (Exp) was a random factor with two levels, and Orientation (Or) was a fixed orthogonal factor with two levels—360°, 90°; $n = 7$ in Experiment 1, and $n = 10$ in Experiment 2. The data were transformed to $\log_e x$ to normalize the data and reduce the differences among variances.

[a] The MS for the interaction between experiment and orientation appeared to be an underestimate ($P > 0.25$); therefore, this term was pooled with the residual to provide a more appropriate test for orientation (*Underwood*, 1997).

dynamic pressure on their inhalant siphons, producing the greatest passive flow through them. Finally, our field experiments confirmed that ascidians oriented into the wave direction had consistently greater feeding rates than those oriented perpendicular to the waves. Taken together, these findings suggest that passive flow is an integral aspect of the feeding strategy of this species. Our study is the first to demonstrate that unstalked ascidians utilize passive flow.

Although most of the *P. stolonifera* were oriented with their inhalant siphons directed into the waves, at some shores the ascidians were also oriented away from the waves. Wave action is the major determinant of flow in this environment; however, at some locations, the flow of water back down the shore after each wave is also substantial. We speculate that this backwash accounts for the bidirectional pattern of orientation observed at some locations (*i.e.*, Towradgi and Bellambi). This ascidian tends to form dense aggregations along rocky shores (Day, 1974; Kott, 1985) and individuals at the back of aggregations (away from the sea) were typically oriented into the backwash, while those at the front of the aggregation were usually oriented into the waves. Among individual ascidians, there was also variation in orientation that may be accounted for by small-scale local variation in flow across rocky shores. That is, the wave direction that individual ascidians experience may differ greatly over short distances due to the structure of the shore or aggregations of the ascidians themselves. The extent of intrapopulation variation in orientation (*r*, Table 1) differed substantially among locations, probably due to underlying differences in the consistency of the flow direction. This was most evident at Bradley's Head, where the orientation of the ascidians varied substantially, with most being oriented between 20° and 160°. This variation seemed to be reflected by the variation in the direction of the wave action due to the swash generated by passing ferries. During several hours of sampling, the direction changed frequently, by about 90°. The apparent correlation between the orientation of the ascidians and the ferry swash suggests that human activities may have altered the orientation of the ascidians at this location. On the other shores, variation in wave direction could be generated naturally, although less frequently, by changes in wind and swell direction.

We predicted that *P. stolonifera* would be able to exploit passive flow not only due to dynamic pressure, but also because of the Bernoulli effect or viscous entrainment. Passive flow-through models did occur when they were oriented perpendicular to or away from the flow. This indicates that the Bernoulli effect or viscous entrainment, or both, can induce passive flow through the ascidian. Nevertheless, the magnitude of the passive flow at these orientations was much smaller for most models than when they were oriented into the flow.

We contend that the results from the models in the flume are a good indicator that the morphology of this ascidian enables it to exploit the movement of water over the rocky shore to induce passive flow. There were, however, several differences between the models and real individuals of *P. stolonifera* and between water movement through the flume and over rocky intertidal shores. For instance, the openings of the siphon in the models were smaller than those of real ascidians (up to 12 mm in diameter in live ascidians; N. Knott, pers. obs.); the exhalant siphons were shorter due to the models being cast from ascidians with partially retracted siphons (a normal reaction to being disturbed); and the models did not have branchial baskets. In relation to water movement, the flow through the flume was laminar with a relatively constant speed of 15 cm s^{-1}, whereas the flow conditions that the ascidians are exposed to on the rocky shore are often likely to be turbulent with flow speed exceeding 15 cm s^{-1} (Denny, 1988). Given these differences, we needed to evaluate whether *P. stolonifera* was actually exploiting passive flow on rocky intertidal shores.

Our field experiments demonstrated enhanced feeding rates for individuals of *P. stolonifera* oriented into the waves on a rocky shore. This pattern was consistent across experiments despite the difference in the feeding rate between experiments, indicating that the ascidian's utilization of passive flow was temporally consistent. We believe, therefore, that it represents a general phenomenon for this ascidian.

The value of passive flow can be further demonstrated by comparing the active pumping rate of *P. stolonifera* specimens from a study in South Africa (Klumpp, 1984) and the passive flow rates measured through the model ascidians in our study. From Klumpp's data, the mean pumping rate of individuals with a dry weight of 3.8 g (the average dry weight of the ascidians used to cast the models in the current study) would be 1245 ml h^{-1}. Passive flow through the models was on average 498 ml h^{-1} when orientated into the flow. Hence, it would appear that if the passive flow through

the models was representative of the passive flow through real ascidians, it could provide about 40% of the active pumping rate at a flow speed of 15.2 cm s^{-1}. Furthermore, passive flow through other facultatively active suspension feeders increases proportionally with external flow velocities (Vogel, 1974, 1977; Young and Braithwaite, 1980). Considering that the flow speed of water over the rocky intertidal is often much greater than that used in our flume experiment and that the actual siphon diameters are greater than those of the tubing we used, passive flow is likely to produce even more than 40% of the pumping rate in live animals.

The potential contribution of passive flow to suspension feeding is rarely considered in studies on invertebrate filtration or clearance rates (Klumpp, 1984; Famme *et al.*, 1986; Riisgard *et al.*, 1993; but see Reiswig, 1971, 1974). These rates are usually measured in still or very slow-moving water. Measurements made under such conditions may be appropriate for suspension feeding invertebrates that inhabit environments with little water motion (Famme *et al.*, 1986; Petersen and Riisgard, 1992); but many suspension feeding invertebrates inhabit environments that are almost continually exposed to fluid movement (Reidle, 1971; Vogel and Bretz, 1972; Vogel, 1976; Wildish and Kristmanson, 1997), which is often consistent in strength and direction (Wainwright and Dillion, 1969; Denny, 1988). Measuring the filtration and clearance rates of these suspension feeders in water with no or little flow will underestimate their real values if they utilize passive flow.

Early estimates of the metabolic costs of suspension feeding suggested that the costs may be only slightly less than the gains in energy (Jørgensen, 1966). Passive flow was, therefore, thought to benefit suspension feeders by reducing the energetic cost of pumping water (Vogel, 1974, 1977; Young and Braithwaite, 1980). Recent estimates of energy expended for suspension feeding have, however, put the costs at less than half a percentage point of the metabolic rate of most suspension feeders (Riisgard *et al.*, 1993; Riisgard and Larsen, 2001). This relatively small cost has led Riisgard *et al.* (1993) to suggest that passive flow is of little energetic consequence to active suspension feeding invertebrates. This view seems to overlook the tremendous potential passive flow has to increase water movement through the filtering structures of active suspension feeders (Vogel, 1974, 1977; LaBarbera, 1977; Young and Braithwaite, 1980; Allanson *et al.*, 1992; the current study) and the subsequent gains in food capture demonstrated for animals utilizing passive flow (Young and Braithwaite, 1980; the current study). Thus, the substantial increases in feeding rates due to passive flow are likely to strongly influence the energetical gains of these organisms, regardless of the magnitude of the effects on feeding costs.

Acknowledgments

We acknowledge Craig Young for the initial observation that *Pyura stolonifera* appeared to be oriented into the waves on the rocky shores of the Illawarra. We thank Maria Punales and Stephen Doggett for help in the field; Ian Gentle and Didier Balez (Faculty of Creative Arts, University of Wollongong) for assistance in producing the models; Jim Britton and Muttucurrama Sivakumar (Faculty of Engineering, UOW) for access to and use of the flume, and Nancy Dawkins for encouragement, food and shelter for NK during the study. This work has benefited from discussions with Todd Minchinton and David Ayre. Two anonymous reviewers made helpful comments on an earlier draft of the paper. This represents contribution 251 from the Ecology and Genetics Group at the UOW.

Literature Cited

Allanson, B., D. Skinner, and J. Imberger. 1992. Flow in prawn burrows. *Estuar. Coast. Shelf Sci.* **35:** 253–256.

Batschelet, E. 1981. *Circular Statistics in Biology.* Academic Press, New York.

Day, R. W. 1974. An investigation of *Pyura stolonifera* (Tunicata) from the Cape Peninsula. *Zool. Afr.* **9:** 35–58.

Denny, M. W. 1988. *Biology and the Mechanics of the Wave-Swept Environment.* Princeton University Press, Princeton, NJ.

Famme, P., H. U. Riisgard, and C. B. Jorgensen. 1986. On direct measurement of pumping rates in the mussel *Mytilus edulis*. *Mar. Biol.* **92:** 323–327.

Jørgensen, C. B. 1966. *Biology of Suspension Feeding.* Pergamon Press, Oxford.

Klumpp, D. 1984. Nutritional ecology of the ascidian *Pyura stolonifera:* influence of body size, food quantity and quality on filter feeding, respiration, assimilation efficiency and energy balance. *Mar. Ecol. Prog. Ser.* **19:** 269–284.

Kott, P. 1985. The Australian Ascidiacea 1. *Mem. Queensl. Mus.* 328–331.

Kott, P. 1989. Form and function in the Ascidiacea. *Bull. Mar. Sci.* **45:** 253–276.

LaBarbera, M. 1977. Brachipod orientation to water movement. I. Theory, laboratory behavior, and field orientations. *Paleobiology* **3:** 270–287.

LaBarbera, M. 1984. Feeding currents and particle capture mechanisms in suspension feeding animals. *Am. Zool.* **24:** 71–84.

Nowell, A., and P. Jumars. 1987. Flumes: theoretical and experimental considerations for simulation of benthic environments. *Oceanogr. Mar. Biol. Annu. Rev.* **25:** 91–112.

Petersen, J. K., and H. U. Riisgard. 1992. Filtration capacity of the ascidian *Ciona intestinalis* and its grazing impact in a shallow fjord. *Mar. Ecol. Prog. Ser.* **88:** 9–17.

Quinn, G. P., and M. J. Keough. 2002. *Experimental Design and Data Analysis for Biologists.* Cambridge University Press, Cambridge, UK.

Reidle, R. J. 1971. Water movement: animals. Pp. 1124–1156 in *Marine Ecology.* O. Kinne, eds. Wiley Interscience, London.

Reiswig, H. M. 1971. *In situ* pumping activities of tropical Demospongiae. *Mar. Biol.* **9:** 38–50.

Reiswig, H. M. 1974. Water transport, respiration and energetics of three tropical marine sponges. *J. Exp. Mar. Biol. Ecol.* **14:** 231–249.

Riisgard, H. U., and P. S. Larsen. 2001. Minireview: ciliary filter feeding and bio-fluid mechanics: present understanding and unsolved problems. *Limnol. Oceanogr.* **46:** 882–891.

Riisgard, H. U., S. Thomassen, H. Jakobsen, J. M. Weeks, and P. S. Larsen. 1993. Suspension feeding in marine sponges *Halichondria panicea* and *Haliclona urceolus*: effects of temperature on filtration rate and energy cost of pumping. *Mar. Ecol. Prog. Ser.* **96:** 177–188.

Sibly, R. M. 1981. Strategies of digestion and defecation. Pp. 109–139 in *Physiological Ecology: An Evolutionary Approach to Resource Use*, C. R. Townsend and P. Calow, eds. Blackwell Scientific, Oxford.

Sibly, R. M., and P. Calow. 1986. *Physiological Ecology of Animals: An Evolutionary Approach.* Blackwell Scientific, Oxford.

Townsend, C. R., and P. Calow. 1981. *Physiological Ecology: An Evolutionary Approach to Resource Use.* Blackwell Scientific, Oxford.

Townsend, C. R., and R. N. Hughes. 1981. Maximising net energy returns from foraging. Pp. 86–108 in *Physiological Ecology: An Evolutionary Approach to Resource Use*, C. R. Townsend and P. Calow, eds. Blackwell Scientific, Oxford.

Underwood, A. J. 1997. *Experiments in Ecology: Their Logical Design and Interpretation Using Analysis of Variance.* Cambridge University Press, Cambridge, UK.

Vogel, S. 1974. Current-induced flow through the sponge, *Halichondria*. *Biol. Bull.* **147:** 443–456.

Vogel, S. 1976. Flows in organisms induced by movements of the external medium. Pp. 285–297 in *Animal Locomotion*, T. J. Pedley, ed. Academic Press, London.

Vogel, S. 1977. Current-induced flow through living sponges in nature. *Proc. Natl. Acad. Sci. USA* **74:** 2069–2071.

Vogel, S. 1978. Organisms that capture currents. *Sci. Am.* **239:** 128–139.

Vogel, S. 1994. *Life in Moving Fluids: The Physical Biology of Flow.* Princeton University Press, Princeton, NJ.

Vogel, S., and W. L. Bretz. 1972. Interfacial organisms: passive ventilation in the velocity gradients near surfaces. *Science* **175:** 210–211.

Wainwright, S. A., and J. R. Dillion. 1969. On the orientation of sea fans (Genus *Gorgonia*). *Biol. Bull.* **136:** 130–139.

Wildish, D., and D. Kristmanson. 1997. *Benthic Suspension Feeders and Flow.* Cambridge University Press, Cambridge, UK.

Young, C. M., and L. F. Braithwaite. 1980. Orientation and current-induced flow in the stalked ascidian *Styela montereyensis*. *Biol. Bull.* **159:** 428–440.

Zar, J. H. 1984. *Biostatistical Analysis.* Prentice Hall, Englewood Cliffs, NJ

Reference: *Biol. Bull.* **207:** 225–232. (December 2004)

Seasonal Acclimatization of Antioxidants and Photosynthesis in *Chondrus crispus* and *Mastocarpus stellatus*, Two Co-Occurring Red Algae With Differing Stress Tolerances

NISSA L. LOHRMANN, BARRY A. LOGAN*, AND AMY S. JOHNSON

Biology Department, Bowdoin College, Brunswick, Maine 04011

Abstract. *Mastocarpus stellatus* and *Chondrus crispus* are red macroalgae that co-dominate the lower rocky intertidal zones of the northern Atlantic coast. *M. stellatus* is more tolerant than *C. crispus* of environmental stresses, particularly those experienced during winter. This difference in tolerance has been attributed, in part, to greater contents or activities of certain antioxidants in *M. stellatus*. We compared the photosynthetic capacities and activities of three antioxidant enzymes—superoxide dismutase (SOD), ascorbate peroxidase (APX), and glutathione reductase (GR)—as well as the contents of ascorbate from fronds of *M. stellatus* and *C. crispus* collected over a year. Photosynthetic capacity increased in winter, but did not differ between species in any season. The activities of the three antioxidant enzymes and the contents of ascorbate were significantly greater in tissues collected during months with mean air and water temperatures below 7.5 °C ("cold" months; December, February, March, April) than in months with mean air temperatures above 11 °C ("warm" months; June, July, August, October). Overall, *C. crispus* had significantly greater SOD and APX activities, while *M. stellatus* had higher ascorbate contents. Species-specific differences in GR activity depended upon mean monthly temperatures at the time of tissue collection; *C. crispus* had higher activities during cold months, whereas *M. stellatus* had higher activities during warm months. Taken together, these data indicate that increased ROS scavenging capacity is a part of winter acclimatization; however, only trends in ascorbate content support the hypothesis that greater levels of antioxidants underlie the relatively greater winter tolerance of *M. stellatus* in comparison to *C. crispus*.

Received 1 July 2004; accepted 22 September 2004.

* To whom correspondence should be addressed. E-mail: blogan@bowdoin.edu

Abbreviations: APX, ascorbate peroxidase; FW, fresh weight; GR, glutathione reductase; ROS, reactive oxygen species; SOD, superoxide dismutase.

Introduction

Mastocarpus stellatus (Stack. in With.) Guiry and *Chondrus crispus* Stackhouse are morphologically similar red macroalgae that occupy the lower rocky intertidal zone of exposed regions of the northern Atlantic coast. *M. stellatus* is more tolerant than *C. crispus* of environmental stresses, particularly those experienced during winter. Photosynthesis recovers more quickly in *M. stellatus* than in *C. crispus* after a bout of freezing in a laboratory setting (Dudgeon *et al.*, 1989, 1995). Frond bleaching and declines in photosynthesis and growth occur in *C. crispus* after long-term experimental exposure to periodic freezing, whereas these parameters remain unaffected in *M. stellatus* (Dudgeon *et al.*, 1990). Thalli of *C. crispus* become larger than those of *M. stellatus*, but the stipes are not as strong, leading to greater biomass loss during winter (Dudgeon and Johnson, 1992; Pratt and Johnson, 2002).

Collén and Davison (1999) reported that a greater capacity to scavenge reactive oxygen species (ROS) might contribute to the relatively greater stress tolerance of *M. stellatus*. ROS are reduced, and highly reactive, species of molecular oxygen such as superoxide and hydrogen peroxide, which are capable of damaging essential macromolecules (Halliwell and Gutteridge, 1999). ROS are by-products of bioenergetic pathways, particularly photosynthesis; however, exposure to environmental perturbations such as thermal stress, especially chilling, can greatly increase the rate of their formation (Niyogi, 1999). This is because

chilling inhibits the enzyme-catalyzed reactions of the Calvin cycle, but has a far smaller effect on photosynthetic light absorption and electron transport (Baker, 1994; Wise, 1995). Therefore, chilling leads to an increase in the absorption of light that exceeds the capacity for photosynthetic utilization (*i.e.,* excess light), and ROS production correlates with excess light absorption (Logan *et al.,* 1998a; Niyogi, 1999).

The primary mechanism for minimizing ROS-mediated cellular damage involves antioxidants, which are enzymes and low-molecular-weight compounds that detoxify ROS (reviewed in Asada, 1999). In the chloroplasts of photosynthetic tissues, superoxide can be safely converted to water *via* the combined activities of superoxide dismutase (SOD; EC 1.15.1.1), which catalyzes the disproportionation of two superoxides to molecular oxygen and hydrogen peroxide; and ascorbate peroxidase (APX; EC 1.11.1.11), which catalyzes the reduction of hydrogen peroxide to water, utilizing ascorbate as a reductant. Chloroplasts possess multiple mechanisms that recycle oxidized ascorbate, including one that couples the oxidation of glutathione to ascorbate reduction. Oxidized glutathione, in turn, is reduced by glutathione reductase (GR; 1.6.4.2).

M. stellatus, in comparison to *C. crispus,* was reported to possess larger pools of ascorbate and β-carotene (a lipid-soluble antioxidant) and greater activities for certain antioxidant enzymes, including GR (Collén and Davison, 1999). These species-specific differences were based upon measurements of fronds harvested in late summer and early autumn. This is relevant because levels of antioxidants undergo seasonal acclimatization. In photosynthetic tissues of algae and plants, acclimatization to colder temperatures generally involves several-fold increases in the activities and contents of antioxidants (Anderson *et al.,* 1992; Logan *et al.,* 1998b, 2003; Mallick and Mohn, 2000; Collén and Davison, 2001). Therefore, the levels of antioxidants in algae harvested when water temperatures are near their peak (late summer) may not be indicative of those in winter. We expanded upon those previous studies by comparing SOD, APX, and GR activities as well as ascorbate contents from *M. stellatus* and *C. crispus* collected on nine occasions over the course of a year. Since photosynthetic activity can influence the rate of ROS production, we also measured the photosynthetic capacities of the two species in all four seasons.

Materials and Methods

Site description and collection protocol

Mastocarpus stellatus (Stack. in With.) Guiry and *Chondrus crispus* Stackhouse were collected about 500 m northeast of the Giant's Stairs on Bailey Island, Maine (43°43′N 69°59′W). All collections were made from a single mixed stand of the two species on an exposed rock face in the intertidal zone. For the measurements of antioxidants, collections were made in 2001 on 16 March, 23 April, 29 June, 27 July, 14 August, 22 October, and 22 December, and in 2002 on 7 February, 25 March (collections are identified by month in the figures and tables, with March 2001 preceding March 2002). The algae were harvested at low tide near noon on clear sunny days. Samples were placed in plastic bags with paper towels moistened with seawater, transported to the laboratory in no more than 45 min, and stored in liquid nitrogen until analysis.

For measurements of photosynthesis, samples were collected from the same site in 2002 on 12 and 18 September (data combined) and 18 December, and in 2003 on 4 March and 20 July. Algae were collected in the afternoon in September and December; collected near dawn in March; and in mid-morning in July. Samples were handled as above and maintained at room temperature in September and July and on ice in December and March. All photosynthetic measurements were completed within 12 h of collection, during which time no systematic loss of photosynthetic activity was observed (data not shown).

Tissue extraction

Frozen frond tissue (0.3–0.6 g fresh weight (FW)) for assays of SOD and GR activity were ground in a prechilled mortar with a small amount of acid-washed sand and extracted with 1.5 ml 50 m*M* potassium phosphate buffer with 0.1 m*M* EDTA, 0.3% (w/v) Triton X-100, and 4% (w/v) soluble PVP-10, pH 7.6, as in Logan *et al.* (1998b). Samples for assays of APX activity were ground in 1.5 ml of the same buffer, with the addition of 1.3 m*M* ascorbate, as in Logan *et al.* (1998b). Samples for assays of ascorbate content were ground in 1 ml 6% H_2SO_4. All samples were centrifuged at 9300 $\times$ *g* for 10 min at 4 °C, and the supernatant was collected and stored on ice until measured. Samples used to measure SOD activity were dialyzed using Slide-A-Lyzer dialysis cassettes (10,000 MWCO, Product # 66425, Pierce Biotechnology, Inc, Rockford, IL). The pH of extracted samples used to measure ascorbate was raised to between 1 and 2 with the addition of Na_2CO_3, as in Logan *et al.* (1998b).

Antioxidant enzymes and ascorbate

All enzyme assays were performed at 25 °C in a temperature-controlled cuvette of a DU640 spectrophotometer (BeckmanCoulter, Fullerton, CA). Total assay volume for SOD, GR, and APX was 2 ml. Total assay volume for ascorbate was 1 ml.

To measure SOD activity, an NADH/phenazine methosulfate superoxide-generating system was employed. SOD activity was monitored as the inhibition of cytochrome *c* reduction. The SOD assay buffer consisted of 50 m*M* potassium phosphate, 0.1 m*M* EDTA, 0.01 m*M* cytochrome *c*,

0.1 m*M* NADH, pH 7.6. To this solution was added 200 μl of sample extract, and the change in absorbance at 550 nm was followed for 1 min after the addition of a sufficient volume of 1 μ*M* phenazine methosulfate to bring about a control rate of cytochrome *c* reduction of 0.125 absorbance units min^{-1}. SOD activity was corrected for the rate of nonspecific cytochrome *c* reduction, which was determined prior to the addition of phenazine methosulfate.

APX activity was quantified as the rate of ascorbate oxidation. The APX assay buffer consisted of 50 m*M* Hepes-KOH, 0.1 m*M* EDTA, 0.5 m*M* ascorbate, pH 7.6. To this was added 40 μl of sample extract, and the change in absorbance at 290 nm was measured for 1 min after the addition of 8 μl of 50 m*M* H_2O_2 (Logan *et al.*, 1998b). APX activity was corrected for the rate of nonspecific ascorbate oxidation, which was determined prior to the addition of H_2O_2.

GR activity was quantified as the rate of NADPH oxidation. The GR assay buffer consisted of 100 m*M* Tris-HCl, 1 m*M* EDTA, 0.5 m*M* oxidized glutathione, pH 8.0. To this was added 100 μl of sample extract, and the change in absorbance at 340 nm was measured for 1 min after the addition of 20 μl of 5 m*M* NADPH (Logan *et al.*, 1998b). GR activity was corrected for the rate of nonspecific NADPH oxidation, which was determined in the absence of oxidized glutathione.

The ascorbate assay buffer consisted of 200 m*M* sodium acetate, pH 5.6; 100 μl of pH-adjusted sample extract was mixed with 900 μl assay buffer, and the change in absorbance at 265 nm was recorded after reaction with 2 units ascorbate oxidase (Logan *et al.*, 1998b). Ascorbate content was determined by comparison to a standard curve.

Measurements of photosynthesis

Frond tissue (0.10–0.12 g FW) was placed in the chamber of a gas-phase oxygen electrode (model LD-2, Hansatech, King's Lynn, Norfolk, UK) on a pad moistened with seawater. Photosynthesis was measured in an atmosphere of humidified 5% CO_2, 21% O_2, and the balance N_2. The temperature of the frond tissue was maintained at 20 °C (the optimum temperature for both species, according to Mathieson and Burns (1971)), *via* the use of a circulating water bath. Tissues were exposed to progressively increasing light intensities for an overall period of about 12 min until the measuring intensity of 1700 μmol photons m^{-2} s^{-1} (saturating light) was reached. Measurements were made after the frond tissue had achieved steady state and rates of oxygen production were linear. Respiratory oxygen consumption was measured by darkening the sample. Gross photosynthetic capacity was calculated as the sum of net photosynthetic oxygen evolution and respiratory oxygen consumption.

Mean monthly temperatures

Temperature data were obtained from the Central Maine Shelf buoy (E0110) (43°42′43″N 69°21′20″W) of the Gulf of Maine Ocean Observing System (GoMOOS) for dates as far back as July 2001, with a gap at Buoy E0110 from October 2001 through December 2001 (Table 1).

Statistical analysis

Differences in antioxidant activities and contents were assessed by using temperature data, and photosynthetic capacities by mean monthly air and water temperature (Table 1). Months with mean monthly air and water temperatures greater than or equal to 11 °C (June, July, August, October) were pooled as "warm" months, and months with mean monthly air and water temperatures less than or equal to 7.5 °C (December, February, March, April) were pooled as "cold" months. ANOVA was followed by *a posteriori* Fisher's protected least significant difference (PLSD) tests when there was a significant interaction between species and temperature. These statistical analyses were followed by *a posteriori* Fisher's PLSD for planned monthly pairwise comparisons of means for each species. All statistics were performed using the statistical software program Statview

Table 1

Mean air temperature and mean water temperatures at 1 m depth for each month in which fronds were collected; all data from buoys in the Gulf of Maine Ocean Observing System (GoMOOS)

	2001							2002	
	Mar.[1]	Apr.[1]	June[1]	July[2]	Aug.[2]	Oct.[3]	Dec.[3]	Feb.[2]	Mar.[2]
Mean Air Temperature (°C)	1.4 ± 0.6	4.1 ± 0.7	11.7 ± 0.4	16.5	17.3	11.0 ± 0.1	3.9 ± 0.2	1.1	2.4
Mean Water Temperature (°C)	3.7 ± 0.5	4.0 ± 0.5	11.0 ± 0.3	15.6	16.1	11.9 ± 0.5	7.5 ± 0.02	5.1	4.7

[1] Mean (± SE of the mean of the means) using data that was averaged from 2002, 2003, and 2004 for GoMOOS Buoy E0110.
[2] Means from GoMOOS Buoy E0110.
[3] Mean (± SE of the mean of the means) using data that was averaged from the two GoMOOS Buoys that are closest to E0110 for that same year.

ver. 5.0.1 (SAS Institute, Cary, NC). Significance refers to $P \leq 0.05$. All statistics are given in the figure legends.

Results and Discussion

The activities of the three measured antioxidant enzymes (SOD, APX, and GR) and the contents of ascorbate were significantly greater in tissues collected during "cold" months (*i.e.*, mean monthly air and water temperatures less than 7.5 °C; December, February, March, April) in comparison to "warm" months (*i.e.*, mean monthly air temperatures greater than 11 °C; June, July, August, October) (Figs. 1–4). Similar up-regulation in antioxidant capacity has been reported for algae (Mallick and Mohn, 2000; Collén and Davison, 2001) and the leaves of many terrestrial plant species after the onset of winter (Anderson *et al.*, 1992; Logan *et al.*, 1998b) or experimentally imposed chilling (de Kok and Oosterhuis, 1983; Schöner and Krause, 1990; Mishra *et al.*, 1993; Xin and Browse, 2000). Cold-induced increases in the levels of antioxidant enzymes compensate for the effect of lower temperatures on their activities. Elevated levels of antioxidants may also be required in winter to cope with an enhanced rate of ROS formation that presumably results when chilling inhibits the use of light energy in the Calvin cycle.

When the data were pooled to examine antioxidant differences between species, *Chondrus crispus* had significantly greater SOD and APX activities than *Mastocarpus stellatus* (Figs. 1 and 2, respectively). *M. stellatus* had higher ascorbate contents than *C. crispus* (Fig. 4). Species-specific differences in GR activity depended upon mean monthly temperatures at the time of tissue collection; *C. crispus* had higher activities during cold months, whereas *M. stellatus* had higher activities during warm months (Fig. 3). Taken together, these data indicate that increased ROS scavenging capacity is a part of winter acclimatization; however, only trends in ascorbate content support the hypothesis that greater levels of antioxidants underlie the relatively greater winter tolerance of *M. stellatus* in comparison to *C. crispus*. Our approach does not allow us to examine the further possibility that either or both species expressed antioxidant enzyme isoforms with differing kinetic characteristics (*e.g.*, lower temperature optimum, or K_m) during colder months, as has been observed in some terrestrial plants (Guy and Carter, 1984).

We have expressed levels of antioxidants per unit frond fresh weight because we believe that this is the most functionally relevant basis of expression and because it allows direct comparison with previously published work (see, for example, Collén and Davison, 1999, 2001). Had we chosen to express our findings on the basis of frond chlorophyll content, seasonal changes in this parameter itself would have unduly influenced seasonal trends in levels of antioxidants. Fronds of *M. stellatus* tend to be thicker than those of *C. crispus* (Dudgeon and Johnson, 1992); therefore, antioxidant enzyme activities expressed per unit frond area may be greater in *M. stellatus* than in *C. crispus*.

Since photosynthetic activity can influence the rate of ROS production, we measured photosynthetic capacities at

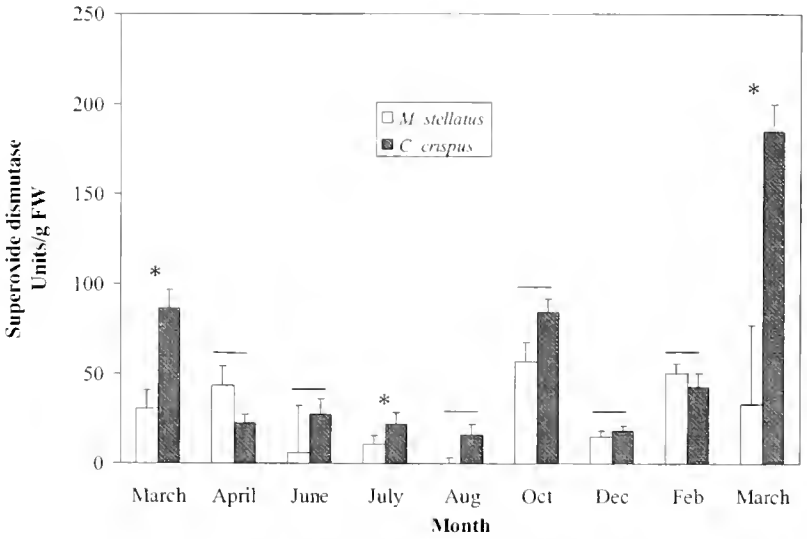

Figure 1. Superoxide dismutase activity, by month, for *Chondrus crispus* (dark bars) and *Mastocarpus stellatus* (white bars). When analyzed by mean monthly temperature, there were significant differences by temperature ($P_{1,86} = 0.003$) and by species ($P_{1,86} = 0.007$) with no significant interaction ($P_{1,86} = 0.7$); overall, both species had higher activities in the cold months, and *C. crispus* had higher activities than *M. stellatus*. A horizontal line indicates no significant difference ($P > 0.05$) between species in a given month, and an asterisk indicates significant difference ($P < 0.05$). Error bars are one standard error; $n = 5$.

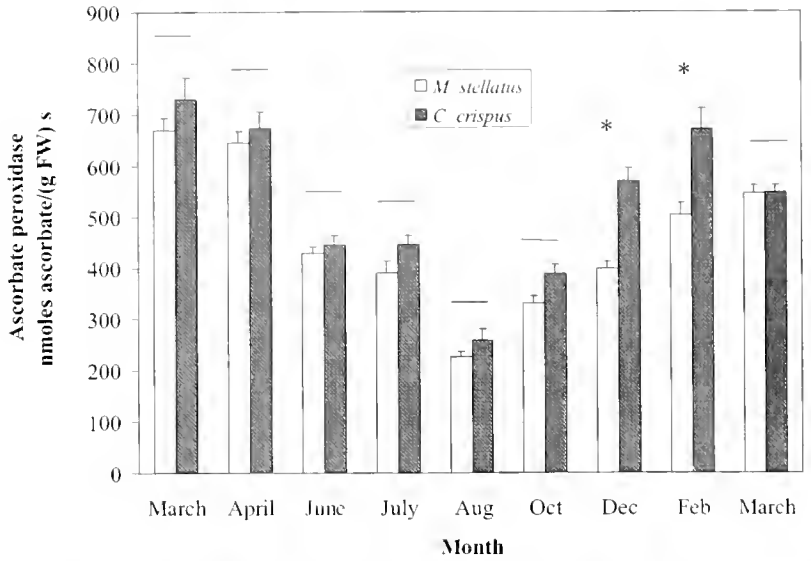

Figure 2. Ascorbate peroxidase activity, by month, for *Chondrus crispus* (dark bars) and *Mastocarpus stellatus* (white bars). When analyzed by mean monthly temperature, there were significant differences by temperature ($P_{1,106} < 0.0001$) and by species ($P_{1,106} = 0.004$) with no significant interaction ($P_{1,106} = 0.4$): overall, both species had higher activities in the cold months (especially in March and April), and *C. crispus* had higher activities than did *M. stellatus* (especially in December and February). A horizontal line indicates no significant difference ($P > 0.05$) between species in a given month, and an asterisk indicates significant difference ($P < 0.05$). Error bars are one standard error; $n = 5$–10.

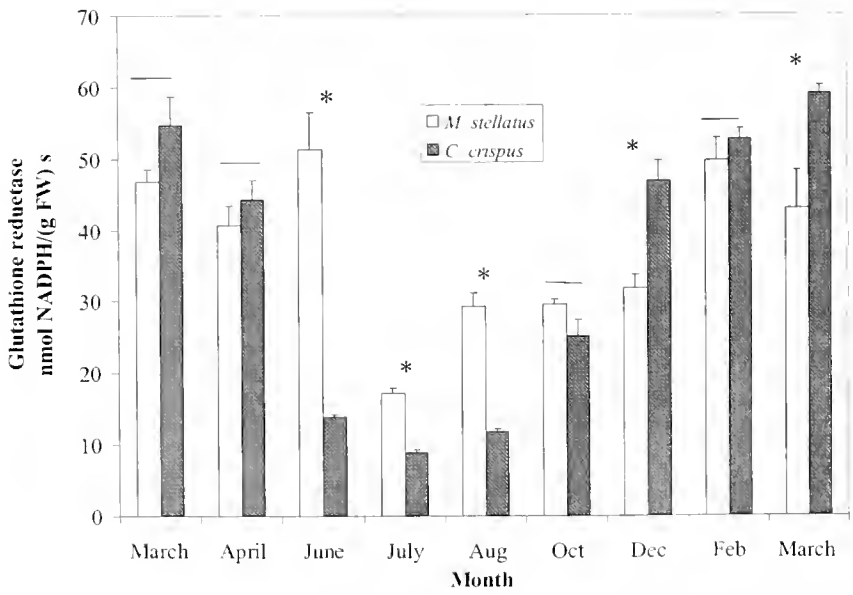

Figure 3. Glutathione reductase activity, by month, for *Chondrus crispus* (dark bars) and *Mastocarpus stellatus* (white bars). When analyzed by mean monthly temperature, there were significant differences by temperature ($P_{1,104} < 0.0001$) and by species ($P_{1,104} = 0.03$) with significant interaction ($P_{1,104} < 0.0001$): overall, both species had higher activities in the cold months, but *C. crispus* had relatively higher activities than did *M. stellatus* in cold months whereas *M. stellatus* had relatively higher activities than did *C. crispus* in the warm months (each *a posteriori* $P < 0.01$). A horizontal line over species in a given month indicates no significant difference ($P > 0.05$) between species in a given month, and an asterisk indicates a significant difference ($P < 0.05$). Error bars are one standard error; $n = 5$.

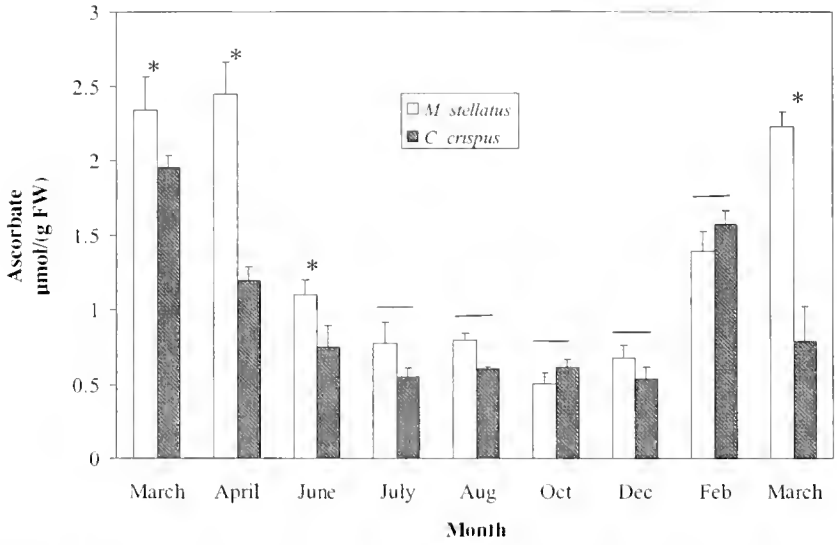

Figure 4. Ascorbate contents, by month for *Chondrus crispus* (dark bars) and *Mastocarpus stellatus* (white bars). When analyzed by mean monthly temperature, there were significant differences by temperature ($P_{1,125} < 0.0001$) and by species ($P_{1,125} = 0.002$) with no significant interaction ($P_{1,125} = 0.2$); overall, both species had higher contents in the cold months, and *M. stellatus* had higher contents than did *C. crispus* (especially in March and April). A horizontal line indicates no significant difference ($P > 0.05$) between species in a given month, and an asterisk indicates significant difference ($P < 0.05$). Error bars are one standard error; $n = 5$–10.

20 °C in all four seasons. Capacities for photosynthetic oxygen evolution underwent 3-fold increases from summer to winter in both species; however, statistically significant differences between species were not observed in any season (Table 2). Significant species-specific differences were also not observed when photosynthesis was measured at 5 °C from fronds collected in March, although rates were lower than at 20 °C (21 ± 7 and 25 ± 1 nmol O_2 (g FW)$^{-1}$ s^{-1} for *M. stellatus* and *C. crispus*, respectively; mean ± SD, $n = 5$).

Cold-induced increases in photosynthetic capacity have been reported for *M. stellatus* and *C. crispus* (Dudgeon *et al.*, 1995) as well as for winter cereal varieties and other terrestrial plants that actively grow in winter (Huner *et al.*, 1993). Such increases are interpreted as a means of compensating for the effects of low temperatures on enzyme activities. Increased photosynthetic capacity in winter may also have been influenced by greater nitrogen availability in this season (Topinka and Robbins, 1976).

Table 2

Photosynthetic oxygen evolution at 20 °C by month for Chondrus crispus *and* Mastocarpus stellatus

	nmol O_2 (g FW)$^{-1}$ s^{-1}			
Species	September	December	March	July
Mastocarpus stellatus	39 ± 6	59 ± 8	40 ± 7	22 ± 4
Chondrus crispus	41 ± 8	60 ± 4	46 ± 8	16 ± 4

Data are means ± standard deviation. There were significant differences in means by month ($P_{3,36} < 0.0001$) but not by species ($P_{1,36} = 0.50$), and there was no significant interaction ($P_{3,36} = 0.86$); all differences between months are significant (each *a posteriori* $P < 0.001$) except for between March and September (*a posteriori* $P = 0.49$); n = 6.

Previous reports that *M. stellatus* is relatively more resistant to freezing damage to the photosynthetic apparatus were based upon freezing regimens imposed experimentally in a laboratory (Dudgeon *et al.*, 1989, 1990, 1995). It is possible that conditions in the field around the time of our collections were not stressful enough for species to show differences in winter tolerance. Alternatively, since our measurements of photosynthetic capacity were performed in humidified air, whereas macroalgal photosynthesis is typically measured from submerged thalli, it may be that winter rates of photosynthesis for *C. crispus* and *M. stellatus* are more similar in air than they are in water. Intertidal algae may perform a significant proportion of total daily photosynthesis during exposure to air at low tide when light intensity is not attenuated by passage through seawater, and there can be species-specific differences in the rates of photosynthesis in air and in water. For example, *Ascophyllum nodosum*, an intertidal brown macroalgae that is also native to the north Atlantic coast, photosynthesizes at slightly greater rates when exposed than when submerged (Johnson and Raven, 1986), whereas the converse occurs in the green alga *Ulva* sp. (Johnson *et al.*, 1974; Quadir *et al.*, 1979).

The potential for tissue freezing may be the most stressful

aspect of the winter season, not cold temperatures *per se*. The tissue damage brought on by freezing is for the most part ultrastructural and results from extreme cellular desiccation induced by extracellular freezing or by the effects of intercellular ice formation (Nilsen and Orcutt, 1996). Antioxidants, on the other hand, protect cells from biochemical damage caused by ROS, whose production increases during imbalances within and between bioenergetic pathways (Wise, 1995). Therefore, one may not expect antioxidants to play a direct role in protection against freezing damage. In *Fucus vesiculosus*, experimental freezing led to an increase in the production of ROS only in thalli that had been acclimated to warm (20 °C) conditions; it did not affect ROS production in thalli that had been acclimated to 0 °C or 0 °C with daily exposure to −10 °C for 3 h (Collén and Davison, 2001).

If levels of antioxidants cannot fully explain the difference in winter tolerance between *M. stellatus* and *C. crispus*, what might? Resistance to freezing damage is greatly enhanced by the accumulation of a class of compounds known as cryoprotectants (Lillford and Holt, 2002). Cryoprotectants serve as osmolites that reduce the shrinkage cells experience when extracellular freezing causes water efflux. They may also stabilize proteins and membranes during cell collapse. Mannitol, a sugar alcohol, is among the most common cryoprotectants. *M. stellatus* contains mannitol, but *C. crispus* does not (Mathieson and Prince, 1973). Perhaps the presence of mannitol explains the relatively greater resistance of *M. stellatus* to freezing damage (Dudgeon *et al.*, 1989, 1990, 1995). This possibility merits more attention, including a comprehensive characterization of the tissue cryoprotectants in these two species.

Conclusions

In *Mastocarpus stellatus* and *Chondrus crispus*, as in other photosynthetic organisms, acclimatization to winter involved profound up-regulation in the capacity to detoxify ROS *via* antioxidants. In winter and early spring, when tolerance to chilling and freezing is important for survival, the activities of SOD, APX, and GR were greater in *C. crispus* than in *M. stellatus* and therefore cannot explain the relatively greater stress tolerance of *M. stellatus*. Of the measured antioxidants, only ascorbate content was significantly greater in *M. stellatus*.

Acknowledgments

We thank Ian Davison, Steve Dudgeon, Olaf Ellers, and two anonymous reviewers for helpful comments, and Jonas Collén for technical assistance. N.L.L. was supported by Doherty Coastal Studies Fellowship from Bowdoin College and a Howard Hughes Medical Institution Undergraduate Research Fellowship.

Literature Cited

Anderson, J. V., B. I. Chevone, and J. L. Hess. 1992. Seasonal variation in the antioxidant system of eastern white pine needles: evidence for thermal dependence. *Plant Physiol.* **98:** 501–508.

Asada, K. 1999. The water-water cycle in chloroplasts: scavenging of active oxygens and dissipation of excess photons. *Annu. Rev. Plant Physiol. Plant Mol. Biol.* **50:** 601–639.

Baker, N. R. 1994. Chilling stress and photosynthesis. Pp. 127–154 in *Causes of Photooxidative Stress and Amelioration of Defense Systems in Plants*, C. Foyer and P. Mullineaux, eds. CRC Press, Boca Raton, FL.

Collén, J., and I. R. Davison. 1999. Stress tolerance and reactive oxygen metabolism in the intertidal red seaweeds *Mastocarpus stellatus* and *Chondrus crispus*. *Plant Cell Environ.* **22:** 1143–1151.

Collén, J., and I. R. Davison. 2001. Seasonality and thermal acclimation of reactive oxygen metabolism in *Fucus vesiculosus* (Phaeophyceae). *J. Phycol.* **37:** 474–481.

de Kok, L. J., and F. A. Oosterhuis. 1983. Effects of frost-hardening and salinity on glutathione and sulfhydryl levels and on glutathione reductase activity in spinach leaves. *Physiol. Plant.* **58:** 47–51.

Dudgeon, S. R., and A. S. Johnson. 1992. Thick *versus* thin: Thallus morphology and tissue mechanics influence differential drag and dislodgement of two co-dominant seaweeds. *J. Exp. Mar. Biol. Ecol.* **165:** 23–43.

Dudgeon, S. R., I. R. Davison, and R. L. Vadas. 1989. Effect of freezing on photosynthesis of intertidal macroalgae: relative tolerance of *Chondrus crispus* and *Mastocarpus stellatus* (Rhodophyta). *Mar. Biol.* **101:** 108–114.

Dudgeon, S. R., I. R. Davison, and R. L. Vadas. 1990. Freezing tolerance in the intertidal red algae *Chondrus crispus* and *Mastocarpus stellatus:* relative importance of acclimation and adaptation. *Mar. Biol.* **106:** 427–436.

Dudgeon, S. R., J. E. Kübler, R. L. Vadas, and I. R. Davison. 1995. Physiological responses to environmental variation in intertidal red algae: does thallus morphology matter? *Mar. Ecol. Prog. Ser.* **117:** 193–206.

Halliwell, B., and J. M. C. Gutteridge. 1999. *Free Radicals in Biology and Medicine*, 3rd ed. Oxford University Press, Oxford, UK. 936 pp.

Huner, N. P. A., G. Öquist, V. M. Hurry, M. Krol, S. Falk, and M. Griffith. 1993. Photosynthesis, photoinhibition and low temperature acclimation in cold tolerant plants. *Photosynth. Res.* **37:** 19–39.

Guy, C. L., and J. V. Carter. 1984. Characterization of partially purified glutathione reductase from cold-hardened and nonhardened spinach leaf tissue. *Cryobiology* **21:** 454–464.

Johnson, A. M., and J. A. Raven. 1986. The analysis of photosynthesis in air and water of *Ascophyllum nodosum* (L.) Le Jol. *Oecologia* **69:** 288–295.

Johnson, W. S., A. Gignn, S. L. Gulmon, and H. A. Mooney. 1974. Comparative photosynthetic capacities of intertidal algae nnder exposed and submerged conditions. *Ecology* **55:** 450–453.

Lillford, P. J., and C. B. Holt. 2002. *In vitro* uses of biological cryoproctectants. *Philos Trans. R. Soc. Lond. B* **357:** 945–951.

Logan, B. A., B. Demmig-Adams, W. W. Adams, III, and S. C. Grace. 1998a. Antioxidation and xanthophyll cycle-dependent energy dissipation in *Cucurbita pepo* and *Vinca major* acclimated to four growth irradiances in the field. *J. Exp. Bot.* **49:** 1869–1879.

Logan, B. A., S. C. Grace, W. W. Adams, III, and B. Demmig-Adams. 1998b. Seasonal differences in xanthophyll cycle characteristics and antioxidants in *Mahonia repens* growing in different light environments. *Oecologia* **116:** 9–17.

Logan, B. A., G. Monteiro, D. Kornyeyev, P. Payton, R. Allen, and A.

Holaday, 2003. Transgenic overproduction of glutathione reductase does not protect cotton, *Gossypium hirsutum* (Malvaceae), from photoinhibtion during growth under chilling conditions. *Am. J. Bot.* **90:** 1400–1403.

Mallick, N., and F. H. Mohn. 2000. Reactive oxygen species: response of algal cells. *J. Plant Physiol.* **157:** 183–193.

Mathieson, A. C., and R. L. Burns. 1971. Ecological studies of economic red algae. I. photosynthesis and respiration of *Chondrus crispus* Stackhouse and *Gigartina stellata* (Stackhouse) Batters. *J. Exp. Mar Biol. Ecol.* **7:** 197–206.

Mathieson, A. C., and J. S. Prince. 1973. Ecology of *Chondrus crispus*. Pp. 53–79 in *Chondrus crispus*, M.J. Harvey and J. McLachlan, eds. Nova Scotia Institute of Science, Halifax, Nova Scotia.

Mishra, N. P., R. K. Mishra, and G. S. Singhal. 1993. Changes in the activities of anti-oxidant enzymes during exposure of intact wheat leaves to strong visible light at different temperatures in the presence of protein synthesis inhibitors. *Plant Physiol.* **102:** 903–910.

Nilsen, E. T., and D. M. Orcutt. 1996. *The Physiology of Plants Under Stress: Abiotic Factors.* John Wiley, New York. 689 pp.

Niyogi, K. K. 1999. Photoprotection revisited: genetic and molecular approaches. *Annu. Rev. Plant Physiol. Plant Mol. Biol.* **50:** 333–359.

Pratt, M. C., and A. S. Johnson. 2002. Strength, drag, and dislodgement of two competing intertidal algae from two wave exposures and four seasons. *J. Exp. Biol. Ecol.* **272:** 71–101.

Quadir, A., P. J. Harrison, and R. E. DeWreede. 1979. The effects of emergence and submergence on the photosynthesis and respiration of marine macrophytes. *Phycologia* **18:** 83–88.

Schöner, S., and G. H. Krause. 1990. Protective systems against active oxygen species in spinach: response to cold acclimation in excess light. *Planta* **180:** 383–389.

Topinka, J. A., and V. Robbins. 1976. Effects of nitrate and ammonia enrichment on growth and nitrogen physiology in *Fucus spiralis*. *Limnol. Oceanogr.* **21:** 659–664.

Wise, R. R. 1995. Chilling-enhanced photooxidation: the production, action, and study of reactive oxygen species produced during chilling in the light. *Photosynth. Res.* **45:** 79–97.

Xin, Z., and J. Browse. 2000. Cold comfort farm: the acclimation of plants to freezing temperatures. *Plant Cell Environ.* **23:** 893–902.

Reference: *Biol. Bull.* **207:** 233–246. (December 2004)

Developmental Dimorphism: Consequences for Larval Behavior and Dispersal Potential in a Marine Gastropod

PATRICK J. KRUG[1,*] AND RICHARD K. ZIMMER[2]

[1] *Department of Biological Sciences, California State University, Los Angeles, California 90032-8201; and* [2] *Department of Ecology and Evolutionary Biology, Neurosciences Program, and Brain Research Institute, University of California Los Angeles, California 90095-1606*

Abstract. Specific effects of alternative developmental programs on swimming and settlement behavior for marine larvae have not been identified experimentally. A major impediment to this research has been the rarity of species with variable development. Here, we compared traits related to movement and habitat selection for different ontogenetic stages of long-lived, feeding larvae (planktotrophic) and short-lived, nonfeeding larvae (lecithotrophic) of the herbivorous gastropod *Alderia modesta.* Newly hatched planktotrophic larvae swam in meandering paths with equal rates of upward and downward movement. As planktotrophic larvae developed towards competence (physiological ability to metamorphose), their swimming paths became straighter, faster, and increasingly directed towards the bottom, traits shared by newly hatched lecithotrophic larvae. Despite differing in developmental history, competent planktotrophic (32-d-old) and lecithotrophic larvae (competent upon hatching) exhibited qualitatively similar swimming behaviors and substrate specificity. However, lecithotrophic larvae moved downward at twice the speed of competent planktotrophic larvae, potentially producing a 5-fold higher rate of contact with the bottom in natural flows. Competent larvae swam downwards rather than passively sinking, even though sinking rates were faster than swimming speeds; active swimming may allow larvae to keep the velum extended, permitting rapid response to chemical settlement cues and promoting successful habitat colonization. Differences between larvae of the two development modes may reflect fine-tuning by selection of traits important for dispersal and settlement into patchy adult habitats.

Received 8 June 2004; accepted 27 September 2004.
* To whom correspondence should be addressed: pkrug@calstatela.edu

Introduction

Many organisms express threshold traits that result in discrete forms differing in morphology, life history, or behavior (Roff, 1996). Such dimorphisms often confer a dispersal advantage on one morph over the other. Numerous examples are known for insects (Harrison, 1980; Zera and Denno, 1997), including winged *versus* wingless aphids (Dixon, 1985), crickets (Crnokrak and Roff, 1995, 1998), plant-hoppers (Denno *et al.,* 1980, 1996), and water striders (Fairbairn and Desranleau, 1987). Some plants produce both nondispersing seeds and seeds that are adapted for increased dispersal from the parent (Payne and Maun, 1981; Morse and Schmitt, 1985; Venable, 1985; Venable and Levin, 1985). In salamanders, paedomorphosis results in an aquatic adult, while metamorphosis produces legged adults that can migrate over land (Semlitsch *et al.,* 1990). One morph generally has a selective advantage over the other under a given set of environmental conditions, but carries a fitness cost (Roff, 1996). The migratory form can locate new food patches or mates, but often has a lower reproductive potential as a trade-off (Denno *et al.,* 1980; Roff, 1986, 1996; Semlitsch *et al.,* 1990; Langellotto and Denno, 2001).

Although well studied in terrestrial organisms, dispersal dimorphisms have received less attention among marine invertebrates (Raimondi and Keough, 1990; Hadfield and Strathmann, 1996). For many benthic marine species, significant dispersal is achieved only during the free-swimming larval stage (Strathmann, 1985, 1990; Levin and Bridges, 1995; Pechenik, 1999). In a few species, some offspring metamorphose prior to hatching, while their siblings hatch and swim into the water column (Gibson and Chia, 1995; Chester, 1996). Intra-clutch differences in set-

tlement requirements may also function as dispersal dimorphisms, with some larvae settling quickly and nonselectively while the rest disperse until encountering a specific environmental cue (Krug, 2001; Toonen and Pawlik, 2001). An extreme dispersal polymorphism occurs in species that produce both feeding (planktotrophic) and nonfeeding (lecithotrophic) larvae in the same population (Levin, 1984; Krug, 1998). The rarity of such species has generally precluded intraspecific comparisons between long- and short-lived larval morphs, however (Hoagland and Robertson, 1988).

The evolutionary significance and biological consequences of planktotrophy *versus* lecithotrophy have long been debated (Thorson, 1950). Planktotrophic larvae are generally much longer-lived than lecithotrophic larvae, often resulting in populations that are demographically open and genetically homogeneous over large areas (Scheltema, 1962; Caley *et al.*, 1996; Todd, 1998). In contrast, lecithotrophic species often show strong genetic differentiation over short spatial scales (Palumbi, 1995; Hellberg, 1996; Todd, 1998; Todd *et al.*, 1998). Demographic effects of development mode may reflect trade-offs between adult fecundity and offspring survivorship (Levin and Bridges, 1995). For habitat selection, models predict that a longer competency period exposes larvae to a larger number of potential settlement sites (Doyle, 1975, 1976); planktotrophic species may offset the costs of dispersal through extended competency and rapid response to cues of habitat suitability (Obrebski, 1979; Pechenik, 1999). An alternative strategy is to limit dispersal from patchy habitats by producing short-lived larvae, thus ensuring local colonization (Todd, 1998; Pechenik, 1999). Lecithotrophic larvae appear unable to extend their competency period without suffering severe post-metamorphic consequences (Pechenik, 1990, 1999), and may exhibit behaviors that minimize dispersal during a brief pelagic interval (Todd, 1998; Todd *et al.*, 1998).

Alternative developmental pathways must ultimately produce a competent larva, but how developmental differences affect the evolution of larval swimming and settlement behavior remains largely unexplored. As Wieczorek and Todd (1998) remarked, "considering only larvae at the attainment of competence, it is probably an article of faith amongst larval biologists that the settlement and metamorphic behaviors of pelagic lecithotrophic species are not fundamentally different from those of species that reproduce by means of planktotrophic larvae." Experimental investigations are clearly needed to test such assumptions. The sea slug *Alderia modesta* (Lovén, 1844) is the only mollusc known to produce both planktotrophic and lecithotrophic larvae in one population (Krug, 1998). After hatching, planktotrophic larvae of *A. modesta* mature for 4 weeks to reach competence, the stage at which larvae are able to settle and metamorphose (Krug and Zimmer, 2000). In contrast, lecithotrophic larvae are competent immediately upon hatching (Krug, 2001). This species thus provides an opportunity to examine the consequences of different development modes on the behavior of distinct but conspecific larval types. A specialist herbivore, *A. modesta* is found in temperate estuaries exclusively upon yellow-green algae of the genus *Vaucheria* De Candolle (Xanthophyta: Xanthophyceae) (Hartog and Swennen, 1952; Bleakney and Bailey, 1967; Trowbridge, 1993). Larvae of *A. modesta* metamorphose in response to bioactive carbohydrates from the adult host alga, *V. longicaulis* Hopp (Krug and Manzi, 1999). A dissolved form of the settlement cue triggered immediate changes in swimming behavior of both larval types; chemically stimulated larvae altered their swimming speeds and increased turning rates, exhibiting site-restricted searches during settlement (Krug and Zimmer, 2000).

In the present study, swimming behavior, physical characteristics, and settlement specificity were compared for the two developmentally distinct larval types of *Alderia modesta*. Our aim was to determine whether development period, which profoundly changes dispersal potential, also results in differences between the two larval types that might affect their distribution in the water column or settlement opportunities. Physical and behavioral characteristics that affect larval movement, such as speed and direction of swimming, were measured for planktotrophic larvae of different ontogenetic stages and for lecithotrophic larvae of several ages. This study is a first step towards linking swimming behaviors associated with alternate dispersal strategies to key components of habitat colonization such as transport, delivery to the bed, and settlement.

Materials and Methods

Collection of organisms and larval culture

Specimens of *Alderia modesta* and patches of *Vaucheria longicaulis* were collected from Mission Bay, a shallow estuary located in San Diego, California, 21 km north of the border between the United States and Mexico. The remaining natural wetlands are confined to the Kendall-Frost Marine Reserve and Northern Wildlife Preserve in the northeastern corner of the back bay. Adult *A. modesta* were collected from mats of *V. longicaulis* on the reserve mudflat. Seawater from the Scripps Institution of Oceanography aquarium was filtered to 0.45 μm (FSW) prior to use.

Several hundred specimens of *A. modesta* were placed in petri dishes overnight, sufficient time for each slug to produce one clutch. Egg masses identified as planktotrophic or lecithotrophic (Krug, 1998) were separated and maintained in FSW, which was changed every other day until hatching. Lecithotrophic larvae from about 50 egg masses were pooled and transferred to fresh FSW upon hatching; larvae were subsampled for use in experiments the next day. From 80–100 planktotrophic egg masses were hatched together

for each batch culture, and the resulting pool of larvae was divided into replicate beakers containing 3 l of FSW at concentrations of 1 larva per milliliter. Aliquots from unialgal suspensions of the phytoplankton *Rhodomonas* sp., *Isochrysis galbana*, and *Pavlova lutheri* were added in a 1:1:1 ratio to cultures to give a final concentration of about 10^4 cells per milliliter. Every 2–3 days, larvae were sieved through a 52-μm mesh and transferred to clean FSW with fresh phytoplankton. Cultures were stirred by pipetting water against the bottom twice daily but were otherwise static. Competence was tested by periodically exposing 10 planktotrophic larvae from a batch to the inductive alga *V. longicaulis* and scoring metamorphosis after 2 d. Larvae did not attain competence earlier than day 26, and the majority became competent after 30 d in culture (Krug and Zimmer, 2000). Experiments were performed promptly after larvae reached competence; replicate trials were conducted using batches cultured in December 1999 and in July 2000.

Quantitative measurements of swimming behavior

Larval swimming behavior was quantified in light and dark for 8-, 16-, and 32-d-old planktotrophic larvae, and for 1-, 2-, and 4-d-old lecithotrophic larvae (larval age is days since hatching from the egg mass). Swimming paths were imaged with a Cohu infrared-sensitive video camera having a Pentax 100-mm macro lens. All video recording was done at 22 °C, using only infrared light for dark treatments. In light trials, an incandescent bulb (GE Daylight Ultra) was placed within a baffled housing to provide diffuse light. An Ocean Optics, Inc. (model S2000) spectroradiometer was connected to a miniature fiber optic probe, and light was measured underwater in an experimental chamber at the same position as video observations of larvae (see below). The mean photon flux (140 μE/m^{2}s), spectral composition (intensity peaks between 435 and 543 nm), and angular distribution (sharp decline in intensity between 40° and 50° relative to the zenith) in the chamber were similar to morning sunlight in a shallow estuary (Lythgoe, 1979; Forward *et al.*, 1984).

Behavioral assays were performed in chambers (3 × 3 × 5 cm) at a concentration of 5 larvae per milliliter. Under these conditions, sufficient swimming paths were recorded over 30 s to permit statistical comparisons between treatments. A total of 8–10 replicates were run for all age classes, using different larvae in each replicate. To minimize the likelihood of recording the same larva more than once, the field size was limited to 0.6 (height) × 0.8 (width) × 0.3 (depth) cm, less than 0.5% of the total chamber volume. All images were captured with the middle of the field placed at 1.5 cm above the bottom, and with the focal plane in the center of the chamber. These images were processed at 10 frames per second through a computer-assisted video motion analyzer (CAVMA) (Motion Analysis Corp. model VP 320, ExpertVision, and custom software) interfaced with a Sun Microsystems SPARC 2 computer workstation.

Analysis consisted of determining the vertical component (Y-dimension only) and total swimming speed for each path of larvae initially suspended in the water column (see methods in Tamburri *et al.*, 1996). Because measurements of speed are scalars, they contain no information on the direction of larval movement. For each path, we therefore subtracted the distance moved downwards from the distance moved upwards, and divided the difference by time to quantify the rate of net vertical displacement as a vector. This quantity may be the most relevant measure relating patterns of swimming and sinking to dispersal and settlement, as it indicates whether an individual tends to move up, down, or remain in suspension. Larval movement was also expressed as net-to-gross displacement (NGD), the ratio of the linear distance from the starting to the ending point in a given path to the total distance traveled. The NGD ratio thus measures the tendency of paths to be circular or twisted; values range from zero, for a path with origin and endpoint at the same spatial coordinates, to a maximum of 1.0 for paths that are completely straight. Ratios were arcsine-transformed to normalize the data before statistical analysis.

To ensure that swimming behavior was not affected by chamber size or larval density, four replicate trials were performed in a 10 × 10 × 20 cm chamber at a concentration of 0.3 larva per milliliter. Lecithotrophic larvae were equilibrated in the chamber for 3 h in the light, prior to video recording for 1 h. They were subsequently held in darkness for 3 h, before an additional 1 h of filming under infrared (IR) illumination. Video records were made with the middle of the field of view (1.5 × 1.8 cm) located 15 cm above the bottom, and with the focal plane in the center of the chamber. Swimming behavior was quantified by CAVMA and compared with data from the 3 × 3 × 5 cm chamber by unpaired two-tailed student's t-tests. No difference in total swim speed was found for larvae in large (1.16 ± 0.05 mm/s, n = 80) and small (1.24 ± 0.04 mm/s, n = 202) chambers ($P > 0.20$). Similarly, vertical speeds ($P > 0.35$) and net vertical displacement rates ($P > 0.75$) also did not differ between chambers. Moreover, the concentration of larvae in the small chamber did not affect behavioral assays, as collisions were never observed. Results were thus independent of larval density and chamber size over the ranges tested. Small chambers were used in subsequent experiments because of limitations in available larvae.

Responses to light and dark

Behavior following a change in illumination was measured for 8-, 16-, and 32-d-old planktotrophic larvae and 1-d-old lecithotrophic larvae, to test whether shadow re-

sponses were present (Young and Chia, 1985) and whether they differed according to age or development mode. For each age class, 40 larvae per replicate were placed in the recording chamber and observed within a 0.6 × 0.8 cm field of view, running 5–10 replicates per class. Larvae were acclimated in the light for 10 min, and were then recorded for 1 min in the light treatment. The light was next extinguished, and larvae were recorded for 1 min in darkness under IR illumination only. The full-spectrum light was then turned back on, and behavior was recorded for an additional 1 min. Through subsequent viewing of the video recordings, the number of larvae observed was scored every 15 s for the full 3 min of each trial. To test for interactions between age class and light/dark treatment, a two-way ANOVA was performed. The number of swimming larvae in each of the four age classes was compared for the following three time points: (1) after 15 s in the initial light treatment, (2) 15 s after the transition to darkness, and (3) 15 s after reexposure to light.

Size and gravitational fall velocity

Planktonic larvae are often modeled as passive particles, vertically distributed by sinking or turbulent mixing. To evaluate the contribution of passive (gravitational fall) *versus* active (swimming) movements to downward transport, sinking rates were measured for precompetent (8-d-old) and competent (32-d-old) planktotrophic larvae, for 1-d-old and 4-d-old lecithotrophic larvae, and for the empty shells of 1-d-old lecithotrophic larvae. Individuals were narcotized in seawater containing excess $MgCl_2$ for 5 min; larvae were then washed twice with seawater and introduced into a temperature-controlled fall velocity apparatus consisting of two nested acrylic plastic chambers (Hannan, 1984). An inner chamber (15 cm square by 40 cm tall) was elevated 5 cm above the bottom and 5 cm below the top of an outer chamber (30 cm square by 50 cm tall); both were filled with 1-μm filtered seawater and equilibrated to 22 °C. Larvae added through a snorkel at the top of the inner chamber were video recorded during the middle 20 cm of their descent. Time from addition through the snorkel to passage through the field of view was about 3 min; controls showed that larvae remained narcotized for more than 5 min after rinsing in fresh seawater, and motion analysis of the video confirmed that larvae were sinking straight downward and not swimming during these measurements. Paths were analyzed using CAVMA to obtain terminal sinking velocities.

The sizes of larvae were also compared. Empty shells were collected after competent planktotrophic ($n = 48$) and lecithotrophic ($n = 89$) larvae had completed metamorphosis, and arranged on a depression slide such that shells lay on their side. The maximum shell dimension was measured on a compound scope using a calibrated ocular micrometer, accurate to ± 3 μm. Precompetent larvae were anesthetized ($n = 36$) prior to shell measurements after 8 days in culture.

Substrate selection and metamorphosis

Larvae of benthic organisms must leave the water column and contact the bottom to colonize new habitats, either initiating metamorphosis or rejecting the encountered substratum and reentering the plankton. A 48-h bioassay was used to compare the metamorphic response of 32-d-old planktotrophic larvae and 2-d-old lecithotrophic larvae to the natural host, *Vaucheria longicaulis*, and four other species of macroalgae. *Enteromorpha clathrata* and *Ulva expansa* co-occur with *V. longicaulis* and thus represent potential habitat cues, whereas *Chaetomorpha linum* and *Codium fragile* are hosts for other local ascoglossan species (Abbott and Hollenberg, 1976). For each treatment, 10–15 larvae were added to each of three replicate dishes containing 4 ml of FSW and a branchlet of a given alga, cleaned of epiphytes. Negative controls were FSW.

Results

Swimming behavior of larvae differing in age and developmental history

Total swimming speed, NGD, and vertical speed were quantified for precompetent planktotrophic larvae after 8 and 16 d in culture, for 32-d-old competent planktotrophic larvae, and for lecithotrophic larvae 1, 2, and 4 d after hatching (Table 1). Within each age class, no significant difference was detected between light and dark treatments for a given behavioral characteristic (Scheffé test: total speed, $P > 0.99$; NGD, $P > 0.46$; vertical speed, $P > 0.99$). There was also no difference in swimming speed, NGD, or vertical speed between batches from different seasons ($P > 0.05$ for each characteristic), indicating that results were not batch-dependent or seasonal (Table 2). Data for light and dark, and from different batches, were therefore pooled prior to statistical comparisons between classes. Lecithotrophic larvae exhibited the highest values for total speed, NGD, and vertical speed, while precompetent larvae had the smallest values for each trait. Competent, 32-d-old planktotrophic larvae consistently exhibited intermediate values. Lecithotrophic larvae of all ages swam significantly faster than 8- and 16-d-old planktotrophic larvae (one-way ANOVA: $F_{5,833} = 12.4$, $P < 0.0001$; Scheffé test, $P < 0.005$). Competent larvae generally swam at similar total speeds, regardless of age or developmental history; the only significant difference was between 2-d-old lecithotrophic and 32-d-old planktotrophic larvae (Scheffé test, $P < 0.05$).

In addition to speed, the trajectories of larval swimming paths may substantially affect distributions in the water column. Precompetent larvae generally swam in meandering paths, whereas competent larvae made primarily vertical

Table 1

Mean (± SE) swimming speeds and net-to-gross displacement (NGD) for planktotrophic and lecithotrophic larvae

	Total speed (mm/s)		NGD ratio		Vertical speed (mm/s)	
Larval class	Light	Dark	Light	Dark	Light	Dark
Planktotrophic						
8-day	0.94 ± 0.07	0.85 ± 0.05	0.74 ± 0.04	0.83 ± 0.03	0.44 ± 0.06	0.42 ± 0.06
16-day	0.79 ± 0.12	0.92 ± 0.09	0.88 ± 0.03	0.85 ± 0.03	0.58 ± 0.15	0.57 ± 0.09
32-day	1.14 ± 0.09	1.03 ± 0.09	0.85 ± 0.02	0.84 ± 0.02	0.73 ± 0.11	0.65 ± 0.07
Lecithotrophic						
1-day	1.22 ± 0.05	1.21 ± 0.04	0.90 ± 0.01	0.92 ± 0.01	1.06 ± 0.12	0.92 ± 0.06
2-day	1.34 ± 0.09	1.42 ± 0.10	0.88 ± 0.02	0.88 ± 0.02	0.97 ± 0.10	1.05 ± 0.15
4-day	1.14 ± 0.07	1.32 ± 0.07	0.88 ± 0.03	0.90 ± 0.03	0.74 ± 0.12	0.99 ± 0.12

NGD is a ratio of the linear distance from the first to the last point of a given path to the actual distance traveled; a value of zero indicates a circle, whereas a ratio of 1.0 represents a straight line. Vertical speed is a measure of larval movement in the *Y*-dimension only.

excursions, swimming mainly upwards or downwards (Fig. 1). To quantitatively describe this behavior, NGD ratios were calculated for larval paths. Lecithotrophic larvae of all age classes had significantly higher NGD ratios than 8-d-old planktotrophic larvae (Table 1, and results of a one-way ANOVA: $F_{5,707} = 9.2$, $P < 0.0001$; Scheffé test, $P < 0.05$). The three ages of planktotrophic larvae did not significantly differ from each other in NGD (Table 1).

Total swimming speeds do not necessarily indicate the capacity of larvae to control their position; the vertical component of swimming speed better represents the ability of a larva to move selectively downward during settlement. Lecithotrophic larvae of *Alderia modesta* swam only about 1.4 times faster than 8-d-old planktotrophic larvae in terms of total speed, but were 2.3 times faster in the vertical dimension (Table 1). Vertical speeds varied significantly among larval classes (one-way ANOVA: $F_{5,651} = 14.1$, $P < 0.0001$). Lecithotrophic larvae had significantly faster vertical speeds than 8-day-old and 16-d-old planktotrophic larvae (Scheffé test, $P < 0.05$), but did not differ from competent planktotrophic larvae (Scheffé test, $P > 0.10$). Competent planktotrophic larvae had significantly faster vertical swimming speeds than 8-d-old precompetent larvae (Scheffé test, $P < 0.05$). Lecithotrophic larvae thus swam in the straightest, fastest paths, and competent larvae of both types moved significantly faster in the vertical dimension than precompetent larvae.

Larvae changed their position in the water column as they developed and became competent to settle. Newly hatched planktotrophic larvae distributed themselves evenly

Table 2

Mean (± SE) swimming speeds and net-to-gross displacement (NGD) ratios for independently reared batches of competent planktotrophic and lecithotrophic larvae

	Total speed (mm/s)		NGD ratio		Vertical speed (mm/s)	
Larval batch	Light	Dark	Light	Dark	Light	Dark
Planktotrophic (32-d)						
Dec. 1999	1.20 ± 0.12	1.16 ± 0.16	0.86 ± 0.04	0.85 ± 0.04	0.95 ± 0.23	0.70 ± 0.20
July 2000	1.04 ± 0.14	0.93 ± 0.09	0.83 ± 0.03	0.84 ± 0.03	0.60 ± 0.10	0.64 ± 0.07
P value	0.40	0.20	0.13	0.59	0.50	0.45
Lecithotrophic (1-d)						
Nov. 1999	1.25 ± 0.07	1.24 ± 0.04	0.90 ± 0.02	0.94 ± 0.01	1.14 ± 0.20	0.93 ± 0.07
June 2002	1.18 ± 0.08	1.14 ± 0.07	0.89 ± 0.02	0.90 ± 0.02	0.97 ± 0.11	0.88 ± 0.09
P value	0.20	0.50	0.37	0.10	0.99	0.93

Planktotrophic larvae were cultured for 32 d and tested during the indicated month. NGD ratios represent the relative straightness of larval paths and were arcsine transformed for comparisons. Vertical speed measures larval movement in the *Y*-dimension only; data were normalized by the function $\ln(x + 0.01)$ prior to statistical analyses.

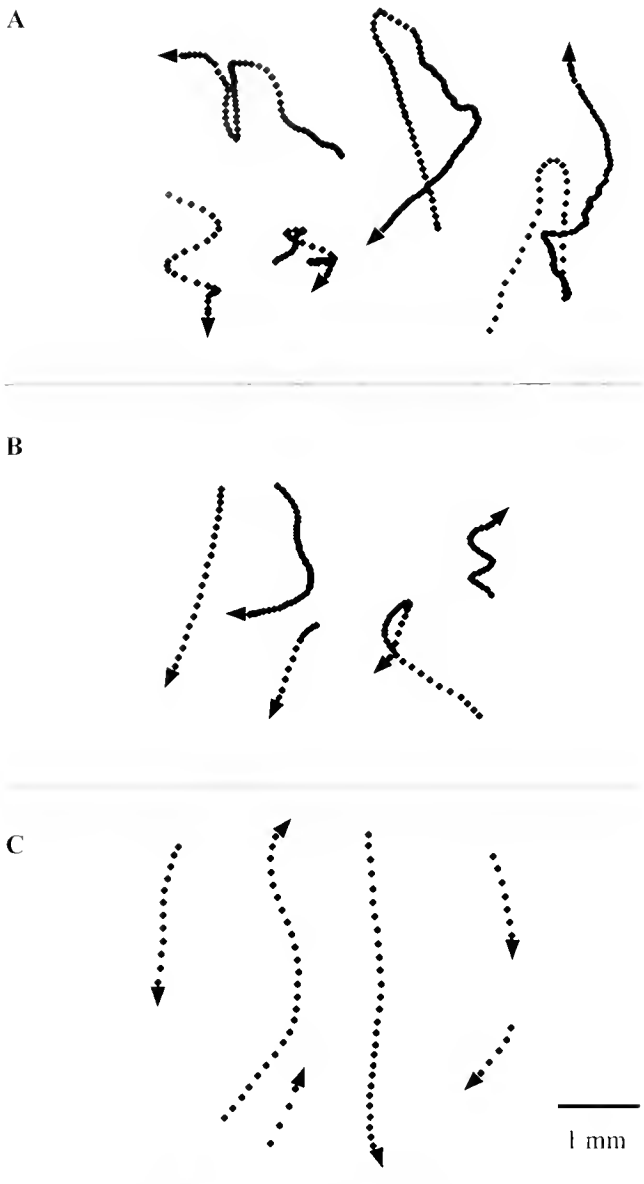

Figure 1. Representative paths of larvae swimming off the bottom in filtered seawater. Data are computer-digitized video records of vertical paths as viewed from the side of a chamber. Each path of dots represents the position of a given larva at consecutive two-frame intervals with video collected at 10 frames per second. The same scale bar applies to all paths. (A) Representative paths of precompetent, 8-d-old planktotrophic larvae, showing the frequent turns and meandering movement typical of immature larvae. (B) Paths of competent, 32-d-old planktotrophic larvae. Larvae increasingly swam towards the bottom in straighter, faster paths as they matured to competence. (C) Swimming behavior of competent, 1-d-old lecithotrophic larvae. Paths show the rapid, vertically oriented swimming that characterizes nonfeeding larvae of *Alderia modesta*.

throughout the water column and did not respond to changing light regimes (Fig. 2A). As planktotrophic larvae neared competence, the trend was for fewer larvae to swim off of the bottom (Fig. 2B). Most competent, 32-d-old planktotrophic larvae remained on the bottom in initial light treatments, as did 1-d-old lecithotrophic larvae (Fig. 2C, D). Competent larvae of both development modes displayed a striking shadow response: both 32-d-old planktotrophic larvae and 1-d-old lecithotrophic larvae immediately swam up into the water column following a transition to darkness (Fig. 2C, D). After 1 min, most larvae settled out of the water column and returned to the bottom, where they remained during a subsequent exposure to light. The effects of age and photostimulation on larval position in the water column were tested using a two-way ANOVA (Table 3). Light or dark treatment had a significant effect on the number of swimming larvae ($P < 0.0001$), and the interactive term for light treatment *versus* larval developmental class was also significant ($P < 0.005$). This result reflects the fact that both competent types responded to alternating light and dark regimes, whereas precompetent larvae were indifferent to changing light conditions.

Role of larval swimming versus *sinking in vertical transport*

Mathematical models of settlement rates are generally based in part on larval (or "particle") characteristics, including gravitational fall velocities or swimming capabilities. Sizes and sinking rates were thus determined for competent planktotrophic and lecithotrophic larvae, and for precompetent, 8-d-old planktotrophic larvae, as a measure of how the three classes compared as passive particles. No difference was found between 1-d-old lecithotrophic larvae and 32-d-old planktotrophic larvae in mean maximum shell dimension, a measure of size (Table 4). Similarly, when competent larvae were anesthetized and introduced into a specially constructed chamber, the two types gave the same mean sinking rate (Table 4). Compared to precompetent larvae, both types of competent larvae were significantly larger (Table 4, and results of a one-way ANOVA: $F_{2,170} = 1081.7$, $P < 0.0001$; Scheffé test, $P < 0.0001$) and sank significantly faster (Table 4, and results of a one-way ANOVA: $F_{2,41} = 11.5$, $P < 0.0001$; Scheffé test, $P < 0.005$).

In terms of time budgets, a similar proportion of precompetent larvae swam downward (57%) as upward (G test for goodness-of-fit: $G = 0.41$, df = 1, $P > 0.50$). The mean rate of net vertical displacement for precompetent larvae, −0.13 mm/s, was not significantly different from a null-expectation of zero net movement (one-tailed t-test: $t = 1.1$, df = 19, $P > 0.20$). On average, immature feeding larvae thus exhibited behaviors expected for dispersing propagules that must remain suspended in the water column to feed during development. In contrast, significantly more competent planktotrophic (71%; $G = 8.11$, df = 1, $P < 0.01$) and lecithotrophic larvae (85%; $G = 27.96$, df = 1, $P < 0.001$) swam down towards the bottom, compared to the 50%:50%

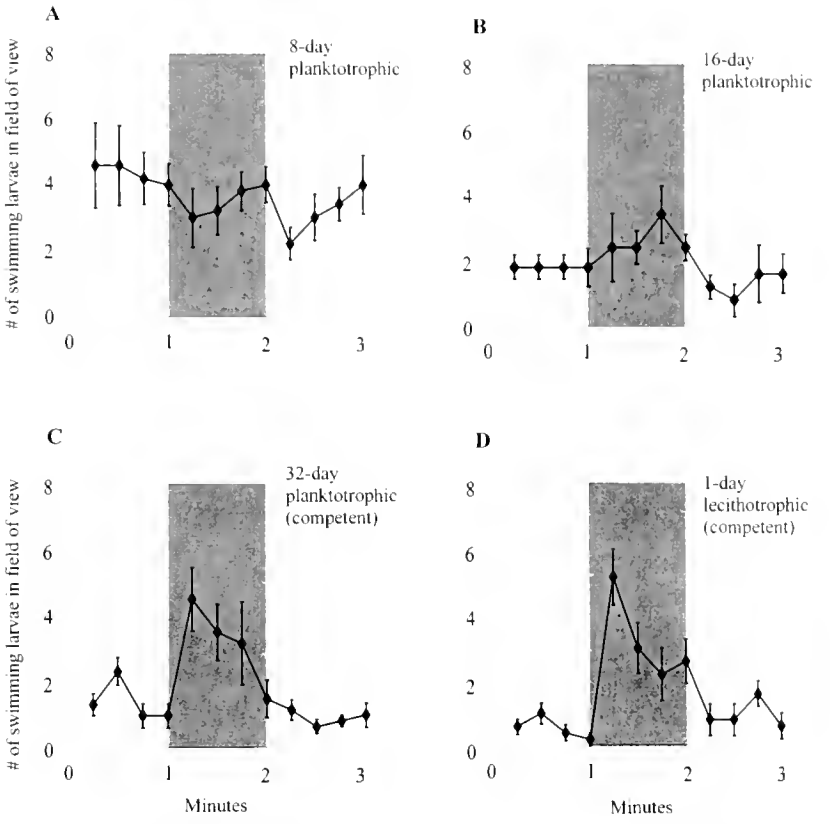

Figure 2. Mean number (± 1 SE) of larvae observed swimming off the bottom in response to light and dark, within a 0.6 × 0.8 cm field of view. Shading indicates observations made in the dark. (A) 8-d-old (precompetent) planktotrophic larvae, in alternating light and dark regimes. (B) 16-d-old (precompetent) planktotrophic larvae. (C) Competent (32-d-old) planktotrophic larvae. (D) 1-d-old lecithotrophic larvae, which are competent upon hatching.

ratio expected for a null-model of equal upward and downward movement. This significant bias in direction, combined with greater speeds and straighter paths, resulted in significant rates of downward displacement for lecithotrophic larvae (one-tailed t-test: $t = 8.3$, df = 57, $P < 0.0005$) and competent planktotrophic larvae (one-tailed t-test: $t = 4.0$, df = 46, $P < 0.0005$) (Table 4).

Table 3

Results of a two-way ANOVA comparing effects of (1) light versus *dark exposure, and (2) developmental age and type (class), on larval position in the water column*

Source of variation	df	SS	MS	F_s	P
Light treatment	2	53.03	26.52	10.61	0.0001
Developmental class	3	18.67	6.22	2.49	0.071
Treatment × class	6	55.63	9.27	3.71	0.004
Error	48	120	2.50		
Total	59	247.33			

Data are the number of larvae observed swimming off the bottom within the video field (0.6 × 0.8 cm) of an experimental chamber.

Competent planktotrophic larvae and 1-d-old lecithotrophic larvae were comparable in size and sinking rate (Scheffé test, $P > 0.90$), and showed similar patterns of downward movement. After 4 d, lecithotrophic larvae sank at a significantly slower rate (Scheffé test, $P < 0.005$), closer to that of empty lecithotrophic shells (−0.88 ± 0.04 mm/s). Older nonfeeding larvae expended their yolk reserves and lost tissue mass during their planktonic period, which likely lowered their density and hence sinking rate. Lecithotrophic larvae of both ages had a significantly faster rate of net vertical displacement than precompetent planktotrophic larvae (one-way ANOVA: $F_{3,195} = 6.5$, $P < 0.005$; Scheffé test, $P < 0.05$). Competent planktotrophic larvae were intermediate in their rate of net vertical displacement, due to swimming behaviors that tended to keep live larvae suspended off the bottom despite a high sinking rate. For all larval classes, video observations revealed that larvae moving straight downward were actively swimming with the velum extended, as opposed to passively sinking with the velum withdrawn as in the gravitational fall chamber.

Table 4

Comparison of mean (± SE) shell sizes, gravitational fall velocities, and net vertical displacement for larvae differing in age and developmental type

Properties	Precompetent	Competent		
	8-day-old planktotrophic	32-day-old planktotrophic	1-day-old lecithotrophic	4-day-old lecithotrophic
Passive properties:				
Shell size (μm)	126 ± 1[a]	194 ± 1[b]	194 ± 1[b]	193 ± 2[b]
Gravitational fall velocity (mm/s)	−0.90 ± 0.09[a]	−1.59 ± 0.12[b]	−1.52 ± 0.10[b]	−0.99 ± 0.10[a]
Active properties:				
Net vertical displacement (mm/s)	−0.10 ± 0.08[a]	−0.40 ± 0.12[ab]	−0.78 ± 0.09[b]	−0.73 ± 0.21[b]

Unlike speeds, which are nondirectional scalar values, net vertical movement is a vector with negative values indicating movement towards the bottom. Statistical comparisons for each larval characteristic were performed using a one-way ANOVA with *post hoc* Scheffé tests. Within each row, means labeled with the same letter did not differ significantly (*post hoc* comparison, $\alpha = 0.05$).

Substrate selection and metamorphosis

To compare substrate selectivity between larval types, competent (32-d-old) planktotrophic and 2-d-old lecithotrophic larvae were exposed to five algal species (Fig. 3). For both larval types, the adult host *Vaucheria longicaulis* induced significantly higher levels of metamorphosis than all other algae (one-way ANOVA: $F_{11,24} = 22.0$, $P < 0.0001$; *post hoc* Scheffé tests, $P < 0.005$). There was no difference in the response of planktotrophic and lecithotrophic larvae to *V. longicaulis*, and no other alga triggered more metamorphosis than FSW controls. Only low levels of spontaneous metamorphosis (1 ± 1%) occurred in cultures of planktotrophic larvae prior to assays.

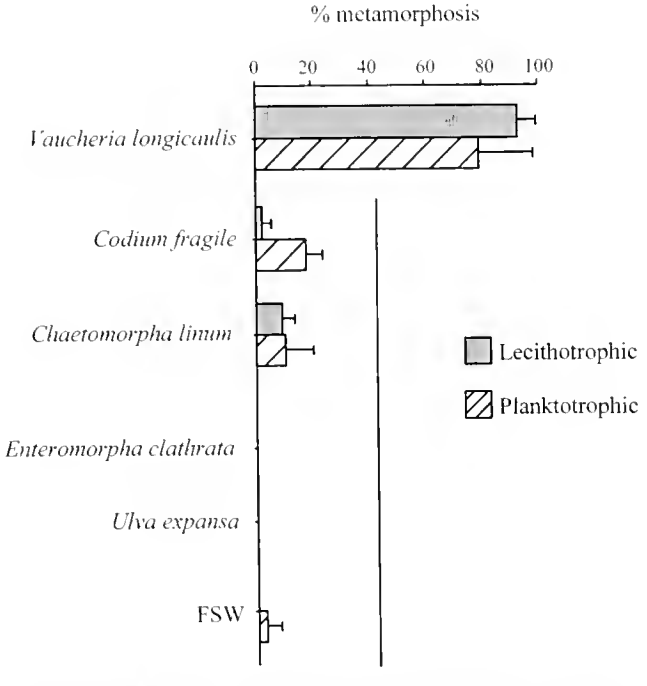

Figure 3. Mean (+1 SD) percent metamorphosis of competent, 32-d-old planktotrophic larvae and 2-d-old lecithotrophic larvae in response to the host alga, *Vaucheria longicaulis*, and four other algae. Means joined by a vertical bar did not differ significantly (one-way ANOVA followed by *post hoc* Scheffé tests, $P > 0.98$).

Discussion

Consequences of swimming behavior and ontogenetic stage for larval transport

The transport and distribution of larvae fundamentally influences patterns of dispersal and settlement, processes that regulate population dynamics and community structure of marine benthic invertebrates (Roughgarden *et al.*, 1988; Pechenik, 1999). To understand how hydrodynamics affect settlement rates, larvae have been modeled as sediment particles, with sinking or swimming speeds used to describe larval movements (Gross *et al.*, 1992; Eckman *et al.*, 1994). Larvae are maintained in suspension by turbulent eddies; high turbulence mixes larvae away from the bed and low mixing allows sinking. Models predict maximal settlement when larvae become concentrated near the bottom due to low turbulent mixing or high downward flux of larvae. Some studies have treated larvae as passive particles, with net downward transport resulting from gravitational sinking; others incorporate conditional downward swimming of larvae in response to light, gravity, or waterborne chemical cues (Butman, 1987; Butman *et al.*, 1988a; Eckman, 1990; Eckman *et al.*, 1994).

In this study, total swimming and sinking speeds were poor predictors of vertical movement. Competent larvae swam only 1.4 times faster than precompetent larvae but, due to behavioral differences, had rates of net vertical displacement that were 6 times higher. Despite swimming at similar speeds, precompetent larvae tended to meander throughout the experimental chambers, whereas competent

larvae had a strong directional bias resulting in rapid downward movement. By swimming towards the seabed, competent larvae can increase the probability of contacting an appropriate settlement site.

Although similar in size and passive sinking speeds, lecithotrophic and competent planktotrophic larvae of *Alderia modesta* exhibited subtle differences in path trajectories and vertical swimming speeds. Lecithotrophic larvae were more uniform in their behavior, and swam downward in faster, straighter paths that resulted in higher rates of vertical movement. In cultures, we observed these short-lived larvae making rapid excursions up into the water column and back down to the bottom, which may allow them to repeatedly sample the substratum during a brief dispersal period. Competent planktotrophic larvae were less consistent in their behavior, swimming with a significant downward bias but at a lower rate. This pattern may result from developmental variation during the month-long maturation period of planktotrophic larvae.

Surprisingly, few studies have documented vertical components of swimming behavior for taxa other than bivalves and crustaceans (Mileikovsky, 1973; Chia *et al.*, 1984). Bivalve larvae typically swim in vertically oriented helical spirals (Mann and Wolf, 1983; Mann *et al.*, 1991; Wang and Xu, 1997), and can lower their sinking rate, without altering swimming speed, by changing rotational velocity (Jonsson *et al.*, 1991). Downward swimming speeds were slower than rates of gravitational sinking in all bivalves examined, as in *A. modesta* and other taxa besides crustaceans (Chia *et al.*, 1984; Young, 1995). These data suggest that live larvae rarely move downward through passive sinking alone, but rather through a combination of gravity and behavior. Prior studies have not measured rates of net vertical displacement for populations of larvae, however. The present investigation demonstrates that larvae differing in ontogeny or life history can express behavioral differences that have potentially large consequences for stage-specific patterns of movement.

To place these data in an ecological context, we developed a numerical model based on sediment transport equations to examine the effects of sinking *versus* swimming on larval distributions (Fig. 4, and Komar, 1976; Gross *et al.*, 1992; Eckman *et al.*, 1994). To first order, the distribution of larvae above the bottom is governed by the same hydrodynamic principles (turbulent mixing and diffusion of momentum) that dictate vertical profiles of suspended sediment (Komar, 1976; Middleton and Southard, 1984). The magnitude of turbulent mixing relative to sinking or downward swimming determines the vertical position of larvae within a one-dimensional bottom boundary layer. We modeled the

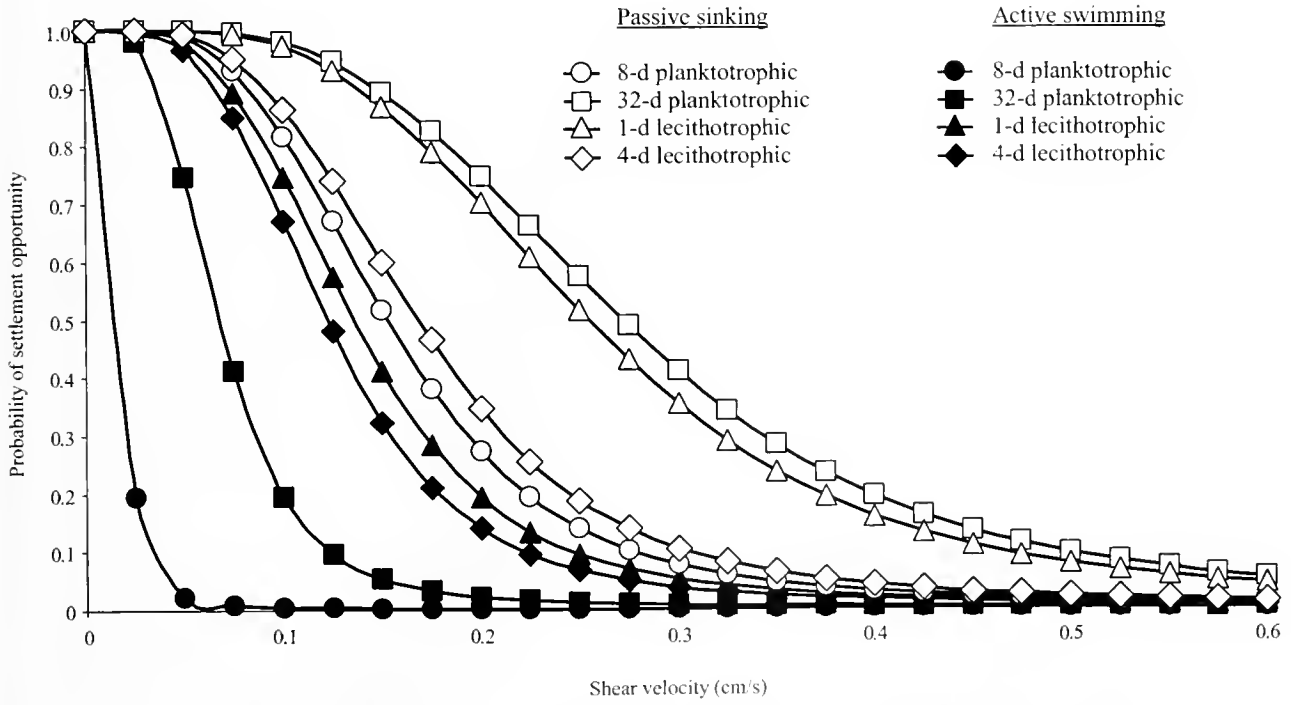

Figure 4. Numerical model of larval settlement opportunity, as a function of active swimming or passive sinking (see text for model description). Settlement opportunity is defined as the probability of a larva coming within one body length (200 μm) of the bottom, computed by vertically integrating larval distributions throughout the entire water column. Open symbols denote probabilities calculated using gravitational fall velocities of anesthetized larvae, and solid symbols represent probabilities calculated using rates of net vertical movement for actively swimming larvae.

equilibrium distribution of suspended larvae in the water column using the steady-state Rouse profile (equation 32, in Komar, 1976). The Rouse parameter indicates the strength of downward larval flux, due to passive sinking or active swimming, relative to the upward larval flux due to turbulent mixing (as characterized by the shear velocity). These profiles were then integrated over the entire water column (set at 1 m). Probability density functions were derived to describe the likelihood of an individual larva being suspended within one body length (200 μm) of the seabed for a given shear velocity. In the southern California estuaries inhabited by *A. modesta*, shear velocities typically range from 0.05 to 0.8 cm/s but are lower than 0.2 cm/s over most (70%) tidal cycles, and water depths at maximum flood tide are 1 m or less (Fingerut *et al.*, 2003). Net vertical displacement rates for live larvae (active) and sinking rates for anesthetized larvae (passive) were taken from Table 4.

Model outputs predicted substantially different results for actively swimming and passively sinking larvae. The concentration profiles generated for passively sinking lecithotrophic and competent planktotrophic larvae were essentially the same, because of comparable gravitational fall velocities. Larvae of both types were concentrated near the seabed at low intensities of turbulent mixing (Fig. 4). When rates of net vertical movement were used rather than sinking speeds, however, lecithotrophic larvae became more bottom-skewed in their distributions relative to competent planktotrophic larvae. A 2-fold difference in active, downward movement between the two types was magnified as a 5-fold difference in predicted concentrations along the bottom for shear velocities commonly found in the field.

The consequences of active swimming *versus* passive sinking were even greater for precompetent larvae (Fig. 4). Anesthetized, 8-d-old larvae sank at −0.9 mm/s, comparable to the downward movement of swimming lecithotrophic veligers. When the passive fall velocity of 8-d-old larvae was used to establish their distribution, the model predicted that most precompetent larvae would sink to the bottom at shear velocities less than 0.2 cm/s. However, when their rate of net vertical displacement (−0.10 mm/s) was used instead, 8-d-old larvae were predicted to mix throughout the water column at most shear velocities. The life-history strategy of planktotrophy requires precompetent larvae to remain suspended for feeding. Although passive sinking would carry newly hatched larvae to the bottom, active swimming will keep such larvae distributed throughout the water column, where they function as dispersing propagules. The behavior of free-swimming larvae must therefore be taken into account when modeling transport and settlement, as swimming speeds and sinking rates do not accurately represent patterns of vertical movement for different developmental stages. Although based on still-water analyses, our data suggest patterns of larval movement to be expected in turbulent water; future studies in sheared flows are needed to test these predictions of behavior and transport for *A. modesta* larvae (Grunbaum and Strathmann, 2003).

It remains controversial at what scale and for which processes larvae can be effectively modeled as passive particles. At least in slower flow regimes, taxonomically diverse larvae and meiofaunal organisms can distribute themselves selectively in the water column and settle in or on preferred substrates along the bed (Butman *et al.*, 1988b; Pawlik and Butman, 1993; Fingerut *et al.*, 2003; Ullberg and Olafsson, 2003). Moreover, experimental studies on larvae of two unrelated molluscs, the Eastern oyster *Crassostrea virginica* and the opisthobranch *Alderia modesta*, reported a remarkably similar suite of behavioral responses to dissolved cues. Larvae of both species increased turning rates, decreased swimming speeds, and swam primarily downward upon stimulation with habitat cues in the water column (Tamburri *et al.*, 1992, 1996; Krug and Zimmer, 2000). These findings are consistent with the present results for competent larvae—those with a biological imperative to stay near the bottom and locate a settlement site. Although passive sinking would seem more effective at bringing larvae into contact with the seabed, live larvae opt to swim rather than sink. This behavior may allow larvae to change their distribution rapidly in response to physical and chemical cues, providing a distinct advantage during habitat selection over random, passive encounters with the bottom (Browne and Zimmer, 2001).

Consequences of developmental dimorphism for dispersal potential and habitat colonization

Developmental dimorphisms are maintained in populations by trade-offs between the advantages of dispersal and costs to the migratory morph (Roff, 1986, 1996; Langellotto *et al.*, 2000). Winged insect morphs can disperse through the air, locating high-quality resources and colonizing habitats after disturbances; however, due to costs of constructing and fueling large flight muscles, winged females have lower fecundities and winged males produce fewer mating calls than wingless conspecifics (Denno *et al.*, 1980, Roff and Fairbairn, 1991; Mole and Zera, 1993; Tanaka 1993; Crnokrak and Roff, 1995; Langellotto and Denno, 2001). Plants that colonize unpredictable environments often produce two types of seeds, one dropping near the parent and the other expressing a structure that can increase drag on a falling seed to aid dispersal by wind (Morse and Schmitt, 1985; Venable, 1985; Venable and Levin, 1985; Telenius and Torstensson, 1989; Imbert, 1999). Some coastal plants have dimorphic fruit segments, parts of which have a buoyant coat that increases dispersal in water (Payne and Maun, 1981). Dispersing seeds may have a reduced capacity for dormancy and phenotypic plasticity as adult plants, how-

ever (Venable and Levin, 1985, Telenius and Torstensson, 1989; Zhang, 1995).

In contrast to terrestrial examples cited above, in marine organisms dispersal dimorphisms involve altered time to competence or settlement preference among larvae, rather than changes in gross morphology (Chia *et al.*, 1996). Larval dispersal by ocean currents is an unavoidable consequence of development occurring in the water column and requires only minor adaptations for long-distance travel (Pechenik *et al.*, 1984; Strathmann, 1985). Physical differences between water and air contribute to the different dispersal strategies of marine and terrestrial organisms. Seawater is 850 times denser than air, providing a buoyant force for suspended organisms, and its 60-fold higher dynamic viscosity results in lower sinking rates for planktonic *versus* airborne particles (Power, 1989; Strathmann, 1990). Due to their physical environment, eggs and larvae of marine organisms can increase flotation by altering ionic or lipid composition, or counteract sinking by increasing drag through simple modifications of ciliated bands or velar lobes (Lambert and Lambert, 1978; Emlet, 1983; Chia *et al.*, 1984; Kelman and Emlet, 1999). Dimorphisms can therefore alter the dispersal potential of marine larvae by changing time to attainment of competence, without major alterations in bodily form or function.

One goal of this study was to compare traits relevant to dispersal and habitat colonization for long-lived, feeding larvae and short-lived, nonfeeding larvae of the same marine animal. Lecithotrophic larvae of *Alderia modesta* metamorphose within 2 d of hatching when *Vaucheria longicaulis* is present, but most die after a week if the alga is not encountered, thus limiting their dispersal potential (Krug, 2001). Extending the larval period by even a few days can result in high mortality and post-metamorphic costs for nonfeeding larvae, which may thus be under selective pressure to locate a high-quality settlement site quickly (Pechenik, 1999). Strong downward swimming should concentrate lecithotrophic larvae of *A. modesta* near the bed, increasing the likelihood of contact with *V. longicaulis* while minimizing the risks of transport from the natal habitat.

In contrast, planktotrophic larvae must survive a 4-week dispersal period before locating and settling in an appropriate environment. Based on drogue studies, Levin (1983) concluded that larvae with a planktonic phase longer than 3 weeks could exit Mission Bay (San Diego, CA) and be transported by along-shore currents. Populations of *A. modesta* are genetically homogenous from San Diego to Tomales Bay, California, indicating that exchange of larvae occurs between estuaries (Ellingson and Krug, unpubl. data). Adult *A. modesta* produce 10-fold more planktotrophic than lecithotrophic larvae (~300 *vs.* 30 larvae per clutch; Krug, 1998), but planktotrophic larvae face a high mortality rate. Only a small percentage of planktotrophic larvae are likely to reach competence, but the survivors have the potential to disperse and colonize distant patches.

In terms of overall size and swimming ability, mature planktotrophic and newly hatched lecithotrophic larvae of *A. modesta* were remarkably similar. Strikingly, competent larvae of both modes exhibited the same shadow response, which was absent in precompetent larvae. Such responses are known from a range of invertebrate taxa (Forward, 1984; Young and Chia, 1985; Buskey *et al.*, 1986), but their ecological significance remains unclear. This behavior is yet another response to an environmental cue that is shared by both types of competent larvae. In a prior study, both types of larvae exhibited qualitatively similar changes in behavior when stimulated with waterborne settlement cues from the host alga (Krug and Zimmer, 2000). Thus, both planktotrophic and lecithotrophic development converge on a phenotypically similar state of competence in this species.

Habitat selection occurs when competent larvae settle to the bottom and then initiate metamorphosis. No differences were observed between the two types of larvae of *A. modesta* in their degree of settlement specificity; competent larvae metamorphosed on the host alga *V. longicaulis*, and not on other macroalgae. Lecithotrophic larvae were previously shown to exhibit a high degree of specificity for the host-associated cue, metamorphosing in response to *V. longicaulis* but not to 17 alternative macroalgae (Krug, 2001). Limited availability of competent planktotrophic larvae precluded testing as many algal species, but long-lived larvae appear similarly able to differentiate among potential habitat cues. The one notable difference was that planktotrophic larvae rarely underwent spontaneous metamorphosis upon reaching competence, as larvae from some lecithotrophic clutches do in the first day after hatching (Krug, 2001). This trait is likely an adaptive response to the different dispersal strategies of the two development modes. Lecithotrophic larvae emerge in a suitable habitat, so combining spontaneous and *Vaucheria*-dependent metamorphosis is a viable bet-hedging dispersal strategy. In contrast, planktotrophic larvae may end up far from a good habitat after their month-long development, and consequently must delay metamorphosis until encountering the *Vaucheria*-associated cue.

In summary, competent planktotrophic and lecithotrophic larvae of *Alderia modesta* are qualitatively similar in swimming behavior and patterns of vertical movement, in their responses to light and waterborne chemical settlement cues, and in their metamorphic requirements. Selection for host-specific colonization has evidently preserved a common suite of traits in alternative developmental pathways, despite the radically different dispersal potentials of the two types. Nevertheless, small differences between the two types of larvae (in rates of net vertical displacement or spontaneous metamorphosis) may represent fine-tuning of

traits important in habitat selection, within the constraints imposed by their respective dispersal strategies.

Acknowledgments

This study was supported by awards from the National Science Foundation (OCE 02-42272, OCE 02-42321, and HRD 03-17772) and UCLA Council on Research. Access to the field site was provided by I. Kay through the Natural Reserve Office of the University of California. We thank J.T. Fingerut for help in modeling larval concentration profiles, and C.A. Zimmer and two anonymous referees for comments that greatly improved earlier drafts of the manuscript.

Literature Cited

Abbott, I. A., and G. J. Hollenberg. 1976. *Marine Algae of California.* Stanford University Press, Stanford, CA.

Bleakney, J. S., and K. H. Bailey. 1967. Rediscovery of the salt-marsh ascoglossan *Alderia modesta* Lovén in eastern Canada. *Proc. Malacol. Soc. Lond.* **37:** 347–349.

Browne, K. A., and R. K. Zimmer. 2001. Controlled field release of a waterborne chemical signal stimulates planktonic larvae to settle. *Biol. Bull.* **200:** 87–91.

Buskey, E. J., C. G. Mann, and E. Swift. 1986. The shadow response of the estuarine copepod *Acartia tonsa*. *J. Exp. Mar. Biol. Ecol.* **103:** 65–75.

Butman, C. A. 1987. Larval settlement of soft-sediment invertebrates: the spatial scales of pattern explained by habitat selection and the emerging role of hydrodynamic processes. *Oceanogr. Mar. Biol. Annu. Rev.* **25:** 113–165.

Butman, C. A., J. B. Grassle, and E. J. Buskey. 1988a. Horizontal swimming and gravitational sinking of *Capitella* sp. I (Annelida: Polychaeta) larvae: implications for settlement. *Ophelia* **29:** 43–57.

Butman, C. A., J. B. Grassle, and C. M. Webb. 1988b. Substrate choices made by marine larvae settling in still water and in a flume flow. *Nature* **333:** 771–773.

Caley, M. J., M. H. Carr, M. A. Hixon, T. P. Hughes, G. P. Jones, and B. A. Menge. 1996. Recruitment and the local dynamics of open marine populations. *Annu. Rev. Ecol. Syst.* **27:** 477–500.

Chester, C. M. 1996. The effect of adult nutrition on the reproduction and development of the estuarine nudibranch, *Tenellia adspersa* (Nordmann, 1845). *J. Exp. Mar. Biol. Ecol.* **198:** 113–130.

Chia, F.-S., J. Buckland-Nicks, and C. M. Young. 1984. Locomotion of marine invertebrate larvae: a review. *Can. J. Zool.* **62:** 1205–1222.

Chia, F.-S., G. D. Gibson, and P.-Y. Qian. 1996. Poecilogony as a reproductive strategy of marine invertebrates. *Oceanol. Acta* **19:** 203–208.

Crnokrak, P., and D. A. Roff. 1995. Fitness differences associated with calling behaviour in the two wing morphs of male sand crickets. *Gryllus firmus*. *Anim. Behav.* **50:** 1475–1481.

Crnokrak, P., and D. A. Roff. 1998. The genetic basis of the trade-off between calling and wing morph in males of the cricket *Gryllus firmus*. *Evolution* **52:** 1111–1118.

Denno, R. F., M. J. Raupp, D. W. Tallamy, and C. F. Reichelderfer. 1980. Migration in heterogenous environments: differences in wing forms of the dimorphic planthopper, *Prokelisia marginata* (Homoptera: Delphacidae). *Ecology* **61:** 850–867.

Denno, R. F., G. K. Roderick, M. A. Peterson, A. F. Huberty, G. D. Hartmut, M. D. Eubanks, J. E. Losey, and G. A. Langellotto. 1996. Habitat persistence underlies intraspecific variation in the dispersal strategies of planthoppers. *Ecol. Monogr.* **66:** 389–408.

Dixon, A. F. G. 1985. *Aphid Ecology.* Blackie, London.

Doyle, R. W. 1975. Settlement of planktonic larvae—theory of habitat selection in varying environments. *Am. Nat.* **109:** 113–126.

Doyle, R. W. 1976. Analysis of habitat loyalty and habitat preference in settlement behavior of planktonic marine larvae. *Am. Nat.* **110:** 719–730.

Eckman, J. E. 1990. A model of passive settlement by planktonic larvae onto bottoms of differing roughness. *Limnol. Oceanogr.* **35:** 887–901.

Eckman, J. E., F. E. Werner, and T. F. Gross. 1994. Modeling some effects of behavior on larval settlement in a turbulent boundary layer. *Deep-Sea Res. II* **41:** 185–208.

Emlet, R. B. 1983. Locomotion, drag, and the rigid skeleton of larval echinoderms. *Biol. Bull.* **164:** 433–445.

Fairbairn, D. J., and L. Desranleau. 1987. Flight threshold, wing muscle histolysis, and alary polymorphism: correlated traits for dispersal tendency in the Gerridae. *Ecol. Entomol.* **12:** 12–24.

Fingerut, J. T., C. A. Zimmer, and R. K. Zimmer. 2003. Larval swimming overpowers turbulent mixing and facilitates transmission of a marine parasite. *Ecology* **84:** 2502–2515.

Forward, R. B. 1984. Occurrence of a shadow response among Brachyuran larvae. *Mar. Biol.* **39:** 331–341.

Forward, R. B., T. W. Cronin, and D. E. Stearns. 1984. Control of diel vertical migration: photoresponses of a larval crustacean. *Limnol. Oceanogr.* **29:** 146–154.

Gibson, G. D., and F.-S. Chia. 1995. Developmental variability in the poecilogonous opisthobranch *Haminaea callidegenita:* life-history traits and effects of environmental parameters. *Mar. Ecol. Prog. Ser.* **121:** 139–155.

Gross, T. F., F. E. Werner, and J. E. Eckman. 1992. Numerical modeling of larval settlement in turbulent bottom boundary layers. *J. Mar. Res.* **50:** 611–642.

Grunbaum, D., and R. R. Strathmann. 2003. Form, performance and trade-offs in swimming and stability of armed larvae. *J. Mar. Res.* **61:** 659–691.

Hadfield, M. G., and M. F. Strathmann. 1996. Variability, flexibility and plasticity in life histories of marine invertebrates. *Oceanol. Acta* **19:** 323–334.

Hannan, C. A. 1984. Planktonic larvae may act like passive particles in turbulent near-bottom flows. *Limnol. Oceanogr.* **29:** 1108–1116.

Harrison, R. 1980. Dispersal polymorphisms in insects. *Annu. Rev. Ecol. Syst.* **11:** 95–118.

Hartog, C. Den, and C. Swennen. 1952. On the occurrence of *Alderia modesta* (Lovén) and *Limapontia depressa* A. & H. on the salt marshes of the Dutch Wadden Sea. *Beaufortia* **2:** 1–3.

Hellberg, M. E. 1996. Dependence of gene flow on geographic distance in two solitary corals with different larval dispersal capabilities. *Evolution* **50:** 1167–1175.

Hoagland, K. E., and R. Robertson. 1988. An assessment of poecilogony in marine invertebrates: phenomenon or fantasy? *Biol. Bull.* **174:** 109–125.

Imbert, E. 1999. The effects of achene dimorphism on the dispersal in time and space in *Crepis sancta* (Asteraceae). *Can. J. Bot.* **77:** 508–513.

Jonsson, P. R., C. André, and M. Lindegarth. 1991. Swimming behavior of marine bivalve larvae in a flume boundary-layer flow: evidence for near-bottom confinement. *Mar. Ecol. Prog. Ser.* **79:** 67–76.

Kelman, D., and R. B. Emlet. 1999. Swimming and buoyancy in ontogenetic stages of the cushion star *Pteraster tesselatus* (Echinoder-

mata: Asteroidea) and their implications for distribution and movement. *Biol. Bull.* **197:** 309–314.

Komar, P. D. 1976. Boundary layer flow under steady unidirectional currents. Pp. 91–106 in *Marine Sediment Transport and Environmental Managements,* D.J. Stanley and D.J.P. Swift, eds. John Wiley, New York.

Krug, P. J. 1998. Poecilogony in an estuarine opisthobranch: planktotrophy, lecithotrophy, and mixed clutches in a population of the ascoglossan *Alderia modesta. Mar. Biol.* **132:** 483–494.

Krug, P. J. 2001. Bet-hedging dispersal strategy of a specialist marine herbivore: a settlement dimorphism among sibling larvae of *Alderia modesta. Mar. Ecol. Prog. Ser.* **213:** 177–192.

Krug, P. J., and A. E. Manzi. 1999. Waterborne and surface-associated carbohydrates as settlement cues for larvae of the specialist marine herbivore *Alderia modesta. Biol. Bull.* **197:** 94–103.

Krug, P. J., and R. K. Zimmer. 2000. Developmental dimorphism and expression of chemosensory-mediated behavior: habitat selection by a specialist marine herbivore. *J. Exp. Biol.* **203:** 1741–1754.

Lambert, C. C., and G. Lambert. 1978. Tunicate eggs utilize ammonium ions for flotation. *Science* **200:** 64–65.

Langellotto, G. A., and R. F. Denno. 2001. Benefits of dispersal in patchy environments: mate location by males of a wing-dimorphic insect. *Ecology* **82:** 1870–1878.

Langellotto, G. A., R. F. Denno, and J. R. Ott. 2000. A trade-off between flight capability and reproduction in males of a wing-dimorphic insect. *Ecology* **81:** 865–875.

Levin, L. A. 1983. Drift-tube studies of bay-ocean water exchange and implications for larval dispersal. *Estuaries* **6:** 364–371.

Levin, L. A. 1984. Multiple patterns of development in *Streblospio benedicti* Webster (Spionidae) from three coasts of North America. *Biol. Bull.* **166:** 494–508.

Levin, L. A., and T. S. Bridges. 1995. Pattern and diversity in reproduction and development. Pp. 1–48 in *Ecology of Marine Invertebrate Larvae,* L. McEdward, ed. CRC Press, Boca Raton, FL.

Lythgoe, J. N. 1979. *The Ecology of Vision.* Oxford University Press, Oxford, UK.

Mann, R., and C. C. Wolf. 1983. Swimming behavior of larvae of the ocean quahog *Artica islandica* in response to pressure and temperature. *Mar. Ecol. Prog. Ser.* **13:** 211–218.

Mann, R., B. M. Campos, and M. W. Luckenbach. 1991. Swimming rate and responses of larvae of three mactrid bivalves to salinity discontinuities. *Mar. Ecol. Prog. Ser.* **68:** 257–269.

Middleton, P. S., and J. B. Southard. 1984. *Mechanics of Sediment Movement,* 2nd ed. Society of Economic Paleontologists and Mineralogists, Tulsa, OK.

Mileikovsky, S. A. 1973. Speed of active movement of pelagic larvae of marine bottom invertebrates and their ability to regulate their vertical position. *Mar. Biol.* **23:** 11–17.

Mole, S., and A. J. Zera. 1993. Differential allocation of resources underlies the dispersal-reproduction trade-off in the wing dimorphic cricket, *Gryllus rubens. Oecologia* **93:** 121–127.

Morse, D. H., and J. Schmitt. 1985. Diaspora size, shape, and fall behaviour in wind-dispersed plant species. *Oecologia* **67:** 372–379.

Obrebski, S. 1979. Larval colonizing strategies in marine benthic invertebrates. *Mar. Ecol. Prog. Ser.* **1:** 293–300.

Palumbi, S. R. 1995. Using genetics as an indirect estimator of larval dispersal. Pp. 369–387 in *Ecology of Marine Invertebrate Larvae,* L. McEdward, ed. CRC Press, Boca Raton, FL.

Pawlik, J. R. and C. A. Butman. 1993. Settlement of a marine tube worm as a function of current velocity: interacting effects of hydrodynamics and behavior. *Limnol. Oceanogr.* **38:** 1730–1740.

Payne, A. M., and M. A. Maun. 1981. Dispersal and floating ability of dimorphic fruit segments of *Cakile edentula* var. *lacustris. Can. J. Bot.* **59:** 2595–2602.

Pechenik, J. A. 1990. Delayed metamorphosis by larvae of benthic marine invertebrates: Does it occur? Is there a price to pay? *Ophelia* **32:** 63–94.

Pechenik, J. A. 1999. On the advantages and disadvantages of larval stages in benthic marine invertebrate life cycles. *Mar. Ecol. Prog. Ser.* **177:** 269–297.

Pechenik, J. A., R. S. Scheltema, and L. S. Eyster. 1984. Growth stasis and limited shell calcification in larvae of *Cymatium parthenopeum* during trans-Atlantic transport. *Science* **224:** 1097–1099.

Power, J. H. 1989. Sink or swim: growth dynamics and zooplankton hydromechanics. *Am. Nat.* **133:** 706–721.

Raimondi, P. T., and M. J. Keough. 1990. Behavioural variability in marine larvae. *Aust. J. Ecol.* **15:** 427–437.

Roff, D. A. 1986. The evolution of wing dimorphism in insects. *Evolution* **40:** 1009–1020.

Roff, D. A. 1996. The evolution of threshold traits in animals. *Q. Rev. Biol.* **71:** 3–35.

Roff, D. A., and D. J. Fairbairn. 1991. Wing dimorphism and the evolution of migratory polymorphisms among the Insecta. *Am. Zool.* **31:** 243–251.

Roughgarden, J., S. Gaines, and H. Possingham. 1988. Recruitment dynamics in complex life cycles. *Science* **241:** 1460–1466.

Scheltema, R. S. 1962. Dispersal of larvae by equatorial ocean currents and its importance to the zoogeography of shoal-water tropical species. *Nature* **217:** 1159–1162.

Semlitsch, R. D., R. N. Harris, and H. M. Wilbur. 1990. Paedomorphosis in *Ambystoma talpoideum:* maintenance of population variation and alternative life-history pathways. *Evolution* **44:** 1604–1613.

Strathmann, R. R. 1985. Feeding and nonfeeding larval development and life-history evolution in marine invertebrates. *Annu. Rev. Ecol. Syst.* **16:** 339–361.

Strathmann, R. R. 1990. Why life histories evolve differently in the sea. *Am. Zool.* **30:** 197–207.

Tamburri, M. N., R. K. Zimmer-Faust, and M. L. Tamplin. 1992. Natural sources and properties of chemical inducers mediating settlement of oyster larvae: a re-examination. *Biol. Bull.* **183:** 327–338.

Tamburri, M. N., C. M. Finelli, D. S. Wethey, and R. K. Zimmer-Faust. 1996. Chemical induction of larval settlement behavior in flow. *Biol. Bull.* **191:** 367–373.

Tanaka, S. 1993. Allocation of resources to egg production and flight muscle development in a wing dimorphic cricket, *Modicogryllus confirmatus. J. Insect Physiol.* **39:** 493–498.

Telenius, A., and P. Torstensson. 1989. The seed dimorphism of *Spergularia marina* in relation to dispersal by wind and water. *Oecologia* **80:** 206–210.

Thorson, G. 1950. Reproductive and larval ecology of marine bottom invertebrates. *Biol. Rev.* **25:** 1–45.

Todd, C. D. 1998. Larval supply and recruitment of benthic invertebrates: Do larvae always disperse as much as we believe? *Hydrobiologia* **375:** 1–21.

Todd, C. D., W. J. Lambert, and J. P. Thorpe. 1998. The genetic structure of intertidal populations of two species of nudibranch molluses with planktotrophic and pelagic lecithotrophic larval stages: Are pelagic larvae "for" dispersal? *J. Exp. Mar. Biol. Ecol.* **228:** 1–28.

Toonen, R. J., and J. R. Pawlik. 2001. Foundations of gregariousness: a dispersal polymorphism among the planktonic larvae of a marine invertebrate. *Evolution* **55:** 2439–2454.

Trowbridge, C. 1993. Local and regional abundance patterns of the ascoglossan opisthobranch *Alderia modesta* (Lovén, 1844) in the Northeastern Pacific. *Veliger* **36:** 303–310.

Ullberg, J., and E. Olafsson. 2003. Free-living marine nematodes actively choose habitat when descending from the water column. *Mar. Ecol. Prog. Ser.* **260:** 141–149.

Venable, D. L. 1985. The evolutionary ecology of seed heteromorphism. *Am. Nat.* **126:** 577–595.

Venable, D. L., and D. A. Levin. 1985. Ecology of achene dimorphism in *Heterotheca latifolia*. I. Achene structure, germination and dispersal. *J. Ecol.* **73:** 133–145.

Wang, W-X., and Z.-Z. Xu. 1997. Larval swimming and postlarval drifting behavior in the infaunal bivalve *Sinonovacula constricta*. *Mar. Ecol. Prog. Ser.* **148:** 71–81

Wieczorek, S. K., and C. D. Todd. 1998. Inhibition and facilitation of settlement of epifaunal marine invertebrate larvae by microbial biofilm cues. *Biofouling* **12:** 81–118.

Young, C. M. 1995. Behavior and locomotion during the dispersal phase of larval life. Pp. 247–277 in *Ecology of Marine Invertebrate Larvae*, L. McEdward, ed. CRC Press, Boca Raton, FL.

Young, C. M., and F.-S. Chia. 1985. An experimental test of shadow response function in ascidian tadpoles. *J. Exp. Mar. Biol. Ecol.* **85:** 165–175.

Zera, A. J., and R. F. Denno. 1997. Physiology and ecology of dispersal polymorphism in insects. *Annu. Rev. Entomol.* **42:** 207–230.

Zhang, J. 1995. Differences in phenotypic plasticity between plants from dimorphic seeds of *Cakile edentula*. *Oecologia* **102:** 353–360.

Reference: *Biol. Bull.* **207:** 247–256. (December 2004)

Chromosomal Rearrangement in Pectinidae Revealed by rRNA Loci and Implications for Bivalve Evolution

YONGPING WANG[1,2] AND XIMING GUO[1,*]

[1] *Haskin Shellfish Research Laboratory, Institute of Marine and Coastal Sciences, Rutgers University, 6959 Miller Avenue, Port Norris, New Jersey 08349; and* [2] *Experimental Marine Biology Laboratory, Institute of Oceanology, Chinese Academy of Sciences, 7 Nanhai Road, Qingdao, Shandong 266071, People's Republic of China*

Abstract. Karyotype and chromosomal localization of major (18–5.8–28S) and minor (5S) ribosomal RNA genes were studied in two species of Pectinidae, zhikong (*Chlamys farreri*) and bay (*Argopecten irradians irradians*) scallops, using fluorescence *in situ* hybridization (FISH). *C. farreri* had a haploid number of 19 with a karyotype of 3m + 4sm + 7sm-st + 4st + 1st-t, and *A. i. irradians* had a haploid number of 16 with a karyotype of 5st + 11t. In *C. farreri*, the major and minor rRNA genes had one locus each and were mapped to the same chromosome—Chromosome 5. In *A. i. irradians*, the major rRNA genes had two loci, located on Chromosomes 4 and 8, and the 5S rRNA gene was found at a third chromosome—Chromosome 10. Results of this and other studies indicate that karyotype of *A. i. irradians* (n = 16, 21 arms) is secondary and derived from an ancestral karyotype similar to that of *C. farreri* (n = 19, 38 arms) through considerable chromosomal loss and rearrangements. The ability to tolerate significant chromosomal loss suggests that the modal karyotype of Pectinidae and possibly other bivalves with a haploid number of 19 is likely tetraploid; *i.e.*, at least one genome duplication has occurred during the evolution of Bivalvia.

Introduction

Chromosomal changes, particularly polyploidy, have played a significant role in the evolution of plants, and most higher plants are recent polyploids (DeWit, 1980). Although polyploidy is relatively rare in animals, chromosomal changes are increasingly recognized as an important force in animal evolution. It is hypothesized that two rounds of genomic duplication occurred during the evolution of vertebrates leading to humans (Furlong and Holland, 2002; Spring, 2002). Chromosomal rearrangements may play a role in reproductive isolation and speciation, by creating barriers to meiotic pairing and reducing the fitness of hybrids (White, 1978; King, 1993). Genic theories, on the other hand, stress the importance of accumulation of genic mutations in reproductive isolation. Recent findings of effects of chromosomal rearrangements on recombination have bridged the gap between the chromosomal and genic theories of reproductive isolation, arguing for a major role of chromosomal changes in speciation (Rieseberg, 2001; Navarro and Barton, 2003). However, the extent of chromosomal changes and their roles in speciation are poorly understood in many animal taxa, including marine bivalves. Many marine bivalves are sympatric broadcast spawners whose mechanisms of reproductive isolation are particularly interesting but largely unknown. Chromosomal studies may provide a unique perspective on the evolution of marine bivalves.

Scallops, members of family Pectinidae, are widely distributed in world oceans. Scallops are characterized by two mostly equal and round valves with a byssal notch and ctenolium on the right valve. Most scallops are free living and mobile, and inhabit the surface of subtidal bottoms. Some species may use byssal threads for temporary attachment or cement themselves permanently onto hard surfaces. The earliest representative of Pectinidae appeared in the Triassic period about 230 million years ago, but most groups did not emerge until the early Paleocene, or 65 million years ago (Waller, 1991). The family contains about 360 living species, and many of them are important for

Received 5 April 2004; accepted 6 August 2004.

* To whom correspondence should be addressed. E-mail: xguo@hsrl.rutgers.edu

fishery and aquaculture production. Chromosome number and karyotype have so far been studied in 16 species of scallops (Beaumont and Gruffydd, 1974; Komaru and Wada, 1985; Insua *et al.*, 1998; Pauls and Affonso, 2000). Chromosome number and karyotype vary considerably. While most of the species have a haploid number of 19 chromosomes, some have 16 (Wada, 1978; Komaru and Wada, 1985), and one species, *Aequipecten opercularis*, has 13 (Beaumont and Gruffydd, 1974). Even among species with 19 pairs of chromosomes, variation in karyotype is apparent, and the number of telocentric chromosomes varies from zero in *Chlamys farreri* to 14 in *Pecten maximus* and *P. albicans* (Beaumont and Gruffydd, 1974; Komaru and Wada, 1985).

Clearly, significant changes in chromosome number and structure occurred during the evolution of Pectinidae. However, detailed analysis of chromosomal changes in scallops is hindered by the inability to identify individual chromosomes. Chromosome identification remains difficult in scallops as well as in most marine bivalves, primarily due to the lack of cell lines needed for preparing elongated chromosomes. Chromosome identification by traditional banding and using embryonic material is possible, but not practical. C-banding analysis has been studied in the queen scallop *Aequipecten opercularis*, but banding characteristics were not distinctive or reliable for routine chromosome identification (Insua *et al.*, 1998). Nucleolar organizer regions (NORs) have been studied in the queen scallop and the chilean-peruvian scallop *Argopecten purpuratus* (Insua *et al.*, 1998; Gajardo *et al.*, 2002), although NOR sites are not always reliable as chromosomal landmarks (Pauls and Affonso, 2000; Wang *et al.*, 2004). Recently, fluorescence *in situ* hybridization (FISH) has been used for chromosomal identification and karyotypic analysis in marine bivalves, providing clear and unambiguous identification of some chromosomes (*e.g.*, Insua *et al.*, 2001; Xu *et al.*, 2001; Wang *et al.*, 2004). The major (18S–5.8S–28S) and minor (5S) ribosomal RNA genes have been assigned to the chromosomes of *Aequipecten opercularis* (Insua *et al.*, 1998).

Major and minor rRNA genes are two distinct families of ribosomal RNA genes in higher eukaryotes. The two gene families are relatively independent of each other and often organized into separate loci on the same or different chromosomes (Martins and Galetti, 2001; Liu *et al.*, 2002). The major rRNA genes correspond to NORs and sometimes can be visualized by silver-staining. Both gene families are present in large numbers of tandem repeats, making them ideal targets for FISH. We studied the karyotype and chromosomal localization of the major and 5S rRNA genes by FISH in zhikong (*C. farreri*) and bay (*A. irradians irradians*) scallops, two Pectinid species with different haploid numbers. Surprisingly, the species with the lower haploid number (*A. i. irradians*, $n = 16$) had three rRNA-bearing chromosomes, while the species with the higher haploid number (*C. farreri*, $n = 19$) had one, suggesting that the karyotype of the latter is pleisomorphic.

Materials and Methods

Chromosome preparation

The zhikong scallops (*Chlamys farreri* Jones and Preston 1904) and bay scallops (*Argopecten irradians irradians* Lamarck 1819) used in this study were from hatcheries in Shandong, China. *C. farreri* is a native species of China and commonly found along much of that country's north and central coasts as well as in waters off Korea and Japan. *A. i. irradians* is native to the Atlantic coast of North America, and it was introduced to China in 1982 (Zhang *et al.*, 1986). *C. farreri* and *A. i. irradians* are the two most important scallop species cultured in China.

Metaphase chromosomes were prepared from early embryos, using the procedures described in Guo *et al.* (1992). Briefly, early embryos were treated with 0.005% colchicine for 15 min and 0.075 *M* KCl for 12 min, before being fixed in freshly prepared fixative, 1:3 (v:v) acetic acid and methanol. The fixative was changed at least twice, with a 15-min duration each time. The fixed samples were stored in the fixative at 4 °C until use. Chromosome samples were prepared by loading the fixed cell suspension onto preheated slides and air-dried. Slides were stored at 4 °C before FISH analysis.

Probe construction

Genomic DNA was extracted from adductor muscle by proteinase K digestion, according to the method described by Doyle and Doyle (1987). A fragment of the targeted ribosomal RNA locus was amplified, labeled with digoxigenin-11-dUTP (alkali-stable) by PCR incorporation. Digoxigenin-11-dUTP and all other PCR reagents were purchased from Roche Diagnostics (Indianapols, IN). Intergenic transcribed spacers between the 18S and 5.8S rRNA genes (ITS1) were used as probes for the major rRNA genes. The primer sequences were 5′-GGTTTCTGTAGGTGAACCTGC and 5′-CTGCGTTCTTCATCGACCC. For the 5S rRNA gene, primers were designed based on the published sequence of mussel *Mytilus edulis* 5S rRNA (GenBank accession no. J01869; Fang *et al.*, 1982): 5′-GTCTACGACCATATCACGTTGAAAA and 5′-TGTCTACAACACCCGGTATTCCC. The PCR reaction mixture (25 μl) contained 1.5 m*M* of $MgCl_2$; 0.2 m*M* each of dATP, dCTP, and dGTP; 0.13 m*M* dTTP; 0.07 m*M* digoxigenin-11-dUTP (for labeling); 0.63U Taq DNA polymerase; 0.4 mg/ml BSA; 1 μM of each primer; and 1 μg of genomic DNA. The PCR reaction was performed using a DeltaCycler II System thermal cycler, with an initial 5-min denaturation at 95 °C; followed by 35 cycles of 1-min denaturation at 95 °C, 1-min annealing at 50 °C, and 1-min extension at 72 °C;

and a final 5-min extension at 72 °C. PCR products were evaluated on 1% (w:v) agarose gels and visualized by 1 μg/ml ethidium bromide staining and ultraviolet illumination.

Fluorescence in situ *hybridization*

FISH was carried out according to Guo and Allen (1997a), with slight modifications. Chromosomes were pretreated by incubating the slides in 2× SSC (0.3 *M* sodium chloride, 0.03 *M* sodium citrate, pH 7.0) for 30 min at 37 °C; dehydrated in 70%, 80%, and 95% ethanol for 2 min each; and air-dried. Chromosomes were denatured in 70% formamide in 2× SSC (pH 7.0) at 72 °C for 2 min and then dehydrated in a cold ethanol series (70%, 80%, and 95%) and air-dried. The labeled probes were diluted in hybridization solution, 65% formamide in 2× SSC, at a ratio of 1:15; denatured at 72 °C for 5 min; and placed immediately on ice. Probe mixture (15–20 μl) was applied to each denatured slide, covered with a glass coverslip, and sealed with rubber cement. For dual-hybridization of two probes on the same metaphase, two probes were denatured and mixed before application. Slides were then incubated at 37 °C in a humidity incubator overnight for hybridization. After hybridization, the coverslips were removed and the slides were washed twice in 2× SSC at 72 °C for 5 min each time, with 1× PBT (0.1 *M* NaH_2PO_4, 0.4% BSA, 0.1% Tween-20, pH 7.4) at room temperature for 2 min. The digoxigenin-labeled probes were detected with fluorescein-labeled anti-digoxigenin antibody. Chromosomes were counterstained with 0.6 μg/ml of propidium iodide (PI) in antifade solution (Vector Laboratories) and viewed under a Nikon epifluorescence microscope. FISH signals and karyotype were captured using a 3CCD camera and analyzed using the Image-Pro Plus 3.0 software. Chromosomes were classified according to the criteria defined by Levan *et al.* (1964).

Results

Probe quality

All PCR amplifications were successful and produced specific fragments as visualized on agarose gels. Amplification with ITS1 primers in *Chlamys farreri* generated a single fragment at about 350 bp (Fig. 1A, Lane 2). The incorporation of digoxigenin-11-dUTP shifted the PCR product to about 480 bp (Fig. 1A, Lane 3), a sign of successful labeling. In *Argopecten irradians irradians*, the ITS1 fragment was slightly longer than that from *C. farreri*, or about 380 bp (Fig. 1B, Lane 2). The labeling with digoxigenin-11-dUTP shifted the fragment to about 500 bp.

PCR amplification with 5S rRNA primers generated a single fragment of about 120 bp, the expected size, in both species (Fig. 1A, B, Lane 4). Similarly, the mobility of the PCR product shifted to about 200 bp after the incorporation of digoxigenin-11-dUTP (Lane 5), indicating that the labeling was successful.

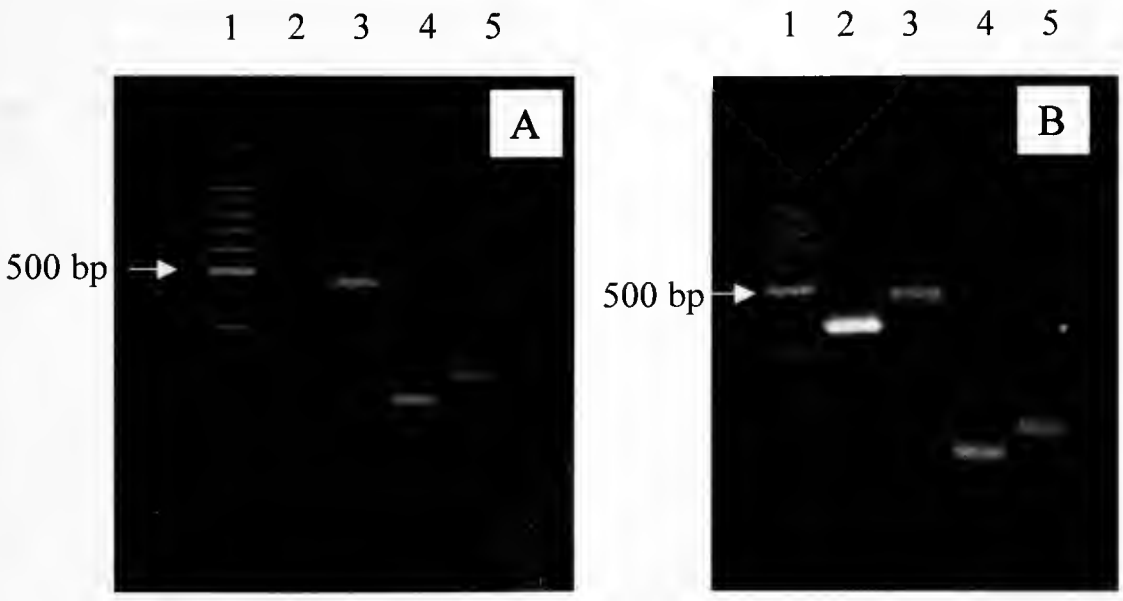

Figure 1. PCR products of intergenic transcribed spacer between 18S and 5.8S rRNA genes (ITS1) and 5S rRNA genes from *Chlamys farreri* (A) and *Argopecten irradians irradians* (B). Lane 1, 100-bp DNA ladder; Lanes 2 and 3, unlabeled and digoxigenin-labeled ITS1 products, respectively; Lanes 4 and 5, unlabeled and digoxigenin-labeled 5S rRNA gene products, respectively. Arrows indicate the location of 500-bp fragment.

Karyotype

Little variation in haploid number was observed among the metaphases screened in this study. The loss of one or two chromosomes was occasionally seen in a few metaphases that appeared to be overly spread. Analyses confirmed the haploid numbers previously reported for both species: 19 for *C. farreri* and 16 for *A. i. irradians*.

Fifteen metaphases that showed no chromosome overlapping or signs of chromosome loss were selected for karyotypic analysis. Chromosomes were measured after FISH. In addition to the difference in haploid number, the two species had strikingly different karyotypes. The karyotype of *C. farreri* consisted of the following chromosome types: three metacentric (m), four submetacentric (sm), seven submetacentric or subtelocentric (sm-st, centromeric index ± SD overlaps two categories), four subtelocentric (st), and one subtelocentric or telocentric (st-t) (Table 1). In comparison, the karyotype of *A. i. irradians*, 5st + 11t, contained only subtelocentric and telocentric chromosomes and no metacentric or submetacentric chromosomes (Table 2). Although the pairing of some chromosomes is subjective because of similarities in length and arm ratio, the number of different types of chromosomes clearly set the two karyotypes apart.

18S-5.8S-28S rRNA genes

The major rRNA genes were easily detected with the ITS1 probes. Strong FISH signals were found on interphase nuclei and metaphase chromosomes in both species. The number of signals per nucleus was variable, which was expected because of varying stages of the cell cycle and overlapping signals. The number of signals per metaphase was consistent. In *C. farreri*, the number of FISH signals per nucleus varied between one and two. For metaphases, FISH signals were consistently found on two (or one pair of) chromosomes (Fig. 2A). Karyotypic analysis indicated that the FISH signals were located on the telomeric region of the short arm of Chromosome 5 (Fig. 2H), a submetacentric or subtelocentric chromosome with a centric index of 0.25 ± 0.03. In *A. i. irradians*, two to four FISH signals were observed in interphase nuclei. For metaphases, FISH signals were observed on two pairs of chromosomes (Fig. 2E). Karyotypic analysis showed that the FISH signals were located on Chromosomes 4 and 8 (Fig. 2I). Both chromosomes were subtelocentric, and the FISH signals were in telomeric regions of the short arms.

Table 1

Karyotype analysis of 15 metaphases in zhikong scallop Chlamys farreri

Chromosome no.	Relative length (mean ± SD)	Centromeric index (mean ± SD)	Classification[1]
1	6.79 ± 0.15	0.31 ± 0.03	sm
2	6.60 ± 0.25	0.23 ± 0.03	sm/st
3	6.46 ± 0.15	0.29 ± 0.04	sm
4	6.17 ± 0.24	0.23 ± 0.02	st
5	5.95 ± 0.32	0.25 ± 0.03	sm/st
6	5.78 ± 0.25	0.31 ± 0.03	sm
7	5.60 ± 0.16	0.23 ± 0.04	sm/st
8	5.36 ± 0.39	0.28 ± 0.05	sm/st
9	5.35 ± 0.35	0.43 ± 0.03	m
10	5.27 ± 0.04	0.25 ± 0.03	sm/st
11	5.03 ± 0.12	0.20 ± 0.04	st
12	4.86 ± 0.20	0.28 ± 0.04	sm/st
13	4.78 ± 0.47	0.11 ± 0.02	st/t
14	4.77 ± 0.32	0.41 ± 0.05	m
15	4.62 ± 0.16	0.25 ± 0.03	sm/st
16	4.45 ± 0.20	0.22 ± 0.01	st
17	4.16 ± 0.11	0.27 ± 0.02	sm
18	4.01 ± 0.24	0.42 ± 0.03	m
19	3.97 ± 0.21	0.15 ± 0.02	st

[1] m = metacentric, sm = submetacentric, st = subtelocentric, t = telocentric; m/sm, sm/st, and st/t are chromosomes overlapping two categories.

Table 2

Karyotype analysis of 15 metaphases in bay scallop Argopecten irradians irradians

Chromosome no.	Relative length (mean ± SD)	Centromeric index (mean ± SD)	Classfication[1]
1	8.40 ± 0.52	0	t
2	8.23 ± 0.59	0.15 ± 0.01	st
3	7.73 ± 0.40	0	t
4	6.95 ± 0.24	0.20 ± 0.02	st
5	6.75 ± 0.06	0	t
6	6.39 ± 0.36	0.20 ± 0.02	st
7	6.23 ± 0.16	0	t
8	6.21 ± 0.39	0.16 ± 0.02	st
9	5.98 ± 0.09	0	t
10	5.82 ± 0.40	0	t
11	5.70 ± 0.11	0	t
12	5.53 ± 0.13	0	t
13	5.34 ± 0.32	0	t
14	5.02 ± 0.29	0.20 ± 0.02	st
15	5.07 ± 0.08	0	t
16	4.64 ± 0.20	—	t

[1] st = subtelocentric; t = telocentric.

5S rRNA genes

Compared with the FISH signals generated by the ITS1 probe for major rRNA genes, those from the 5S probe were relatively weak, but strong enough for unambiguous chromosomal assignment. As with ITS1, the number of signals varied in interphase nuclei but was consistent on metaphase chromosomes. In both species, FISH signals were found on two (or one pair of) chromosomes (Fig. 2B, F). In both species, the 5S locus was at an interstitial site on the long arms, about 1/3 arm length away from the telomere and 2/3 arm length from the centromere.

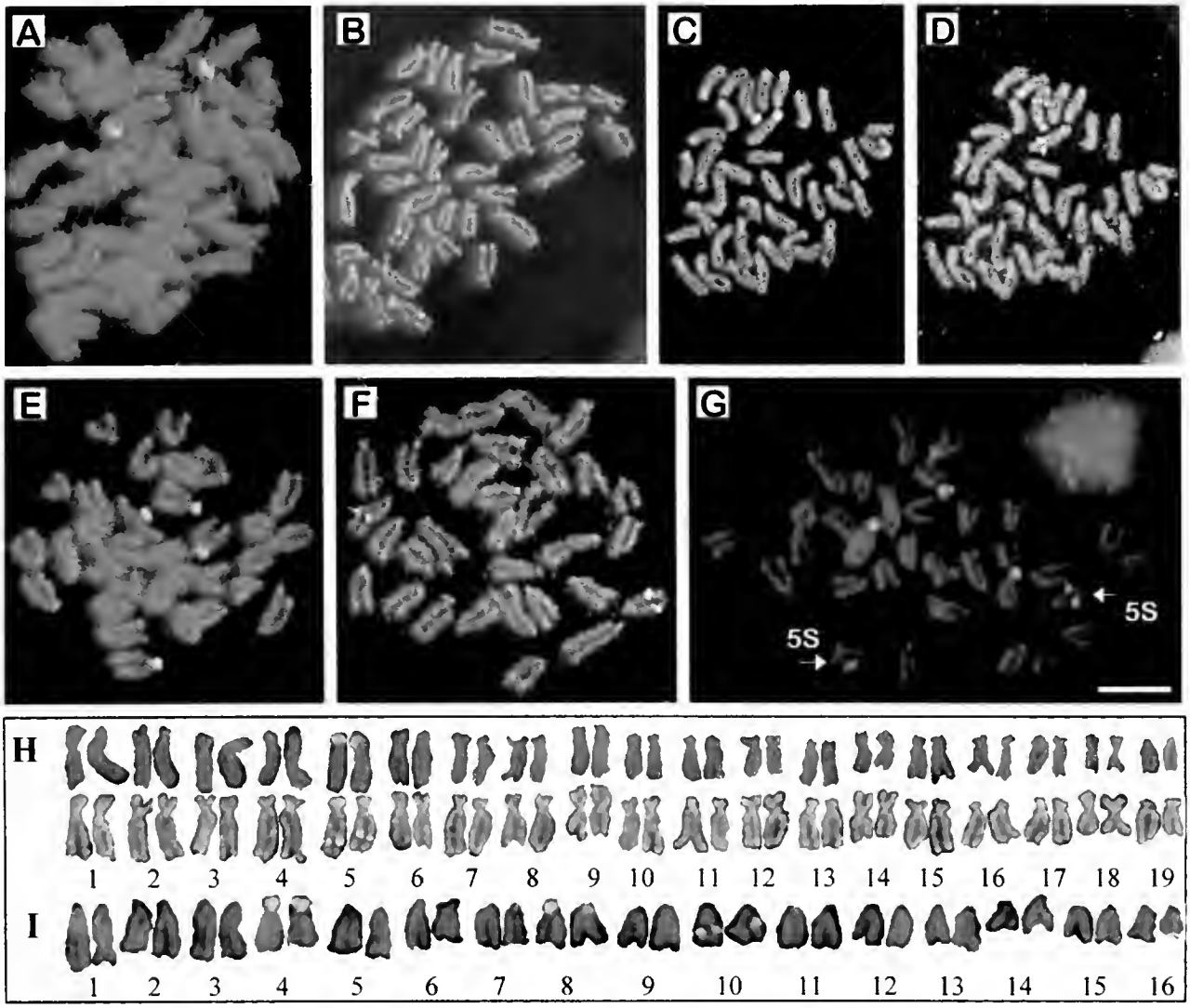

Figure 2. FISH signals and chromosomal location of the major rRNA genes (ITS1) and 5S rRNA genes in *Chlamys farreri* and *Argopecten irradians irradians*. (A) ITS1 in *C. farreri;* (B) 5S rRNA in *C. farreri;* (C and D) ITS1 and 5S on the same metaphase in *C. farreri;* (E) ITS1 in *A. i. irradians;* (F) 5S in *A. i. irradians;* (G) ITS1 and 5S on the same metaphase in *A. i. irradians* with arrows pointing to signals from 5S rRNA; (H) karyotypes of *C. farreri;* and (I) karyotype of *A. i. irradians*. Scale bar = 5 μm.

To determine whether the 5S and the major rRNA genes are linked on the same chromosome, the two gene families were located on the same metaphase by dual-hybridization. In *C. farreri*, the two genes were located on the same chromosome (Fig. 2C, D), but in different regions. The rRNA gene-bearing chromosome was Chromosome 5 (Fig. 2H), as previously shown. In *A. i. irradians*, the 5S genes were not associated with the two chromosome pairs that carried the major rRNA genes (Fig. 2G). Instead, they were located on Chromosome 10, a telocentric chromosome (Fig. 2H).

The karyotypic characteristics of *C. farreri* and *A. i. irradians* are summarized in Table 3, along with those of 14 other species studied so far. In addition to differences in haploid number and chromosome morphology, the number and distribution of rRNA gene loci represent another major difference between *C. farreri* and *A. i. irradians*. *C. farreri* had only one chromosome carrying rRNA genes, while *A. i. irradians* had three. *C. farreri* had 38 chromosomal arms, while *A. i. irradians* had 21.

Discussion

Karyotype and rRNA loci

This study provides unambiguous chromosomal mapping of the major (18S–5.8S–28S) and minor (5S) rRNA genes in *Chlamys farreri* and *Argopecten i. irradians*. As far as we can determine, this is the first time that specific genes have

been assigned to chromosomes in the two scallop species. Before this study, chromosomal location of ribosomal RNA genes had been determined using FISH in only one species of scallops—*Aequipecten opercularis* (Insua *et al.*, 1998). In *Nodipecten nodosus* and *Argopecten purpuratus*, two to three Ag-NOR sites were reported at variable locations (Pauls and Affonso, 2000; Gajardo *et al.*, 2002). NORs are supposed to be actively transcribed rRNA sites; however, the number and location of NORs are often variable and may not always provide accurate location of the major rRNA genes (Wang *et al.*, 2004).

This study provides a karyotype for *A. i. irradians*, which has not been described before. The karyotype we describe, 5st + 11t, is identical to that of another species of the same genus, *A. purpuratus*, described by Gajardo *et al.* (2002); it differs, however, from the *A. purpuratus* karyotype of Von Brand *et al.* (1990) (Table 3). As pointed out by Gajardo *et al.* (2002), the karyotype of Von Brand *et al.* (1990) may not be based on proper measurements. The karyotype of *C. farreri* we describe is similar to that described by Komaru and Wada (1985) for the same species.

Modal haploid number and karyotype of Pectinidae

The findings of this study, along with available data from the literature (Table 3), support the hypothesis that the haploid number, $n = 19$, is the modal or ancestral number for Pectinidae. This hypothesis is based on the fact that most of the species across four genera studied so far have a haploid number of 19 (White, 1954; Beaumont and Zouros, 1991). The other chromosome numbers, $n = 13$ in *Aequipecten opercularis* and $n = 16$ in *Argopecten purpuratus*, were considered as derived primarily because they were less frequent (Beaumont and Gruffydd, 1974; Insua *et al.*, 1998; Gajardo *et al.*, 2002). The assumption that common features are pleisomorphic is not necessarily true. This study provides another and perhaps more convincing evidence that 19 is the modal haploid number of Pectinidae. The finding that *C. farreri* ($n = 19$) has one major rRNA locus and one rRNA-bearing chromosome while *A. i. irradians* ($n = 16$) has two major rRNA loci and three rRNA-bearing chromosomes suggests that the karyotype of *C. farreri* is pleisomorphic and that of *A. i. irradians* is derived. A single locus for rRNA genes is considered as the ancestral state within taxa (Hsu *et al.*, 1975). It is more likely that the one rRNA-bearing chromosome in *C. farreri* splits into three chromosomes than that the three chromosomes consolidate into one. In vertebrates, the major and 5S rRNA genes are rarely located on the same chromosome (Schmid *et al.*, 1987; Lucchini *et al.*, 1993; Mäkinen *et al.*, 1997). The two gene families are found on the same chromosome in the nematode *Meloidogyne arenaria* (Vahidi *et al.*, 1991) and in the gastropod periwinkle *Melarhaphe neritoides* (Colomba *et al.*, 2002).

Given that $n = 19$ is the ancestral haploid number, the

Table 3

Summary of karyotypic data from 16 species of Pectinidae

Species	Haploid number	Arm number	Karyotype[1]							18S	5S	Reference
			m	m/sm	sm	sm/st	st	st/t	t			
Aequipecten opercularis	13	19	2	4	0	0	0	0	7	7q	1q,1q	Insua *et al.*, 1998
Argopecten i. irradians	16	21	0	0	0	0	5	0	11	4p,8p	10q	This study
Argopecten purpuratus	16	21	0	0	0	0	5	0	11			Gajardo *et al.*, 2002
	16	28	2	7	0	0	3	0	4			Von Brand *et al.*, 1990
Chlamys nobilis	16	19	3	0	0	0	0	0	13			Komaru and Wada, 1985
Chlamys glabra	14	—										Rasotto *et al.*, 1981
Chlamys farreri	19	38	3	0	4	7	4	1	0	5p	5q	This study
	19	38	3	0	1	6	7	2	0			Komaru and Wada, 1985
Chlamys distorta	19	—										Beaumount and Gruffydd, 1974
Chlamys islandica	19	—										Beaumount and Gruffydd, 1974
Chlamys varia	19	—										Beaumount and Gruffydd, 1974
Euvola ziczac	19	37	5	0	6	0	7	0	1			Basoa *et al.*, 2000
Nodipecten nodosus	19	38	6	0	6	0	7	0	0			Pauls and Affonso, 2000
	19	35	4	0	5	0	7	0	3			Basoa *et al.*, 2000
Patinopecten yessoensis	19	35	2	1	4	6	3	0	3			Komaru and Wada, 1985
Pecten albicans	19	24	1	1	0	3	0	0	14			Komaru and Wada, 1985
	19	26	0	3	0	0	4	0	12			Ieyama, 1975
Pecten maximus	19	24	2	0	2	0	1	0	14			Beaumount and Gruffydd, 1974
Pecten jacobeus	19	—										Rasotto *et al.*, 1981
Placopecten magellanicus	19	30	0	0	5	0	10	0	4			Xiang *et al.*, 1993

[1] m = metacentric, sm = submetacentric, st = subtelocentric, t = telocentric; m/sm, sm/st, and st/t are chromosomes overlapping two categories.

karyotype of *C. farreri*, which has the highest number of chromosomal arms (38, Table 3), is probably the closest representative of the ancestral karyotype of Pectinidae. Karyotypes with metacentric or submetacentric chromosomes are considered as more pleisomorphic than those with telocentric and subtelocentric chromosomes (Thiriot-Quiévreux, 1994). We argue that karyotypic changes in Pectinidae started with a karyotype with a haploid number of 19 and 38 arms, similar to that of *C. farreri*, and involved gradual loss of arms by deletion and of whole chromosomes by fusion, leading to all other variant karyotypes in Pectinidae.

Fossil records suggest that the *Aequipecten* group (including *Argopecten*) is a descendent of the *Chlamys* stem group from about 60 million years ago (Waller, 1991). Phylogenetic trees constructed using molecular data are consistent with fossil records and also indicate that the *Aequipecten* group is derived from the *Chlamys* group (Rice *et al.*, 1993; Barucca *et al.*, 2004). Interestingly, three species with reduced chromosome numbers, *Aequipecten opercularis*, *A. i. irradians* and *Chlamys glabra* (Table 3), are found in a single clade distal from the root on the phylogenetic tree of Barucca *et al.* (2004), supporting our conclusion that karyotype of *A. i. irradians* is derived.

Chromosomal rearrangements in Pectinidae

Robertsonian centric fusion has been used to explain chromosome number reductions in Pectinidae. Beaumount and Zouros (1991) postulated that the *Chlamys nobilis* karyotype ($n = 16$), which has 3 metacentric and 13 telocentric chromosomes (Komaru and Wada, 1985), may be derived from the $n = 19$ karyotype, by Robertsonian fusion of three pairs of telocentric chromosomes. Similarly, the karyotype of *Aequipecten opercularis* ($n = 13$), which has 6 metacentric and submetacentric chromosomes and 7 telocentric chromosomes, can also be explained by Robertsonian fusion (Beaumont and Gruffydd, 1974; Insua *et al.*, 1998).

There is no question that centric fusion plays a role in chromosome number reduction in Pectinidae. However, the karyotype of *A. i. irradians* described in this study and that of *A. purpuratus* (Gajardo *et al.*, 2002), both with a reduced haploid number of 16 and without any metacentric chromosomes, cannot be explained by centric fusion alone. They have to involve the loss of chromosome arms after centric fusion. Furthermore, fusion alone cannot explain chromosomal arm losses in scallops with the haploid number of 19, but chromosomal deletion can (Table 3).

We argue that chromosomal deletion is a major feature of karyotypic changes in Pectinidae, as indicated by the wide range of chromosomal arms (19–38, Table 3) and DNA contents (2.23–3.28 pg per diploid genome) (Rodríguez-Juíz *et al.*, 1996; Gonzáles-Tizón *et al.*, 2000; Thiriot-Quiévreux, 2002). The four species with reduced haploid numbers (13 or 16) have an average of 20 chromosome arms, ranging from 19 to 21 (Table 3). On the other hand, the four species with the ancestral haploid number ($n = 19$) have an average of 30 chromosome arms, ranging from 24 to 38. The loss of chromosome arms is likely caused by chromosomal deletion, rather than relocation, as the reduction in arm number in *Aequipecten opercularis* (by 20.8%) corresponds to a similar reduction in DNA content (by 21.2%), using *Pecten maximus* as a reference species (Rodríguez-Juíz *et al.*, 1996). More data on DNA content from other species are needed to verify the correlation.

Results of this study also suggest that chromosomal translocation and duplication may play a role in karyotypic evolution in Pectinidae. The finding that the major and minor rRNA genes are located on the same chromosome in *C. farreri* but on two different chromosomes in *A. i. irradians* can be explained by translocation. The fact that *A. i. irradians* has two loci for the major rRNA genes while *C. farreri* has only one points to chromosomal duplication, possibly through unequal translocation.

We speculate that the karyotype of *A. i. irradians* is evolved from an ancestral karyotype of $n = 19$, similar to that of *C. farreri*, possibly involving the following steps: (1) loss of the chromosomal arms and emergence of telocentric chromosomes; (2) fusion of telocentric chromosomes; (3) deletion of chromosomal arms after fusion; and (4) translocation and duplication of the major rRNA loci. Further studies involving more species may improve our understanding of karyotypic changes in Pectinidae.

Evolutionary implications: Is the ancestral karyotype tetraploid?

Assuming that the karyotype of *C. farreri* represents the ancestral/modal form ($n = 19$, 38 arms), evolution leading to the *Aequipecten* ($n = 13$) and *Argopecten* ($n = 16$) is accompanied by significant loss of chromosomal arms (by about 50%). If this is true, it raises the question of why scallops can tolerate so much chromosomal loss. The most obvious explanation is that the ancestral karyotype, $n = 19$, may be polyploid. Polyploid species are known to tolerate considerable loss of chromosomes (White, 1978). We hypothesize that the ancestral karyotype of Pectinidae ($n = 19$) is tetraploid and evolved by genome duplication from an ancestral bivalve with a haploid number of about 10, similar to that of Ostreidae ($n = 10$). During or soon after the genome duplication, one pair of chromosomes was lost, leading to a relatively stable karyotype of $n = 19$. Since most bivalves studied so far have a haploid number of 19 chromosomes (Nakamura, 1985; Rodríguez-Juíz *et al.*, 1996; Thiriot-Quiévreux, 2002), it is possible that all bivalve groups with a modal haploid number of 19 are tetraploid and derived from a common diploid or triploid

ancestor. Bivalve species with variant haploid numbers between 13 and 16 represent a triploid state, either derived from the diploid species or formed through chromosome reduction from the tetraploid form by a process similar to that found in Pectinidae.

Ostreidae, with a haploid number of 10 in most member species studied so far (Nakamura, 1985; Thiriot-Quiévreux, 2002), may represent the closest relative of the diploid ancestor. Triploid and tetraploid oysters are fully viable and phenotypically indistinguishable from diploids (Stanley *et al.*, 1981; Guo *et al.*, 1996). Triploid and tetraploid oysters can easily tolerate the loss of two chromosomes in one generation without obvious deleterious effects, while diploids can rarely tolerate the loss of one (Wang *et al.*, 1999). Polyploid oysters can lose chromosomes *de novo* and can even revert from triploidy to diploidy or from tetraploidy to triploidy (Allen *et al.*, 1997). Tetraploids in the Pacific oysters produce significant proportions of aneuploid gametes with chromosome losses due to multivalent formation (Guo and Allen, 1997b). Therefore, genome duplication from $n = 10$ to $n = 19$ is theoretically possible. A quick examination of limited data on DNA content seems to support the genome duplication hypothesis. DNA content per diploid nucleus ranged from 1.82 to 2.33 pg in Ostreidae, compared to 2.83–3.94 pg in bivalves with a haploid number of 19 chromosomes (Rodríguez-Juíz *et al.*, 1996; Gonzáles-Tizón *et al.*, 2000; Thiriot-Quiévreux, 2002). Minor deviations in DNA content and chromosome numbers can be explained by chromosomal losses or gains, and the pattern is in general agreement with the genome duplication hypothesis.

In summary, we suggest that at least one genome duplication event has occurred during the evolution of bivalves. The tetraploid hypothesis is primarily based on the findings that (1) the ancestral karyotype of Pectinidae ($n = 19$) can tolerate significant amount of chromosome loss, leading to the formation of *A. i. irradians* (this study); (2) most bivalves have a haploid number of 19 (Nakamura, 1985; Rodríguez-Juíz *et al.*, 1996; Thiriot-Quiévreux, 2002), while Ostreidae has a modal haploid number of 10; and (3) there is a general correlation between chromosome number and DNA content, and variations can be explained by chromosomal deletion, fusion, translocation, and limited duplication, as shown for Pectinidae in this study. Although our hypothesis on genome duplication is somewhat speculative, it is the most logical explanation of available data and provides a theoretical framework for further testing and analysis. Phylogenetic relationships among most bivalve groups are not well understood (Schneider, 2001). Recently, molecular studies have produced phylogenetic trees that are in general agreement about the relationship among most major groups (Adamkewicz *et al.*, 1997; Giribet and Wheeler, 2002; Giribet and Distel, 2003). Supporting our genome duplication hypothesis, the basal positions of the phylogenetic trees are dominated by species with low haploid numbers, including Ostreidae ($n = 10$) and Solemya ($n = 11$); the derived branches are dominated by species with $n = 19$; and species with $n = 14$ lie in between. Two of the three trees are rooted with Polyplacophora (Adamkewicz *et al.*, 1997; Giribet and Distel, 2003), which has a modal haploid number of $n = 12$ (Patterson, 1969) and is a close relative of the bivalves. It is possible that Polyplacophora and Bivalvia share a common ancestor which, after genome duplication, gave rise to scallops and clams with haploid numbers of 19.

Clearly, significant chromosomal rearrangements occurred during the evolution of Pectinidae and Bivalvia. Whether these changes are the driving forces for speciation or merely byproducts of other evolutionary events remains unclear. It is possible that scallops with reduced chromosome numbers evolved as a result of chromosomal rearrangements, but supporting data are yet to be collected. *C. farreri* and *A. i. irradians* can cross-fertilize with a success level of up to 90%, and the larvae can survive for 12 days (Chen *et al.*, 1991), but no viable hybrids have been reported. It is not known if the postzygotic barrier to hybridization is chromosomal or genic. This study does demonstrate the usefulness of FISH analysis and the need for similar studies in more species of pectinids and other bivalves.

Acknowledgements

The authors thank Drs. Ning Gong and Xiaojun Zhang, Institute of Oceanology, Chinese Academy of Sciences, for kindly providing metaphase material from bay scallops. We thank Dr. Ken Halanych and anonymous reviewers for constructive comments. This study is conducted at Rutgers University and supported by grants from the U.S. Sea Grant (B/T-9801; R/OD-2003-1), U.S. Department of Agriculture (96-35205-3854), and New Jersey Commission on Science and Technology (02-2042-007-11). Part of the work is supported by grants from China's Natural Science Foundation (39825121 and 30230280), the 863 program (2001AA628150) and Chinese Academy of Sciences. This is Publication IMCS-2004-11 and NJSG-04-566.

Literature Cited

Adamkewicz, S. L., M. G. Harasewych, J. Blake, D. Saudek, and C. J. Bult. 1997. A molecular phylogeny of the bivalve mollusks. *Mol. Biol. Evol.* **14:** 619–629.

Allen, S. K., Jr., X. Guo, G. Burreson, and R. Mann. 1997. Heteroploid mosaics and reversion among triploid oysters, *Crassostrea gigas*: fact or artifact? *J. Shellfish Res.* **15:** 514.

Barucca, M., E. Olmo, S. Schiaparelli, and A. Canapa. 2004. Molecular phylogeny of the family Pectinidae (Mollusca: Bivalvia) based on mitochondrial 16S and 12S rRNA genes. *Mol. Phylogenet. Evol.* **31:** 89–95.

Basoa, E., C. Alfonsi, J. E. Perez, and H. Cequea. 2000. Karyotypes on the scallops *Euvola ziczac* and *Nodipecten nodosus* from the Gulf of

Cariaco, Sucre State, Venezuela. *Bol. Inst. Oceanogr. Venez.* **39:** 49–54.

Beaumont, A. R., and L. D. Gruffydd. 1974. Studies on the chromosomes of the scallop *Pecten maximus* (L.) and related species. *J. Mar. Biol. Assoc. UK* **54:** 713–718.

Beaumont, A. R., and E. Zouros. 1991. Genetics of scallops. Pp. 585–623 in *Scallops: Biology, Ecology and Aquaculture*, S. E. Shumway, ed. Elsevier, Amsterdam.

Chen, Q., J. Xiang, Y. Qin, B. Kou, and H. Wang. 1991. Study on the possibility of hybridization and breeding between *Argopecten irradians, Chlamys farreri*, and *Patinonecten yessoensis* 1. The affinity of heterogametes between the three species of scallops and early development of hybrids. Pp. 122–128 in *Annual Research Report of the Experimental Marine Biology Laboratory Institute of Oceanology, Academia Sinica*, C. Zeng, and X. Feng, eds. Qingdao Ocean University Press, Qingdao, China (in Chinese).

Colomba, M. S., R. Vitturi, L. Castriota, R. Bertoni, and A. Libertini. 2002. FISH mapping of 18S–28S and 5S ribosomal DNA, $(GATA)_n$ and $(TTAGGG)_n$ telomeric repeats in the periwinkle *Melarhaphe neritoides* (Prosobranchia, Gastropoda, Caenogastropoda). *Heredity* **88:** 381–384.

DeWit, J. M. J. 1980. Origins of polyploids. Pp. 3–15 in *Polyploidy, Biological Relevance*, W. H. Lewis, ed. Plenum Press, New York.

Doyle, J. J., and J. L. Doyle. 1987. A rapid DNA isolation procedure for small quantities of fresh leaf tissue. *Phytochem. Bull.* **19:** 11–15.

Fang, B.L., R. De Baere, A. Vandenberghe, and R. De Wachter. 1982. Sequences of three molluscan 5 S ribosomal RNAs confirm the validity of a dynamic secondary structure model. *Nucleic Acids Res.* **10:** 4679–4685.

Furlong, R. F., and P. W. H. Holland. 2002. Were vertebrates octoploid? *Philos. Trans. R. Soc. B* **357:** 531–544.

Gajardo, G., M. Parraguez, and N. Colihueque. 2002. Karyotype analysis and chromosome banding of the Chilean-Peruvian scallop *Argopecten purpuratus* (Lamarck, 1819). *J. Shellfish Res.* **21:** 585–590.

Giribet, G., and D. L. Distel. 2003. Bivalve phylogeny and molecular data. Pp. 45–90 in *Molecular Systematics and Phylogeography of Mollusks*, C. Lydeard and D.R. Lindberg, eds. Smithsonian Books, Washington, DC.

Giribet, G., and W. C. Wheeler. 2002. On bivalve phylogeny: a high-level analysis of the Bivalvia (Mollusca) based on combined morphology and DNA sequence data. *Invertebr. Biol.* **121:** 271–324.

Gonzáles-Tizón, A. M., A. Martínez-Lage, I. Rego, J. Ausió, and J. Méndez. 2000. DNA content, karyotypes, and chromosomal location of 18S-5.8S-28S ribosomal loci in some species of bivalve molluscs from the Pacific Canadian coast. *Genome* **43:** 1065–1072.

Guo, X., and S. K. Allen, Jr. 1997a. Fluorescence *in situ* hybridization of the vertebrate telomere sequence to chromosome ends of the Pacific oyster, *Crassostrea gigas* Thunberg. *J. Shellfish Res.* **16:** 87–89.

Guo, X., and S. K. Allen, Jr. 1997b. Sex and meiosis in autotetraploid Pacific oyster, *Crassostrea gigas* (Thunberg). *Genome* **40:** 397–405.

Guo, X., K. Cooper, W. K. Hershberger, and K. K. Chew. 1992. Genetic consequences of blocking polar body 1 with cytochalasin B in fertilized eggs of the Pacific oyster, *Crassostrea gigas*: I. Ploidy of resultant embryos. *Biol. Bull.* **183:** 381–386.

Guo, X., G. DeBrosse, and S. K. Allen, Jr. 1996. All-triploid Pacific oysters (*Crassostrea gigas* Thunberg) produced by mating tetraploids and diploids. *Aquaculture* **142:** 149–161.

Hsu, T. C., S. E. Spirito, and M. L. Pardue. 1975. Distribution of 18 + 28 S ribosomal genes in mammalian genomes. *Chromosoma* **53:** 25–36.

Ieyama, H. 1975. Chromosome number of three species in three families of Pteriomorphia (Bivalvia). *Venus Jpn. J. Malacol.* **34:** 26–32.

Insua, A., M. J. Lopez-Pinon, and J. Mendez. 1998. Characterization of *Aequipecten opercularis* (Bivalvia: Pectinidae) chromosomes by different staining techniques and fluorescent *in situ* hybridization. *Genes Genet. Syst.* **73:** 193–200.

Insua, A., R. Freire, J. Rios, and J. Mendez. 2001. The 5S rDNA of mussels *Mytilus galloprovincialis* and *M. edulis:* sequence variation and chromosomal location. *Chromosome Res.* **9:** 495–505.

King, M. 1993. *Species Evolution: The Role of Chromosome Change.* Cambridge University Press, Cambridge.

Komaru, A., and K. T. Wada. 1985. Karyotypes of four species in the Pectinidae (Bivalvia: Pteriomorphia). *Venus Jpn. J. Malacol.* **44:** 249–259.

Levan, A., D. Fredga, and A. A. Sandberg. 1964. Nomenclature for centromeric position on chromosomes. *Hereditas* **52:** 201–220.

Liu, Z., D. Zhang, D. Hong, and X. Wang. 2002. Chromosomal localization of 5S and 18S-5.8S-25S ribosomal DNA sites in five Asian pines using fluorescence *in situ* hybridization. *Theor. Appl. Genet.* **122:** 1007–1024.

Lucchini, S., I. Nardi, G. Barsacchi, R. Batistoni, and F. Andronico. 1993. Molecular cytogenetics of the ribosomal (18 + 28S and 5S) DNA loci in primitive and advanced urodele amphibians. *Genome* **36:** 762–773.

Mäkinen, A., C. Zijlstra, N. A. Haan, C. H. M. Mellink, and A. A. Bosma. 1997. Localization of 18S + 28S and 5S ribosomal RNA genes in the dog by fluorescence *in situ* hybridization. *Cytogenet. Cell Genet.* **78:** 231–235.

Martins, C., and P. M. Galetti, Jr. 2001. Two 5S rDNA arrays in neotropical fish species: Is it a general rule for fishes? *Genetica* **111:** 439–446.

Nakamura, H. K. 1985. A review of molluscan cytogenetic information based on the CISMOCH-computerized index system for molluscan chromosomes. Bivalvia, Polyplacophora and Cephalopoda. *Venus Jpn. J. Malacol.* **44:** 193–226.

Navarro, A., and N. H. Barton. 2003. Evolution in rearranged chromosomes. *Science* **300:** 321–324.

Patterson, C. M. 1969. Chromosomes of molluscs. Pp. 635–689 in *Proceedings of the 2nd Symposium of Mollusca.* Marine Biological Association of India, Ernakulam, Cochin, India.

Pauls, E., and P. R. Affonso. 2000. The karyotype of *Nodipecten nodosus* (Bivalvia: Pectinidae). *Hydrobiologia* **420:** 99–102.

Rasotto, M., D. Altieri, and D. Colombera. 1981. I chromosomi spermatocitari di 16 species appartenenti alla classe Pelecypoda. *Atti Congr. Soc. Malac. Ital.* **1198:** 113–127.

Rice, E. L., D. Roddick, and R. K. Singh. 1993. A comparison of molluscan (Bivalvia) phylogenies based on palaeontological and molecular data. *Mol. Mar. Biol. Biotechnol.* **2:** 137–146.

Rieseberg, L. H. 2001. Chromosomal rearrangements and speciation. *Trends Ecol. Evol.* **16:** 351–358.

Rodríguez-Juíz, A. M., M. Torrado, and J. Méndez. 1996. Genome-size variation in bivalve molluscs determined by flow cytometry. *Mar. Biol.* **126:** 489–497.

Schmid, M., L. Vitelli, and R. Batistoni. 1987. Chromosome banding in Amphibia. IV. Constitutive heterochromatin, nucleolus organizers, 18S + 28S and 5S ribosomal RNA genes in Ascaphidae, Pipidae, Discoglossidae and Pelobatidae. *Chromosoma* **95:** 271–284.

Schneider, J. A. 2001. Bivalve systematics during the 20th century. *J. Paleont.* **75:** 1119–1127.

Spring, J. 2002. Genome duplication strikes back. *Nat. Genet.* **31:** 128–129.

Stanley, J. G., S. K. Allen, Jr., and H. Hidu. 1981. Polyploidy induced in the American oyster, *Crassostrea virginica*, with cytochalasin B. *Aquaculture* **23:** 1–10.

Thiriot-Quiévreux, C. 1994. Advances in cytogenetics of aquatic organisms. Pp. 369–388 in *Genetics and Evolution of Aquatic Organisms*, A. R. Beaumont, ed. Chapman and Hall, London.

Thiriot-Quiévreux, C. 2002. Review of the literature on bivalve cytogenetics in the last ten years. *Cah. Biol. Mar.* **43:** 17–26.

Vahidi, H., A. Purac, J. M. Leblanc, and B. M. Honda. 1991. Characterization of potentially functional 5S rRNA-encoding genes within ribosomal DNA repeats of the nematode *Meloidogyne arenaria*. *Gene* **108:** 281–284.

Von Brand, E., G. Bellolio, and K. Lohrmann. 1990. Chromosome number of the Chilean scallop *Argopecten purpuratus*. *Tohoku J. Agric. Res.* **40:** 91–95.

Wada, K. 1978. Chromosome karyotypes of three bivalves: the oysters, *Isognomon alatus* and *Pinctada imbricata*, and the bay scallop, *Argopecten irradians irradians*. *Biol. Bull.* **155:** 235–245.

Waller, T. R. 1991. Evolutionary relationships among commercial scallops (Mollusca: Bivalvia: Pectinidae). Pp. 1–73 in *Scallops: Biology, Ecology and Aquaculture*, S. E. Shumway, ed. Elsevier, Amsterdam.

Wang, Y., Z. Xu, and X. Guo. 2004. Differences in the rDNA-bearing chromosome divide the Asian-Pacific and Atlantic species of *Crassostrea* (Bivalvia, Mollusca). *Biol. Bull.* **206:** 46–54.

Wang, Z., X. Guo, S. K. Allen, Jr., and R. Wang. 1999. Aneuploid Pacific oyster (*Crassostrea gigas* Thunberg) as incidentals from triploid production. *Aquaculture* **173:** 347–357.

White, M. J. D. 1954. *Animal Cytology and Evolution.* Cambridge University Press, Cambridge. 454 pp.

White, M. J. D. 1978. *Modes of Speciation.* W.H. Freeman, San Francisco.

Xiang, J. H., R. R. Desrosiers, and F. Dube. 1993. Studies on the chromosomes of the giant scallop *Placopecten magellanicus* (Gmelin) and the surf clam *Spisula solidissima* (Dillwyn). *Cytologia* **58:** 125–132.

Xu, Z., X. Guo, P. M. Gaffney, and J. C. Pierce. 2001. Chromosomal location of the major ribosomal RNA genes in *Crassostrea virginica* and *Crassostrea gigas*. *Veliger* **44:** 79–83.

Zhang, F., Y. He, X. Liu, J. Ma, S. Li, and L. Qi. 1986. The introduction, hatchery rearing and culture of bay scallops. *Oceanol. Limnol. Sinica* **17:** 367–374 (in Chinese with English Abstract).

INDEX

D

E

F

G

H

I

J

K

L

M

N

O

P

Q

R

S

T

U

V

W

Y

Z

THE

BIOLOGICAL BULLETIN

2005 Subscription Form

Volumes 208-209, 6 issues

(Please print)

NAME: _____

INSTITUTION: _____

ADDRESS: _____

CITY: _____ STATE: _____ POSTAL CODE: _____

COUNTRY: _____ TELEPHONE: _____

FAX: _____ E-MAIL ADDRESS: _____

Please send me a 2005 subscription to *The Biological Bulletin* at the rate indicated below:

Price includes both print and online versions. All subscriptions run on the calendar year.

❒ Individual: $120.00 (6 ISSUES) ❒ Institutional: $360.00 (6 ISSUES)

❒ Individual: $70.00 (3 ISSUES) ❒ Institutional: $180.00 (3 ISSUES)

Check one: ❒ February, April, June or ❒ August, October, December

Please send me the following back issue(s): _____

❒ Individual: at $25.00 (PER ISSUE) ❒ Institutional: at $75.00 (PER ISSUE)

Delivery Options

❒ Surface Delivery (Surface delivery is included in the subscription price.)

❒ Air Delivery (Please add the correct amount to your payment.)

U.S. and Canada: $45.00 Mexico: $60.00 All other locations: $100.00

Payment Options

❒ Enclosed is my check or U.S. money order for $ _____

payable to Marine Biological Laboratory (with reference *The Biological Bulletin*)

❒ Please charge my ❒ VISA ❒ MasterCard ❒ Discover Card $ _____

Account No.: _____ Exp. Date: _____

Signature: _____ Date: _____

❒ Please send me an invoice. (Note: Payment must be received before subscription commences.)

Return this form with your check or credit information to:

Subscription Administrator, *The Biological Bulletin*
Marine Biological Laboratory, 7 MBL Street
Woods Hole, MA 02543 U.S.A.
Fax: 508-289-7922 • Tel: 508-289-7402 • E-mail: lreuter@mbl.edu

www.biolbull.org

Published by the Marine Biological Laboratory
Woods Hole, Massachusetts, 02543 U.S.A.

Brilliant Signals.

ew. Axio Imager.
iscover New World

A new generation of microscopes is setting new standards in digital imaging. Through ultimate optimization of components, flawless integration of digital imaging and pioneering developments in optics – Axio Imager from Carl Zeiss.

Carl Zeiss MicroImaging, Inc. zeiss/axio-imager.com 800.233.2343

ZEISS

We make it visible.